Developments and applications of solid phase microextraction (SPME) coupled to direct analysis in real time (DART) and approaches towards small volume analysis

by

Tijana Vasiljevic

A thesis

presented to the University of Waterloo

in the fulfillment of the

thesis requirement for the degree of

Doctor of Philosophy

in

Chemistry

Waterloo, Ontario, Canada, 2019

Examining Committee Membership

The following served on the examining committee for this thesis. The decision of the examining committee is by majority vote.

External Examiner

Prof. Karl Jobst
Adjunct Professor
Department of Chemistry & Chemical Biology
McMaster University

Supervisor

Prof. Janusz Pawliszyn
University Professor and Canada Research Chair
Department of Chemistry, University of Waterloo

Committee Member

Prof. Mario Gauthier
Professor
Department of Chemistry, University of Waterloo

Committee Member

Prof. Scott Hopkins
Associate Professor
Department of Chemistry, University of Waterloo

Committee Member

Prof. Juewen Liu
Professor
Department of Chemistry, University of Waterloo

Internal-external member

Prof. Brendan McConkey
Associate Professor
Department of Biology, University of Waterloo

Author's Declaration

This thesis consists of material which has been authored or co-authored by myself: see Statement of Contributions included in the thesis. This is the true copy of the thesis, including any required final revisions, as accepted by my examiners.

I understand that my thesis may be made electronically available to the public.

Statement of Contributions

Chapter 2 has already been published in three articles, and two manuscripts are currently pending acceptance. Chapter 2.3 includes the following manuscript "On the performance of solid-phase microextraction (SPME) fibers vs transmission-mode (TM) meshes for direct analysis in real time (DART) coupled to mass spectrometry (MS): Differences in analytical sensitivity", submitted for potential publication to *Journal of Separation Science*. The manuscript was co-authored/supervised by prof. Janusz Pawliszyn. In all cases, experimental planning, its execution, data analysis, data interpretation and writing of the manuscript was carried out by the author of this thesis. Chapter 2.4 includes the following manuscript "Direct Analysis in Real Time (DART) and Solid-Phase Microextraction (SPME) Transmission Mode (TM): A Suitable Platform for Analysis of Prohibited Substances in Small Volumes" which has been sent to *Analytical Methods* and is pending response. The manuscript was co-authored/supervised by prof. Janusz Pawliszyn. In all cases, experimental planning, execution, data analysis, data interpretation and writing of the manuscript was carried out by the author of this thesis. Chapter 2.5 includes the following manuscript "Towards on-site analysis of complex matrices by solid-phase microextraction-transmission mode coupled to a portable mass spectrometer via direct analysis in real time" (*Analyst, **2017**, 142 (16), 2928-2935*) which was co-authored by Gómez-Ríos, G.A.; Gionfriddo, E. and Yu, M. and supervised by prof. Janusz Pawliszyn. German A. Gómez-Ríos, Tijana Vasiljevic and Emanuela Gionfriddo share equal contribution to this manuscript, whereby experimental planning, execution, data interpretation and writing for analysis of drugs-of-abuse in oral fluid section is carried by the author of this thesis. Chapter 2.6 includes the following manuscript "High-Throughput Quantification of Drugs of Abuse in Biofluids via 96-Solid-Phase Microextraction–Transmission Mode (SPME-TM) and Direct Analysis in Real Time- Mass Spectrometry (DART-MS)" (*Rapid Comm. in Mass Spectrometry, **2019***) which was co-authored by Gómez-Ríos, G.A; Li, F.; Liang, P. and supervised by prof. Janusz Pawliszyn. In all cases, experimental planning, its execution, data analysis, data interpretation and writing of manuscript was carried out by the author of this thesis. Chapter

2.7 is dedicated to "Single Use Polyetheretherketone (PEEK) Solid-Phase Microextraction-Transmission Mode (SPME-TM) devices for rapid screening and quantitation of drugs of abuse in oral fluid and urine via direct analysis in real time-tandem mass spectrometry (DART-MS/MS)" *(Anal.Chem., **2018**, 90 (1), 952-960)* which was co-authored by Gómez-Ríos, G.A. and supervised by prof. Janusz Pawliszyn. In all cases, experimental planning, its execution, data interpretation and writing of the manuscript was carried out by the author of this thesis.

Section of chapter 3 has already been published as "Miniaturized SPME tips directly coupled to mass spectrometry for targeted determination and untargeted profiling of small samples" *(Talanta, **2019**, 199, 689-697)* and was co-authored by Singh, V. and supervised by prof. Janusz Pawliszyn. In all cases, experimental planning, execution, data interpretation and writing was carried out by the author of this thesis.

Chapter 4 describes a collaboration between University of Waterloo and Toronto General Hospital and has been submitted for potential publication to *Anaesthesia & Analgesia*. Tijana Vasiljevic completed the sampling, sample processing, instrumental run, data processing and data interpretation of 2015 and 2016/17 patient cohort. Dr. Barbara Bojko completed the sampling, processing, instrumental run, data processing and data interpretation of mice cohort. Dr. Sheila Riazi was crucial in providing the grant for the human and mice sampling. Dr. Anna Roszkowska and Dr. Ezel Boyaci contributed to experimental work and discussion. Dr. Natalia Kraeva aided in the sampling of the human cohorts. Dr. Susan Hamilton and Dr. Amy Hanna were instrumental in providing mice samples and aiding in their sampling. Tijana Vasiljevic also wrote the manuscript for submission to *Anaesthesia & Analgesia*, with contributions from Dr. Bojko and Dr. Riazi.

Abstract

Solid phase microextraction (SPME) has been rapidly developing since its invention in 1990. Due to a flexible design and the ability to implement various extractive coatings, SPME has found use in numerous applications. One such application is the coupling of SPME to Direct Analysis in Real Time (DART), an ambient ionization mass spectrometry (AIMS) technique. AIMS techniques completely eliminate the use of chromatography, reducing lengthy workflows and improving time-efficiency. SPME coupled to DART-MS has been quite successful in achieving low detection limits and reproducible results in bioanalytical applications. These successes are mostly due to the excellent preconcentrating and interference resisting abilities of SPME coatings and detection capabilities of DART-MS. Certainly, as a novel technique, many aspects of SPME-DART-MS are yet to be explored. Hence, this thesis investigated fundamental aspects of SPME-DART-MS, in addition to exploring novel applications, such as detection of prohibited substances in small bio-volumes (i.e., ≤ 25 µL of oral fluid (OF) and human blood) and implementation of SPME-DART-MS as high-throughput technology for quantitation of opioids in urine and human plasma in less than 1.5 h for a set of 96 samples. Coupling of SPME to portable DART-MS instrumentation was investigated for on-site, *in vivo* drug detection in samples of OF as a potential tool of law enforcement, reporting detection limits that are below those proposed by regulatory agencies. Additionally, the use of biocompatible plastic materials such as polyetheretherketone (PEEK) was investigated as a potential alternative material for the manufacturing of SPME devices for DART-MS, which are usually made of stainless steel (SS). Performance of the PEEK devices was similar to those of SS, allowing for their use in quantification of drugs-of-abuse (DoAs) in OF and urine at low parts-per-billion levels (ppb). In addition, OF samples following coffee consumption from a female volunteer were used to monitor caffeine half-life. The results were in compliance with established half-life of caffeine reported in literature, and highlighted the potential of the PEEK devices for *in vivo* buccal swabbing testing.

Another novel application of SPME described in this thesis was the development of miniaturized SPME devices "minitips" for analysis of small volumes. The analysis of small sample volumes (biofluids, tissues, and cells) has become more common within the scientific community in the last few years. For this type of analysis, very sensitive instrumental platforms and sample preparation methods are required to obtain qualitative and quantitative information. Hence, the SPME minitip format was introduced, and the tip apex was coated with 1 millimeter (mm) of polyacrylonitrile (PAN) and in-house-synthesized N-vinylpyrrolidone-co-divinylbenzene, also known as hydrophilic lipophilic balance (HLB) particles. Robustness, extraction efficiency, repeatability, reusability, and matrix effect (ME) assessment yielded good results. Benzodiazepines were extracted from 15 µL of phosphate buffer saline (PBS) and urine, and certain DoAs were extracted from 1 µL of OF using LC-MS/MS. Very good figures of merit were obtained, with limits of detection (LODs) and quantitation (LOQs) in the lower ppb range. DoAs were also extracted from 1 µL of blood by directly coupling the SPME minitips to nanoelectrospray ionization (nESI) devices. The SPME HLB minitips were also used for untargeted metabolomic profiling of caviar eggs via liquid chromatography high resolution mass spectrometry (LC/HRMS), thereby showing that despite introduced dilution, satisfactory results can be obtained. Indeed, good statistical separation of caviar eggs was observed, in addition to extracting well over a hundred significant features.

Lastly, this thesis also details application of SPME for untargeted metabolomics profiling of patient affected with a genetic condition known as malignant hyperthermia (MH). Small human muscles obtained from Toronto General Hospital were sampled using SPME fibers and analysed via LC/HRMS using an untargeted metabolomics approach. Potential disease related compounds (i.e., biomarkers) were found, aiding in the elucidation of the biochemical pathways affected in patients with MH. The accepted diagnostic tool of MH is a highly invasive procedure which involves excision of a portion of the Gracilis muscle. Hence the prospect of using SPME as minimally invasive diagnostic tool was discussed.

As this thesis shows, the opportunities of SPME are many; and its continuous development will most likely require efforts and collaboration from experts in numerous fields.

Acknowledgement

I would like to take this opportunity to express my appreciation to all who have supported and assisted me in the completion of my PhD.

Firstly, I would like to thank my supervisor, prof. Janusz Pawliszyn, for letting me be a part of his research team. My learning experience has been exceptional, and I would like to thank prof. Pawliszyn for helping me in the development of my skills as an analytical chemist and for always encouraging me to think critically. I am very grateful for the opportunity to participate in a range of projects, and for being allowed to participate in international conferences and meetings to present my research to the scientific community.

I would like to thank my committee members, prof. Mario Gauthier, prof. Scott Hopkins and prof. Juewen Liu for their continuous support over the last five years and for the time and effort spent reading my thesis. I would also like to thank my external committee member, prof. Karl Jobst and my external-internal committee member, prof. Brendan McConkey for accepting the invitation to be a part of reading and evaluation of my thesis.

I would also like to thank my University of Waterloo colleagues, who have helped me tremendously and in different ways during my doctoral studies including Ms. Nikita Looby, Ms. Sofia Lendor, Dr. German Augusto Gómez-Ríos, Dr. Nathaly Reyes-Garces, Dr. Emanuela Gionfriddo, Dr. Varoon Singh, Dr. Marcos Tascon, Dr. Ezel Boyaci, Mr. Daniel Rickert, Dr. Miao Yu, Dr. Anna Roszkowska, Ms. Dominika Gruszecka, Mr. Alexander Kasperkiewicz and Mr. Emir Nazdrajic.

I would also like to thank our industrial collaborators including Dr. Brian Musselman, Mr. Frederick Li, Mr. Paul Liang, Mr.Joseph Tice, Dr. Dragan Vuckovic and Mr. Craig Aurand.

Gratitude also goes to Dr. Sheila Riazi of Toronto General Hospital's Pain Management unit for collaboration on the Malignant Hyperthermia project.

Dedication

I dedicate this thesis to

my parents, Fatima and Dragan Vasiljevic

my grandparents, Bosko & Zora Vasiljevic and Ibrahim & Ajsa Zajkic

my brother, Sanjin Vasiljevic

and my husband, Karlos Geljic

for their love, support and understanding.

"Znaš li šta je najljepše u životu? Želja, prijatelju."
Eng. translation: "Do you know what the most beautiful thing in life is? Aspiration, my friend."
(Meša Selimović, The Fortress, 1970, Bosnia & Herzegovina)

Table of Contents

List of Figures

xix

List of Tables

List of Abbreviations

+ve	Positive
-ve	Negative
ACN	Acetonitrile
AIMS	Ambient ionization mass spectrometry
BZDs	Benzodiazepines
C18	Octadecyl
DART	Direct analysis in real time
DBS	Dried blood spots
DMF	Dimethylformamide
DoAs	Drugs of abuse
DRUID	Driving under the Influence of Drugs, Alcohols and Medicines
ESI	Electrospray ionization
FA	Formic acid
GC	Gas chromatography
H_2O	Water
HCl	Hydrochloric acid
HLB	Hydrophilic lipophilic balance
HRMS	High resolution mass spectrometry
HV	High voltage
IPA	Isopropanol
IE	Ionization energy
IS	Internal standard
LC	Liquid chromatography
LDR	Linear dynamic range
LOD	Limit of detection
LOQ	Limit of quantitation
m/z	Mass-to-charge
ME	Matrix effects

MeOH	Methanol
MH	Malignant hyperthermia
MM	Mixed mode
MRM	Multiple reaction monitoring
MS	Mass spectrometry
MS/MS	Tandem mass spectrometry
N$_2$	Nitrogen
OF	Oral fluid
PA	Proton affinity
PAN	Polyacrylonitrile
PBS	Phosphate buffer saline
PCA	Principal component analysis
PEEK	Polyetheretherketone
PLS-DA	Partial least square discriminant analysis
PoA	Percentage open area
PQC	Pooled quality control
PS	Paper spray
QC	Quality control
Q-TOF	Quadrupole time of flight
QqQ	Triple quadrupole
RSD	Relative standard deviation
SA	Surface area
SiNPs	Silica nanoparticles
SPME	Solid phase microextraction
SS	Stainless steel
SVP	Standard voltage and pressure
TDM	Therapeutic drug monitoring
TM	Transmission mode
UW	University of Waterloo

Chapter 1: Introduction

1.1 The importance of analytical chemistry

Many researchers in scientific- and engineering-based fields often seek the aid of analytical chemists to identify and quantitate specific compounds. The obtained results often contribute significantly to the research in question, as they can play a large role in establishing conclusions and/or next step(s). This involvement extends to a variety of areas, including monitoring and evaluating the safety and quality of water, food(s), and pharmaceutical products. For example, analytical chemists can evaluate the extent of meat spoilage by examining compounds like glucose and lactic acid, which can be found in bacterial microflora.[1] Analytical chemists also play a key role in criminal trials, as their forensic findings are often critical in determining whether or not a defendant is innocent. Specialized investigations can also aid in solving particular analytical problems. For instance, the causes of cracks and fissures in roads and sidewalks can be determined by examining the chemical composition of the asphalt that was used to make them. Such approaches not only allow the asphalt to be accurately characterized, but they also allow us to better understand the factors that impact asphalt quality.[2] Furthermore, analytical chemists can help to study the underlying mechanisms of cancer by screening and quantifying the chemical markers, known as biomarkers, associated with the disease.[3] Most recently, the legalization of marijuana use in Canada has created a need for research by analytical chemists, especially in relation to quality control of cannabis products, which is being strictly regulated by Health Canada.[4,5] Such analytical work could include testing for unauthorized pesticides, microbial/chemical contaminants, solvent residues, percentage of Δ-9-tetrahydrocannabinol (Δ-9-THC), Δ-9-tetrahydrocannabinolic acid, cannabidiol, and cannabidiolic acid.[4,5] Certainly, none of the above-mentioned applications would be possible without the continuous effort of scientists around the world to advance analytical technology. It is clear that analytical chemistry (AC) aims to improve quality of life by developing strategies that allow us to analyze a number

1

of different compounds. The work presented in this thesis reflects some of the most popular areas of inquiry in modern 21st century AC.

1.2 The basic protocol of analytical chemistry

AC is a branch of chemistry that focuses on the qualification and/or quantification of various compounds (analytes) in different media, commonly referred to as "matrices" (matrix, sing.). Matrices range in complexity from pure, interference-free samples (e.g., H_2O), to solid matrices containing high amounts of endogenous/exogenous components (e.g., biologicals, foodstuff, soil, crude oil, etc.) that can interfere with analytical measurements. For example, analyzing Δ-9-THC in "pot brownies" is challenging due to the complexity of the matrix (i.e., high level of fats and carbohydrates).[6] In order to develop a robust method for analyzing target analyte(s), it is imperative to devise a comprehensive protocol that includes an adequate sampling strategy (proper sampling of sufficient amounts of the true matrix representative), sample preparation method (isolating and preconcentrating the compounds of interest from the matrix), separation technique (partitioning complex mixtures into smaller fractions, which is also known as chromatography), identification/quantitation approaches (use of analytical instrumentation and statistical tools to establish the presence of specific compounds and to assess their quantities), and decision-making processes (the use of obtained data to form a conclusion and, if needed, to determine the next step).[7] It is critical to optimize each step in the protocol, as they are prone to a "domino effect"; that is, the actions performed in each step impact all subsequent steps.[7] For example, an error in the sample preparation stage could result in errors in the quantitation of target compound(s). While the sampling protocol is often considered to be the least difficult step, certain situations can make it very challenging to obtain a true representation of the matrix (in proper amounts). One example of this occurs when a tiny needle must be maneuvered in order to sample a specific area of a microscopic cell.[8] As mentioned above, sample preparation aims to provide a truly "representative, reproducible and homogeneous solution" that is appropriate for instrumental analysis.[9] Figure 1.1 outlines some of the main points to consider when

2

choosing a sample preparation strategy, including the physical state of the matrix (gaseous, solid, liquid, mixtures), the available volume and/or mass, and the presence of interfering components. For example, certain sample preparation approaches will not be applicable if the matrix is a gas (e.g., human breath, car exhaust, roasted coffee). Similarly, analysts should avoid exhaustive approaches- which destroy and/or consume the sample when sufficient amounts of matrix are unavailable.[7]

Important factors to consider for method development

1.) What is the matrix?
➢a. Is the matrix gaseous, solid, liquid or a suspension?
➢b. What is the volume/mass of the matrix?
➢c. What are potential interferences that might arise from the matrix?

2.) What is the analytical instrumentation?
a. Which analytical technique is being used?
b. What is the expected run-time?
c. Are there requirements imposed on sensitivity/detection limits?

3. What are the evaluation requirements?
a. Is qualitative or quantitative information needed?
b. What is the accuracy and precision?

Figure 1.1 *Outline of major considerations in choosing a sample preparation approach.*

If the matrix is highly complex, yet valuable (e.g., meconium—the first feces of a newborn), its impact on the extraction process and the qualitative/quantitative analysis of target compounds should be assessed.[10] For example, some matrices can even "stick" to sample preparation tools, thus interfering with their capabilities.

The selection of analytical instrumentation usually involves carefully assessing a given platform's suitability for analyzing the compounds of interest. This is an important consideration, as certain techniques are inappropriate for analyzing certain compounds. For example, determining concentrations of metallic species (e.g., As, Cd, Cu, Pb, Mo, Se, and Zn) requires instruments capable of very low detection limits (parts-per-trillion), as these analytes are often toxic at very low levels. Hence, inductively

coupled plasma MS is often used to analyze metallic species due to its excellent detection capabilities. Instrumental run time should also be determined and, if possible, measures should be taken to reduce it. This is particularly important for assays wherein a large number of samples must be analyzed. Furthermore, the instrument's sensitivity and detection limits should also be evaluated, particularly in cases where specific performance requirements must be satisfied, for example, the Food and Drug Administration's (FDA) bioanalytical method validation guidance.[11]

Ultimately, the choice of sample preparation method and analytical instrumentation will depend on the requirements of the evaluation. In other words, is the method being used for screening applications (qualitative analysis), or is it being used to determine the actual concentrations (quantitative analysis) of target analytes? The answers to these questions play a central role in determining the complexity of the sample preparation step and the level of sophistication required for the analytical instrumentation. Finally, the accuracy and precision of the analytical method should be provided, as these metrics allow for a fair assessment of the method's success and allow for suggestions on future improvements.

1.2.1   Common sample preparation strategies

According to Pawliszyn, sample preparation consists of an "extraction procedure that results in isolation and enrichment of components of interest from a sample matrix."[12] The extraction procedure primarily depends on the choice of the extraction phase, which is directly responsible for analyte isolation.[12] The extraction phase and the matrix may be in different phases (i.e., solid, liquid, or gas), but they remain in contact with each other during the extraction procedure while the analytes are being transported between the two.[7,12] For example, liquid-solid extraction uses a liquid (e.g., a strong solvent like MeOH) to extract analytes from a solid matrix (e.g., soil). The extraction rate and the distribution of the analyte(s) between the two phases will depend on the distribution constant, temperature, and volume of the phases, and their diffusion rates.[7,12,13] A summary of commonly employed sample preparation strategies can be seen in

Figure 1.2.[13,14] As mentioned above, liquid-based extractions rely on the use of a solvent to perform extractions. These methods—which include liquid-liquid extraction (LLE), liquid-solid extraction, enhanced liquid extraction, single drop extraction, and "assisted" liquid extraction—are easy and cheap, but it is necessary to evaluate their specificity and sensitivity for target compounds prior to performing any experiments, as their preconcentrating ability is limited. Additionally, liquid-based methods offer little to no sample clean-up, which progressively contaminates the MS and results in elevated instrumental noise.
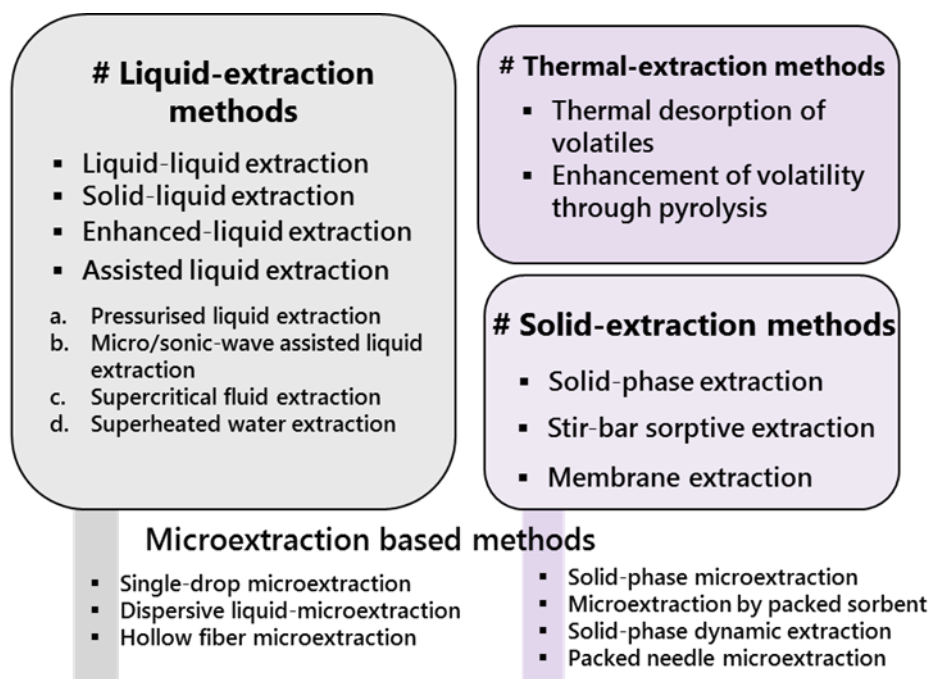
Figure 1.2 *Summary of commonly used sample preparation approaches.*

Solid-based extractions, which include solid-phase extraction (SPE), stir-bar sorptive extraction, and membrane extraction, rely on the use of an extractive solid phase to isolate/preconcentrate analytes of interest. The most popular solid-based approach is SPE, which consists of an extractive solid phase (also known as a cartridge) that is immobilized within a plastic container. However, SPE is hampered by a number of drawbacks, including a laborious, time-consuming workflow that becomes even more arduous when sample pretreatment is required for more complex matrices (e.g., blood, plasma, tissue).

In contrast to the aforementioned strategies, which are mostly exhaustive, microextraction-based approaches only require the extraction of a small portion of the analyte. The extraction phases used in microextraction are quite small (< 100 μL or 100 mg) and are usually insufficient for exhaustive analyte removal.[7,15] In recent years, microextraction approaches have begun to be utilized more frequently due to their simplicity, need for fewer resources, cost-effectiveness, and increased sample throughput, which is largely due to the elimination of the time-consuming steps required for traditional sample preparation methods (i.e., LLE or SPE). Examples of microextraction approaches include dispersive liquid-liquid microextraction, hollow-fiber microextraction, microextraction by packed sorbent, solid-phase dynamic extraction, packed-needle microextraction, and SPME.[7,14]

1.3   SPME: the fundamentals

SPME is sample preparation technique that was developed by Arthur and Pawliszyn in 1990, and it has become a source of inspiration for researchers in many fields in the nearly 30 years since that time.[7,16] SPME's appeal is largely due to its simple operation (i.e., a minimal number of steps implemented in the workflow), which provides significantly improved accuracy and precision. As its name suggests, SPME consists of a solid phase (i.e., extractive phase, also referred to as a coating), which is firmly fixed onto a support/base.[7,16] The support can be made of many different materials (optical fiber,[16] nickel-titanium (nitinol),[17] SS,[18] plastics,[19] etc.) with the coating typically being deposited onto it externally. Most SPME configurations utilize this "open-bed" format,[7] with the exception being in-tube SPME wherein the coating is deposited inside of a capillary.[20] The most popular SPME format is the SPME fiber. Figure 1.3 shows an example of a fiber used for LC-SPME applications, wherein the support consists of a flexible nitinol fiber and a solid C18 coating. A variety of other SPME formats are also available for a number of different applications (Figure 1.4).[20–30] For example, membrane SPME probes can be placed directly on human skin for the *in vivo* detection of skin volatiles.[21] In general, two main extraction

strategies are used in SPME: direct exposure to the matrix (e.g., immersion into urine), or indirect exposure via headspace sampling (e.g., extraction of volatiles).[7]
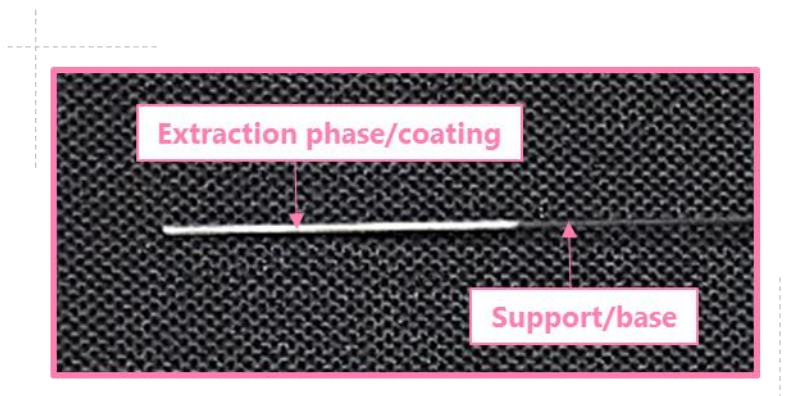
Figure 1.3 *Example of one of the most popular formats of SPME, the "fiber." The depicted device consists of a C18 coating and a nitinol support.*
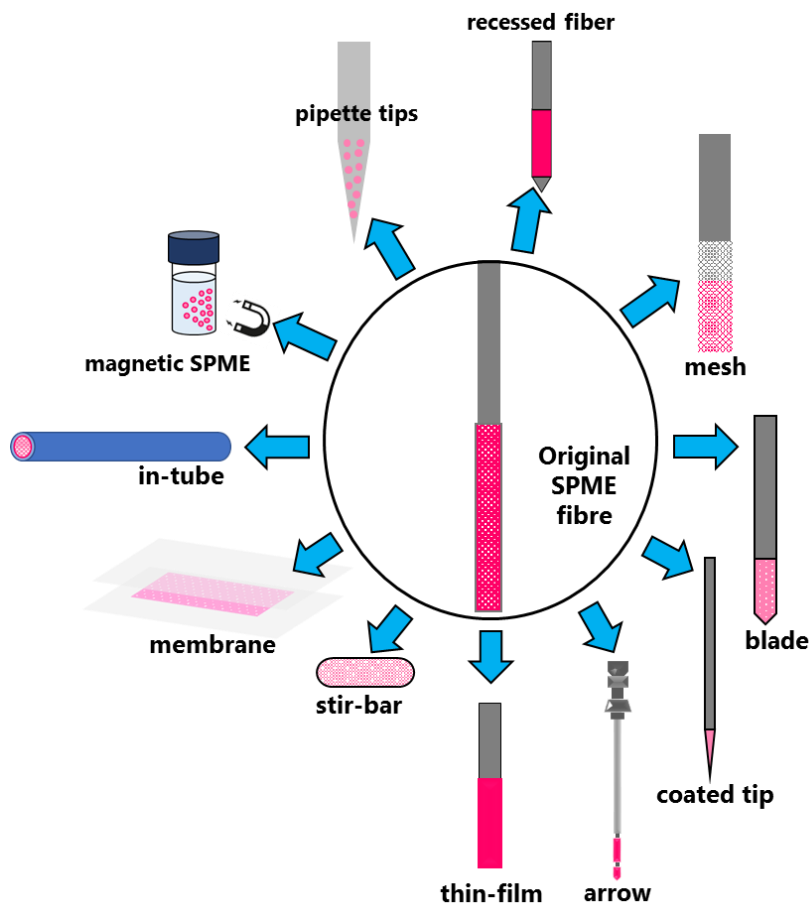
Figure 1.4 *Various different formats that were inspired by the original design of the SPME fiber (represented in the white circle).*

When the device is ready for use, it is exposed to a sample of interest for a pre-determined amount of time in order to extract the analytes. Figure 1.5A contains a schematic of an SPME used for direct-exposure extraction from a liquid sample, with *'a'* denoting the fiber support's inner radius, *'b'* denoting the coating's radius, and *'L'* denoting the entire coating length.[7] The sample volume to which the fiber is exposed is labeled *'Vs'*, while the initial analyte concentration in the sample is labeled *'C_S^0'*.[7] The coating volume is labeled *'V_e or V_f'*, and the interaction between the coating and the analytes can be described using *'K_{es} or K_{fs}'*, which are known as the fiber partitioning coefficient/constant.[7] The analytes present in the sample have their own diffusion coefficients *'D_s'* as well as diffusion towards the fiber, which is labeled *'D_f'*.[7] The kinetic theory of SPME states that the amount of analyte that can be extracted depends on their diffusion constants and the agitation (convection) conditions present in the system.[7,12]
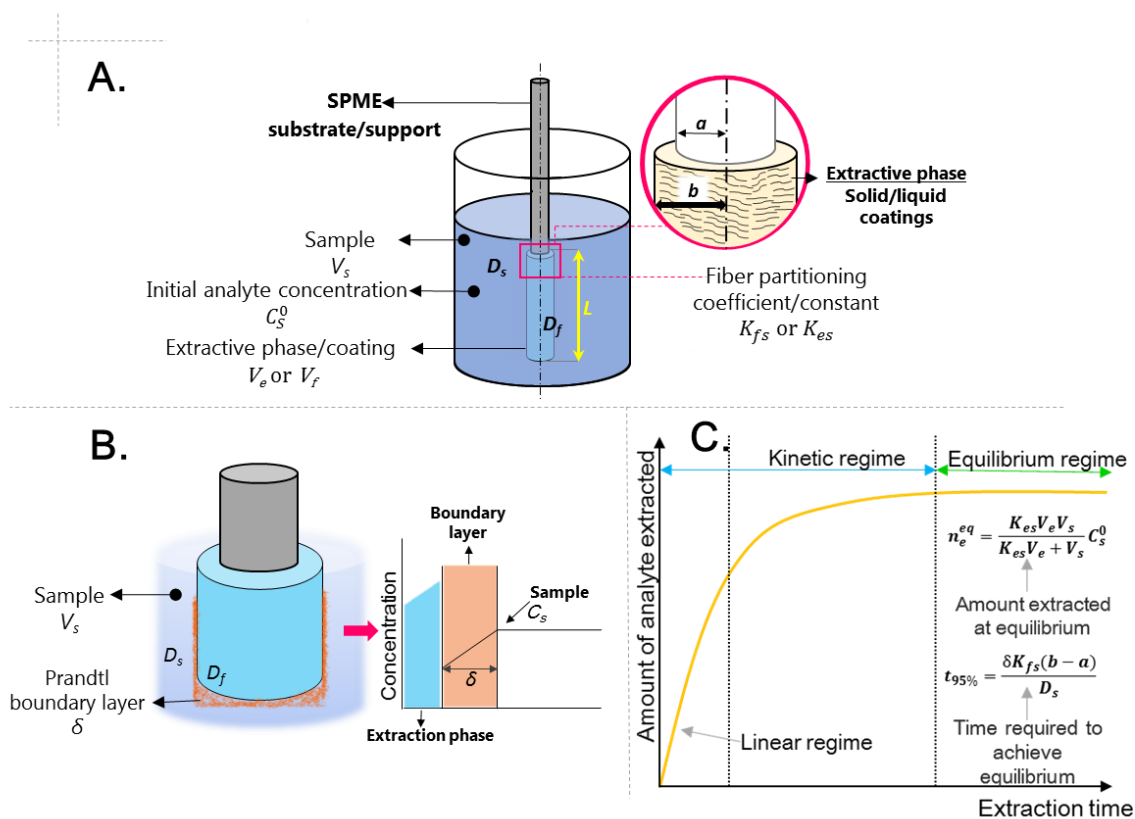
Figure 1.5 *Schematic of SPME components and main principles governing its extraction mechanism. Figure 1.5**A**. shows the basic configuration of an SPME being used in direct-exposure mode with a liquid solution. Figures 1.5**B-C**. show some thermodynamic and kinetic principles of SPME.*

Although SPME can use either static or agitated extraction to suit the situation, the fluid contacting the fiber surface will always be stationary, regardless of which one is chosen.[7] The stationary fluid labeled δ and represented by an orange coating in Figure 1.5B is known as Prandtl's boundary layer.[7] This layer can have different thicknesses depending on the agitation and diffusion of the analytes. The concentration gradient in Figure 1.5B shows that analyte concentration tends to drop as it approaches the δ, resulting in a lower concentration near the fiber surface.[7] The amount of analyte ultimately extracted by SPME is largely time dependent, as analyte molecules diffuse progressively deeper into the coating as extractions increase in duration.[7] Hence, the amount of analyte extracted by the SPME coating (which is also the basis of its quantitative application) can be expressed using the following equation:

Equation 1.1

$$n_e^{eq} = \frac{K_{es}V_eV_s}{K_{es}V_e + V_s} C_s^0$$

where n_e^{eq} is the amount of analyte extracted at equilibrium conditions.[7] According to physical chemistry, chemical equilibrium is a state in which "both reactants and products have no tendency to change their concentrations over time"; but dynamic fluctuations can still exist in the system.[31] Once the SPME device has been exposed to the sample, the analytes will diffuse into the coating until only an insignificant amount is extracted. This condition is known as equilibrium extraction.[7] Performing extractions past the equilibrium point will not increase the amount of analyte that is extracted. As Pawliszyn notes, "equilibration time is assumed to be achieved when 95% of equilibrium amount of the analyte is extracted from the sample," with the 5% accounting for the possibility of experimental error.[7] However, it is not always necessary to achieve equilibrium, particularly when sampling is challenging (e.g., *in vivo* sampling of live animals). In such cases, a kinetic or linear regime, also known as pre-equilibrium, can be employed.[7] Figure 1.5C shows a typical SPME extraction-time profile, where the x-axis represents the extraction time and the y-axis represents the amount of analyte extracted. A kinetic regime is defined

by a steady increase in the amount of analyte extracted, while an equilibrium regime exhibits an extraction plateau after a specific period.[7] The main factors that influence the time required to achieve equilibrium can be expressed using the following equation:

$$t_{95\%} = \frac{\delta K_{fs}(b - a)}{D_s}$$

where $t_{95\%}$ denotes the time required to extract 95% of the analytes under equilibrium conditions.[7] As Equation 1.2 shows, extraction time is directly proportional to the distribution coefficient, $K_{fs}(\frac{c_e^{eq}}{c_s^{eq}})$, the boundary layer, δ, and the thickness of the extraction phase, b-a.[7] In other words, extraction times can be very long if analytes have very high affinity for the coating (high K_{fs} value); δ is too large (e.g. no agitation); and the coating on the SPME device is too thick. These factors must be carefully considered and adjusted accordingly prior to any experiments. Once the analytes have been extracted through SPME, they are removed from the coating via a desorption step, which can be done with a heated gas (e.g., GC applications) or a strong solvent (e.g., LC applications).[7] The desorption-time profile is often derived by examining different desorption time points and it is crucial for ensuring that the extracted analytes are completely removed from the SPME device.

Lastly, it is important to note that SPME extracts via free concentration, which refers to the fraction of the analyte(s) that are not bound to matrix components.[7] When analytes are present in a specific matrix, they do not simply "drift" within it; rather, they tend to bind to matrix components.[7] For example, analytes spiked to matrices like water and PBS have high free concentrations, as they do not contain significant analyte-binding components. In contrast, analytes have a tendency to bind to human plasma because it is made of plasma proteins (~7 to 8% v/v), which have analyte-binding properties.[7,32] Analyte-matrix binding can be expressed numerically via matrix-binding constants.[15] Significantly, analyte-

matrix binding reduces the amount of free concentration available for SPME extraction, which can result in decreased sensitivity for SPME methods.[7,15]

1.3.1 Commonly employed calibration methods of SPME

A number of calibration options have been devised for SPME that allow it to be used in different sampling scenarios. For example, SPME has successfully been used to determine an average 3-month concentration of biocides and UV-blockers in wastewater,[33] the presence of the "earthy" off-flavor compounds, geosmin and 2-methylisoborneol, in live fish,[34] and concentrations of the anti-cancer drug, doxorubicin, in pig lungs.[35] While a number of different calibration strategies exist for SPME, the present discussion will be limited to "traditional" calibration methods, specifically the spiking of external standards and the use of ISs for correction. A detailed review on SPME calibration methods is available for those interested.[36]

External-standard calibration involves preparing standard solutions of working analytes at a range of concentrations and then spiking them into the matrix. The spiked analytes are then extracted by SPME, and a calibration plot is obtained by plotting the response for the amount extracted (y-axis) against the spiked concentration (x-axis). This approach is also known as matrix matched calibration, as the matrix is used in the construction of the calibration plot.[7,36] Matrix matched calibration is valuable because it considers the extent to which the matrix influences the amount of analyte that is extracted. Extractions from a "blank matrix" are also performed in order to determine the level of instrumental noise. If an IS is used for a matrix matched external-standard calibration, it is usually spiked at a single concentration across the range of the spiked external standards. The calibration plot is then obtained by plotting the response of the spiked concentration (x-axis) against the ratio of external standard area to IS area (y-axis).[7,36]

1.3.2   SPME coatings

Coating type is a major factor that impacts SPME sensitivity. Since compounds have greater affinity for coatings with similar polarities, their logP values (octanol-water partition coefficient, often used to describe polarity)[37] can be used as an indicator for selecting an appropriate coating.[7,38] Another critical aspect to consider when selecting a coating is durability. For example, if the coatings are to be used in applications involving thermal desorption, robust heat-stable coatings should be employed. If desorption is to be done using a strong solvent, then it is important to select a coating that will not crack, swell, or strip-off upon solvent exposure. Device robustness and flexibility are also critical, particularly when the coating is being used to penetrate solid materials; for such applications, it is important to ensure that the coating will not strip off during withdrawal from solid matrices, such as tissue or animal skin.[7] In addition, it is imperative that the coatings maintain adequate repeatability, which can be assessed by evaluating inter (many) and intra-device (single) reproducibility.[7] In some cases, SPME coatings can be re-used if a proper cleaning procedure is employed.

In the last decade, there has been a tremendous increase in the number of coatings reported for SPME use. These materials consist of either solid or liquid polymers,[15] nanomaterials (e.g., metal organic frameworks),[39,40] specialized coatings (e.g., molecularly imprinted polymers),[41] conductive polymers[42] and ionic liquids.[43] Various approaches have also been devised for depositing the coatings onto the support, including dipping,[24] brush-painting,[44] spraying,[44] electrodeposition,[25] sorbent adhesion[45] and sol-gel.[46] Over the last few years, the Pawliszyn group has been investigating the use of SPE sorbent particles as SPME coatings.[44,45,47–50] These particles, which have a powder-like consistency, can be mixed with a binding material to create a coating slurry. This idea originated in the work of Musteata et al., who proposed using biocompatible polymer PAN as a binding material for the sorbent particles.[48] By definition, biocompatible materials are materials that do not cause toxic shock within living systems.[48] Conveniently, PAN contains nitrile groups with hydrophilic and negatively charged properties that

prevent unwanted biologicals from adhering to the surface; thus, PAN acts as a restricted access material.[7,15,49,51,52] A schematic detailing PAN's action is presented in Figure 1.6. When foreign material is exposed to blood, the first event that occurs is the adsorption of hydrophobic materials and proteins to its surface.[53] This poses a problem, as the adsorption of unwanted material to the SPME coating hinders the extraction process by slowing the transfer of analytes. Fortunately, the electronegative nitrogen in PAN significantly reduces the attachment of biomolecules.[49] The development of biocompatible coatings has allowed SPME fibers to be used in minimally invasive applications, such as the *in vivo* sampling of beagles[54] and muskellunge fish,[55] which provides SPME with a distinct advantage over other commonly employed techniques, such as SPE and LLE.
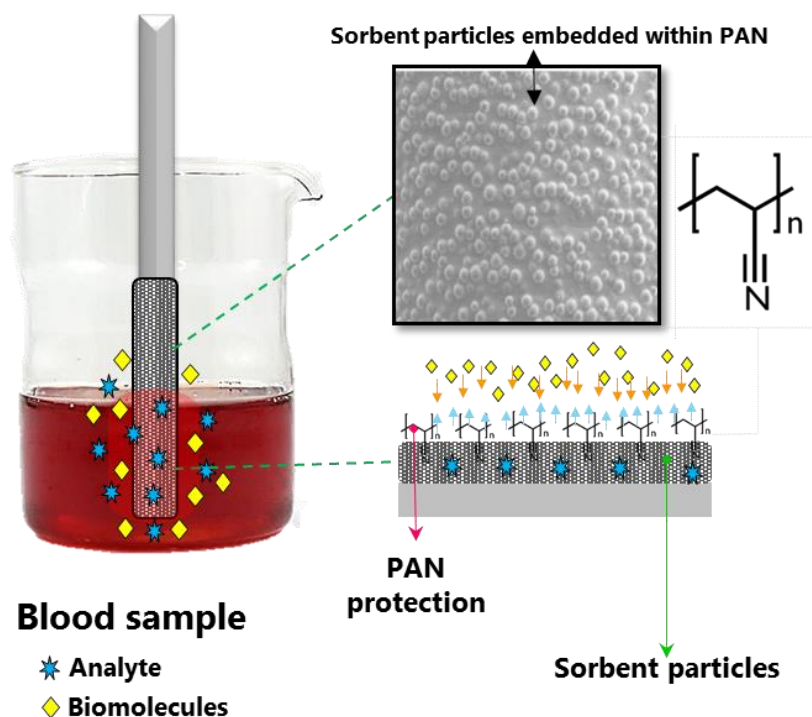
Figure 1.6 *Schematic representation of the application of PAN in blood.[48]*

1.3.3 SPME's growth in bioanalytical chemistry and metabolomics

The term bioanalytical chemistry (also known as bioanalysis) refers to the "analysis of drugs, their metabolites and low molecular weight biomarkers in biological matrices such as plasma, serum, whole blood, urine, oral fluid, tissues, etc."[9] Bioanalysis is somewhat challenging due to the complexity of

biological matrices, which consist of numerous components, such as salts, acids, bases, proteins, cells, lipids, and lipoproteins.[9] Each bio-matrix contains different degrees of interference and should be carefully assessed in terms of matrix effects (ME),[56] which is a phenomenon that occurs when matrix components interfere with the analysis of compounds of interest.[56] These components either increase (matrix-enhancement) or decrease (matrix-suppression) signals that arise from the analyte(s) of interest.[56] Fortunately, SPME employs a small amount of extractive phase, which limits the amount of interferences co-extracted, thus reducing ME. In addition, the use of PAN coatings mentioned in the previous section is crucial in reducing the adherence of unwanted biologicals, which also contributes to the reduction of the ME. Since Musteata et. al.'s 2007 publication on the use of PAN, a number of studies have detailed its use with SPME for analysis of urine,[26] plasma,[44] OF[57] and blood.[49] Another important characteristic of SPME is its ability to equally extract analytes of varying polarities, also known as "balanced coverage."[15] Nonpolar (hydrophobic) compounds have a greater tendency to bind to matrix components, thus having a lower free concentration in the matrix.[15] In contrast, polar (hydrophilic) compounds bind less to matrix components, resulting in a higher free concentration in the matrix.[15] Hence, analytes with a lower binding constant for the matrix are extracted more rapidly by SPME, while analytes with higher binding constants require more time to be extracted in the same amounts.[15] Hydrophilic analytes that have already been extracted do not become displaced by hydrophobic analytes due to their extended extraction times and reduced free concentrations.[15]

SPME's ability to provide balanced coverage has enabled it to be used successfully in the field of metabolomics. Metabolomics is concerned with extraction of small molecules (MW ≤ 1000 Da) called metabolites, which provide a representative snapshot of a particular subject's metabolism at the time of extraction.[58] As such, metabolites can provide insight into the healthy and diseased states of humans by revealing important information about the biochemical pathways involved with a given disease, which can ultimately be used in therapy development.[58] Global (untargeted) metabolomics (i.e., fingerprinting)

aims to extract as many metabolites as possible,[15] while targeted (i.e., profiling) metabolomics seeks to examine specific metabolite(s).[15] For untargeted metabolomics, the idealistic aim of an extraction protocol, or sample preparation strategy, is to be as unselective as possible.[59] In 2010, Vuckovic and Pawliszyn provided support for the balanced coverage theory of SPME by showing that mixed-mode coatings (C18 with benzenesulfonic acid group as cation exchanger ($C_6H_6O_3S$)) are capable of extracting a range of metabolites with logP values ranging from -7.9 to 7.4.[45] In the time since Vuckovic and Pawliszyn published their findings, SPME has been used in a variety of untargeted metabolomics investigations.[50,57,60–62]

1.3.4 General workflow of SPME method development in bioanalysis

SPME method development begins with the selection of a coating. To this end, analysts must consider the logP values of the analytes of interest, and then choose a coating with a proper affinity for these analytes. If sensitivity is problematic, other SPME formats with greater surface areas (e.g., SPME thin-films)[23] could be a viable option. Once a coating has been determined, a preconditioning procedure is used to "wet" the coating surface to ensure that the material is primed prior to extraction. Before extraction, the SPME device should be washed with H_2O to remove any residual solvent, as this could interfere with the partitioning equilibria if it comes into contact with the sample.[7] The total volume of standards spiked into the sample should not exceed 1% of the sample's total volume in order not to disturb partitioning equilibria.[7] The extraction process is then optimized with respect to sample volume, extraction time, agitation, and potential matrix modifications.[38] Sample volume and the number of replicates that can be achieved both depend on the quantity of available matrix. Extraction-time profiles are built by assessing whether adequate sensitivity was obtained at different time points. While extraction times can be decreased by using agitation, static extraction is more appropriate in certain scenarios (e.g., *in vivo* sampling). In addition, matrix modifications might be required if there is significant sample-to-sample variation (e.g., normalization of urine pH when samples from multiple individuals are used).[63]

After the extraction is completed, the devices should be washed with H_2O for a pre-determined amount of time to remove any unwanted biologicals. Finally, the optimum desorption solution or mixture is identified in order to guarantee that the analytes will be completely removed from the SPME device. Desorption conditions must be evaluated to identify the optimum solvents or mixtures, which guarantees that the analytes are completely removed from the SPME device. Additionally, failure to optimize the volume of the desorbing solution can result in excessive analyte dilution. Lastly, the presence of carry-over should be examined. This is particularly important in cases of "sticky compounds," which are those with very high logP values.[64] These steps are summarized in Figure 1.7.
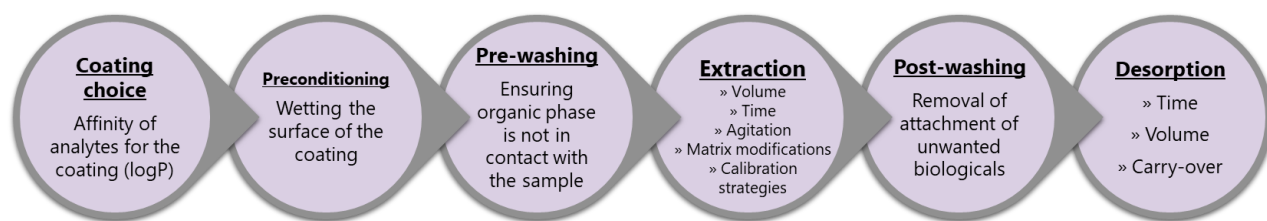
Figure 1.7 *Summary of main steps involved in SPME method development for bioanalytical applications.*

1.4   General workflow of untargeted metabolomics

As mentioned in section 1.3.3, untargeted metabolomics aims to extract as many metabolites as possible in an effort to understand the biochemistry of living systems. Although metabolomics research often occurs within the context of biological investigations, environmental[65] and food[66] metabolomics have also been reported. SPME has been coupled to both GC and LC platforms for metabolomics; for such couplings, the platform choice is dictated by the physico-chemical properties of the metabolites (i.e., volatile, semi-volatile or non-volatile).[67] Since chapter 4 of this thesis is solely devoted to an untargeted metabolomics investigation, it is important to provide some background relating to its basic workflow (Figure 1.8). Every investigation begins with the selection of a biological matrix, which in turn establishes the working volumes. Next, metabolite extraction is performed. While most of the sample preparation options discussed in Section 1.2.1 can be used during this step, it is important to be mindful

BIOLOGICAL SAMPLE

METABOLITE EXTRACTION

INSTRUMENTAL ANALYSIS

PRELIMINARY DATA PROCESSING

- conversion of output format
- processing with data packages (e.g. XCMS)
- data filtering

D A T A   A N A L Y S I S

RESOLUTION
Understanding of biochemical pathways
Potential outcome: clinical trials

METABOLITE IDENTIFICATION

tentative identification

MS validation

STATISTICAL ANALYSIS

- univariate analysis
- multivariate analysis

D A T A   A N A L Y S I S

Figure 1.8 *Typical workflow of an untargeted LC/MS-based metabolomics investigation.*

of the fact that the sample preparation method can impact metabolite extractability.[59] After extraction,

the metabolites are converted to a form that is suitable for instrumental analysis. In the case of SPME,

this conversion process simply consists of desorbing the extracted materials from the device into a

desorbing solution. Once instrumental analysis has been completed, an immense amount of data is

generated. In LC-MS based metabolomics, this data consists of chromatograms containing thousands of

different peaks, which can be attributed either to system noise (also known as artifacts, and can include

solvents, instrument plumbing, glass or plastic vials, etc.) or to the sample itself. The next step entails

time-consuming data analysis consisting of preliminary data processing, statistical analysis, and

metabolite identification. Preliminary data processing involves converting the instrument's raw output

into a format that can be read by the software used for metabolomics data processing. One example of

such software is R, which can be used in conjunction with a special XCMS package that was specifically

developed to process metabolomics data.[68,69] Once the raw output has been converted, filters can be

applied to the data in order to reduce irrelevant information, such as noise peaks arising from the mobile

phase, vials, and LC tubing. Next, statistical analysis is conducted to determine which metabolites are

statistically significant (i.e., much more elevated in disease samples). Univariate analysis consists of

statistical tests (e.g., Mann-Whitney, Wilcoxon signed rank, Kruskal-Wallis, Friedman, etc.) that examine the integrated peak areas of two groups of samples (control vs disease) and calculate whether the difference between them is significant.[68] If the difference is significant, the m/z values are placed into a separate group. Further statistical analysis can be performed using multivariate tools like principal component analysis (PCA) and partial least squares discriminant analysis (PLS-DA). PCA and PLS-DA are tools of exploratory data analysis, which is an approach that summarizes main data characteristics using visual methods. Within the context of metabolomics, PCA and PLS-DA are used to examine whether there is any separation or clustering between the data obtained from control and diseased samples. PCA is an unsupervised method, which means that the samples are not assigned any classes; in contrast, PLS-DA is a supervised method, which means that samples are assigned classes. In other words, the software "tells" PLS-DA that some samples come from the control group and that others come from the diseased group. An example of a PLS-DA plot used to examine data clustering in vitreous humor samples from healthy (control) and diseased subjects (rhegmatogenous retinal detachment (RD) and diabetic retinopathy (DR)) can be seen in Figure 1.9.[70] A strict validation of models generated by PLS-DA should be done. Namely, PLS-DA has a tendency to "over-fit" data, or in other words, separate samples due to class assignment and not the inherent biological differences. Simply put, PLS-DA can make the data "look better" than it actually is. To assess whether PLS-DA models are true, different validation strategies can be used; they usually depend on the type of data processing software. Since Metaboanalyst was predominantly used in this thesis (Chapters 3 and 4), its tools will be mentioned. The first PLS-DA validation test is done by looking at the predictive ability of the model. The data is often partitioned into two different sets, whereby one is used to build a training set, while the other is used to test the model, as is often referred to as a validation set. Two strategies are often employed to perform the cross-validation test, and these include k-fold cross-validation and/or leave one out cross-validation
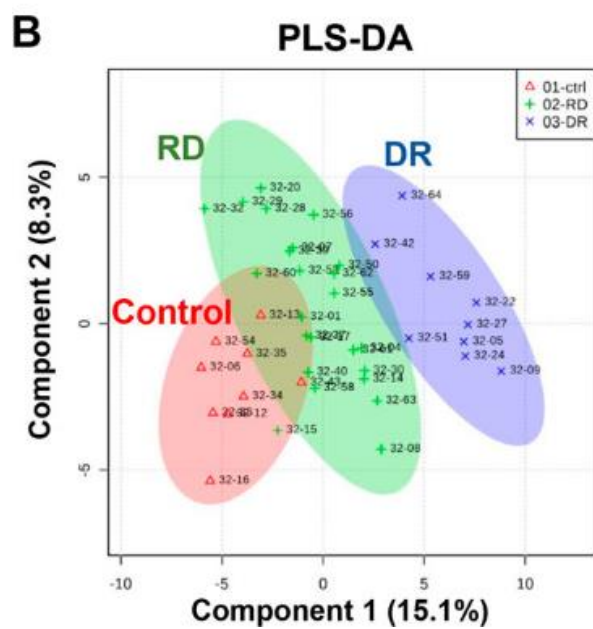
Figure 1.9 *An example of a PLS-DA plot used to examine similarities/differences between vitreous humor of heathy (control), rhegmatogenous retinal detachment (RD), and (diabetic retinopathy) DR samples. Adapted from Haines et al., and reprinted with permission from Haines, Nathan R., et al. Journal of Proteome Research, vol. 17, no. 7, 2018, pp. 2421–2427, doi:10.1021/acs.jproteome.8b00169. Copyright (2019) American Chemical Society.*

(LOOCV). The default k-fold cross-validation of Metaboanalyst is 10-fold cross-validation, whereby the data is split into 10 different subsets. The predictability of the model (for a set number of components) is then tested by building a training set consisting of 9 subsets, while 1 subset is used to assess the model.[436] LOOCV is similar to k-fold cross-validation, whereby a training set is made of *n* samples, while the left out sample is used to assess the model.[436] In either case, both cross-validation strategies generate R2 and Q2 values.[436] R2 is defined as a goodness of fit whereby R2 = 1 indicates a perfect fit, while Q2 is used to assess the predictability of the model and Q2 = 1 indicates a perfect predictability.[436] While a general consensus of the scientific community has not yet been reached, it is generally acceptable that a Q2 value $\geq$ 0.4 is acceptable for biological models and that difference between R2 and Q2 should not be $\geq$ 0.2.[71] Large discrepancy between R2 and Q2 values means that the model has been over fitted due to use of too many components.[436] The second validation test is a permutation test; whereby statistical significance of the PLS-DA model is examined by looking at its Q2 value and comparing it to its null reference distribution which can be obtained through H_0 testing.[437] For permutation tests, the sample

labels are permuted (random) and a new classification is generated, hence model performance can be assessed by examining the Q2 value.[437] By repeating the permutation N times, H_0 becomes a distribution of Q2 values.[437] The statistical significance of the PLS-DA model can then be examined by assessing the Q2 values of the model calculated with the original (non – permuted data set) set to H_0 distribution of the Q2 values which have been obtained for the permuted data set.[437] In Metaboanalyst, permutation test can be done based on separation distance based on sum of squares between and sum of squares within ratio (B/W).[438]

Once statistical analysis is completed, metabolites must be identified. This can be aided using search engines (HMDB, Metlin)[72,73] that generate potential identifications based on the obtained m/z values. This is known as tentative identification. While these search engines are useful, it is widely agreed that the best way to identify a metabolite is through targeted MS/MS experiments, also known as validation. In this stage, significant metabolites are broken down in order to examine fragment production. These fragments are then compared for potential matches using open-source databases (e.g., Metlin & HMDB). Ultimately, the goal of the entire investigation is to understand which biochemical pathways are involved with a particular disease or condition. If a certain set of metabolites is found to be linked to a disease, special therapies can be devised to target them or the biochemical pathway they affect. For example, metabolomics has already been used as a tool in pre-clinical and clinical trials aimed at assessing the glutamate, antioxidant, lipid, and creatinine levels of patients with amyotrophic lateral sclerosis.[74–76]

1.5   Advancements in mass spectrometry: ambient ionization mass spectrometry

Progress in the development of MS technologies has been crucial for the advancement of modern AC. In particular, developments in MS that allow the identification of compounds through ionization and m/z ratios have proved to be extremely valuable, as they have enabled the use of MS for applications such as trace analysis,[77] radiocarbon dating,[78,79] clinical diagnostics,[80] space exploration[81] and proteomics[82] were

possible thanks to MS. One of the most interesting newer developments in MS has been AIMS.[83] In conventional MS, samples are ionized using an enclosed ion source before entering the vacuum region of the mass spectrometer. However, AIMS does not require an ion source in order to ionize the samples; rather, as its name suggests, sample ionization in AIMS occurs in the open, atmospheric air.[84] Although AIMS is sometimes viewed as a "direct-to-MS" approach, the two should not be combined as the latter involves directly injecting the sample into the instrument (e.g., infusions, loop injections) and offers a lower degree of "ambience"[84], i.e., sample ionization does not occur in open air.

The term, AIMS, first appeared in a publication by Takats et al. in 2004 to describe a novel approach called desorption electrospray ionization (DESI). In DESI, charged solvent droplets are deposited onto surfaces of different materials in order to extract, desorb, and ionize compounds of interest, which are then "sucked-in" by the vacuum pull of the MS for analysis in real time.[85] The development of techniques like DESI is largely aimed at minimizing lengthy workloads associated with sample preparation and chromatographic analysis. Figure 1.10 provides a generalized comparison of the time required to complete sample preparation, instrumental runs, and data interpretation for conventional chromatographic approaches and AIMS. Sample preparation and instrumental run time are usually main sources of bottlenecks in chromatographic investigations. In contrast, AIMS is easier to operate, produces results more rapidly, and is less likely to contaminate instrumental interfaces, thus minimizing carry-over.[84] Since Takats's initial publication in 2004,[85] many different AIMS approaches have been developed; the various AIMS approaches and their classifications are discussed in detail in an excellent review by Venter et al.[84] In general, AIMS can be divided into methods that use liquid extraction, laser ablation and thermal desorption for sample processing.[84] For example, ambient nanoelectrospray (nESI) can be classified as a liquid extraction. In nESI, sharp, extremely small (2-100 μm tip diameter) hollow tips are used for sampling, with electrospray being performed on the extracted components by filling the tips with solvent and applying HV to achieve ionization (Figure 1.11).[86] Such techniques can also be

Conventional chromatographic approaches	AIMS	
Minutes or hours	Minimal or no preparation	Sample preparation
Varies (Minutes to hours)	Seconds or minutes	Instrumental run
Depends on length of run	Immediate	Data interpretation
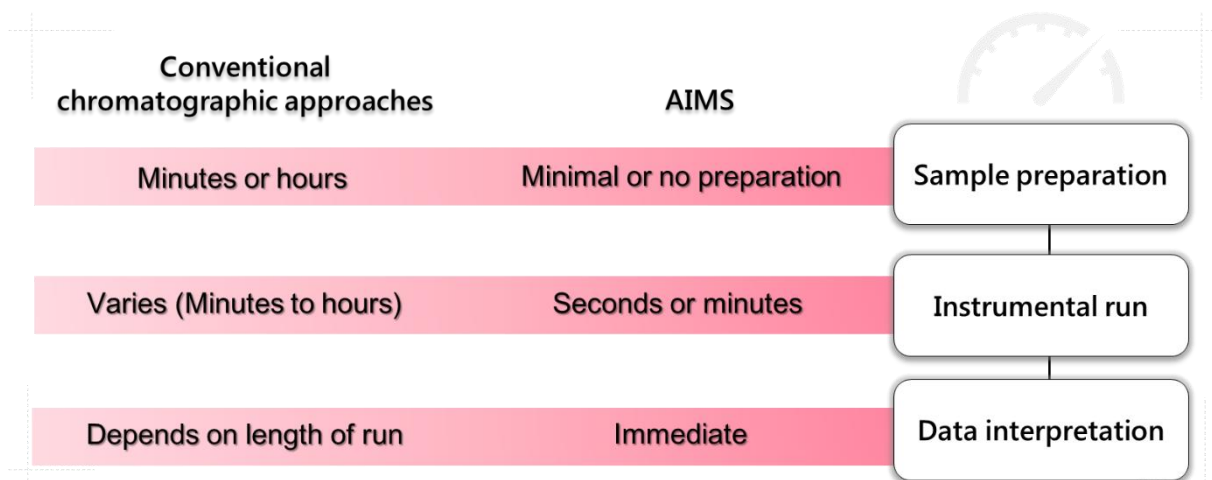
Figure 1.10 *Overview of steps involved in the development of conventional chromatographic approaches and AIMS methods.*

referred to as substrate spray, as a "substrate" (nESI emitter in this case) is used to induce an electrospray.[84] DESI is also classified as a liquid extraction approach because its sample processing procedure uses a strongly charged solvent to extract components from a sample.[84] Even though no extensive sample preparation takes place, one could argue that some sample preparation (liquid-solid extraction) does take place during both nESI and DESI (liquid-solid extraction). In fact, the term, "sample preparation," is avoided in some AIMS publications due to its association with laborious workflows,

nESI emitter
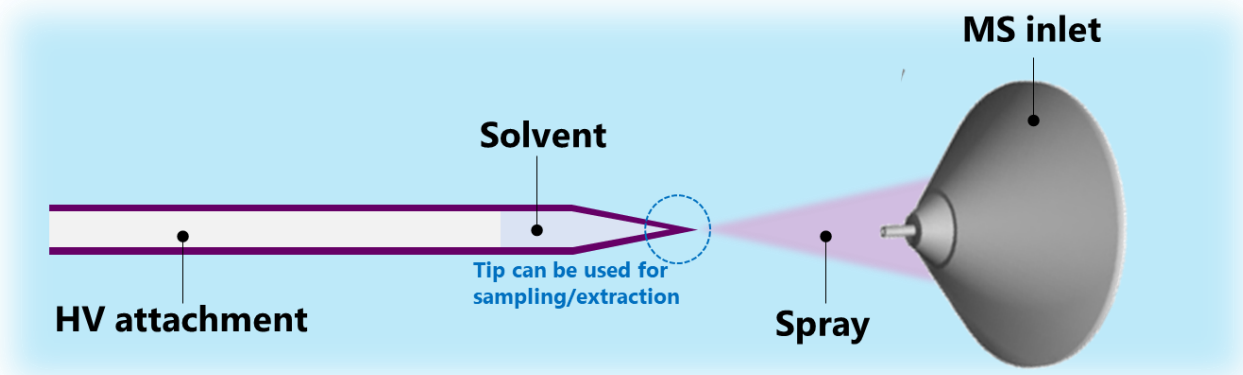
Figure 1.11 *Schematic of a nESI emitter used as a "substrate" spray.*

with authors instead preferring to use the term, "sample processing". Indeed, there are AIMS approaches that allow analysts to process a sample without the need for significant sample preparation. For example,

DART uses heated gases to thermally desorb analytes of interest from various surfaces (e.g., pesticide residues on a whole orange). [87]

1.5.1 Direct analysis in real time (DART)

DART is a thermal desorption/ionization ambient mass spectrometric technique co-invented by Cody and Laramée.[87] The rights to this technology are currently under the ownership of Jeol USA (Peabody, MA, USA) and IonSense, Inc. (Saugus, MA, USA).[88] DART grew to prominence rather quickly in 2005 following its introduction in an article published in *Analytical Chemistry*; indeed it is one of the few analytical chemistry technologies to be featured on a TV show ("CSI:NY").[88] DART is a rapid, simple-to-use, reliable tool that offers tremendous potential for on-site applications. In addition, DART-MS does not require the use of solvent in the desorption process, which also makes it environmentally friendly. A schematic of a DART source can be seen in Figure 1.12.[88] The left portion of the source contains an opening that fits a gas line (typically N_2 or helium (He)) which introduces the gas into the chamber, as
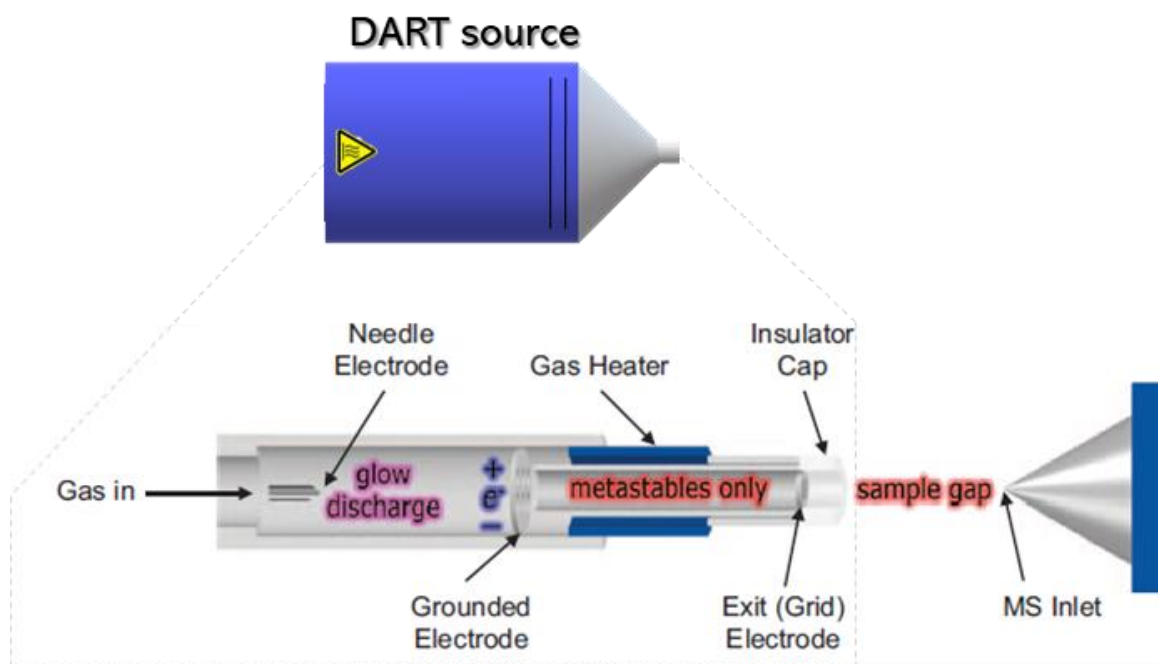
Figure 1.12 *Schematic of DART source and its inside components. Lower portion of the schematic reprinted from "Ambient Ionization Mass Spectrometry", Chapter 2. (Reprinted with permission from Royal Society of Chemistry. Copyright Royal Society of Chemistry, 2015).*

shown in Figure 1.12. As gas is pumped during operation, the needle electrode in the first chamber is exposed to a high potential (−3.5kV) while the perforated counter-electrode remains grounded.[88] The high potential creates a discharge containing metastable (excited-state) species, which ionize the samples.[88] The gas heater heats the gas (50-550 °C), which exits the source and aids in the desorption of less volatile analytes.[88] The exit (grid) electrode is thought to prevent plasma recombination (positive ions combining with free electrons or negative ions to release neutral species) arising from Penning ionization.[88] In Penning ionization, an electronically excited atom or molecule in gas phase (E*) interacts with a neutral species (N) to yield positive ions ($N^{+\bullet}$) and electrons (e^-).[88] This can be expressed with the chemical equation:[88]

$$E^* + N \rightarrow N^{+\bullet} + e^- + E$$

In order for Penning ionization to occur, the ionization energy (IE) of 'N' must be lower than the internal energy of 'E*'.[88] He is the most commonly used gas (E*) for DART. He has an energy of 19.8 eV in the 2^3S_1 state, with a lifetime of ~8000 s, which is enough to ionize many organic compounds.[88,89] The DART source can ionize compounds in both positive (+ve) and negative (−ve) ionization modes. Since +ve ionization mode was maintained for all the DART-MS research in this thesis, −ve ionization mode will not be discussed. Ions generated by DART-MS in +ve ionization mode are usually the product of atmospheric H_2O undergoing Penning ionization:[88]

$$He\ (2^3S) + H_2O \rightarrow H_2O^{+\bullet} + He\ (1^1S) + e^-$$

$$H_2O^{+\bullet} + H_2O \rightarrow H_3O^+ + OH^\bullet$$

$$H_3O^+ + nH_2O \rightarrow [(H_2O)_nH]^+$$

$$[(H_2O)_nH]^+ + M \rightarrow [M+H]^+ + nH_2O$$
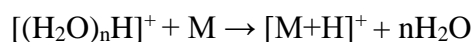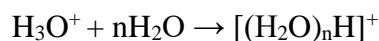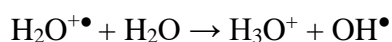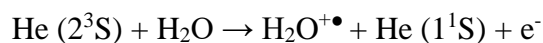
H_2O has an IE of 12.62 eV,[90] and as the above equations indicate, protonated H_2O clusters $[(H_2O)_nH]^+$ can readily undergo proton transfer reactions with molecules/analytes (M) that have proton affinities (PA) higher than those of H_2O clusters.[88] A schematic of DART's ionization process can be seen in Figure 1.13. Analytes of interest (M) are formed mostly through protonation reactions. Current commercial DART sources also incorporate nitrogen (N_2) to keep the source purged while in stand-by mode. Finally, the insulator cap is a safety feature that prevents the user from coming into contact with exit electrode.[88]
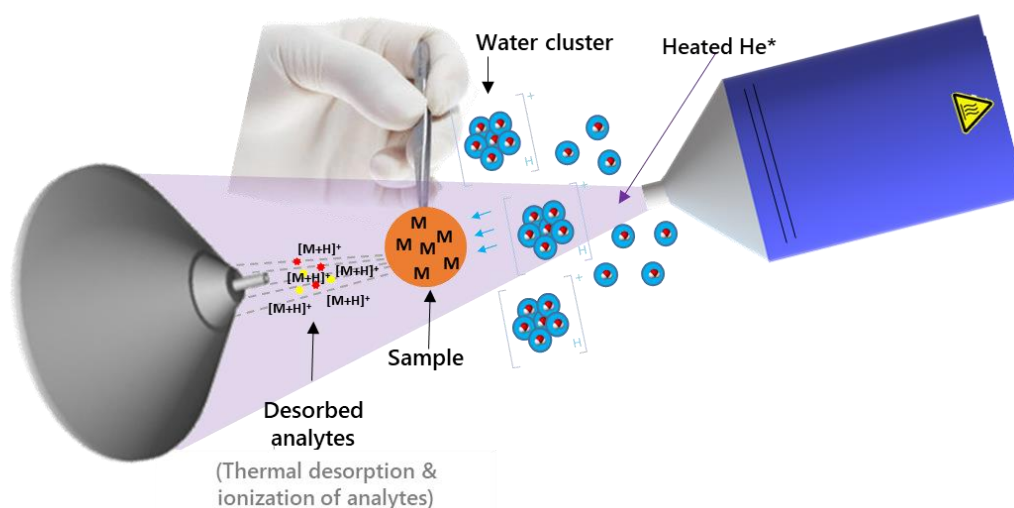
Figure 1.13 *Schematic of the desorption/ionization process in DART for +ve ionization mode.*

1.5.1.1 Interfacing DART to MS

DART sources are commercially available with an atmospheric pressure interface known as the Vapur® interface. This interface was designed to allow the MS vacuum pump to efficiently handle the entrance of He, as too much He can compromise the vacuum system's operating pressure. In addition, newer DART sources are equipped with an SVP® source with pre-optimized voltage and pressure. Figures 1.14 and 1.15 illustrate the coupling of a DART-SVP® Vapur® interface and an MS. The DART source is always placed directly in front of the MS inlet. Hollow Teflon tubing is inserted into the aperture in the middle of the Vapur® interface in order to allow the passage of the ions formed in the gap between the DART source and the MS inlet. This tubing is also secured by a special ring.[91] The vacuum and the
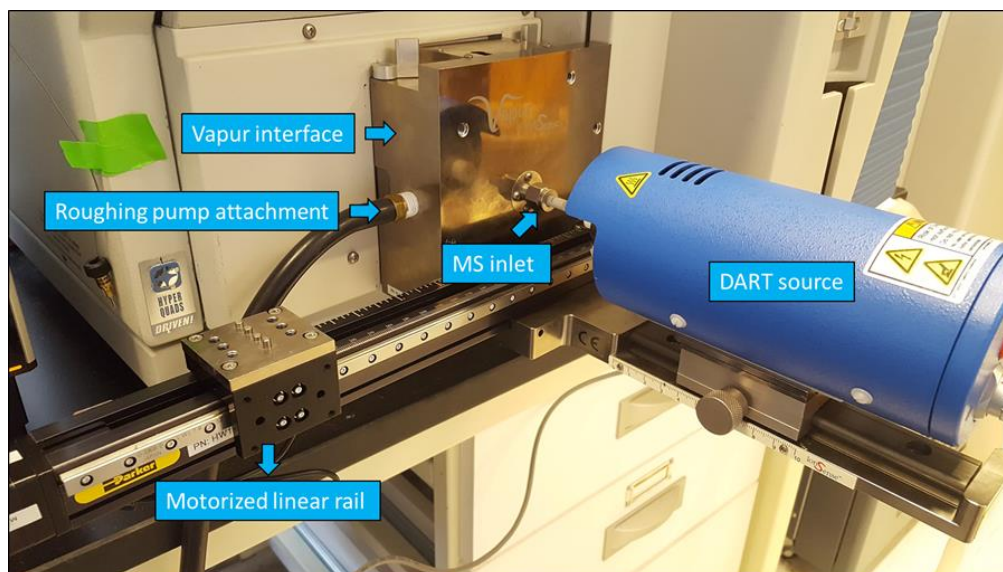
Figure 1.14 *Schematic of DART-SVP Vapur interface coupled to a MS.*
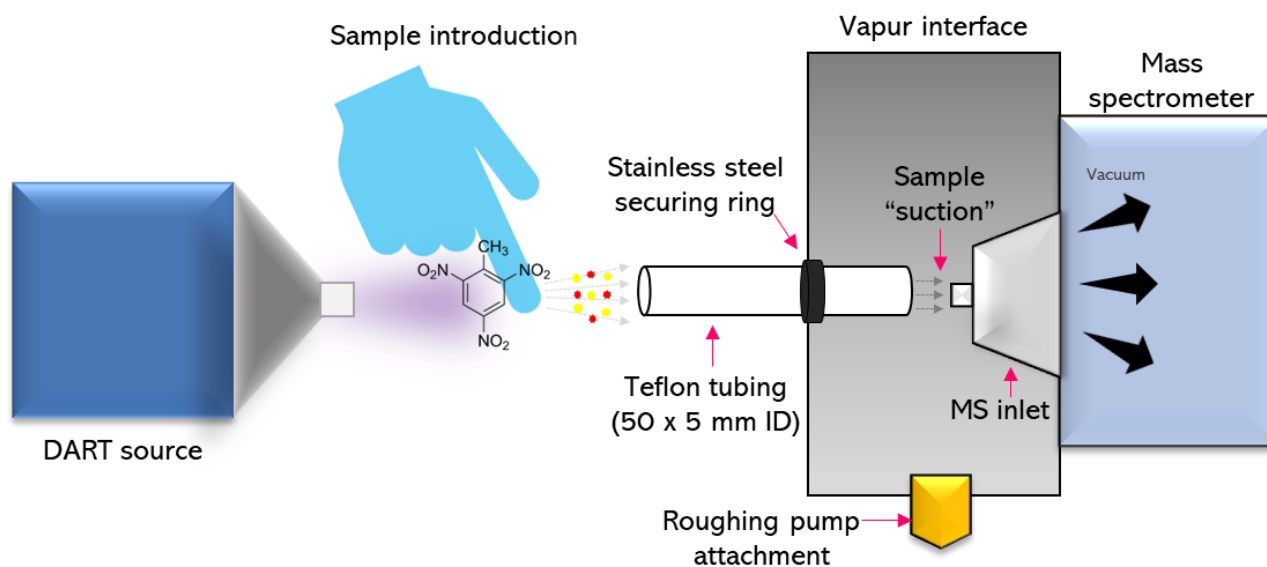
Figure 1.15 *Schematic of Vapur® interface components.*

additional pull provided by the roughing pump "sucks" the sample into the MS for analysis. As shown

in Figure 1.14, the interface is also equipped with a motorized linear rail that can be adjusted/modified

for movements in x, y and z-directions. This is a particularly useful feature, as special holders can be

immobilized onto the rail to carry several samplers at the same time for enhanced analysis throughput.

26

1.5.1.2 Sample preparation for DART-MS

Since first being reported in 2005, a number of publications have detailed the use of DART-MS for a variety of applications, including forensics,[92] food and beverage quality control,[93] environmental assesments,[94] art conservation,[95] natural product analysis[96] and pharmaceutical[97] and material analysis.[98] As mentioned in Section 1.5, DART allows intact samples to be analyzed in their native state(s); as such, many publications report the use of the source in this manner.[47,99–104] While this approach is useful, it is also somewhat underwhelming because it does not capitalize on DART-MS's highly sensitive analytical capacities. Many drug regulatory agencies [e.g., the World Anti-Doping Agency (WADA)] have established minimum concentration levels (also known as cut-offs), which are on the parts-per-billion (ppb) scale.[105] An analytical method can demonstrate its practicality by meeting or providing even lower detection limits than the imposed cut-offs. Native sample analysis via DART-MS insufficiently isolates/preconcentrates analytes of interest, yielding mostly qualitative information on the parts-per-million (ppm) detection scale. As noted in Section 1.5, significantly lower detection limits can be achieved by combining sample preparation with AIMS. This is especially true for complex samples (e.g., blood or plasma), as detection limits tend to increase in these cases. Therefore, numerous efforts have been made to devise sample preparation strategies for DART-MS. To this end, several authors have attempted to pre-concentrate analytes prior to analysis, but these approaches proved to be technically cumbersome.[106–108] For example, Jagerdeo et al. used microextraction by packed sorbent (MEPS), which consists of sorbent conditioning, sample loading, washing, and, finally, elution.[107] Following elution, a glass capillary is dipped into the eluted solvent and desorbed in front of DART-MS for analysis.[107] Others have reported semi-quantitative results with higher detection limits (mg L^{-1})[109–111] while fully quantitative results with low detection limits (ng mL^{-1}) were also reported, albeit with pre-treated matrices.[112–114]

1.5.1.3 SPME in DART-MS

It is somewhat unsurprising that SPME has emerged as an excellent sample preparation tool for DART-MS. Besides its preconcentrating ability, SPME devices can easily be placed in a holder for a higher sample throughput using the DART-MS's motorized linear rail. The main SPME format for DART-MS is SPME-TM meshes. In essence, TM technology utilizes a controlled device geometry (i.e., reproducible nets and/or meshes) to normalize the introduction of samples into the MS, which allows for a more repeatable response from the DART-MS system.[115] Figure 1.16 provides a schematic of the mesh's structure, which consists of a woven, intertwined network of wires with a diameter 'd'. The area between two adjacent wires is the aperture width, w, while pitch denotes the distance between the center points of two adjacent wires. The coated wires are used to extract the analytes, which are then desorbed via
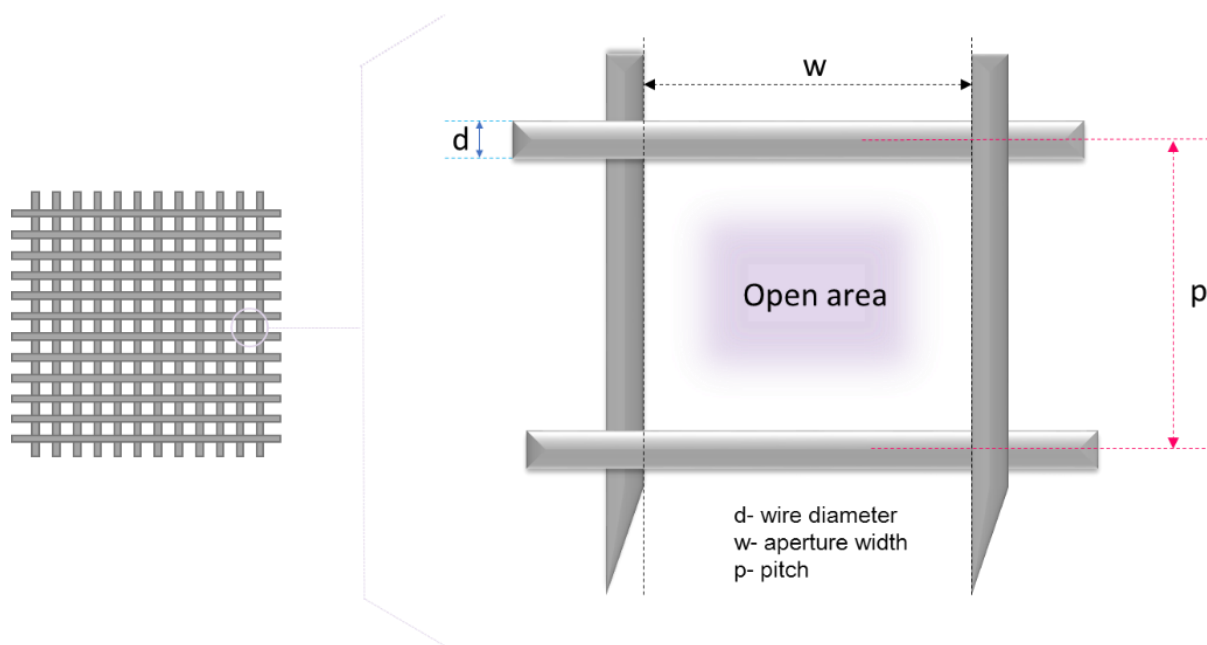
Figure 1.16 *Schematic representation of the mesh format.*

exposure to heated He. The open area of the meshes allows the analytes to pass safely into the MS, thus ensuring successful transmission (hence the name, TM). The open areas vary in size and are usually expressed in percentages that define the total hole area to total screen area of the mesh. The TM format was utilized in the first two publications to document the use of DART-MS-SPME. The first two attempts

28

to use DART-MS-SPME, published by Mirnaghi et al.[49] and Rodriguez-Lafuente et al.[116] were conducted using the TM format and used SS meshes coated with C18-PAN (Figure 1.17). However, the coating strategy was not completely optimized in either study; specifically, the coating was applied using a brush-painting procedure,[49] which is not optimum for the mesh as it results in an incomplete coating. Mirnaghi et al. used meshes to extract diazepam from 5 µL of blood and were able to achieve an LOD of 0.3 mg L^{-1}.[49] The high LOD was probably partially attributable to blood's complexity, but the lack of coating material on the mesh very likely undermined the extraction process as well. As seen in Figure 1.17, the SS strands were not completely covered by the coating slurry; instead the coating tends to be localized around the wire junctures.[49] Despite the flaws in Mirnaghi et al.'s design, it would nevertheless provide a blueprint for the future development of the device. In 2014, Gómez-Ríos et al. enhanced the mesh's analytical performance by devising a dip-coating protocol in order to improve the distribution of coating on the mesh's individual wires (Figure 1.18). For easier handling, an electric soldering tool was used to attach the meshes to a SS blade (Figure 1.19).[26] Gómez-Ríos et al.'s design significantly improved the preconcentrating abilities of SPME-TM, enabling extremely low detection limits (pg mL^{-1}) for cocaine
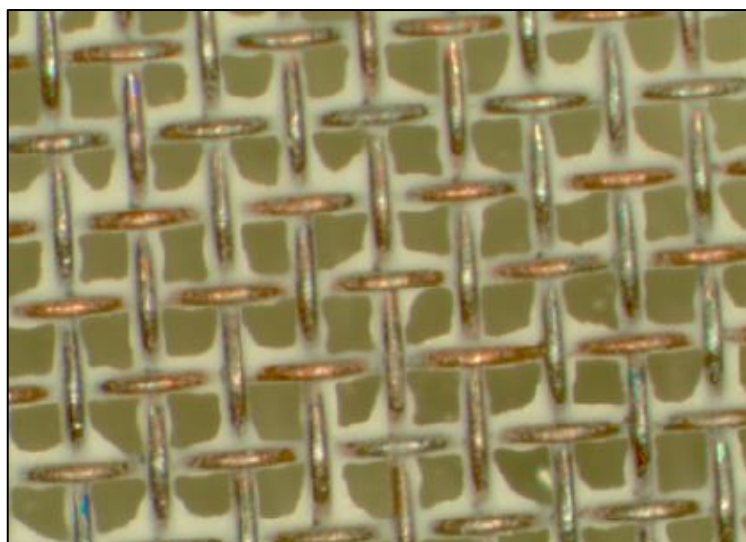
Figure 1.17 *SS mesh coated with PAN-C18 particles, suited for use in TM-DART-MS. Original design by Mirnaghi et al.. Reprinted with permission from Mirnaghi, Fatemeh S., and Janusz Pawliszyn. Analytical Chemistry, vol. 84, no. 19, 2012, pp. 8301–8309, doi:10.1021/ac3018229. Copyright (2019) American Chemical Society.*

and diazepam in urine[26] and pesticides in environmental and food matrices[117] were reported using an extraction time of only one minute.
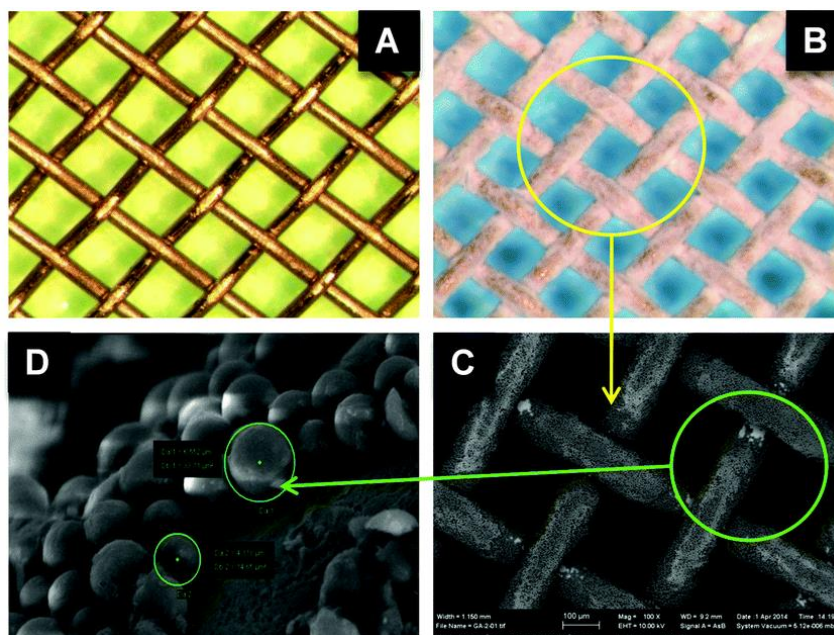
Figure 1.18 *SS mesh coated with PAN-C18 using a dip-coating procedure devised by Gómez-Ríos et al. Figure **A** shows the uncoated mesh, **B** shows the mesh coated by C18-PAN, while **D**-**C** show the SEM images of the coated mesh. Reproduced with permission from Gómez-Ríos, German A. and Janusz Pawliszyn. Chemical communications, vol. 50, no. 85, 2014, pp. 12937-12940. doi: 10.1039/C4CC05301J. Published by The Royal Society of Chemistry under the Creative Commons license (CC BY 3.0).*
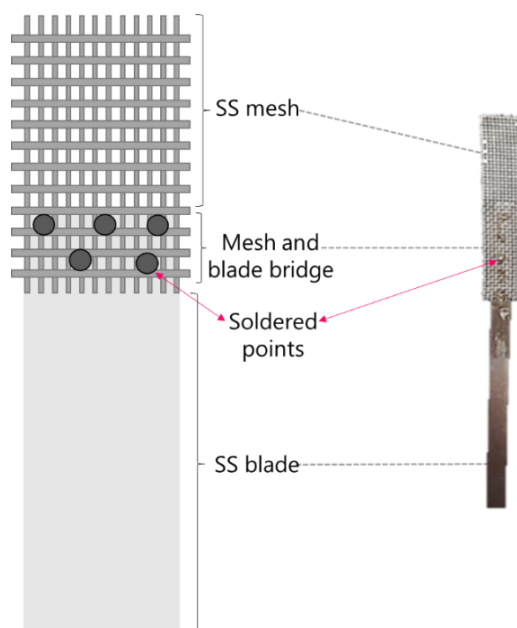
Figure 1.19 *Schematic representation of the SPME-TM design by Gómez-Ríos et al. An SS blade is attached to the mesh via an electric soldering tool.*

1.6 Small volume analysis

Small volume analysis is one the most challenging tasks in contemporary analytical chemistry. Small volume analysis aims to minimize the overall amount of sample required for a particular analysis, while still yielding sufficiently sensitive and reliable data.[118] Reducing sample volumes is beneficial, especially in scenarios that require individuals to frequently provide biological samples for monitoring purposes, such as therapeutic-drug monitoring (TDM)[119-120] and neonatal screening.[119,121] Small-volume analysis can also be useful for applications involving animals, as the reduction of sample volumes would allow individual animals to be monitored over extended periods of time.[122] Hence, the pharmaceutical industry is expending considerable effort to develop analytical methods that will allow scientists to work with very small sample volumes.

Two emerging fields that fit within the small-volume scope are single-cell and cell-population analysis. As its name suggests, single-cell analysis aims to obtain meaningful information from tiny cellular organisms in order to elucidate the cellular activities involved in metabolic pathways.[123] While there is no consensus as to what qualifies as a "small volume," a large number of publications within this field work with volumes that are ≤ 20 µL. Small-volume analysis is particularly important for matrices like blood and plasma, which are more difficult to obtain. Techniques like SPE and LLE are inappropriate sample preparation strategies for small volume analysis, since they are developed to work with much larger sample volumes. In some publications, the term, "microsampling," is sometimes used to describe small-volume analysis techniques.[124–126] Figure 1.20 provides an overview of these microsampling approaches, as well as the strategies implemented for single-cell analysis.[8,127–133] It is important to point out that the microsampling approaches described in Figure 1.20 (with the exception of some microfluidic approaches) cannot be construed as sample preparation approaches, as they are more concerned with sample collection rather than preconcentration and clean-up. Cell-analysis approaches can utilize microfluidics or different probe approaches, wherein a probe is used to extract meaningful compounds

31

directly from a cell. However, since the majority of probe-based approaches do not use preconcentrating materials, the extraction is based on unselective interaction between cell materials and the probe. Hence, there is a need to develop a miniaturized coated probe that can handle both small volumes and single cells, while providing adequate extraction for analytes of varying polarities and yielding robust qualitative and quantitative results. A microextraction technique like SPME is an ideal choice for small-volume sampling because it requires fewer sample preparation steps. This is significant because reducing the number of sample preparation steps helps to reduce errors and improve accuracy and precision, which is crucial for small-volume analysis.
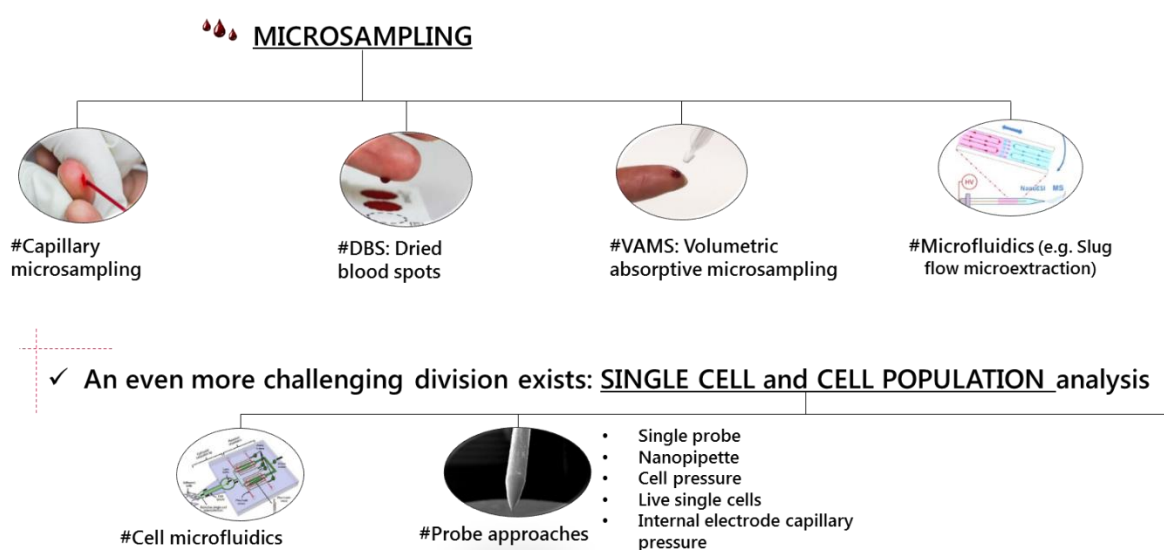
Figure 1.20 *Commonly reported sample processing strategies used for microsampling and single cell analysis.*

1.7   Research objectives

At the forefront of every scientific discipline is the eagerness to improve people's day-to-day lives. Some of the more prominent topics currently being explored in AC are direct-to-MS technology, small-volume analysis, and metabolomics. The push to refine AIMS technology reflects the need to develop strategies that will allow us to obtain quality results more rapidly, which is significant as laboratories are becoming

increasingly strained in terms of workload by the ever-growing population. Many tests in these laboratories are still being performed via conventional chromatography, which requires considerable time and materials and yields long turnaround times. The criminal and forensic sectors would also benefit from AIMS technologies, as timely results are of the highest importance in the early resolution of casework. Thus, coupling technology like DART-MS to an efficient sample preparation approach like SPME could be an immense help in achieving robust results and faster throughput. With respect to small-volume analysis, it must be remembered that it is a humane approach that is dedicated to preserving the well-being of animals and humans alike. As such, it is particularly valuable for patients who are required to provide blood samples every day. However, the analysis of small volumes (including cells) is not straightforward; it requires elevated levels of analytical sensitivity, accuracy, precision, and robustness. Even the sampling process can be challenging for inexperienced analysts. Hence, the development of a miniaturized SPME tool that satisfies the above-described criteria and that can comfortably be used with small volumes is highly desirable, though it will be equally important to examine its limitations and shortcomings in order to continue to refine it. Lastly, advancements in mass spectrometry and sample preparation have allowed metabolomics to flourish as a field, which has enhanced our ability to understand the mechanisms of diseases through the identification of various biomarkers. Thus, the continued development of techniques like SPME could be critical in furthering our ability to understand the metabolic profiles of individuals and ultimately lead to the development of more powerful diagnostic tools in the medical field.

The main objectives of this thesis include examining studies and developments dedicated to the coupling of SPME and DART-MS, and advancing the application of SPME technology for the analysis of small sample volumes. Chapter 2 exclusively focuses on the work that has been done on SPME-DART-MS. Specifically, Chapter 2 examines prior work that details the experimental basics of SPME-DART-MS, as well as work that has broadened its scope of applications. Section 2.2 investigates certain experimental

factors that must be considered for SPME and DART-MS, and how they impact signal responses. A deeper understanding of these factors' effects is important because it will allow scientists to optimize the experimental parameters for SPME-DART-MS more efficiently. Section 2.3 provides a comparison of the analytical performance of the two most popular SPME formats for DART-MS: fibers and meshes (SPME-TM). One of this section's main goals is to identify applications where meshes outperform fibers, and applications where fibers outperform meshes. Sections 2.4-2.7 focus on novel developments/applications of the SPME-DART-MS technology. Section 2.4 examines the coupling of SPME meshes to a portable MS (Waters-QDa) for the on-site, *in vivo*, roadside drug testing of samples. Section 2.5 assesses the sensitivity of both formats by examining their suitability for the analysis of small volumes (Vs ≤ 25 µL) such as OF and blood. One of the greatest benefits of DART-MS is that it enables high sample throughput; thus, in Section 2.6 we demonstrate how SPME-TM can be coupled to DART-MS in a 96-format in order to quantify opioids in 96 biological samples in less than 1.5 hours. While SS mesh is most commonly used to fabricate SPME-TM meshes, alternative materials like biocompatible plastics are worth investigating as they can be less costly and more comfortable when used for *in vivo* buccal swabbing. As such, Section 2.7 details the development and application of SPME-TM meshes made of PEEK for OF and urine sampling. Chapter 3 is dedicated to the development and application of SPME miniaturized tips, or minitips, which were specifically designed to be used in small volume analysis. This chapter details all aspects of the challenging production process, from the dip-coater designed at UW's machine shop to the development of the formulation for the coating-slurry. The results of preliminary performance assessments, as well as the devices' limitations are also addressed in Chapter 3. Furthermore, three different minitip applications are presented, each highlighting different aspects of the device's analytical ability. These include the analysis of DoAs in 1 µL of OF via LC-MS/MS; directly coupling the minitips to nanoelectrospray (nESI), and metabolomics sampling of four different types of fish eggs (caviar). Chapter 4 details an untargeted metabolomics investigation conducted in collaboration

with the Toronto General Hospital (TGH). This chapter describes the use of SPME fibers to collect miniscule muscle samples from patients with the metabolic disorder, MH. The purpose of this study aimed to investigate the biochemical pathways that define the pathophysiology of the MH condition and to examine the SPME's potential as a diagnostic tool. As a part of the examination of the diagnostic aspect of SPME, extensive validation of the PLS-DA models generated is provided. Finally, Chapter 5 summarizes the main findings of the current work and proposes future directions and potential challenges that might arise.

Chapter 2: Studies, developments and applications of SPME coupled to DART-MS

2.1 Preamble

Chapter 2 consists of 6 sections out of which 3 have been published in *Analyst, Analytical Chemistry,* and *Rapid Communications in Mass Spectrometry*. Two sections have been submitted to journals *Analytical Methods* and *Journal of Separation Science*. Most of the data presented herein has already been included in the manuscripts mentioned below. Section 2.2 is not published anywhere as it is an ongoing investigation which focuses on the impact of different factors which influence the sensitivity of the SPME-DART-MS. Section 2.3 compares the analytical performance of SPME meshes against those of SPME fibers by examining sensitivity for a set of model analytes spiked to PBS and was submitted to *Journal of Separation Science*. Section 2.4 describes the application of a portable DART-MS system Waters-QDa which was used for semi-quantitation of 7 DoAs in OF and has been published in *Analyst*.[134] Section 2.5 describes the applicability of SPME-TM meshes for analysis of DoA(s) in small volume biofluids like OF and blood, and has been submitted for potential publication to *Analytical Methods*. Section 2.6 details the development and application of a HT 96-SPME-TM system coupled to DART-MS for quick detection and quantitation of opioids in urine and plasma and has been published in *Rapid Communications in Mass Spectrometry*.[135] Section 2.7 describes the development and application of plastic SPME-TM meshes, made of PEEK which were used for analysis of DoAs in OF and urine and has been published in *Analytical Chemistry*.[136]

Section 2.2 includes the following portion:

"Some investigations of factors impacting the sensitivity of DART-MS coupled to SPME"

I participated in all stages of experimental design including its planning, execution, data analysis and interpretation.

Section 2.3 includes the following submitted manuscript:

"On the performance of solid-phase microextraction (SPME) fibers vs transmission-mode (TM) meshes for direct analysis in real time (DART) coupled to mass spectrometry (MS): Differences in analytical sensitivity."

I participated in all stages of experimental design including its planning, execution, data analysis and interpretation. The manuscript was entirely written by me and submitted to *Journal of Separation Science*.

Section 2.4 includes the following manuscript:

Gómez-Ríos, G.A., Vasiljevic, T., Gionfriddo, E., Yu, M., Pawliszyn, J., *Towards on-site analysis of complex matrices by solid-phase microextraction-transmission mode coupled to a portable mass spectrometer via direct analysis in real time*, Analyst, 2017, 142, 2928-2935, doi: 10.1039/C7AN00718C

This manuscript was published under an agreement of equal contribution by Dr. German A. Gómez-Ríos, Tijana Vasiljevic and Dr. Emanuela Gionfriddo. Dr. German A. Gómez-Ríos used the material discussing pesticide detection and milk profiling in his thesis, while Tijana Vasiljevic is using the material discussing detection of DoA(s) in OF for her thesis. The authors had already agreed on this before conducting any experiments. Dr. German A. Gómez-Ríos and Dr. Emanuela Gionfriddo participated in experimental planning, execution, data interpretation, analysis and manuscript writing for the pesticide data and milk profiling. Tijana Vasiljevic participated in experimental planning, execution, data interpretation, analysis and manuscript writing for the drug detection in OF portion. Dr. Miao Yu participated in the statistical analysis of the data which was used for milk profiling (not presented herein, used for Gómez-Ríos's thesis).

I, German A. Gómez-Ríos, authorize Tijana Vasiljevic to use this material for her thesis.

I, Emanuela Gionfriddo, authorize Tijana Vasiljevic to use this material for her thesis.

I, Miao Yu, authorize Tijana Vasiljevic to use this material for her thesis.

Section 2.5 includes the following submitted manuscript:

DART and SPME-TM: A Suitable Platform for Analysis of Prohibited Substances in Small Volumes

I participated in all stages of experimental design including its planning, execution, data analysis and interpretation. The manuscript was entirely written by me and submitted to *Analytical Methods*.

Section 2.6 includes the following manuscript:

Vasiljevic, T.; Gómez-Ríos, G.A.; Li, Frederick; Liang, P. and Pawliszyn, J. *High-Throughput Quantification of Drugs of Abuse in Biofluids via 96-Solid-Phase Microextraction–Transmission Mode (SPME-TM) and Direct Analysis in Real Time- Mass Spectrometry (DART-MS)*, Rapid Com. in Mass Spectrometry*, doi: 10.1002/rcm.8477*

Text, tables and figures are reprinted from this publication with permission from Wiley (Copyright 2019 Wiley).

Tijana Vasiljevic participated in all stages of the experimental design, its execution, data interpretation and manuscript writing. Dr. German A. Gómez-Ríos participated in some experimental design, data interpretation and aided in the manuscript writing. Mr. Frederick Li and Mr. Paul Liang aided in certain aspects of experimental design (3D-printed holder) and portions of the manuscript writing.

I, German A. Gómez-Ríos, authorize Tijana Vasiljevic to use this material in her thesis.

I, Frederick Li, authorize Tijana Vasiljevic to use this material in her thesis.

I, Paul Ling, authorize Tijana Vasiljevic to use this material in her thesis.

Section 2.7 includes the following manuscript:

Vasiljevic, T.; Gómez-Ríos, G.A. and Pawliszyn, J. *Single-Use Poly(etheretherketone) Solid-Phase Microextraction–Transmission Mode Devices for Rapid Screening and Quantitation of Drugs of Abuse in Oral Fluid and Urine via Direct Analysis in Real-Time Tandem Mass Spectrometry*, Anal. Chem., 90 (1), 952-960, doi: 10.1021/acs.analchem.7b04005

Tijana Vasiljevic participated in all stages of the experimental design, its execution, data interpretation and manuscript writing. Dr. German A. Gómez-Ríos participated in some aspects of experimental design, data interpretation and aided in the manuscript writing.

I, German A. Gómez-Ríos, authorize Tijana Vasiljevic to use this material in her thesis.

2.2 Some investigations of factors impacting the sensitivity of DART-MS coupled to SPME

2.2.1 Introduction

For nearly 30 years, SPME has been on the forefront of novel developments and applications in the world of sample preparation. Part of SPME's continued success is the fact that its format can be altered to fit the needs of different sampling strategies. One of such formats with a rising number of publications is SPME-TM coupled to DART-MS.[26,117,137–139] DART-MS is a relatively novel, simple to operate, thermal desorption AIMS technique whose operational mechanisms are still being investigated.[87–89] There are even some studies suggesting that thermal desorption is not the only ionization mechanism of DART-MS, as evidence of chemical sputtering has also been reported.[140,141] It is known that the primary ionization mechanism of DART-MS is Penning ionization, which leads to protonation of target analytes ($[M+H]^+$) when used in +ve ionization mode.[88] Deprotonation is the main ionization mechanism of –ve ionization mode ($[M-H]^-$).[88] Indeed, DART-MS is capable of forming other ions such as $[M+NH_4]^+$, $[M]^+$, $[M]^-$ and $[M+Cl]^-$ which is largely influenced by compound properties.[88,89] For example, alcohols, large alkenes, mono- and di-triglycerides are thermally labile and not easily ionized by DART-MS.[88] Certain alcohols, carbohydrates, compounds with labile phosphate/sugar groups, metals and proteins are incapable of desorption due to large MWs and lack of volatility.[88] Hence, it is important to acknowledge that compound specific parameters are crucial for determining their ionization success by DART-MS. These factors include proton affinity (PA), thermal stability, ionization energy (IE), vapor pressure (VP), MW, ME(s), internal energy (IU), electron affinity (EA), anion affinity and acidity/basicity. These are summarized in Figure 2.1 as compound properties.[88] It is also important to understand that signal responses in DART-MS are governed by additional factors which include hardware settings (or system properties), sample preparation specifics and even ambient air (i.e., moisture which aids in analyte protonation).[88,89] These can also be seen in Figure 2.1. System properties such as DART gas[142,143] and its

DART/MS

Ambient air
- Humidity

Compound properties
- Proton affinity
- Thermal stability
- Ionization energy
- Vapor pressure
- Molecular weight
- Matrix effect
- Internal energy
- Electron affinity
- Anion affinity
- Acidity/basicity

System properties
- DART gas & flow
- DART temperature
- DART rail speed
- Angle of gas desorption
- Sample positioning
- Choice of mass analyser
- Teflon tubing diameter
- Doping additives

Sample preparation (SPME)
- Compound affinity for coating
- Choice of substrate
- Extraction settings

Figure 2.1 Summary of main factors which influence the response of DART-MS.

flow,[144,145] temperature,[93,146,147] rail speed,[143,148] angle desorption,[115,149,150] sample positioning,[115,150,151]

choice of mass analyzer,[152] Teflon tubing diameter and dopant use[104] for enhancement of ionization. For

example, Dane et al. have used argon gas (instead of commonly employed He) in combination with

acetylacetone and pyridine to selectively ionize melamine.[142] Vaclavik et al. used NH_4 to enhance

protonation and analysis of triacylglycerols in olive oil.[104] Additionally, Duvivier et al., compared

different mass analyzers (Q-TOF, QqQ, orbitrap and QqQ-orbitrap) for forensic hair analysis, finding

that highest sensitivity was obtained using a high resolution QqQ.[152] Sample preparation also contributes

significantly to the analytical capabilities of DART-MS[153] and discussions are strictly limited to SPME

in this thesis. The main contributors to system response with respect to SPME include coating and

substrate choice and extraction settings. Coating choice is the key factor which determines the sensitivity

of any SPME approach, and polarity of target analytes should be considered when choosing coating

chemistry. Essentially, non-polar coatings (e.g., C18) work well for hydrophobic compounds while

hydrophilic compounds have better affinity for polar coatings (e.g., HLB). Substrate refers to the choice

of the SPME format for DART-MS analysis (i.e., fibers, meshes, in-tube SPME, stir-bars, etc.) and is

usually chosen based on the sampling requirements.[7] For example, for *in vivo* sampling SPME fibers are the most appropriate choice due to easy insertion in living systems. Ultimately, extraction settings (e.g., extraction time, agitation, matrix pH, etc.) also contribute. Hence, the goal of research in this section is to use SPME-TM meshes to investigate influence of some (but not all) of the factors listed in Figure 2.1. Compound dependent properties such as PA and IE can be calculated using computational *ab initio* approaches,[154] which are complex calculations that require a higher level of mathematical and programming skills. For this reason, such properties were not evaluated but will be considered in the future. Considering the number of factors involved, investigation was simplified, using a one-at-a-time factor[155] investigation approach. DART source temperature, SPME coating chemistry, positioning of the meshes between the DART source and the MS inlet and the impact of pH manipulation were investigated. DART source temperature was evaluated in the 250-500 ˚C range, while coating's influence was examined using C18, HLB and MM chemistry. MM coatings were made by mixing C18 and HLB particles (5μm) in a 1:1 ratio. Positioning of the mesh was examined by placing the mesh at different locations with respect to the DART source and the MS entrance. Additionally, the desorption angle of the mesh was investigated. To examine the influence of pH, samples were adjusted to acidic, neutral and basic conditions. The results obtained indicated that each factor contributes to the analytical sensitivity, yet our findings also pointed that these factors interact with each other, thus displaying a synergistic effect during DART desorption/ionization.

Additionally, 3 consecutive desorption tests were done from the same position of SPME-TM mesh to examine the extent of release of analytes during exposure to heated gas. The goal was to observe whether incomplete desorption of SPME-TM meshes was occurring. Indeed, it was found that some analytes require more than 2 desorptions to release the extracted analytes from the SPME-TM mesh.

2.2.2 Experimental section

Materials/Chemicals

 The following chemicals were purchased from Cerilliant (Round Rock, TX, USA) as certified reference standards (in methanol) at a concentration of 1000 mg L^{-1}: 2-Ethylidene-1,5-dimethyl-3,3-diphenylpyrrolidine (EDDP), cocaethylene, methamphetamine, nicotine, codeine, methadone, oxycodone, cotinine, morphine, 3,4-Methylenedioxymethamphetamine (MDMA), cocaine, lysergic acid diethylamide (LSD), fentanyl, RSC-4, RSC-8, JWH-210; JWH-015, JWH-250, JWH-203, JWH-200, AM-2233, and heroin. PAN, DMF, sodium chloride (NaCl), potassium chloride (KCl), potassium phosphate (K_3PO_4) and sodium phosphate (Na_3PO_4) were obtained at $\geq$ 99 % purity from MilliporeSigma (Burlington, MA, USA). MeOH, IPA, ACN, FA, ammonium hydroxide (NH_4OH) and H_2O were obtained from Fisher Scientific (Hampton, NH, USA). FA and NH_4OH were used to adjust the pH of the samples. SS meshes (74x74 wire $inch^{-1}$, diameter: 0.004 inch, length: 30 mm, width: 4 mm) were obtained from IonSense (Saugus, MA, USA). PBS was made by combining 8 g of NaCl, 0.2 g of KCl, 0.2 g of K_3PO_4, and 1.44 g of Na_3PO_4 with 1L of LC/MS grade H_2O.

Preparation of the meshes

The original recipe for coating of the meshes was adapted from Musteata et al.[48] PAN solution was prepared by dissolving 7 g of PAN powder in 100 mL of DMF via periodical vortexing to ensure uniform dissolution without "dry patches" (clusters of undissolved PAN powder). C18 particles (5 μm size) were obtained from MilliporeSigma while 5 μm Oasis HLB particles were obtained from Waters (Milford, MA, USA). MM coatings were made by mixing 0.5 g of C18 and 0.5 g of HLB particles. Then, 1 gram of C18, HLB and MM particles were mixed (separately) with 10 mL of PAN solution to obtain 10% C18-PAN, HLB-PAN and MM-PAN slurry. The slurries were then agitated with stir-bars for 12 hours at 1800 rpm in order to ensure adequate mixing of PAN with the extractive particles. The SS meshes

were then etched in concentrated HCl for 5 minutes using the aid of a sonicator, followed by 5 minute

sonicated washes in MeOH (1x) and deionized H_2O (2x). The etched meshes were then dried at 100 ˚C

for 30 minutes, purged with N_2 and kept in a desiccator to prevent surface oxidation. The slurries were

deposited on the meshes via dip-coating method published by Gómez-Riós et al.[26] After the mixture had

been deposited, excess slurry was removed by blasting the open area with pressurized gas. This prevents

blockage of the open area, i.e., transmission holes. The coating was then cured at 100 °C for 1 minute

and the whole procedure was repeated for the other side. The meshes were then cleaned twice in a solvent

mixture consisting of MeOH/IPA/ACN (50/25/25) at 1500 rpms for 15 minutes to remove potential

interferences which could have occurred due to the dip-coating procedure. To activate the extractive sites

on the particles, the meshes were preconditioned in MeOH/H_2O (50/50) and kept in it until use.

Extraction procedure for PBS

Methanolic stock solution of the analyte standards were made to a concentration of 100 mg L^{-1}. The stock

solution was then diluted to proper concentrations used to spike PBS. PBS was used as extraction media

due to lack of interfering components. Spiking was done in such a manner that the percentage of organic

solvent spiked was below 1% in order not to disturb any partitioning equilibria between SPME and PBS.[7]

No IS(s) were used in this investigation, and all the data represented in this section is the raw uncorrected

data obtained from the ion chronograms. All extractions were carried out according to a procedure

published by Gómez-Riós et al.,[26] which consists of rapid agitation of a single mesh (3200 rpm) in a glass

or plastic vial filled with 1500 μL of the sample. Except for pH experiments, all extractions were carried

out from PBS samples spiked with 25 ng mL^{-1} of target analytes. For the pH experiments, extractions

were carried out from a PBS sample spiked at 200 ng mL^{-1}. After the extractions were completed, a brief

5-sec wash in H_2O was used to clean the mesh. The meshes were then gently blot-dried with a KimWipe

(to remove H_2O residues) and inserted into a custom-made holder (UW-12) able to allocate up to 12

SPME-TM devices.[26] DART source temperatures were evaluated by examining the responses at 250,

300, 350, 400, 450 and 500 ˚C. Sample positioning was assessed with respect to the distance of the

SPME-TM mesh from the DART source and MS entrance. Additionally, we examined whether changes

in mesh angle impact the signal. Figures 2.2-2.3 provide a schematic of how the positioning experiments

were done. As seen in Figure 2.2, position '1' describes the position in which the mesh is closest to the

Position 1: Mesh closest to DART source

Position 2: Mesh in the middle

Position 3: Mesh closest to MS inlet
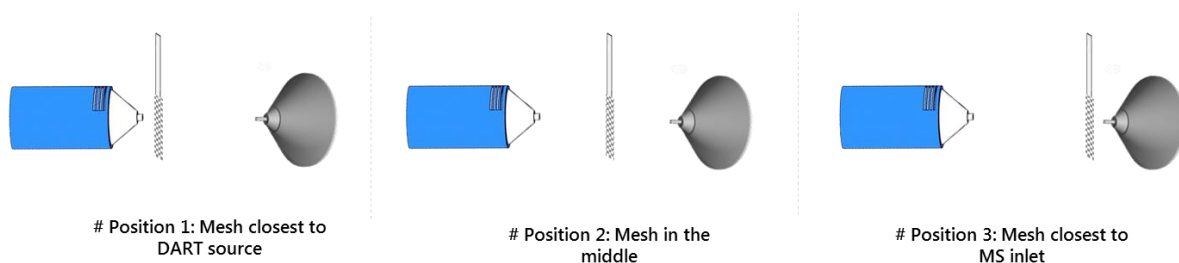
Figure 2.2 *Schematic representation of sampling for determination of the optimum signal response with respect to mesh positioning between the DART source and the MS inlet. The distance between the DART source and the MS inlet is 1 cm. In position 1, the mesh is 0.1 cm away from the DART source. In position 2, the mesh is 0.5 cm away from the DAR source, while in position 3 the mesh is 0.9 cm away from the source.*

DART source. In position '2' the mesh is located in the middle, i.e., between the DART source and MS

inlet. In position '3' the mesh is located closest to the MS entrance. The impact of mesh angle on signal

was assessed by performing desorption in 2 different ways (Figure 2.3). In scenario I., the gas hits the

mesh at an angle about 90 ˚ horizontal to the mesh surface, which is the commonly used desorption

Angle I

Angle II

SPME mesh →

SPME mesh →

DART source

DART source
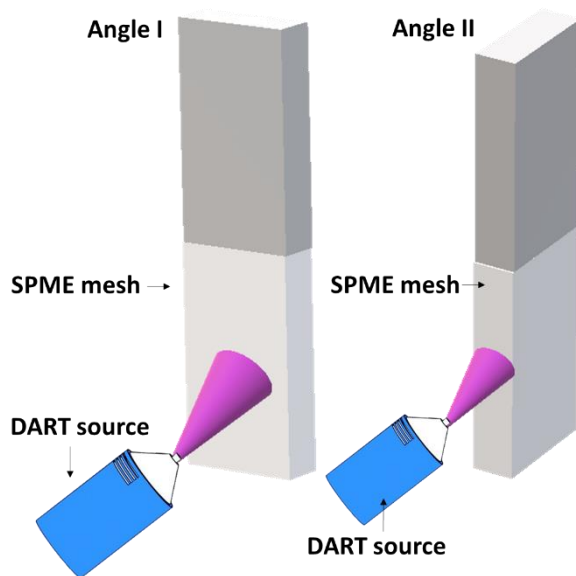
Figure 2.3 *Schematic of 2 different angles of SPME-TM meshes used for desorption of SPME-TM meshes via DART-MS.*

approach. However, in scenario II., the mesh's angle is shifted by 90˚, so the gas hits the mesh at an angle corresponding to the gas flow. Impact of pH on signal response was assessed by modifying the pH of PBS by directly spiking small amounts (~5 μL) of FA or NH_4OH. The pH of PBS was evaluated using pH strips from MicroEssential Laboratory (Brooklyn, NY, USA). All of the experiments were done in triplicates (n = 3).

DART-MS/MS

A DART-SVP® model from IonSense, Inc. was coupled to a QqQ mass spectrometer (TSQ Vantage) from Thermo Scientific (San Jose, California, USA) via Vapur® interface (IonSense, Inc.) and an auxiliary membrane pump. The needle valve of the membrane pump used with the Vapur® interface was adjusted according to the "Vapur Pump Optimization Protocol" suggested by the manufacturer whereby blue indicator at position 4 was used to maintain adequate vacuum in the MS and provide sufficient sensitivity via DART-TM. Table 2.1 provides logP values of the analytes used for the research, alongside their parent and product m/z values and settings (S-lens & CE) for experiments on TSQ-Vantage. DART-SVP was fitted with a single-dimensional motorized linear rail that was controlled through the web-based software of IonSense, Inc. The custom-made holder was then immobilized into the linear rail, which was operated at a speed of 0.2 mm s^{-1} for all the experiments. DART source temperature was maintained at 450 ˚C for all the experiments, with the exception of the temperature experiment. Desorptions were then done by operating the DART source in +ve ionization mode using the following voltage conditions: high-voltage (HV) electrode at −3000 V, discharge electrode at +350 V and a grid voltage at +350 V.

Table 2.1 *Details of the model analytes used, including logP, parent and product m/z values as well as S-lens and CE values adjusted for TSQ Vantage. Class and logP information was obtained from PubChem.[156]*

Compound	Class	logP	Parent m/z	Product m/z	S-lens	Collision energy (eV)
Oxycodone	Morphinans	0.30	316.1	241.1	124	28
Cotinine	-	0.39	177.1	80.1	98	24
Nicotine	-	0.87	163.1	117	75	28
Morphine	Morphinans	0.89	286.1	152.1	121	59
Codeine	Morphinans	1.21	300	152.1	120	60
MDMA	Benzodioxoles	1.65	194.1	135	55	20
Methamphetamine	Benzenes	2.23	150	91.1	63	20
Heroin	Morphinans	2.3	370.1	165	165	29
Cocaethylene	-	2.53	318.1	195.7	78	20
LSD	Ergolines	2.95	324.1	223	118	23
Methadone	Benzenes	3.93	310.2	265.1	93	14
Cocaine	Benzenes	3.93	304.1	182.1	91	19
Fentanyl	Piperidines	4.05	337.1	188	101	22
JWH-200	Cannabinoids	4.21	385	155	123	20
EDDP	-	5.26	278.1	233.9	78	31
JWH-250	Cannabinoids	5.30	336	121.1	114	19
JWH-015	Cannabinoids	5.66	328	155.01	115	22
RCS-4	Cannabinoids	5.68	322.1	135	135	23
RCS-8	Cannabinoids	6.12	376.1	121.1	141	23
JWH-203	Cannabinoids	6.22	340	125	114	33
AM-2233	Cannabinoids	6.44	459	98	82	33
JWH-210	Cannabinoids	7.47	370.1	183	112	25

2.2.3 Results and discussion

Impact of DART source temperature on signal response

Certain authors, such as Maleknia et al. examined desorption of volatile organic compounds (VOCs) from surfaces of eucalyptus leaves, demonstrating that progressive increases in temperature led to desorption of semi-volatile, higher MW terpenes.[147] They concluded that lower boiling point compounds

were desorbed at lower temperatures while higher boiling point compounds were desorbed at higher temperatures.[147] It is important to acknowledge that the temperature set up in the DART software and the one which exits the hot source are not of the same value. In fact, Prof. Fernandéz's group found that the temperature which leaves the source is nearly half of the value set up in the DART software (i.e., 250 °C set in software, 125-150 °C exits the source).[145] In fact, the heat becomes attenuated by the ambient air as it exits the source. During experimental optimizations, the temperature of the DART source can be increased incrementally (i.e., 50 °C) to desorb the less volatile analytes or to simply desorb greater amounts of the analytes. Setting the DART gas source to highest temperature offered (550 °C) does not necessarily equate to the best response. This is evidenced by Figure 2.4, whereby signal responses for a set of model analytes were tested in 50 °C increments, ranging 250 to 500 °C. As it can be seen, increasing the source temperature does not lead to an increased signal intensity for all the analytes involved. Cotinine (with exception of 250 °C) maintains a signal that changes insignificantly over the range of
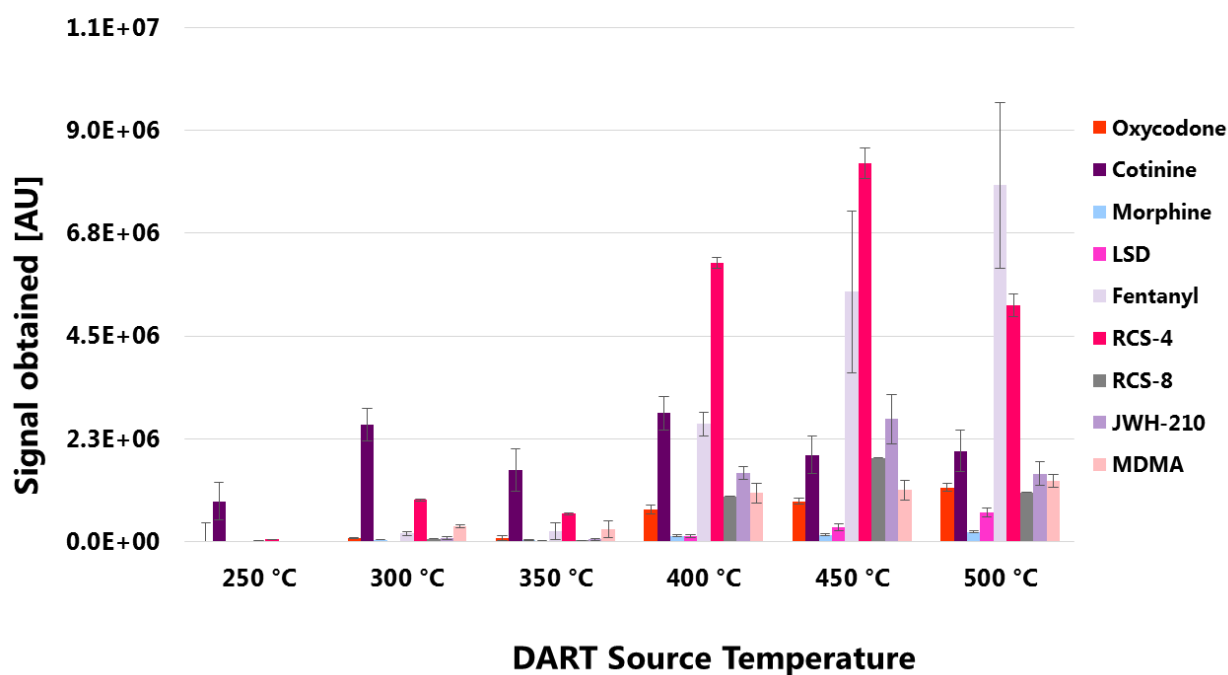
Figure 2.4 *Assessment of signal responses (n = 3) for a set of model analytes spiked at 25 ng mL^{-1} and extracted with HLB meshes from a 1500 μL PBS sample with incremental increases in the DART source temperature.*

temperatures tested. Oxycodone, morphine, LSD and MDMA display similar signal patterns, i.e., steady

lower intensities up to 400 °C followed by an increase at 450 °C and 500 °C. Fentanyl and RCS-4 display

the highest intensity for all the analytes examined, with an almost consistent increase in signal intensity

up to 500 °C. In case of RCS-4 a drop is observed at 500 ˚C. In fact, RCS-4, RCS-8 and JWH 210 share

similarities in signal behavior. Their signals are somewhat low until a temperature of 400°C is reached.

This indicates poorer volatility of RCS-4, RCS-8 and JWH-210 at lower temperatures. Regardless, it

would appear that increasing the source temperature benefits the analysis of some, but not all analytes.

Another observation is tendency of polar to mid-polar analytes (oxycodone, morphine, MDMA at 0.3,

0.89 and 1.65 logP, respectively) to yield lower intensities. Figure 2.5 shows the structure of oxycodone,

morphine and MDMA as well as fentanyl and RCS-4, which yielded the most sensitive responses. The

poorer response of polar analytes could be related to the fact that oxycodone, morphine and MDMA
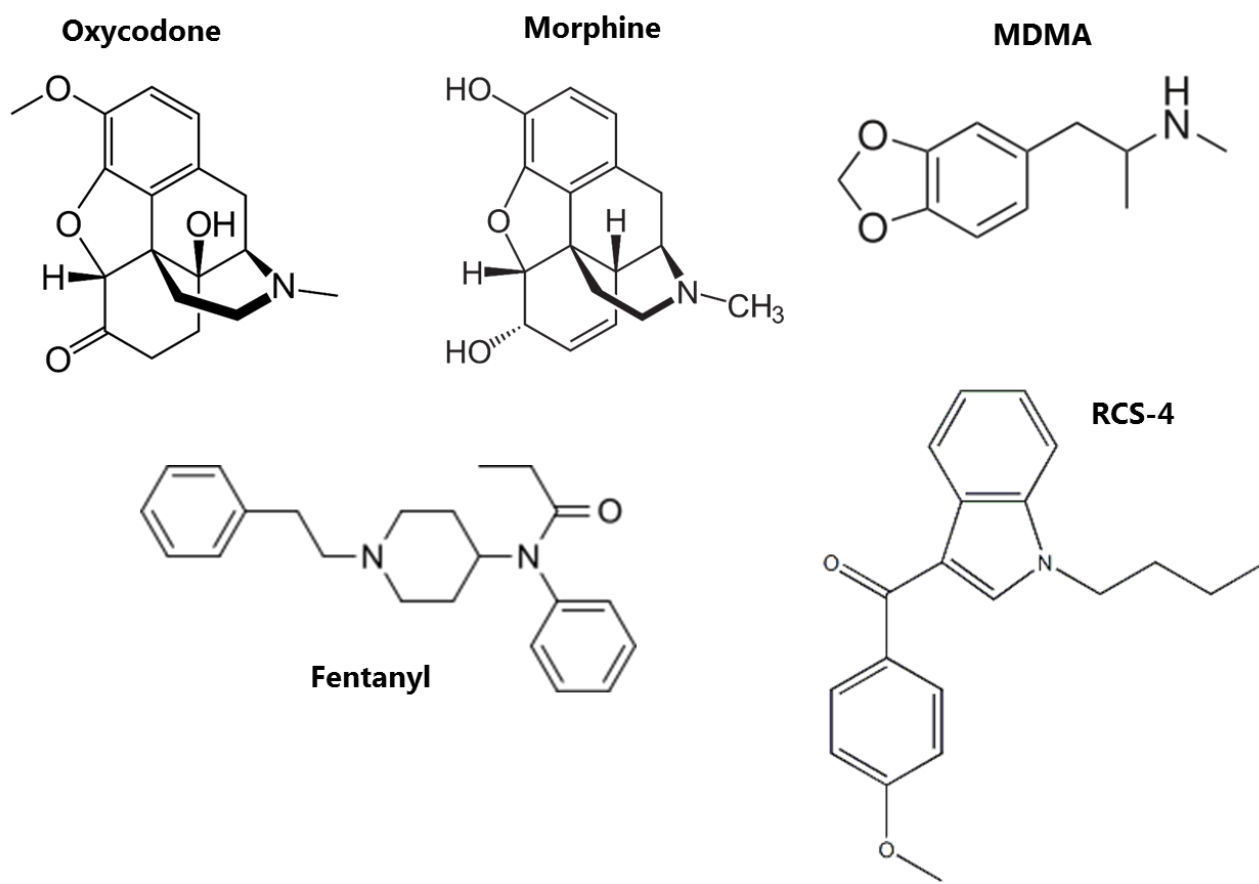
Figure 2.5 *Chemical structures of oxycodone, morphine, MDMA, fentanyl and RCS-4. Structures were obtained from DrugBank.*

contain polar functional groups (-OH, -NH), which require higher temperatures to increase the volatility. Interestingly, LSD (2.95 logP) and RCS-8 (6.12 logP) are mid to non-polar analytes whose sensitivity is lower or comparable to MDMA and oxycodone, suggesting involvement of other more sophisticated factors such as PA, IE and thermal stability.

Evaluation of coating chemistry

Selection of coating chemistry is the most important factor determining the sensitivity of the SPME method.[7] As mentioned in the experimental section, three different coating chemistries consisting of MM, C18 and HLB extractive particles were used. MM coatings were used to examine whether a combination of non-polar and polar material would result in balanced extraction of polar and non-polar analytes. For example, Mousavi et al. already investigated mixing of different chemistries (polystyrene, divinylbenzene (DVB), HLB, ionic liquids, etc.) in an effort to find the optimum coating recipe for extraction of a range of metabolites from *Escherichia Coli* (*E.Coli*) cultures.[50] C18 coating has more affinity towards non-polar compounds, owing to its long hydrocarbon chain (Figure 2.6, ChemDraw).[157] HLB is a polar polymer which contains hydrophilic N-vinylpyrrolidone (NVP) and hydrophobic DVB groups (Figure 2.7, ChemDraw),[157] making HLB suitable for extraction of polar, mid-polar and some
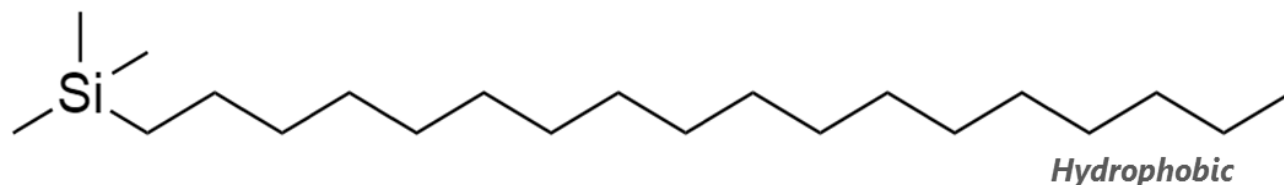
Figure 2.6 Basic chemical structure of the C18 chain. Drawn using ChemDraw JS.

non-polar analytes.[158] Figure 2.8 shows the results obtained for comparison of signal areas obtained by extracting via HLB, MM and C18 coatings from a PBS sample spiked at 25 ng mL^{-1}. It is noticeable that polar compounds (oxycodone, cotinine, morphine, MDMA) produce a higher signal area when extracted with HLB coatings. As expected, C18 provided a better signal for the non-polar compounds (cocaine,

LSD, fentanyl, RSC-4, RSC-8, JWH-210). MM does not significantly outperform C18 or HLB in terms of intensity for polar and non-polar analytes. In case of morphine, a significant difference in signal
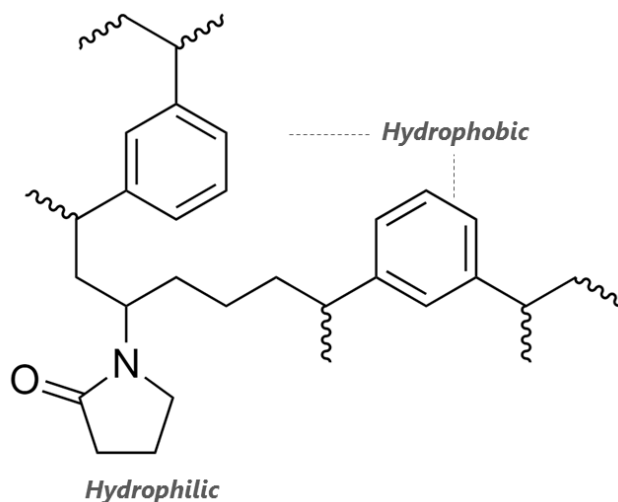
Figure 2.7 *Chemical structure of the HLB polymer, consisting of hydrophobic DVB and hydrophilic NVP groups. Drawn using ChemDraw JS.*

intensity between all three coatings is not observed. Morphine is a polar compound, and by inspecting its response more closely (Figure 2.8 cut-out) one can note that a somewhat higher response is obtained (although statistically insignificant, one-way ANOVA, p = 0.29) using HLB. Interestingly, for
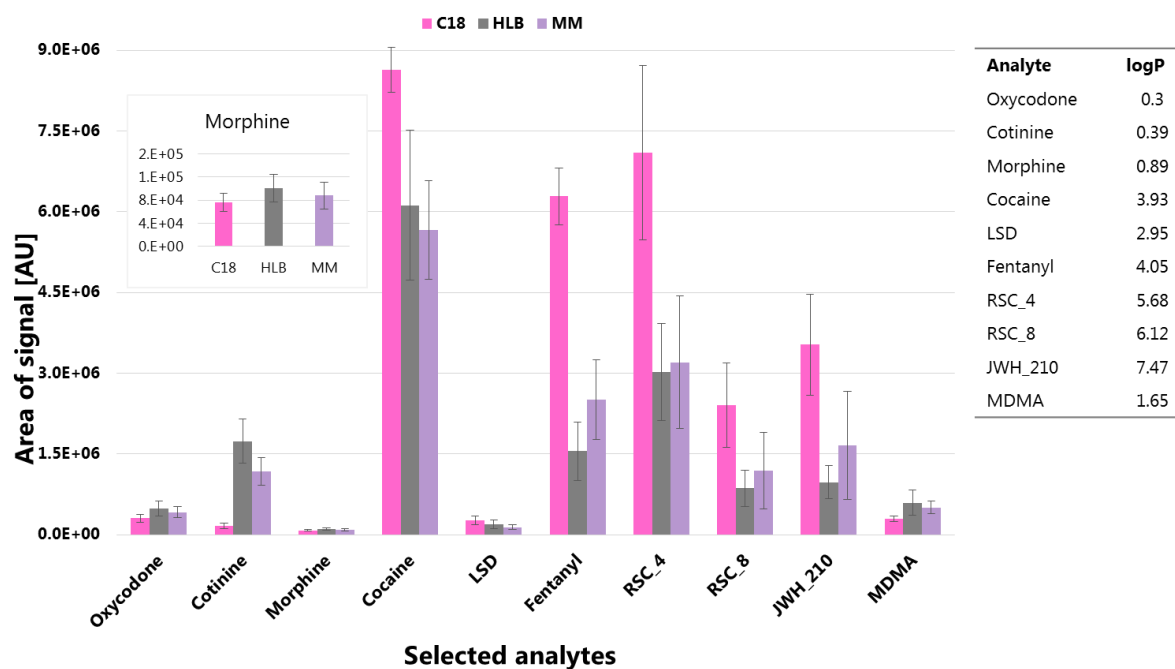
Figure 2.8 *Assessment of signal responses (n = 3) for the model analytes spiked at 25 ng mL^{-1} to PBS and extracted using C18, HLB and MM coatings.The right side of the chart indicates the logP values of the analytes used. logP information obtained from PubChem.*

oxycodone, morphine, LSD and MDMA coating choice does not appear to contribute significantly to the sensitivity. In the previous investigation (influence of temperature), it was discovered that the same analytes produced the lowest intensities. This furthers the notion that compound specific factors (PA, VP, IE, etc.) play a key role in influencing the signal sensitivity.

Mesh positioning and its influence on the signal

In DART-MS, responses typically depend on the proximity of the sample to the source and the MS inlet. This can be very problematic because slight variation in sample positioning could lead to also a problem because slight variation in sample positioning or turbulences could lead to increased % RSDs.[159] To determine the influence of mesh positioning on the signal, 2 different types of experiment were done. As mentioned in Section 2.2.2, the first experiment consisted of mesh placement in different positions with respect to the DART source and the MS inlet. In position 1, the mesh was closest to the DART source and furthest from the MS inlet. Theoretically, position 1 would likely result in the fastest thermal desorption of the analytes as it is closest to the gas source. Position 2, whereby the mesh was placed between the DART source and the MS inlet was used as compromise of positions 1 and 3. The results obtained for this test can be observed in Figure 2.9. As it can be seen, position 3 gives the least sensitive response, while 1 and 2 yielded comparable responses. Position 3 is not optimal for efficient thermal desorption of the analytes due to its proximity to the MS inlet. Positions 1 and 2 yielded somewhat similar responses, demonstrating that mesh proximity to the heated ionizing source is more important than its proximity to the MS inlet. Newsome et al. have also found that analyte signals decrease significantly when the source is furthest from the sample surface.[160]
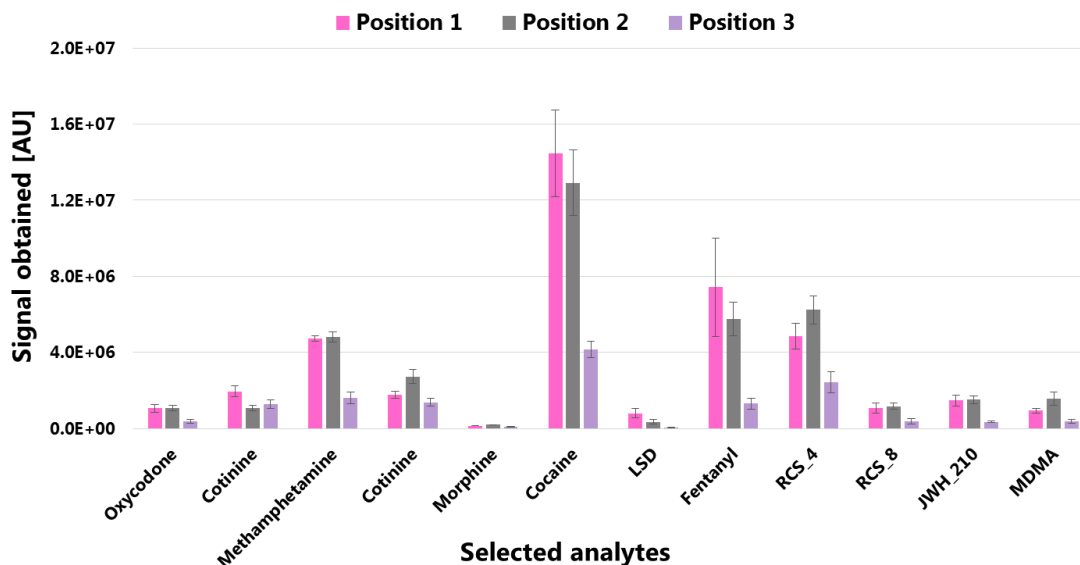
Figure 2.9 *Signal areas [AU] obtained for a set of model compounds (n = 3) tested at three different positions with respect to DART source and MS inlet.*

Influence of mesh angle on signal response was examined in the second part of the investigation. By changing the mesh angle, the interaction of the gas plume with the sample is changed. The question is whether different mesh desorption angle produces a more sensitive response? Recall, in scenario I gas hits the mesh at an angle about 90 ˚ horizontal to the mesh surface, while in scenario II, the mesh's angle is shifted by 90˚, so the gas hits the mesh at an angle corresponding to the gas flow, i.e., gas flow is parallel to mesh surface. Ion chronograms of MDMA were monitored for this purpose, and as it can be seen from Figure 2.10II., a change in the angle yielded a sharper, but not a more sensitive chronogram
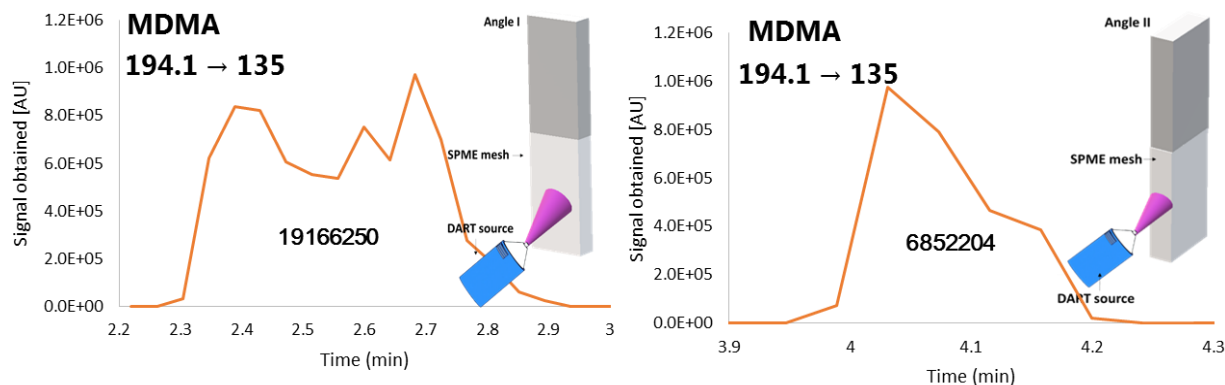
Figure 2.10 *Ion chronograms obtained for extraction of 25 ng mL^{-1} of MDMA spiked to PBS and analyzed using two different mesh angles in I. and II.*

peak, as evidence by signal area shown inside the chronograms. The response is better when the stream is perpendicular to the SA of the mesh, as it can be seen in Figure 2.10I. This proves that SPME-TM-DART-MS responses and are heavily influenced by the angle of incidence of the gas flow. In other words, the greater the SA of the coated SPME device, the greater the response obtained from DART-MS.

Impact of pH manipulation

The pH is an important extraction parameter of SPME.[7] According to the theory of SPME, only the undissociated (neutral) form of the analyte can be extracted by the coating.[7] If the analyte is charged, coatings with anion or cation exchanger sites can be used. In this section, experiments were done using a PBS sample spiked with 200 ng mL^{-1} of methadone, EDDP, cocaine, cocaethylene, and codeine. HLB meshes were used for the extraction (n = 3). The results obtained can be seen in Figure 2.11, alongside respective pKa values of the analytes (obtained from DrugBank).[161] Noticeably, the least sensitive response is obtained when the samples are acidified (pH = 3). The majority of the analytes are present in
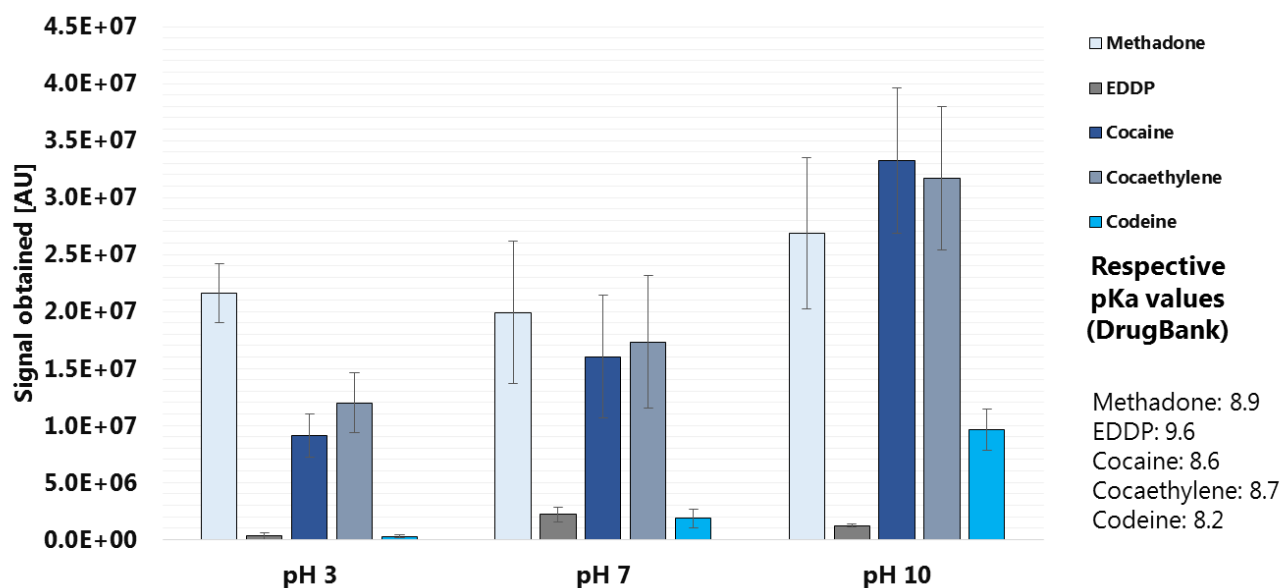
Figure 2.11 *Signals obtained for methadone, EDDP, cocaine, cocaethylene and codeine (200 ng mL^{-1}) at pH's of 3, 7 and 10 using SPME HLB meshes coupled to DART/MS (n = 3). pKa values are shown on the right.*

a dissociated state at this pH, which leads to reduction of extraction capability of the HLB meshes. EDDP is the only analyte that does not show major changes in signal response at the different pH values tested.

It is possible that other factors (e.g., PA) are responsible for this observation. Codeine's response was the least sensitive out of all of the analytes examined, particularly at the pH of 3. Methadone, cocaine and cocaethylene yielded the highest responses, which were most apparent at the pH of 10. However, adjustment of sample pH may not be necessary in every sampling scenario. Nonetheless, it is important to keep in mind that certain matrices like urine (tends to vary with different lots) may require a dedicated evaluation of the impact of pH on responses of DART-MS-SPME-TM.

Multiple desorption tests

In order to examine the extent of "loss" of target analytes during DART desorption, three consecutive desorptions of the same mesh (at the same location) were done for MM, C18 and HLB coatings. The main concern was that incomplete desorption of the analytes was occurring after/during the initial desorption. Due to the volume of the data, a table representing the signal area (in AU) after three consecutive desorptions for C18, HLB and MM is shown in Table 2.2. Please note that the values provided are the averages of three different meshes used. The blank desorption (desorption from unused mesh) was used as a control. As it can be seen from Table 2.2, complete desorption of all analytes does not occur upon initial exposure to the heated gas. While the large majority of the extract is desorbed during initial exposure, 2nd and 3rd desorption indicate that some analyte still remains on the mesh. This is more apparent in the case of the 2nd desorption, since signal for the 3rd desorption is only slightly higher or comparable to the blank for the majority of the analytes. Examination of Table 2.2 reveals that C18 coating (with the exception of methadone and JWH-250) does not yield the same responses as the blank by the time that 3rd desorption is done. It is also possible that heat permeation through the steel wires of the mesh causes partial desorption of the surrounding area of the mesh thus potentially resulting in elevated signal areas for the 3rd desorption. From Table 2.2 it can be seen that HLB's signal for 3rd desorption is comparable to blank desorption in case of nicotine, cotinine, morphine, codeine, RCS-8, JWH-250, and JWH-203. MM coatings reach a near-blank signal for methamphetamine, morphine,

codeine, methadone, RCS-4, JWH-015, JWH-250 and JWH-203 by the time 3rd desorption is done. Interestingly, JWH-250 reaches a near-blank value by the 3rd desorption for all 3 coating chemistries. To provide a better visualization of these trends, a few analytes were selected to show signals from all desorptions involved. These can be seen in Figure 2.12, whereby the left side shows results for the blank and all 3 desorptions, while the right side shows the blank, 2nd and 3rd desorption signals. Figure 2.12A. shows methamphetamine's response with a noticeable comparability between signals of 2nd, 3rd and blank desorption for all 3 coating types. In case of codeine (Fig. 2.12B.), a comparable signal upon 1st desorption for HLB and MM coatings are observed, while 3rd desorption is comparable to the blank

Table 2.2 *Signals obtained (in AU, n = 3) for blanks, first, second and third desorption from C18, HLB and MM coatings for a set of selected analytes.*

Desorption	Blank			First desorption			Second desorption			Third desorption		
Analyte	C18	HLB	MM	C18	HLB	MM	C18	HLB	MM	C18	HLB	MM
Methamphetamine	8.4E+04	7.4E+04	1.1E+05	1.5E+06	7.1E+05	9.5E+05	9.4E+04	6.4E+04	5.3E+04	1.1E+05	9.5E+04	1.1E+05
Nicotine	9.1E+04	1.1E+05	1.0E+05	2.5E+05	1.2E+05	1.4E+05	1.2E+05	1.3E+05	1.1E+05	1.1E+05	1.2E+05	1.3E+05
Cotinine	2.0E+04	2.5E+04	1.6E+04	4.1E+05	7.5E+04	7.1E+04	5.9E+04	3.4E+04	2.9E+04	3.6E+04	2.9E+04	2.9E+04
Morphine	1.0E+04	9.2E+03	1.2E+04	1.1E+05	9.3E+03	8.7E+04	2.4E+04	6.7E+03	1.9E+04	1.8E+04	5.7E+03	1.4E+04
Codeine	5.5E+03	7.3E+03	7.0E+03	1.3E+05	3.1E+04	1.3E+05	1.5E+04	1.0E+04	1.0E+04	1.0E+04	6.8E+03	7.2E+03
Cocaine	4.0E+03	3.5E+03	6.7E+03	2.5E+06	8.9E+05	4.3E+06	7.6E+04	2.1E+04	2.0E+04	3.6E+04	8.5E+03	1.1E+04
Methadone	1.3E+05	8.3E+04	4.9E+05	1.7E+06	1.3E+06	3.4E+06	1.5E+05	1.3E+05	3.5E+05	1.5E+05	1.1E+05	3.7E+05
Oxycodone	3.0E+03	4.5E+03	3.3E+03	2.2E+05	4.7E+04	3.6E+05	3.0E+04	1.7E+04	2.5E+04	1.9E+04	1.2E+04	1.3E+04
RCS-4	1.7E+04	1.6E+04	9.9E+04	1.0E+06	6.3E+05	2.0E+06	1.5E+05	7.4E+04	1.6E+05	9.9E+04	4.0E+04	9.9E+04
RCS-8	1.5E+04	1.1E+04	2.8E+04	2.5E+05	1.6E+05	5.6E+05	5.9E+04	2.0E+04	9.2E+04	4.3E+04	1.3E+04	5.3E+04
LSD	8.4E+03	5.2E+03	5.3E+04	3.2E+05	6.1E+04	1.5E+06	4.7E+04	7.4E+03	5.7E+04	2.2E+04	6.3E+03	3.3E+04
Heroin	1.5E+03	1.9E+03	3.1E+03	1.7E+05	6.5E+04	2.7E+05	1.3E+04	9.8E+03	6.9E+03	7.4E+03	5.1E+03	4.4E+03
JWH-015	1.7E+04	8.4E+03	1.1E+05	9.5E+05	5.3E+05	2.1E+06	1.5E+05	6.9E+04	1.7E+05	9.9E+04	3.5E+04	1.1E+05
JWH-250	1.1E+03	1.1E+03	1.6E+03	5.1E+03	4.3E+03	1.4E+04	2.0E+03	9.7E+02	2.1E+03	1.8E+03	1.0E+03	1.8E+03
JWH-203	8.8E+03	1.1E+04	4.0E+04	3.7E+05	2.2E+05	4.6E+05	6.8E+04	1.9E+04	7.4E+04	4.7E+04	1.2E+04	5.3E+04
JWH-210	4.2E+03	5.3E+03	1.3E+04	1.9E+05	1.5E+05	4.7E+05	5.3E+04	2.3E+04	8.9E+04	3.7E+04	1.3E+04	5.7E+04
JWH-200	6.9E+03	4.7E+03	1.3E+04	6.6E+05	4.1E+05	1.7E+06	2.0E+05	5.3E+04	3.3E+05	1.3E+05	2.3E+04	1.7E+05
AM-2233	1.5E+03	1.2E+03	5.4E+03	1.4E+05	1.6E+05	4.3E+05	3.9E+04	1.8E+04	2.8E+04	1.9E+04	7.5E+03	1.3E+04

signal. For cocaine (Fig. 2.12C.), C18 and MM coatings have desorbed the majority of the extracted analyte by the 3rd desorption while HLB retains some of the analyte past 3rd desorption. In case of JWH-250 (Fig. 2.12D.), a progressive drop in signal can be observed for all 3 coatings, although HLB and MM appear to retain only slightly more in comparison to C18. JWH-200 retains a larger amount of analytes

after 1st desorption, particularly for HLB and MM, and even after 3rd desorption, signals are still elevated for HLB and MM coatings (Fig. 2.12E.). Certainly, it is apparent that incomplete desorption of the analytes occurs after 1st desorption for all 3 coating types. It must be kept in mind that a 0.2 mm sec^{-1} speed was used to move the meshes in front of the DART source, and it possible that this speed is not suitable for desorption of all analytes. In fact, a longer exposure time would likely be required to desorb all of the analytes. For example, Harding et al. analyzed transmission of N-(4-hydroxyphenyl)ethanamide (HPE) and N-phenylbenzamide (PB) on bare SS meshes.[146] The standards were directly deposited onto the SS mesh and desorbed over 60 mins to examine the desorption behavior.[146] Interestingly, signal intensity peaked after 2-3 mins of exposure and continued to release the analytes with a progressive drop up to 60 mins.[146] Of course, signal intensity from desorption of a pure standard tends to be high, but desorption occurring after nearly an hour of exposure indicates that incomplete desorption should not be directly linked to SPME only. It is likely that compound and specific factors play a role too. Certainly, using longer exposure times would allow for a more complete desorption but this becomes time consuming. In fact, it would defeat the whole purpose of AIMS, which are rapid quality results.
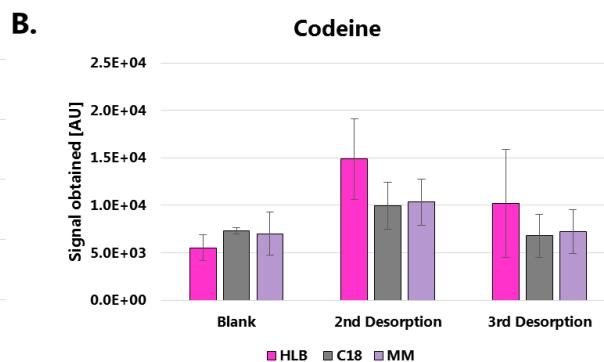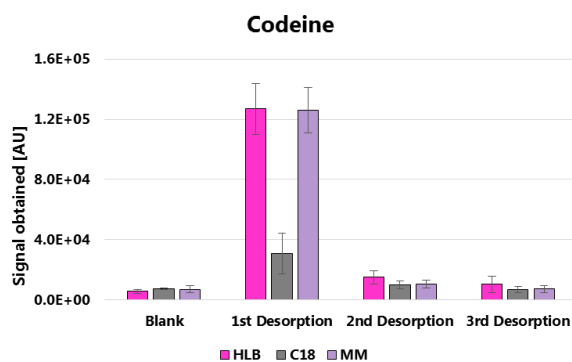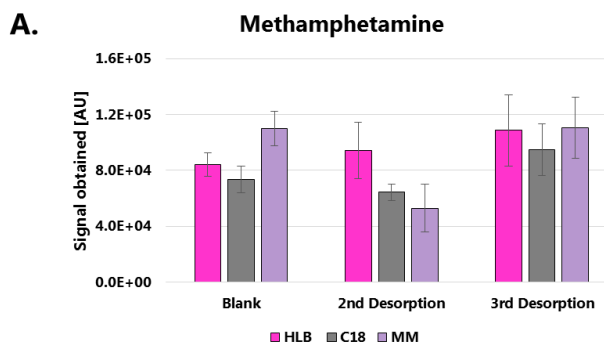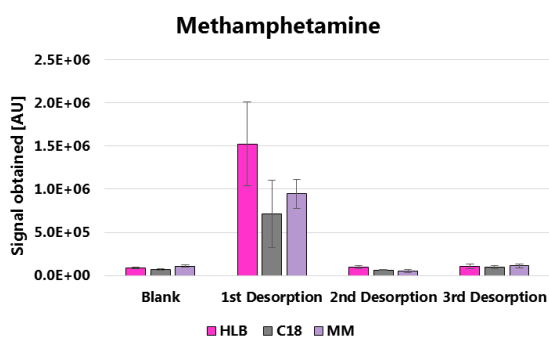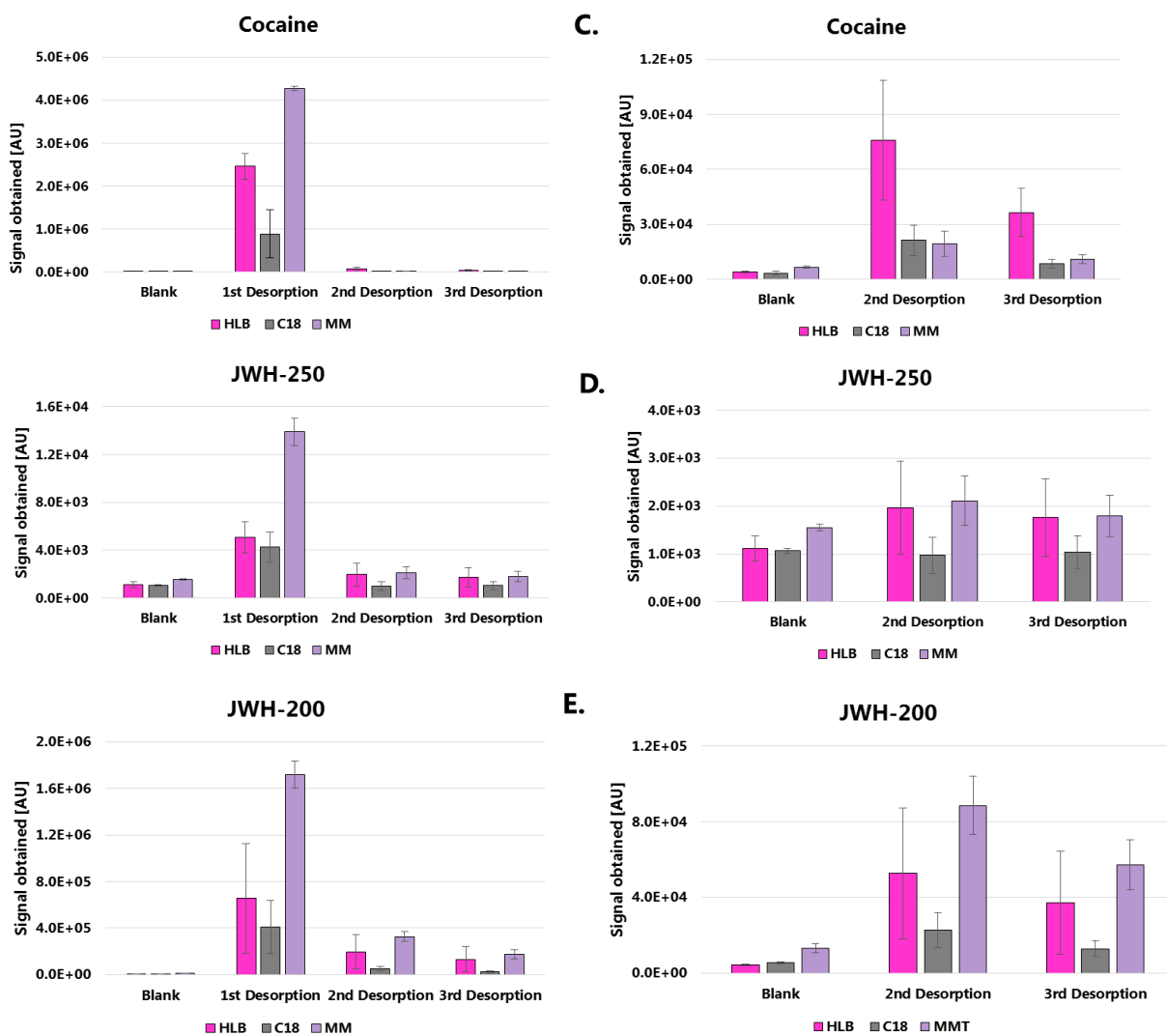
Figure 2.12 *Individual charts showing signals obtained (n = 3) for methamphetamine (**A.**), codeine (**B.**), cocaine (**C.**), JWH-250 (**D.**) and JWH-200 (**E.**) for blank, 1st, 2nd and 3rd desorption on the left and for blank, 2nd and 3rd desorption for better visualization of signal comparability to the blank on the right.*

A future perspective: factorial experimental design

Considering the number of different factors that influence the signal response of DART-MS, it is fair to say that the best way to investigate their impact would be through the use of factorial experimental designs.[155] The aforementioned allows investigators to choose several different factors at fixed levels (e.g., high, medium or low) to determine which factors have the greatest impact on the result.[155] Using a "one-at-a-time" approach is acceptable towards examination of a single factor, but it provides responses at selected and/or fixed conditions of other factors and it must be assumed that the outcome is the same

at all other settings for the remainder of the factors.[155] In case of DART-MS, it is more than likely that the factors mentioned in Section 2.2.1 interact with each other. Hence factorial experimental design would allow for detection of interactions between the factors, in addition to saving both time and resources. As mentioned in the introduction, calculation of certain parameters such as PAs require computational skills, so efforts from programmers, mathematicians and analytical chemists are required to obtain a more complex understanding of DART-MS mechanisms.

2.2.4   Conclusion for Section 2.2

Impact of different DART and SPME parameters with respect to source temperature, coating chemistry, sample positioning, and pH were investigated in this section. Additionally, a multiple desorption test was done to examine the extent of loss of analytes during the desorption process. It has been found that all of the aforementioned factors influence responsiveness of SPME-TM-DART-MS system. These findings highlight the importance of proper optimization of experimental factors before conducting any work. Considering the number of factors involved, the use of full factorial experimental designs would be an excellent method to discover the most important factors and their potential interactions.

2.3 On the performance of solid-phase microextraction (SPME) fibers vs transmission-mode (TM) meshes for direct analysis in real time (DART) coupled to mass spectrometry (MS): Differences in analytical sensitivity

2.3.1 Introduction

Invented by Cody in 2005, DART quickly became popular in numerous fields due to its friendly interface and ability to provide rapid results.[87] DART can be used to analyze unaltered samples, but this approach hinders the achievement of trace-level detection limits. However, the use of a sample-preparation strategy[162] can significantly reduce detection limits and bring them in line with the levels offered by GC and LC-MS. Of the various reported sample preparation options that can be coupled to DART-MS, SPME has proven to be one of the most efficient, as it combines preconcentration, sampling, clean-up, and desorption into a single step.[7,26,49] Different formats of SPME have been coupled to DART-MS, including in-tube SPME,[163] stir bars,[164] fibers,[165,166] and meshes.[26,117,134,136–139] In-tube SPME, which consists of a coating deposited within a capillary device,[7,163] has great potential for application in small volume analysis.[167] Despite this potential, in-tube SPME has some drawbacks; for example, it is relatively cumbersome to prepare, and it is prone to tubular clogging when used with complex matrices, like blood.[163] Stir-bar sorptive extraction has been used for the detection of organic UV filters[164] and phosphoric acid esters.[106] While the detection limits offered by this technique are on the lower side of the ppb scale, its application can sometimes be limited due to the size of the stir bar. For example, it would be challenging to perform small-volume extractions with stir bars, even though smaller-sized stir bars are also available. Additionally, the stir bars are usually manually held or placed inside specially designed glass tubes for introduction within DART's desorbing stream,[106,164] which could pose problems with regards to reproducibility and sample-throughput. Other researchers, such as LaPointe et al. and Cajka et al., have used fibers for detecting synthetic cathinones in urine (synthetic source) and beer profiling, respectively.[165,166] Conversely, Pawliszyns' and Sacks' groups have been diligently using the SPME mesh format for drug, food, and environmental analyses.[26,117,134,136–139] The idea to use a "net-

like" or "mesh-like" device to introduce the sample into AIMS was first reported by Pérez et al., who used it for DESI and DART. This method is known as TM.[115] By depositing samples onto nets or meshes with controlled geometries, Pérez et al. were able to normalize sample introduction into the MS, therefore allowing better analyte "transmission". The major outcome of this approach was enhanced reproducibility.[115] Since fibers and meshes are the two SPME formats most amenable to DART-MS, we conducted a study that aimed to concomitantly examine and compare their analytical performance. To the best of our knowledge, such a study has not yet been published. Obtaining greater insight into the analytical performance of fibers and meshes is desirable because it can provide a more robust understanding of the operating principles of SPME coupled to DART-MS. To examine the performance of these two formats, two separate studies were conducted using two randomized protocols. Protocol #1 was designed to investigate the analytical sensitivity of custom-made fibers and meshes. Both devices were dip-coated in a slurry consisting of 10% PAN binder and 7% of 5 µm C18 particles using a uniform procedure. Nitinol wire served as support for the fibers, while stiff SS mesh with a dense network, named "wire-mesh," was used as a substrate. Analytical performance was then examined using a set of model compounds spiked to PBS, which were then extracted via agitation and a static approach and examined using MRM mode. Ultimately, the meshes outperformed the fibers, reaching lower detection limits and providing sensitivity that was nearly 10x higher. Protocol #2 used commercial SPME fibers (SPE-its™) coated with C18 particles and meshes made of thin metallic sheets with large hexagonal apertures, which were aptly named "sheet-meshes." This mesh design contrasted that of meshes used in Protocol #1. The sheet-meshes were coated in-house using dip-coating (10% PAN, 7% 5 µm C18 particles). PBS was also used as the model matrix, and the analysis was performed using full-scan mode. The results of Protocol #2 were more ambiguous, with the fibers outperforming the meshes in some instances, and the meshes outperforming the fibers in others. Overall, however, the meshes and the SPE-its™ fibers produced comparable results. We postulate that these results were likely related to the mesh design, which indicates

that the wire-mesh format is the superior option for DART-MS-SPME-TM analysis. A discussion of the applications of these two formats (mesh and fiber) is also presented herein, as each contain factors that may limit their applicability.

2.3.2 Experimental

Materials/Methods

The chemicals used in Protocol #1 were ordered from Cerilliant at a concentration of 1000 mg L^{-1}. These chemicals included: fentanyl, oseltamivir, oxycodone, pseudoephedrine, and methadone. The chemicals used in Protocol #2 were also ordered from Cerilliant (1000 mg L^{-1}) and included: EDDP perchlorate, cocaine, cocaethylene, methadone, and codeine. All the chemicals were ordered as methanolic standards. NaCl, KCl, K_3PO_4, Na_3PO_4, PAN, and DMF were obtained from MilliporeSigma at a purity $\geq$ 99 %. C18 particles (5 µm) were also ordered from MilliporeSigma. LC/MS-grade solvents were obtained from Fisher Scientific, including: IPA, ACN, MeOH, and H_2O. Wire-format SS mesh was purchased on Amazon (see Figure 2.13 for a detailed visualization of this format; aperture: 280 µm, wire diameter: 140 µm, pitch: 400 µm, 39% percent open area (POA). Nitinol wire (diameter: 198 µm, lot #2086856-2A) was purchased from Confluent (Freemont, CA, USA). SS meshes in sheet format (see Figure 2.14) were obtained from IonSense, Inc. The sheet meshes had a diameter of 843 µm, a length of ~ 5mm, and an estimated POA of ~ 62%. The SPE-its™ fibers were also obtained from IonSense, Inc. and can be seen in Figure 2.15. PBS was prepared according to procedure described in Section 2.2.2. The preconditioning and cleaning solutions for the devices were made by combining 50/50 of MeOH/H_2O and 50/25/25 of MeOH/ACN/IPA, respectively. Human urine was obtained from a female volunteer. Optical images were taken with an Olympus microscope (SZX10) with a SC30 digital camera (Olympus, Tokyo, Japan), and SEM images were acquired using a Zeiss FESEM 1530 (Carl Zeiss, Oberkochen, Germany).
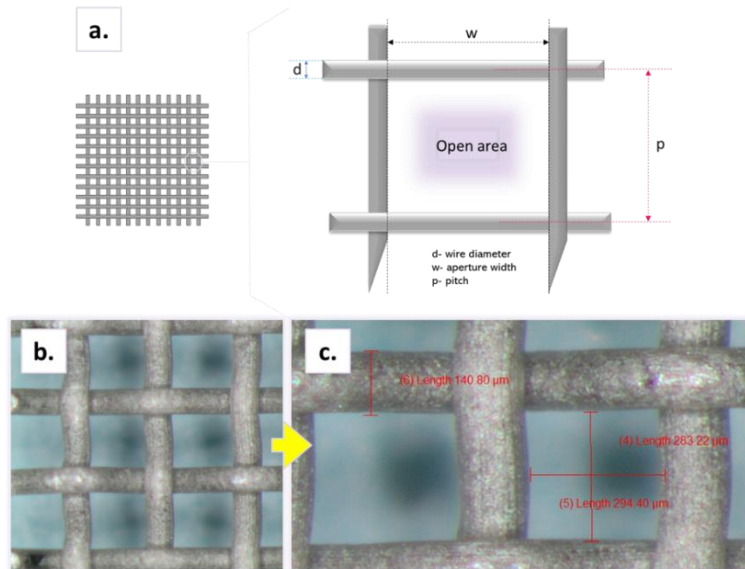
Figure 2.13 *The basic design of the SS wire mesh is shown in image **a.**, which provides an enlarged view of one section of the mesh and its structural features. Image **b.** shows the bare mesh substrate that was used in this research. Figure **c.** provides highly magnified view of the mesh, along with its aperture width (~ 283-294 μm), pitch (400 μm), and wire diameter (140 μm).*
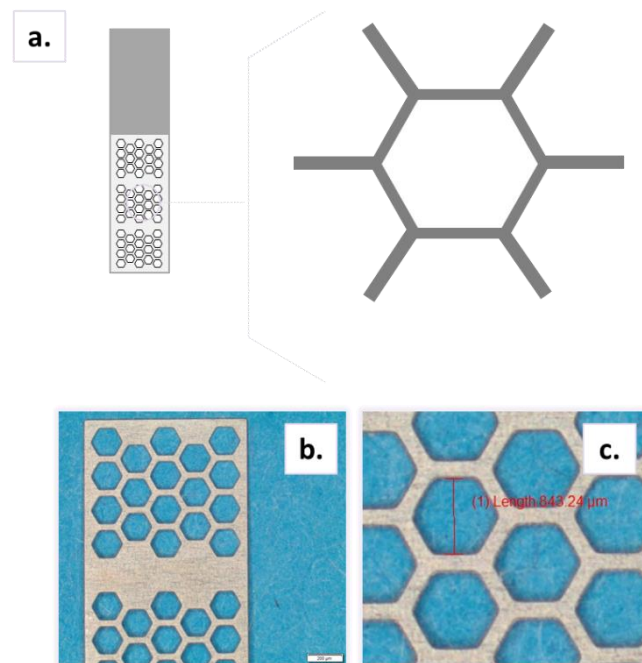
Figure 2.14 *Design of SS mesh used for Protocol #2. Image **a.** shows the basic design of the aperture, which is structured with very characteristic hexagonal shape. Images **b.** and **c.** show the uncoated mesh, with c. providing a highly-magnified view of the structure. As can be seen, the width of the aperture is ~843 μm.*
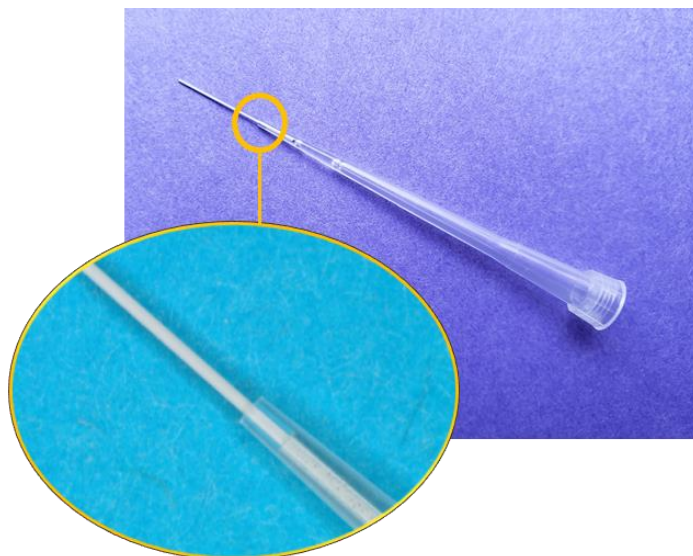
Figure 2.15 *Optical image of SPE-its® coated with a C18 extractive phase.*

Preparation of meshes and fibers

The wire-format meshes were prepared according to the protocol developed by Gómez-Riós.[26] Briefly, the meshes were carefully cut into 2.5 x 0.5 cm strips, etched in concentrated HCl (5 min), cleaned in MeOH and deionized H_2O (5 min, 2x), dried in an oven at 100 °C, and then stored in IPA (to prevent oxidation) until the coating process. The fibers were prepared by cutting the nitinol wires to a length of 5 cm, cleaning them in the cleaning solution, drying at 100 °C, and then storing them in IPA until use. A coating slurry was made by dissolving 10% of PAN powder in DMF and then heating the solution to 100 °C to obtain a uniform glue-like consistency. Once the desired consistency had been achieved, 7% of C18 particles were added and the solution was vigorously agitated and vortexed overnight (12 h, 1500 rpm) with a stir-bar. This slurry was used to coat fibers and meshes used in Protocol #1. The meshes and fibers were immersed in the coating solution and then carefully withdrawn in order to ensure a uniform layer on the device surface. Following dipping, the fibers were immediately placed in the oven for drying (100 °C), while the meshes were blasted with pressurized N_2 to remove any excess slurry from the openings between the wires. Afterwards, the meshes were also placed in the oven for drying (100 °C). This constituted 1 preparation cycle, with a total of 4 cycles being employed for both devices. Coating

64

length was maintained at 1 cm for both devices. For convenient desorption in front of DART source, the fibers were immobilized into plastic 200 μL pipette tips using epoxide glue.

The metallic sheet meshes for Protocol #2 were etched using the following sequence: MeOH (2x, 20 min), HCl (1x, 20 minutes with brief shaking every 5 min), MeOH again (1x, 10 min), and, finally, deionized H_2O (2x, 10 min). Following this procedure, the meshes were dried for 30 minutes at 100 ˚C and kept in a desiccator (under N_2) until use. A slurry made of 10% PAN and 7% C18 particles (different than one used in Protocol #1 as different batches of the material were used) was implemented to coat the sheet meshes with the exception that 2 dip-cycles were implemented (due to a visually acceptable adherence of C18 particles). The coating procedure consisted of dispensing 1 mL of coating slurry (via plastic disposable pipettes) into 12 slots of a 96-well plate (2 mL capacity). This allowed for immersion of 12 pins simultaneously followed by a careful manual withdrawal and blasting with N_2 to remove excess slurry. Once all the devices had been fabricated, cleaning solution was used to remove any interference attachments and the devices were stored in a preconditioning solution until use.

DART-MS/MS

A TSQ-Vantage from Thermo Scientific was used to perform the MRM analysis (+ve ionization mode) in Protocol #1. Table 2.3 provides selected details of the analytes' physico-chemicals properties, as well as the settings that were used for their analysis in Protocol #1. Protocol #2 utilized an Exactive Orbitrap (Thermo Scientific) which was operated in full scan +ve ionization mode (Table 2.4-2.5). A DART SVP® source with a Vapur® interface was obtained from IonSense, Inc. and coupled to both instruments. The DART source was operated at a temperature of 400 °C for Protocol #1, and a temperature of 350 °C for Protocol #2. Custom-made holders (UW) were used for the wire-meshes[26] and the sheet-meshes (Figure 2.16), while fibers were immobilized into a holder made by IonSense, Inc. (Figure 2.17). A linear

rail was used to move the holders along the x-plane at a speed of 0.2 mm s^{-1} for Protocol #1, and a speed

of 0.3 mm s^{-1} for Protocol #2.

Table 2.3 *Details relating to the analytes chosen for Protocol #1, including their respective classes, logP values, parent and product m/z values, along with the S-lens and collision energy used on the TSQ-Vantage. Compound details obtained from PubChem.*

Compound	Class	logP	Parent m/z	Product m/z	S-lens	Collision energy (eV)
Fentanyl	Piperidines	4.05	337.1	188	101	22
Oxycodone	Morphinans	0.30	316.1	241.1	124	28
Methadone	Benzenes	3.93	310.2	265.1	93	14
Oseltamivir	Carboxylic acid and derivatives	1	313	166	70	18
Pseudoephedrine	Benzenes	0.89	166	148.1	64	11

Table 2.4 *Exactive-Orbitrap settings used for the experiments in Protocol #2.*

Resolution	50,000
Mass range	100 - 500
Polarity	+ve
Microscans	1
Capillary temperature	250 °C
S-lens RF level	-
AGC target	1,000,000
Max injection time	-

Table 2.5 *Details relating to the analytes used in Protocol #2, along with their respective classes, logP values, vapor pressure, and boiling and melting points (PubChem).*[156] *Parent m/z values are also provided.*

Compound	Class	logP	Vapor pressure (mmHg)	Boiling point	Melting point	Parent m/z
Methadone	Benzenes	3.93	1.21e-6	-	235°C	310.2171
Cocaine	Benzenes	3.93	1.91e-7	-	219°C	304.1549
EDDP	n/a	5.26	n/a	-	-	278.1909
Cocaethylene	n/a	2.53	n/a	-	-	318.1705
Codeine	Morphinans	1.21	5.54e-9	482°F	309-313°F	300.1599
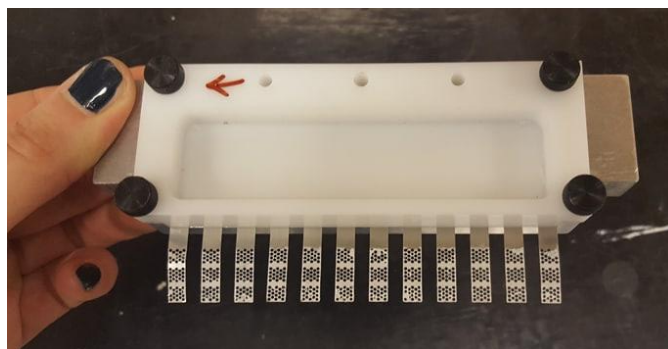
Figure 2.16 *Holder used for the sheet-format SS meshes.*
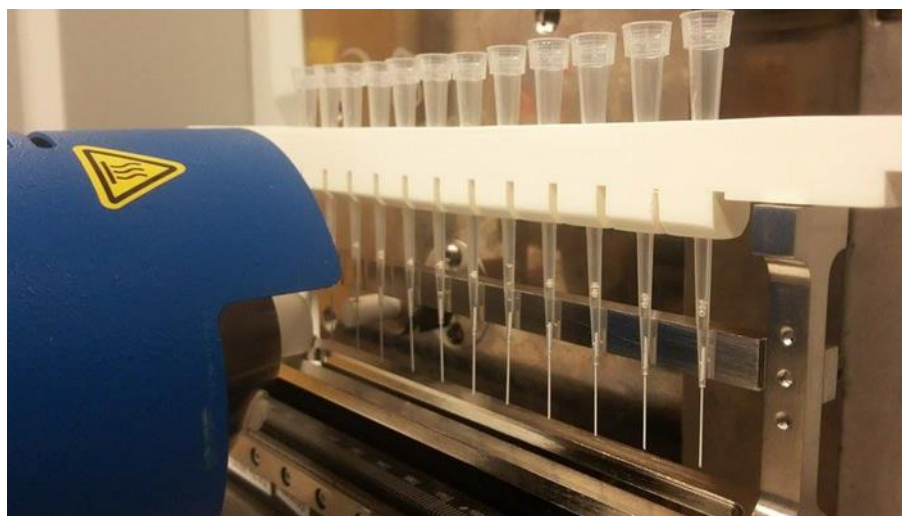
Figure 2.17 *Holder used to immobilize the SPME fibers for DART-MS.*

Extraction procedure

A 100 mg L^{-1} stock solution of analytes (Protocol #1 and #2) was prepared in MeOH and then diluted to adequate concentrations, which were used to spike PBS. Spiking was performed carefully in order to ensure that the percentage of organic solvent content in the PBS comprised ≤ 1 % of the total sample volume.[7] Since the aim of this study was to examine sensitivities at a lower concentration range, the following spiking points were used for Protocol #1: 0.01, 0.05, 0.1, 0.5, 1, 2.5, 5, 10, 15, 20, 35, and 50 ng mL^{-1}. The extractions in Protocol #1 were carried out from a 1 mL sample using agitated (vortex, 3000 rpm, 1 min) and static approaches (10 min) for meshes and fibers. Both approaches were used in conjunction with each device. For Protocol #2, the 100 mg L^{-1} stock mixture was further diluted so that

spiked PBS concentrations equated to 0.1, 1, and 10 ng mL^{-1}. The mesh and fiber extractions were performed using a 96-well-plate with 1.5 mL of spiked PBS in each well for a total of five repetitions (n = 5) per point. The extraction was carried out for 10 minutes on an orbital shaker (~500 rpm). For both protocols, a 5-10 second agitated wash in LC/MS-grade H$_2$O was performed once the extractions had been completed. The devices were then blotted with a KimWipe to remove any remaining H$_2$O, dried, and placed into holders to carry out DART-MS desorption. Signals obtained from blank PBS were acquired for both formats to establish the S/N ratios. Since the aim of this study was to examine raw signal responses, no ISs were used. A summary of details pertaining to the instruments and extraction procedures used in Protocol #1 and #2 is provided in Table 2.6.

Table 2.6 Summary of experimental parameters used in Protocol #1 and #2.

	Protocol #1	**Protocol #2**
Instrument	TSQ-Vantage	Exactive-Orbitrap
Scan mode (+ve ionization)	MRM	Full scan
Matrix (volume used)	PBS (1 mL)	PBS (1.5 mL)
Analytes	Fentanyl, oxycodone, oseltamivir, methadone and pseudoephedrine	Cocaine, cocaethylene, EDDP, methadone and codeine
Choice of fiber	Custom-made	Commercial, SPE-its®
Meshes	Custom made, wire design	Custom made, metallic sheet design
Coating chemistry	C18 (5 µm)	C18 (5 µm)
DART source temperature	400 °C	350 °C
DART rail speed	0.2 mm s^{-1}	0.3 mm s^{-1}
Extraction mode	Agitated (vortex ~ 3200 rpm, 1 min) & static (10 min)	Agitated (orbital shaker ~ 500 rpm, 10 min)
Wash time	5-10 sec (vortex ~ 3200 rpm)	5-10 sec (orbital shaker ~ 500 rpm)

2.3.3 Results/Discussion

Protocol #1

According to the theory of SPME, increasing the SA of the extraction phase should improve sensitivity, as it will allow the device to extract more analyte in a shorter period of time.[7,23,168] Thinner coatings are also more desirable since thicker coatings take longer to equilibrate.[23,168] This is particularly true for SPME thin films developed for GC (also known as membranes) and LC. A comparison of the analytical performance of SPME fibers, thin-films, and stir-bars has already been done by Qin et al. using GC-electron impact.[168] In their study, Qin et al. showed that thin films outperformed both fibers and stir bars due their relatively larger SA and thinner coatings.[168] Given these findings, it is worthwhile to investigate whether this same principle (i.e., higher SA = higher sensitivity) applies within the context of DART-MS analyses of meshes and fibers. Aside from the apertures on the mesh surface that contribute to POA, meshes and thin films are structurally similar. POA, which can be defined as the percentage (or ratio) of the mesh's total hole area to total screen area,[169] is important for the efficient transmission of analytes into the MS. The smaller the POA, the greater the extent to which the wires intertwine (see Figure 2.18 for a visualization). The meshes used in Protocol #1 contained an intertwined network of solid wires (Figure 2.13), with each wire providing a unique desorption point. A visual comparison of meshes and
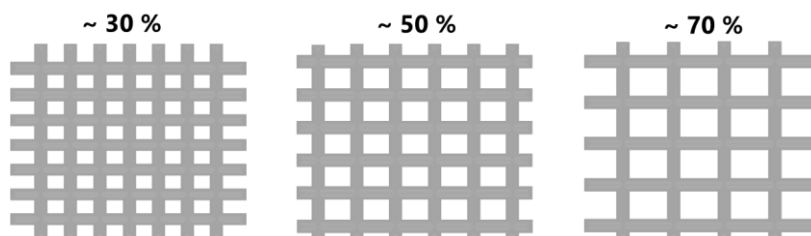
Figure 2.18 *Visualization of how POA changes in response to varying levels of wire intertwining. Note that the percentages presented above the figures are arbitrary and are only used to emphasize the visualization.*

fibers is available in Figure 2.19. Since DART relies on the interaction between a heated gas and an exposed surface (i.e., mesh or fiber) to attain a signal, it was of interest to examine the surface topology
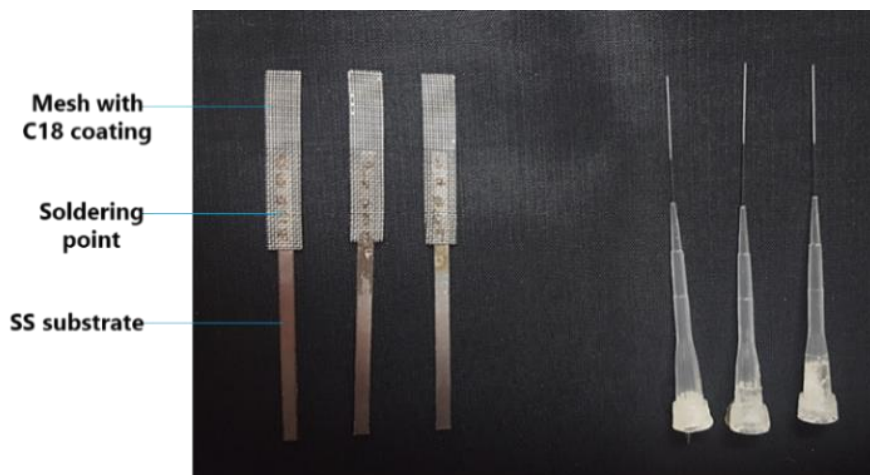
of both devices. Specifically, we were interested in examining the distribution of C18 particles on the individual wires of the meshes and fibers. We wanted to see whether the surface of the devices contained irregularities in the dispersion of the particles. Figure 2.20 provides a detailed illustration of the mesh network. Figure 2.20a. shows an optical image of a network of solid wires coated with C18 particles, while Figure 2.20b. shows an enlarged segment of the mesh. As can be seen, there are slight coverage imperfections along the junction portions of the wires. Optical images of the mesh taken prior to and after coating were used to estimate the thickness, which was found to be ~20 µm. Figures 2.20c-h. show detailed SEM images of the mesh. As can be seen, a dense network of C18 particles is present on the surface. An examination of individual portions of the wire (Figure 2.20f-h.) also revealed uniform particle distribution on the surface. As noted earlier, each individual wire provides a desorption point; hence, adequate extractive particle coverage is important for producing a robust ion chronogram. In addition, the mesh's length of ~5mm allows a greater amount of extracted material to come into contact with the desorbing gas of the DART-MS. Furthermore, the rail speed also contributes to the ion chronogram. Specifically, lower speeds produce broader peaks by allowing for longer interaction times between the desorbing gas and the exposed material. In contrast, the fiber does not have an intertwined wire-network, and instead relies on desorption from a single substrate. Hence, ion chronograms for fibers

70
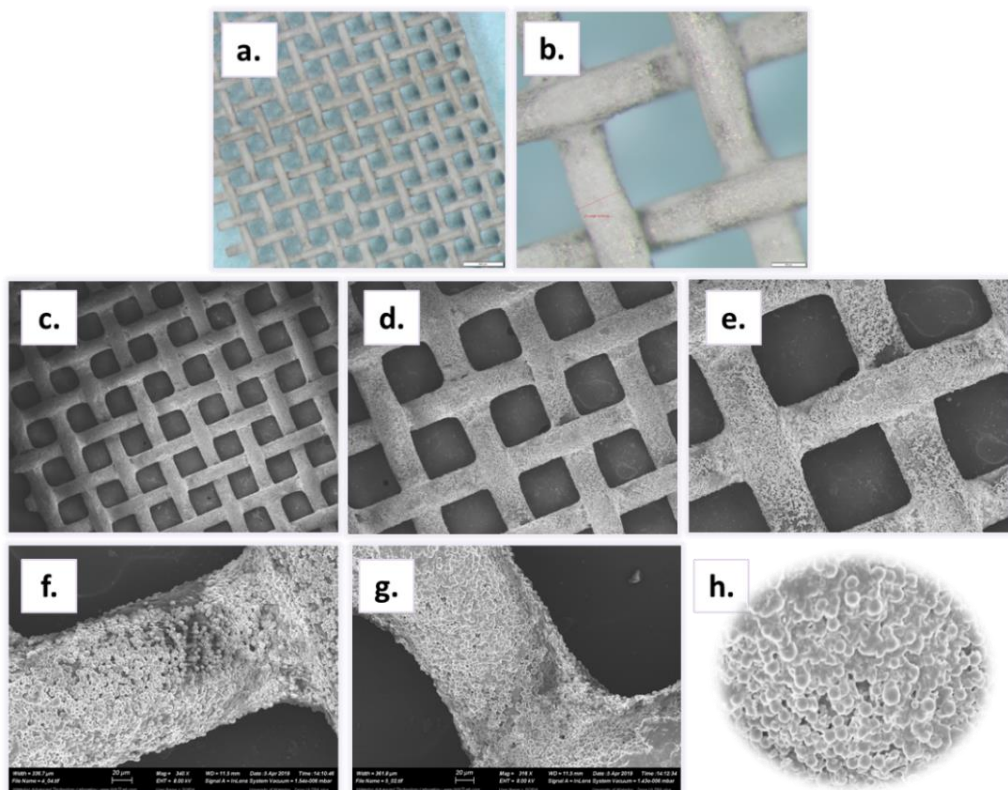
Figure 2.20 *Optical and SEM images of a wire-format SS mesh. Images **a.** and **b.** are optical images, with **b.** providing a magnified view of a mesh segment. Images **c-e.** show the wire strands adequately covered by C18 particles. Images **f-g.** provided a highly magnified view of a section of SPME wire, while Image **h.** provides shows a condensed area of C18 particles.*

tend to be taller and narrower with sharper peaks. Figure 2.21 provides optical and SEM images of the

fibers used in Protocol #1. Figures 2.21a-b. provide optical images of nitinol and a coated fiber,

respectively. Figures 2.21c-d., which were obtained via SEM analysis, show images of a coated fiber

with a surface topology that features a dense network and distribution of C18 particles. Coating thickness

was evaluated by stripping-off a portion of the coating (Figure 2.21e.-f.). An estimation obtained via

SEM analysis revealed that the coating thickness was ~ 12.4-13.8 µm. As discussed above, the devices

used in Protocol #1 were prepared using the same coating slurry in an effort to eliminate and/or reduce

batch effects. This is an important measure because the presence of batch effects (different lot of C18

particles and PAN, differences in slurry preparation) could lead to variation in coating homogeneity,

which could potentially lead to erroneous conclusions. One major difference between DART-SPME and

GC and LC applications using SPME thin-films is the manner in which desorption is conducted. In the
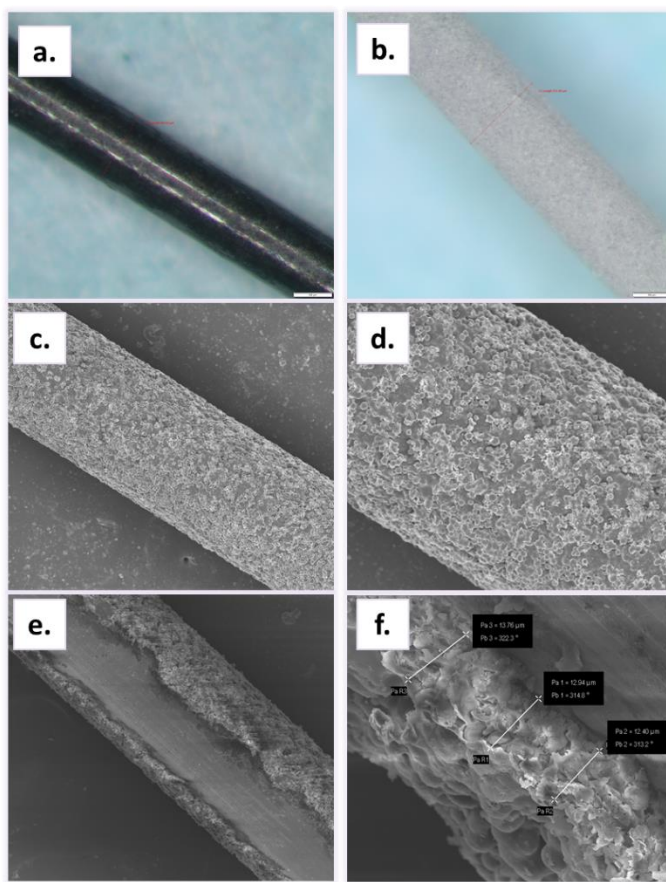
Figure 2.21 *Optical and SEM images of the fibers used in Protocol #1. Image **a.** shows a bare nitinol wire, which was used as a substrate for the SPME fibers. Image **b.** shows the coated SPME fiber. Images **c-d**. show SEM images of the fiber depicted in **a.** and **b.** Image **e.** shows the fiber with a section stripped-off in order to enable an estimation of thickness, as indicated in image **f.***

latter applications, the entire coating is usually exposed to a desorbing gas or solution, ideally removing

all of the extracted analytes.[7] During DART acquisition, the ion chromatogram is created via desorption
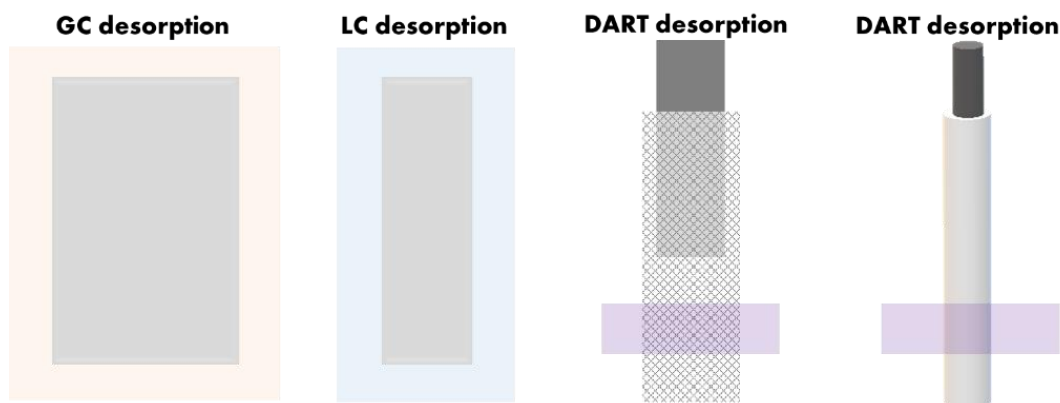
Figure 2.22 *Schematic representation of the desorption strategies used for GC, LC, and DART-MS. GC and LC thin-films are entirely exposed to thermal and solvent desorption, while only a segment of mesh or fiber is exposed to desorbing He* gas in DART-MS.*

from only a segment of the mesh or fiber (illustrated by Figure 2.22). Hence, only a portion of the extracted analytes are analyzed when DART-MS is used. Although the surrounding area may contribute to the signal due to heat transfer, it is unlikely that this would account for signal from the entire coating. Figure 2.23 provides an ion chronogram and the signal areas for agitated extractions performed with a mesh and a fiber using PBS samples spiked with 20, 30, and 50 ng mL^{-1} of methadone. As can be seen, the response of the mesh was nearly a magnitude larger than those of the fiber, with much broader ion chronograms. Figure 2.24 provides a summary of the S/N ratios for the mesh and the fiber, with meshes evidently yielding higher ratios and therefore lower detection limits. For methadone, LODs were achieved at 0.5 and 10 ng mL^{-1} for mesh and fiber, respectively. Detectable signals for fentanyl were observed at 0.01 (S/N of 5) and 0.5 ng mL^{-1} (S/N of 24) for mesh and fiber, respectively. Nonetheless, these findings were based on raw signals (n = 3) obtained without IS correction. In addition, some
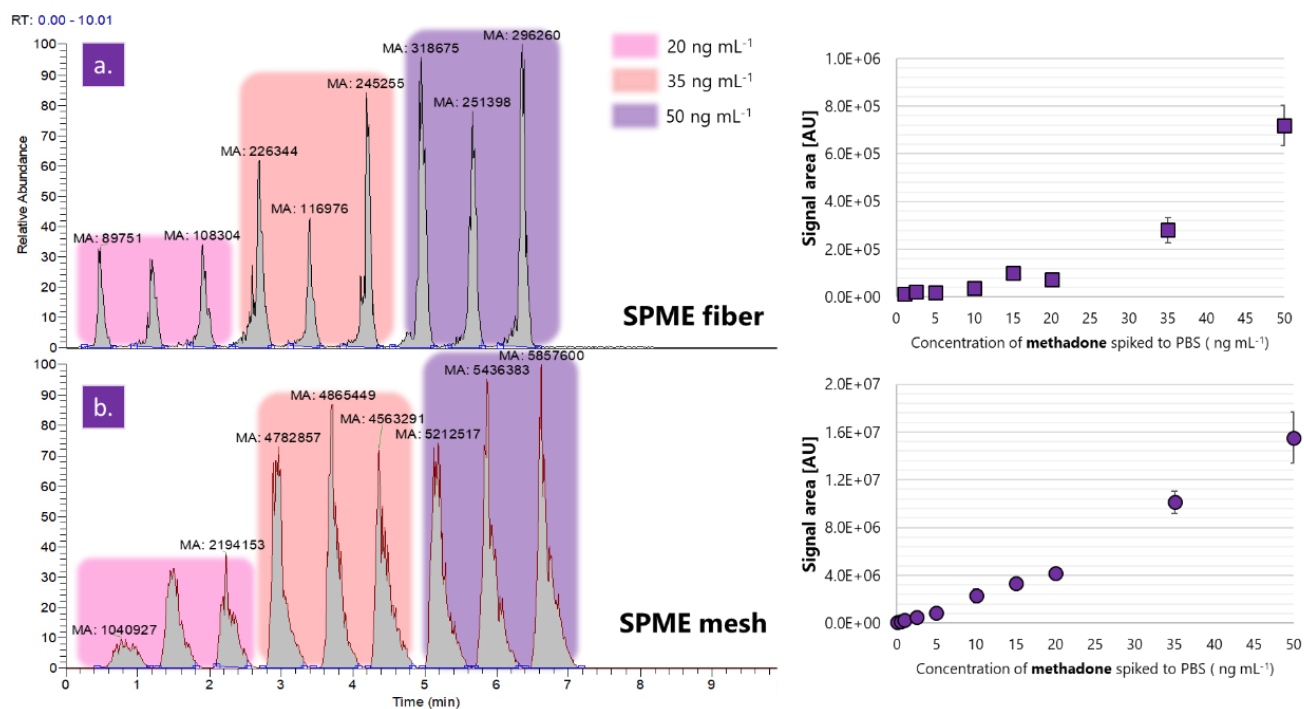
Figure 2.23 *Ion chronogram obtained for methadone (310 → 265) in PBS at concentrations of 20, 35, and 50 ng mL^{-1} using SPME fiber (**a.**) and mesh (**b.**).*

73

Signal-to-noise ratios

Analyte	Format	0.01	0.05	0.1	0.5	1	2.5	5	15	20	35	50
Fentanyl	Mesh	5	26	20	155	365	652	1336	5397	5259	12622	19913
Fentanyl	Fiber	Not detected	Not detected	Not detected	24	20	143	398	692	646	1650	1747
Oseltamivir	Mesh	Not detected	Not detected	Not detected	3	5	9	22	62	56	110	215
Oseltamivir	Fiber	Not detected	Not detected	Not detected	Not detected	Not detected	Not detected	Not detected	19	21	34	54
Oxycodone	Mesh	Not detected	Not detected	Not detected	8	18	33	78	250	245	509	769
Oxycodone	Fiber	Not detected	Not detected	Not detected	Not detected	Not detected	Not detected	Not detected	Not detected	4	34	39
Methadone	Mesh	Not detected	Not detected	1	3	6	11	19	76	95	231	354
Methadone	Fiber	Not detected	Not detected	Not detected	Not detected	1	2	2	10	7	27	68
Pseudoephedrine	Mesh	Not detected	Not detected	Not detected	Not detected	Not detected	Not detected	1	2	2	4	5
Pseudoephedrine	Fiber	Not detected	Not detected	Not detected	Not detected	Not detected	Not detected	Not detected	Not detected	Not detected	Not detected	Not detected

Concentration spiked (ng mL^{-1})

Figure 2.24 *S/N ratios obtained for the extraction and analysis of fentanyl, oseltamivir, oxycodone, methadone, and pseudoephedrine from PBS spiked at 11 different concentrations for meshes and fibers.*

discrepancies were observed in the S/N ratios; for example, the S/N ratios were slightly higher at lower spiked-concentration points. Such discrepancies tend to be more prevalent when signal correction (no IS) is not employed. While other factors may have contributed to these errors (extraction irregularities and coating imperfections), ambient-air turbulence during analysis can be considered as one of the main culprits for such errors. LODs of 15 and 20 ng mL^{-1} were achieved for oseltamivir and oxycodone, respectively, while pseudoephedrine went undetected. In the case of the meshes, LODs of 0.5, 0.5, and 35 ng mL^{-1} were achieved for oseltamivir, oxycodone, and pseudoephedrine, respectively. The performance of the devices was also tested using a static approach, which produced S/N ratios that indicated a slight drop in sensitivity for both formats. However, the static tests also revealed that the meshes yielded better responses than fibers (Figure 2.25), as the fibers were unable to produce a signal for oxycodone and pseudoephedrine. In general, it is not surprising that the meshes outperformed the fibers, as they offer a much larger SA for desorption. After all, DART-MS is a thermal-desorption technique in which response quality depends on time and surface exposure. Several authors have already

demonstrated DART's tremendous ability in surface analysis.[101,149,170] For example, Chernetsova et al. showed that performing angled DART desorptions allowed for greater interaction between the desorbing gas and the sample, thus improving sensitivity.[149] In the case of SPME-TM wire meshes, a greater proportion of the particles are exposed to the desorbing gas, which ultimately yields a better response.
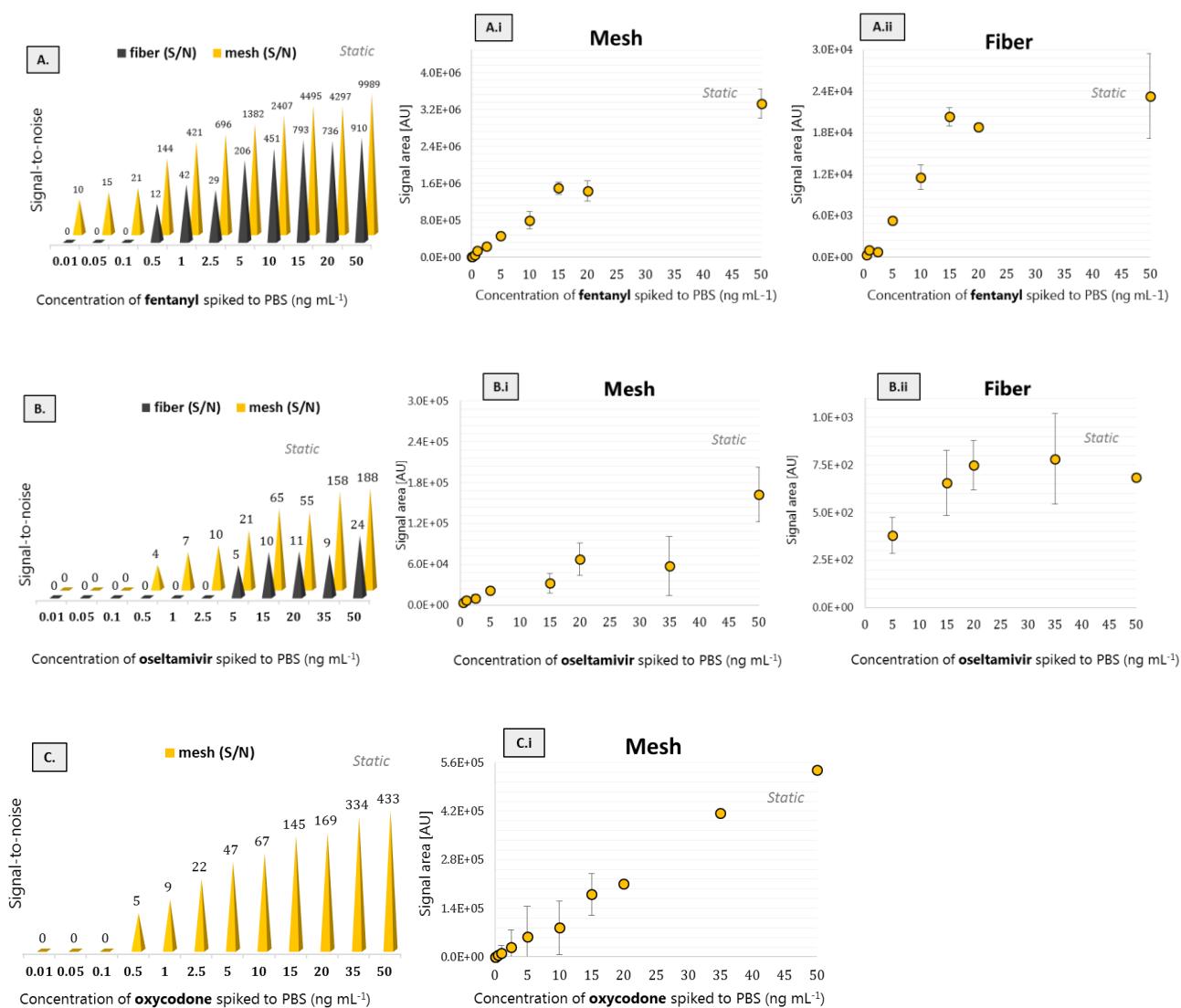
Figure 2.25 *Responses of meshes and fibers (Protocol #1) used for static extractions of fentanyl (**A.**), oseltamivir (**B.**) and oxycodone (**C.**). Please note that log scale is used for the signal-to-noise figures.*

Protocol #2

The goal of Protocol #2 was very similar to the goal of Protocol #1; that is, we sought to examine whether more SA would provide an increase in sensitivity, even with changes in the experimental parameters. Specifically, Protocol #2 used different instruments, DART settings, and extraction strategies, as well as C18 particles from 2 different purchasing sources. Perhaps the biggest change was the use of a different mesh format (Figure 2.14). For these tests, we used a thinner substrate that was made of smooth metallic sheets, which had been perforated with hexagonal apertures approximately ~ 0.8 mm in diameter. Hexagonal apertures were recommended by the manufacturer due to their better "structural stability" when dealing with complex samples and high agitation speeds. These characteristics have not yet been investigated, but will be examined in future studies. In addition, the sheet mesh had relatively fewer desorbing points compared to the wire-mesh. Figures 2.26 and 2.27 provide detailed images of the surface topologies of the sheet meshes and SPE-its®. Figures 2.26a-b. provide optical images of the coated sheet mesh, showing what appears to be a good coating. Figures 2.26c-g. show the SEM images used to perform a thorough visual examination of surface topology, while Figure 2.26c. shows that the sheet mesh appears to have a slightly less dense network of C18 particles, unlike wire-meshes of Protocol #1. As can be seen in Figure 2.26d., the lower section of the three-point junction highlighted in purple appears to have minor variability in the amount of deposited C18 particles, which is likely caused by smoother surface of the photochemically etched sheet-mesh. Exposing the mesh to longer or more aggressive etching could have made the surface rougher, but it could have also compromised its structural integrity. Figure 2.26e. shows a portion of the coated mesh with variations in how the particles "protrude." For example, i. shows a dense area of particles and ii. shows particles that are more embedded within the PAN glue. Figures 2.26f-g. show the mesh with portions of coating removed, indicating an estimated thickness of ~18-22 µm. Figure 2.27 shows the SEM image obtained for a stripped-off portion of the SPE-it®, which had an estimated thickness of ~ 69-77 µm. The findings of Protocol #2 revealed
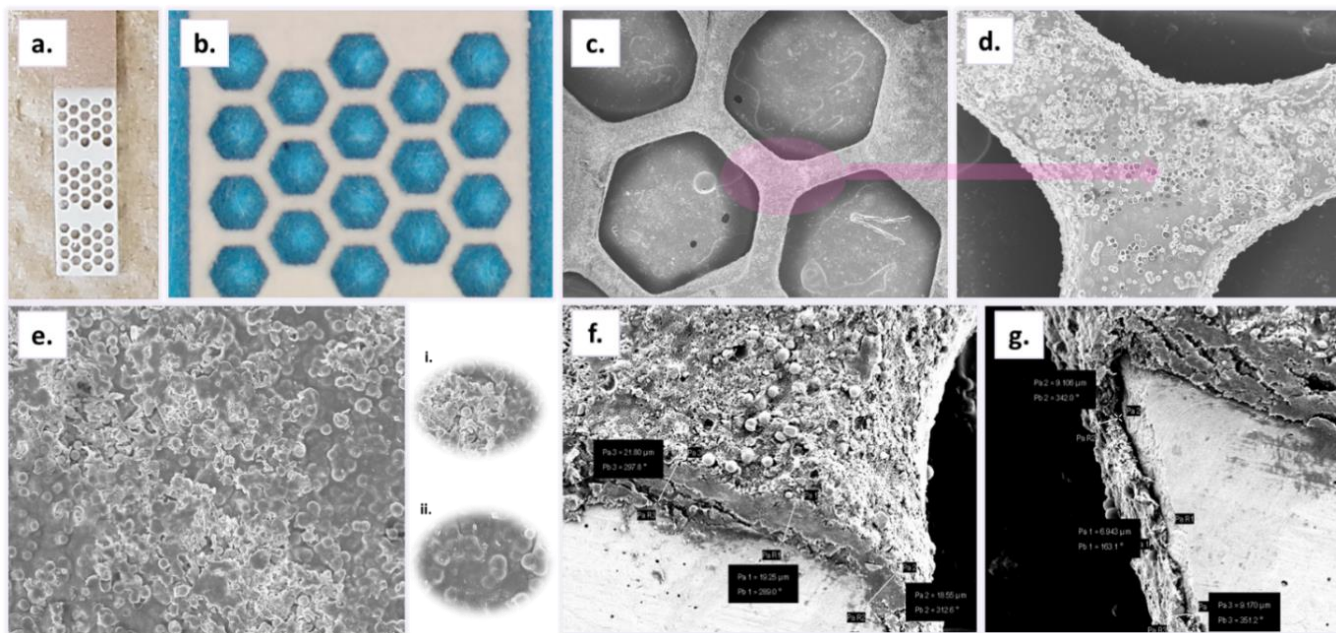
Figure 2.26 *Visual examination of meshes used for experiments conducted in Protocol #2. Figures 2.26a-b. show the pin coated with C18 particles. Figures 2.26c-d. show SEM images of the mesh, with d. depicting an enlarged portion of a three-point junction. This junction point is highlighted with purple in c. Figures 2.26e., 2.26i., and 2.26ii. show an enlarged image of a cluster of C18 particles obtained from the mesh, while f. and g. show cross-sections of the mesh.*

comparable performance for both devices, with the meshes and fibers outperforming each another for specific concentrations and/or analytes. Figure 2.28 provides a chart showing the signal response (in AU) for sheet-meshes and SPE-its® for 0.1, 1, and 10 ng mL^{-1} of model analytes extracted from PBS. As can be seen, neither format produced a signal for methadone at 0.1 ng mL^{-1}, but the fibers produced an elevated response (6e3) at 1 ng mL^{-1} when compared to the sheet mesh (1e3). However, sheet mesh's
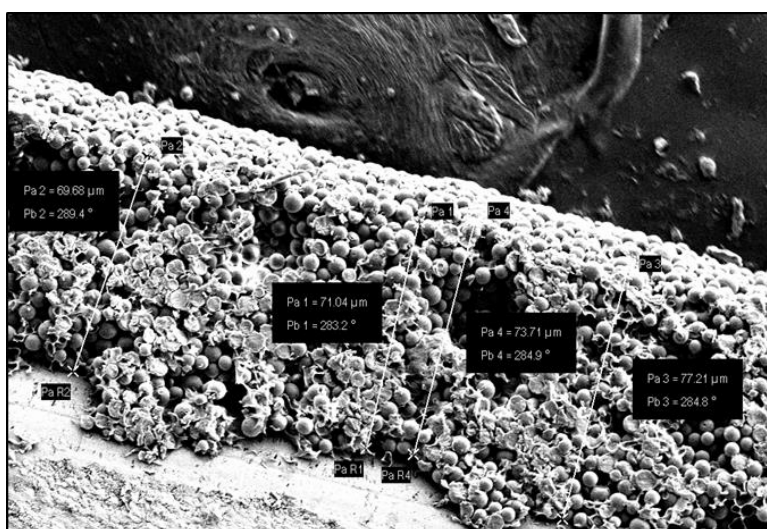
Figure 2.27 *SEM image obtained from a stripped-off section of an SPE-it® fiber, providing an estimated coating thickness between ~ 69 and 77 µm.*

response at 10 ng mL^{-1} (2.4e5) was greater than that of SPE-its® (1.4e5). No signal was observed for EDDP at 0.1 ng mL^{-1}, while SPE-its® showed a better response at 1 ng mL^{-1} and the sheet meshes provided superior response at 10 ng mL^{-1}. Furthermore, sheet mesh was able to detect cocaine at 0.1 ng mL^{-1}, while SPE-its® was able to do so at 1 ng mL^{-1} and 10 ng mL^{-1}. In fact, at 10 ng mL^{-1} of cocaine, SPE-its® produced a greater response than sheet-mesh.

In the case of cocaethylene and codeine, SPE-its® showed a greater response for all the spiked concentrations. Figure 2.29 also provides ion chronograms obtained for 10 ng mL^{-1} of EDDP monitored via sheet-mesh and SPE-its®; it is clear that SPE-its® performed better in this scenario. As it can be seen, the sheet-mesh yields a non – linear response, which could be potentially related to turbulence that occurs during introduction of He* gas. As the SEM image in Figure 2.27 clearly shows, SPE-its® has a dense distribution of C18 particles on the surface. Although the sheet mesh also appears to have adequate

	Methadone		EDDP		Cocaine		Cocaethylene		Codeine	
	Mesh	SPE-its	Mesh	SPE-its	Mesh	SPE-its	Mesh	SPE-its	Mesh	SPE-its
0.1 ng/mL	0.0E+00	0.0E+00	0.0E+00	0.0E+00	1.2E+03	0.0E+00	5.0E+02	4.7E+02	0.0E+00	0.0E+00
1 ng/mL	1.1E+03	6.0E+03	5.0E+02	2.6E+03	1.8E+04	2.2E+04	5.1E+02	1.7E+04	0.0E+00	2.7E+03
10 ng/mL	2.4E+05	1.4E+05	1.5E+05	8.5E+04	1.6E+05	3.1E+05	2.0E+05	2.9E+05	0.0E+00	3.8E+04
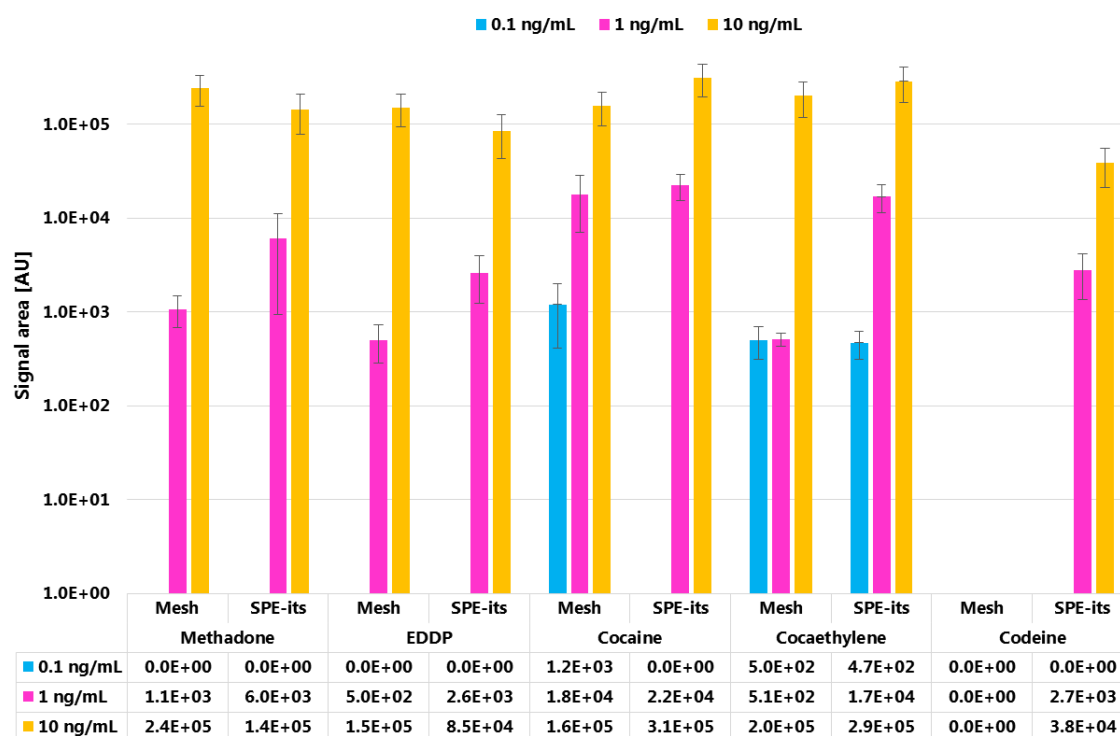
Figure 2.28 *Chart obtained from the experiments conducted in Protocol #2. The bars (log scale) indicate signal response (in AU) of sheet meshes and SPE-its® for extractions from PBS samples spiked with of 0.1, 1, and 10 ng mL^{-1} of methadone, EDDP, cocaine, cocaethylene and codeine.*
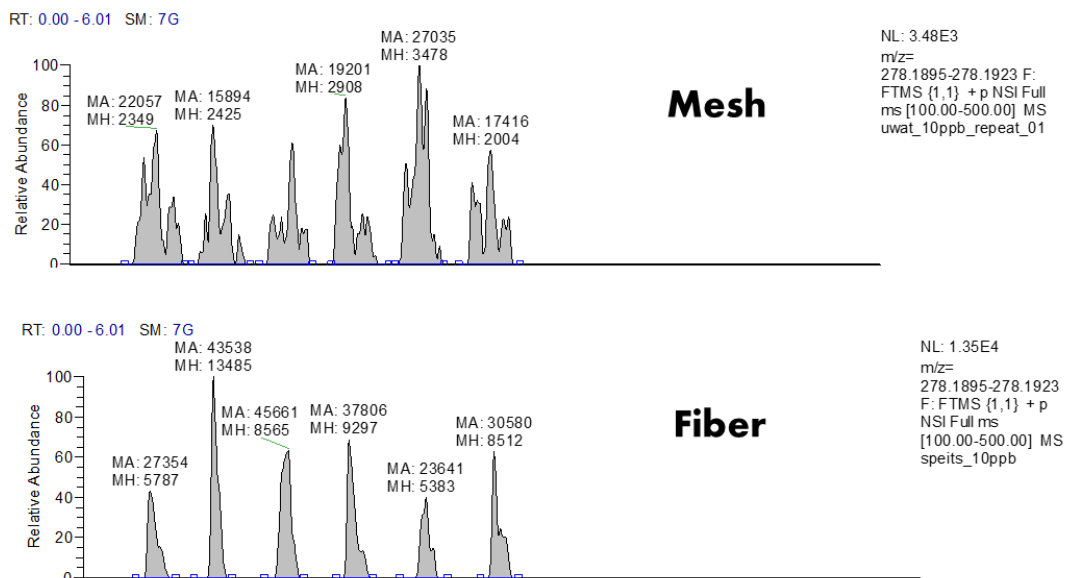
Figure 2.29 *Ion chronogram obtained on an Exactive-Orbitrap for the monitoring of EDDP (278.1909) via mesh and fiber.*

particle distribution, a large POA, combined with fewer desorption points and much thinner coatings, may be to blame for its sub-par performance. Protocol #1 used SS meshes that consisted of a dense network of cylindrical wires, which significantly contributed to the signals of the ion-chronogram; in contrast, Protocol #2 used meshes made from metallic sheets with wider open areas, thus reducing the mesh's interaction with the desorbing gas. Figure 2.30 provides a side-by-side comparison of two types of mesh [Canadian 10-cent coin used to emphasize the size (1.8 cm diameter)]. It is also possible that

Figure 2.30 *SPME-TM meshes: "wire-mesh" design represented on the left and "sheet-mesh" represented on the right.*

the mesh design—that is, the circular geometry of the wire-mesh vs the "flat"geometry of sheet mesh (Figure 2.31)—interacts differently with the heated gas, thus resulting in different heat transfers.

As such, it may be useful to investigate "depth of penetration" of the desorbing gas in order to determine how deeply the gas penetrates the extraction phase. Although studies focusing on heat transfer are beyond the scope of this investigation, it is nevertheless important to consider this aspect, perhaps via modelling studies and follow-up experiments.
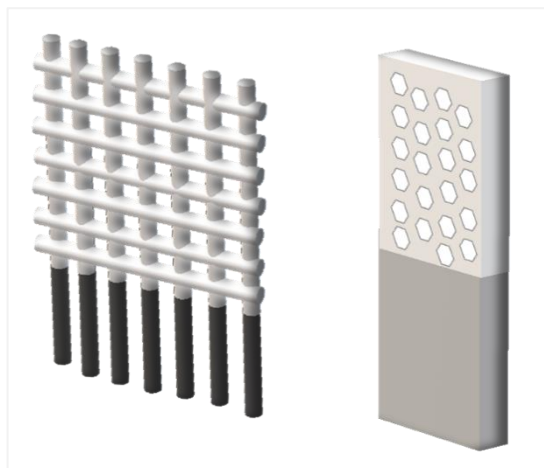
Figure 2.31 *Visualization of the wire mesh's "circular" geometry (left, 0.12 mm thickness), and the sheet mesh's "flat" geometry (right, 0.06 mm thickness).*

A consideration of both approaches

When evaluating SPME formats for coupling to DART-MS, it is important to ascertain the differences between them with regards to performance and compatibility. Ignoring the application aspect for the moment, one must be cognizant of the fact that, while the larger SA offered by the mesh may enhance sensitivity, it may also extract more interferences from biological matrices. Although protecting the coating using PAN and an optimized wash step can reduce the attachment of interferences, this approach can become challenging for increasingly complex matrices (i.e. viscous, fatty and/or solid). Figure 2.32 shows an excerpt of an ion chronogram obtained for monitoring of pseudoephedrine and fentanyl transitions in blank urine via mesh (2.32a-b., 3x) and fiber (2.32c-d., 3x). Notably, mesh yielded greater noise levels for extractions from blank urine. Therefore, preliminary investigations to evaluate noise levels should be conducted before using meshes. These tests could be done by performing extractions from a blank sample and a sample spiked at the lowest concentration point, which is based on the
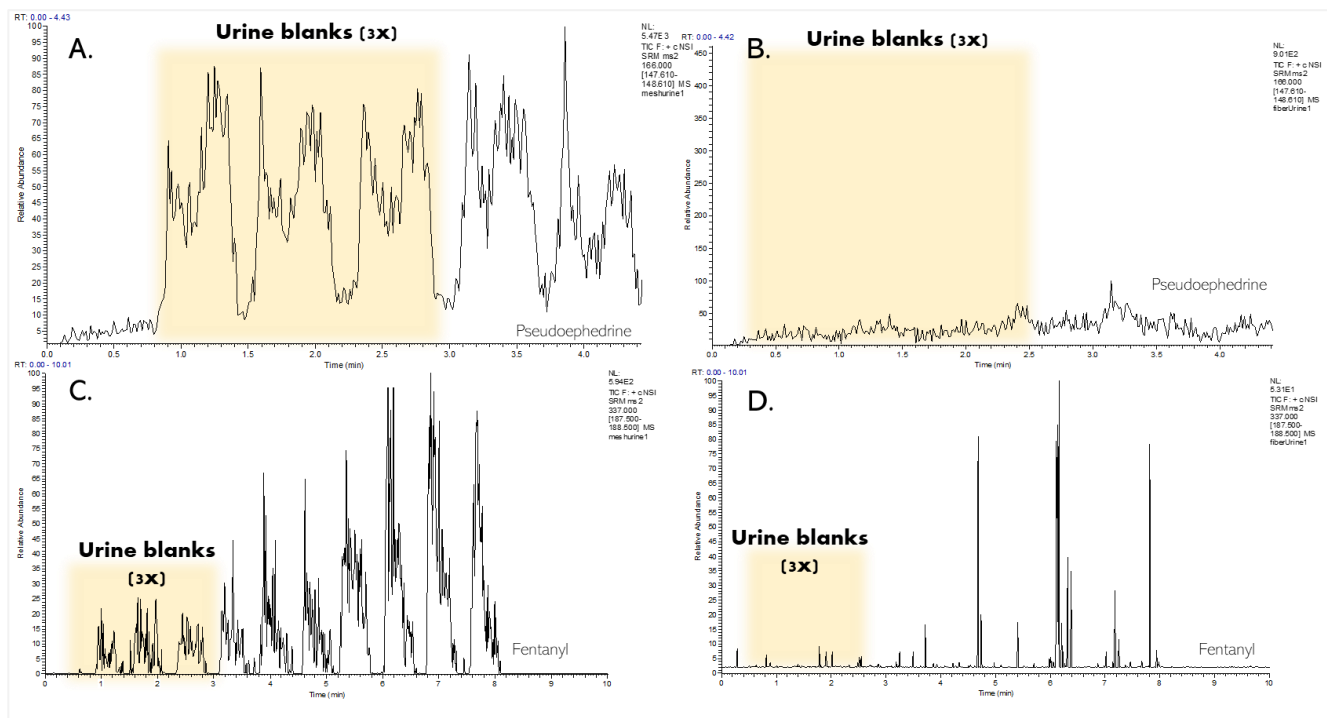
Figure 2.32 *Ion chronograms obtained for blank extractions from urine for pseudoephedrine with meshes (**A.**) and fibers (**B.**). Images **C.** and **D.** show ion chronograms obtained for blank urine extractions for fentanyl with mesh and fiber, respectively.*

predetermined analytical cut-offs of established techniques like GC and LC-MS. This preliminary step would help ensure that realistic detection goals can be established.

As this research has shown, mesh's properties can be best taken advantage of by employing adequate design and coating topology. In other words, when it comes to trace-level detection, meshes will likely provide better sensitivity than fibers. SPME-TM's ability to yield very low detection limits in biological, food, and environmental matrices has already been demonstrated.[26,117] Metabolomics, for example, is a field that has not yet been sufficiently explored via SPME-TM. In addition, while Gómez- Ríos et al. have profiled different types of milk (from dairy and non-dairy sources) using a portable MS,[134] no large-scale studies have been reported thus far. As Mousavi et al. have shown,[50] using thin films for metabolomics significantly enhanced sensitivity, proving capable of reporting well over 1000 cellular metabolites of *E.Coli.* Hence, it would be worthwhile to investigate how metabolomics would respond to SPME-TM coupled to a thermal-desorption platform like DART-MS.

With respect to fiber applicability, it is fair to say that they have great potential for *in-vivo* sampling. In fact, SPME fibers have already been used to obtain samples from living systems in multiple studies.[34,171,172] Compared to fibers, the use of SPME meshes might be more challenging for *in vivo* analysis, as their design is somewhat inconvenient for insertion into living systems. Nonetheless, this does not completely preclude the use of meshes for *in vivo* sampling. For instance, meshes could be used in biological surface analysis, such as skin sampling[21] or oral swabbing. Jiang et al. used polydimethylsiloxane SPME thin films for GC analysis of *in vivo* profiling of skin volatiles,[21] while Park et al. demonstrated the applicability of DART-TOF-MS for profiling of skin metabolites in mice following UVB irradiation.[167] Furthermore, HLB-coated SPME-TM meshes have been used for a simulated semi-quantitative *in vivo* analysis of caffeine in OF[136] wherein OF samples were collected from a volunteer at different time points; this study was able to confirm that caffeine has a half-life of about 5-6 h after initial consumption. In addition, meshes also have great potential for small-volume analysis such as biofluidic spot sampling. Spot sampling allows meaningful information to be obtained from very small sample volumes (Vs ≤ 20 µL), as the sample (i.e., blood, plasma, OF) can be deposited as a droplet onto the mesh for fast extraction and desorption. The Pawliszyn group has recently designed "miniaturized tips," which allow the detection of analytes in as little as 1-20 µL of biofluids.[25,173] However, desorption of the afore-mentioned devices in front of DART-MS is challenging due to size of the miniaturized tip (< 1000 µm), which has to be carefully aligned between the heated gas output and the MS inlet. Hence, using SPME-TM meshes for biofluidic spot analysis would be more feasible.

2.3.4 Conclusion for Section 2.3

In this research, meshes (wire and sheet format) and fibers (custom-made and SPE-its®) were tested using two different protocols to examine which format yielded better results with respect to sensitivity and detection limits. All devices were manufactured under tightly controlled conditions in order to eliminate batch effects. The results of Protocol #1 revealed that the wire meshes yielded better responses

than the custom fiber, while the results of Protocol #2 indicated that the SPE-its® fiber slightly outperformed the sheet meshes. This result suggests that the SPME sheet mesh is not optimal for DART-MS applications. These results highlight the importance of investigating different parameters that may influence signal response in approaches that couple SPME to DART-MS.

2.4 Towards on-site analysis of complex matrices by solid-phase microextraction-transmission mode coupled to a portable mass spectrometer via direct analysis in real time

2.4.1 Introduction

Within the setting of a forensic laboratory, the analysis of controlled substances has a major impact on both the workload and evidence back-log.[174] Controlled substance analysis can be time consuming, which is inconvenient for the criminal justice system. Hence, increasing the throughput of routine drug evidence analysis is of great interest.[174] The "golden standards" or established laboratory methods (i.e., hyphenated techniques like GC and LC) are known for their accuracy and robustness but are very time and material consuming.[174] Over the course of the last few years, the scientific community has invested significant effort in the development of AIMS techniques. In AIMS, sample processing occurs in the open air, thereby removing the need for chromatography and significantly decreasing analysis times.[84] AIMS could be done without sample preparation, but sample preparation substantially decreases detection limits allowing analysts to approach trace-level detection limits, even with very complex matrices.[162] Considering the reduction in analysis time and implementation of a facile sample preparation technique, AIMS would be an ideal workhorse for forensic experts and law enforcement. In fact, portable MS instrumentation amenable to ambient analysis would provide great benefits to forensics.[174] Portable MS are miniaturized instruments ideal for *in-situ* analysis.[175] An exact definition of a miniature MS is not available, but the term is typically used to describe analyzers that are significantly smaller than those used in conventional laboratories.[175] Such analyzers would enable efficient field testing by performing immediate evidence analysis at the crime scene and thus allowing for an increase in sample throughput,[174] thereby creating an opportunity to prevent delays which happen when evidence is dispatched to forensic laboratories.[176] In fact, the first few hours of a crime scene investigation are of crucial importance for obtaining important information as timely responses of law enforcement are vital for establishment of

criminal intent.[174,176] Many miniaturized platforms for analysis of forensic-related samples already exist and include electrochemical sensors, paper-tests, microfluidics and portable systems (Raman and near-infrared).[176] However, portable MS offers greater specificity and sensitivity. Some of them are already implemented in airports, sea-ports, police operations, and border inspections.[176] Several researchers have already investigated portable MS in forensic applications. O'Leary et al. used an ion-trap for monitoring of clandestine synthesis of methamphetamine[177] and building of reference libraries for the portable MS.[178] Mach et al. even mounted a portable MS to vehicles for detection of residues associated with clandestine laboratories.[179] Some applications relied on strict analysis of chemical standards,[179] while some attempted to employ a sample introduction strategy like Bruno et al., who used swab analysis prior to portable MS coupling.[180] In order to efficiently use a portable MS outside of a laboratory setting, one should implement simple procedures that allow for proper sample introduction to the MS.[181] For example, Zhang et al. reported LOQs of 10-20 µg L^{-1} for a set of selected drugs using DBS coupled to Mini 11, a portable ion trap MS.[182] Ren et al. also used DBS for analysis of sitaglipin in whole blood, reporting an LOQ of 10 µg L^{-1}.[183] Another increasingly popular technique amenable for on-site analysis is DART-MS. DART has already been extensively introduced in Section 1.5.1, so its basics will not be provided here. Portable DART-MS has been employed by Brown et al.[184] for testing of pure drug standards and mixtures (Percocet tablets and cherry cough syrup); and by Bernier et al.[185] whereby DART-MS was used for fingerprinting of falsified anti-malarial medicines. Reports of quantitative work via portable DART-MS are still scarce, due to lack of use of preconcentrating, interference isolating sample preparation techniques. In this section, coupling of a portable DART-MS system Waters Q-Da to SPME-TM is presented. Previous DART-MS-SPME-TM publications demonstrated very good results for analysis of complex matrices.[26,117] Therefore, the goal was to investigate both specificity and sensitivity of the aforementioned portable system when coupled to a concentration enriching technique such as SPME-TM. OF was used as a matrix of interest due to its potential for use in drug detection

85

following recent drug use. SPME-TM meshes were coated with 5 µm HLB particles which were imbedded within 10% of PAN binder. Extractions were carried out for one minute prior to analysis by DART-Waters-QDa. Satisfactory semi-quantitative results were obtained for a total of seven drugs, with LODs ranging from 10-25 µg L^{-1} and LOQs ranging from 25-75 µg L^{-1}. Acceptable accuracy (83-119%) and precision (2-13% was also achieved) for the validation point examined (100 µg L^{-1}). The results of this research highlight the potential that SPME-TM has for use in scenarios amenable to portable MS use, such as roadside drug testing whose aim is to prevent driving under the influence of drugs (DUID) accidents.

2.4.2 Experimental

Materials/Methods

OF was obtained from five male and five female volunteers (n = 10) and pooled together. A set of DoAs was obtained from Cerilliant at a concentration of 1000 mg L^{-1}: morphine, oxycodone, codeine, heroin, cocaine, methamphetamine and methadone. The respective ISs were also obtained from Cerilliant at a concentration of 100 mg L^{-1}: morphine-d6, oxycodone-d3, codeine-d3, heroin-d9, cocaine-d3, methamphetamine-d5 and methadone-d3. A stock solution consisting of aforementioned analytes was made in MeOH at a concentration of 100 mg L^{-1}, while the IS stock solution was made to 10 mg L^{-1}. The IS stock was spiked to a final concentration of 100 µg L^{-1} for all samples, while DoAs were spiked at 25, 50, 75, 100, 250, 500, 750, and 1000 µg L^{-1} to build matrix matched IS-corrected calibration plots. A 100 µg L^{-1} was used as a QC for the validation. After spiking, OF was gently agitated (800 rpm) on an orbital shaker to allow for analyte and matrix binding to occur. The percentage of organic content spiked to OF was ≤ 1%. SS meshes were obtained from IonSense, Inc. and HLB particles were obtained from Waters, Inc. PAN and DMF were obtained from MilliporeSigma. LC/MS grade MeOH, H_2O, ACN, and IPA were obtained from Fisher Scientific. Section 2.2.2 explains the mesh manufacturing protocol in detail.

Extraction process

The SPME-TM meshes were kept in a preconditioning solution (MeOH/H_2O, 50/50). Before use, they were removed from the solution and washed with H_2O to remove solvent residuals. Afterwards, the meshes were placed in vials containing 1.5 mL of OF and the extraction was carried out for 1 minute under strong agitation (3000 rpm). After completion of extraction, the meshes were washed with 1.5 mL of H_2O (under agitation as well), dried and placed in the mesh holder. The whole procedure was adapted from Gómez-Riós.[26] A schematic of the process is provided in Figure 2.33.
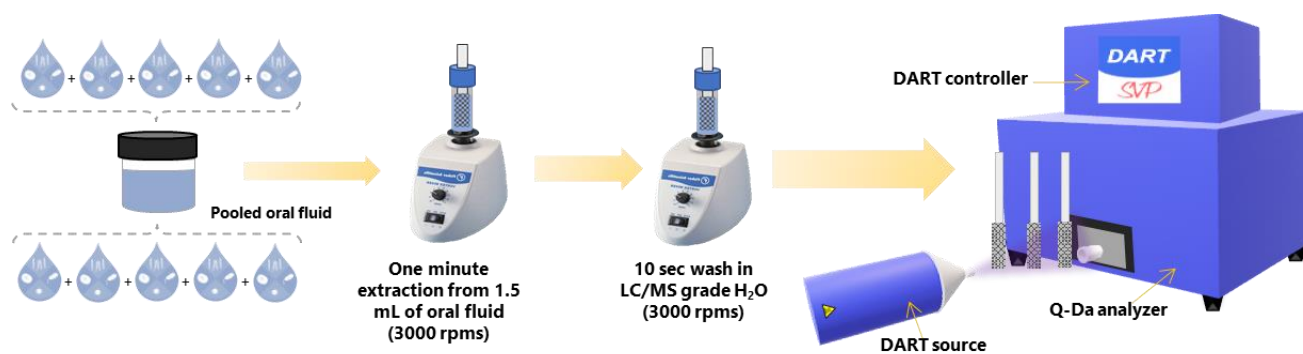
Figure 2.33 *Schematic of the workflow used for detection of DoAs in OF via SPME-TM and DART-QDa mass analyzer.*

DART-MS analysis

DART-SVP® with a Vapur® interface was obtained from IonSense, Inc. and coupled to a single quadrupole Waters-QDa with an Acquity Q-Da mass detector. Full scan and single reaction monitoring (SIR) mode were explored for the semi-quantitative experiments with full scan mode yielding better results. Details on performance specifications of Acquity Q-Da are available elsewhere.[186] DART was run in +ve ionization mode, over a 50-500 m/z range. The source temperature was maintained at 350 °C while the linear rail was operated at a speed of 0.2 mm s^{-1}. MassLynx software was used to monitor the runs in real time and perform the data analysis.

2.4.3 Results/Discussion

The ability to perform on-site testing of suspects would allow law enforcement to exercise immediate administrative and precautionary measures, including driving suspension, thereby reducing the chance of an accident occurring.[187] OF is a good alternative matrix choice, its collection is non-invasive and the matrix has little potential for adulteration.[188] Certain weakly basic and smoked drugs might even have a larger detection window in OF.[188] However, OF collection might yield small volumes due to reduced salivary flow after use of certain drugs (amphetamines and/or cannabis).[187] In this case, SPME-TM would be an ideal tool for OF analysis due to its ability to work with small volume samples. Although previous DART-MS-SPME-TM publications of the Pawliszyn group have demonstrated good quantitative results,[26,117] it is important to point out that those were obtained on benchtop instruments, which are analytically superior with regards to sensitivity and specificity. Hence, results presented herein can be deemed as semi-quantitative, as the technology still requires further investigations of its ability to provide accurate analytical responses on-site. In the preliminary experiments, a high background noise was noticed in the spectra using SIR mode. The noise level in the SIR mode was overlaying the signal from the actual analytes at low to mid-concentrations and yielding higher LOD values. Full scan mode proved to be more useful, as lower LODs were achieved using this approach. The full spectrum of an OF sample spiked with 500 µg L^{-1} of methamphetamine, morphine, codeine, cocaine, methadone, oxycodone, and heroin can be seen in Figure 2.34. It was also important to maintain adequate spiking concentrations, since detector saturation started occurring for certain analytes at higher concentration points. For example, methamphetamine started saturating the detector at 500 µg L^{-1} (see Figure 2.35A.). As can be seen, the inclusion of a 1000 µg L^{-1} point for methamphetamine calibration led to detector saturation and, consequently, to cumbersome calibration at higher concentration levels. Hence, the 1000 µg L^{-1} calibration point was excluded from the plot (Figure 2.35A.i). In addition, one may note a progressive
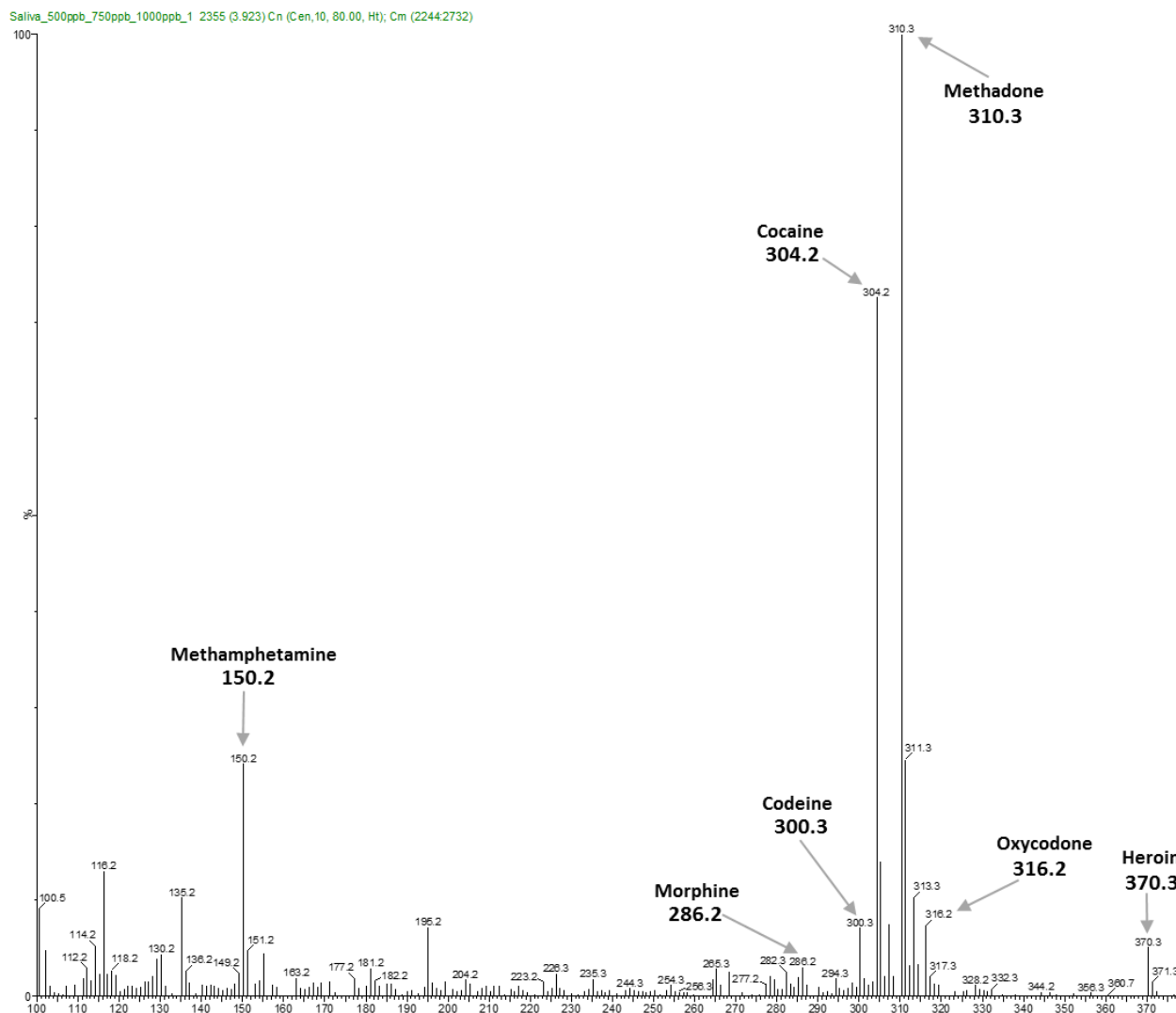
Figure 2.34 *Mass spectrum profile obtained on a Waters-QDa after 1 min extraction from OF sample spiked with DoAs at 500 µg L^{-1}. The gray arrows represent the analytes of interest.*

drop in the IS response as the target analyte concentration increases (Figure 2.35A.ii). In other words, if the concentration of the spiked standard is too high, the signal area of the IS drops significantly and nearly equates to the ambient air signal. At that point, data correction would no longer be feasible. This demonstrates that the selection of the IS concentration must be carefully evaluated, as certain analyte correction might require higher IS concentrations. Similar pattern is also observed in case of codeine (Fig. 2.35B.), whereby saturation appears to occur at 800 µg L^{-1}. Hence, the LDR was maintained in the 50-500 µg L^{-1} range (Figure 2.35B.i). Examination of codeine-d3 area at 500, 750, and 1000 µg L^{-1} reveals a higher signal (7.5e5, 1.1e6 and 8.6e5, respectively) in comparison to the area obtained for

concentrations spiked for lower levels (50, 75, and 250 µg L^{-1} at 5.6e5, 6.3e5, and 7.7e5, respectively (Figure 2.35B.ii)). Ideally, the IS area should be dropping at higher concentration points and not vice-versa. The calibration plots for the remainder of the drugs can be seen in Figure 2.35C-G. The results are summarized in Table 2.7, which also showcases the analytes' logP values, LOD, LOQ, accuracy, and precision at 100 µg L^{-1}. In fact, the LODs obtained for the analytes were lower than the cut-off levels
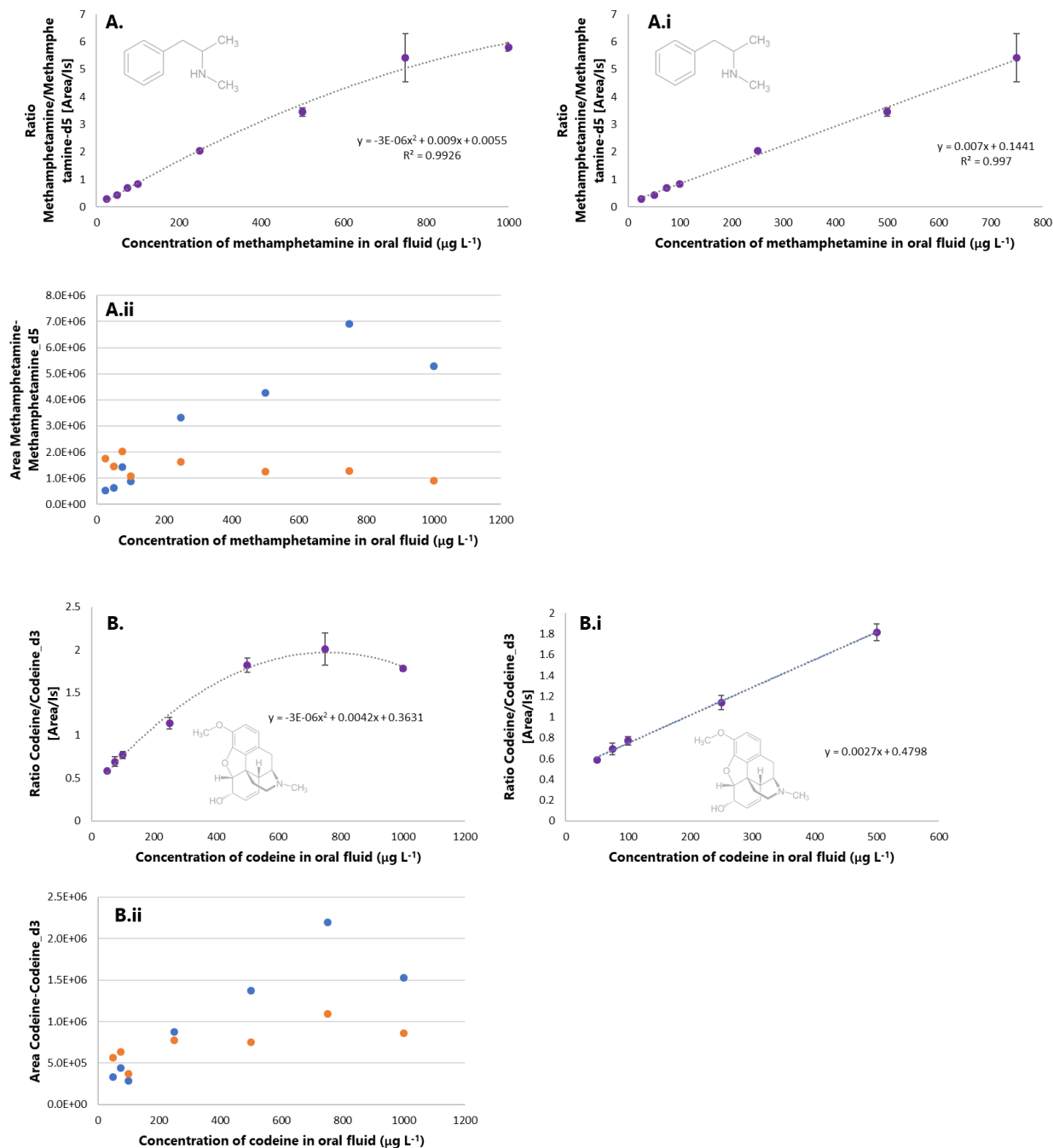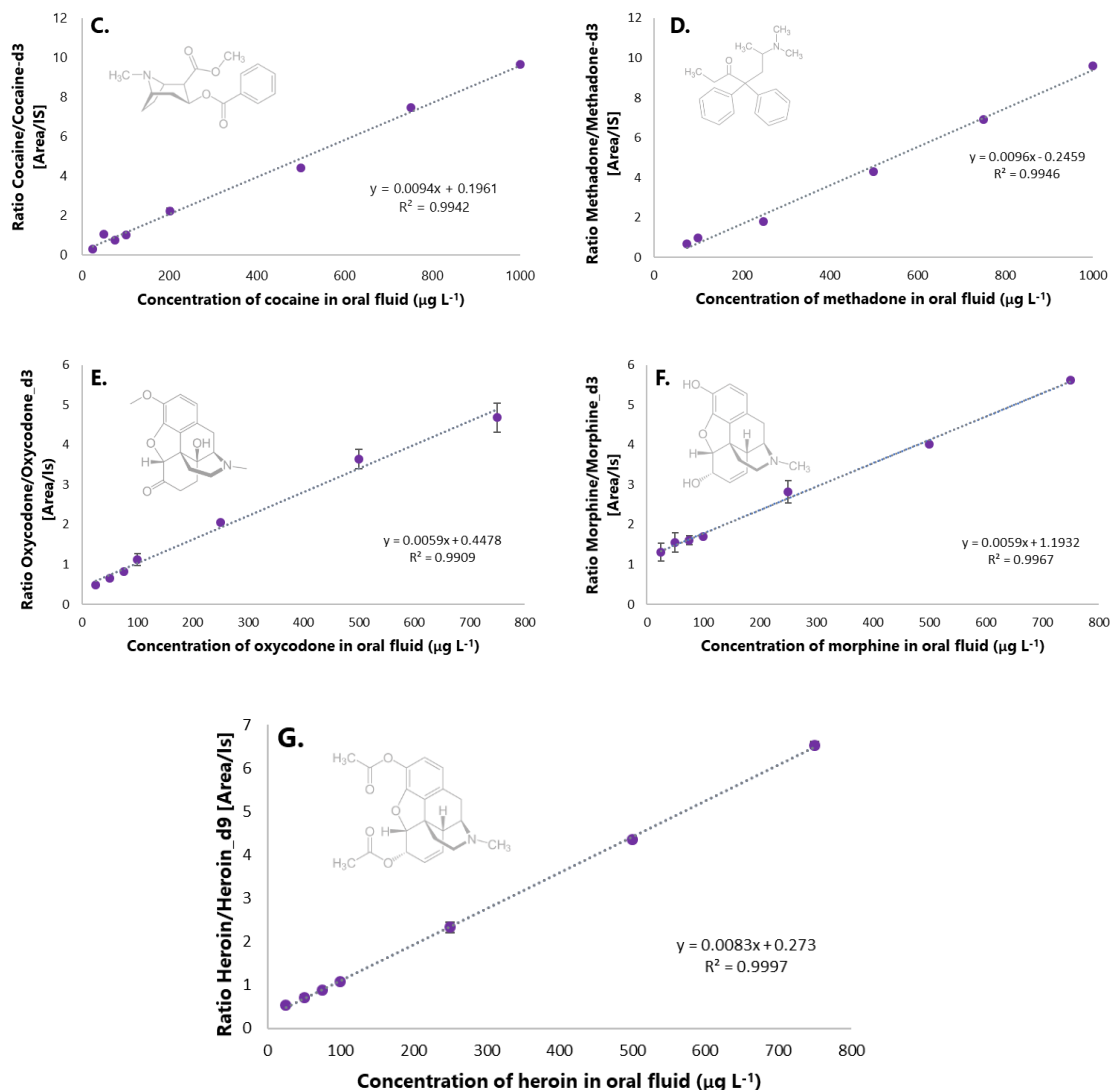
Figure 2.35 *Calibration plots and signal areas of methamphetamine and codeine in OF in **A**., and **B**., respectively. Calibration plots of cocaine, methadone, oxycodone, morphine, and heroin are shown in **C**., **D**., **E**., **F**., and **G**., respectively.*

used by the Substance Abuse and Mental Health Services Administration (SAMHSA)[189] as seen from

Table 2.7. In addition, the LODs obtained can be compared to cut-off levels used the by the Driving

under the Influence of Drugs, Alcohols and Medicines (DRUID)[190] project (Table 2.7). The cut-off levels

imposed by the DRUID project have been met in this study, with some of the LODs being below what

is required (morphine, codeine, cocaine, methamphetamine) by the regulatory agencies. The observed

accuracy (83-119 %) and precision (<13 %) for the tested validation point (100 µg L^{-1}) was good, which

demonstrates this approach's potential for on-site use. Certainly, modifications to the workflow of SPME

(i.e., greater extraction times and different coating chemistries) could be used towards improving the S/N

ratios. However, the hardware components of Q-Da contribute the most in this case. As stated in the beginning of this section, Waters Q-Da is a single quadrupole MS analyzer. Its detection limits could be improved by using noise filtering components, i.e., MS/MS. For example, Wright et al. developed a miniaturized portable QqQ MS system, which yielded a 10 µg L^{-1} LOD for detection of thiabendazole in apple homogenate.[191] It is fair to say that analysis of complex matrices via portable MS has not yet been fully explored due to technical difficulties. Maintaining reproducible responses and simple instrumentation at the same time is challenging.[192] Regardless, this study represents the first application of SPME-TM for on-site detection of DoAs in OF samples using a portable MS, and the promising results demonstrated this approach's potential in roadside drug testing and crime scene investigations contexts where obtaining rapid and reliable information is of crucial importance.

Table 2.7 *Figures of merit for the semi-quantitation of several DoAs spiked to OF by using SPME-TM coupled to a portable MS (Waters-QDa) via DART.*

Compound	logP[*]	IS	Cut-off [µg L^{-1}]	LOD [µg L^{-1}]	LOQ [µg L^{-1}]	QC point [100 µg L^{-1}]	
						Accuracy (%)	Precision (RSD, %)
Morphine	0.90	Morphine-d6	2000[**], 95[***]	25	75	83	2.7
Oxycodone	1.04	Oxycodone-d3	-	25	50	117	13
Codeine	1.20	Codeine-d3	2000[**], 94[***]	25	50	112	5.5
Heroin	1.54	Heroin-d9	-	10	25	97	1.9
Cocaine	1.97	Cocaine-d3	170[***]	10	25	101	5.2
Methamphetamine	2.23	Methampethamine-d5	250[**], 410[***]	10	25	99	8.4
Methadone	4.14	Methadone-d3	22[***]	25	50	119	4.4
[*]*Data source: https://www.drugbank.ca*							
[**]*SAMHSA. Analytes and their cut-offs.*[189]							
[***] *Schulze, H.; Schumacher, M.; Urmeew, R.; Auerbach, K. Final Report: Work performed, main results and recommendations.*[190]							

2.4.4 Conclusion for Section 2.4

In this research, the first reported application of SPME-TM for coupling to a portable single quadrupole MS system DART-QDa for detection and semi-quantitative analysis of drugs in OF is presented. Satisfactory figures of merit were obtained for seven different drugs used in the study. Accuracy and

precision were very good for the tested validation point. Further improvements could be made to some aspects of sample preparation involved in SPME-TM, but use of a portable MS with MS/MS abilities would make the biggest contribution.

2.5 DART and SPME-TM: A Suitable Platform for Analysis of Prohibited Substances in Small Volumes

2.5.1 Introduction

Interest in small-volume analysis has largely increased due to advancements in personalized medicine, which includes disease diagnostics and therapeutic drug monitoring (TDM).[153,193] TDM is used to develop optimal therapy programs for patients based on individual phenotypes.[153] Unfortunately, this form of therapy requires blood to be withdrawn from the patient each day, which can become physically and mentally taxing over extended periods of time. The development of novel drugs would also benefit from new approaches that require lower sample volumes. For example, many clinical trials and pharmacokinetic studies are performed using blood, which requires large volumes of blood and/or plasma to be collected from small animals.[118] With animal welfare becoming a more prominent concern, attention is shifting to a focus on developing methods that reduce the need for animal subjects.[194]

Immunoassays and chromatography are two analytical approaches that have previously been used for small-volume processing.[195] However, both of these methods require relatively large amounts of time and materials in addition to being expensive and unsuitable for analysing a large number of samples. In contrast, stand-alone MS is capable of providing good results at trace levels in a matter of minutes, even for complex matrices.[153] Furthermore, one stand-alone MS format, known as AIMS,[84] may offer a fool-proof method for small-volume analysis. As the name suggests, AIMS approaches ionize/desorb samples in open/ambient air.[84] Moreover, AIMS techniques are able to rapidly analyse numerous samples in addition to offering unique methods for introducing/processing small-volume samples. Although a partial understanding of AIMS may lead one to believe that it does not involve sample preparation, this assumption would be erroneous as the scientific community has been expending considerable effort to developing/improving sample preparation strategies for AIMS.[162] Many AIMS strategies have been used for small-volume analysis, but one of the more commonly used approaches is the coupling of dried blood

spots (DBS) with DESI or paper spray (PS).[120,196,197] Notably, plasma[198] and OF[199] have also been analysed using a paper-drying approach. DBS coupled to PS (DBS-PS) is an enticing, low-cost approach that features a simplified operation protocol. Small biofluidic volumes are spotted onto a paper matrix, where they are dried and then analysed via spray desorption, which is induced through the addition of a strong solvent and the application of a high voltage (HV).[196] Although DBS-PS lacks a sample clean-up step (which could be accomplished by incorporating an extra SPE step),[200] it nevertheless provides satisfactory quantitative performance.[201] Despite its advantages, DBS-PS is hampered by some minor workflow-related inconveniences. For example, paper drying, accurate biofluid spotting, and the manual deposition of strong solvent are inconvenient and/or harmful to the environment.[201,202] Other suitable AIMS approaches for small-volume analysis include microfluidic interfaces,[203–205] nESI,[206] coated-blade spray (CBS),[27] thermal desorption ESI,[207] and DART.[87] Selecting the best approach to use in a clinical/drug-development setting will necessarily depend on difficulty level with respect to the approach. In general, techniques featuring easy operation and minimal technical elements are highly desirable in such settings. In this respect, DART has been a pioneering technology as it features a user-friendly interface and is simple to operate. DART is a thermal-desorption technique that does not require the use of solvents, has great potential for high-throughput (HT) analysis, and maintains adequate levels of repeatability by normalizing sample introduction.[87,115] In DART, normalization can be achieved using a TM format,[115] wherein the introduction of the sample into the MS is controlled by depositing it onto meshes with precisely controlled geometries.[115]

Unsurprisingly, DART has been coupled to DBS to screen for phenylketonuria in newborns using Dip-its® (glass-tips).[208] Although satisfactory results were obtained, an LOQ of 3 µmol L^{-1} was reported for phenylalanine. In addition, concerns related to reproducibility were raised.[208] This approach also required the samples to be pre-treated prior to analysing the Dip-its®. In a slightly different approach, blood spots were deposited on a glass slide, dried, and desorbed in front of a DART source.[209] An LOQ of 10 ng mL^{-1}

for verapamil in blood and plasma was obtained, and a significant reduction in signal response was achieved by desorbing blood directly from paper.[209]

Coupling DART to SPME can make it a suitable option for small-volume analysis. Over the last few years, the Pawliszyn group has pioneered the use of biocompatible SPME devices coated with PAN. PAN is a polymeric material with properties that minimize the attachment of interfering biologicals to the device's surface,[19,44,48,49,63,210] and that allow it to conveniently act as a biocompatible glue for a range of extracting phases/particles for the SPME substrate.[50] These properties enable analyses of very complex samples like blood and plasma that yield trace-level detection limits, while also offering reduced device fouling.[19,206] Gómez-Rios et al. incorporated these properties into the design of SPME-TM meshes for DART-MS that fully maximized the advantages offered by SPME's preconcentration step and DART's desorbing/ionizing power.[26] Since developing these meshes, a number of reports detailing novel applications and further design configurations for this technology were published.[117,134,136] However, there have been no reports for using SPME-TM for small volume analysis.[159] This section documents the first reported use of SPME-TM HLB extractive particles for quantifying DoAs in small volume OF and human blood samples. Droplet extraction was performed in open-air conditions, and the experiment was carefully optimized with regards to extraction time. Satisfactory figures of merit were obtained for the examined analytes, and QC points were implemented to inspect the validity of calibration curves. In addition, OF from two male volunteers was examined for nicotine levels, thus showing SPME-TM's usefulness for detecting substances following recent smoke inhalation/exposure. Percent recovery was also examined to investigate whether exhaustive extraction was achieved using this approach. The evidence presented herein—particularly the rapidity with which the low detection limits were obtained—suggests that DART may have good applicability for small-volume analysis.

2.5.2 Experimental

Chemicals/Materials

The following standards and their isotopic analogues were ordered from Cerilliant at concentrations of 1000 mg L^{-1} and 100 mg L^{-1}, respectively: nicotine, benzoylecgonine, cocaethylene, EDDP, cocaine, LSD, methamphetamine, methadone, morphine, heroin, oxycodone, codeine, fentanyl, nicotine-d4, benzoylecgonine-d3, cocaethylene-d3, EDDP-d3, cocaine-d3, LSD-d3, methamphetamine-d5, methadone-d3, morphine-d3, heroin-d9, oxycodone-d3, codeine-d3, and fentanyl-d5. Human blood (stabilized with K2-EDTA) was ordered from BioreclammationIVT (Westbury, NY, USA). OF was obtained from 10 healthy volunteers (5 male and 5 female) through non-stimulated (chemical free) expectoration into 10 mL glass vials. A pooled batch was then made by combining 5 mLs of OF from each volunteer. The blood and OF samples were kept refrigerated at $^{\circ}$4 C until use (no more than 7 days). SS meshes were obtained from IonSense, Inc. and HLB particles (5 µm) were obtained from Waters. LC/MS-grade solvents (H$_2$O, MeOH, ACN, IPA) were obtained from Fisher Scientific. Finally, PAN, DMF, and HCl were obtained from MilliporeSigma.

Mesh manufacturing protocol

Meshes were made using a procedure that was already publishedand Section 2.2.2 provides greater details of the protocol.[26] Microscopic images of the mesh were taken with an Olympus microscope (SZX10) with a SC30 digital camera, while SEM images were taken with a Zeiss FESEM 1530.

Extraction procedure

A stock mixture of all analytes was made to 100 mg L^{-1}, with a corresponding IS stock mixture being made to 10 mg L^{-1}. The stock mixture was then diluted to create OF spiking points (0.5, 1, 2.5, 5, 10, 25, 50, 75, and 100 ng mL^{-1}) and blood spiking points (0.5, 2.5, 5, 12.5, 25, 75, 150, and 325 ng mL^{-1}). QC points of 3, 30, and 90 ng mL^{-1} were used for OF, while points of 37.5 and 250 ng mL^{-1} were used for

blood. The matrices were spiked with the appropriate concentrations of the stock standards and left to equilibrate for 2~4 h. Spiking was conducted using a method designed to keep organic content below 1%, so as to not disturb the drug and matrix binding equilibria.[7] IS was spiked at 25 and 50 ng mL^{-1} for OF and blood, respectively. To perform the droplet extractions, the meshes were removed from the preconditioning solution, washed with H_2O, blotted with a KimWipe, and placed horizontally into an immobilization device. Fifteen µLs of OF and 25 µL of blood were then carefully deposited onto the horizontally imbedded mesh using a small pipette (10-100 µL). The calibration plots were built using a matrix-matched approach with IS correction, and the LODs and LOQs were determined based on S/N ratios of 3 and 10, respectively. Noise was determined using blank extractions of the matrices. Extraction times were done at 5, 10, 15, and 20 min for OF, and 5, 7, 9, 11, and 13 min for blood. Following extraction, the mesh containing OF was washed with LC/MS-grade H_2O using a 10 s vortex-assisted wash (3200 rpm); the meshes containing blood droplets were washed for 15 s on a vortex (3200 rpms), which was followed by an additional 5-10 s wash under a pressurized stream of LC/MS-grade H_2O. The meshes were then dried and placed in a custom-made DART holder for desorption/analysis. A schematic of this process is represented in Figure 2.36. To examine percent recovery, 25 µL of PBS, OF and blood spiked with 25 ng mL^{-1} of model analytes were placed onto an HLB mesh and the extraction was carried out for 10 minutes. Following a wash, the meshes were desorbed to 300 µL of ACN/MeOH/FA (80/20/0.1) for LC-MS/MS analysis.[211] All extractions were done in triplicates (n = 3). SEM images of
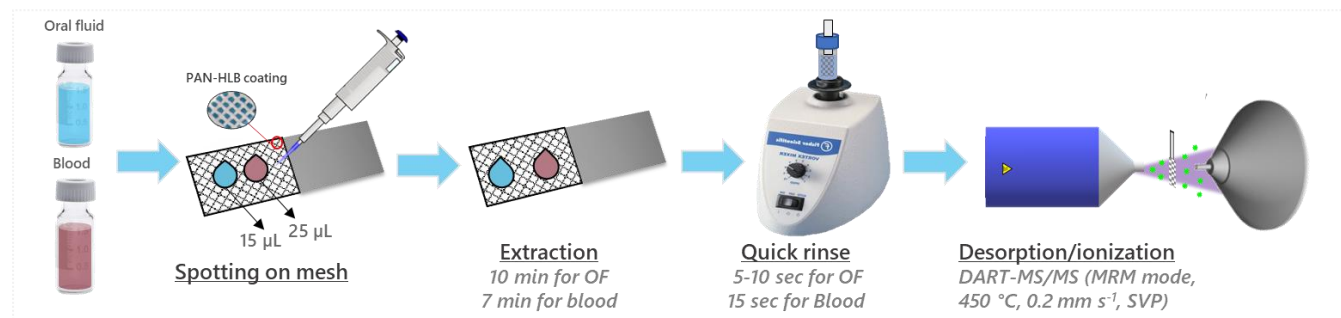
Figure 2.36 *Schematic representation of droplet extraction for OF and blood via SPME-TM coupled to DART-MS/MS.*

the mesh were taken following blood-droplet extraction and DART desorption in order to assess red blood cell (RBC) attachment to the mesh's surface.

Instrumentation

DART-MS/MS experiments were performed using a QqQ MS system (TSQ Vantage) from Thermo Scientific, while a DART-SVP® source and a Vapur® interface was obtained from IonSense, Inc. and coupled to the MS to perform MRM acquisitions. The Vapur® interface was coupled to a membrane pump (blue, position 6) in order to maintain the integrity of the MS vacuum. DART runs were conducted using a source temperature of 450 °C and a rail speed of 0.2 mm s^{-1}. He gas was used during acquisition, and N_2 was used during standby. Details on the TSQ Vantage specifics of the standards used can be accessed in Section 2.2.2, while Table 2.8 offers details on the specifics of benzoylecgonine and respective ISs. LC-MS/MS runs were also done on a TSQ Vantage, which consisted of an Accela autosampler and pump. Chromatographic run details were obtained elsewhere (Reyes-Garcés et al.),[211] and Table 2.9-2.10 provides a summary of conditions used.

Table 2.8 *TSQ-Vantage specifics of benzoylecgonine and IS(s).*

Analyte	Precursor m/z	Product m/z	S-lens	Collision energy (CE)
Benzoylecgonine	290.1	168.1	11	18
Benzoylecgonine-d3	293.1	171.1	98	18
Methadone-d3	313.1	268.1	93	13
Morphine-d3	289.5	152.2	125	58
Heroin-d9	379.2	272.1	171	46
Oxycodone-d3	319.1	244.1	117	28
Codeine-d3	303.1	152	125	68
LSD-d3	327	226	116	23
Fentanyl-d5	342	188	124	22
Nicotine-d4	167.1	121.1	71	28
Cocaethylene-d3	321.1	198.7	120	20
EDDP-d3	281.1	233.9	140	31

Table 2.9 *Chromatographic and ESI conditions used for the LC-MS/MS evaluation of mesh reproducibility and reusability.*[211]

Column	Phenomenex: Pentafluorophenyl [PFP] (1.7µm, 2.1 mm x 10 mm)
Mobile phase	A: H_2O + 0.1 % FA B: ACN + 0.1 % FA C: MeOH + 0.1 % FA
Flow rate	400 µL/min
Column temperature	35 °C
Injection volume	10 µL
Injection mode	Full loop
Spray voltage	1300 V
Vaporizer temperature	275 °C
Sheath gas	45 units
Auxiliary gas	30 units
Capillary temperature	280 °C

Table 2.10 *Summary of the ternary gradient used for the LC portion of the method.*[211]

	Mobile phase		
Time	A	B	C
0- 0.51 min	90 %	5 %	5 %
0.51- 9.50 min	0 %	50 %	50 %
9.51- 15.0 min	0 %	37.5 %	62.5 %
15.1- 17.3 min	90 %	5 %	5 %

2.5.3   Results/Discussion

Spot sampling using the mesh: OF analysis

Over the last few years, OF has become more common for use in work-place and road-side drug testing, as well as in toxicology, pain management, and epidemiological research.[212] OF's main advantage is that it is easy to collect, which reduces both invasiveness and the potential for sample adulteration.[212] Although OF is easier to obtain than blood, it is not readily available in large quantities (especially when individuals have difficulties expectorating), which makes it a suitable matrix for small volume analysis.

The main experimental concern during the initial stages of this study was whether the droplet would be sufficiently sustained on the mesh surface; that is, would the surface tension of the mesh prevent the droplet from leaking through the mesh holes? This concern proved to be unnecessary, as the initial experiments demonstrated that the mesh was capable of sustaining the droplet. Next, an adequate extraction time for selected analytes in OF was determined using 5, 10, 15 and 20 min points; time points past 20 mins were not considered due to the potential of OF drying on the mesh surface. The extraction time profile for 15 µL of OF spiked with 1 ng mL^{-1} of codeine, heroin, and oxycodone can be seen in Figure 2.37, which shows a gradual increase in signal as extraction time increases (see also Table 2.11 for S/N ratios of examined analytes). Although higher responses were obtained at 15 and 20 min, 10 min was deemed adequate to achieve acceptable sensitivity and was used for the remainder of the experiments. With an adequate extraction time having been established, quantitation experiments were
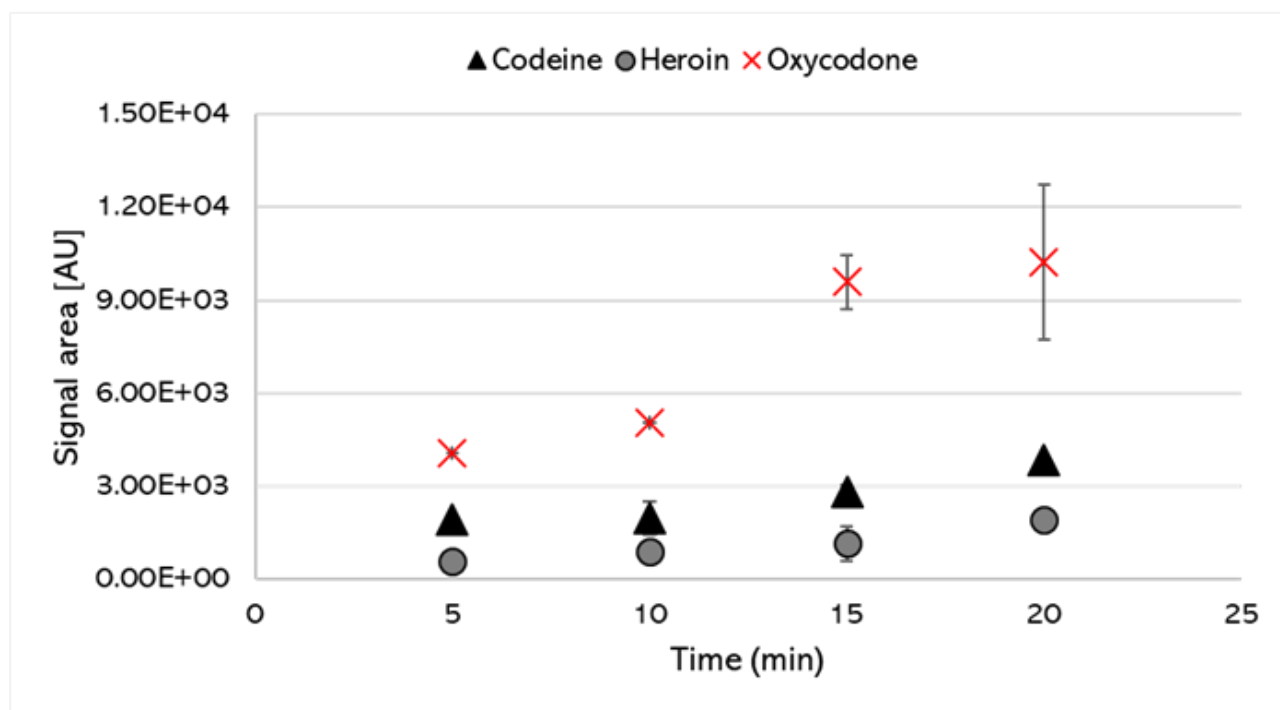
Figure 2.37 *Extraction time plots for selected analytes spiked to 15 µL of OF at a concentration of 1 ng mL^{-1} and analysed via DART-MS/MS (source temperature of 450 °C and rail speed of 0.2 mm s^{-1}).*

Table 2.11 *S/N ratios obtained for the time points examined in Figure 2.37.*

Extraction time (min)	S/N Ratios		
	Codeine	Heroin	Oxycodone
5	3.7	13.4	18.1
10	3.8	19.7	22.4
15	5.4	25.4	42.6
20	7.3	41.8	45.5

then conducted by carefully placing the droplet onto the middle section of the mesh (to maintain spotting position). The results of the quantitation experiments are presented in Table 2.12. The LDR was maintained in the 0.5-100 ng mL^{-1} range, while the LODs and LOQs ranged from 0.1-1 ng mL^{-1} and 0.5-5 ng mL^{-1}, respectively. The lower detection limits obtained for such a small volume (15 µL) are primarily the result of two factors: sensitive DART desorption and SPME's preconcentration ability, which is enhanced by the use of HLB particles. HLB is a very wettable material, which allows it to interact favourably with polar matrices. OF is mostly composed of H_2O (99%),[213] with a contact angle (estimated ~70-90°) initially being present when it is placed onto an HLB-coated mesh. As the extraction time increases, the contact angle progressively drops until it is nearly 0° by the end of the extraction process. A similar occurrence has also been noted by Reyes-Garcés for pure H_2O samples.[19] Additionally, the droplet interacts with the mesh's large SA, thereby enabling greater extraction and contributing to lower detection limits. Higher LOQs were obtained for methamphetamine, methadone, morphine, codeine, LSD (5 ng mL^{-1}), and nicotine (10 ng mL^{-1}) and were compared to the cut-off levels outlined by the DRUID project of the European Commission.[190] The concentrations of the analytes listed in Table 2.12 are all below the cut-off levels proposed by DRUID.[190] For example, LOQs of 1 and 0.5 ng mL^{-1} were achieved for codeine and methadone, respectively, which are both well below the recommended

cut-off levels[190] (94 and 22 ng mL^{-1}, Figure 2.38A-B.). The examined QC levels can be observed in Table 2.12, with accuracies ranging from 80.6-126.9%. The accuracy of 126.9% was obtained for oxycodone at 3 ng mL^{-1}. This result indicates the presence of potentially co-extracted salivary constituents, which can lead to ionization enhancement. The process's repeatability was found to be acceptable, with an % RSD range of 0.1-17.8%. In order to demonstrate the approach's effectiveness in real-life applications, we used it to screen for nicotine in OF acquired from two male volunteers, one smoker and one non-smoker. Five minutes after smoking a cigarette, each volunteer provided us with a 100 µL OF sample (via expectoration). Fifteen µLs of the sample were then placed onto the mesh and extraction

Table 2.12 *Figures of merit obtained for quantitative analysis of 15 µL of OF on SPME-TM mesh and DART-MS/MS.*

Analyte	LOD (ng mL^{-1})	LOQ (ng mL^{-1})	R^2	LDR (ng mL^{-1})	Calibration plot equation y = mx+b	Accuracy (%), RSD (n=3) Levels			Cut-off (DRUID)[190]
						3 ng mL^{-1}	30 ng mL^{-1}	90 ng mL^{-1}	
Cocaine	0.1	0.5	0.9978	0.5-100	y=0.1614x+0.1881	90.7 (9)	93.7 (13.9)	97.5 (6.4)	170
Methamphetamine	1.0	5.0	0.9989	5-100	y=0.2776x+0.2182	-	91 (2.9)	89.6 (3.9)	410
Methadone	0.5	5.0	0.9989	5-100	y=0.1017x+0.1072	-	88.6(4.9)	95.1 (0.1)	22
Morphine	0.5	5.0	0.9982	5-100	y=0.2944x+0.5293	-	91.7(6)	102.4(1.8)	95
Heroin	0.5	1.0	0.9969	1-100	y=0.2216x-0.0564	90.4(17.8)	88.6(7.8)	99.4(3.1)	-
Oxycodone	0.1	0.5	0.9994	0.5-100	y=0.2201x+0.4048	126.9(5.5)	114.8(11.8)	112.9(3.4)	-
Codeine	1.0	5.0	0.9973	5-100	y=0.0775x-0.0004	-	87(1.3)	96.9(3.8)	94
LSD	0.5	5.0	0.9915	5-100	y=0.105x+0.1222	-	92.2 (5.5)	94.8 (2)	-
Benzoylecgonine	0.1	0.5	0.9929	0.5-100	y=0.0849x+0.0227	89.4(6.22)	109.6 (6)	93.2(2.7)	95
Fentanyl	0.1	0.5	0.9934	0.5-100	y=0.2292x-0.3538	92.3 (7.6)	80.6 (9)	91.6 (9)	-
Nicotine	5.0	10.0	0.9912	10-100	y=0.0448x+0.1160	-	92.4 (3.9)	112.6 (1.3)	-

was performed for 10 mins. The obtained ion chronogram, which can be seen in Figure 2.39, shows desorption from a blank mesh (n = 2), desorption for the smoker's OF (n = 2), and desorption for the non-smoker's OF (n = 2). Predictably, a nicotine signal (163 → 130.1) was not observed for the blank

mesh and the non-smoker, while a very high signal was observed for the smoker. With the introduction of the Cannabis Act in Canada in October 2018,[5] an increase in incidents related to driving under the influence of marijuana can be expected. As such, members of the law enforcement community could benefit from the availability of simple-to-use samplers, like SPME meshes, that can be coupled to portable MS instruments, like DART-QDa, as they offer a convenient way of detecting recent drug exposure/consumption QDa, as they offer a convenient way of detecting recent drug exposure/consumption.[134]
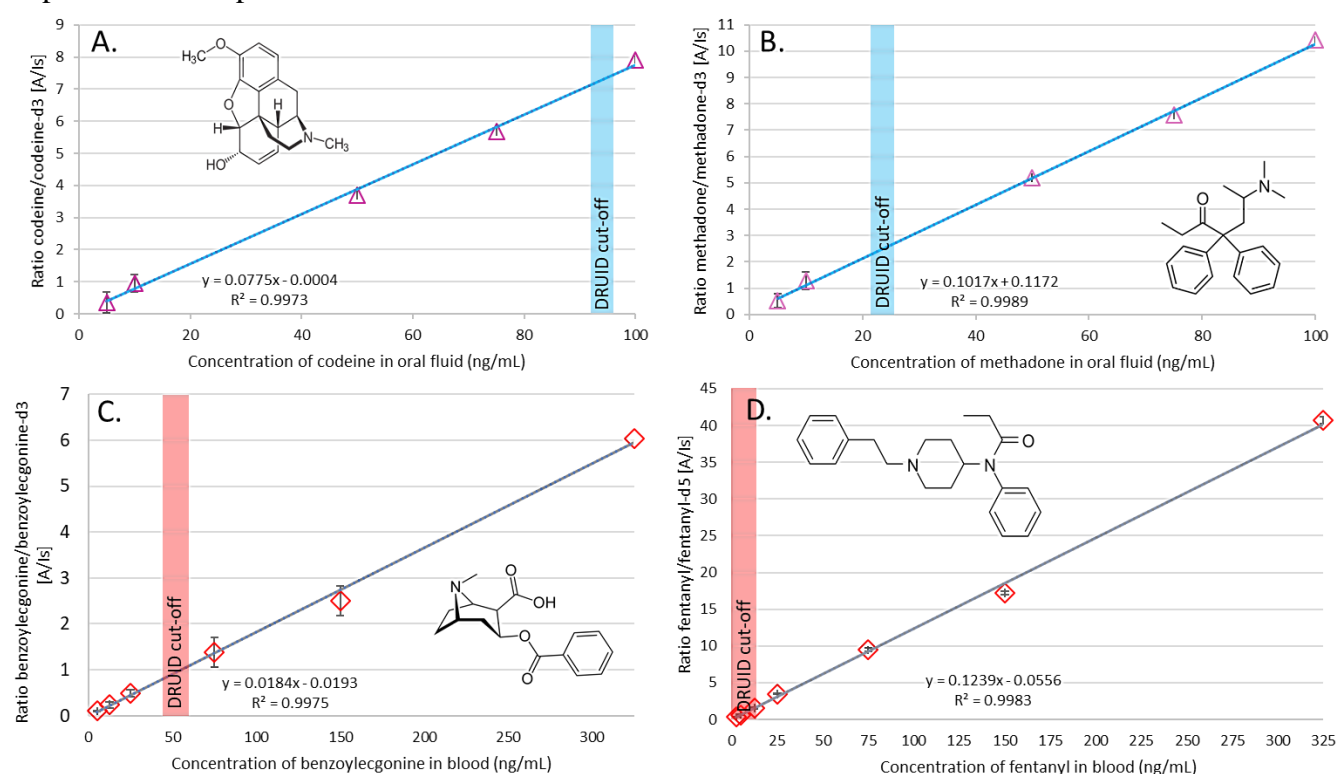
Figure 2.38 Selected examples of calibration plots obtained for the quantitative analysis of DoAs in OF (A. and B.) and blood (C. and D.). The cut-offs for codeine and methadone in OF suggested by DRUID[190] are highlighted in blue (94 and 22 ng mL^-1), while those for benzoylecgonine and fentanyl in blood are highlighted in red (50 and 10 ng mL^-1).

Spot sampling using the mesh: Blood analysis

Many clinical trials are done using blood,[118] but there are difficulties that accompany the use of blood for analytical purposes. For instance, blood is a very complex matrix. It is a colloidal suspension[214] that
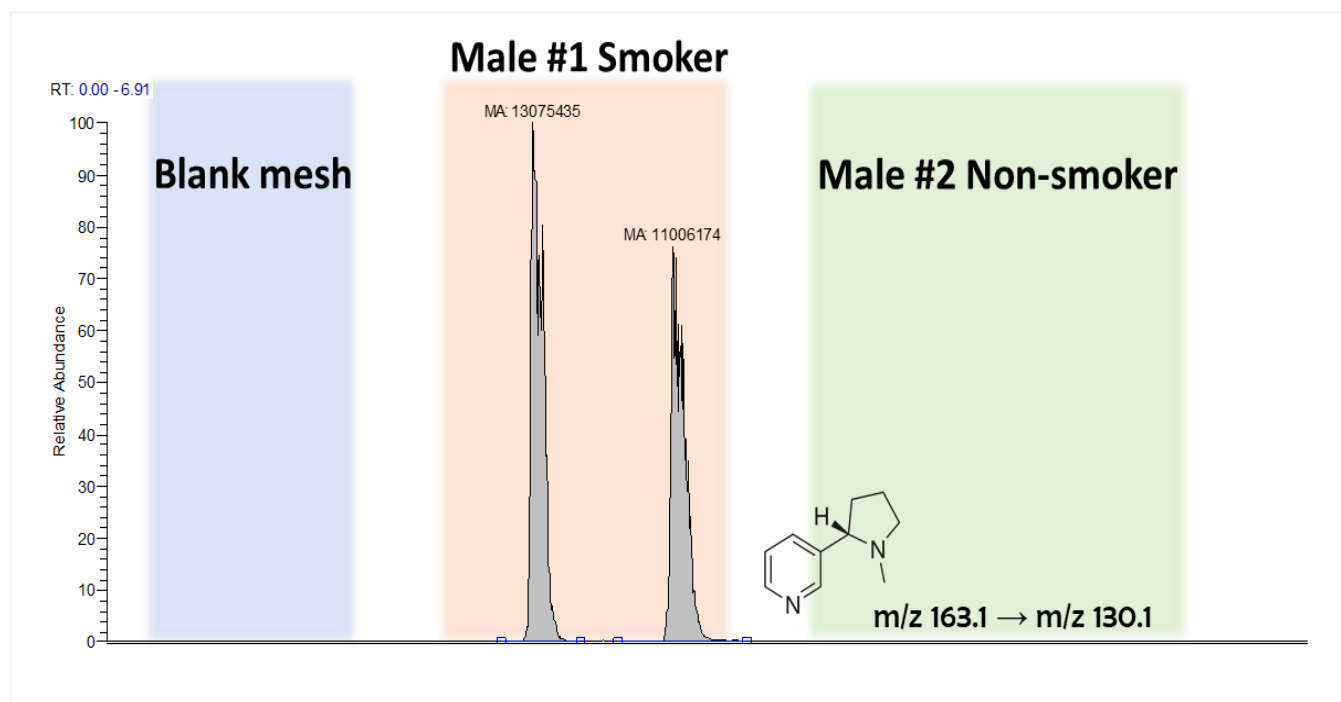
Figure 2.39 *Ion chronogram obtained for measurements of nicotine signal in blank mesh and OF samples from a male smoker and a male non-smoker male (n = 2, for all).*

contains a number of elements: blood plasma, which contains H_2O, proteins, glucose, minerals, hormones, carbon dioxide, and blood cells,[215] which consist of red (RBCs) and white blood cells (WBCs), as well as platelets.[215] Once in open air, blood tends to attach to surfaces, with the adhesion of RBCs and proteins being irreversible in some cases.[216,217] Droplet sampling can also be exacerbated due to blood drying,[216,218] which tends to lead to the appearance of a ring on the edges of a bloodstain within 50 s.[216] While the drying process depends on volume, SA, temperature, humidity, air circulation, and VP, the appearance of the ring (known as the skeletonization effect) is almost immediate[216,218] and can negatively affect the performance of sampling devices.[219] Hence, different strategies have been developed to aid with blood analysis. For example, Zhang et al. used silica-coated chromatography paper (enhances resolving power) in combination with a DBS-PS approach to improve the recovery efficiency for a set of therapeutic drugs in 5 µL of blood.[182] Huang et al. tried heating the DBS before coupling it to PS in order to enhance its detection limits for propranolol.[220] Strategies for blood analysis with SPME have also been documented. For instance, Reyes-Garcés et al. were able to avoid significant RBC attachment

105

or ionization suppression/enhancement by using HLB-PAN and a post-extraction washing protocol in their analysis of a range of compounds in blood.[19] Similarly, Gómez-Rios et al. implemented HLB-PAN CBS devices to analyse small volumes of blood and plasma.[221] To reduce detection limits, small amounts of ACN were added to blood spots,[221] as strong solvents disrupt drug-protein binding equilibria, which in turn enables lower detection limits.[7,221] Zinc sulphate may also be used to reduce detection limits.[222] Since present study is the first examination of blood-spot extraction with SPME-TM and DART-MS, no matrix modifications (other than analyte spiking) were done. During the optimization stage, 15 µL of blood were initially used for the sampling. However, dry "patches" quickly formed on the droplet surface, leading to rapid drying. This issue was ameliorated by increasing the volume to 25 µL of blood. To reduce potential issues during the transmission portion of the experiments (arising from "stuck" blood cells), the meshes were cleaned post-extraction using a two-step wash procedure. Extraction time was evaluated for time points of 5, 7, 9, 11, and 13 min, with the highest signal being obtained for the 7 min time point (results are shown in Figure 2.40). When the droplet is initially placed on the mesh, a high
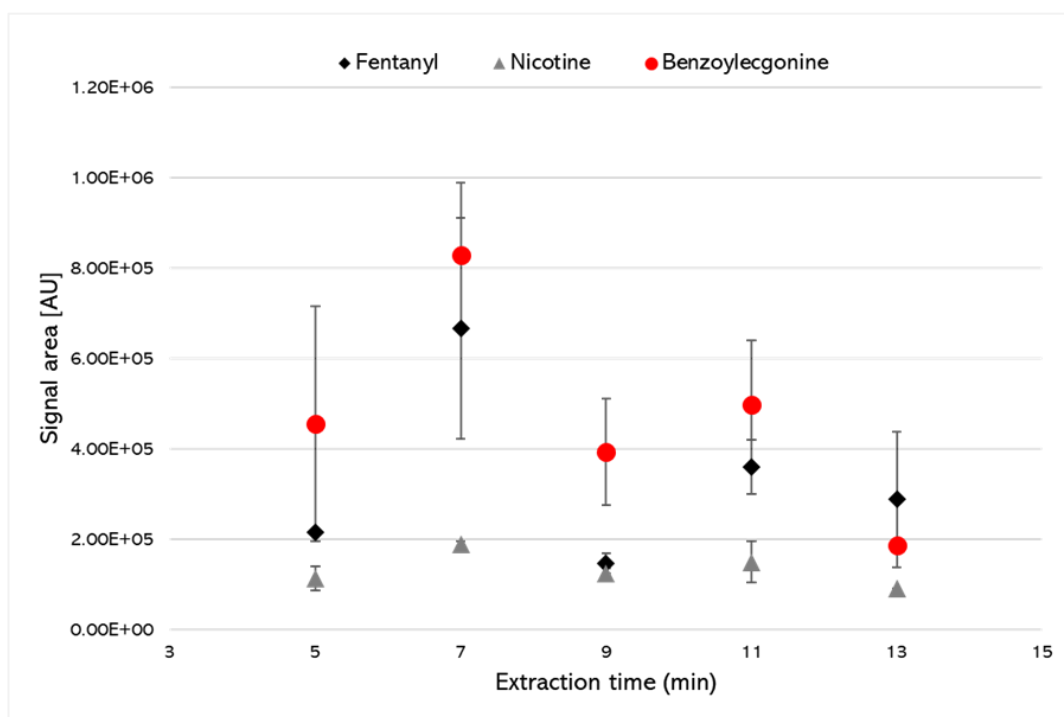
Figure 2.40 *Extraction time plots for selected analytes (25 ng mL^{-1}) spiked to 25 µL of blood and analysed via DART-MS/MS with a source temperature of 450 °C and a rail speed of 0.2 mm s^{-1}.*

contact angle is present (est. >90°) due to HLB's poor interaction with non-polar matrices like blood. Consequently, a skeletonization ring starts to appear past the 7 min mark, with significant skeletonization being observable on the mesh surface after 10 min. At 11 and 13 min, the washing protocol is unable to remove the blood ring (see Figure 2.41 for blood ring observed on dummy mesh). Table 2.13 provides
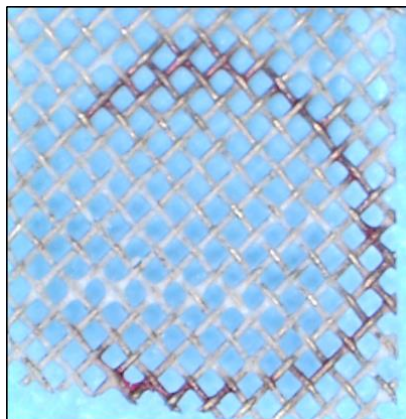
Figure 2.41 *Formation of a "blood ring" or "skeletonization effect" on a dummy-mesh occurring in extractions exceeding ten minutes.*

the S/N ratios obtained for extraction at different time points. Extending the wash time, even with vortex assistance, does not eliminate the dry ring. Conversely, applying an additional layer of PAN to mesh surface may somewhat circumvent unwanted blood attachment, but this would also decrease SPME's extraction kinetics.[19,219] Therefore, no modifications were applied to the mesh; instead, the washing protocol and the extraction time of 7 minutes were tightly controlled, as the presence of unwanted blood constituents on the washed mesh represents a significant problem for DART desorption. Directing the heated gas flow of a DART source onto a mesh with unwanted blood attachment could cause blood "charring", which can contribute to a significant level of ionization suppression and/or enhancement. This issue did not arise during this investigation, as no residual blood attachment was detected in SEM examinations of the mesh surface after blood extraction (Figure 2.42: A. unused mesh; B. used mesh). The results relating to the mesh's quantitative performance are presented in Table 2.14, which shows LODs in the 0.5-5.0 ng mL^{-1} range, and LOQs in the 2.5-25.0 ng mL^{-1} range. These higher detection limits are unsurprising considering that blood is significantly more complex than OF. Extraction

efficiency of analytes from the blood into the HLB polymer was reduced, with the drug-protein binding equilibria that took place in the blood resulting in a reduced amount accumulating on the coating. Examinations of the DRUID project cut-off values for blood analysis[190] are available for 2 out of the 8 analytes that were analysed in this study. The obtained LOQ for benzoylecgonine (5 ng mL^{-1}) was well below DRUID's recommended threshold (50 ng mL^{-1}), but the LOQ for fentanyl (2.5 ng mL^{-1}) fell between DRUID's cut-off (1-3 ng mL^{-1}, see Figure 2.38C-D.), indicating that the technology would require further improvements to be able to quantify lower concentrations. Furthermore, a comparison of oxycodone's LOQ (25 ng mL^{-1}) and the cut-off outlined by the Clinical Reference Laboratory[223] (CLR, 10-100 ng mL^{-1}) reveals no significant reduction in detection limits. Lastly, the results of the QC validation were quite satisfactory for the points examined (37.5 and 250 ng mL^{-1}), with accuracy ranging between 85.1-118.6 % and a repeatability between 1.5-18.5 % RSD. Ultimately, the higher detection limits obtained for blood analysis do not undermine the assay presented herein, but they do highlight the need to continue to develop more efficient and rapid methods for processing complex matrices like blood. The Pawliszyn lab is currently focused on investigating the mechanisms that take place during blood extractions via SPME-TM in order to gain a thorough understanding of the process, which will in turn enable enhancement of the technique.

Table 2.13 *S/N ratios obtained for the time points examined in Figure 2.40.*

Extraction time (min)	S/N Ratios		
	Codeine	Heroin	Oxycodone
5	3.7	13.4	18.1
10	3.8	19.7	22.4
15	5.4	25.4	42.6
20	7.3	41.8	45.5

Table 2.14 *Figures of merit obtained for quantitative analysis of 25 µL of blood on SPME-TM mesh and DART-MS/MS.*

Analyte	LOD (ng mL^{-1})	LOQ (ng mL^{-1})	R^2	LDR (ng mL^{-1})	Calibration plot equation y = mx + b	Accuracy (%), % RSD (n=3) Levels		Cut-off (ng mL^{-1}, DRUID;[190] CLR)[223]
						37.5 ng mL^{-1}	250 ng mL^{-1}	
Nicotine	5.0	12.5	0.9980	12.5-325	y=0.017x+0.0182	96.6 (10.2)	107.7 (2.2)	-
Benzoylecgonine	0.5	5.0	0.9975	5-325	y=0.0184x-0.0193	118.6 (8)	96.7 (2.9)	50[190]
Cocaethylene	5.0	12.5	0.9996	12.5-325	y=0.0222x-0.0262	114 (9.4)	96.9 (3)	-
EDDP	2.5	5.0	0.9934	5-325	y=0.028x-0.0255	116.7 (13.8)	107.6 (3.6)	-
LSD	2.5	25	0.9998	25-325	y=0.0186x+0.0226	95.9 (1.5)	98.8 (4.9)	-
Fentanyl	0.5	2.5	0.9983	2.5-325	y=0.1239x-0.0556	110.2 (6.9)	94 (5)	1-3[190]
Oxycodone	2.5	25	0.9956	25-325	y=0.0144x+0.1550	85.1 (18.5)	95.6 (10)	10-100[223]
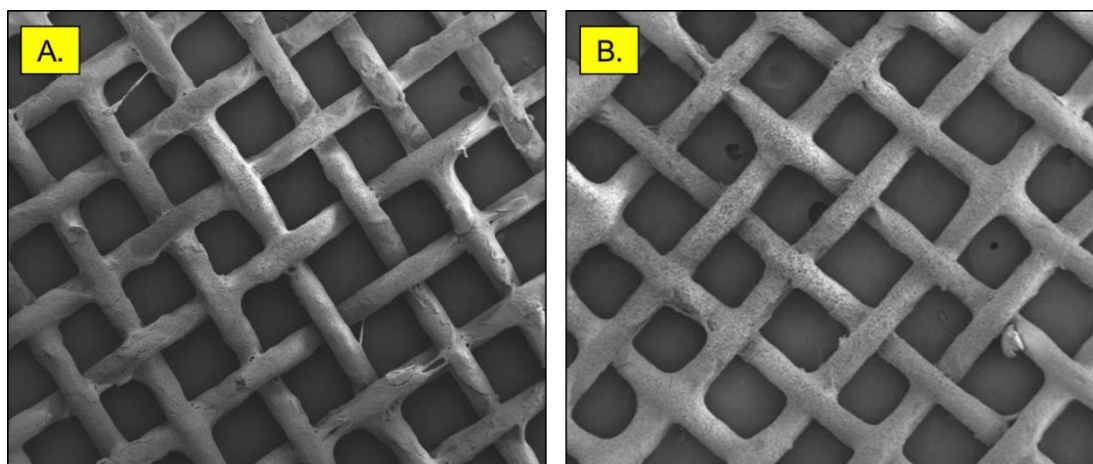
Figure 2.42 A. *SEM image of a never-used HLB-coated mesh;* **B.** *image of a mesh used for a 7-minute blood extraction. Both images depict the mesh after the application of a wash step and DART desorption.*

Extent of recovery

Percent recovery of model compounds was also investigated for potential exhaustive extraction. Percent recovery is defined as ratio of the amount of analyte extracted vs amount of analyte spiked to the sample and can be calculated by building an instrumental calibration curve (which covers expected concentration range) and injecting the samples which contain the portion extracted by SPME. Exhaustive extraction occurs when majority of the analyte is extracted, i.e., probe capacity is high and sample volume/concentration is low, allowing $\geq$ 90 % of the analyte to be extracted.[7] Negligible depletion is

achieved when ≤ 10 % of the analyte is extracted.[7] For this section, recovery was assessed by performing extractions from 25 µLs of PBS, OF, and blood. The results obtained can be seen in Figure 2.43 for all three matrices. Slightly greater recovery of more polar analytes is observed in case of PBS (morphine,
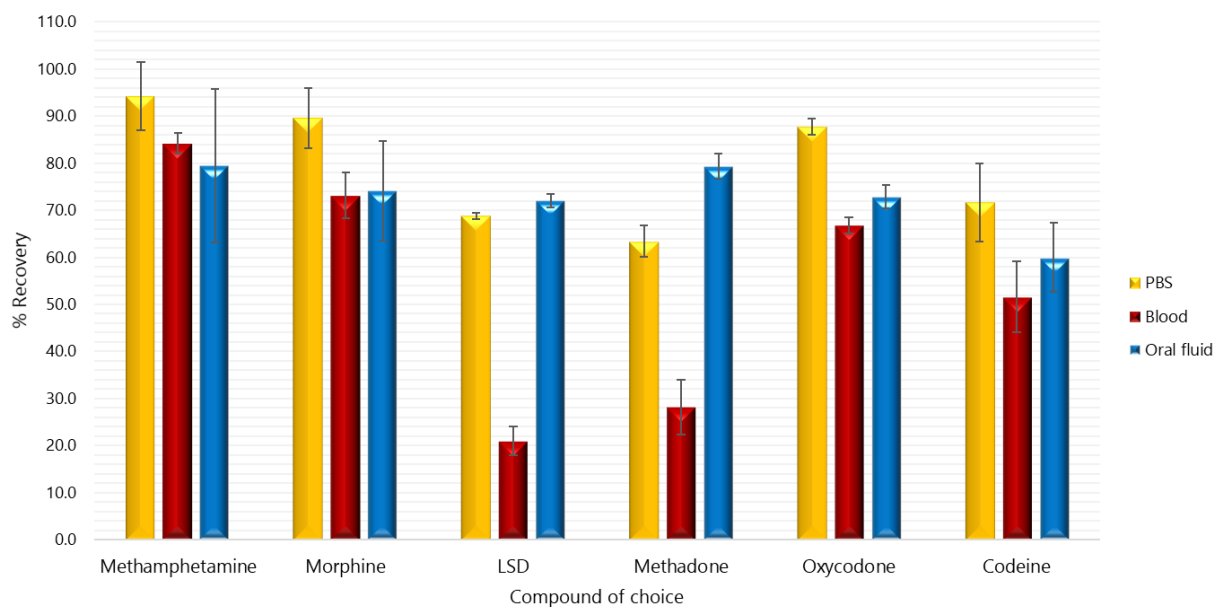
Figure 2.43 *Assessment for % of recovery for a set of model compounds in 15 µL of PBS, blood and OF.*

oxycodone). Codeine, despite its logP of 1.19, shows poorer recovery in comparison to the afore-mentioned polar compounds. Analytes of medium polarity show some variability with regards to recovery for PBS, with methamphetamine being 94.2 %, LSD being 68.8 % and methadone being 63.4%. A slight trend is observed whereby non-polar analytes are extracted less by the HLB coating for PBS. For blood, the lowest recovery is observed for LSD (21%) and highest for methamphetamine (84.2 %). The poorer recovery appears to be related to the increase in logP value of the analytes. In general, recovery of analytes from blood is lower when compared to PBS and OF. In OF, the recoveries for compounds like LSD and methadone are slightly higher (72% and 79.3%, respectively) than those of PBS (69 % and 63.4 %, respectively), which might be caused by MEs, or in other words, co-extracted components with similar MRM transitions of LSD and methadone. Recovery for the remainder of analytes in OF is either comparable or slightly lower than the ones observed for PBS. Ultimately, truly

exhaustive extraction is achieved for methamphetamine in the case of PBS (94.2 %), while the remainder of recoveries for analytes examined in all three matrices ranges between 21.0-89.6 %. Hence, it is safe to say that spot extractions do not fully approach exhaustive extraction, but certainly are not within the negligible extraction regime.

2.5.4 Conclusion for Section 2.5

In this investigation, SPME-TM was applied for analyses of OF and blood droplets via DART-MS/MS, with satisfying figures of merit being obtained for both matrices. Unsurprisingly, the LODs and LOQs were lower for OF because it is a less complex bio-matrix. As a part of a real-life application, nicotine was successfully detected in a 15 µL OF sample obtained from a cigarette smoker. Conversely, the analysis of blood proved to be more challenging, but extraction parameters with regards to extraction time and washing procedure were carefully optimized to ensure reasonable analytical response. As demonstrated in this research, combining DART's excellent sensitivity and high-throughput capabilities with SPME-TM can be an effective tool for small-volume analysis. This report is limited to body fluids, but it is not difficult to imagine use of the SPME/DART technology to screen for pesticide residues in small samples of food products, contaminants in environmental samples in or even impurities in drinking H_2O.

2.6 High-Throughput Quantification of Drugs of Abuse in Biofluids via 96-Solid-Phase Microextraction–Transmission Mode (SPME-TM) and Direct Analysis in Real Time Mass Spectrometry (DART-MS)

2.6.1 Introduction

As mentioned in the introductory chapter, AIMS comprises a group of direct-to-MS techniques that focus on open-air sample processing (desorption/ionization).[84] Within this field, the combination of minimal or no sample preparation, real-time sample processing, and subsequent data acquisition allows analysts to obtain information in a matter of minutes or even seconds.[84] Given AIMS's ability to provide speedy analysis and results, it is anticipated that a demand for such methods will continue to grow in clinical laboratories.[193,224] The development and implementation of high-throughput (HT) methods is perhaps the most efficient approach to managing these ever-growing workloads and producing shorter turnaround times.[225] While there is no official definition of HT as it pertains to laboratory testing, certain authors, such as Shevlin, have defined it as a set of techniques that allow many experiments to be completed simultaneously.[225] Modern MS systems are capable of analyzing many samples in a short amount of time, but bottle-necking often occurs during sample preparation for hyphenated approaches. In response, researchers have invested much effort to making sample preparation more suitable for HT applications. These efforts have produced an array of approaches, including SPE,[226,227] LLE,[228] protein precipitation,[229] and automated disposable-pipette extraction.[230] With the exception of SPE and automated disposable-pipette extraction, these methods carry an increased chance of ME(s). SPE and automated disposable-pipette extraction are less prone to MEs, but they are also exhaustive approaches that contain potential clogging issues, as well as the need for additional sample preparation steps for highly complex matrices (e.g., fibrous or viscous).[231] Similar limitations also apply to certain highly automated systems, such as Agilent's integrated SPE-MS RapidFire™ platform.[232] Although RapidFire™ can easily accommodate an instrumental injection time of 15 seconds for a single sample,

there are a number of factors to consider when selecting this technology for HT applications, including: potential system clogging when working with extremely complex samples (e.g., plasma, blood, and meconium); restricted cartridge chemistry, and high operational and maintenance costs (particularly when decommissioned).[231]

The coupling of AIMS and HT approaches offer a perfect solution to the issues that laboratories worldwide are experiencing today, as the decreased turnaround times would allow researchers to focus more intently on matters of critical thinking.[233] DART is a very popular AIMS approach that has tremendous potential for HT implementation due to its easy operation, speedy analysis, and high sensitivity.[87] DART is a "dry" approach, which means that that it does not use any solvents; instead, heated gas is used to thermally desorb/ionize different sample surfaces.[87] The DART module is able to analyze several samples simultaneously due to its cleverly designed interface, which consists of a motorized linear rail (x-direction or xy-directions) that carries samples between the DART source and the MS inlet.[91] Among the devices that can be interfaced via this rail system, TM technology is particularly notable.[115] TM's potential has yet to be fully explored, with only a limited number of research papers having been published to date.[83,115,234] In contrast, a number of publications have documented the implementation of DART for HT applications via the use of other sample introduction methods. For example, Danhelova et al. analyzed caffeine using a simple exposure method wherein Dip-it tips® were inserted into a hot water/coffee mixture and then processed using an AUTO/DART-96, which is a robotic system from CTC Analytics.[235] Alternately, Grange et al. built a 91 cm long square aluminum rod capable of holding 76 cotton swabs in order to analyze 2-aminobiphenyl, 2-(methylthio)benzothiazole, and N-butylbenzenesulfonamide[236] but this apparatus consumes a fair amount of laboratory space. Furthermore, an additional problem commonly encountered with the sample-introduction methods used in many DART applications (including the ones mentioned above) is the lack of preconcentration of analytes of

interest,[237] which is important given that the cut-off levels of certain compounds are on the lower ppb scale.[223]

SPME is a sample preparation tool that is capable of solving this preconcentration issue and facilitating the development of a robust HT-DART method. SPME is renowned for its structural flexibility, as its format can be re-shaped in order to comply with the requirements of varying direct-to-MS approaches.[27,205,238–240,241] SPME sampling only extracts a fraction of analyte, and the use of biocompatible protective coatings, such as PAN, helps to prevent the adherence of unwanted biologicals (reducing clogging issues and artifact formations), thus enabling a "cleaner" introduction of the sample to the MS.[7,15] The coupling of SPME and DART is not novel,[159,238] as applications using the classical fibre format[165,244] (commercially known as SPE-its^{TM}) have previously been documented. In 2014, the TM format for SPME was optimized, which allowed analytes to be efficiently preconcentrated and quantified at low ppb levels.[26] Since then, SPME-TM has been employed to detect pesticides in H_2O, consumer beverages, and milk,[117,134] and it has also been coupled to a portable MS for detecting DoAs in OF and urine.[134] Sacks group at Cornell University has also explored its application towards determination of volatiles from wine samples.[137,237]

DART, with its simple operation and ruggedness, is an AIMS approach that may have a long-lasting impact in the field. At the same time, SPME is a very efficient sample pre-concentration tool that can provide sufficient selectivity and sensitivity. Thus, these two technologies would seem to be the perfect partners for establishing a robust HT-AIMS technique. Given this potential, SPME-TM was arranged as a "96-brush" in order to enable the HT collection and quantification of analytes of interest from varying matrices. The 96-SPME-TM, described herein for DART, consisted of SS meshes with meticulous geometry (i.e., hexagonal honey-comb apertures), which were carefully etched and coated using C18 particles embedded within PAN solution. Device features (i.e., coating stability, extraction capacity, collection capacity, and effect of sample pH) and DART parameters (i.e., source temperature and rail

114

speed) were investigated to identify the configuration that offered maximum instrumental sensitivity while also maintaining reliable operation throughout the analytical workflow. Finally, the 96-brush SPME-TM devices were implemented for the simultaneous extraction and quantification of opioids from PBS, urine, and blood plasma. Approximately 1.5 h were required to complete the analyte collection, desorption/ionization, and data analysis steps for a set of 96 samples. Our results demonstrate that the coupling of 96-SPME-TM to DART-MS can allow laboratories to handle large workloads while significantly reducing turnaround times.

2.6.2 Experimental

Chemicals and Materials

The following standards (1000 mg L^{-1}) and respective ISs (100 mg L^{-1}) were obtained from MilliporeSigma: fentanyl, cocaine, cocaethylene, codeine, EDDP, oxycodone, meperidine, methadone, dihydrocodeine, hydrocodone, fentanyl-d5, cocaine-d3, cocaethylene-d3, codeine-d3, EDDP-d3, oxycodone-d3, meperidine-d4, methadone-d3, dihydrocodeine-d6, and hydrocodone-d3. Compound details and instrumental settings are documented in Section 2.2.2, 2.5.2 and Tables 2.15-2.17. Table 2.15 lists compounds that were used for preliminary examination of mesh extraction efficiency as a part of a standard operating procedure (SOP) for interlaboratory assessment of the mesh performance at IonSense, Inc. and the University of Waterloo. PAN, DMF, and concentrated HCl were also obtained from MilliporeSigma, while LC/MS-grade MeOH, ACN, IPA, and H$_2$O were obtained from Fisher Scientific. Bare photochemically etched custom-manufactured SS meshes and C18 particles (5 µm) were kindly provided by IonSense, Inc. and MilliporeSigma, respectively. A custom-designed N$_2$ blower (see Figure 2.44) was made at the UW machine shop in order to facilitate a speedy coating process for the meshes. A dedicated mesh holder (for desorption in front of the DART source) featuring three different immobilization positions was also custom made (see Figure 2.45). Details on preparation of PBS are

Table 2.15 *Compounds used in preliminary mesh-performance assessments using an Exactive Orbitrap, including their logP values and exact mass.*

Analyte	LogP	Exact mass (m/z)
Cocaine	2.30	304.1549
Cocaine-d3	-	307.1737
Cocaethylene	2.64	318.1705
Cocaethylene-d3	-	321.1894
Codeine	1.19	300.1599
Codeine-d3	-	303.1788
EDDP	5.26	278.1909
EDDP-d3	-	281.2097
Methadone	3.93	310.2171
Methadone-d3	-	313.2359

Table 2.16 *Acquisition conditions used to obtain data on the Exactive Orbitrap for the DART-MS experiments.*

Resolution	50,000
Mass range	100 - 500
Polarity	+ve
Microscans	1
Capillary temperature	250 °C
S-lens RF level	-
AGC target	1,000,000
Max injection time	-

Table 2.17 *List of opioids used in the quantification experiments for the 96-SPME-TM, including their logP values, TSQ Vantage perimeters and structures.*

Analyte	logP[1]	Parent (m/z)	Product (m/z)	CE	S-lens
Hydrocodone	1.2	300.4	199	28	87.9
Hydrocodone-d3	-	303.1	199.1	29	199.1
Meperidine	2.7	248.1	219.8	29	110.7
Meperidine-d4	-	252.1	223.8	20	68.6
Dihydrocodeine	1.6	302.1	199.0	30	133.2
Dihydrocodeine-d6	-	308.1	202.0	32	143.9

provided in Section 2.2.2. These materials were all obtained from MilliporeSigma. The pH of the samples was adjusted using acetic acid (AA) and NH_4OH, which were also obtained from MilliporeSigma. Surine[TM] negative urine control was obtained from MilliporeSigma. Human urine was collected from

two healthy volunteers in their mid-20s (male and female) and kept at 4 ˚C until use, while human plasma

(K2-EDTA stabilized) was obtained from BioIVT and kept at -30 ˚C until use.
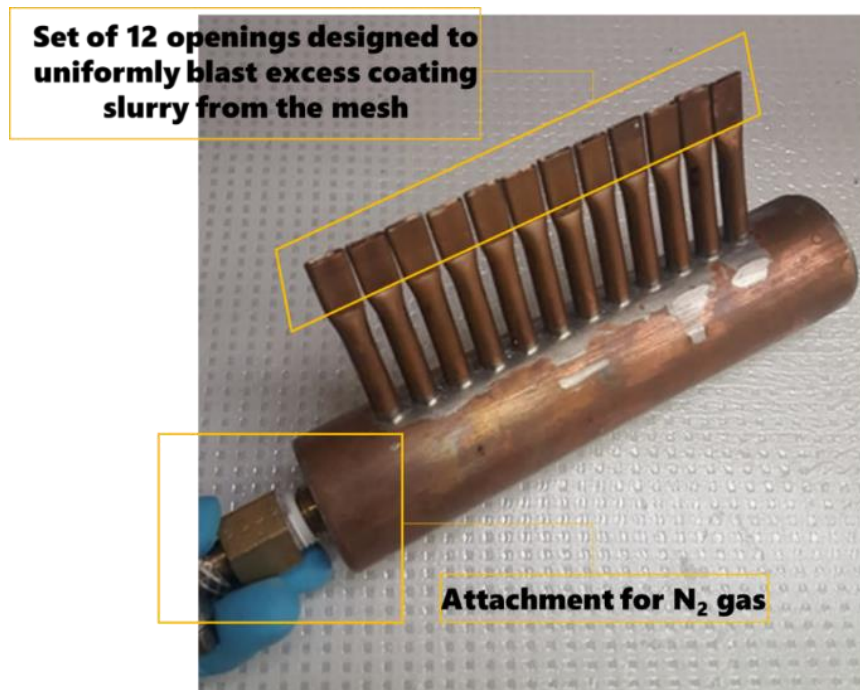
Figure 2.44 *N₂ blower designed for the high-throughput fabrication of the 96-SPME-TM meshes. Tubing was attached to the holder on the side of the blower and to a N₂ tank. The valve on the N₂ tank was opened each time excess slurry had to be blown out.*
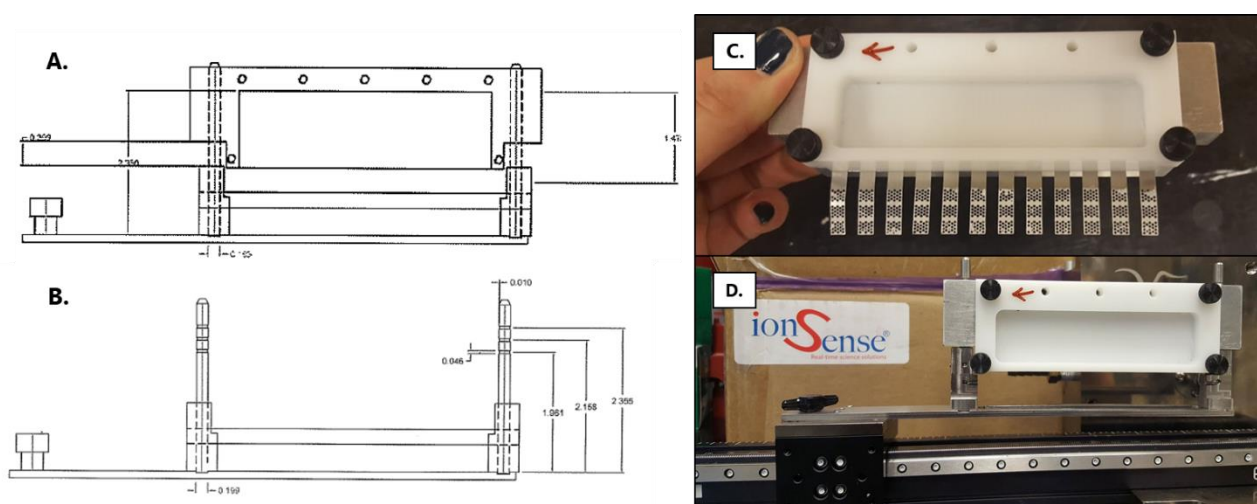
Figure 2.45 *The holder setup for the 96-SPME-TM mesh. Figures A. and B. show the schematic of the holder, with B. showing the "mounting stage". Figures C. and D. show the completed 96-SPME-TM mesh holder, with Figure D. showing the holder immobilised on the linear rail.*

Preparation of Stock Solutions and Samples

The selected standards were combined to make a 100 mg L^{-1} methanolic stock, and the ISs were also combined into a separate 10 mg L^{-1} methanolic stock. The standards were further diluted with MeOH to create samples for use in preliminary examinations of mesh performance, as well as for the construction of a calibration curve consisting of 14 points (0.5, 1, 2.5, 5, 7.5, 10, 25, 50, 75, 100, 120, 150, and 200 ng mL^{-1}). The IS stock was also diluted in order to ensure that the final concentration in the samples was kept at 10 ng mL^{-1}. All dilutions were performed using LC/MS-grade MeOH. In accordance with the guideline recommending that the partitioning equilibria for SPME not be disturbed, the spiking of organic content to the samples for extraction (PBS, urine, and plasma) was kept ≤ 1 %.[7] After spiking, the samples were gently agitated at 200 rpm for 2-4 h to achieve matrix-drug equilibration.

Preparation of the SPME-TM 12 Mesh Strip

Unlike the previous work, which used hand-cut SS meshes,[26,117,134] we employed photoetched SS meshes with a well-defined geometry in order to remove errors introduced from human handling. As can be seen in Figure 2.46, each pin on the SS mesh "comb" is divided into three areas, or desorption sites, which allows for the production of three distinct replicates for each sample using a single extraction step. Hence, it is important to investigate whether "loss of analyte" occurs on other coated areas of a given pin during desorption due to heat transfer on the metal surface. The SS sheets had very smooth surfaces as a result of being fabricated via photochemical milling; as such, the photomask that was used on the surfaces needed to be removed through extensive wet-etching in order to obtain the desired surface roughness. This process consisted of four stages of mesh sonication in various fluids: MeOH (2x, 20 min), HCl (1x, 20 min with brief shaking every 5 min), MeOH again (1x, 10 min), and, finally, deionized H_2O (2x, 10 min). After these steps, the meshes were dried for 30 minutes at 120 ˚C and kept in a desiccator (under N_2 atmosphere) until use. A slurry consisting of 10% PAN in DMF was mixed with 7% of 5 µm C18
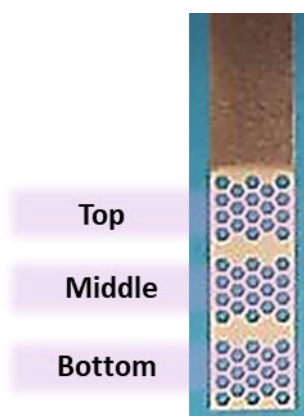
particles and agitated overnight at 700 rpm to achieve homogeneity. The coating process was performed using a 2 mL 96-well plate that had 1 mL of coating slurry deposited into twelve of the wells. The brush was dipped into the wells, carefully withdrawn, and the excess slurry was removed using an N_2 blower that uniformly blasted all twelve pins at the same time. Afterwards, the brush was pinched with a holder (to avoid tumbling) and cured at 100 ˚C in a fan-controlled oven. In order to establish a homogenous coating on both sides of mesh, the coating protocol was repeated for the other side as well. Before being used in real samples, the meshes underwent two 15 minute cleanings in a mixture of MeOH/ACN/IPA (50/25/25) and preconditioning in MeOH/H_2O (50/50) for at least 30 minutes prior to use. These steps aim to remove any material remaining from the manufacturing step (e.g. oligomers, uncured PAN, among others).

Extraction Procedure for Surine, PBS, Urine, and Plasma

Prior to extractions, the meshes were immobilised and kept in a preconditioning solution using a 3D-printed holder. A simplified schematic of the 96-well plate can be seen in Figure 2.47. PBS spiked with 50 ng mL^{-1} of oxycodone was used for the evaluation of extraction repeatability via LC-MS/MS. The entire 96-well plate was filled with 0.9 mL of PBS spiked with 50 ng mL^{-1} of oxycodone, followed by washing of the meshes in H_2O to remove residuals of the preconditioning solution. The meshes were then immersed into PBS to perform an agitated 10 minute extraction on an orbital shaker (500 rpm).
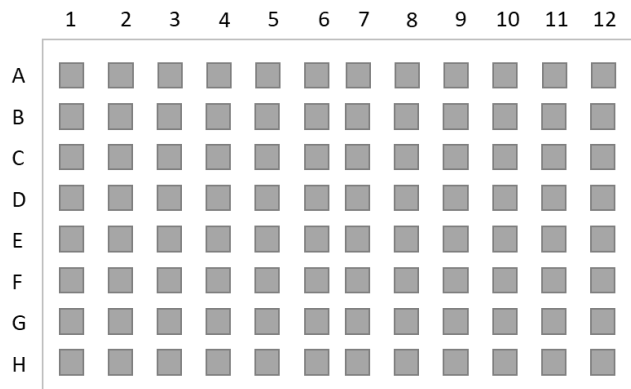
Figure 2.47 *Schematic of a 96-well plate.*

After extraction was completed, the meshes were washed for 5 seconds in H_2O (separate 96-well plate, 1.5 mL) and immersed into another 96-well plate filled with 0.9 mL of ACN/H_2O/FA (90/10/0.1%) for a 10 minute desorption (also agitated). Once desorption was completed, the 96-well plate was analysed via LC-MS/MS. For DART experiments, three 2 mL 96-well plates were prepared: two plates were filled with 1.5 mL of H_2O to perform the pre- and post-washing steps, while the extraction plate was filled with 1.2 mL (n = 3) of sample (0.9 mL of plasma was diluted with 0.3 mL of PBS to reduce viscosity). Matrix pH was adjusted by adding droplets (< 20 µL) of either AA or NH_4OH. To ensure that all solvent components were removed, the meshes in the preconditioning solution were pre-washed for 10 secs using an orbital shaker (200 rpm) and then gently blotted with a Kimwipe to remove excess H_2O. The extraction was carried out by fully immersing the brush into the 96-well plate and agitating via orbital shaking (500 rpm). A schematic of this process can be seen in Figure 2.48. Extraction time profile was evaluated at seven different time points (1, 3, 5, 10, 20, 30, and 60 min) for n = 4. After the extraction was completed, the samples were washed for 10 seconds using the orbital shaker (200 rpm) and then inserted into the custom-made holder for DART analysis.
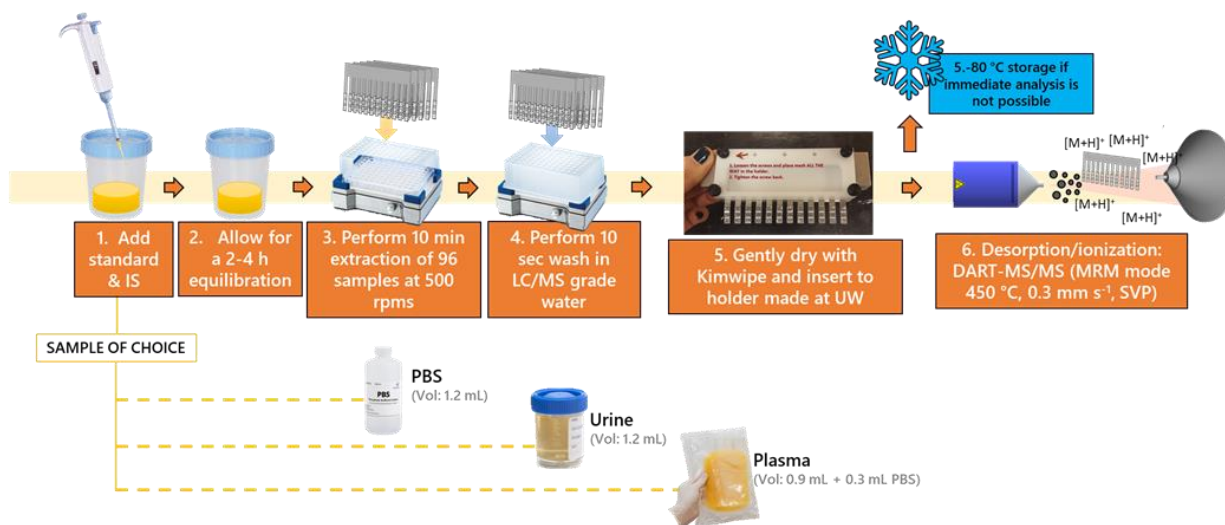
Figure 2.48 *Schematic representation of the extraction and desorption process used for 96-SPME-DART-TM.*

LC/MS, DART-MS & MS/MS Conditions

LC/MS experiments were conducted on API 3000 (Sciex, Framingham, MA, USA) equipped with a Shimadzu binary pump (LC-10ADvp, Kyoto, Japan) and a HTC PAL autosampler (CTC Analytics, Leap Technologies, Zwingen, Switzerland). A binary gradient consisting of 20 mM ammonium acetate and 0.1 % FA in H_2O was used for phase A, while 0.1 % FA in ACN was used for phase B. The following gradient at 400 µL min^{-1} was used with a PFP column (1.7 µm, 2.1 mm x 10 mm): 0.5 min 95 % A, 3.5 min 60% A, 5 min 0% A and 7 min 95% A ending with an re-equilibration for 1 min at 100% A. An injection volume of 10 µL was used, and oxycodone was monitored using SRM mode ($316 \rightarrow 241$) at a 55 V declustering potential (DP), 175 V focusing potential (FP), 5 V entrance potential (EP), 39 V collision energy (CE) and 16 V cell exit potential (CXP).

All of the DART-MS experiments were performed using a DART-SVP® ion source set to the following conditions: +ve ionization mode, high-voltage electrode at −3000 V, discharge electrode at +350 V, and a grid voltage of +350 V. The DART-SVP® source was coupled to an Exactive Orbitrap (Thermo

Scientific) and a TSQ Vantage. Since DART-SVP® utilises N_2 and He gas during active runs, the amount of gas entering the MS was reduced using a membrane pump (adjusted to blue indicator, position 4) to avoid compromising the vacuum. The meshes that had been placed in the holder were mounted on a linear rail for desorption, while maximum sensitivity was obtained by adjusting the rail speed (0.2, 0.3, and 0.4 mm s^{-1}) and the DART source temperature (350, 450, and 500 °C). Prior to any DART-MS/MS, the level of noise was assessed by obtaining a background signal of ambient air for the MS/MS transitions of the monitored analytes. Additionally, ion chronograms of monitored analytes were also obtained for unused meshes, i.e. meshes that had only been cleaned and preconditioned.

2.6.3 Results/Discussion

Initial performance of the 96-SPME-TM meshes for HT analysis

In comparison to other AIMS methods, DART has the benefit of not requiring the addition of solvent post-extraction in order to desorb samples, thus eliminating the need for extraneous input. SPME-TM DART has already demonstrated its ability to handle time efficiently, but analyses had yet to be carried out on a one-by-one basis.[26,117,134] It should be noted that, the use of a 96-SPME format is not a novel concept. In fact, it has garnered interest for nearly a decade, and almost every SPME configuration can be augmented to fit a 96 format.[19,63,245,246] Our results demonstrate that SPME-TM can also be used to further decrease the total time required for DART. Figure 2.49 depicts the 96-SPME-TM design. Panel A shows an uncoated mesh pin with hexagonally-shaped apertures (opening diameter ~ 843 μm) and a single coated pin in the insert. Panel B shows the coated 12-pin set, alongside its dimensions. Panel C shows the entire coated 96 set, which can be immobilized into a 3D printed holder so that the analyst can control the stages of SPME extraction and potentially implement Concept-96, which is a robotic arm used to control the preconditioning, washing, and extraction steps of the SPME protocol.[246] The initial mesh performance evaluations focused on coating stability and visual examination whether strong agitation caused the coating to strip off. The results of these tests showed no significant issues related to
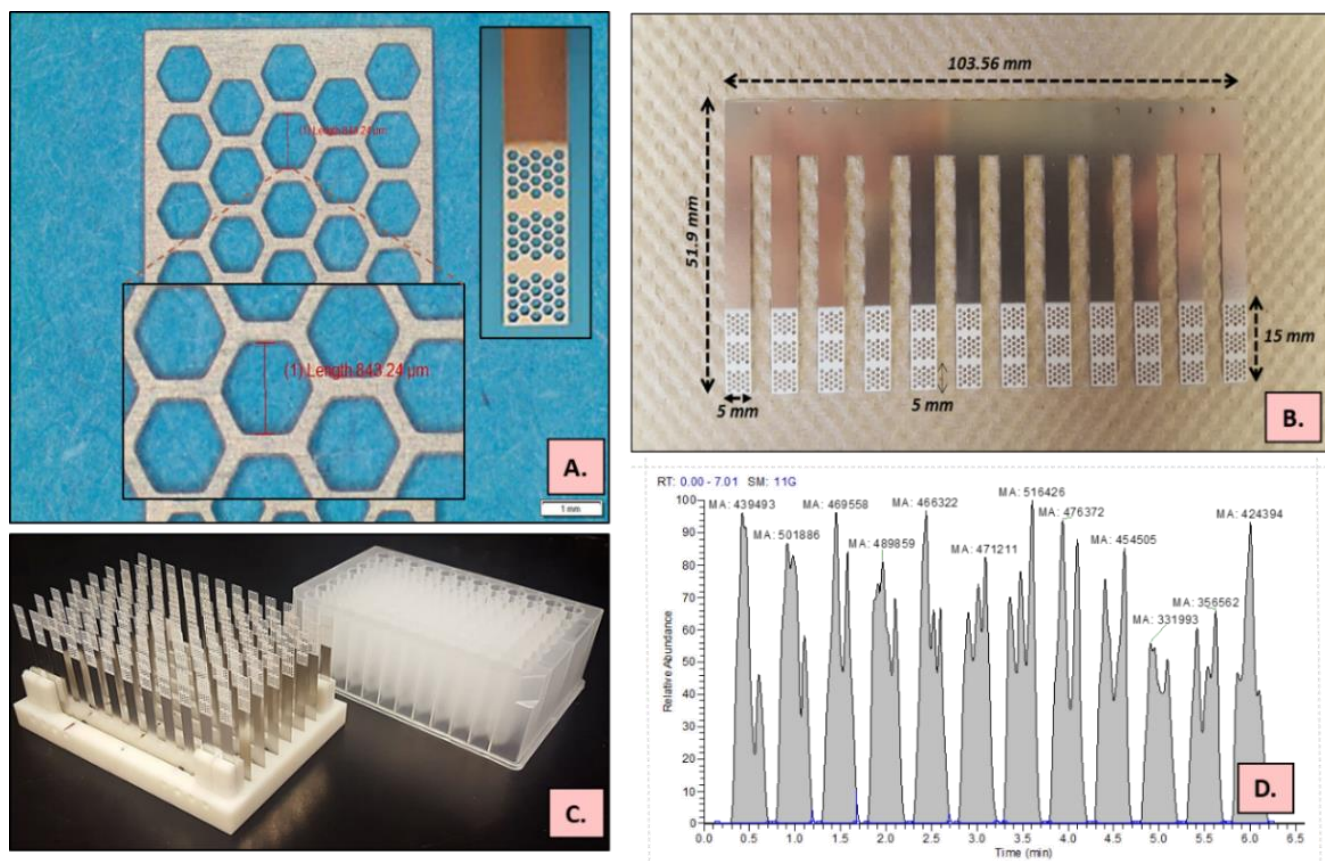
Figure 2.49 *The overall assembly of the 96-SPME-TM is shown in panels **A**., **B**., and **C**. Panel **A**. shows a close-up image of the uncoated mesh, while the insert shows a coated pin. Panels **B**. and **C**. show the dimensions and the full 96-SPME-TM "brush" designed to fit within a 96-well plate. Panel **D**. shows the signals obtained from 12 pins for extraction of 25 ng mL^{-1} of cocaine from surine which served as a preliminary assessment of the mesh's performance.*

mesh stability. The next step was to perform assessment of extraction efficiency using LC-MS/MS. A plot for amount of oxycodone extracted (in ng) versus each pin (n = 96) can be seen in Figure 2.50. It is noticeable that the combs positioned in A_{1-12} and H_{1-12} extracted less oxycodone, likely related to improper positioning of the comb which resulted in insufficient interaction of the mesh pins with the bulk of the solution. Hence, it is important that the analyst ensures that the mesh movement is not obstructed in the well plate. The mean amount of oxycodone extracted (taking into consideration the afore-mentioned positions) was 19 ng, with a % RSD of 41.9 %. Excluding A_{1-12} and H_{1-12} positions yields a mean of 22.7 ng for extraction of oxycodone, with a % RSD of 20.9 %. The Shewhart chart observed in Figure 2.51 indicates amounts extracted for each pin with the exclusion of A_{1-12} and H_{1-12}.
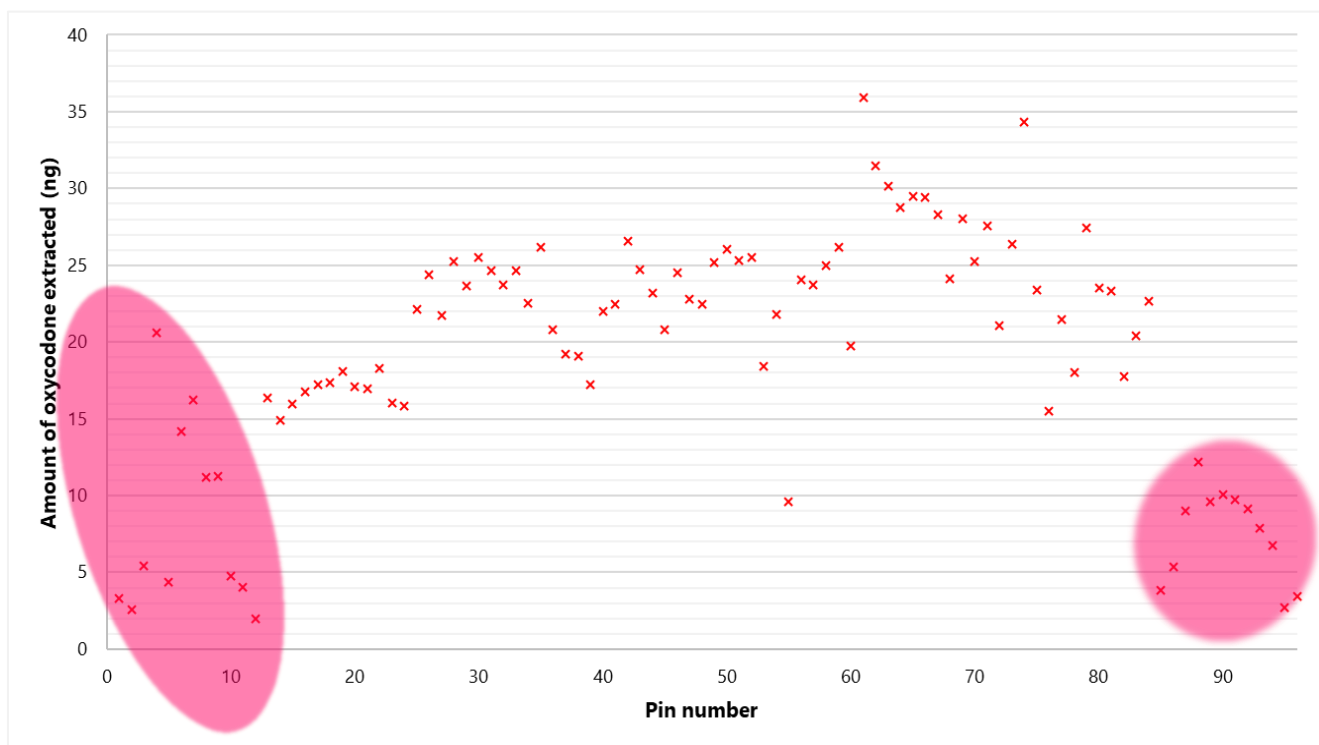
Figure 2.50 *Amount of oxycodone extracted (ng) from 0.9 mL of PBS spiked with 50 ng mL^{-1} of oxycodone for a full brush set of SPME-TM meshes (n = 96) analysed via LC-MS/MS.*

The discrepancy observed due to positioning on the orbital shaker may not represent a major issue during

DART desorption since only a portion of the mesh is actually exposed to the desorbing stream
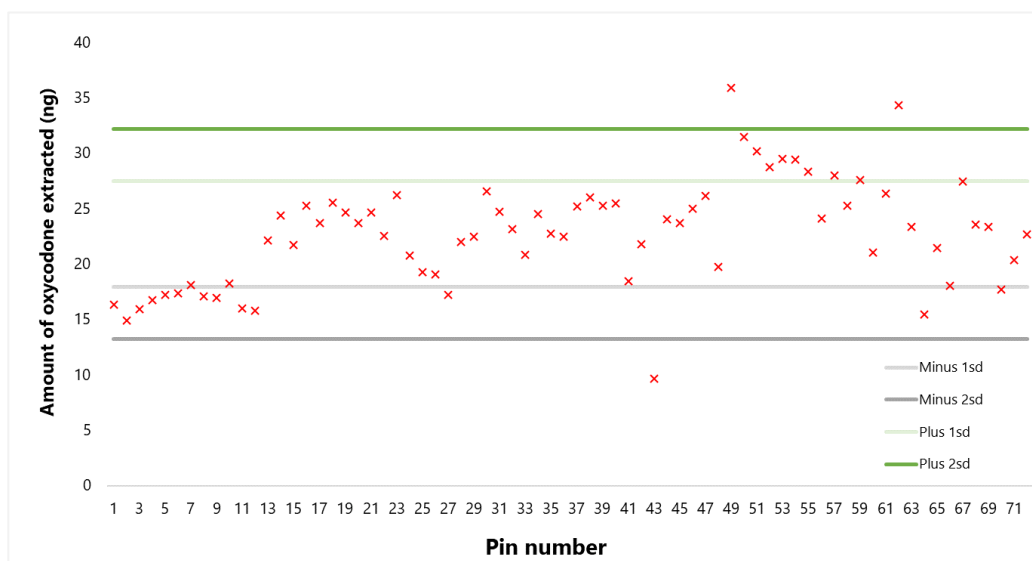
Figure 2.51 *Amount of oxycodone extracted (ng) from 0.9 mLs of PBS spiked with 50 ng mL^{-1} of oxycodone for a full brush set of SPME-TM meshes (n = 96) analysed via LC-MS/MS.*

of DART and the IS may conveniently correct for such discrepancy. Nonetheless, it is important to

emphasize the fact that the agitation mode, i.e. orbital shaking could cause variance in the data. Next, extraction efficiency of meshes was assessed using DART-MS and an inter-laboratory SOP developed between IonSense, Inc. and UW which involved the use of Exactive-Orbitrap, surine negative control and methadone, cocaine, codeine, EDDP, and cocaethylene as model compounds. Figure 2.49D. shows the ion chronogram (Gaussian smoothing, seven points) along with the signal areas of cocaine (arbitrary units, AU) that was obtained from extraction of a 25 ng mL^{-1} spiked sample (10 minute extraction, 300 °C, 0.3 mm second^{-1}). A relatively repeatable trend in chronogram signal area (12.3 % RSD) can be observed, with a slight drop on the 10th and 11th pins. This drop could be attributed to either small amounts of turbulence that occur during the desorption process or a structural deviation in the device itself (i.e., differences in coating thickness). Ion chronograms for the remainder of the tested compounds can be seen in Figure 2.52. Since DART is very sensitive to small changes in air flow, a robust immobilization of the device is absolutely necessary in all serious efforts to implement it as a HT technique for clinical settings.
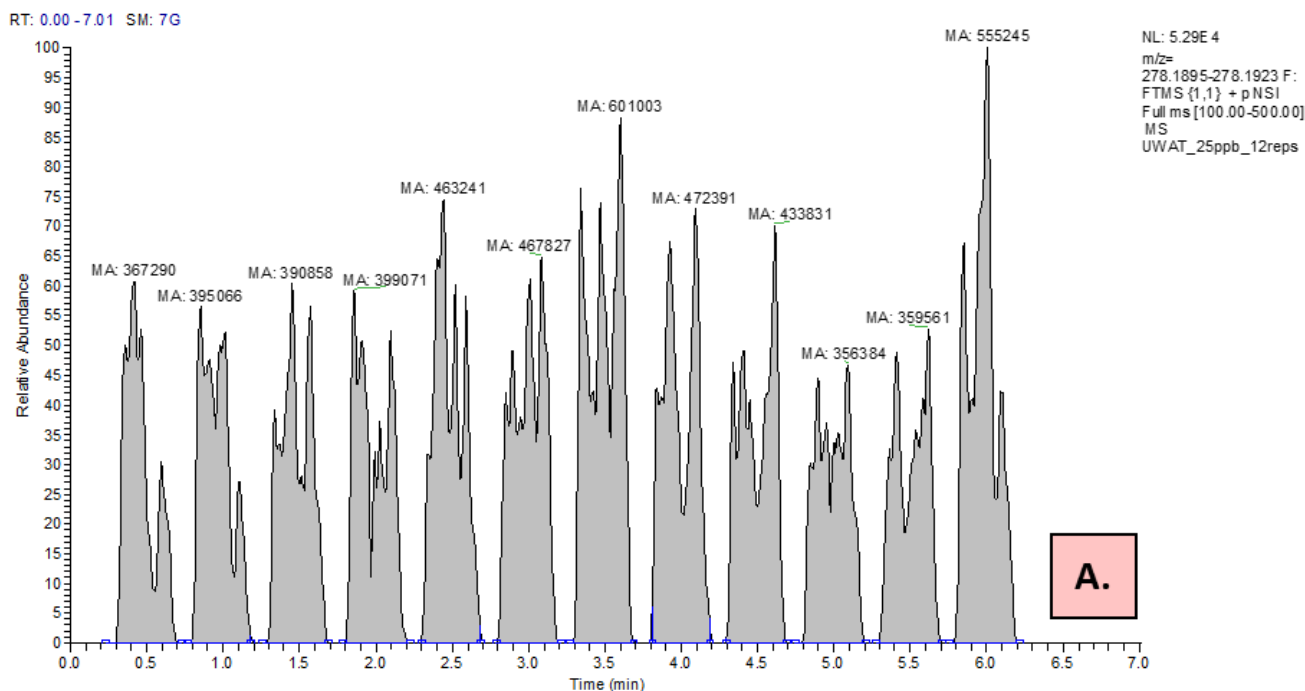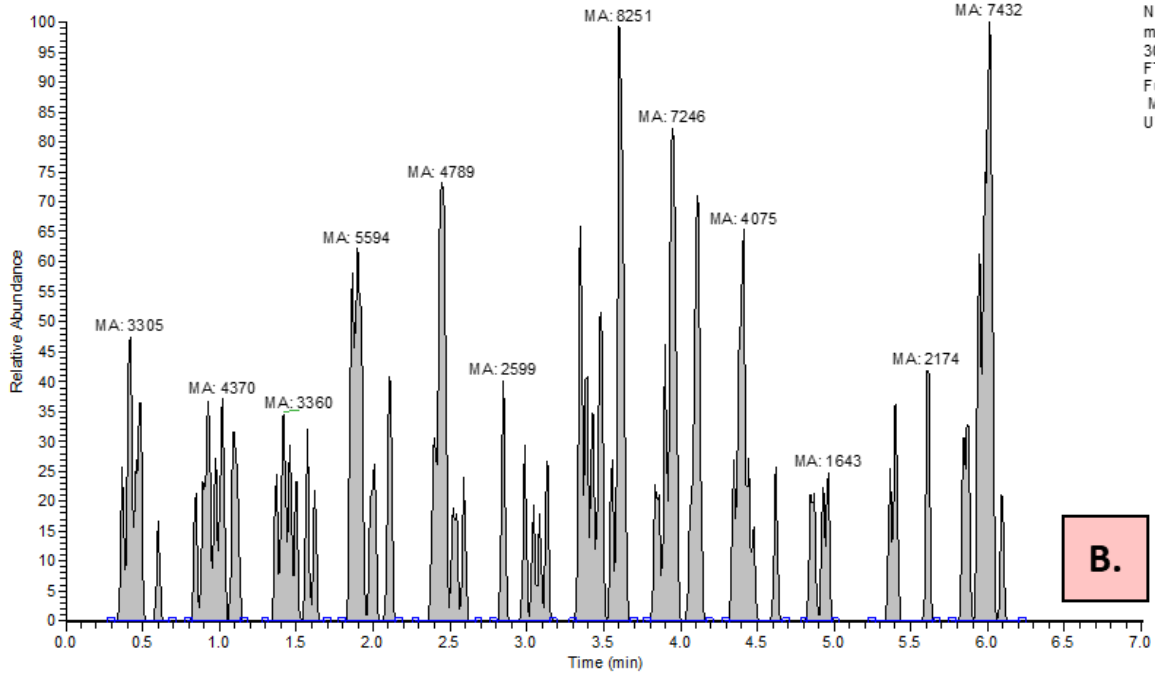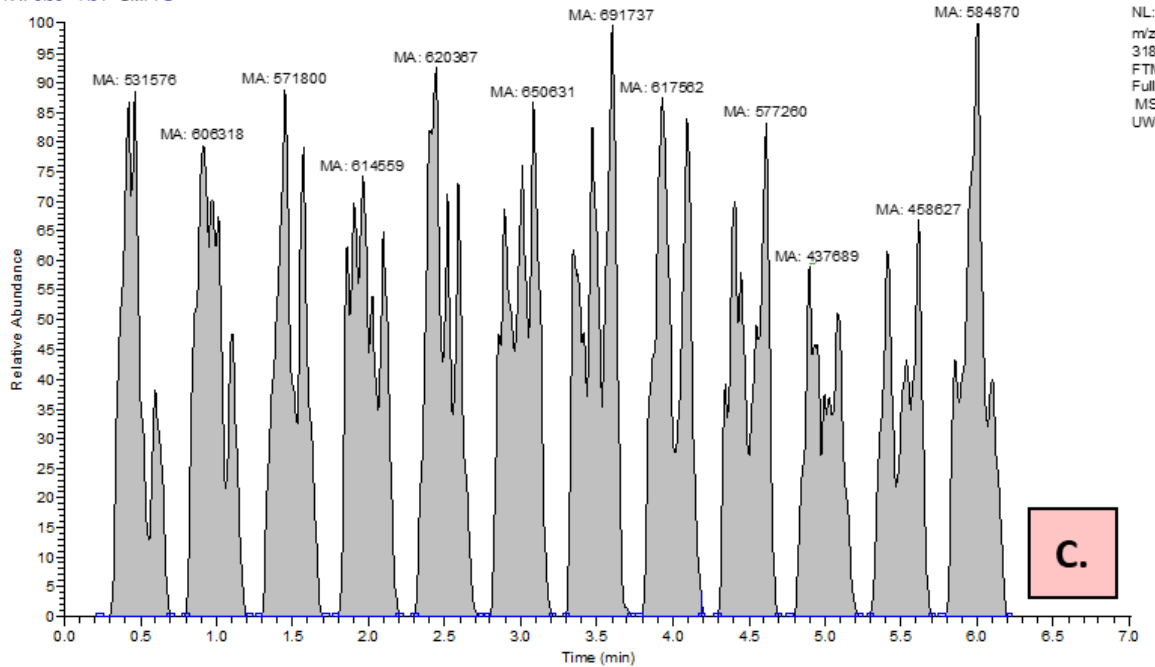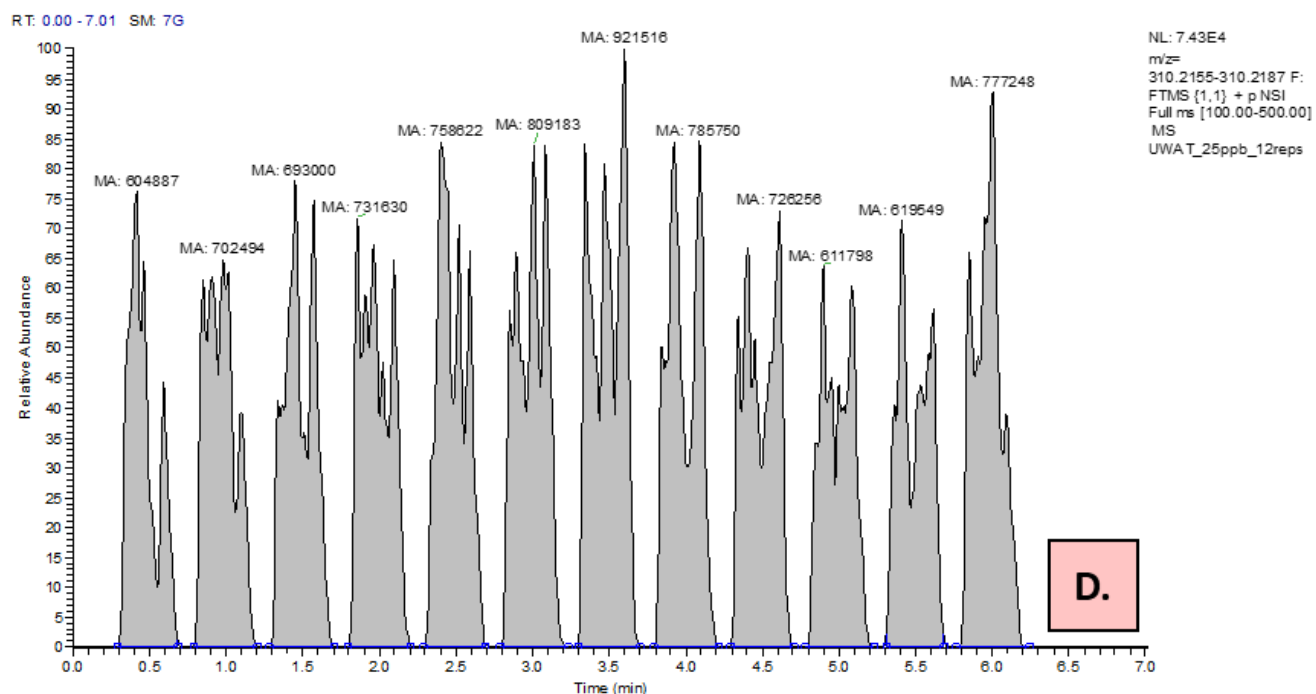
*Figure 2.52 Ion chronograms of extracts from surine spiked with 25 ng mL^{-1} of EDDP, codeine, cocaethylene and methadone in **A., B., C., and D.***

A Single Mesh for Multiple Desorptions?

While HT is one important topic investigated by this study, another is the exciting idea that a single device could be used to obtain replicate measurements. In addition to being able to perform HT analysis, we wanted our mesh to be capable of obtaining three replicate measurements per pin, thus avoiding the need to use a new mesh when a replicate measurement is required. It was anticipated that thermal conductivity would be an important parameter in understanding how this concept would function. Thermal conductivity measures a material's ability to transfer heat via conductance, with denser materials like metals and alloys usually providing better heat transfer. The thermal conductivity of SS is different at different temperatures; however, for reference purposes, the thermal conductivity of SS at 25 °C is ~16 W mK^{-1}[247], while that of paper is 0.05 W mK^{-1}.[247] Harding et al. examined how long it takes to heat different materials, such as aluminium and cardboard, for use with DART and found that cardboard reached a higher temperature faster than aluminum due to its thermal conductivity.[146] Therefore, the present investigation also examined whether the three sections of the mesh pin would be

affected by surrounding heat transfer. Specifically, we were interested in determining whether a pin's sensitivity would be negatively affected by subsequent desorptions. In order to examine this, desorptions were performed on ten pins on n = 3 different meshes such that the ordering of the desorption sites was alternated for each mesh (i.e., mesh #1- bottom, top, middle; mesh #2-top, bottom, middle; mesh #3-middle, top, bottom). Fentanyl spiked at 25 ng mL^{-1} in PBS (1.2 mL, 10 min extraction) was used as a model compound, and no IS was used to assess the response, as the aim was to investigate the uncorrected signal. The obtained results can be seen in Figure 2.53. While it may appear that the middle position produces the least sensitive response, statistical analysis (single factor ANOVA, p = 0.96) did not show significant differences amount the three sites. Responses observed in the signal could be contributed to slight heat transfer, differences in coating homogeneity or both. Thus, further work shall focus on investigating effect of coating choice and substrate thickness in potential heat transfer and as a cause of irreproducibility.
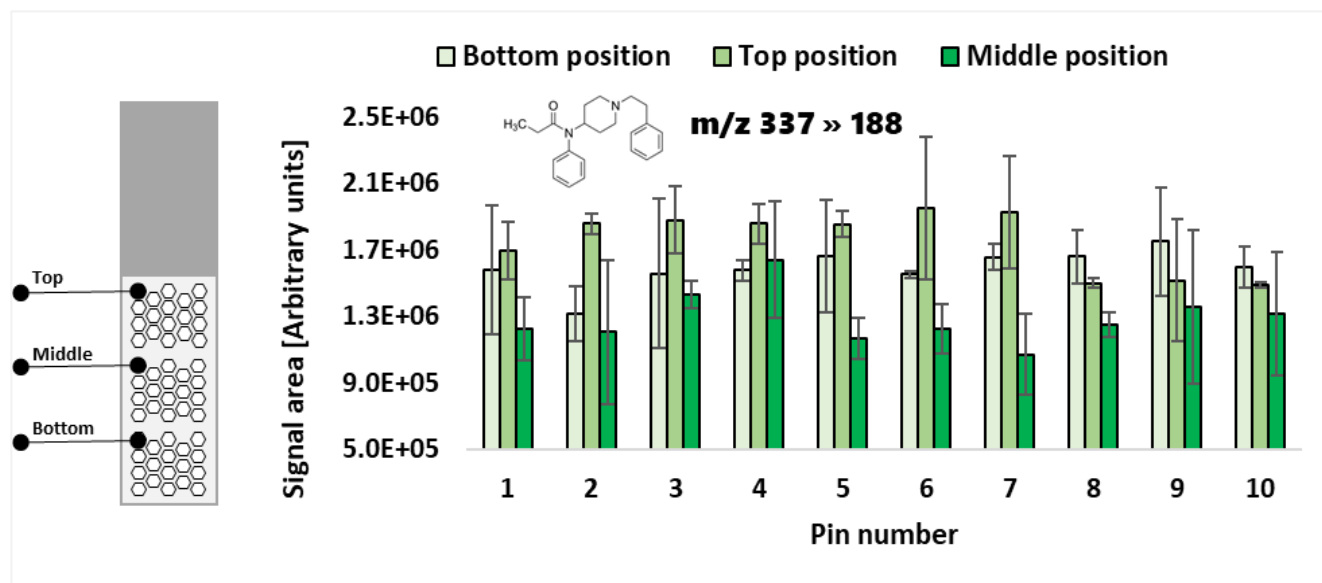
Figure 2.53 *Assessment of signal response for 25 ng mL^{-1} of fentanyl (spiked to PBS, 1.2 mL, 10 min extraction) obtained after using 3 different desorption sites (top, middle, and bottom, indicated on left side of figure) per pin. Ten pins were used in total per mesh, and the experiment was repeated for a total of three meshes, starting with a different desorption site each time. No IS was used for data correction.*

Investigation of Factors Impacting the Sensitivity of DART-MS/MS

The response for the targeted analytes was optimised with respect to sample pH, DART source temperature, and SPME-TM rail speed relating to MS entrance. As Figure 2.54 indicates, the highest
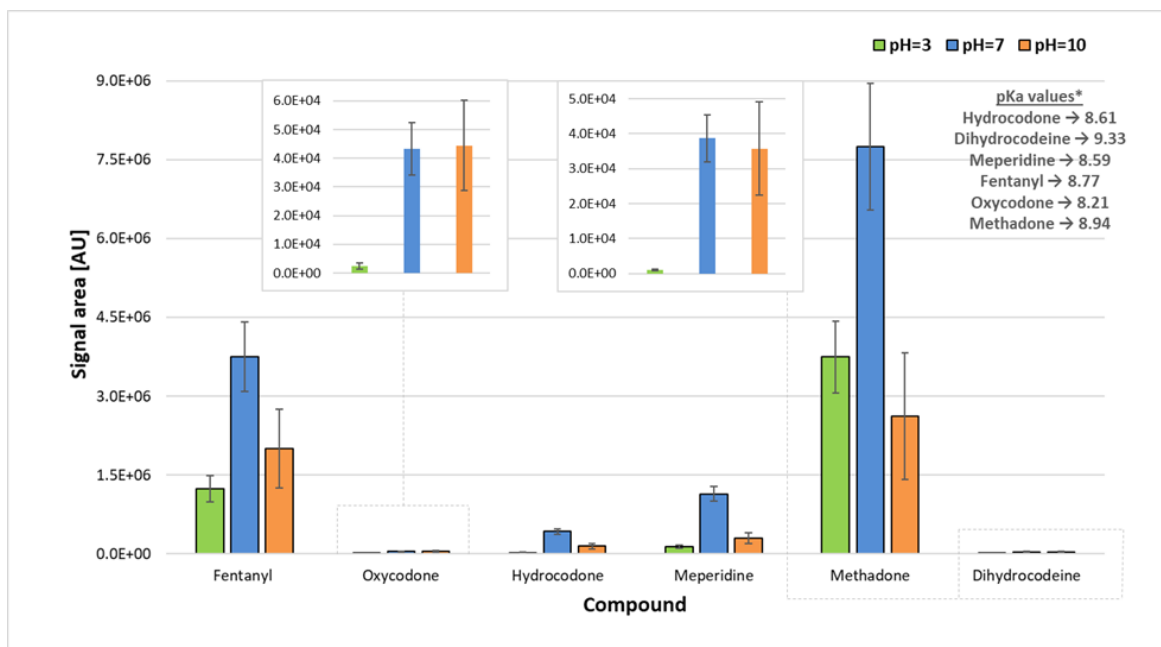
Figure 2.54 *Assessment of the signal response (n = 12) obtained for selected opioids (25 ng mL^{-1} in 1.2 mL PBS, 10 min extraction, 500 rpm agitation on orbital shaker, 450 °C, 0.3 mm s^{-1}) at pH levels of 3 (treated with AA) 7, and 10 (treated with NH$_4$OH). Respective pKa values of the compounds are shown on the right side.*

response was obtained at pH 7, which correlates to the pKa values of the majority of the targeted compounds. SPME coatings without cation/anion exchange moiety extract mainly the undissociated form of an analyte. Hence, considering the pKa values of analytes of interest, extraction from an acidified environment would be the worst option as predominantly dissociated forms of the analytes would be present. With regards to temperature, 3 different settings were used at 350, 450, and 500 °C to investigate the signal response. The greatest response was obtained at 450 °C, providing an adequate compromise for the majority of the analytes (Figure 2.55). Usually, the optimum DART source temperature is compound-specific.[89] However, certain analytes, such as dihydrocodeine and oxycodone, did not show an increase in sensitivity as temperature was increased. The lower signal attained for these analytes may be due to a combination of a number of factors, including low VP, low PA, and poor thermal stability.
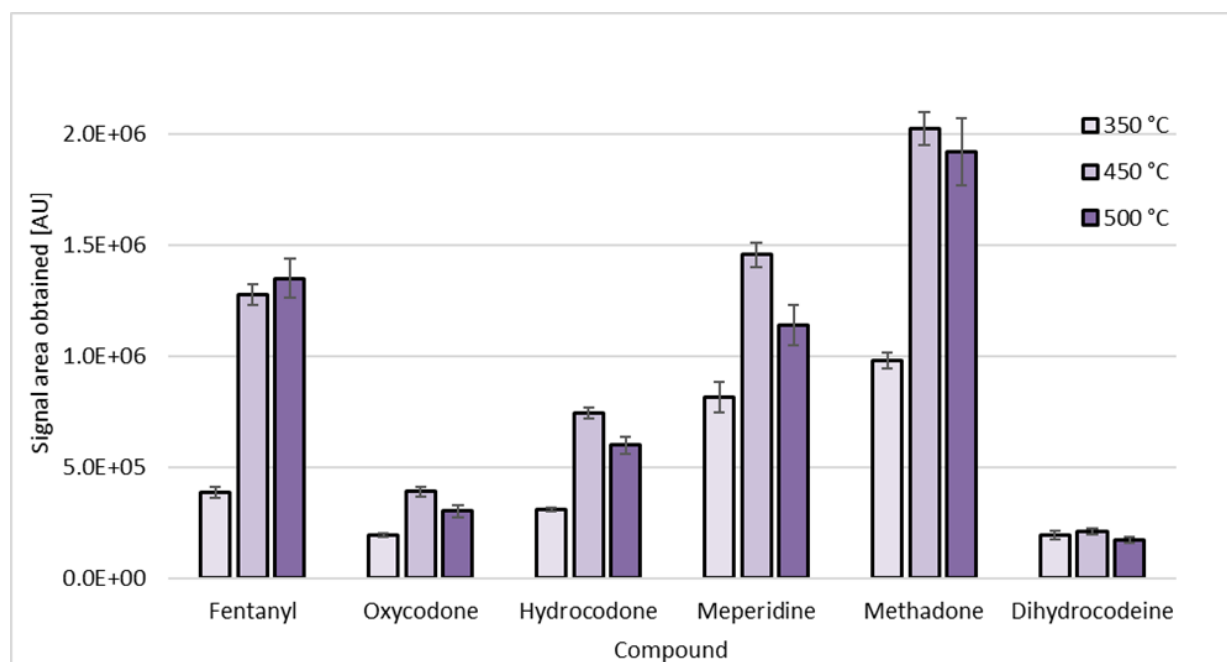
Figure 2.55 *Determining the optimum DART source temperature (n = 4) in order to maximize sensitivity using selected opioids (25 ng mL^{-1} in 1.2 mL PBS, 10 min extraction, pH 7, 500 rpm agitation on orbital shaker, 0.3 mm sec^{-1}).*

Indeed, the National Institute of Standards and Technology lists dihydrocodeine as a trimethylsilyl-derived molecule (i.e., for GC analysis), which indicates that it is a potentially poorly volatile and a heat-labile compound.[248,249] On-coating derivatization could potentially be implemented prior to DART analysis to enhance ionization of labile analytes since certain authors have demonstrated derivatization feasibility with DART applications.[144,250] The influence of rail speed was investigated at speeds of 0.2, 0.3, and 0.4 mm sec^{-1} to determine whether significant sensitivity loss would occur at higher speeds, as this would reduce the amount of time the mesh was exposed in front of the DART source. As shown in Figure 2.56, the results indicate that there is no significant difference between speeds. Therefore, 0.3 mm sec^{-1} was used for further experiments, as a slight drop in intensity did occur when the speed was increased to 0.4 mm sec^{-1} (see Figure 2.57).
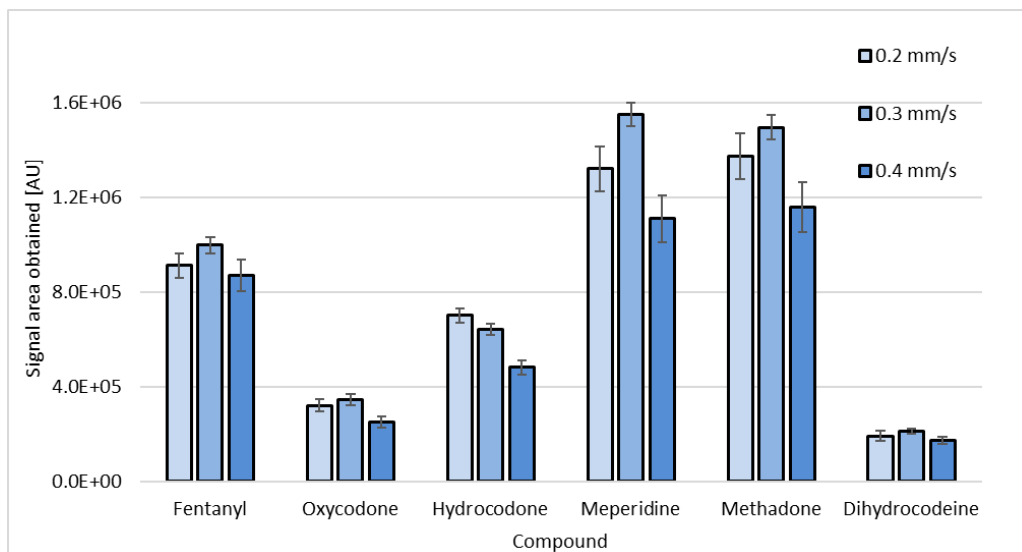
***Figure* 2.56** *Determining optimum DART rail speed (n = 4) to maximize sensitivity using selected opioids (25 ng mL^{-1} in 1.2 mL PBS, 10 min extraction, pH 7, 500 rpm agitation on orbital shaker, 450 °C).*
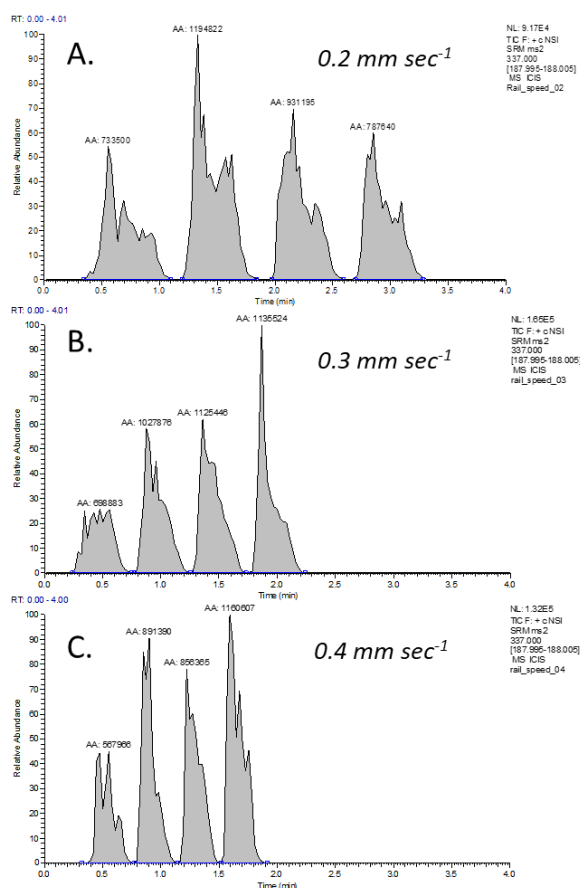
***Figure* 2.57** *Ion chronogram showing the peak shape and areas obtained during the monitoring of fentanyl's signal (n = 4) at 0.2, 0.3, and 0.4 mm s^{-1} rail speed in **A.**, **B.**, and **C.**, respectively.*

Extraction Time Profile of Selected Opioids

It is important to establish an adequate extraction time because it significantly influences SPME's sensitivity.[7] However, it is not always necessary to achieve full equilibrium between the extraction device and the analyte of interest, especially if sufficient sensitivity can be obtained in the kinetic regime (i.e. pre-equilibrium).[7] Thus far, SPME-TM publications have focused on using rapid agitation of each mesh on a vortex (i.e., 3000 rpm).[26,115,159] This approach has worked well due to the mesh's high SA, which allows for adequate pre-concentration in a short period of time. However, it is not feasible to use such high speeds for the 96-SPME-TM format at present, as it may lead to collisions between the mesh and the well walls, which would result in the dispersal of samples from and into surrounding wells. To avoid this problem, an orbital shaker set at 500 rpm was used for all the experiments, as this speed provided adequate agitation without compromising the meshes and/or samples. Figure 2.58 shows the extraction time profile for 25 ng mL^{-1} of spiked opioids obtained at seven different extraction time points (1, 3, 5, 10, 20, 30, and 60 min) for PBS. As can be seen, sensitivity peaks at 30 min, with a drop occurring by the 60 min mark. Further analysis of this drop using a t-test (two sample unequal variance) revealed that it was not statistically significant. Although ten minutes was deemed sufficient for achieving adequate
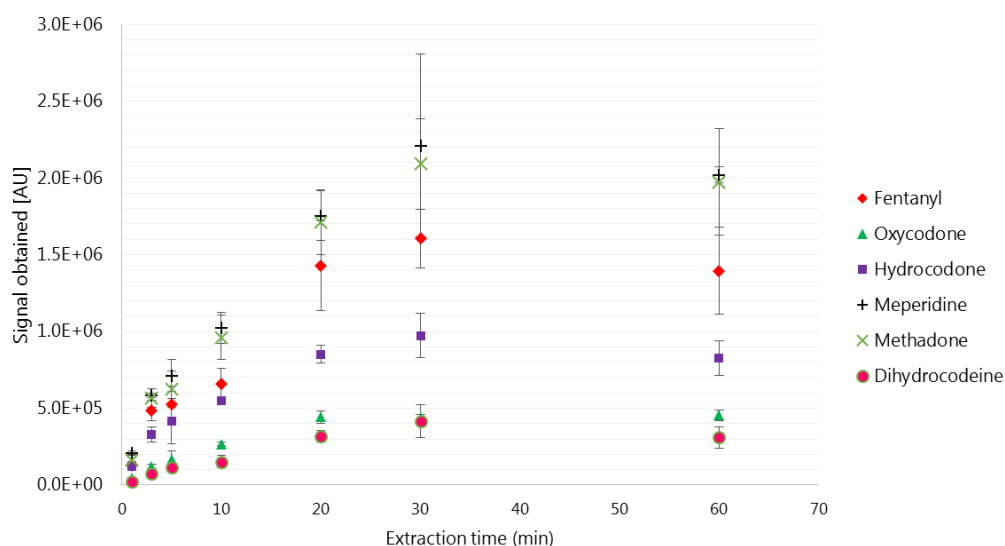
Figure 2.58 *Extraction time profile of opioids.*

sensitivity in our experiments, one should keep in mind that the potential for extracting matrix components that can generate larger noise may become greater with longer extraction times.[159]

High-Throughput Quantification of Opioids in PBS, Urine, and Plasma

PBS

AIMS techniques are generally regarded as methods that offer limited quantitative abilities, but over the last few years there has been a rise in publications reporting otherwise, particularly for DART applications.[139,237,251–254] As mentioned in the introduction of this thesis, and as shown by Pérez et al.,[115] sample preparation devices that have been normalized (i.e., TM device with a defined geometry and coated area) are one of the crucial components for guaranteeing reproducible quantitative results. Several articles published by the Pawliszyn[26,117,134] and Sacks[137,139,237] groups have documented how coupling SPME-TM to DART-MS can provide analysts with reasonable quantitative results.

The decision to select opioids as the model compounds for our quantification experiments was strongly influenced by the ongoing opioid crisis.[255] In 2018, the United Nations Office on Drugs and Crime report indicated that in 2015 450,000 people around the world died due to drug abuse, with 167,750 of those deaths being related to opioid abuse.[256] These startling figures indicate a potentially great demand for opioid testing within clinical settings. All LODs and LOQs obtained in this research were determined based on S/N ratios of 3 and 10, respectively. In order to dismiss any signals coming from the device itself, the response obtained from the coated mesh only (no extraction) was assessed. This result can be seen in Figure 2.59. To assess calibration quality, the first set of 96-SPME-TM mesh strips was used with PBS. Since PBS is an interference-free matrix, it can provide an insight into the mesh's calibration ability without the interfering biologicals. The figures of merit obtained for PBS can be seen in Table 2.18. Low LODs and LOQs were obtained, with validation levels (0.5, 30, and 90 ng mL^{-1}) confirming very good accuracy (71.4-124.4 %) and repeatability (1.9-18.2 % RSD). The data in Table 2.18 was

obtained using deuterated analogs for each analyte, but calibration without an IS was also examined using

PBS (selected analytes can be seen in Figure 2.61). DART relies on surface desorption, and the analyst

is typically unable to control what happens outside of the MS region. If random/uncontrolled movements

occur during the desorption process, the ion chronograms will be affected, causing fluctuations in the
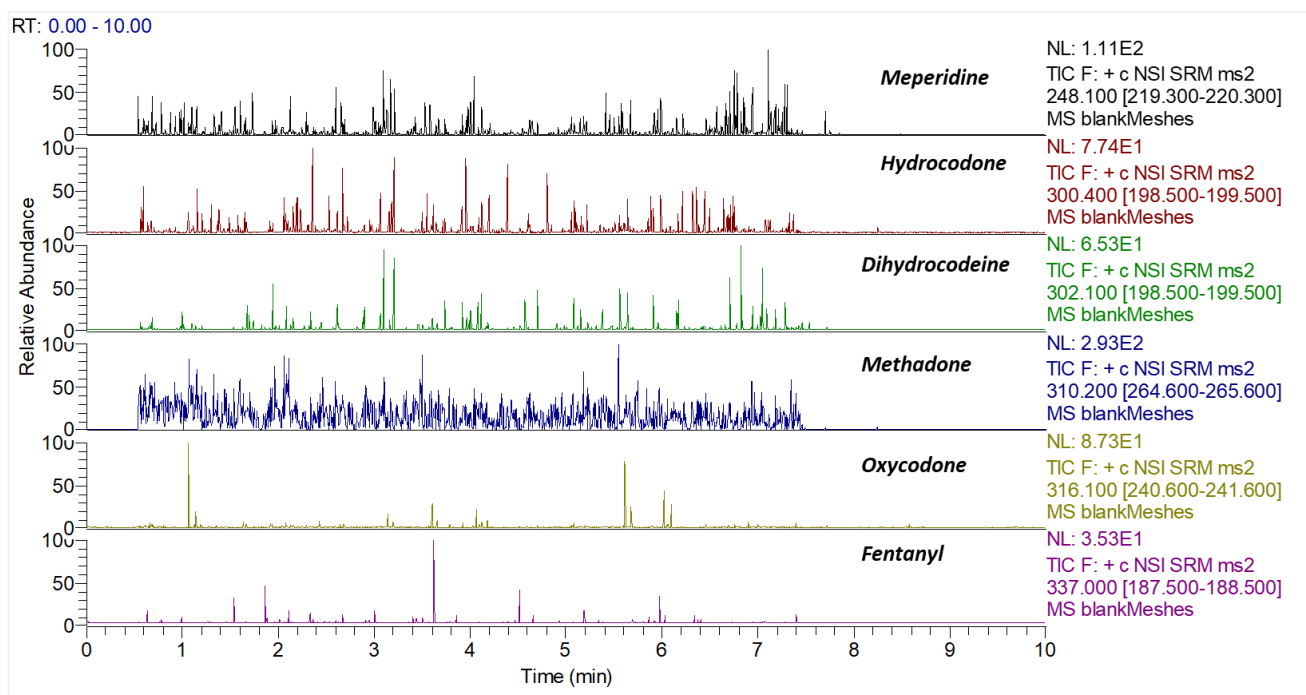
Figure 2.59 *Ion chronogram obtained for the signal assessment of mesh only (i.e. no extraction, only cleaning and preconditioning of the mesh) for the targeted analysis of meperidine, hydrocodone, dihydrocodeine, methadone, oxycodone, and fentanyl.*

signal areas and leading to higher % RSDs.[257,258] Therefore, quantitative analysis for DART is more

robust if an IS implemented. However, ISs can be quite expensive for a single compound or may require

special synthesis. Therefore, it is worthwhile to investigate calibration without the use of an IS. Gómez-

Ríos et al.[117] examined IS-free calibration for the quantification of pesticides (metalaxyl, pyrimethanil,

cyprodinyl, and pyriproxyfen) in grape juice, finding that linearity was maintained up to 10 ng mL^{-1} (on

a LDR up to 100 ng mL^{-1}). The loss of linearity observed in this study was attributed to either source or

detector saturation.[117] Figure 2.60 shows uncorrected calibration plots of the target analytes used in this

research. The obtained calibration plots showed that linearity was predominately maintained at lower

concentration levels (up to 50 ng mL^{-1}), while deviation was observed at higher concentration levels (mostly beginning at 100 ng mL^{-1}). As with the loss of linearity, this deviation could also be attributed

Table 2.18 Figures of merit obtained for the quantification of selected opioids in PBS.

Analyte	LOD (ng mL^{-1})	LOQ (ng mL^{-1})	R^2	LDR	Validation level; accuracy (RSD, %, n = 3)		
					0.5 ng mL^{-1}	30 ng mL^{-1}	90 ng mL^{-1}
Fentanyl	0.1	0.5	0.9995	0.5-200	115.0 (3.5)	108.6 (4.5)	109.5(2.6)
Oxycodone	0.1	0.5	0.9981	0.5-200	123.6 (11.4)	89.8 (4.0)	100.3 (3.0)
Hydrocodone	0.1	0.5	0.9952	0.5-150	71.4 (18.2)	129.4 (6.2)	110.3 (2.4)
Meperidine	0.1	0.5	0.9975	0.5-200	97.3 (2.7)	82.9 (1.9)	97.9 (5.7)
Methadone	0.1	0.5	0.9996	0.5- 200	84.8 (4.5)	104.8 (3.4)	109.5 (5.9)
Dihydrocodeine	1.0	2.5	0.9986	2.5- 200	-	93.5 (3.7)	98.2 (3.1)

to detector saturation. In order to increase the method's LDR, one could desorb a smaller amount of SPME extraction phase into the MS by either using a faster rail speed or decreasing the extraction times.[117]
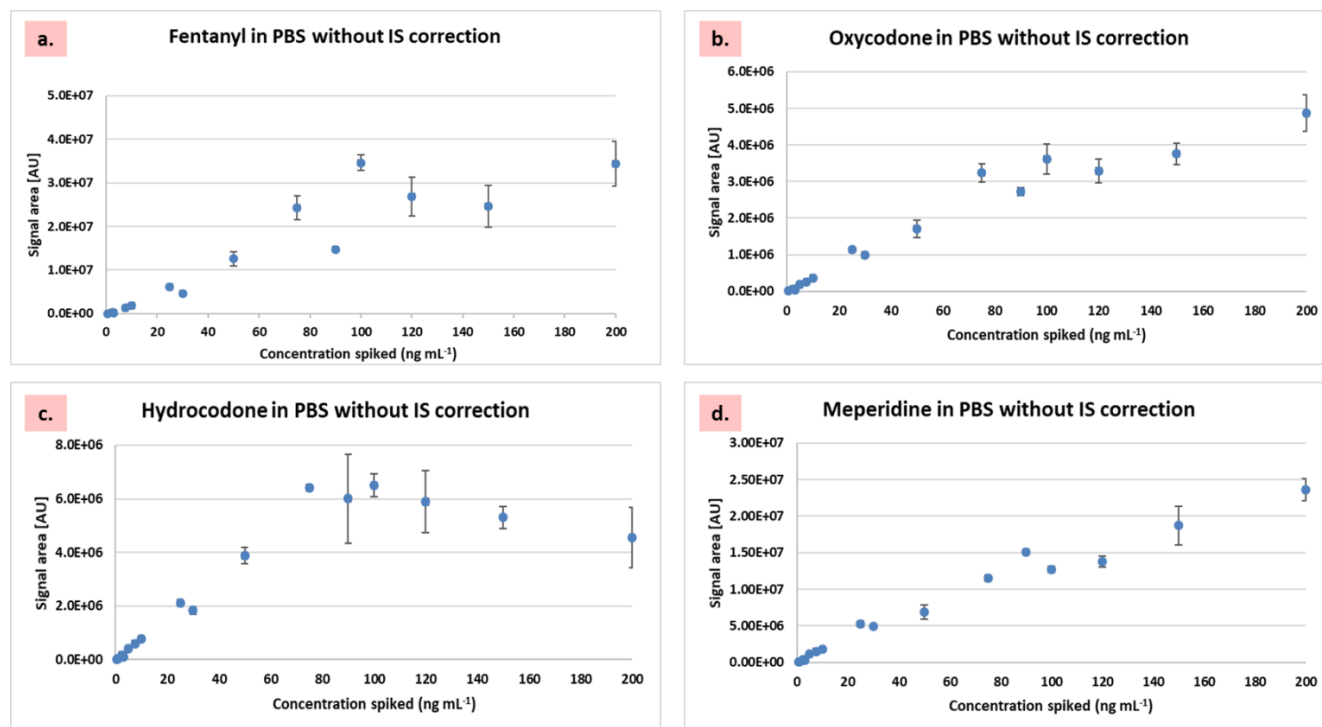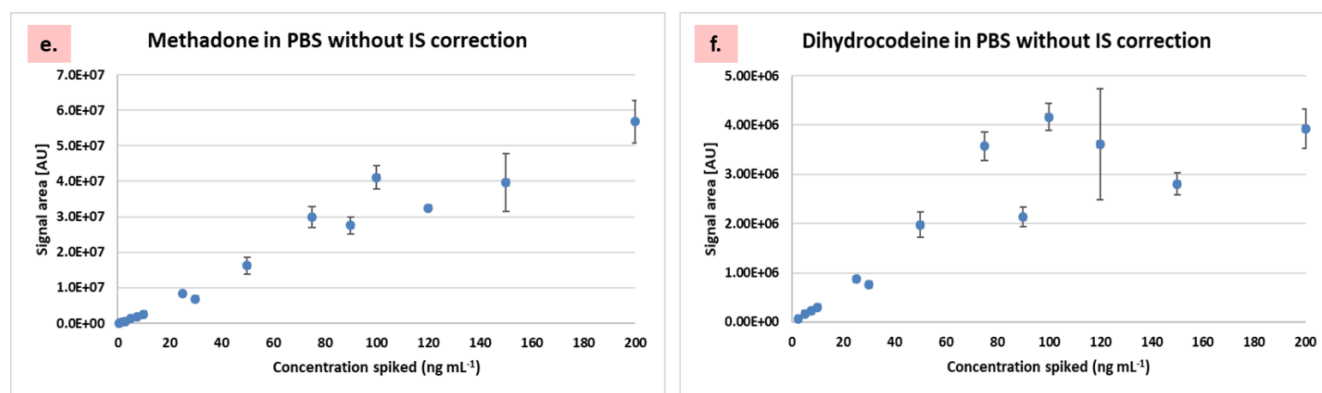
Figure 2.60 *Assessment of opioid (n = 3) quantification in PBS (1.2 mL, 10-min extraction, 450 °C, pH 7, and 0.3 mm s^{-1}) without the use of an IS for: **a.**) fentanyl, **b.**) oxycodone, **c.**) hydrocodone, **d.**) meperidine, **e.**) methadone, and **f.**) dihydrocodeine.*

Urine

At present, the drug market is experiencing a marked supply-driven expansion (particularly for cocaine and opioids), and this expansion has highlighted the need to increase the throughput of certain tests, like urine toxicology.[256] Urine toxicology is one of the most common procedures performed in analytical laboratories worldwide, as the matrix is available in large quantities, collection is minimally invasive, and its analysis can accurately detect the presence of drug metabolites.[259] Hence, tools like 96-SPME-TM-DART-MS could alleviate the high workloads faced by toxicology labs. Table 2.19 lists the obtained results for the quantification of selected opioids in urine. As can be seen, there is a notable increase in the LOQs of oxycodone and hydrocodone (25 ng mL^{-1}) when compared to mere PBS. In the case

Table 2.19 *Figures of merit obtained for the quantification of selected opioids in urine.*

Analyte	LOD (ng mL^{-1})	LOQ (ng mL^{-1})	R^2	LDR	Validation level; accuracy (RSD, %, n=3)		
					0.5 ng mL^{-1}	30 ng mL^{-1}	90 ng mL^{-1}
Fentanyl	0.1	0.5	0.9989	0.5-200	76.6 (4.6)	102.6 (3.0)	103.5 (4.3)
Oxycodone	5.0	25.0	0.9923	25-200	-	93.7 (9.7)	101.5 (1.8)
Hydrocodone	5.0	25.0	0.9789	25-150	-	96.2 (9.8)	105.3 (1.3)
Meperidine	2.5	7.5	0.9976	7.5-200	-	87.4 (4.6)	103.1 (24.0)
Methadone	0.5	2.5	0.9996	2.5-200	-	103.1 (0.7)	100.6 (1.6)
Dihydrocodeine	-	-	-	-	-	-	-

of dihydrocodeine, the selected MS/MS transitions (see Fig. 2.61) produced an elevated signal for the blank urine sample, thus making it difficult to quantify this compound. This difficulty could be due to a combination of factors, including the co-extraction of an interference with the same transition and/or the poor ionization of the analyte when it is in the presence of the matrix. Nonetheless, the validation levels for all of the other compounds provided good accuracy (71.4-129.4 % RSD) and repeatability (1.3-24 % RSD). In addition, the LOQs obtained are below the urine cut-off points suggested by CLR.[223]
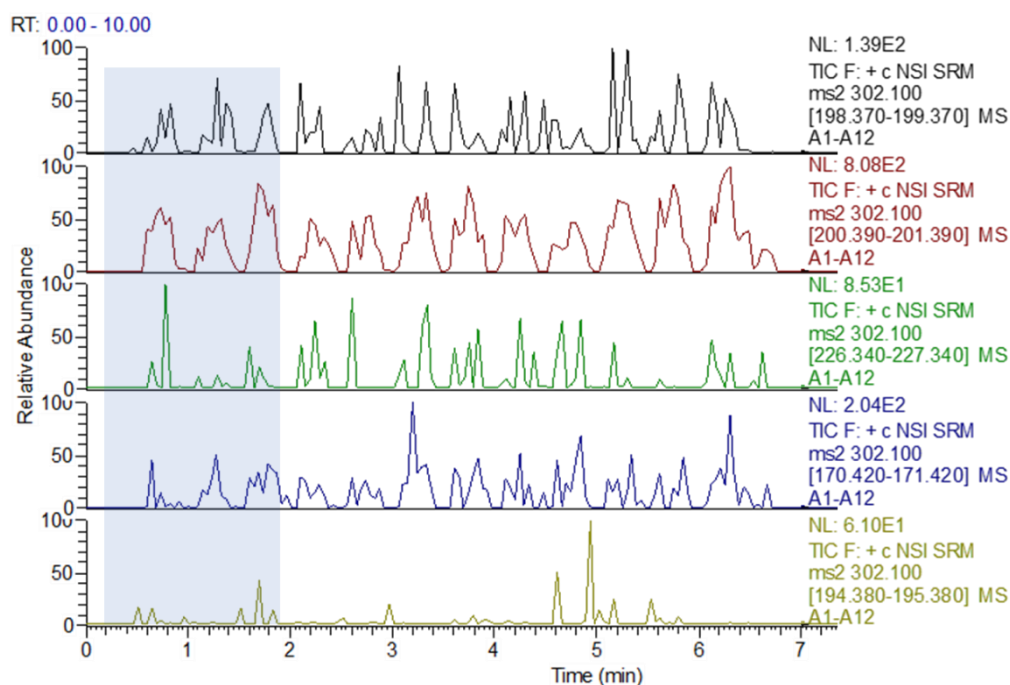
Figure 2.61 *Monitoring of different MS/MS transitions for dihydrocodeine (302.1 → 198.9, 200.9, 194.8, 170.9, 226.8) in urine for a blank sample and 0.5, 1, and 2.5 ng mL^{-1} spiked samples (all tests were performed in triplicate using 1.2 mL of sample, a 10-minute extraction time, a pH of 7, agitation on an orbital shaker at 500 rpm, 450 °C, and a track speed of 0.3 mm s^{-1}). The portion highlighted in blue indicates extractions from urine blanks. The transitions obtained from the TSQ Vantage during the optimization procedure included 198.9, 200.9, 194.8, 170.9, and 226.8, with 198.9,[3] 200.9,[4] and 226.8 being the most commonly reported transitions in the literature.*

Plasma

Given plasma's complexity[260] and the heavy binding of some target analytes to its constituent proteins,[32] one can expect the detection limits to increase when compared to PBS and urine. For the plasma experiments, we utilised a 3/4 dilution with PBS. Although the majority of reports indicate an expected drop in plasma protein binding when a dilution is utilised,[32] this study was not concerned with

determining the % of plasma protein binding . Table 2.20 lists the results for the quantification of opioids in plasma. Certain analytes, such as oxycodone, meperidine, and dihydrocodeine, had higher LOQs when compared to PBS, which is partially associated with the elevated signal of the target compound on plasma blank (i.e., the co-extraction of a compound with a similar MS/MS transition). The obtained values for the validation point assessments had an accuracy of 86.6-108% and a repeatability of 2-11.2 % RSD. The 0.5 ng mL^{-1} validation point was not examined as it was below LOQ values. Except for methadone, the LOQs of the reported opioids are higher than cut-offs proposed by Marin et al. for serum or plasma.[261]

Table 2.20 *Figures of merit obtained for the quantification of selected opioids in plasma.*

Analyte	LOD (ng mL^{-1})	LOQ (ng mL^{-1})	R^2	LDR	Validation level; accuracy (RSD, %, n = 3)		
					0.5 ng mL^{-1}	30 ng mL^{-1}	90 ng mL^{-1}
Fentanyl	0.5	1.0	0.9950	1-200	-	86.6 (4.0)	93.0 (2.3)
Oxycodone	2.5	25.0	0.9938	25-200	-	89.6 (11.3)	101.3 (2)
Hydrocodone	0.5	2.5.0	0.9974	2.5-75	-	104.2 (13.2)	-
Meperidine	5.0	25.0	0.9998	25-200	-	114.8 (6.8)	94.1 (5.2)
Methadone	2.5	10.0	0.9974	10-200	-	90.9 (5.4)	105.5 (8.5)
Dihydrocodeine	2.5	25.0	0.9797	25-200	-	73.4 (4.3)	103 (1.1)

Considering the extraction and desorption time taken to perform analysis of 96 samples with the system presented herein, the total analysis time is approximately 30 s per sample. This includes extraction and desorption time. This is comparable to other SPME-AIMS technologies like CBS (29 s)[245] and open port probe (15-20 s).[205] In PS, drying time (minutes, in some cases hours)[182,196,262] and spraying times[196,263] (seconds to minutes) tend to vary with applications, but total analysis times usually is not excessively long. When compared to hyphenated techniques like LC/MS[264,265] (where processing can take hours), analysis time is significantly reduced with the 96-SPME-TM. Techniques like RF report analysis time of 45 minutes for 384 wells or 7 s per sample,[266] but it is important to keep in mind that, unlike SPME, RF

138

requires significant plasma pre-processing.[267] Hence, one must carefully consider processing times as well as limitations of techniques prior to proceeding with a choice.

2.6.4   Conclusion for Section 2.6

A HT 96-SPME-TM system for DART-MS analysis was developed as a potential solution to the growing demands related to clinical testing faced by laboratories worldwide. This study has not only shown how HT and AIMS can play a key role in solving this demand issue, but it has also highlighted some of the challenges that must be addressed before AIMS can be considered a viable validated option for commercial laboratories. Significantly, the proposed system's applications are not limited to clinical settings; rather, it can be used in the environmental and food-safety sectors, which also face high demands[242]. Regardless of which field this system is applied in, its ability to reduce the amount of time spent on sample preparation and monitoring direct coupling reactions will enable analysts to utilize their time more efficiently. The development of a fully automated robotic system that can take the 12-mesh strip (with extracts), mount it onto the rail, trigger the desorption step, and repeat the procedure for the next strip is one example of an innovation that could make DART and HT 96-SPME-TM even more productive. Moreover, the development of an integrated SPME-DART system, wherein one robotic component handles the extraction stage while the other performs mesh mounting and subsequent desorption, may prove to be an even more effective option. While there are existing engineering challenges to realizing this vision, the availability of such systems would undoubtedly prove extremely useful for the industry.

2.7 Single-Use Poly(etheretherketone) Solid-Phase Microextraction-Transmission Mode Devices for Rapid Screening and Quantitation of Drugs of Abuse in Oral Fluid and Urine via Direct Analysis in Real-Time Tandem Mass Spectrometry

2.7.1 Introduction

Within the field of forensic science, there is a great need for a highly-robust and reliable tool that can rapidly detect the presence of DoAsx in biofluids.[92] Driving under the influence of drugs (DUID) is a very serious criminal offense that can have dire consequences. According to the Canadian Centre on Substance Abuse, substance use played a primary role in approximately 34.2 % of fatal car crashes in 2010.[268] Due to an increase in such accidents, many methods have been developed to detect commonly abused prohibited substances in OF[269–274] and urine.[269,275,276] These methods generally use a chromatographic step as a confirmatory test, which places a time restraint on the whole procedure. This is especially problematic in DUID cases where obtaining reliable results rapidly is of prime importance. While still requiring extensive validation procedures for wide acceptance as a confirmatory method, it is unsurprising that AIMS[84,193] has received considerable attention from forensic scientists, as this group of technologies is capable of rapidly determining target compounds while also reducing or avoiding the need for sample preparation, eliminating the chromatographic step, requiring minimal or no solvent use, and decreasing the overall time required to complete the process. Among the diverse array of AIMS techniques, DART has been of particular interest in forensic science. This technology uses heated and highly energetic He gas to desorb/ionize compounds from surfaces of various materials.[87,91,277] Although DART can reveal important qualitative information about the forensic sample, its applicability for quantitative analysis was plagued in the beginning because it lacked the ability to normalize the sample (*i.e.,* a homogenous and reproducible mechanism for introducing the analytes into the MS-system from one sample to the other). In an attempt to solve this issue, Prof. Fernandez's group developed a mesh-like device with fixed geometrical characteristics (*i.e.,* strand size, pitch-to-pitch distance, percentage

opening) that provided better control over sample introduction.[115] This device, known as TM, allowed gas to flow more efficiently through the mesh, which permitted better ion-transmission and reproducibility.[115] Although this technology enabled the sample to be pragmatically positioned in front of the MS system (*i.e.,* a spot of the sample is dried on the mesh prior to analysis), its lack of sample preparation prevented a dramatic enhancement in the limits of detection. In this regard, one of the sample preparation tools that has been successfully implemented with many AIMS techniques is SPME.[27,117,278] Depending on the experimental conditions, compounds of interest, and matrices under investigation, SPME can extract either a "small" amount of analyte (also known as negligible depletion), or it can be used in cases in which a significant amount of analyte is extracted (i.e., exhaustive extraction).[7] SPME is cleverly designed, comprising the immobilization of a small amount of extractive material (coating) onto a designated substrate.[7] This sample preparation tool has seen a rapid increase in bioanalytical applications over the last few years due to the development of matrix-compatible coatings[49,63,211,279,280] that allows SPME devices to be directly introduced into complex matrices, which in turn leads to negligible biofouling and remarkable target analyte extraction. In addition, SPME features efficient sample cleanup, which reduces issues related to ionization suppression and ionization enhancement.[281,282] Indeed, SPME is no stranger to DART, and diverse geometrical SPME formats (e.g., fiber, in-tube, mesh) have been interfaced with DART in numerous applications.[63,165,283–285] Nonetheless, as the Pawliszyn team has recently demonstrated,[26,117,134] the best results are obtained when SPME is implemented as a TM substrate. For instance, cocaine and diazepam were quantified in sub ng mL^{-1} levels in urine and plasma samples using SS meshes that were adequately coated only on the strands with a C18-PAN slurry.[26] Furthermore, it has been documented elsewhere how mesh coated with HLB particles can be used to efficiently detect pesticides in different food matrices.[117,134] Over the last few years, various substrates have been used for the immobilization of extractive materials in SPME[17,286–288] devices, the most recent example being polybutylene terephthalate (PBT) plastic support, which was

developed by Reyes-Garcés et al.[19] PBT proved to be a very useful material for single-use SPME, as the device provided satisfactory results for drug quantitation in plasma, urine, and blood, while also being very robust. PBT-based devices also showed no interferences from being used as a material in the method.[19] It is evident that the use of alternative materials opens up a diverse array of potential applications for SPME; for example, on-site road testing. Given the rise in DUID accidents over the last few years, the primary goal of this research was to develop a single-use device that can be interfaced with DART, and that can eventually be used for rapid, *in vivo*, on-site drug detection. In order to fulfill such a requirement, it is essential to use a biocompatible material. As such, PEEK was selected in order to fulfill the substrate biocompatibility requirement.[289] PEEK is a semi-crystalline polymer known for its great mechanical stability, a property arising from its aromatic structure,[290] which can be seen in Figure 2.62. In addition, PEEK is thermoplastic material, with a melting temperature of 343 °C,[291] and, with the exception of 98 % sulfuric acid, it is chemically inert to most solvents and acids.[292] It is important to note however that in certain cases target analytes can be highly non- polar, so a careful investigation
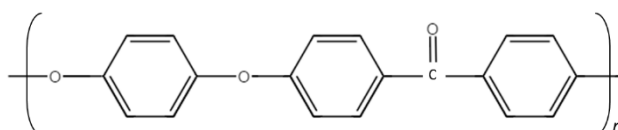
Figure 2.62 Structural formula of PEEK

of potential analyte adherence to plastics should be done prior to their use.[259] PEEK's biocompatible feature has allowed it to be used in dental surgery[293] and maxillofacial reconstruction,[294] as well as in spinal,[295] orthophedic,[296] and cardiac implants.[297] Given PEEK's many benefits, we decided to apply SPME coating to a PEEK-based mesh to rapidly detect and quantitate drugs in OF and urine via DART-MS/MS. Different parameters were evaluated, such as coating robustness under strong agitation or high temperatures, as well as mesh reusability. Encouraging results led us to apply disposable SPME-TM meshes to quantitatively determine DoAs in *ex vivo* OF and urine analysis. In addition, we attempted a

semi-quantitative analysis of caffeine concentration in an OF sample obtained from a volunteer who had recently consumed coffee. Certainly, the results obtained show that SPME has tremendous potential as a simple, effective device for roadside drug testing.

2.7.2 Experimental

Chemicals/Materials

The following standards were obtained from Cerilliant (all standards had a concentration of 1000 mg L^{-1}): cocaine, methamphetamine, nordiazepam, fentanyl, MDMA, heroin, phencyclidine (PCP), oxazepam, methadone, oxycodone, lorazepam, LSD, heroin, diazepam, caffeine and nicotine. The respective IS(s) were also ordered from Cerilliant (all at a concentration of 100 mg L^{-1}), namely: cocaine-d3, methamphetamine-d5, MDMA-d5, PCP-d5, nordiazepam-d5, oxazepam-d5, methadone-d3, oxycodone-d3, lorazepam-d4, LSD-d3, heroin-d9, diazepam-d5, fentanyl-d5, caffeine-C^{13}, and nicotine-d4. A pooled batch of urine and OF was collected by having 10 healthy individuals (5 male and 5 female) each expectorate into a 10 mL vial. PBS was made in lab and details are available for Section 2.2.2. In addition, a female volunteer provided 1mL of OF to measure for caffeine levels. For this test, OF was collected after a 24h caffeine fast, followed by collection at 5 minutes, 1 hour, 3 hours, and 5 hours post coffee consumption. PAN, DMF, NaCl, KCl, KH_2PO_4, Na_2HPO_4, and FA were all purchased from Sigma Aldrich. LC/MS-grade H_2O, IPA, ACN, and MeOH were purchased from Fisher Scientific. The HLB particles were purchased from Waters and removed from the SPE cartridge for use.

DART-MS/MS and LC-MS/MS

A DART-SVP® model ion source (IonSense, Inc.) was coupled to a QqQ mass spectrometer (TSQ Vantage) by Thermo Scientific via a Vapur® interface (IonSense, Inc.). The needle valve of the membrane pump used with the Vapur® interface was adjusted to the blue indicator at position 4 in order to maintain adequate MS vacuum and provide sufficient sensitivity required for quantitative analysis via DART-TM. The DART-SVP® was fitted with a single-dimensional motorized linear rail that was

controlled through the DART-SVP® web-based software in order to reproducibly and consecutively automatically position the SPME-TM devices in front of the DART source (a speed of 0.2 mm s^{-1} was used). In order to guarantee good reproducibility and higher throughput of the desorption process, a custom-made holder (UW-12) able to allocate up to 12 SPME-TM devices was used.[26] The DART source was operated using the following conditions: +ve ionization mode; HV electrode (−3000 V); discharge electrode (+350 V); and a grid voltage of +350 V. The gas heater was optimized at 350 °C in order to yield the optimum intensities for most of the analytes. LC-MS/MS conditions are detailed in section 2.5.2. MRM details are listed in Tables 2.1, 2.8 and Table 2.21.

Table 2.21 *TSQ Vantage details of model analytes used in this investigation. logP obtained from PubChem.*[156]

Analyte	logP	Parent (m/z)	Product (m/z)	CE	S-lens
MDMA-d5	-	199.1	165.0	12	61
PCP	4.69	244.2	86	12	49
PCP-d5	-	249.2	86	12	55
Nordiazepam	2.9	271	243	20	141
Nordiazepam-d5	-	276	213	28	111
Oxazepam	2.24	287	241	21	133
Oxazepam-d5	-	292	246	22	101
Lorazepam	2.39	321	275	21	117
Lorazepam-d4	-	325	279	21	117
Diazepam	2.82	285	193	30	139
Diazepam-d5	-	290	198	21	139
Caffeine	−0.07	195	138	19	64
Caffeine-C13	-	198	148.1	19	19.3

Preparation of PEEK mesh for SPME-TM coating

A 12×12 cm mesh piece was cut and cleaned in IPA and H_2O for 15 minutes by sonication. The meshes were then dried (100 °C) and etched for 90 s on both sides using an ATC-2020-IM ion mill (AJA International, Scituate, MA) at a setting of 400 V and 190 mA. The meshes were then purged with N_2 and left in a desiccator to ensure that the coating application remained unaffected by possible contaminants and moisture. A paper cutter was used to obtain mesh strips (2.5 × 0.5 cm, length by width).

Images of the mesh were taken using an Olympus microscope (SZX10) with a SC30 digital camera, and SEM images were acquired using a Zeiss FESEM 1530.

Application of HLB-PAN coating to the meshes

PAN solution was prepared by dissolving 7 g of PAN powder with 100 mL of DMF via periodical vortexing to ensure uniform dissolution. Oasis HLB particles were used to prepare the slurry for the coating application. Since the size of the particles (30 μm) was large for the application, the particles were ground using a ball mill for 2 h at 240 rpm. The ground particles were then collected, and 1 g was mixed with 10 mL of PAN solution to obtain a final HLB-PAN slurry. The slurry was then stirred for 12 hours at 1800 rpm to provide adequate mixing of particles with PAN. The mixture was applied to the meshes by dip-coating using an in-house method[26] developed at the UW. After the mixture had been applied, excess solvent was removed via gas pressure, and the coating was then cured at 100 °C. In order to facilitate the handling of the meshes, the meshes were attached to PBT with soldering tool to provide extra support (*i.e.,* thermally attached). The meshes were then cleaned twice in a solvent solution consisting of MeOH/IPA/ACN (50/25/25) at 1500 rpm for 15 minutes to remove any leftover chemicals from the polymerization or coating procedures. To activate the extractive sites on the particles, the meshes were preconditioned in a mixture of MeOH/H_2O (50/50).

Evaluation of coating mesh endurance

 The evaluation was conducted by exposing a new set of coated PEEK meshes to DART's thermal desorption (350 °C, 0.2 mm s^{-1}). After the first thermal desorption, the meshes (n = 5) were preconditioned and used to perform extraction from a PBS sample that had been spiked with 50 ng/mL of cocaine. After extraction, the meshes were desorbed in solvent (MeOH/ACN/FA, 80/20/0.1) for 20 minutes using an agitator at 1800 rpm.[211] LC-MS/MS analysis[211] was then used to determine the meshes' ability to retain their extractive capacity after one exposure to the DART source. Once the solvent had been desorbed, the same meshes were cleaned with the MeOH/IPA/ACN (50/25/25) mixture and

exposed to thermal desorption using the DART source (350 °C, 0.2 mm s^{-1}) for a second time. The meshes were then preconditioned, and a PBS sample spiked with 50 ng mL^{-1} of cocaine was once again used to perform the extractions. The amount extracted was determined using solvent desorption. LC-MS/MS analysis was conducted to determine the extractive ability of the meshes after a second exposure to DART source. The entire procedure was repeated until the total number of thermal desorptions for the meshes was five. The amount extracted after each thermal desorption was compared to the amount extracted from a mesh that was never exposed to thermal desorption.

Extractive procedure for OF and urine

Stock solutions for all studied analytes and their respective deuterated analogues were made and the two matrices were spiked at the appropriate concentrations (0.5, 1, 2.5, 5, 10, 25, 50, 75, 100, 125, 150, 175, 200 ng mL^{-1}) for the calibration plot and the validation points (8, 40, 80, 140 ng mL^{-1}). The IS was spiked at a fixed level of 10 ng mL^{-1}, and all spiking was conducted so as to keep the organic content in the matrices below 1 % in order to simulate a "real" sample and to prevent any effects from the solvent during the extraction step.[7] For the semi-quantitative measurements of caffeine, a calibration plot for caffeine was made in PBS; this calibration plot consisted of nine calibration levels (*i.e.,* 1, 5, 10, 50, 100, 250, 500, 750, 1000 ng mL^{-1}). Caffeine-C$^{13}_3$, spiked at 50 ng mL^{-1}, was used as an IS. After spiking, both complex matrices, urine and OF, were gently agitated on a vortex at 200 rpm for at least 2 hours to allow for proper equilibration between the analytes and the matrix. Prior to extraction, the meshes were briefly washed with H$_2$O to remove the organic content which can affect the extractive capabilities of the mesh (i.e., disturbance of partition equilibria between analytes and coating)[7,20] and then gently blotted with a KimWipe. The extractions were conducted by directly immersing the mesh into the vials containing the spiked samples. The extraction process was carried out according to a published procedure that consists of rapidly agitating the sample at 3200 rpm for 1 minute.[26]A 700 µL sample was used for urine analysis following a 10 sec agitated wash step in H$_2$O. OF analysis was also carried out under the same agitation

conditions for 1 minute; however, a smaller volume (300 µL) and a longer wash step of 12 s were used. The longer wash step was employed due to OF's viscosity and to remove any potential food residue that may have adhered to the mesh. Extraction of caffeine was done under the same agitation conditions described above, but, as with OF, a smaller volume was used (300 µL), and the extraction time was also reduced to 30 s in order to reduce the prospect of detector saturation. It is important to note that caffeine concentration in OF is very high (mg L^{-1} levels) immediately following coffee consumption.[298] Thus, in order to avoid potential detector saturation and to fit the instrumental calibration, OF samples were diluted 1/100 with PBS. The dilution factor was chosen according to Liguori et al.'s results.[298] Upon completion of the above extractions, the meshes were inserted into an in-house-developed mesh holder and subsequently analysed.[26]

2.7.3 Results/Discussion

Evaluation of PEEK as material for TM

PEEK was chosen as a substrate for this study due to its attractive properties, which include: biocompatibility, inertness to the majority of solvents, and relatively greater stability when exposed to high temperatures. When choosing the proper PEEK substrate, it is worth remembering that the mesh robustness is extremely important, as sturdy connections between the filaments within the mesh are essential for a successful extraction and desorption process. Initially, the robustness of two meshes from two different providers was tested by exposing them to 100 °C in an oven. Although the first mesh tested (mesh opening: 450 µm, strand size: 200 µm, open area: 48 %; GoodFellow, Mississauga, ON, Canada, part #346-012-62, Figure 2.63a.,c.) allowed for successful coating application, it was not chosen for further experimentation because the filament attachment weakened after exposure to 100 °C (see Figure 2.63e., g., and i.). Conversely, the second PEEK mesh, ordered from Building Materials Express (mesh opening: 220 µm, strand size: 75 µm, open area: 56 %), exhibited much better performance following

exposure to a high temperature (see Figure 2.63b., d., f., h., j. and 2.64); therefore, it was chosen for further experimentation.
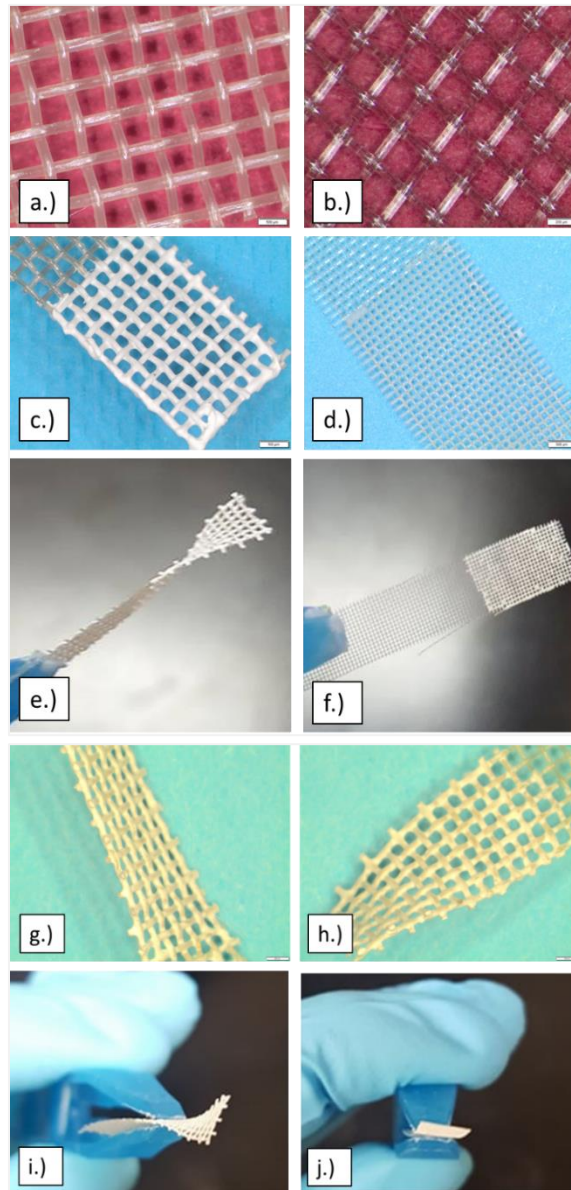
Figure 2.63 *Mesh models assessed for the study. Bare PEEK mesh (part #346-012-62) ordered from Goodfellow **(a.)** with a 450 µm mesh size, 200 µm monofilament diameter, and an open area of 48 %, and bare mesh ordered from Building Materials **(b.)** with a 220 µm mesh size, 75 µm monofilament diameter, and an open area of 56 %. Inserts **(c.)** and **(d.)** show both mesh types coated with HLB particles from Waters. The meshes were exposed to 100 °C for two minutes in a GC oven, and, as can be seen in **(e.)**, the mesh from Goodfellow showed significant filament deformation, while the mesh from Building Materials **(f.)** remained the same. Figures **(g.)** and **(h.)** show a more detailed view of the deformed mesh purchased from Goodfellow. Figures **(i.)** and **(j.)** represent top view of the deformed Goodfellow mesh, and the Building Materials mesh, respectively.*

Stability and analytical performance of PEEK SPME-TM

Ultimately, PEEK meshes were developed for the purpose of performing *in vivo* OF sampling. To achieve the full potential of such an application, we had to ensure that proper coating stability was achieved. In order to examine proper coating attachment on the meshes, the meshes were inserted into a vial containing a mixture made of MeOH/IPA/ACN (50/25/25) and agitated at high speed in a vortex (*i.e.,*3200 rpm) for one minute and then again at 1800 rpm overnight (~12 h). After agitation, the meshes were observed under a microscope, which revealed no changes in the coating. In addition, the SEM images show good attachment between the particles and the substrate (Figure 2.64d-e.). The PBT support that had been affixed to the mesh via soldering iron also proved stable as no de-attachment occurred (Figure 2.64f). Another important point of consideration in assessing stability was whether the meshes would be able to withstand exposure to the DART source's high temperature. Thus, a stability test was
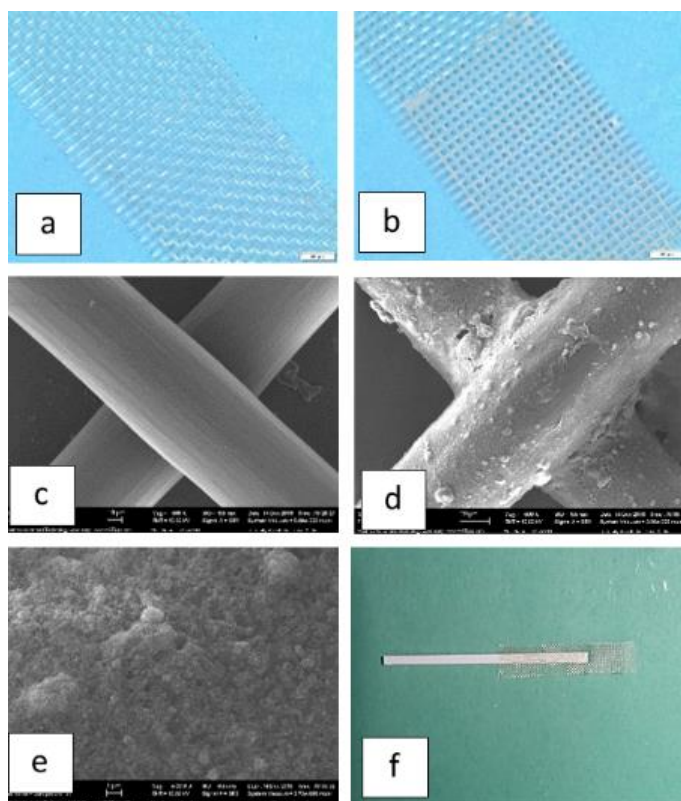
Figure 2.64 (a.) Bare PEEK mesh without any coating attached; (b.) mesh coated with the HLB particles; (c.) SEM of bare mesh at 500x magnification; (d.) SEM of coated mesh at 500× magnification; (e.) close-up of HLB particles attached to mesh at 5k× magnification; and (f.) coated mesh attached to the PBT support.

conducted by exposing the meshes to the DART source at 250, 300, and 350 °C. Temperatures beyond 400 °C were not explored due the PEEK's reported melting point of 343°C.[289–291] However, as noted by prof. Fernandez's group the temperature indicated by the DART software is generally higher than the temperature of the region where the heated gas comes into contact with the coated surface;[145] hence, it was not a concern that the material would be compromised at the set temperature of 350 °C. Indeed, the unravelling of mesh filaments was not observed (see Figure 2.63f. and Figure 2.64).

Mesh repeatability was assessed by performing a rapid extraction (1 min) from a vial containing PBS solution spiked with 50 ng mL^{-1} of cocaine. Analysis was performed via LC-MS/MS to eliminate any errors associated with the desorption/ionization step, and, as such, to enable a strict evaluation of the coating's repeatability. To determine the amounts of cocaine extracted, the meshes were desorbed in a 80:20:0.1 MeOH/ACN/FA solvent mixture already described elsewhere.[211] After the first desorption, the meshes were cleaned twice using the above-mentioned cleaning solution mixture, and the obtained samples were additionally analysed for carry-over. The results obtained for mesh repeatability (n = 5) can be seen in Figure 2.65. The amount of cocaine extracted by the meshes varied from 12.5-16 ng, with
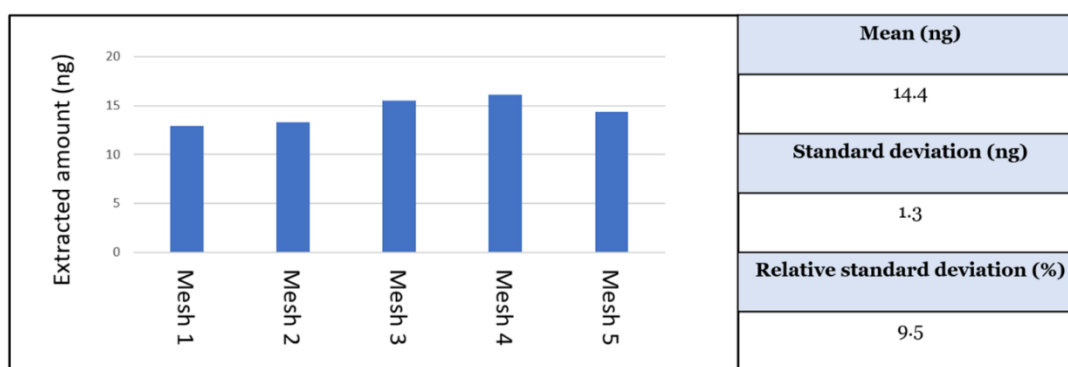
Figure 2.65 *Assessment of mesh repeatability performed by extracting cocaine from a 50 ng mL^{-1} PBS spiked sample and subsequently desorbing it in 80/20/0.1 MeOH/ACN/FA solvent mixture for LC-MS/MS analysis.*

a mean of 14.4 ± 1.3 ng, and a % RSD of 9.5 % (without IS correction). These results were quite satisfactory given the short and non-automated extraction process. The cleaning solutions were tested for carryover, but the amounts remaining on the mesh were below the LOQ of the experiment. The analytical

performance of the PEEK meshes was further compared to that of SS meshes[26] (mesh opening: 250 μm, strand size: 90 μm, open area: 55%). For this comparison, both the SS and PEEK meshes were coated with the same ground particles and analyzed under same DART parameters. A sample of PBS was spiked with 50 ng mL^{-1} of heroin, and extraction was carried out for one minute under the above-mentioned conditions (n = 3 for PEEK meshes; n = 3 for SS meshes). The two meshes were compared by monitoring the product ion of heroin (m/z 370→165), with the resultant ion chronograms revealing comparable analytical performance between PEEK and SS meshes (see Figs. 2.66 and 2.67).
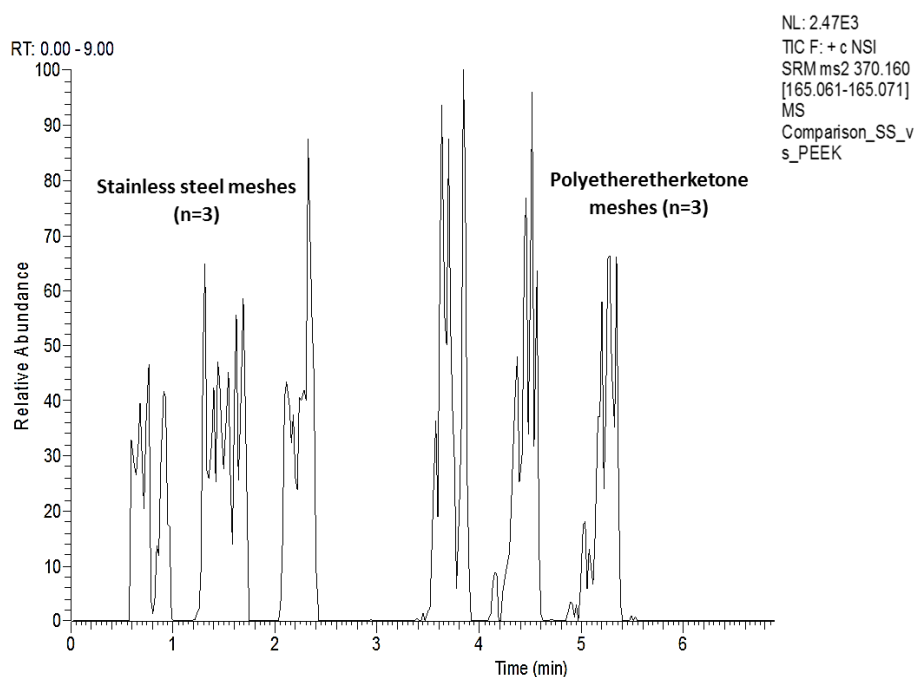
Figure 2.66 *Comparison of signal responses of SS meshes, and PEEK meshes. Ion chronograms obtained after extraction from 1.5 mL of PBS spiked with heroin (50 ng mL^{-1}) when using SS meshes (left) and PEEK meshes (right).*

Assessment of potential re-usability

Even though the plastic meshes are intended to be single use, the possibility of reusability was also investigated. Reusability was assessed by running the meshes in front of the DART source six times at 350 °C at a rail speed of 0.2 mm s^{-1}. After each run, the meshes were washed in a MeOH/IPA/ACN mixture and preconditioned in MeOH/H$_2$O for at least thirty minutes. After the preconditioning step, the
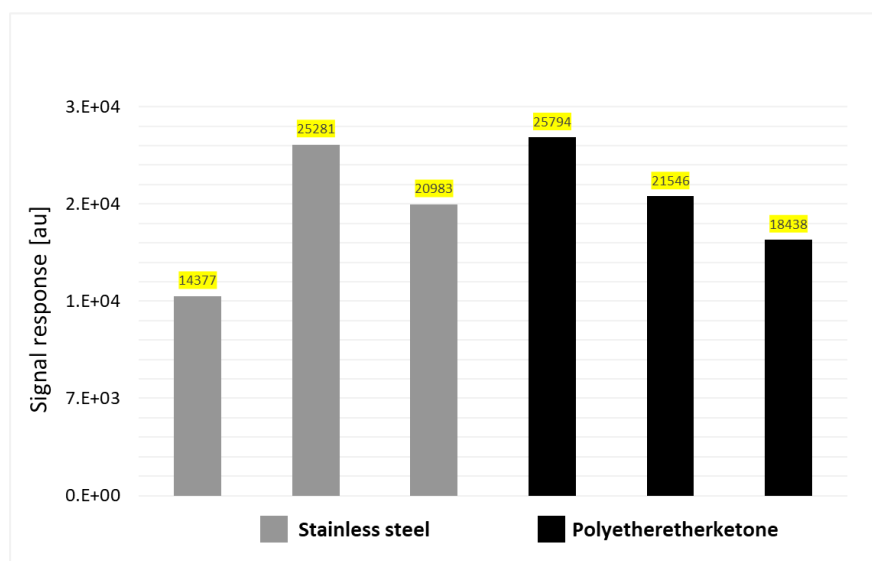
Figure 2.67 *Signal response (in arbitrary units; au) obtained for ion chronogram in Figure 2.66 for SS meshes (n = 3) and PEEK meshes (n = 3). The respective values obtained for each mesh are highlighted in yellow above the bars.*

meshes were used to perform an extraction from PBS spiked at 50 ng mL^{-1} with cocaine, followed by a brief wash step and solvent desorption in 300 µL of MeOH/ACN/FA (80/20/0.1) mixture. The LC-MS/MS conditions used for the run have already been described (see Section 2.5.2). As can be observed in Figure 2.68, extraction capability drops by approximately 37 % after DART desorption. A one-tailed student's T-test and a one factor analysis of variance (ANOVA) was conducted ($\alpha = 0.05$) to assess whether there is a significant difference between the meshes prior to and after exposure. The calculated p-values (< 0.001) revealed a significant difference in the amounts of cocaine extracted after the meshes had been re-used. An SEM image was also obtained in order to investigate the mesh surfaces and revealed that noticeable cracking in the coating occurs after five exposures (Figure 2.69). Nonetheless, this instrumental drop is expected due to the solid coating's repeated exposure to a DART source temperature of 350 °C. Ultimately, the meshes still retain their extractive ability and can be easily implemented as screening tools. Therefore, mesh reusability was only tested aiming to evaluate the robustness of the device. Yet, PEEK SPME-TM devices are not intended to be reused when dealing with real samples so to prevent false positives/negatives due to inadequate performance.
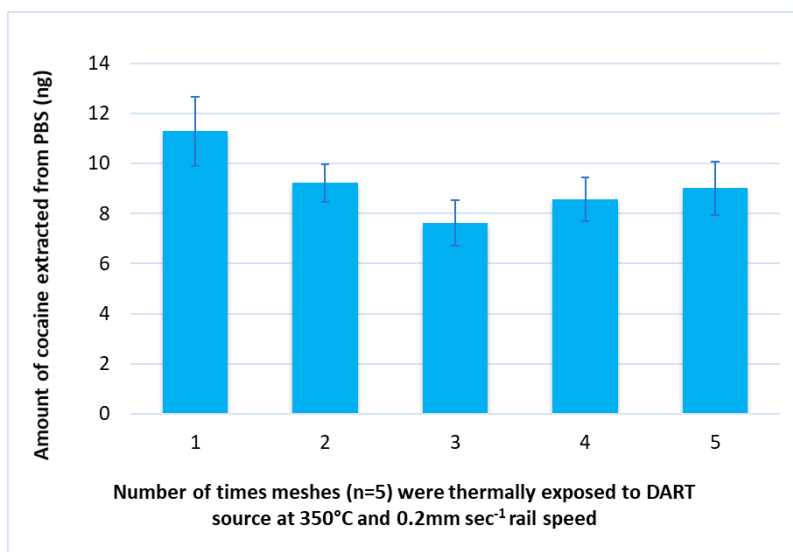
Figure 2.68 *Assessment of mesh reusability and retainment of extractive capacity done by performing repeated exposure of the mesh to DART source. The chart shows the amount of cocaine extracted in ng after five different meshes were exposed and run in front of the DART source five times at 350 °C using a rail speed of 0.2 mm s^{-1}.*
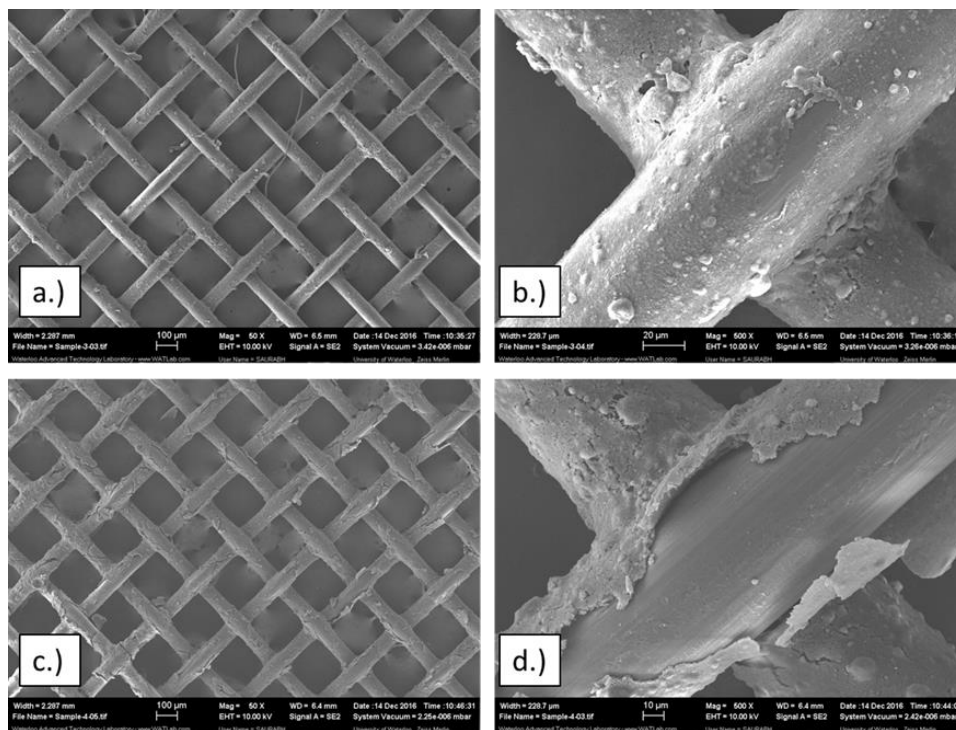
Figure 2.69 *SEM images of PEEK mesh in (**a.**) and (**b.**) before exposure to DART source. Images obtained after a single mesh has been exposed to the DART source five times (**c.** and **d.**) at 350 °C and 0.2 mm s^{-1}.*

153

Detection and quantification of drugs of abuse in urine and oral fluid

Oral fluid

The successful demonstration of the PEEK meshes' robust performance paves the way for further *ex vivo* quantitative studies with both OF and urine. The use of OF as an alternative matrix in drug detection has been on the rise in the last few years due to ease of collection, minimum invasiveness, and remote potential for adulteration given that the collection can be carried out by the authority.[299] Recently, there has been a rise in the number of publications on AIMS and OF drug analysis[300–302] focusing on screening-related questions, as well as some quantitative studies. The primary motivation for using OF in this work is to contribute to efforts to make rapid on-site detection with simple tools a reality. SS meshes could be used for *in vivo* application, but the sharp edges and the metallic flavor (potentially enhanced by the use of concentrated HCl for mesh etching) may be inconvenient for *in vivo* use. For example, filaments can become damaged and cause an injury to oral cavity. In addition, storage of SS meshes for extended times in strong solvents may lead to corrosion. Hence, PEEK has an advantage in relation to potential *in vivo* sampling due to its smoother surface, inertness and flexibility. These characteristics make the placement of the mesh on the tongue or buccal mucosa more convenient. Additionally, the use ion milling for etching makes PEEK mesh fabrication more environmentally friendly. The volume used for OF analysis was maintained at 300 µL in order to simulate this matrix's limited availability. In general, OF is relatively less complicated to work with when compared to more complex matrices such as blood and plasma, which consist of higher amounts of protein.[280] In fact, OF is composed of 99 % H_2O, with the remaining 1% consisting of proteins, electrolytes, enzymes, urea, ammonia, and immunoglobulins.[213] As it can be seen in Table 2.22, remarkable figures of merit were obtained for the selected analytes despite their diverse physicochemical properties (*e.g.,* logP). Although extraction was rapid (1 min), it was nevertheless sufficient for preconcentrating the analytes and establishing very low detection limits.[26] The LODs and LOQs were calculated based on S/N ratios of 3 and 10, respectively. The majority of values

Table 2.22 *Figures of merit for the determination of drugs of abuse in OF using coated PEEK mesh via DART-MS/MS*

Analyte	LOD (ng mL^{-1})	LOQ (ng mL^{-1})	R^2	LDR (ng mL^{-1})	Cut-off (ng mL^{-1})[223]	Validation levels; accuracy (RSD, %, n=3)			
						8 (ng mL^{-1})	40 (ng mL^{-1})	80 (ng mL^{-1})	140 (ng mL^{-1})
Oxycodone	0.5	1.0	0.9956	1.0-200	100-300	113.2 (1.7)	106.7 (3.5)	99.7 (4.8)	94.2 (1.6)
Heroin	0.5	2.5	0.9978	2.5- 100	-	96.4 (10.7)	88.7 (10.1)	100.9 (6.8)	-
MDMA	2.5	10	0.9913	10- 200	5	-	90.5 (1.8)	106.4 (0.8)	99.4 (4.8)
Methamphetamine	2.5	25	0.9955	25- 200	500	-	95.5 (4.6)	95.8 (3.4)	102.3 (5)
Oxazepam	1.0	2.5	0.9963	2.5- 200	100	126.8 (3.6)	114.8 (8)	107.1 (3)	103 (2.3)
Cocaine	0.1	0.5	0.9924	0.5-100	150	114.8 (6.1)	101.2 (6.8)	100.7 (1.8)	-
Lorazepam	0.5	2.5	0.9936	2.5- 75	100	121.9 (2.7)	120.1 (0.6)	-	-
Diazepam	0.5	2.5	0.9999	2.5- 125	100	81 (6.6)	121.8 (2.8)	116.4 (5.5)	-
Nordiazepam	1.0	2.5	0.9983	2.5- 200	-	86.1 (10.2)	91.7 (3.3)	94.1 (4.9)	97.3 (3.5)
LSD	0.5	2.5	0.9906	2.5- 200	0.1	93.5 (10.4)	116.1 (4.4)	111.1 (4.3)	100.8 (3.4)
Methadone	0.5	1.0	0.9952	0.5- 200	200	119.3 (3.5)	90 (4)	83.2 (1.5)	97.6 (2.2)
Fentanyl	0.5	2.5	0.9978	2.5- 125	1-5	88.3 (11.8)	94 (3.1)	88.1 (6.8)	-
PCP	1.0	2.5	0.9980	2.5- 175	25	121.6 (3.3)	112.1 (4)	108.3 (4.8)	102.8 (0.8)
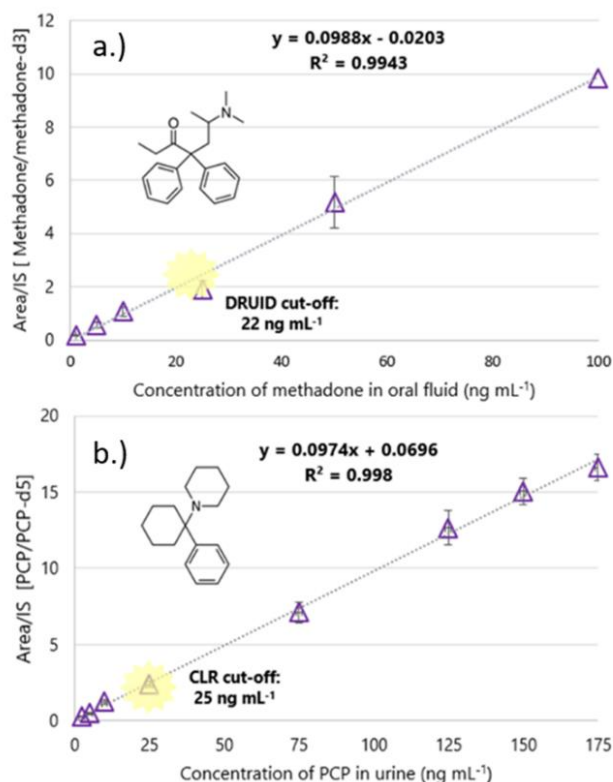
Figure 2.70 *Detection and quantification of methadone (**a.**) and PCP (**b.**) in OF and urine, respectively. The highlighted points in (**a.**) and (**b.**) represent the cut-off levels used for these drugs by regulatory agencies, such as DRUID and CLR.*

reported in this research are considerably lower than the values required by agencies such as SAMHSA,[189] and DRUID.[190] To account for any variation during the desorption ambient ionization process, IS calibration was chosen.[303] The method's LDR was maintained in the 0.5-200 ng mL^{-1} range, with acceptable precision (< 11 %). Regarding validation points for OF, the majority of data accuracy falls within the 83-115.1 % range. Validation points such as 8 ng mL^{-1} and 140 ng mL^{-1} could not be tested for some analytes because they fall below the LOQ or above the upper LOQ. At the lowest validation point of 8 ng mL^{-1} certain analytes (oxazepam, lorazepam and oxycodone) exhibit accuracy between 79.6-121.1 %, while MDMA's accuracy lies at 75.1 %. At 40 ng mL^{-1} some analytes (methamphetamine, diazepam, fentanyl and PCP) lie in the 119-128 % accuracy range, which could be related to co-extracted small molecules from OF with similar SRM transitions to the ones of the target analytes. An example of a calibration curve for quantifying methadone in OF can be seen in Figure 2.70(a.). In addition, it is worth noting that the 12 s rinsing step successfully removed food debris remaining on the mesh, which could have potentially caused major interferences in the analysis. Another notable factor was the use of HLB, which is a highly-wettable material that is capable of providing wide analyte coverage.[19,117,134] Calibration plots of some selected analytes (nicotine, MDMA and fentanyl) are shown in figure 2.71b., d. and f., respectively.

Urine

Although OF shows great promise for use in toxicological investigations, urine is most commonly used for drug detection at present due to its availability in large quantities. The regulatory limits for urine cut-off levels were taken from cut-off & toxicity levels for DoAs testing from the CLR;[223] as Table 2.23 shows, the large majority of LODs and LOQs achieved by the tests in this study were lower or close to those imposed by the CLR (with the exception of LSD where regulatory level of 0.1 ng mL^{-1} was not met). For example, we managed to achieve an LOQ for PCP in urine that was ten times lower than the level required by the CLR (Figure 2.70(b)). The SPME-TM device's large SA allows for improved sensitivity,[26,117,134] particularly at low ng mL^{-1} levels when compared to the fiber geometry.[165] The LDR

of the method was maintained in the 0.5-200 ng mL^{-1} range, with acceptable precision (< 11 %). The validation points for urine gave satisfactory results, with the accuracy levels ranging from 83.9-115.1 %. However, certain analytes (oxazepam, lorazepam, nordiazepam, methadone, PCP) ranged from 119-127

Table 2.23 *Figures of merit for the determination of drugs of abuse in urine using coated PEEK mesh via DART-MS/MS.*

Analyte	LOD (ng mL^{-1})	LOQ (ng mL^{-1})	R^2	LDR (ng mL^{-1})	Cut-off (ng mL^{-1})	Validation levels; accuracy (RSD, %, n=3)			
						8 (ng mL^{-1})	40 (ng mL^{-1})	80 (ng mL^{-1})	140 (ng mL^{-1})
Oxycodone	0.5	5.0	0.9970	0.5-100	-	79.6 (1.8)	86.3 (7.1)	99.7 (4.8)	92.8 (6)
Nicotine	2.5	5.0	0.9941	5-175	-	108.4 (7.2)	107.8(11.1)	105.9 (6.6)	92.0 (9)
MDMA	1.0	5.0	0.9949	5-200	270[190]	75.1 (4.8)	108.8 (5.6)	111.5 (6.8)	101.5 (10.2)
Methamphetamine	1.0	5.0	0.9917	5-200	410[190]	115.9 (4.3)	119.3 (2.4)	115.1 (3.2)	107 (5.9)
Oxazepam	0.5	1.0	0.9948	1-100	13[190]	121.2 (7.1)	106.8 (4.9)	109.9 (4.6)	-
Cocaine	0.1	0.5	0.9930	0.5-100	170[190]	112.2 (10.9)	111.6 (6.3)	103.1 (8.3)	-
Lorazepam	0.5	1.0	0.9935	1-50	1.1[190]	120.8 (5.8)	97.0 (2.6)	-	-
Diazepam	2.5	5.0	0.9924	5-125	5[190]	83.9 (5.8)	123.2 (4.7)	119 (2.8)	-
Nordiazepam	0.5	1.0	0.9962	1-100	1.1[190]	87.1 (12.3)	86.6 (5.5)	105.5 (3.5)	-
LSD	0.5	1.0	0.9994	5-200	-	101.5 (5.8)	106.7 (1.9)	104.9 (12)	101.6 (5.9)
Methadone	0.5	1.0	0.9943	1-100	22[190]	117.9 (6.6)	88.8 (3.4)	106.6 ((4.8)	-
Fentanyl	0.5	2.5	0.9988	2.5-125	-	109.7 (8.1)	128.1 (1.8)	110.1 (8.7)	-
PCP	0.5	5.0	0.9923	5-200	25[189]	115.4 (3.7)	122.0 (1.5)	108.1 (5.2)	93.4 (5.0)

% at 8 ng mL^{-1}. At 40 ng mL^{-1}, lorazepam and diazepam were slightly elevated, giving an accuracy of 120.1 % and 121.8 %, respectively. The cause of these elevated levels could be contributed to MEs (particularly at lower validation levels) carrying the same MS/MS transition as the analytes of interest. It is possible that matrix enhancement occurred due to co-extraction of small molecules present in urine.[304] Additional calibration plots for selected analytes nicotine, MDMA and fentanyl are shown in Figure 2.71a., c. and e., respectively. It is worth mentioning that the detection of compounds with lower molecular weights (m/z < 150) at low concentration levels may yield higher detection limits due to the intrinsic level of background signal exhibited by DART for such compounds (e.g. when monitoring an extraction from a blank sample or even ambient air). For instance, the LOQ of a compound with small
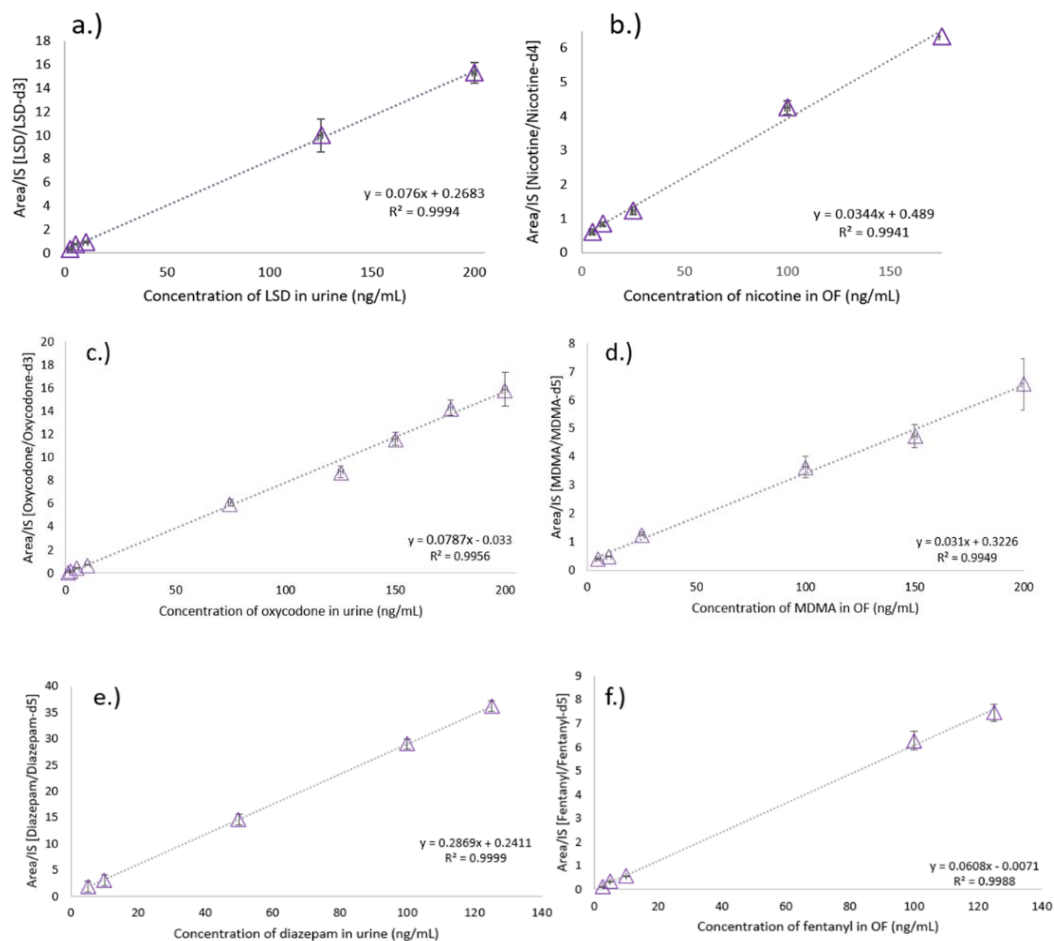
Figure 2.71 *External calibration curves with IS correction of selected analytes in urine for LSD (**a.**), oxycodone (**c.**) and diazepam (**e.**) and OF for nicotine (**b.**), MDMA (**d.**) and fentanyl (**f.**).*

m/z value, like methamphetamine, was 25 ng mL^{-1} in the case of urine, and 5 ng mL^{-1} for OF. In cases where major product ion yields higher background noise, it is advisable to investigate other transitions as they may give better results for quantification using DART (see Figure 2.72 for an example of monitoring of 2 transitions of amphetamine). It is important to note that the LDR for the majority of the compounds was adequate up to the highest calibration point (i.e., 200 ng mL^{-1}); the lone exception to this was lorazepam, for which detector saturation started occurring at lower concentration levels (~ 50 ng mL^{-1}; see Figure 2.73). When compared to OF, urine required a shorter rinsing step of 10 s to allow for sufficient mesh clean-up. It is possible that some co-extracted components were additionally introduced into the MS, but the use of MS/MS capabilities significantly reduces the chances that those co-extracted components will interfere with the analysis process. In addition, it is also worth noting that

the meshes are miniaturized, which allows for simple and less troublesome on-site handling for authorities.
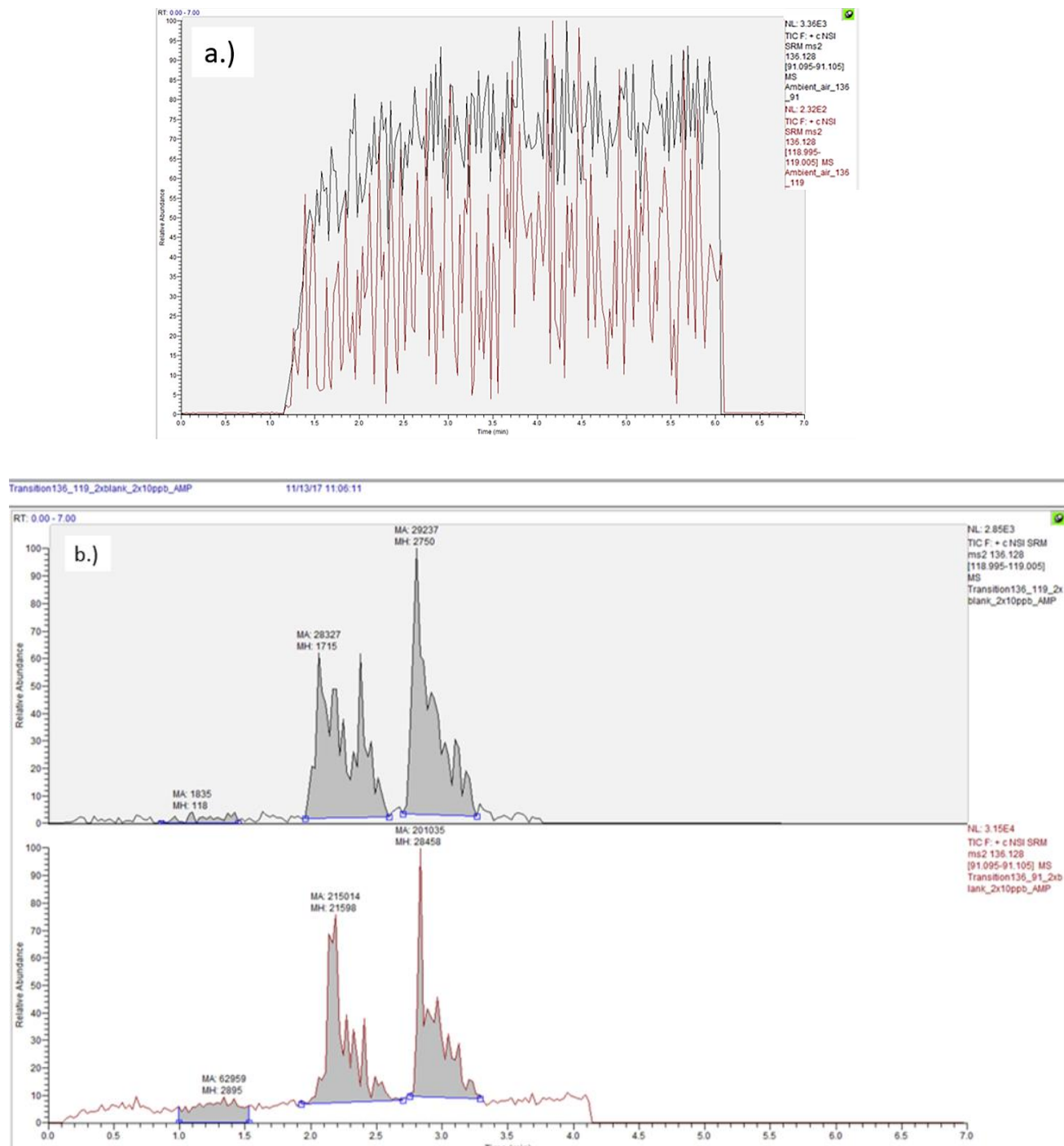
Figure 2.72 MS signal obtained for the SRM channels of amphetamine with DART-MS/MS. Figure (*a.*) shows the overlay of normalized chronograms for amphetamine for monitoring of m/z 136 » 119 and m/z 136 » 91 for ambient air in DART. Figure (*b.*) shows the ion chronograms obtained for desorption of 2 replicates of blank PBS extract and 2 replicates of 10 ng mL^{-1} of amphetamine spiked in PBS for m/z 136 » 119 and m/z 136 » 91. Note that m/z 136 » 119 transition exhibits lower background signal and higher S/N ratio.
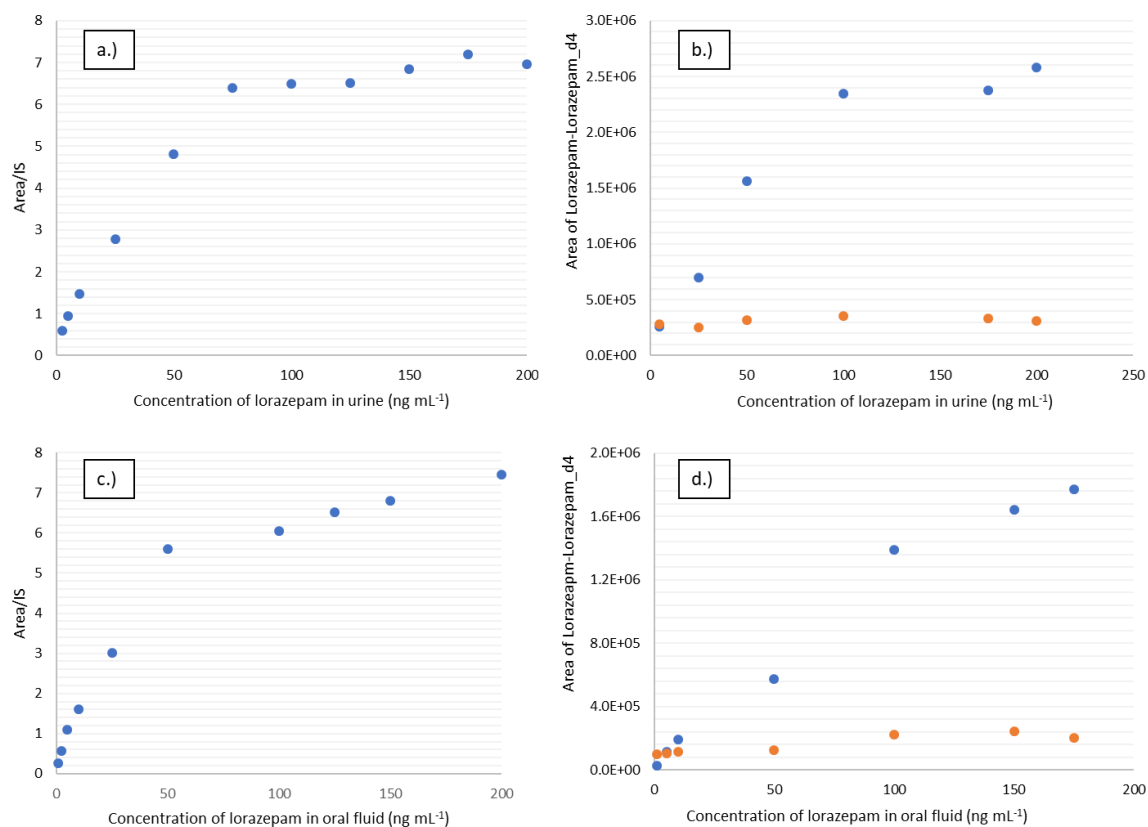
Figure 2.73 *Data obtained for detecting lorazepam in urine and OF with IS correction in (**a.**) and (**c.**), with visible saturation after 75 ng mL^{-1} and 50 ng mL^{-1}, respectively. Figures (**b.**) and (**d.**) show the area obtained for lorazepam (blue) and its IS (orange). The concentration of the IS (Lorazepam-d4) was kept at 10 ng mL^{-1}.*

For example, sample extraction can be carried out on site and immediately processed using a portable instrument for drug detection.[33] If portable instrumentation is not available, the meshes can be stored in a container that allows temperature to be carefully controlled. The influences of diverse storage conditions for these types of samples are currently under investigation in our laboratory.

Caffeine analysis

Since the major objective in developing these meshes is to provide law enforcement officers with a tool for *in vivo* OF analysis, an experiment was conducted in our lab wherein we semi-quantitatively measured caffeine levels in OF from a volunteer at different time points following the consumption of a single cup of coffee. Given that the literature points out that caffeine is typically concentrated in OF at mg L^{-1} levels, the samples were diluted with PBS in order to ensure they were within the instrument's LDR. As a result,

160

a calibration curve was constructed in PBS as shown in Figure 2.74(a.). Furthermore, as can be seen in Figure 2.75, detector saturation was only observed above 1000 ng mL^{-1}. Therefore, a calibration plot with an LDR of 5-1000 ng mL^{-1} was used to calculate the caffeine levels in the diluted OF samples. The results obtained for each point (n = 3) can be seen in Figure 2.74(b.). It is worth noting that the volunteer's history reveals frequent coffee consumption (approximately 2 cups daily), and that 4.6 mg L^{-1} of caffeine were present in the OF sample following 24 hours of caffeine fasting. Five minutes after coffee consumption, the caffeine level was calculated to be 15.3 mg L^{-1}; this figure fell to 7.6 mg L^{-1} one hour after coffee consumption, which is consistent with caffeine's average half-life of 6.2 ± 1.6 hours.[305] The figures for 3 and 5 hours post consumption revealed a small drop to 7.4 and 6.5 mg L^{-1}, respectively. However, it is possible that other processes take place too, such as distribution of caffeine in OF immediately after drinking as well as slower metabolism of caffeine (~ 12 h). The ion chronograms obtained at the different time points can be seen in Figure 2.76. It is important to highlight that this experiment was used to perform a semi-quantitative analysis of caffeine levels in OF, and that one must
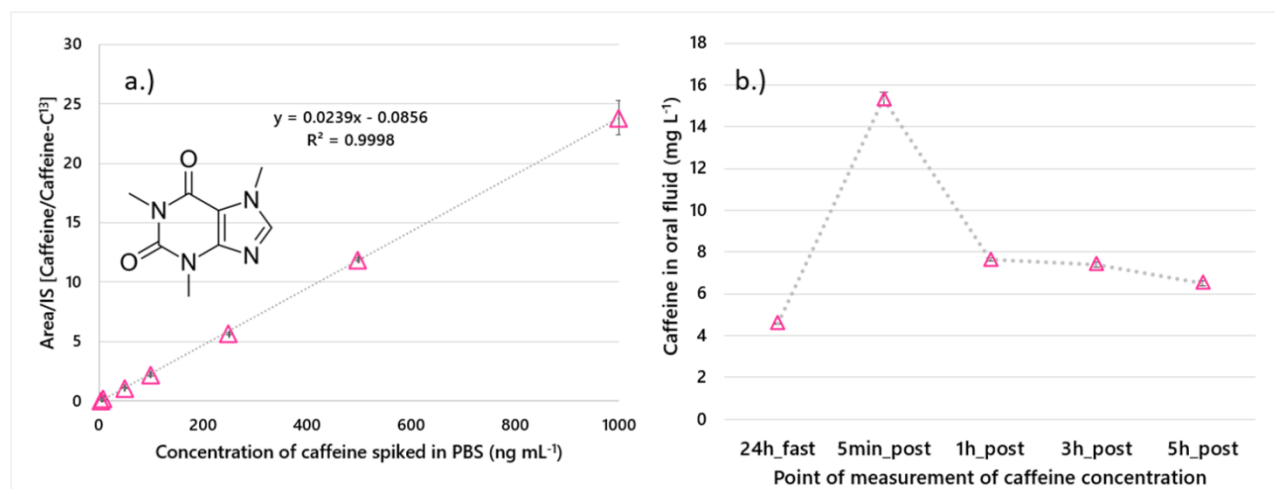
Figure 2.74 *Semi-quantitative caffeine levels measured in the OF of a female volunteer after consumption of a single cup of coffee. Figure (**a.**) shows the calibration curve obtained for spiking caffeine in PBS, while Figure (**b.**) shows the semi-quantitative trend in caffeine levels measured (without the dilution factor) by monitoring caffeine ion's product (m/z 195.1→135.1). The chart includes caffeine levels (n = 3) measured after a 24 h caffeine fast, followed by measurements at 4 different post-consumption time points.*
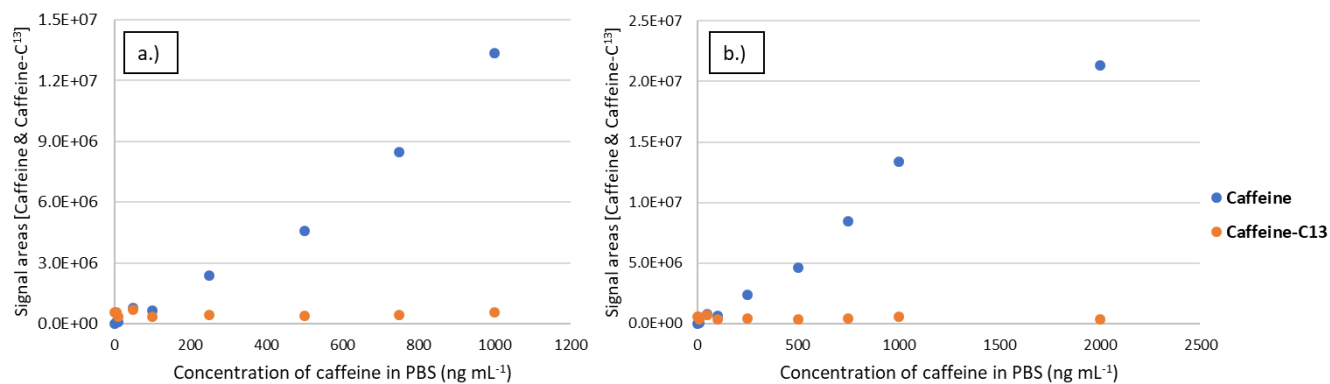
Figure 2.75 *Figure (a.) shows the signal response in au (arbitrary units) of caffeine and caffeine-C^{13} respectively up to 1000 ng mL^{-1} while (b.) shows the same as (a.) but with detector saturation caused by the inclusion of the 2000 ng mL^{-1} point. The concentration of IS (Caffeine-C^{13}) was kept at 50 ng mL^{-1}.*

be cognizant of the fact that MS systems can experience detector saturation at high analyte concentration

levels. As such, the careful planning and execution of experiment is the key to obtaining reliable data.
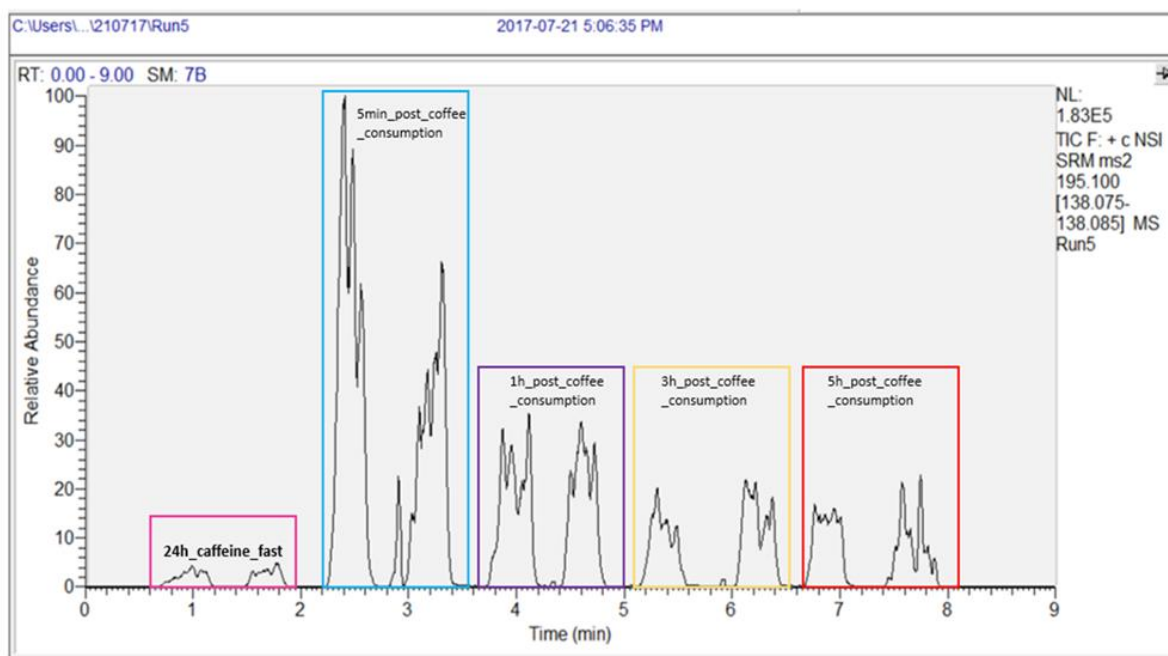
Figure 2.76 *Example of the ion chronogram obtained for detection of caffeine (m/z 195.1 → 138.1) in OF for a 24 h caffeine fast period (2x), 5 min post coffee consumption (2x), 1 h post coffee consumption (2x), 3 h post coffee consumption, and 5 h post coffee consumption (2x).*

162

2.7.4 Conclusion for Section 2.7

This work details the development and application of biocompatible coated SPME plastic mesh for use in screening and quantitating prohibited drugs in OF and urine. The chosen material provided mechanical robustness and good resistance to high temperatures. Furthermore, the gentle ion milling method proved to be appropriate for etching the plastic material prior to the adhesion of the coating. A stability test for SPME-TM-PEEK revealed good coating attachment, as no fall-out was observed during the test conditions, and no issues were observed upon exposure to high temperatures from the DART source. The assessment of the coated PEEK mesh's repeatability provided us with acceptable results, with a % RSD of less than 10 % without IS correction. Similar results were obtained when the plastic mesh was compared to the traditional SPME-TM SS-coated meshes. Drug quantification was successfully performed, allowing us to reach lower or comparable LODs and LOQs required by all the regulatory agencies with the exception of LSD cut-off for urine detection imposed by CLR. In addition, the detection of caffeine levels in OF obtained from a volunteer proved the method's feasibility for on-site analysis. Tests for reusability showed that, although the meshes are intended for single use, they can be reused for screening purposes. This work demonstrates the great potential of these meshes for used in roadside drug testing, given the availability of proper portable DART instrumentation.[134] Currently, our efforts are focused on demonstrating SPME-TM's advantages as an analyte sampling technology for use following conventional sampling protocols with cotton swabs or polymeric adsorbents. Future work will be focused on demonstrating that coated meshes can collect analytes, either from pure OF, or from OF stored in clinically-accepted containers (i.e., stabilizing solution after sampling with adsorbent).

Chapter 3: Development of miniaturized SPME tips coupled to mass spectrometry for targeted determination and untargeted profiling of small samples

3.1 Preamble

Chapter 3 consists of content which has already been published in *Talanta*. The majority of content published in *Talanta* has been included in this chapter, but it also includes portions which have not been published elsewhere. Majority of chapter 3 is published as:[173]

Vasiljevic, T.; Varoon, S. and Pawliszyn, J. *Miniaturized SPME tips directly coupled to mass spectrometry for targeted determination and untargeted profiling of small samples,* Talanta, 2019, 199, 689-697, doi: 10.1016/j.talanta.2019.03.025.

Text, table and figures are reprinted with the permission from Elsevier (Copyright 2019 Elsevier).

I participated in all stages of the development of the SPME minitips, including optimization of its substrate and the coating recipe. I designed all of the experiments and carried them out with the aid of Dr. Varoon Singh. Dr. Varoon Singh provided crucial expertise for the synthesis of the required microporous HLB particles and their characterization. I prepared the manuscript, submitted it and carried out communication with reviewers of Talanta. Dr. Singh aided me in the manuscript writing process.

I, Varoon Singh, authorize Tijana Vasiljevic to use this material for her thesis.

3.2 Introduction

Mass-spectrometric-based small volume analysis has recently become popular within analytical chemistry, with a growing number of publications exploring the development of suitable methods for analyzing small liquid volumes or sampling extremely small organisms (i.e., single cells).[118,130,306,307] Generating sensitive and reliable data for this type of analysis requires a high level of sophistication when it comes to equipment, materials, sensitivity, and even sampling, which may pose a challenge for an inexperienced analyst.[8] To this end, several sample-preparation techniques have emerged as being potentially suitable for analyses of small volumes, including microsampling,[308] DBS,[119] microfluidics,[204] and probe-based sampling.[307]

As the name suggests, probe-based sampling uses a dimensionally reduced probe to perform investigations, either by exposure to a small volume, penetration of the organism under study, or the removal of its contents via aspiration.[309] Removing cell contents via hollow probes (like nESI) is an emerging field,[128,129,131,310–312] but issues related to probe clogging, cost, instrument cleanliness, and associated MEs (no sample clean-up, all cellular contents directly sprayed into MS) have scarcely been addressed. In addition, such approaches are plagued by a lack of selectivity, with trace metabolites being difficult to detect due to ion suppression.[309] In contrast, solid-probe-based approaches rely on directly exposing the probe to the desired sample and performing nonspecific or specific extraction via the probe's coating material. As with nESI tips, solid probes can be ordered, but the material cost is often high.[307,313,314]

Solid probes can be coated with extractive materials, which allows for the pre-concentration of analytes of interest and improved sensitivity. This is important because the coating material ultimately determines the quality of the information obtained. Therefore, in order to achieve optimal selectivity, the physicochemical characteristics of the extractive material should be as close as possible to those of the analytes of interest (in case of charged analytes, coating with ion exchange groups can be used). It is

interesting that many authors have reported using un-coated probes, which rely on non-specific binding between the material (commonly metallic tips) and the compounds.[127,131,307] Although this approach produces results that identify highly concentrated,[25,313,314] mostly lipid-based (500-1000 m/z range), or pre-spiked compounds, it tends to ignore compounds with lower m/z values. As such, the information produced is limited at best. Additionally, a lack of preconcentration means that hyphenated approaches (i.e., chromatography) are generally avoided, which become problematic as sample and data complexity increase. Hence, there is a need for interference-resistant, cost-effective, reproducible and pre-concentrating tool which offers adequate sensitivity and selectivity.

SPME is one technology that meets these criteria. SPME is ideal for probe-based small-volume analyses because its simple design is easily customizable. Its dimensions can be conveniently reduced, and different coatings deposited depending on analytes being investigated. Undoubtedly, drop in sample volume challenges sensitivity of any sample preparation method. For SPME, this issue can be resolved by exploring more efficient extraction phases such as nanomaterials.[315–318] However, the structure of these materials is often altered in order to obtain better extraction efficiency,[319–322] which precludes investigations into the material's ability to provide a broad range of coverage for analytes with different physico-chemical properties. Additionally, some of these materials raise problems, like large biomolecule adsorption,[323,324] batch-to-batch variability and deterioration in the homogeneity of the material,[325] limited extraction capability[326,327] and release of heavy metals into surroundings which can be highly toxic for living organisms.[328] Piri-Moghadam et al. reported the development of SPME "coated tips," which consist of acupuncture needles with tips that have been electrochemically coated in the 150-500 µm range using a biocompatible nanostructured conductive polymer polypyrrole (PPy).[25] The tips were used to extract selected drugs from biological samples (Vs ≤ 20µL), as well as quercetin (70 mg g^{-1} mean, onion skin)[329] from a single cell of onion (*Allium cepa L*). PPy is a conductive polymer that is frequently used for SPME, but, similar to the above-mentioned materials, its properties must be tailored

through the addition of dopants in order to meet different mechanical and extractive requirements.[42] Furthermore, PPy's robustness may pose problems, as the material has poorer stability (breakage) when it is immobilized onto a material like SS.[7]

In this chapter, development of biocompatible HLB-coated miniaturized SPME probes—conveniently named "minitips"—that can be used in small-volume/organism studies, is detailed. Our goal was to develop a tool that would be able to perform three tasks: 1.) efficiently analyze small liquid volumes (Vs < 20μL); 2.) extract samples from small subjects/organisms; and 3.) provide adequate coverage of polar and non-polar analytes. Mousavi et al.[50] extracted over 1000 cellular *E.coli* metabolites within a broad logP range spanning from −7 to 15 using HLB coated SPME thin-film. HLB is a highly wettable (i.e., good interaction with aqueous samples) co-polymer that contains lipophilic non-polar DVB and polar hydrophilic NVP groups, which makes it an ideal sorbent for extracting both polar and non-polar compounds. In this study, we used in-house synthesized microporous (1.3 µm particle size) HLB particles that had been imbedded within an interference-resistant biocompatible binder PAN in order to assess how well HLB performs in small volume analyses, specifically in relation to extraction efficiency, sensitivity, and selectivity (i.e., extracting as many compounds as possible). Cost-effective SS acupuncture needles were used as substrates, carefully etched and dip-coated in the 100-1000 µm length range. The minitips proved to be robust during preliminary performance assessments, which led us to apply the minitips for quantification of DoAs in 1 µL of OF via LC-MS/MS as well as 1 µL of human blood via ambient nESI-MS/MS. Next, a proof-of-concept study investigating the metabolomic profile of four different individual caviar eggs was conducted using the minitips and LC/HRMS. The results showed that this method was able to provide good statistical discrimination between the samples (PCA & PLS-DA), in addition to identifying over 140 significant features.

3.3 Experimental

Chemicals/Materials for the Synthesis of HLB particles

The HLB particles were synthesized using DVB, NVP, and 2,2-Azo bis(isobutyronitrile) (AIBN). HPLC-grade MeOH and ACN were purchased from Millipore-Sigma, and a mechanical stirrer with regulated speed controls (50-2200 rpm) was purchased from Scilogex LLC (Rocky Hill, Connecticut, USA). Temperature was controlled using a magnetic hot plate that was equipped with a temperature sensor; a stirring controller was also purchased from Scilogex LLC. All the monomers were passed through an alumina column to remove inhibitors before being stored in amber coloured vials at −23 °C until further use.

Chemicals/Materials for the Remainder of the Experiments

PAN, DMF, and mesoporous silica nanoparticles (SiNPs) with particle and pore sizes of 200 nm and 4 nm, respectively, were all ordered from MilliporeSigma. LC/MS-grade MeOH, ACN, H_2O, FA and IPA were also purchased from MilliporeSigma. The following compounds were ordered from Cerilliant at concentrations of 1000 mg L^{-1}: diazepam, nordiazepam, oxazepam, lorazepam, cocaine, oxycodone, propranolol, carbamazepine, fentanyl, clenbuterol, cocaethylene, testosterone, benzoylecgonine, and LSD. Corresponding ISs were also ordered from Cerilliant at concentrations of 100 mg L^{-1}: diazepam-d5, nordiazepam-d5, oxazepam-d5, lorazepam-d4, cocaine-d3, oxycodone-d3, propranolol-d7, carbamazepine-d10, fentanyl-d5, clenbuterol (HCl)-d9, cocaethylene-d3, testosterone-C13, benzoylecgonine-d3, and LSD-d3. Diazepam, nordiazepam, oxazepam, lorazepam and their respective ISs constituted a group entitled benzodiazepines (BZDs). A pooled urine sample was created using contributions from one male and one female volunteer, while a pooled OF sample was created using contributions from five healthy individuals (three females, two males). Both matrices were kept at -20 °C prior to use. Human blood stabilised with K2-EDTA and plasma was ordered from BioreclammationIVT

168

and kept at 4°C until use. The caviar samples, which consisted of black lumpfish, red lumpfish, herring, and salmon, were purchased from a local supermarket (Waterloo, ON) and kept at 4 °C until sampling was conducted.

Preparation of the SPME minitips substrates

An MTS50/M-Z8E-Metric-Tapped 50 mm motorized stage with a controller and a PSU was purchased from ThorLabs, Inc. (Newton, MA, USA) and was used to construct an in-house coating station for tip fabrication (Figure 3.1). To ensure repeatability, a liquid-level sensor (conductivity based) was developed at UW (Figure 3.2) and was used to detect the contact point between the tip and the solution. SS acupuncture needles (gauge: 0.18 mm, length: 40 mm), shown in Figure 3.3, were ordered from Electro-Therapeutic Devices Inc. (Markham, ON, Canada). Etching parameters were optimized with respect to etching solution type and concentration, voltage, and time required to etch one tip to a desired shape. With respect to solution type, both KOH and sodium hydroxide were tested, with KOH providing better results. The optimum etching concentration was determined to be 1M KOH, and voltage and etching time were kept at 11 V and 40 s, respectively. After 40 s, the needle was carefully withdrawn from the
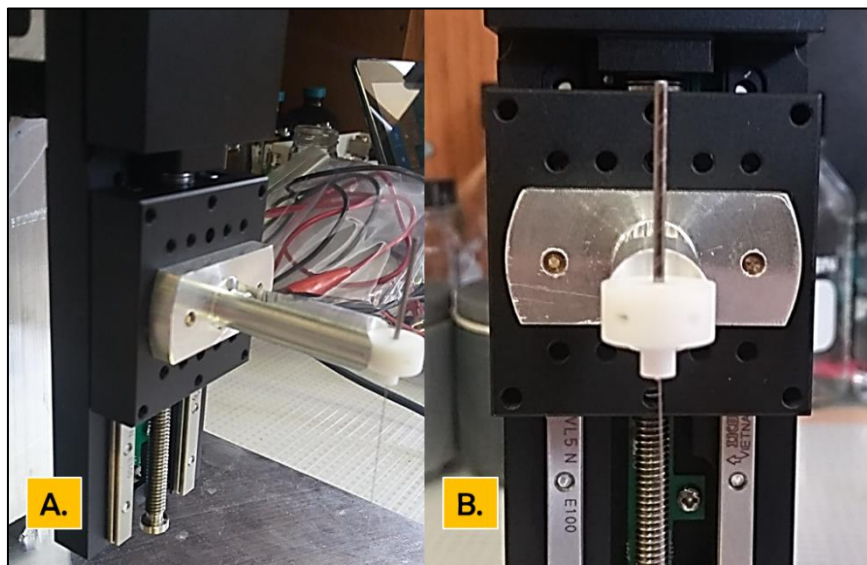
Figure 3.1 *Stage developed in-house at UW for manufacturing the SPME minitips. **A.**) motorized portion of the stage that controls the movement in z-axis; **B.**) Teflon-made holder used to accurately position the acupuncture needles for etching and dip-coating.*
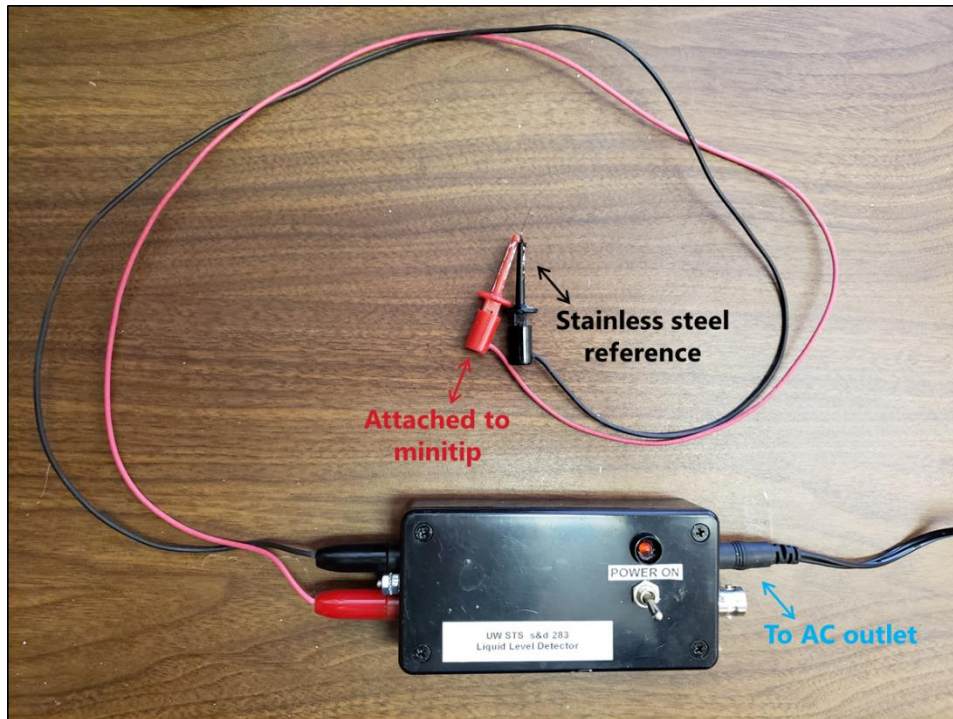
Figure 3.2 *Liquid level sensor developed at the electronic shop at UW.*
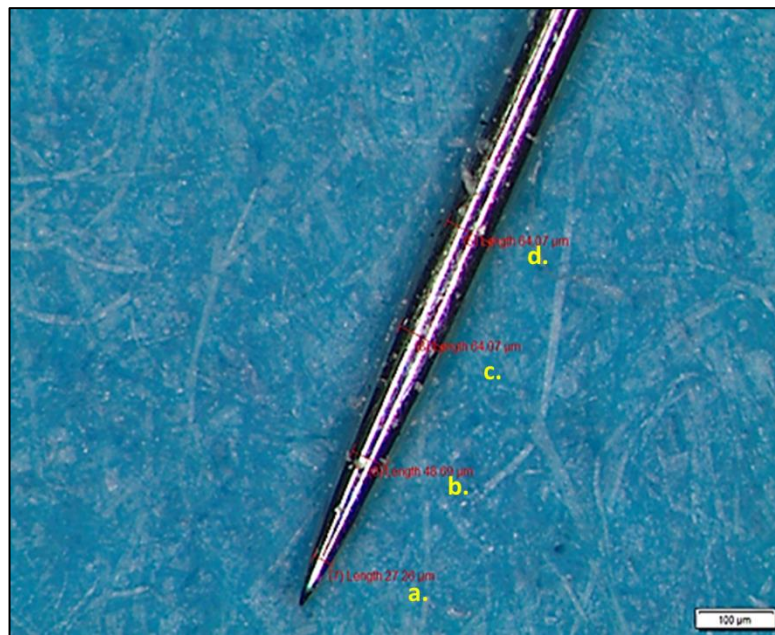
Figure 3.3 *Acupuncture needles ordered from Electro Therapeutic Devices (gauge: 0.18 mm, length: 40 mm). The needle shown here has not undergone any pre-treatment to enhance binding of HLB particles to the tip. Note how smooth the surface of the needle appears. Measurements were made at different points to examine tip diameter, which were 27.2, 48, and 64 μm at **a.**, **b.**, **c.**, and **d.**, respectively.*

etching solution (with voltage still applied) at 0.2 mm s^{-1} to produce a conical shape. The tip was then gently sanded and sequentially cleaned in IPA, acetone (ACE), and H$_2$O. Finally, the tips were dried at 100 °C for 15 min and stored in IPA (to prevent oxidation) until further use.

Synthesis of HLB particles

HLB particles were synthesized via a modified form of precipitation polymerization.[330] In the setup used in this study, 4 mL of DVB and 1 mL of NVP were added to a 500 mL three-necked round bottom flask containing 200 mL of ACN and degassed for 30 min. After 30 min, the reaction was immersed in a preheated oil bath at 70 °C. After immersion, AIBN (20 mg) dissolved in 1 mL ACN was added to the solution, which was then stirred for 24 h using an overhead stirrer equipped with a SS stirring rod containing a Teflon stirring blade. During stirring, the solution is sealed using polytetrafluoroethylene (PTFE) stirring seals for overhead stirrers to preserve the inert environment inside the flask. To avoid losing initiators during the reaction, the polymerization solution was jacketed with N$_2$ above the reaction mixture throughout the reaction. After 24 h, the precipitated particles were separated from the reaction mixture via centrifugation at 10,000 rpm. The obtained HLB particles were then washed with ethanol (EtOH) to remove excess unreacted monomer, oligomers, and/or short chain polymers. The HLB particles were then dried in a vacuum oven at 80 °C for 24 h before being characterized by fourier transform infrared spectroscopy (FTIR) using a Tensor II spectrometer (Bruker Corp., Billerica, MA, USA). Spectrums ranging from 400-4000 cm^{-1} were collected in powder form using a Standard Pike ATR cell. Surface morphology and size were determined via SEM with a Zeiss FESEM 1530, and SA analysis was done using a Quantachrome Autosorb iQ-MP (Boynton Beach, FL, USA) for BET analysis on nitrogen adsorption isotherms obtained at 77.35 K and outgassing at 373 K.

SPME-minitip HLB Coating Procedure

In order to create effective coatings for the minitips, it was necessary to optimize the percentage of PAN binder and HLB particles in the slurry. To this end, the following PAN-to-DMF percentages were

evaluated to determine the optimum binder viscosity: 5, 6, 7, 10, 12, and 20 %. Furthermore, the following percentages of HLB-particles-to-PAN binder were also tested for this purpose: 7, 10, 12, and 20%. The optimum ratio was determined to be 6 % of PAN mixed with 15% of HLB particles. The minitips were coated via dip coating, wherein 6 repeated dips were performed with a withdrawal speed of 3.5 mm s^{-1} (a = 5 mm s^{-2}). Following dipping, each tip was cured at 100 °C for 20 s before being cleaned in a solvent mixture consisting of MeOH/ACN/IPA (50/25/25) and stored in MeOH/H$_2$O (50/50) until further use. Subsequent images of the minitips were taken with an Olympus microscope (SZX100) equipped with an SC30 digital camera (Olympus, Tokyo, Japan).

Preparation of stock standards

Stock mixtures of the studied analytes and their corresponding ISs were made at concentrations of 100 mg L^{-1} and 10 mg L^{-1}. Urine and PBS (used for preliminary investigations) were spiked with appropriate concentrations of the stock solution to construct a 13-point calibration plot (0.1, 0.5, 1, 5, 10, 25, 50, 75, 100, 200, 300, 400, and 500 ng mL^{-1}) for the quantitation of BZDs in these matrices. BZD's internal standards were spiked at a concentration of 100 ng mL^{-1} and a QC point of 100 ng mL^{-1} was used to assess accuracy and repeatability. DoA compounds were added to OF at a wider concentration range (1, 5, 10, 25, 50, 75, 150, 300, 500, 650, 700, 850, and 1000 ng mL^{-1}), as well as to blood at 0.5, 2.5, 5, 12.5, 25, 37.5, 75, 150, 250, 325, and 425 ng mL^{-1}. IS concentrations were kept at 100 ng mL^{-1} for OF and 50 ng mL^{-1} for blood analysis, with selected QC points of 150 ng mL^{-1} and 37.5 ng mL^{-1} for OF and blood, respectively. Spiking was carried out in a manner that limited the organic content in the matrices to less than 1 % in order not to disturb any partition equilibria that may occur during the extraction process.[7] After spiking, the matrices were gently agitated at 200 rpm for at least 2 h to establish drug-matrix equilibration. No other modifications were made to the matrices under study. A pooled QC (PQC) sample for the metabolomics analysis was created using 10 µL of each desorbed caviar sample post-extraction. MEs in this study were assessed according to protocol by Mateuzewski et al.[331]

Preliminary assessment of HLB minitip performance using BZDs as model compounds

Before the quantitative and profiling studies could be performed, we had to assess the stability, robustness and extraction efficiency of the tips. Potential coating fall-out was examined via rapid agitation at 1800 rpm overnight (12 h) and by puncturing a piece of clay. Intra-tip (repeatability of a single minitip used multiple times) and inter-tip reproducibility (repeatability of multiple minitips) were investigated with and without IS for correction, by performing five subsequent extractions from both 50 µL of PBS and urine (200 ng mL^{-1} of BZDs, 10 min extraction, 5 min desorption to 50 µL of ACN/H$_2$O (50/50). The same experimental conditions were used to: 1.) examine how sensitivity is influenced by the preconditioning solvents (MeOH/H$_2$O at 50/50, 80/20, 100/0 and 20/80 %; ACN at 100 %; IPA at 100 %; Ethanol (EtOH) at 100 % and MeOH/IPA at 50/50%), and 2.) whether tip pre-treatment (preconditioned, preconditioned & washed, cleaned only had an impact on the sensitivity. Furthermore, extraction (0.5, 1, 2.5, 4, 5, 10, 30, and 60 min) and desorption (0.5, 1, 5, 10 min) time profiles for BZDs (200 ng mL^{-1}, 50 µL of PBS, desorption: 50 µL ACN/H$_2$O (50/50)) were performed to examine the extraction kinetics and the desorption process. The influence of sample volume on the signal response was examined by performing 10 min extractions from 1, 2, 3, 5, 10, and 50 µL of PBS spiked with 200 ng mL^{-1} of BZD(s) and desorbing them to 50 µL of ACN:H$_2$O (50:50). Finally, preliminary investigation of quantitative capabilities of the minitips were done extracting from a 15 µL PBS sample for 5-mins, followed by a 1-min desorption to 15 µL of ACN/H$_2$O (50/50). All of the afore-mentioned experiments were done on an API 4000 equipped with a Shimadzu binary pump and a CTC PAL autosampler. Instrumental details can be seen in Tables 3.1-3.3.

Table 3.1 Summary of chromatographic conditions used for BZD separation via API 4000.[7]

Column	Agilent-Zorbax: Extend-C18 (3.5 µm, 2.1 mm x 50 mm)
Mobile phase	A: 90/10 H_2O/ACN + 0.1 % AA B: 90/10 ACN/H_2O + 0.1 % AA
Flow rate	150 µL min^{-1}
Injection volume	20 µL
Injection mode	Full loop
Spray voltage	5000 V
Source temperature	450
CAD	8
CUR	10
GS1	20
GS2	5

Table 3.2 Summary of binary gradient used for BZDs separation via API 4000.[7]

Time	Mobile phase	
	A	B
0-0.51 min	90 %	10 %
0.51-2.50 min	10 %	90 %
2.51-5.00 min	10 %	90 %
5.01-6.00 min	90 %	10 %

Table 3.3 *List of analytes monitored via API 4000, including logP values (PubChem),*[156] *parent and product ions (m/z), DP, EP, CE and CXP.*

Analyte	logP	Parent (*m/z*)	Product (*m/z*)	DP (V)	EP (V)	CE (V)	CXP (V)
Diazepam	2.82	285	154	118.7	11.7	37	11.2
Diazepam-d5	-	290.3	262.1	117.2	9.9	34.6	20.1
Oxazepam	2.24	287.1	241	121	12.8	32.7	39
Oxazepam-d5	-	292	246	107.1	11	35	21.5
Nordiazepam	2.90	271	140	60.8	8.5	42.8	11.3
Nordiazepam-d5	-	276	213	117.2	6.8	39.3	16.1
Lorazepam	2.39	321.1	275.1	65.1	5.7	27	42.2
Lorazepam-d4	-	325	279	94.5	10.8	34.4	20.2

Extraction from 1 µL of OF

The quantitation of DoAs in OF was performed using static 5 min extractions from 1 µL of sample placed into a 300 µL vial, followed by a wash step (10 s, 3200 rpm) and 1 min desorption to 50 µL of MeOH/ACN/FA (80/20/0.1). Schematic of this process is shown in Figure 3.4. Instrumental analysis was also performed using LC-MS/MS. Details on the chromatographic method used are available in section 2.5.2.[211] Details on compound specific optimization parameters are available in Section 2.2.2, 2.5.2 and Table 3.4.

Pooled oral fluid → 1. Five minute extraction from 1 µL of oral fluid → 2. Ten second wash in 300 µL of LC/MS grade H_2O → 3. Five minute desorption to 50 µLs of MeOH:ACN:FA (80:20:0.1) → 4. LC-MS/MS analysis on TSQ Vantage
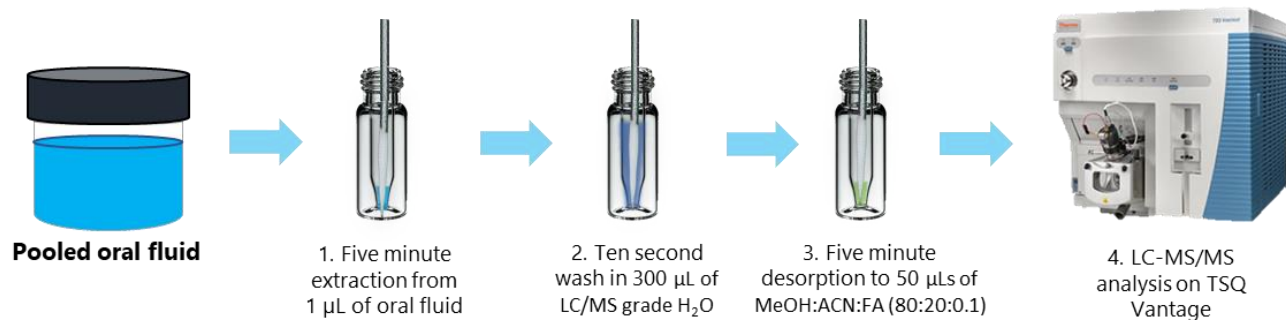
Figure 3.4 *Schematic of sampling conducted with 1 µL of OF, analysed via LC-MS/MS.*

Table 3.4 *List of analytes monitored via TSQ Vantage, including log P values, parent and product ions (m/z), collision energy (CE) and S-lens.*

Analyte	log P	Parent (*m/z*)	Product (*m/z*)	Collision energy (eV)	S-lens
Carbamazepine	2.45	237.1	194.1	19	86
Carbamazepine-d10	-	247.1	204.1	20	127
Clenbuterol HCl	2.94	277.1	202.9	14	91
Clenbuterol-d9 HCl	-	286.1	204.0	15	83
Testosterone	3.21	289.1	97.0	23	114
Testosterone-C^{13}_3	-	292.1	100.0	23	114
Propanolol	3.48	260.1	116.1	17	92
Propanolol-d7	-	267.1	116.1	17	87

Nanoelectrospray experiments

Standard coated nESI sprayers (PicoTip, BG10-58-2-CE-20) were ordered from New Objective (Woburn, MA, USA). Prior to conducting the nESI experiments, the instrument was run overnight using a single solvent mixture (MeOH/ACN/FA, 80/20/0.1), a flow rate of 400 µL min^{-1}, a spray voltage of 1300 V, a vaporizer temperature of 275 °C, sheath gas of 45 (AU), auxiliary gas of 30 (AU), and capillary temperature of 280 °C. This was done in order to provide a primed environment for the nESI experiments (i.e. reduce noise from analytes previously run by other users on the TSQ-Vantage). Prior to performing the experiments, the optimum spraying voltage was determined by monitoring the signal of different analytes at varying voltages, i.e. at 500, 600, 700, 800, 900, 1000, 1100, 1200, 1300, 1400, and 1500 V. After 1500 V, a drop in signal was observed; therefore, 1300 V was used for the experiments. One µL of blood was placed into a 300 µL glass vial using a 0.5-2.5 µL Eppendorf pipette. The experiments were carried out by inserting the minitip into 1 µL of blood for a 5 min static extraction, which was followed by a 10 s wash under a stream of LC/MS-grade H_2O and a 1 min offline desorption (static) into 3 µL of MeOH/ACN/FA (80/20/0.1). Following desorption, the solvent was transferred to the nESI sprayers using a 10 µL capillary syringe. The sprayers were then immobilised into a stage that had been specially

designed at UW for nESI desorptions.[206] Next, a voltage of 1300 V was applied to the nESI tip, and the signal was acquired for 20 s. A schematic of this process can be observed in Figure 3.5. The calibration plots were generated using a matrix matched approach with IS correction, and the LODs and LOQs were determined based on S/N ratios of 3 and 10, respectively. Analysis was performed via MRM mode in +ve ionization mode using a TSQ Vantage (Thermo Scientific). Compound specific details pertaining to TSQ-Vantage can be accessed in Section 2.2.2, 2.5.2 and Table 3.4.
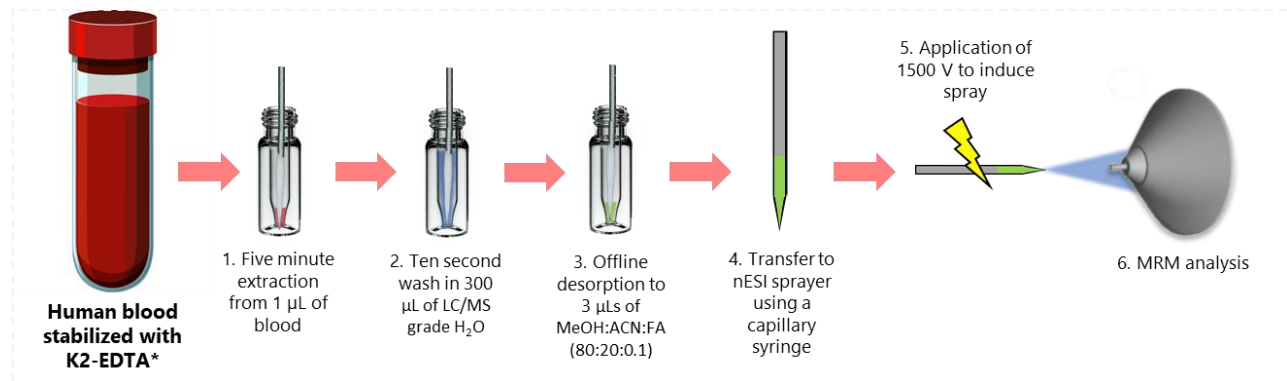
Figure 3.5 *Schematic of sampling of 1 µL of blood with SPME minitips coupled to nESI-MRM.*

Caviar sampling

Caviar samples were purchased randomly from the store while ensuring that egg diameter was < 3.0 mm. Each caviar egg was measured as having a diameter of ≤ 2.9 mm. A single egg was carefully removed from the container, placed onto a microscope slide, and penetrated with a minitip that had been preconditioned and washed with H_2O. Each extraction was carried out for twenty minutes, with a total of six (n = 6) replicates being performed for each caviar type. The sampling process is illustrated in Figure 3.6. Desorption was performed in 90 µL of LC/MS-grade ACN/H_2O (50/50) for a total of 10 min via agitation at 500 rpm. The desorbed samples were analyzed in +ve ionization mode on an Exactive Orbitrap that was equipped with an Accela autosampler and a pump, using a generic method that had been developed and published by the Pawliszyn research team for global metabolomics (PFP column, binary gradient, 300 µL/min flow).[45] The stability of the run was monitored by injecting a pooled QC (PQC) every 7th injection. Details pertaining to the instrumental run can be found in Table 3.5-3.6.

1. Black lumpfish
Egg size: 2.34 mm

2. Red lumpfish
Egg size: 2.20 mm

3. Salmon
Egg size: 2.98 mm

4. Herring
Egg size: 2.73 mm
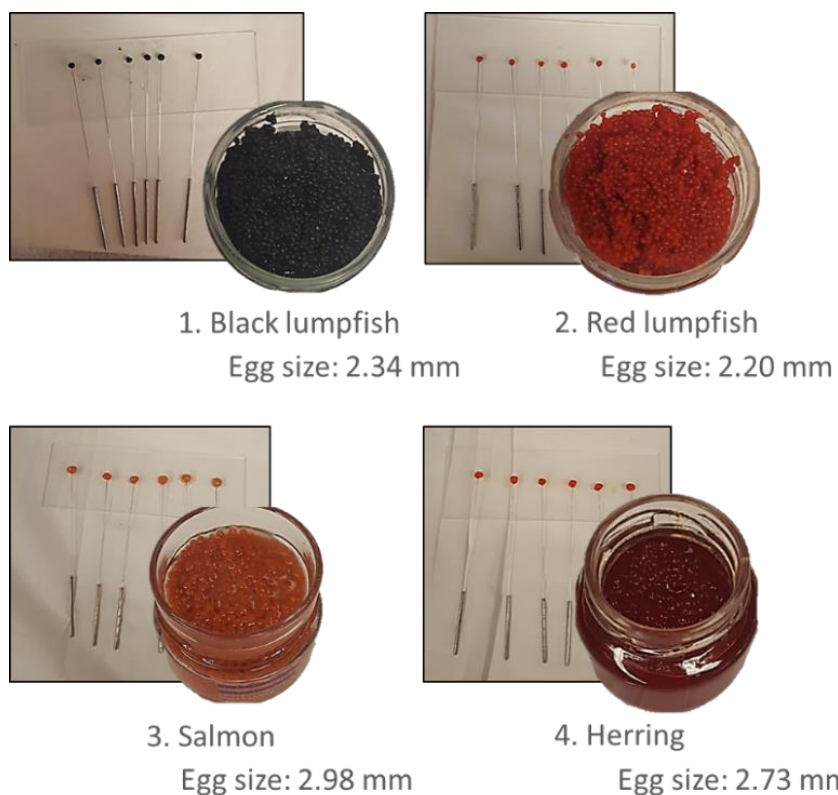
Figure 3.6 *The set of samplings performed for the metabolomic profiling of caviar.*

Table 3.5 *Summary of chromatographic conditions used for the separation of caviar samples via Thermo Exactive.*[45]

Column	Phenomenex: PFP (1.7μm, 2.1 mm x 10 mm)
Mobile phase	A: 100 % H_2O + 0.1 % FA B: 100 % ACN + 0.1 % FA
Flow rate	300 μL/min
Column temperature	25 °C
Injection volume	10 μL
Spray voltage	4 kV
Vaporizer temperature	300 °C
Sheath gas	30 AU
Auxiliary gas	10 AU
Capillary temperature	300 °C

Table 3.6 *Summary of the binary gradient used for the separation of caviar samples via Thermo Exactive*[45]

Time	Mobile phase	
	A	B
0-3 min	100 %	0 %
3-25 min	10 %	90 %
25-34 min	10 %	90 %
34-40 min	100 %	0 %

3.4 Results/Discussion

Characterization of the HLB particles

FTIR was used to examine the presence of the monomers that were used to synthesize the HLB particles used in this study. The peak at 1687 cm^{-1} indicates the presence of C=O groups of lactams in NVP in the polymer backbone (Figure 3.7), while the peaks at 1603, 1507, and 1446 cm^{-1} confirmed the stretching frequency of the conjugated C=C bonds in the benzene ring. The peaks at 2921 cm^{-1} and 3100 cm^{-1} were respectively created by the –CH stretching of the alkane chain following polymerization and the terminal –CH$_2$ groups of terminal alkenes that arise from the residual –HC=CH$_2$ of the vinyl groups; these peaks also confirm the presence of DVB and NVP monomers in the final HLB particles. The size and shape of the HLB particles were imaged using SEM (Figure 3.8), and, as this image shows, the particles are monodisperse, spherical, and smooth on the surface with an average size of 1.33 µm. Furthermore, the particles do not show any signs of agglomeration or the formation of a core-shell structure consisting of two different monomers. Surface-area analysis revealed that the synthesized HLB particles were porous, with a specific SA of 335.23 m^2 g^{-1} and had a pore diameter and volume of 1.3 nm and 0.201 mL g^{-1}, respectively.
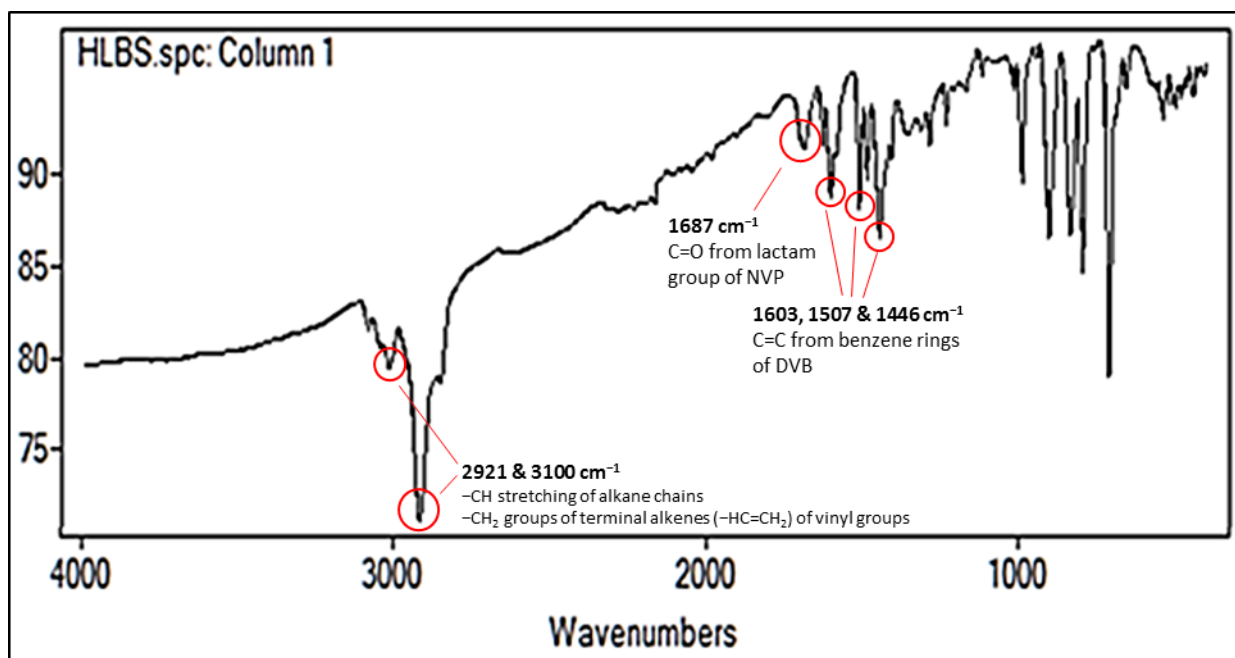
Figure 3.7 *FTIR image obtained from Tensor II spectrometer for the analysis of HLB particles.*
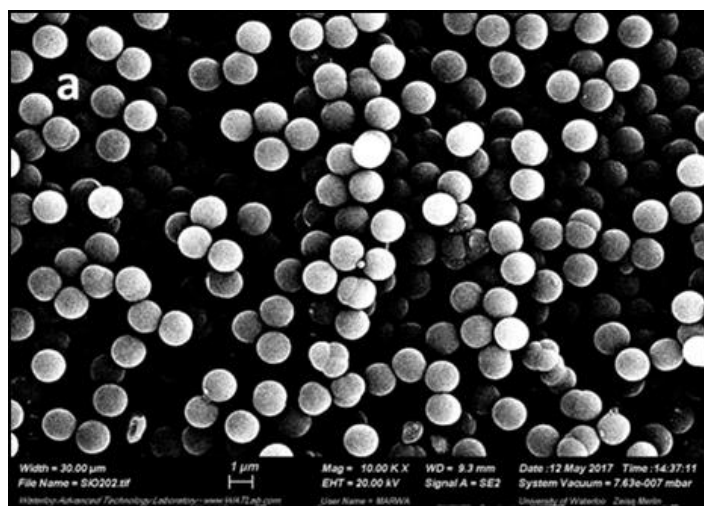
Figure 3.8 *SEM image of HLB particles captured at 10kX.*

Preparation of the SPME minitips: Optimization of etching conditions

The development of a protocol for manufacturing of SPME minitips was an integral step in this study, as it is important to establish a controlled production setting. Given the difficulty of manually fabricating SPME minitips on a very small scale, a motorized stage and sensor were constructed at UW to ensure that the tip shape could be normalized and that a coating length of 1 mm could be reliably reproduced.

180

SS acupuncture needles were selected for use in order to avoid the need for expensive materials (i.e., titanium tips). Since the diameter of the acupuncture needles was greater than required, we developed a protocol for diameter reduction via electrochemical etching that would also allow for the robust adherence of HLB particles. The fabrication protocol enables tip diameter manipulation through immersion in the etching solution at a fixed position. For instance, a sharper tip can be obtained by withdrawing it from the etching solution (1 M KOH) at a speed of 0.2 mm s^{-1} while voltage (11 V) is still being applied. The SEM images obtained for the untreated, etched, and sanded tips can be seen in Figure 3.9, and, as can be seen, the tip surfaces exhibit a tendency towards a coarser morphology. In
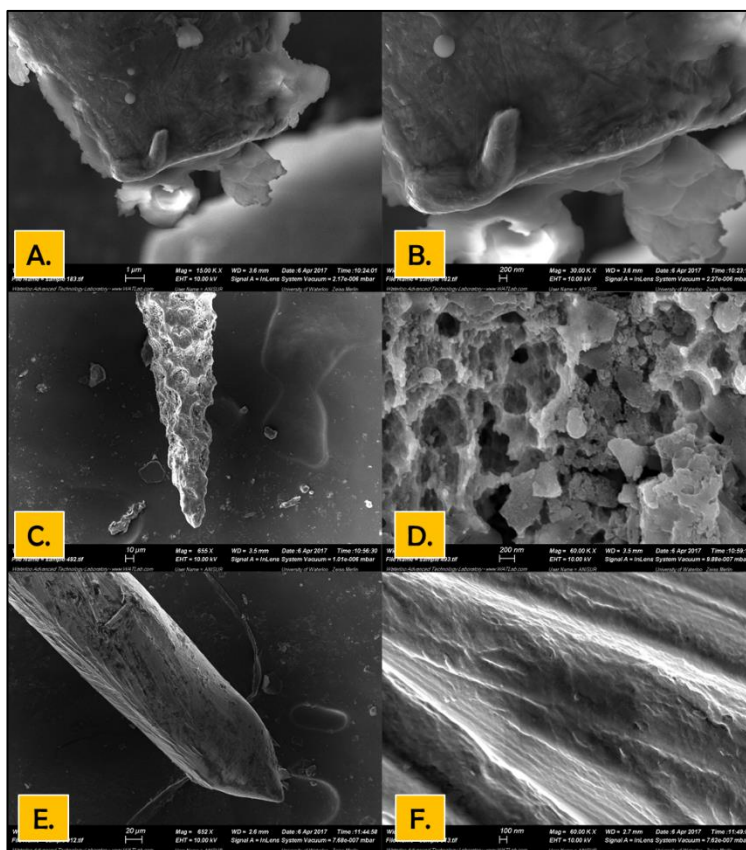
Figure 3.9 *SEM images of acupuncture needles obtained from Electro-Therapeutic Devices. **A.**) Untreated acupuncture needle (no etching); **B.**) Close-up of untreated acupuncture needle (no etching); **C.**) Needle surface topology after etching in KOH for 40 s; **D.**) Close up of needle surface after etching in KOH for 40 s; **E.**) Topology of previously etched needle after sanding; **F.**) Close up of topology of previously etched needle after sanding revealing a rougher surface suitable for dip-coating.*

controlling the etching conditions, it becomes possible to make tips with varying diameters, including diameters small enough that they can be applied for extractions from very small sample volumes (i.e.

small organisms or single cells). However, it is important to keep in mind that very thin SS tips can be more prone to bending and breakage, which can make sampling more difficult. As such, it would be useful to consider alternative materials for applications that require smaller minitips.

Preparation of the SPME minitips: Dip coating procedure

Initial attempts at ≤ 1 mm coating lengths proved troublesome. These attempts were carried out using a procedure established by the Pawliszyn group[48] and commercially available HLB particles (particle size range: 5-30 µm) from Waters. The commercial particles were ground using a ball mill, but the resulting slurry did not produce positive results (even after ten dip coats). Further attempts to increase the solution's viscosity and particle percentage were unsuccessful, as they only yielded coagulated clusters (Figure 3.10). It became apparent that the thickness of the minitip's cone region (d < 130 µm) posed significant challenges to the dip-coating process, as it resisted the viscous pull drag. Another contributing factor to these difficulties was the attempt to coat the minitip at a length of ≤ 1mm. According to Brinker,[332] the process of dip-coating depends on factors such as particle size and structure, surface
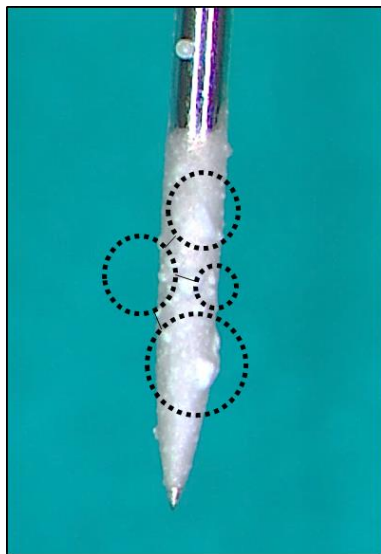
Figure 3.10 *Attempt to coat an acupuncture needle using solution with higher viscosity and particle percentage. Note that simply increasing viscosity and the percentage of particles is insufficient to obtain a smooth-surfaced SPME minitip.*

tension, dipping speed, and gravitational draining. To the best of our knowledge, there is no reported research that has investigated how substrate size influences the dip-coating process. Several researchers have reported that the dip coating process becomes more difficult on a microscale due to surface-tension forces.[333,334] It is important to note that we used the "draining regime" dip-coating process (withdrawal speeds > 1 mm s^{-1}, Landau-Levich model).[334] As such, the minitips were coated using the highest withdrawal speed offered by our device (3.5 mm s^{-1}). Fang et al.[333] reported that film thickness could be increased by increasing the concentration of polylactic acid (PLA), as the amount of PLA coated onto the tip will be greater due to increased drag force, which is directly proportional to solution viscosity. Given this relationship, we decided to investigate whether reducing particle size (< 5 µm) and increasing the percentage of particles in the slurry would result in a successful dip-coat. To test this idea, we used 200 nm sized silica nanoparticles (SiNPs) and adjusted the coating recipe to 6 % PAN viscosity and 15 % particles, which produced a successful minitip coating process (Figure 3.11). However, since SiNPs are limited in terms of extraction efficiency, we synthesized HLB particles at a size of 1.3 µm and used them with the same recipe that we used for SiNPs. The coated SPME minitips and the respective SEM images can be seen in Figure 3.12. The dip-coating process causes a gradual reduction in coating thickness, which is most evident at the thinnest parts of the minitip. Therefore, the solid coating does not have a uniform thickness; rather, the coating thickness decreases as the substrate thickness decreases. As

Figure 3.11 SPME minitip coated with SiNPs (particle size: 200 nm; pore size: 4 nm) using a recipe consisting of 6% PAN and 15% SiNPs.

can be seen in the SEM images in Figures 3.13-3.14, the thickness of the coating is 4.1-4.6 µm at roughly 100 µm in length and 10.5 µm at 300 µm in length. This could be attributed to diminishment of gravitational pull at such a small scale. Hence, one must be aware that coating very thin probes (d ≤ 30 µm) may require nanosized particles. Furthermore, the minitips were also tested by using them to puncture a piece of clay and then performing a microscopic examination to see whether the coating had been compromised. The results of these tests showed that the minitip coating remained intact throughout the insertion and removal from the clay. It was important to ensure that the device was robust, as this study would require them to maintain their performance despite being exposed to conditions that would challenge their durability (i.e., rigid solid samples & aggressive agitation potentially causing strip-off). For example, a limitation was found such that the minitip's mechanical strength decreased when etched (diameter reduction) to extremely small   dimensions (i.e., tip apex diameter ≤ 30 µm). This resulted in the apex bending somewhat easily upon contact with sources of external pressure (finger pressure, contact with well-walls and rigid samples). It is important to highlight this issue, as it may be avoided in the future by using probe substrates with very sturdy characteristics. Potential highly sturdy substrates could include titanium and tungsten tips, but their cost and coating logistics (i.e., how to create a rougher substrate surface to allow coating deposition on a microscale) must be considered. To best of our knowledge, these practical aspects are rarely addressed in publications focusing on coated probes.[313,314] Lastly, once the SPME-HLB minitips were made, we compared their performance to those of SiNPs. A chromatogram showing extracted BZDs with SiNPs and HLB can be seen in Figure 3.15.
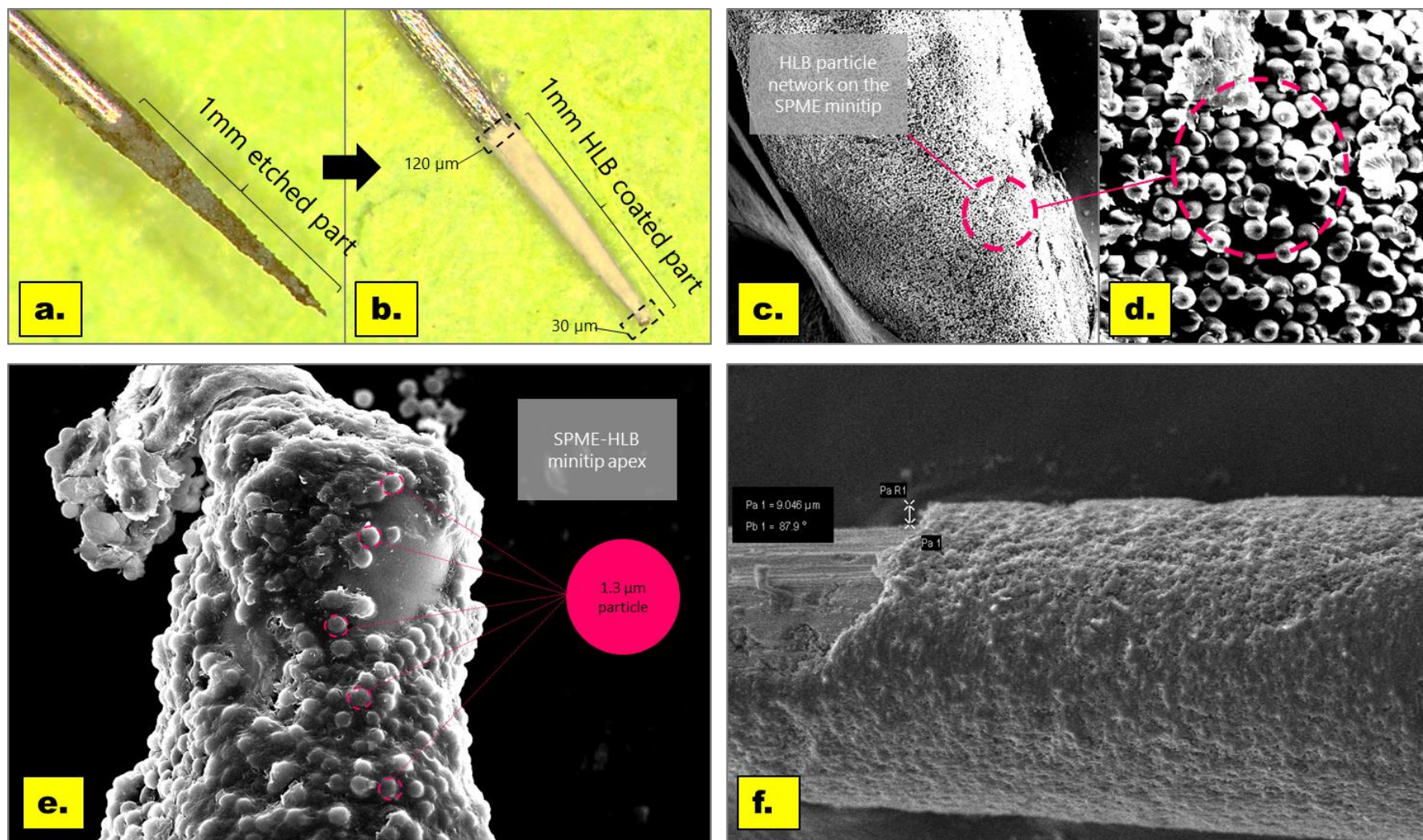
Figure 3.12 *SPME minitips coated with 1.3 μm HLB particles.* ***a.****) Minitip obtained after etching 1 mm of a SS needle with KOH;* ***b.****) 1 mm coated HLB minitip obtained after sanding and 6 dip-coats of the 6% PAN & 15 % particle slurry;* ***c.****) SEM image of minitip surface after six layers have been deposited and cured;* ***d.****) close-up SEM image of the dense particle network on the minitip's surface;* ***e.****) close-up view of tip apex;* ***f.****) partially stripped-off coating present on the surface of the etched SS needle.*
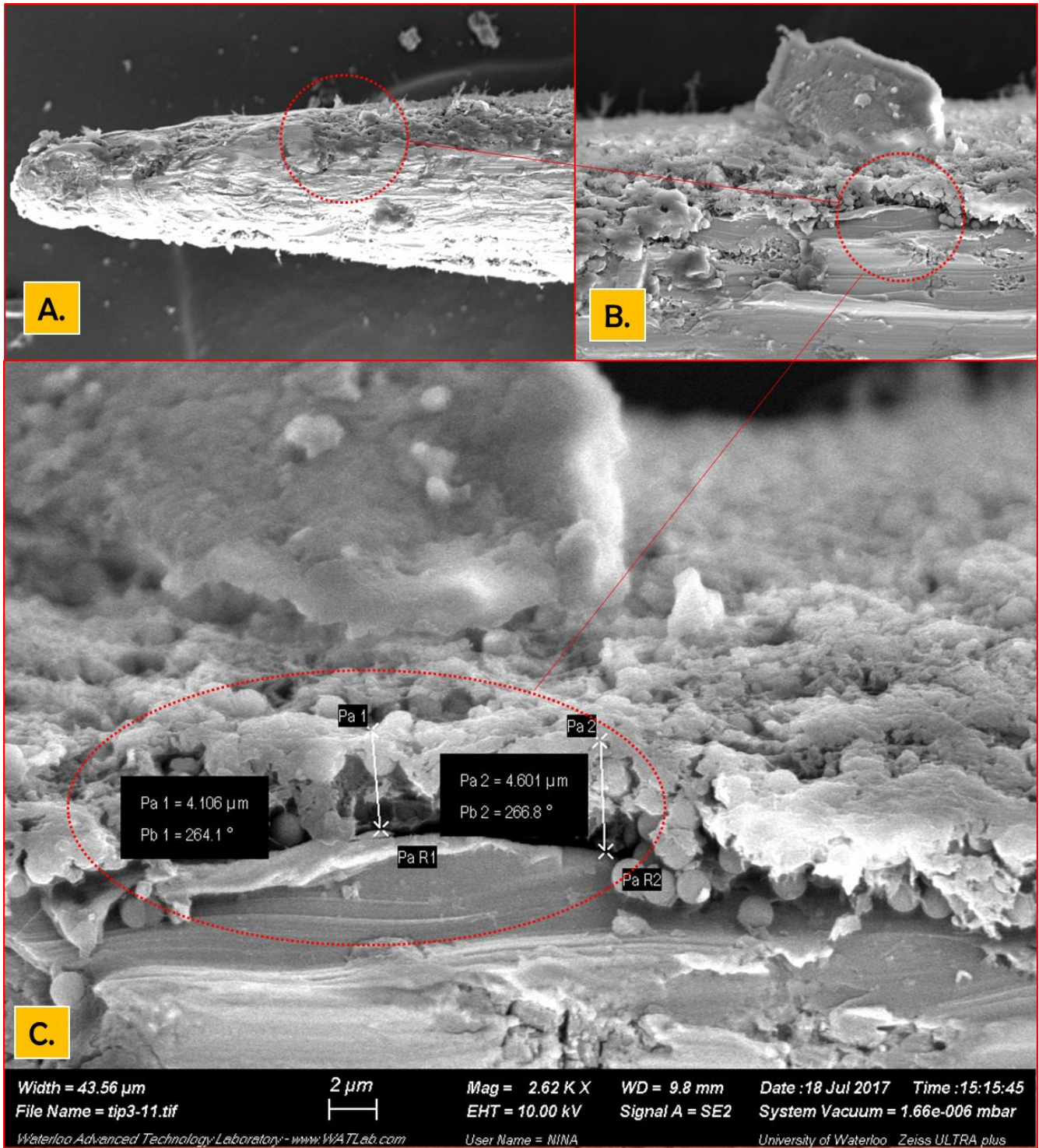
Figure 3.13 *Determination of coating thickness near the minitip apex (roughly 100 µm away from the apex). Figures **A.** and **B.** show the portion from which the tip thickness was determined, while **C.** shows that the coating thickness at this portion was roughly estimated to be between 4.1 – 4.6 µm.*
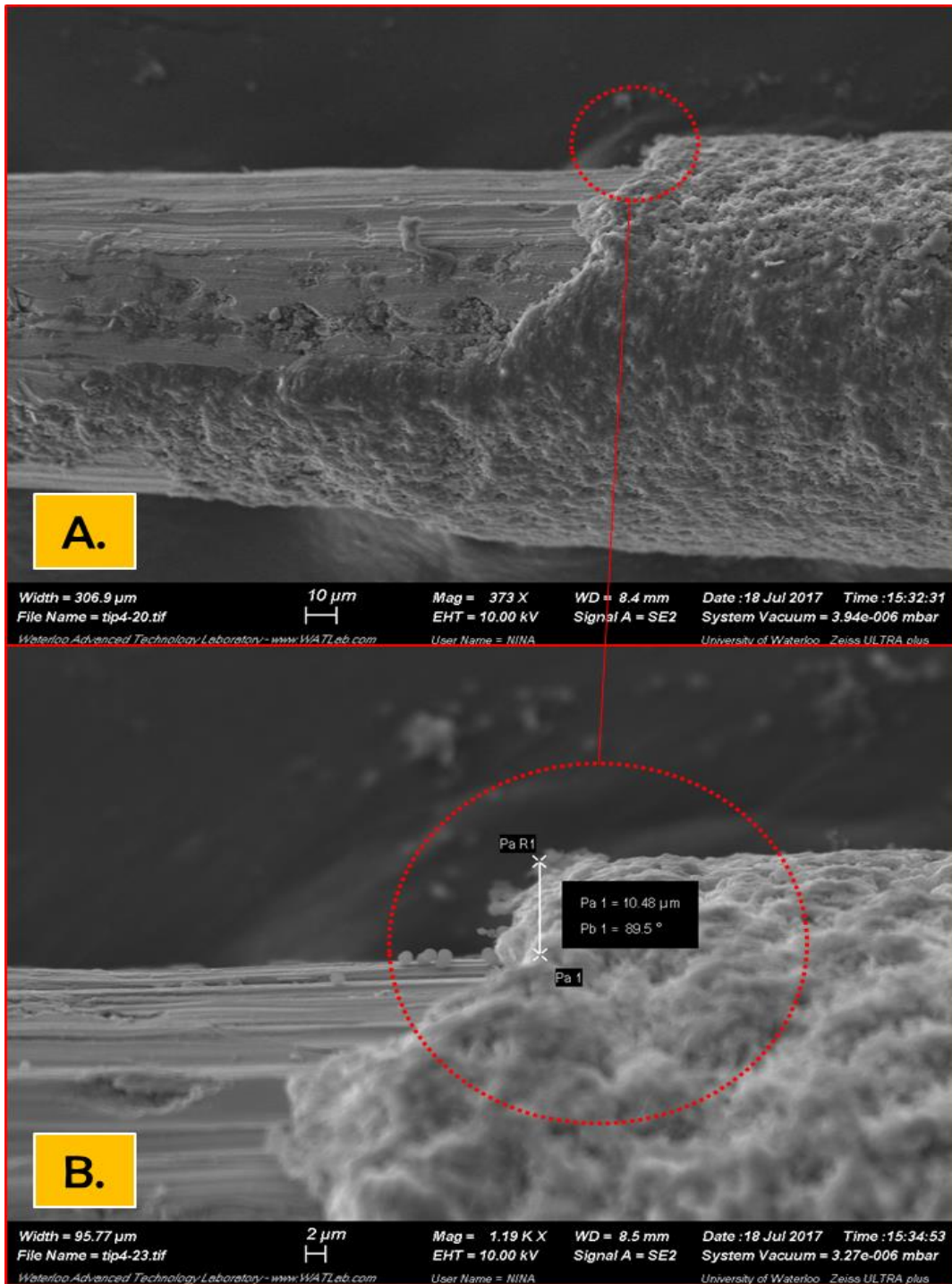
Figure 3.14 *Determination of the coating thickness further away from tip (roughly 300 µm away from tip apex). **A.**) Portion of tip that was used to determine the coating thickness; **B.**) Coating thickness at Portion **A.** shows measurement of ~ 10.5 µm.*

Blue: Diazepam; **Gray: Nordiazepam**, **Red: Lorazepam**; **Green: Oxazepam**
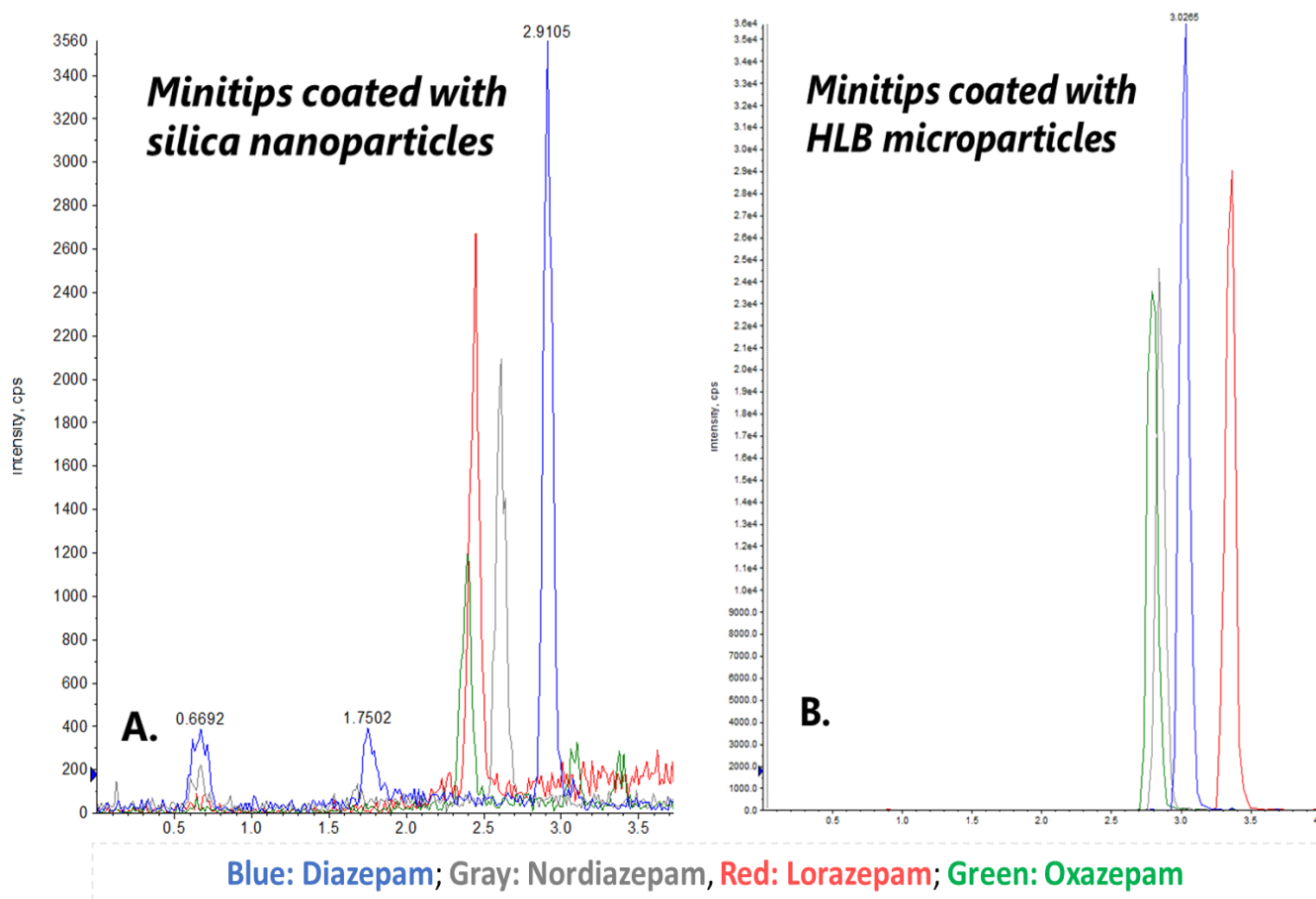
Figure 3.15 *Chromatograms obtained for extraction of 500 ng mL⁻¹ of BZDs from a PBS sample for SiNPs in **A**. and HLB minitips in **B**.*

Preliminary performance assessments: Repeatability of the SPME minitip

Intra-tip repeatability was tested by performing five extractions (cleaned in-between each trial), while inter-tip repeatability was tested by performing eight individual extractions. The results of these tests, which used BZDs as model compounds, are presented in Tables 3.7-3.8. As can be seen, intra-tip repeatability was ≤ 26.4 % RSD (n = 6 tips, 5 re-uses of each) without IS correction, and ≤ 6.9 % RSD (n = 6 tips, 5 re-uses of each) with IS correction. While assessing the repeatability of a single tip is important in establishing whether a good manufacturing protocol has been achieved, it is also important to keep in mind that re-using sample-preparation devices is usually appropriate for screening applications but should be avoided when real biological samples are used. Therefore, we elected to use a cheaper material like SS rather than titanium and/or tungsten. Inter-tip repeatability was found to be ≤ 20% RSD (n = 8) without IS correction, and ≤ 5.4 % RSD (n = 8) with IS correction. This variability can be

188

attributed to deviations that may occur during fabrication, particularly during the etching and coating process (i.e., small differences in dip-coating process may result in thinner/thicker coatings). The thinner/thicker coating will extract either more or less of the analyte, which contributes to an elevated % RSD at a microscale. Therefore, the use of an IS is highly encouraged for this type of analysis. In addition, manufacturing protocols (including issues encountered), mechanical robustness, and repeatability should all become a greater focus of discussion, as the optimization of these elements would lead to the development of better micro-sized probes.[309] It is unfortunate that most approaches that focus on small volume and single cell analysis discuss the resultant biological information but fail to rigorously assess the quality of sample preparation (robustness and repeatability). Indeed, such oversights are problematic because they prevent the establishment of standards of quality regarding the information that is being reported.

Table 3.7 *Assessment of intra-tip repeatability was conducted by using five different tips to perform 25 extractions (5 per tip). Extraction was performed for 10 mins from 50 μL of a PBS sample (spiked with 200 ng mL⁻¹ of BZDs and 100 ng mL⁻¹ of corresponding IS's) and desorbed for 5 min to ACN/H₂O (50/50). Repeatability was assessed using the signal obtained for the area of a chromatogram (Au), as well as an IS (Area/IS) for correction: diazepam-d5, lorazepam-d4, oxazepam-d5 and nordiazepam-d5.*

Tip number	Diazepam (RSD %, n = 5)		Lorazepam (RSD %, n = 5)		Oxazepam (RSD %, n = 5)		Nordiazepam (RSD %, n = 5)	
	Area [AU]	Area/IS	Area [AU]	Area/IS	Area [AU]	Area/IS	Area [AU]	Area/IS
1	4.6	3.5	21.1	2.0	18.4	3.9	25.4	6.2
2	18.6	4.5	18.6	2.7	18.2	2.9	8.4	4.2
3	18.6	5.1	26.2	4.5	22.7	5.1	22.4	4.6
4	24.9	2.0	2.4	1.3	8.0	3.6	26.3	5.4
5	13.6	2.3	6.5	3.2	7.1	6.9	9.7	3.3

Table 3.8 *Assessment of inter-tip repeatability was conducted according to the same extraction/desorption conditions described in Table 3.7. Eight different tips were used for this evaluation, and RSDs (%) were assessed with (diazepam-d5, lorazepam-d4, oxazepam-d5 and nordiazepam-d5) and without IS correction.*

Diazepam (RSD %, n = 8)		Lorazepam (RSD %, n = 8)		Oxazepam (RSD %, n = 8)		Nordiazepam (RSD %, n = 8)	
Area [AU]	Area/IS	Area [AU]	Area/IS	Area [AU]	Area/IS	Area [AU]	Area/IS
18.8	5.4	18.0	3.7	19.2	4.2	20.0	4.4

Preliminary performance assessments: Reusability of the SPME minitip

Considering the intricacy and time invested in the process of making the SPME minitips, reusability was of special interest. Hence experiments were conducted to test the afore-mentioned by performing 5 consecutive cycles of extraction (Vs = 50 µL, 200 ng mL^{-1} BZDs, 10 min) and desorption (50 µL desorption volume, 50/50 ACN/H$_2$O, 5 min). These extractions were completed using PBS and urine. In between each cycle, the tips were cleaned and preconditioned. The data obtained from re-using a single

RSD (%)			
Diazepam	Lorazepam	Oxazepam	Nordiazepam
4.6	18.6	18.4	22.4
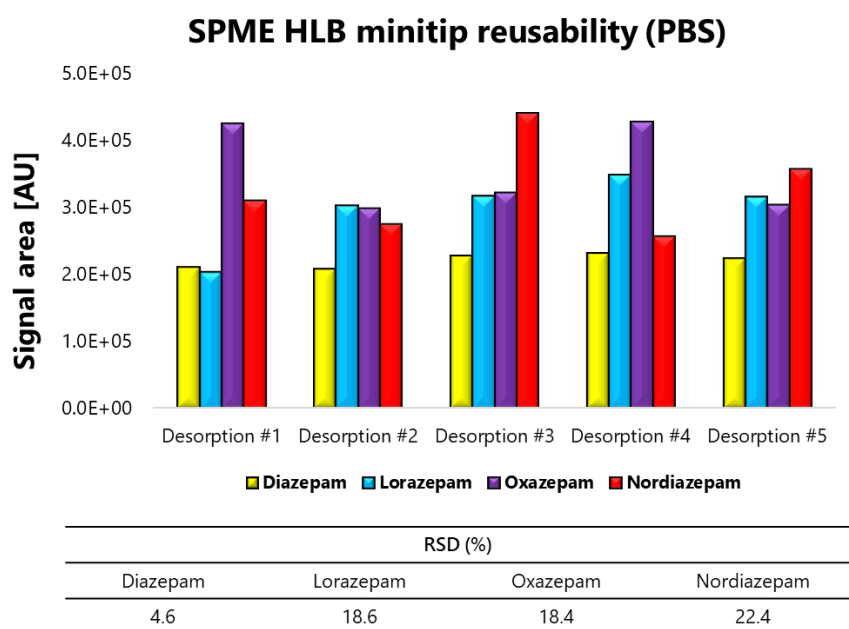
Figure 3.16 *Assessment of tip reusability (n = 5) performed via 10 min extractions from a 50 µL PBS sample spiked with 200 ng mL^{-1} of BZDs and 5 min of desorption to 50 µL of ACN/H$_2$O (50/50).*

SPME HLB minitip reusability (Urine)

	RSD (%)		
Diazepam	Lorazepam	Oxazepam	Nordiazepam
17.8	17.4	19.8	41.5
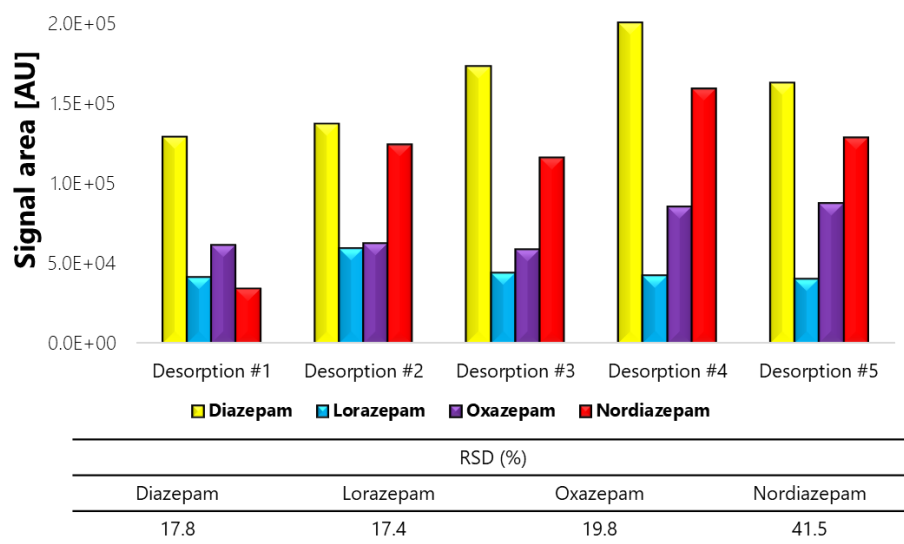
Figure 3.17 *Assessment of tip reusability (n = 5) performed via 10 min extractions from a 50 µL urine sample spiked with 200 ng mL^{-1} of BZDs and 5 min of desorption to 50 µL of ACN/H$_2$O (50/50).*

HLB minitip in both PBS and urine is presented in Figures 3.16-3.17, with the % RSD values for each analyte presented beneath the figure. These values appear to be satisfactory, as the data suggests that the tips retain their extraction ability. Furthermore, a visual inspection of the tips after 5 extractions/desorptions revealed no coating fall-out. It should be noted that the repeatability of nordiazepam in urine was 41.5 %, which could be due to the fact that a much smaller amount was extracted on the first desorption than on subsequent iterations.

Preliminary performance assessments: Preconditioning of the SPME minitip

The influence of the preconditioning solvent was also investigated, as the solvent's properties can affect the minitip's extractive ability. To conduct this assessment, we analyzed eight different preconditioning solvents. The results of these analyses are presented in Figure 3.18, and, as can be seen, a mixture of 50/50 MeOH/H_2O produced the best results. Given the micro-scale of the device, we conducted further experiments to evaluate whether a preconditioning step is required in sample preparation process by testing the minitips in a "dry form", i.e., without preconditioning (cleaning only). We compared the performance of the "dry form" tips to "washed tips" that had been cleaned, preconditioned, and washed with H_2O prior to extraction. Tips were also "conditioned" whereas only preconditioning was done without a wash step. As shown in Figure 3.19, the tips that were washed with H_2O demonstrated better analyte extraction ability. Conversely, the active sites on the coating did not
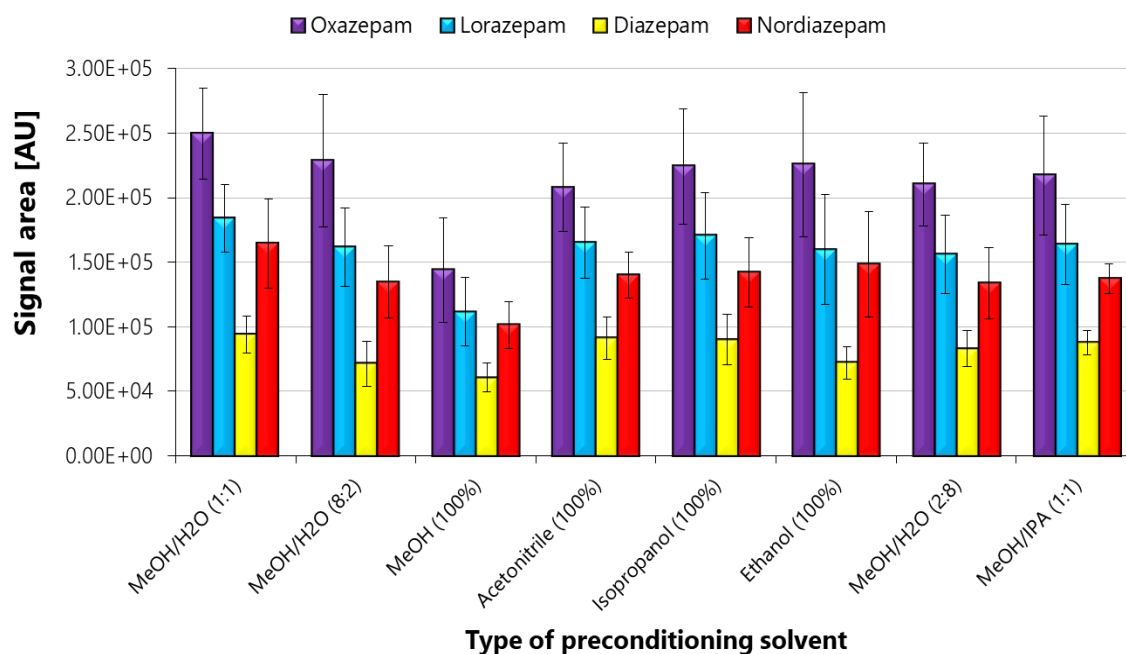
Figure 3.18 *Investigation of the influence of eight different preconditioning solvents on the signal obtained (n = 4) for 10 min extractions from a 50 μL PBS sample spiked with 200 ng mL^{-1} of BZDs and 5 min of desorption to 50 μL of ACN/H_2O (50/50).*

appear to be fully activated on the dry tips. When a tip is preconditioned but not washed, it is possible

that some preconditioning solvent remains on the tip, which could potentially interfere with the partitioning equilibria.
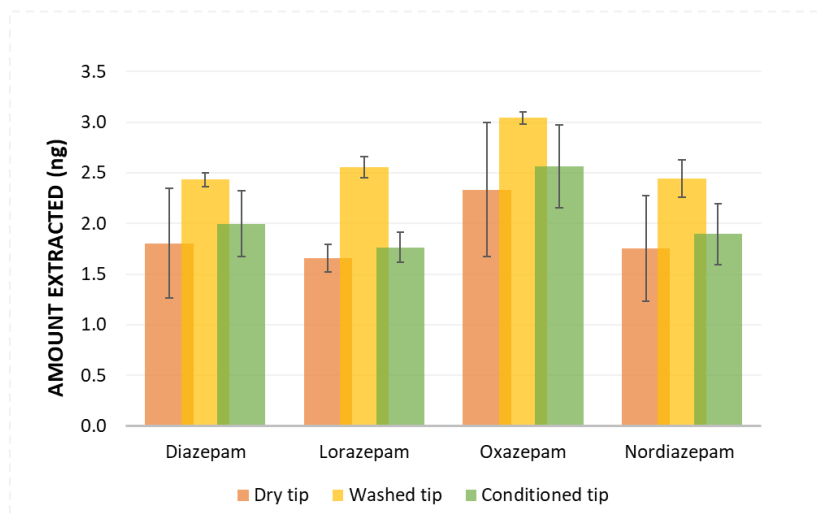
Figure 3.19 *Investigation of the influence of tip pre-treatment on amount extracted (n = 3) using 10 min extractions from a 50 µL PBS sample spiked with 200 ng mL^{-1} of BZDs and 5 minutes of desorption to 50 µL of ACN/H$_2$O (50/50).*

Preliminary performance assessments: Influence of sample volume

According to the underlying theory of SPME, the amount of extracted analyte increases with the sample volume up to a certain point, after which sensitivity plateaus.[7] To investigate how sample volume influences the response, we performed extractions from 1, 2, 3, 5, 10, and 50 µL of PBS spiked with 200 ng mL^{-1} of BZDs. The results obtained can be seen in Figure 3.20. As can be seen, signal obtained (in AU) increases alongside sample volume up to 10 µL, where it appears to plateau. These results are in agreement of those obtained by Piri-Moghadam et al., who also found that sensitivity increased up to a certain volume.[25]
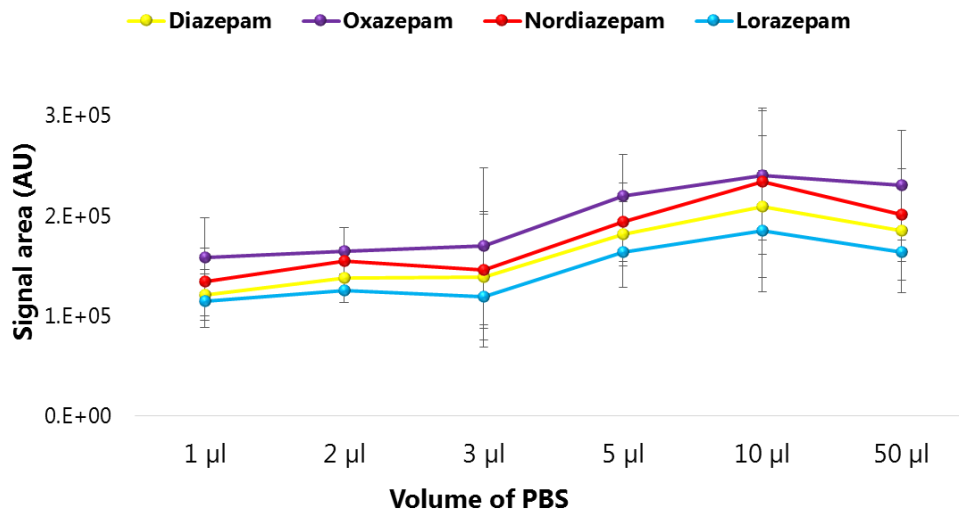
Figure 3.20 *Assessment of the influence of sample volume (1, 2, 3, 5, 10, and 50 µL) on the signal obtained for BZD extraction from a PBS sample spiked with 200 ng mL^{-1} using a 10 min static extraction and a 1 min desorption.*

Preliminary performance assessments: A Note on Biocompatibility, Matrix Effects, and Extraction Kinetics

As it pertains to SPME, biocompatibility refers to an extractive coating's ability to resist the adherence of unwanted biologicals and to not cause toxic shocks within studied organisms.[15] Overcoating SPME devices is one way to establish biocompatibility.[335]

A number of investigations over the past 10 years have supported PAN's suitability for use with SPME.[19,44,48,49,336,337] While biocompatibility is not always a key requirement of general sample preparation, one must keep in mind that biocompatible coatings offer number of benefits, such as enabling *in vivo* sampling (in addition to reducing the level of biological interferences in the MS). In this study, the MEs of the minitips were assessed using human plasma and urine. In order to determine whether any significant ionization suppression and/or enhancement occurred, blank urine and plasma extractions were performed using the minitip. The extractions were then desorbed and spiked with neat

standard, and the obtained signal area was compared to the area of neat standard (i.e., blank extraction not performed). This assessment was done using BZDs at 5, 50, and 100 ng mL^{-1}. The results obtained for urine and plasma can be seen in Tables 3.9 and 3.10, respectively. The obtained ME was acceptable for the BZDs examined in urine, with a range of 103-128.5 %. The exception to this result was nordiazepam, which showed an enhancement of 134 % at 50 ng mL^{-1}, thus potentially indicating greater interference from either an exogeneous or endogenous source. The tested BZDs produced a ME range of 95.8-109.7 %, which indicates that the minitips are not significantly affected by protein-dense matrices like plasma. While these are promising results, one must keep in mind that different analytes/matrices could yield a different response. Therefore, it is appropriate to investigate whether matrix co-extracts could interfere with analytes of interest.

Extraction kinetics are also important in the development of SPME methods, as they directly influence method sensitivity. In this study, we examined the extraction time profile of BZDs in PBS by evaluating extraction times of 0.5, 1, 2.5, 4, 5, 10, 30, and 60 min. The extraction time profile and the desorption time profile can be seen in Figures 3.21-3.22. We observed a consistent increase in the amounts extracted, which may be attributable to the highly porous nature of the minitip. The desorption time profile shows

Table 3.9 *Results obtained for the assessment of the absolute MEs for the SPME-HLB minitips. Absolute ME was assessed by examining the signal response after blank extraction from urine, followed by desorption, and spiking the desorbate with 5, 50, and 100 ng mL^{-1} of diazepam, oxazepam, and nordiazepam (analysis done on an API 4000).*

Compound	Absolute matrix effect for urine (Precision, RSD %, n = 3)		
	Spiked level		
	Low (5 ng mL^{-1})	Medium (50 ng mL^{-1})	High (100 ng mL^{-1})
Diazepam	106.4 (5.0)	123.5 (15.0)	126.7 (11.8)
Oxazepam	103.9 (2.5)	128.5 (14.3)	119.8 (12.4)
Nordiazepam	104.8 (13.8)	134.0 (21.1)	120.7 (23.7)

Table 3.10 *Results obtained for the assessment of the absolute ME arising from blank plasma extractions via SPME-HLB minitips, followed by spiking of 5, 50, and 100 ng mL^{-1} of diazepam, oxazepam and nordiazepam to the desorbate. Analysis was performed using an API 4000, and both ME analysis approaches were conducted according to procedure proposed by Matuszewski et al.[331]*

Compound	Absolute matrix effect for plasma (Precision, RSD %, n=3)		
	Spiked level		
	Low (5 ng mL^{-1})	Medium (50 ng mL^{-1})	High (100 ng mL^{-1})
Diazepam	100.2 (12.1)	108.0 (7.0)	104.5 (2.5)
Oxazepam	105.8 (12.5)	101.3 (6.5)	109.7 (8.2)
Nordiazepam	98.4 (12.2)	102.7 (6.2)	95.8 (6.2)
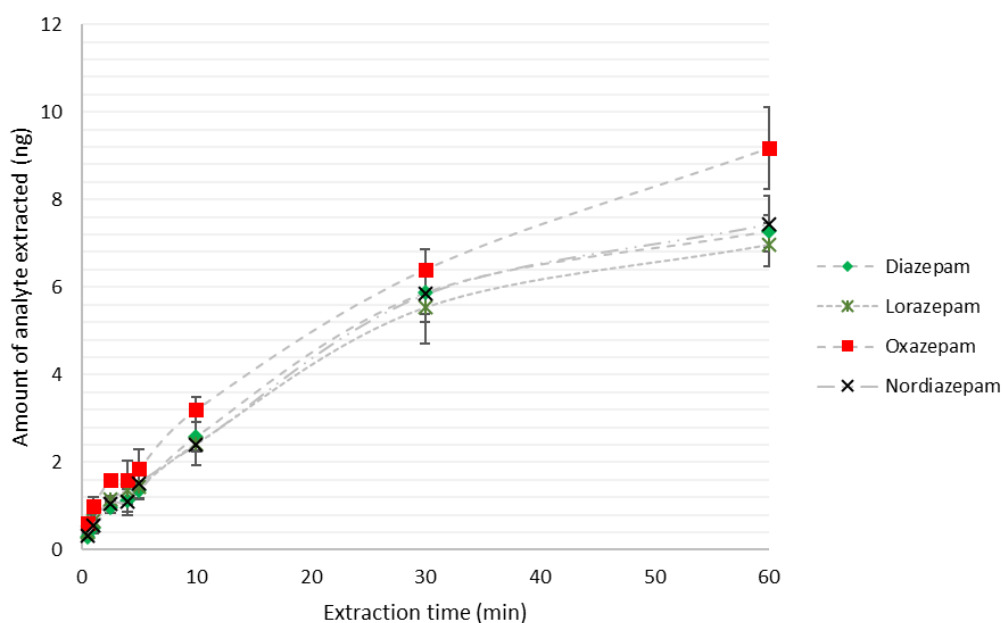
Figure 3.21 *Extraction time profiles obtained at 0.5, 1, 2.5, 4, 5, 10, 30, and 60 min (n = 4) for the extraction of 200 ng mL^{-1} of BZDs spiked to a 50 µL sample and desorbed to a 50 µL solvent mixture (ACN/H$_2$O, 50/50) for LC-MS/MS analysis. Desorption was performed for five minutes. The highly porous nature of the HLB coating suggests that longer extraction times are needed to achieve full equilibrium due to the coating's small pore size.[435] However, the achievement of full equilibrium is not always a pre-requisite for successful SPME extraction, especially if sufficient sensitivity is obtained in the pre-equilibrium regime.*

that the analytes rapidly release from the minitips (i.e., one minute). This result is similar to those obtained by Piri-Moghadam[25] and could be related to the device's scale, i.e., very small amount of extractive phase allowing rapid release of analytes to desorbing solvent. The minitips' ability to provide

quick desorption times is very useful for real-time direct-to-MS approaches that aim to produce rapid results.
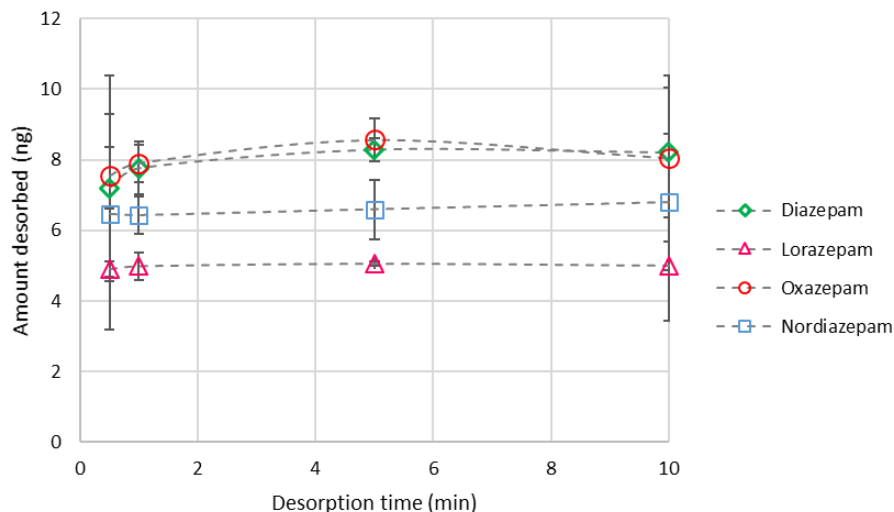
Figure 3.22 *Desorption time profile obtained at 0.5, 1,5, and 10 min for a 10 min extraction of 500 ng mL^{-1} of BZDs spiked to a 50 μL sample and desorbed to a 50 μL solvent mixture (ACN/H$_2$O, 50/50) for LC-MS/MS analysis.*

Preliminary performance assessments: Is the quantitation with SPME minitips satisfactory?

Before proceeding with further experimentation, it was important to conduct assessments of quantitative performance of the minitips. These were performed using PBS as the interference free matrix and urine, as the more complex matrix. A matrix matched calibration with and without IS correction was employed. While it was in our interest to examine calibration without correction, the use of an IS is highly beneficial when working with small sample volumes because micro-scale analyses inevitably produce a greater
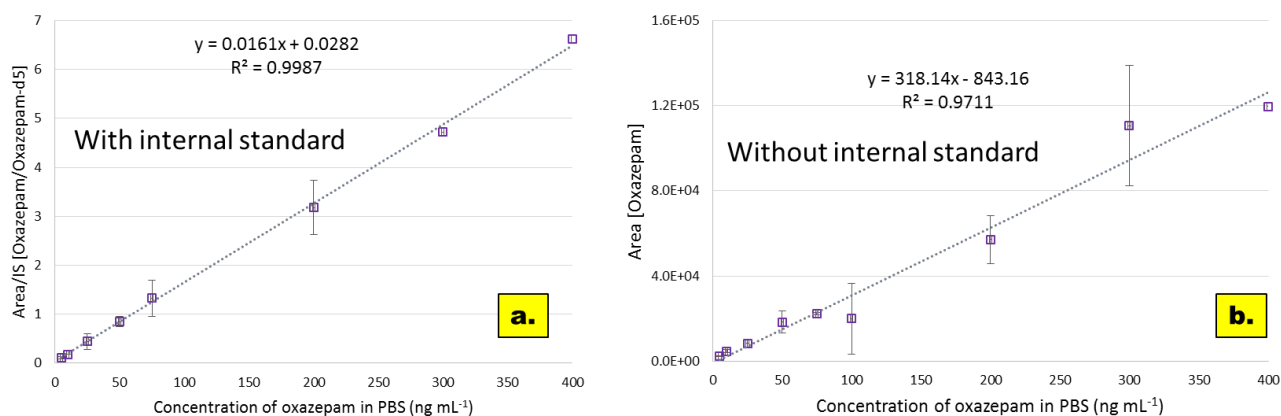
Figure 3.23 *Quantitation of oxazepam in PBS using a.) IS correction approach (Area of standard/ area of IS, i.e., A/IS); b.) no IS correction (area of standard only) (note: same points are used in both cases).*

number of errors. The calibration plots for oxazepam in PBS with and without IS correction are shown in Figure 3.23. As it can be seen, the plot with the IS (Figure 3.23a.) included yields a better R^2 value (0.9987) in comparison to plot that does not employ an IS (Figure 3.23b.) for correction ($R^2 = 0.9711$). Linearity appears to be maintained up to 100 ng mL^{-1} in the uncorrected plot, but then starts to veer off at subsequent concentration points (100, 200, 300, and 400 ng mL^{-1}), which potentially could be caused by variation in coating homogeneity on some minitips. However, it would appear that the use of an IS provides adequate correction for the calibration. As it can be seen from Table 3.11, satisfactory figures of merit are obtained for diazepam, oxazepam and nordiazepam in both PBS and urine. The tested QC level (100 ng mL^{-1}) was in the 95-127.5% accuracy and 3.4-15.8% repeatability range for PBS. For urine, accuracy and repeatability were in the 104-116.4% and 5.7-12.5% ranges, respectively. Lorazepam was excluded from the quantitation due to a higher LOQ (50 ng mL^{-1}). All the LODs and LOQs determined in this research were calculated based on S/N ratio of 3 and 10, respectively. The LODs (1 ng mL^{-1} for PBS, 1-5 ng mL^{-1} for urine) and LOQs (5 ng mL^{-1} for PBS, 5-10 ng mL^{-1} for urine) are satisfactory. Higher LOQs were obtained for urine which is not surprising since urine is a more complex matrix. It is also important to keep in mind that the sensitivity is influenced by desorption volume and the flow of mobile phase employed for LC-MS/MS analysis. For this analysis, we employed a flow rate of 150 µL min^{-1} and injected 20 µL of sample. This appears to have been adequate, as satisfactory detection limits were achieved. Nonetheless, it is important to emphasize the fact that dilution free instrumental analysis techniques could yield better results.

Table 3.11 *Figures of merit obtained for the detection of diazepam, oxazepam, and nordiazepam in PBS and urine.*

Matrix	PBS						QC point (RSD, %, n = 3)	Urine						QC point (RSD, %, n = 3)
Compound	LOD	LOQ	R^2	LDR	Slope	Intercept	100 ng mL^{-1}	LOD	LOQ	R^2	LDR	Slope	Intercept	100 ng mL^{-1}
Oxazepam	1	5	0.9987	5-400	0.0161	0.0282	95.0 (6.7)	1	5	0.9996	5-400	0.0136	0.1443	104.0 (5.7)
Diazepam	1	5	0.9994	5-400	0.0484	-0.0793	105.6 (15.8)	1	5	0.9990	5-400	0.0429	0.3236	107.1 (12.5)
Nordiazepam	1	5	0.9984	5-400	0.0497	0.3457	127.5 (3.4)	5	10	0.9994	10-400	0.0544	0.4882	116.4 (8.5)

Applications of the SPME minitip: Quantitative Detection of DoAs in 1μL of Oral Fluid via LC-MS/MS

To demonstrate the minitips' efficiency in applications where sample volume is highly limited, we simulated an experiment wherein only 1 µL of OF was available for extraction. Such a scenario may be encountered in forensic settings, i.e., trace amounts of biological evidence. In addition to working with a very challenging sample volume, we also decided to employ an LC-MS/MS approach whose flow rate was 400 µL min^{-1}.[211] Higher flow rates provide greater sample dilution, thus resulting in an inevitable reduction or complete loss of sensitivity. In a way, the analytical capabilities of the minitips were pushed to their limits. Ten DoAs (logP: 0.3-4) were chosen for the investigation. Despite increased dilution, analysis of the afore-mentioned compounds was successful. Owing to the use of HLB microparticles, SPME minitips possess very good preconcentrating power. This allowed us to obtain LODs in the 5 - 50 ng mL^{-1} range and LOQs in 10 - 75 ng mL^{-1} range (Table 3.12). The highest LOD and LOQ in each case is obtained for testosterone (50 and 75 ng mL^{-1}), which could be related to poorer ionization efficiency of this compound. Furthermore, we performed QC analysis at 150 ng mL^{-1} and obtained accuracy in the 79.4 - 113.3 % range and repeatability in the 5.2-20.2 % range. Additionally, MEs were assessed at the following levels: 5, 50, and 100 ng mL^{-1}. The results are shown in Table 3.13, and, as can be seen, they exhibited a range of 85.8-131.6 %. Certain compounds, such as oxycodone and cocaine,

exhibited higher MEs (i.e., 130.6 and 131.6 %, respectively), which demonstrates a tendency towards matrix enhancement.

Table 3.12 Figures of merit obtained for the quantitation of DoAs in 1 µL of OF using LC-MS/MS.

Analyte	LOD (ng mL^{-1})	LOQ (ng mL^{-1})	R^2	LDR (ng mL^{-1})	Slope	Intercept	QC level 150 ng mL^{-1}; accuracy (RSD, %, n = 3)
Oxycodone	10	25	0.9952	25-1000	0.0115	-0.3608	113.3 (17.8)
Benzoylecgonine	25	50	0.9929	50-1000	0.0085	0.0835	96.0 (15.7)
Cocaine	10	25	0.9940	25-1000	0.0279	-0.9347	104.0 (8.8)
Carbamazepine	25	50	0.9930	50-1000	0.0484	-1.5198	110.4 (9.0)
Cocaethylene	10	25	0.9955	25-1000	0.0177	0.1090	112.4 (20.2)
Clenbuterol	10	25	0.9927	25-1000	0.0076	0.2060	79.4 (5.2)
LSD	5	10	0.9948	10-1000	0.0106	-0.2005	100.7 (7.6)
Testosterone	50	75	0.989	75-1000	0.0116	-0.5946	99.9 (18.7)
Propanolol	25	50	0.9925	50-1000	0.0210	-0.8611	112.4 (7.1)
Fentanyl	10	25	0.9947	25-1000	0.1200	4.1730	81.4 (11.1)

Table 3.13 Absolute MEs and precision calculated for extraction from 1 µL of OF at 5, 50, and 100 ng mL^{-1} for selected DoAs.

Compound	Absolute matrix effect (precision, RSD %, n = 3)		
	Spiked level		
	Low (5 ng mL^{-1})	Medium (50 ng mL^{-1})	High (100 ng mL^{-1})
Oxycodone	100.8 (22.1)	98.1 (27.6)	130.6 (10.1)
Benzoylecgonine	110.9 (25.4)	123.3 (6.4)	123.0 (18.3)
Cocaine	105.3 (19.8)	121.4 (24.5)	131.6 (20.3)
Carbamazepine	95.7 (15.2)	104.1 (21.0)	119.3 (16.5)
Cocaethylene	120.1 (27.1)	116.3 (5.9)	114.3 (8.2)
Clenbuterol	106.6 (25.2)	122.2 (4.7)	121.6 (16.6)
LSD	97.4 (14.9)	98.6 (20.7)	121.0 (8.1)
Testosterone	107.5 (29.8)	85.8 (12.2)	101.2 (16.1)
Propanolol	93.4 (9.4)	118.5 (19.4)	123.3 (2.6)
Fentanyl	114.6 (15.4)	115.3 (10.8)	122.5 (2.4)

Applications of the SPME minitip: Quantitation of DoA(s) in 1 µL of Human Blood via nESI Ionization

nESI ionization is a nanoscaled form of ESI wherein specialized nESI tips are filled with a small volume of solvent solution, which is then sprayed to produce a mist of charged droplets.[86] nESI tips can be coupled to chromatography[338] or AIMS,[204] and are ideal for small-volume analysis because they produce a significant increase in sensitivity. nESI provides enhanced sensitivity through minimal dilution, which increases ionization efficiency and ion transmission due to the reduction of droplet sizes during the ESI process.[339] SPME and nESI have already been used together in applications where the nESI tips functioned as spray emitters, with the SPME device being introduced to the emitter through either online or offline means.[25,206,240] These applications are notable for their ability to obtain low LODs, despite using complex matrices such as blood, urine, or plasma. For example, Gómez-Ríos et al.[206] were able to achieve a detection limit of 5 ng mL^{-1} for amitriptyline by performing extractions from 20 µL of blood using 4 mm SPME MM fibers. Additionally, Piri-Moghadam's use of PPy microtips yielded detection limits of 0.3 (cocaine), 5 (oxycodone), and 25 ng mL^{-1} (amitriptyline) from 5 µL samples of urine, plasma, and blood, respectively.[25] These detection limits are primarily attributable to SPME's ability to efficiently pre-concentrate the analytes in addition to the "clean" introduction of the sample to MS (i.e., implementing a post-extraction wash step to remove any potential biological interferences that may have adhered to the coating). Given the results obtained by Gómez-Ríos[206] and Piri-Moghadam,[25] as well as the ever-present need for a sample preparation tool that can efficiently sample small volumes, an investigation was conducted to examine HLB's suitability as a new sorbent for SPME-nESI. To this end, 1 µL of blood was spiked with DoA(s) with different logP values (PubChem)[156] and protein binding percentages (PB%) (DrugBank).[161] PB% indicates the actual free concentration of an analyte that is available for extraction. SPME extracts via free concentration, which means that sensitivity may be compromised in scenarios where analytes are highly bound to proteins, as only a small portion of the analyte will available for extraction.[7] Due to the complexity of blood and the use of static SPME

extraction (i.e. potentially reduced mass transfer to SPME), we opted to use a longer extraction time (5 min), while keeping the desorption time at 1 min. The results for the quantification of the DoAs and the QC point (37.5 ng mL^{-1}) are provided in Table 3.14 and calibration plots can be seen in Figure 3.24. We did not examine a greater number of compounds due to the TSQ Vantage's limitations on the number of scans that can be monitored simultaneously. Lower detection limits (< 2.5 ng mL^{-1}) were obtained for most drugs, despite higher PB% for certain ones. For example, while propranolol is bound to proteins at $> 90\%$, the obtained LOD was 1 ng mL^{-1}. Certain drugs, such as clenbuterol and cocaethylene, had higher LOQs (12.5 and 25 ng mL^{-1}, respectively), but a further review of the literature (PB % unavailable on DrugBank)[161] revealed that these compounds also have a tendency towards higher PB %.[340,341] It was not necessary to perform additional steps like diluting blood viscosity, which alters the matrix's intrinsic properties, in order to achieve low detection limits. An examination of the tested validation point (37.5 ng mL^{-1}) revealed accuracy and repeatability in the 96.5-125.8 % and 1.7-7.7 % ranges, respectively. A higher response (125.8 %) was observed for cocaethylene, which could be attributed to co-extracted components from blood. Nonetheless, when compared to more conventional microsampling techniques (i.e., DBS and volumetric absorptive microsampling), SPME's matrix-compatible coating and washing step allow for more efficient pre-concentration and sample clean-up. Since the need for smaller volumes of blood benefits animal welfare, child screening, and TDM, it comes as no wonder that the pharmaceutical industry is shifting towards the use of volume-effective tools.[194] SPME could be integrated into an all-in-one package, allowing simultaneous sample collection and extraction. In fact, SPME offers the potential to make diagnostics more convenient for both the patient and laboratory personnel, as it can allow patients to collect samples in the comfort of their own home through a simple finger prick. In a sense, SPME and point-of-care MS could pave the way for a future where simply providing 1 µL of blood will be sufficient for diagnostic testing, thus alleviating physical distress for patients and allowing health-care professional to make faster decisions.[193]

Table 3.14 *Figures of merit obtained for the quantitation of DoAs in 1 µL of blood using nESI.*

Analyte	LOD (ng mL^{-1})	LOQ (ng mL^{-1})	R^2	LDR (ng mL^{-1})	Slope	Intercept	QC level 37.5 ng mL^{-1}; accuracy (RSD, %, n = 3)
Oxycodone	2.5	5.0	0.9945	5.0-425.0	0.0173	0.0003	96.6 (2.7)
Cocaine	1.0	2.5	0.9994	2.5-425.0	0.0243	-0.0754	99.5 (1.7)
Carbamazepine	0.5	2.5	0.9991	2.5-425.0	0.0502	-0.1804	96.5 (5.1)
Cocaethylene	2.5	25	0.9975	25.0-425.0	0.0246	0.0001	125.8 (7.7)
LSD	1.0	2.5	0.9999	2.5-425.0	0.0212	-0.0250	96.4 (4.7)
Clenbuterol	2.5	12.5	0.9926	12.5-425.0	0.0168	0.1447	106.6 (3.1)
Propanolol	1.0	2.5	0.9938	2.5-425.0	0.0458	-0.0107	95.1 (4.4)
Fentanyl	0.5	2.5	0.9990	2.5-425.0	0.1685	0.8156	118.0 (4.9)
EDDP	0.1	0.5	0.9977	0.5-500.0	0.0191	0.1117	111.2 (1.5)

A. protein binding: 80-85 % y = 0.1685x + 0.8156 R² = 0.999

B. protein binding: 76 % y = 0.0502x - 0.1804 R² = 0.9991

C. protein binding: >90 % y = 0.0458x - 0.0107 R² = 0.9938

D. protein binding: N/A y = 0.0168x + 0.1447 R² = 0.9926
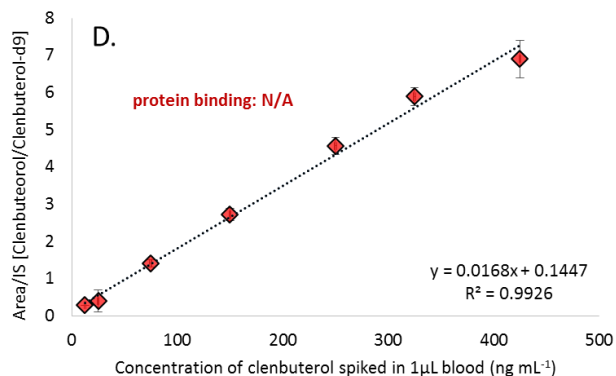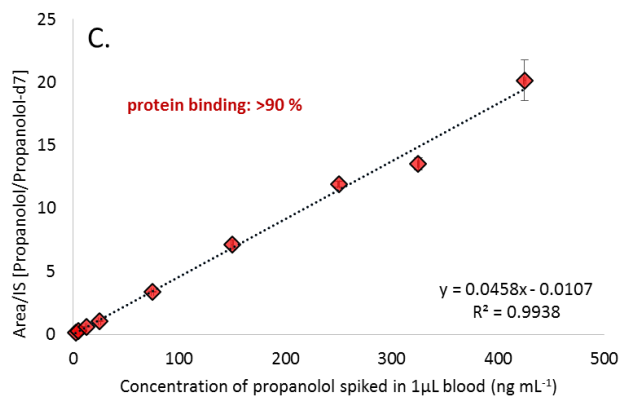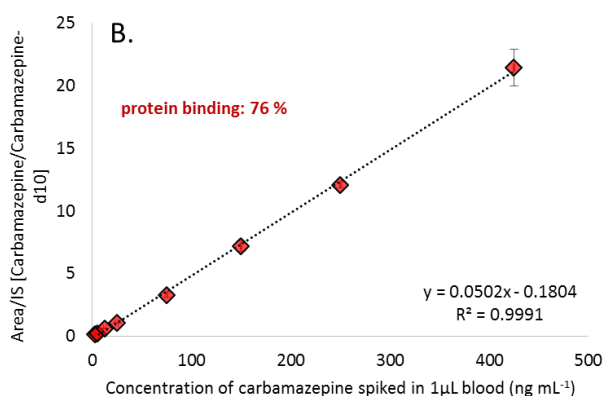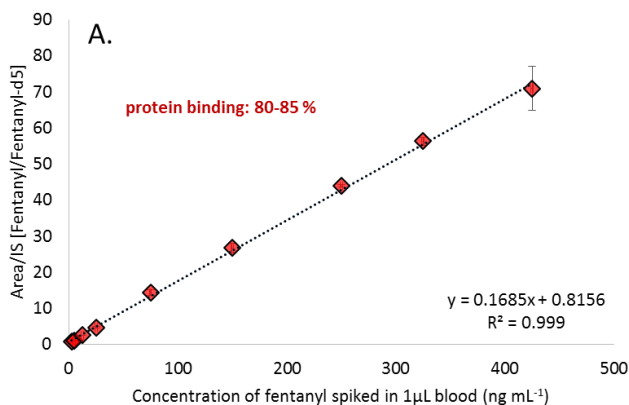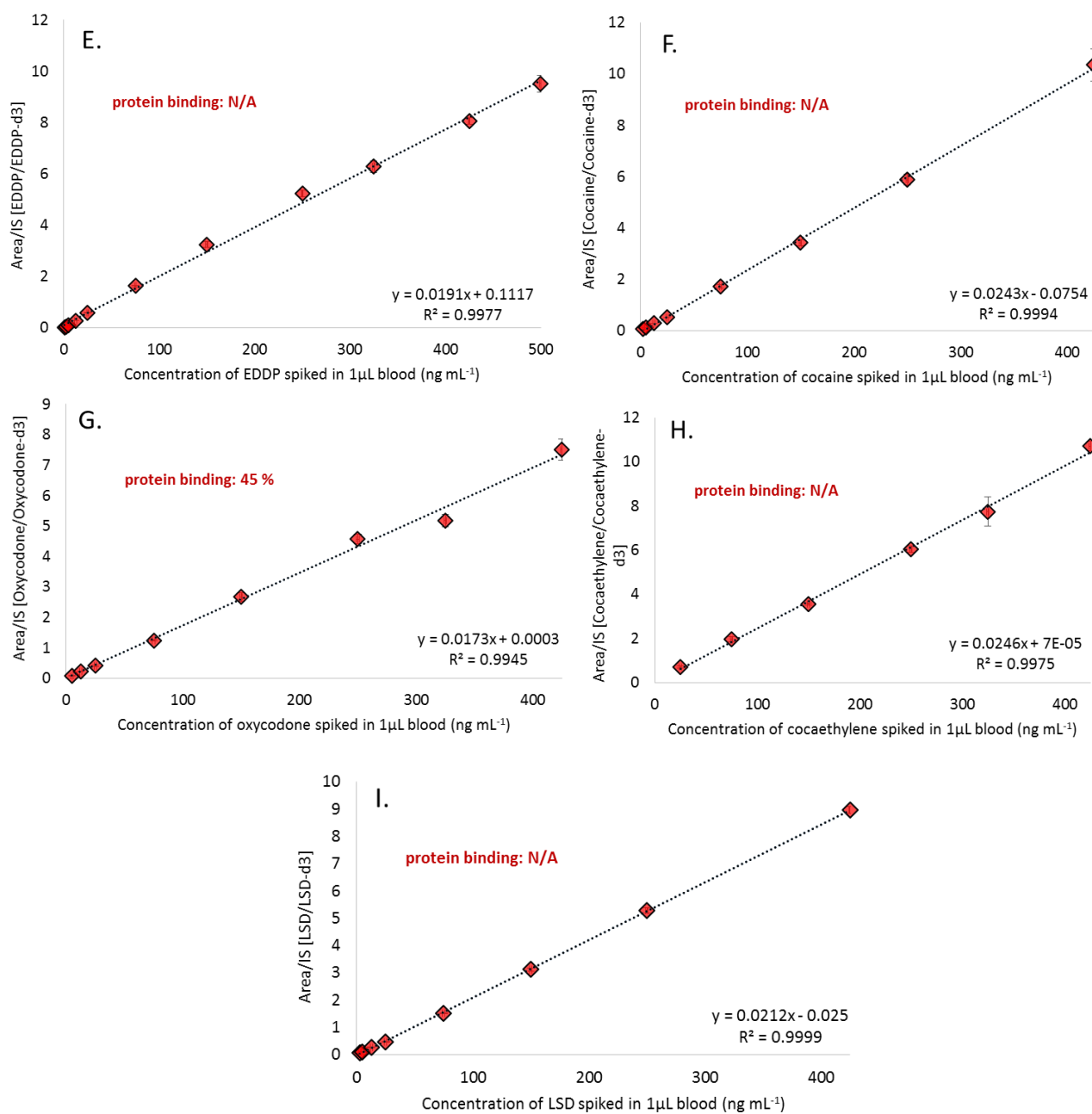
Figure 3.24 Calibration plots obtained for DoAs sampling from 1 μL of blood via SPME-HLB-minitips and nESI using a matrix-matched IS correction approach. Fentanyl, carbamazepine, propranolol, clenbuterol, EDDP, cocaine, oxycodone, cocaethylene, and LSD can be seen in plots **A.-I.**, respectively.

Application of the SPME minitip: Metabolic Profiling of Selected Caviar Species

Since the goal of untargeted metabolomics is to obtain as much information about a system as possible,

the key sample preparation requirement is to ensure reduced selectivity,[59] as this allows for the extraction

of compounds with the widest range of physico-chemical characteristics. While common metabolomic sample preparation methods like LLE and SPE are inconvenient for small-volume analysis, SPME may offer a viable alternative.[342] Since SPME's format can be tailored for specific applications, it offers considerable potential for use in volume-limited metabolomics. Previous SPME applications for untargeted metabolomics have involved the use of C18 or MM (C18 with benzenesulfonic acid particles) (5-30 μm sized) embedded on nitinol wires. Due to their size, such particles proved unsuccessful for coating the extremely thin substrates used in our study. Nanomaterials were also considered, but they provide higher selectivity, hence reducing their effectiveness for untargeted metabolomics. This reduced effectiveness is also evidenced in the lack of reports on their use.[343] Therefore, SPME minitips coated with micro-sized HLB particles were utilised as a compromise between selectivity and sensitivity. Their potential was investigated by sampling four different types of caviar eggs and performing LC/HRMS analysis using an Exactive Orbitrap. To the best of our knowledge, there has only been one other study that has investigated the lipidomic profile of caviar using a combination of direct-to-MS approaches, focusing mostly on high MW species.[344]

The data obtained for caviar sampling from the Exactive was converted to mzXML format using MSConvert[345] and processed using R-software.[69] Without using any data filters, a total of 3034 features were detected. A table of m/z vs retention time (min) can be seen in Figure 3.25. A strict data treatment was then applied wherein peaks with an S/N < 5 when compared to PQC were first eliminated, which was followed by the elimination of peaks with a % RSD greater than 30%. This data treatment process left us with 177 features, which were subjected to analysis with Metaboanalyst.[346] A PCA plot seen in Figure 3.26 was used to observe the data clustering trends. The best PCA plot was obtained based on an overview that Metaboanalyst provides that demonstrates which combination of components provides the best PCA model. For our data, we found that 2 PCs on the x-axis (24 %) and 1 PC on the y-axis (43.3%) provided us with a satisfactory PCA model (Figure 3.27a. shows a 3D PCA plot created for the further

inspection of data variance). A separation between salmon, herring and lumpfish can be observed in the

2D plot, while the 3D plot reveals a slight separation between the black and red lumpfish. As shown in
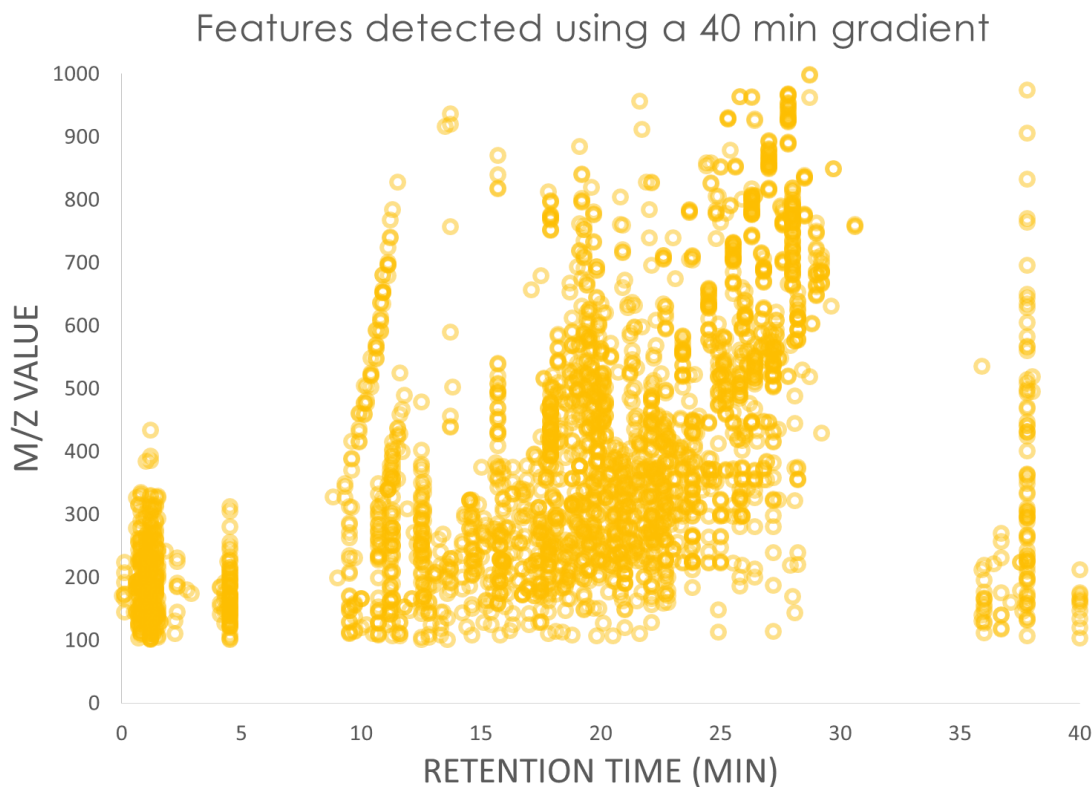
Figure 3.25 *m/z values (total of 3034 features) vs their respective retention times (minutes). The data shown in this figure was obtained via an LC/MS-based approach wherein analysis was performed using a chromatographic 40-min binary gradient method with a flow of 300 μL min^{-1}. We highlight this because over 3000 features were found in the data, despite the small size of the sample (fish egg).*

Figure 3.27b., the supervised PLS-DA model shows better separation between the red and black

lumpfish, although a single replicate of the black lumpfish does fall within the red lumpfish region. To

ensure that the PLS-DA plot was not "forced" into separation, we performed a LOOCV using Q2 as a

performance measure. The optimum number of components was two, with R2 and Q2 being 0.61 and

0.45, respectively. A permutation test using separation distance (B/W) and a permutation number of 100

gave us a value of $p < 0.01$, indicating that the PLS-DA model was not the product of randomness

(validation results can be seen in Figures 3.28-3.29). The "cleaned" features were subjected to one-way,

rigorous, non-parametric ANOVA, resulting in 149 significant metabolites (a detailed list of these

analytes can be found in Table 3.15). Next, the "blank" desorptions of the minitips (n = 3) were inspected
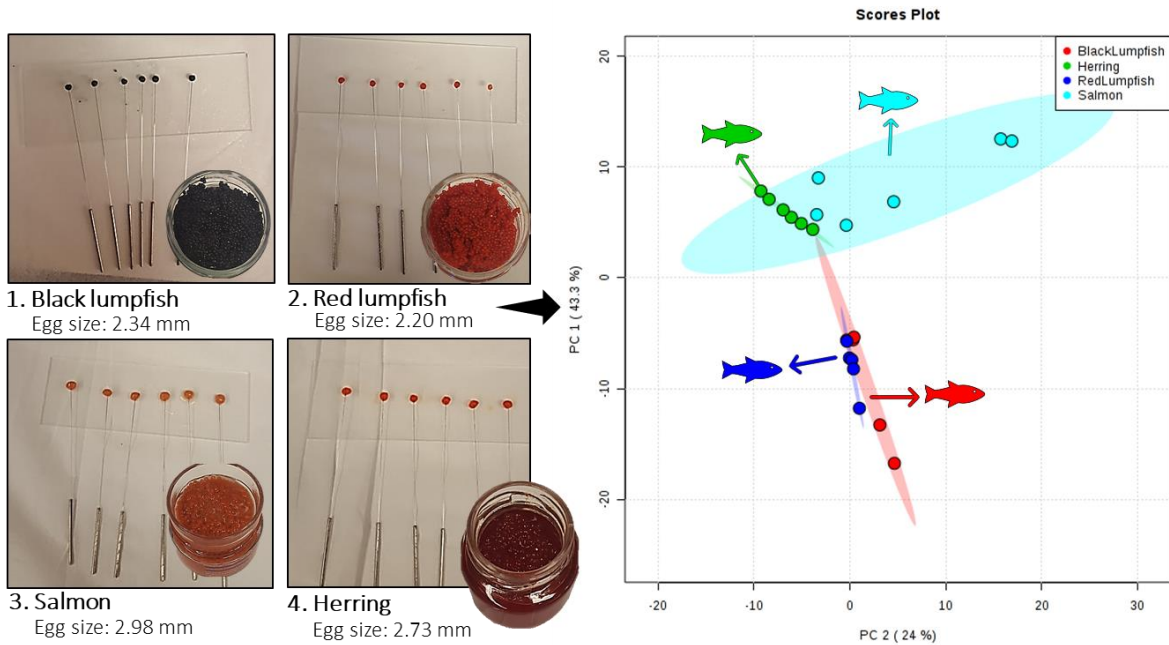
Figure 3.26 PCA plot obtained for the untargeted metabolomic analysis of four different types of caviar (light blue: salmon; green: herring; red: black lumpfish; dark blue: red lumpfish) with two components on the x-axis and one component on the y-axis. Notable separation between salmon, herring, and lumpfish (with exception of one black lumpfish sample) can be observed.

for false positives. Features were searched using the Metlin database,[73] with a number of compounds commonly found in fish being detected, including:eicosapentaenoic acid (EPA), L-tryptophan, retinoic acid, 3,4-dimethyl-5-pentyl-2-furannonanoic acid, cholesterol, N-acetylhistidine, and octadecadienoic
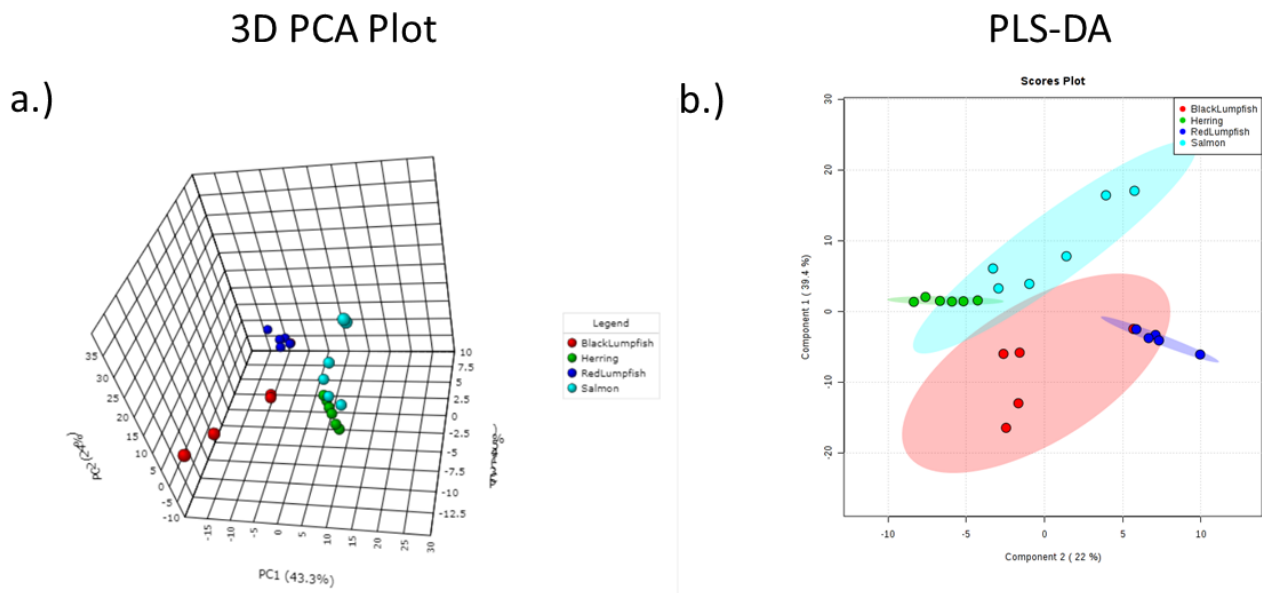
Figure 3.27 3D PCA plot in a. and PLS-DA plot in b. for the untargeted data obtained from sampling different types of caviar roe.

207
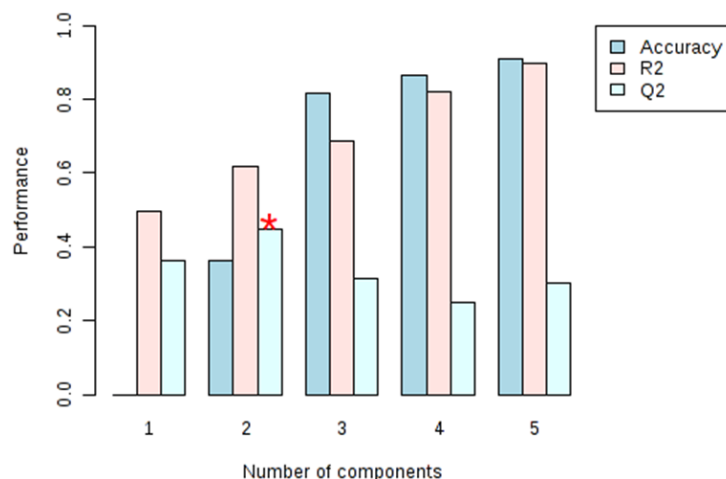
Figure 3.28 *Results obtained for assessment of the PLS-DA model used to examine untargeted metabolomic data from caviar sampling. The model was examined using a LOOCV approach with Q2 as a performance measure. Note the red star marking that the model is best fitted using two components. The R2 and Q2 values read 0.61 and 0.45, respectively.*

acid. The distinguished chromatographic peaks of L-tryptophan (red lumpfish) and EPA (black lumpfish) are shown in Figure 3.30, alongside their normalized concentrations. Given potential compositional similarity between the fish, it is unsurprising that shared metabolites were found for both black and red
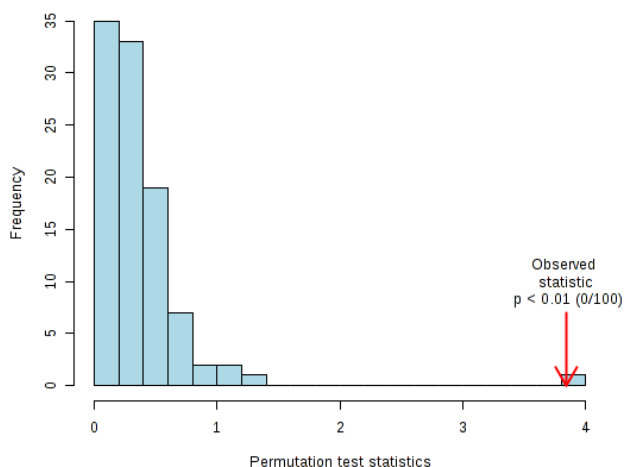
Figure 3.29 *Permutation test conducted using separation distance (B/W) and a permutation number of 100. Note that the observed test statistic (p) lies to the right of the test, indicating that the PLS-DA model built for the study is not the product of randomness. It is important to examine the validity of a PLS-DA model, as untargeted data may often be "over-fitted" using this approach.*

lumpfish, as well as salmon and herring (Fig. 3.31). It is important to note that the discovered significant features are not mostly characterized by high MW species. Minitips could also be potentially useful for

detecting environmental pollutants. For example, they could be used to detect the presence of toxic arseno-containing lipids in marine species (particularly caviar eggs), which is an issue that is rapidly becoming more prominent.[347] It is important to keep in mind that this study used dilution (LC) to profile caviar species and that the size of the sampled subjects could have significantly undermined detection capability. Nonetheless, satisfactory separation with defined chromatographic peaks and rich metabolomic information was still obtained. It is rather difficult to imagine the development of an optimum analysis agenda for trace compounds in complex matrices without using some sort of separation.[348] Undoubtedly, separation would aid in resolving some of the issues associated with complex mass spectra, discrimination between isomeric and isobaric species, and elevated MEs.[306] MEs cannot be completely eliminated, but they can be minimised, and using improved chromatography is an efficient way to eliminate interfering compounds from analytes.[349] For example, combining the use of narrow-bore columns with reduced internal diameters and nanoflow ultra-high performance LC and nESI can not only allow peaks to elute at greater concentration,[339] but it has also been shown to efficiently reduce suppression effects.[349,350] In fact, Kajiyama et al. have already implemented nanoflow LC and excision-based sampling for analyses of certain low MW compounds in the petal tissues of Torenia hybrida.[351] In addition, Dovichi's team and others have also made efforts to introduce hyphenation into cell analysis by implementing both LC and capillary electrophoresis in the analysis of 1000-4000 proteins in Xenopus laevis embryos.[352,353] While work is currently undergoing in our laboratory to produce probes with even thinner substrates, we anticipate that our minitips will best be implemented in studies involving larger single cells.

Table 3.15 *List of features and their adducts whose class, parent, and ID were tentatively identified using the Metlin and FoodBank databases. In addition, p values, false discovery rate (FDR) values, number of possible species, and the error associated with each feature have also been provided. Please note that identifications on databases are still unavailable for many m/z values. Hence, these fields were left as "N/A", but they do show the number of significant features identified by SPME.*

Mass of the adduct	Class	Direct parent(s)	Positive mode adduct(s)	p value	FDR	# of possible species	Tentative ID	Error (ppm)
170.5484	N/A	N/A	N/A	0.00049	0.001622	N/A	N/A	N/A
190.56	N/A	N/A	N/A	0.00021	0.001622	N/A	N/A	N/A
201.1489	Lipids	Medium chain FAs	[M+H]⁺	2.2E-03	3.0E-03	9	*2-oxo-undecanoic acid*	1
233.1357	N/A	N/A	N/A	5.3E-03	6.6E-03	N/A	N/A	N/A
241.0681	N/A	N/A	N/A	1.1E-03	1.7E-03	N/A	N/A	N/A
241.6326	N/A	N/A	N/A	2.7E-02	3.1E-02	N/A	N/A	N/A
249.0613	Indoles & derivatives	Indolyl carboxylic acids & derivatives	[M+2Na-H]⁺	1.8E-03	2.5E-03	3	*L-Tryptophan*	0
250.0646	N/A	N/A	N/A	3.6E-03	4.7E-03	N/A	N/A	N/A
262.9872	N/A	N/A	N/A	1.0E-03	1.7E-03	N/A	N/A	N/A
281.0948	N/A	N/A	N/A	1.8E-02	2.1E-02	N/A	N/A	N/A
288.1606	N/A	N/A	N/A	0.00065084	1.6E-03	N/A	N/A	N/A
290.6395	N/A	N/A	N/A	0.00039774	1.6E-03	N/A	N/A	N/A
296.1875	Glycerophospholipids	PSs'	[M+3Na]⁺	0.00014526	1.6E-03	6	N/A	5
298.6257	N/A	N/A	N/A	0.0002552	1.6E-03	N/A	N/A	N/A
301.2164	Lipids	Retinoids	[M+H]⁺	9.3E-04	1.6E-03	3	*Retinoic acid*	0
303.2322	Lipids	Long chain FA	[M+H]⁺	4.1E-02	4.4E-02	5	*Eicosapentaenoic acid*	1
304.0136	N/A	N/A	N/A	1.4E-03	2.0E-03	N/A	N/A	N/A
304.1733	Carboxylic acids & derivatives	Alpha amino acids and derivatives	[2M+ACN+H]⁺	6.2E-03	7.7E-03	4	*Creatine*	2
304.2356	N/A	N/A	N/A	9.4E-03	1.2E-02	N/A	N/A	N/A
323.2582	Lipids	Long chain FA, Furanoid FA	[M+H]⁺	2.6E-02	3.0E-02	3	*3,4-Dimethyl-5-pentyl-2-furannonanoic acid*	0
324.6870	N/A	N/A	N/A	2.7E-03	3.6E-03	N/A	N/A	N/A
327.2524	Lipids	Medium chain FA	[M+H]⁺	1.2E-03	2.5E-03	2	*8-methoxy-13-hydroxy-9,11-octadecadienoic acid*	1

328.2559	Diazines	Pyrazines	[2M+2H+3H$_2$O]$^+$	0.0049364	6.2E-03	7	_2,3-Diethyl-5-methylpyrazine_	4
339.2137	N/A	N/A	N/A	0.0031428	4.1E-03	N/A	N/A	N/A
341.2322	N/A	N/A	N/A	0.0016672	2.4E-03	N/A	N/A	N/A
344.0644	n/a	N/A	N/A	0.00052005	1.6E-03	N/A	N/A	N/A
355.2837	Fatty acyls	Long chain FA	[M+CH$_3$OH+H]$^+$	0.0031494	4.1E-03	11	_3,4-Dimethyl-5-propyl-2-furanundecanoic acid_	2
357.2914	N/A	N/A	N/A	0.018092	2.2E-02	N/A	N/A	N/A
367.2454	Glycerolipids	1,2-DAGs'	[M+Na]$^+$	0.00065496	1.6E-03	2	_DG (8:0/8:0/0:0)_	0
369.2630	N/A	N/A	N/A	0.033549	3.7E-02	N/A	N/A	N/A
369.3511	Steroids and steroid derivatives	Cholesterols and derivatives	[M+H-H$_2$O]$^+$	0.018769	2.2E-02	10	_Cholesterol_	3
370.3553	N/A	N/A	N/A	0.028431	3.2E-02	N/A	N/A	N/A
371.2268	Lipids	1,2-DAG-3-phosphates	[M+H+Na]$^{2+}$	9.2E-04	1.6E-03	10*	~	0
373.1854	N/A	N/A	N/A	3.0E-03	4.0E-03	N/A	N/A	N/A
373.2743	N/A	N/A	N/A	1.5E-04	1.6E-03	N/A	N/A	N/A
383.3163	Glycerolipids	1,3-DAGs'	[M+H-H$_2$O]$^+$	7.0E-04	1.6E-03	10	N/A	0
388.2547	Lipids	PEs'; 1,2-DAG-3-phosphates	[M+ACN+2H]$^{2+}$	8.0E-04	1.6E-03	9	~	0
389.2576	N/A	N/A	N/A	5.1E-04	1.6E-03	N/A	N/A	N/A
395.1670	Carboxylic acids and derivatives	Histidine and derivatives	[2M+H]$^+$	1.8E-03	2.5E-03	-	_N-Acetylhistidine_	1
401.3414	Glycerolipids	Alkyl-DAGs'	[M+H+K]$^+$	2.4E-03	3.3E-03	5	N/A	N/A
402.3440	N/A	N/A	N/A	1.5E-03	2.2E-03	N/A	n/a	n/a
402.3491	Glycerolipids	1,2-DAGs', alkyl-DAGs'	[M+H+K]$^+$; [M+2ACN+2H]	1.1E-03	1.7E-03	27	N/A	2-5
404.2871	Lipids	PEs'	[M+ACN+2H]$^{2+}$; [M+H+NH4]$^{2+}$	2.1E-02	2.5E-02	50	~	3
415.2535	Lipids	PGPs'	[M+H+Na]$^{2+}$; [M+2H]$^{2+}$	9.2E-04	1.6E-03	4	~	0
416.2857	Lipids	PEs'; PSs'	[M+ACN+2H]$^{2+}$; [M+H+NH$_4$]$^{2+}$; [M+3ACN+2H]$^{2+}$	2.1E-03	3.3E-03	38	~	1-4
432.2800	N/A	N/A	N/A	8.7E-04	1.6E-03	N/A	N/A	N/A

437.2363	Lipids	PGPs'	[M+H+Na]²⁺; [M+2Na]²⁺; [M+2H]²⁺	7.7E-04	1.6E-03	21	~	0-3
439.3571	Prenol lipids; Fatty acyls	Kaurane diterpenoids; linoleic acids and derivatives	[M+H]⁺; [M+H+K]⁺	4.5E-03	5.8E-03	23	*Thujyl 19-trachylobanoate*	0-3
440.2085	N/A	N/A	N/A	1.5E-04	1.6E-03	N/A	N/A	N/A
454.3291	Lipids	PCs'	[M+H]⁺	2.6E-04	1.6E-03	5	~	N/A
455.2956	Lipids	PEs'	[M+3ACN+2H]²⁺	7.5E-04	1.6E-03	12	~	3
457.3684	Glycerolipids	TAGs'	[M+2H]⁺; [M+H+Na]⁺	6.0E-03	7.4E-03	45	N/A	2-4
459.2806	Lipids	PIs'	[M+H+Na]²⁺	8.7E-04	1.6E-03	1	*PI(P-18:0/22:6(4Z,7Z,10Z,13Z,16Z,19Z))*	2
460.2827	Lipids	PEs'; LPEs'	[M+H-H₂O]⁺	2.5E-03	3.8E-03	4	~	0-1
460.3124	N/A	N/A	N/A	9.1E-04	1.6E-03	N/A	N/A	N/A
461.3145	Fatty acyls; Glycerophospholipids	Long chain fatty alcohols; PIs'	[M+2K-H]⁺; [M+2ACN+2H]⁺	7.4E-04	1.6E-03	3	*Erythro-6,8-Pentacosanediol*	3; 5
468.3093	Lipids	PCs'; PEs'; PAs'; LPCs'	[M+H]⁺; [M+NH4]⁺	7.1E-04	1.6E-03	8	~	1
469.3112	Lipids	PEs'	[M+3ACN+2H]²⁺	2.0E-04	1.6E-03	14	~	2
476.3077	Glycerophospholipids; fatty acyls	PSs'; furanoid FAs'	[M+ACN+2H]⁺²; [2M+2H+3H2O]⁺	7.8E-04	1.6E-03	11	*3-Methyl-5-pentyl-2-furanpropanoic acid*	1-4
477.3102	Lipids	PIs'	[M+2H]²⁺	8.3E-04	1.6E-03	1	*PI(22:6(4Z,7Z,10Z,13Z,16Z,19Z)/21:0)*	1
479.0499	N/A	N/A	N/A	4.8E-03	6.1E-03	N/A	N/A	N/A
480.3083	Lipids	PEs'; Monoacylglycerophosphates; PAs'; LPEs'	[M+H]⁺; [M+NH4]⁺; [M+ACN+H]⁺	9.8E-04	1.6E-03	8	~	0
481.2627	N/A	N/A	N/A	8.5E-04	1.6E-03	N/A	N/A	N/A
481.3126	Lipids	PEs'	[M+3ACN+2H]²⁺	9.2E-04	1.6E-03	4	~	0
482.3236	Lipids	LPCs'; LPEs'	[M+H]⁺	4.6E-04	1.6E-03	3	~	1
482.3597	Lipids	PCs'	[M+H]⁺	8.0E-04	1.6E-03	6	~	1
483.3275	Lipids	PEs'	[M+3ACN+2H]²⁺	1.1E-03	1.7E-03	4	~	2
483.3631	N/A	N/A	N/A	4.4E-04	1.6E-03	N/A	N/A	N/A
485.3471	N/A	N/A	N/A	1.7E-02	2.1E-02	N/A	n/a	N/A
488.3958	Glycerolipids	TAGs'	[M+NH₄]⁺	1.2E-03	1.8E-03	1	*2,3-bis(Acetyloxy)propylicosanoate*	3

489.3969	Glycerop hospholip ids	PSs'	[M+H+NH$_4$]$^+$	1.7E-03	2.4E-03	1	_PS(24:0/24:0)_	3
490.4006	Lipids	PCs'	[M+3ACN+2H]$^{2+}$	1.1E-03	1.7E-03	7	~	1
493.3501	Glyceroli pids	TAGs'	[M+Na]$^+$	6.5E-04	1.6E-03	1	_2,3-bis(Acetyloxy)prop ylicosanoate_	0
494.3251	Lipids	PSs'; PEs'; PAs'; PCs'; LPCs'	[M+H]$^+$	2.8E-04	1.6E-03	5	~	0; 1
494.3545	N/A	N/A	N/A	1.5E-04	1.6E-03	N/A	N/A	N/A
495.3267	Lipids	PCs'	[M+H+K]$^{2+}$	2.0E-04	1.6E-03	3	~	2
496.3410	Lipids	PCs'; PEs'; LPCs'	[M+H]$^+$	1.2E-03	1.8E-03	11	~	2
497.2731	N/A	N/A	N/A	3.3E-04	1.6E-03	N/A	N/A	N/A
497.3442	Glycerop hospholip ids	DimethylPEs'	[M+3ACN+2H]$^{2+}$	9.6E-04	1.6E-03	4	~	1
498.3466	N/A	N/A	N/A	7.9E-04	1.6E-03	N/A	N/A	N/A
500.2777	Lipids	LPEs'; PAs'; PEs'	[M+H]$^+$; [M+NH4]$^+$; [M+ACN+H]$^+$	6.1E-04	1.6E-03	5	~	1
501.2814	N/A	N/A	N/A	2.2E-04	1.6E-03	N/A	N/A	N/A
502.2913	Lipids	PEs'; LPEs'; PCs'; PAs'; LysoPAs'	[M+Na]$^+$; [M+ACN+Na]$^+$	2.4E-04	1.6E-03	1	~	1-3
502.3748	N/A	N/A	N/A	3.3E-04	1.6E-03	N/A	N/A	N/A
503.3054	N/A	N/A	N/A	8.5E-04	1.6E-03	1	N/A	2
504.3371	Lipids	Furanoid FAs'	[2M+3H$_2$O+2H]$^+$	8.4E-04	1.6E-03	1	_3,4-Dimethyl-5-pentyl-2-furanpropanoic acid_	0
505.3416	Lipids	PCs'	[M+2Na]$^{2+}$	8.5E-04	1.6E-03	2	~	4
507.3290	N/A	N/A	N/A	6.8E-04	1.6E-03	N/A	N/A	N/A
508.3314	N/A	N/A	N/A	3.4E-04	1.6E-03	N/A	N/A	N/A
508.3389	Lipids	PEs'; PCs'; LPEs'; PAs'	[M+H]$^+$; [M+NH4]$^+$	6.0E-04	1.6E-03	7	~	1
509.3437	n/a	N/A	N/A	2.2E-04	1.6E-03	N/A	N/A	N/A
510.3554	Lipids	LPCs'; LPEs'; PCs'; PAs'; PEs'	[M+H]$^+$; [M+NH4]$^+$	4.0E-04	1.6E-03	14	~	0
516.3088	Lipids	PCs'; LPCs'; PSs'	[M+H]$^+$; [M+H-H$_2$O]$^+$	3.6E-04	1.6E-03	4	~	0-1
517.3120	N/A	N/A	N/A	2.8E-04	1.6E-03	N/A	N/A	N/A
518.3219	Lipids	PCs'; PEs'; LPEs'	[M+H]$^+$; [M+Na]$^+$	9.7E-04	1.6E-03	17	~	0-4
519.3247	N/A	N/A	N/A	2.6E-04	1.6E-03	N/A	N/A	N/A

520.3387	Lipids	PCs'; LPCs'; PSs'; PEs'	[M+H]+; [M+H-H2O]+	8.7E-04	1.6E-03	13	~	2-3
521.3353	Lipids	PEs'; LPEs'	[M+ACN+H]+; [M+NH4]+	8.4E-04	1.6E-03	12	~	0
521.3825	N/A	N/A	N/A	1.5E-04	1.6E-03	N/A	N/A	N/A
522.3551	Lipids	PAs'; PCs'; LPCs'; PSs'	[M+ACN+H]+; [M+H]+; [M+H-H2O]+	6.0E-04	1.6E-03	20	~	0; 1
523.3253	N/A	N/A	N/A	8.9E-04	1.6E-03	N/A	N/A	N/A
523.3577	N/A	N/A	N/A	5.2E-04	1.6E-03	N/A	N/A	N/A
524.3712	Lipids	PCs'; LPCs'; LPEs'	[M+H]+	6.4E-04	1.6E-03	12	~	0
525.2869	N/A	N/A	N/A	9.9E-04	1.6E-03	N/A	N/A	N/A
525.3027	N/A	N/A	N/A	0.00093127	0.001622	N/A	N/A	N/A
525.3392	N/A	N/A	N/A	0.0028319	0.003769	N/A	N/A	N/A
525.3756	N/A	N/A	N/A	0.00039774	0.001622	N/A	N/A	N/A
525.3994	N/A	N/A	N/A	0.00025482	0.001622	N/A	N/A	N/A
526.2936	Lipids	PEs'; LPEs'	[M+H]+	7.7E-04	1.6E-03	3	~	1
527.2956	N/A	N/A	N/A	1.2E-03	1.9E-03	N/A	N/A	N/A
535.3596	N/A	N/A	N/A	2.2E-03	3.0E-03	N/A	N/A	N/A
537.3764	N/A	N/A	N/A	1.1E-03	1.7E-03	N/A	N/A	N/A
542.3246	Lipids	PCs'; PSs'	[M+H]+; [M+H-H2O]+	6.5E-04	1.6E-03	2	~	0-1
543.3263	N/A	N/A	N/A	8.5E-04	1.6E-03	N/A	N/A	N/A
543.4017	N/A	N/A	N/A	1.5E-04	1.6E-03	N/A	N/A	N/A
544.3298	N/A	N/A	N/A	4.4E-04	1.6E-03	N/A	N/A	N/A
544.3384	Lipids	PCs'; PAs'; LPCs'	[M+Na]+; [M+H]+; [M+ACN+Na]+	2.7E-05	1.2E-04	25	~	1-4
544.4572	N/A	N/A	N/A	1.5E-04	1.6E-03	N/A	N/A	N/A
545.4604	N/A	N/A	N/A	1.1E-03	1.7E-03	N/A	N/A	N/A
548.3349	N/A	N/A	N/A	7.4E-04	1.6E-03	N/A	N/A	N/A
548.3650	N/A	N/A	N/A	8.7E-04	1.6E-03	N/A	N/A	N/A
549.3396	N/A	N/A	N/A	1.5E-04	1.6E-03	N/A	N/A	N/A
550.3866	Lipids	PCs'; LPCs'	[M+H]+	2.9E-04	1.6E-03	11	~	0
551.3572	N/A	N/A	N/A	8.1E-03	1.0E-02	N/A	N/A	N/A
551.3890	N/A	N/A	N/A	3.9E-04	1.6E-03	N/A	N/A	N/A
553.3347	N/A	N/A	N/A	5.1E-04	1.6E-03	N/A	N/A	N/A

564.3061	Lipids	PCs'; LPCs'	[M+Na]+; [M+2Na-H]+	4.6E-04	1.6E-03	5	~	0-4
565.3104	N/A	N/A	N/A	5.1E-04	1.6E-03	N/A	N/A	N/A
568.3388	Lipids	PCs'; LPCs'	[M+H]+; [M+Na]+	3.7E-04	1.6E-03	6	~	1-2
569.3445	N/A	N/A	N/A	4.2E-04	1.6E-03	N/A	N/A	N/A
570.3163	N/A	N/A	N/A	1.6E-03	2.3E-03	N/A	N/A	N/A
570.3476	N/A	N/A	N/A	3.6E-04	1.6E-03	N/A	N/A	N/A
570.3569	Lipids	LPCs'	[M+H]+	5.5E-04	1.6E-03	2	~	2
571.3597	N/A	N/A	N/A	4.4E-04	1.6E-03	N/A	N/A	N/A
572.4878	Glycerolipids	TAGs'	[M+NH4]+	3.2E-02	3.6E-02	1	*TG(10:0/10:0/10:0)*	1
590.3224	Lipids	PEs'; PCs'; LPEs'	[M+K]+; [M+Na]+	9.8E-06	9.2E-05	13	~	0-1
591.3245	Carboxylic acids and derivatives	Dicarboxylic acids and derivatives	[M+2K-H]+	2.4E-04	1.6E-03	1	*Didodecyl thiobispropanoate*	0
631.4812	Phospholipids	PEs'	[M+H-H2O]+; [M+H]+	2.2E-02	2.5E-02	4	N/A	0
668.4142	N/A	N/A	N/A	9.0E-04	1.6E-03	N/A	N/A	N/A
675.5427	Lipids	Ceramide PEs'	[M+H]+	3.2E-04	1.6E-03	3	~	1
719.5337	Lipids	PCs'; PEs'	[M+ACN+H]+ ; [M+NH4]+	0.02127	0.025096	51	N/A	0
764.5218	Lipids	PAs'; PCs'; PEs'; PSs'	[M+NH4]+; [M+H]+; [M+ACN+H]+; [M+H-2H2O]+; [M+ACN+Na]+;[M+Na]+	0.02623	0.029758	120	N/A	0-2
778.5396	Lipids	PAs'; PCs'; PEs'; PSs'	[M+NH4]+; [M+H]+; [M+ACN+H]+; [M+H-2H2O]+; [M+ACN+Na]+; [M+Na]+	0.00032	0.001622	108	N/A	0-4
806.5703	Lipids	PAs'; PCs'; PEs'; PSs'	[M+NH4]+; [M+H]+; [M+ACN+H]+; [M+H-2H2O]+; [M+ACN+Na]+; [M+Na]+	0.00053	0.001622	111	N/A	0-4
807.5713	Lipids	PIs'	[M+H-H2O]+	0.00053	0.001622	3	N/A	4
826.536	Lipids	PAs'; PCs'; PEs'; PSs'	[M+NH4]+; [M+H]+; [M+ACN+H]+; [M+H-2H2O]+; [M+ACN+Na]+; [M+Na]+	0.00031	0.001622	91	N/A	0-3
827.5412	Lipids	PIs'	[M+H-H2O]+	0.03785	0.041608	23	N/A	3
852.554	Lipids	PCs'; PSs'	[M+H]+; [M+H-2H2O]+ ; [M+Na]+	0.00136	0.002004	32	N/A	0; 3

853.5569	Lipids	PIs'	[M+ACN+H]$^+$; [M+H-2H$_2$O]$^+$; [M+H-2H$_2$O]$^+$	0.00147	0.002144	21	N/A	2; 3

Phosphatidylserine (PS); Fatty acid (FA); Phosphatidylethanolamines (PE); Diacylglycerols (DAG); Phosphatidylglycerophosphate (PGP), Phoshatidylcholine (PC); Phospatidylinotisol (PI); Phosphatidic acid (PA); Triacylglycerol (TAG); Lysophosphatidylethanolamine (LPE); Lysophosphotidylcholine (LPC); Phosphoethanolamines (PEA)
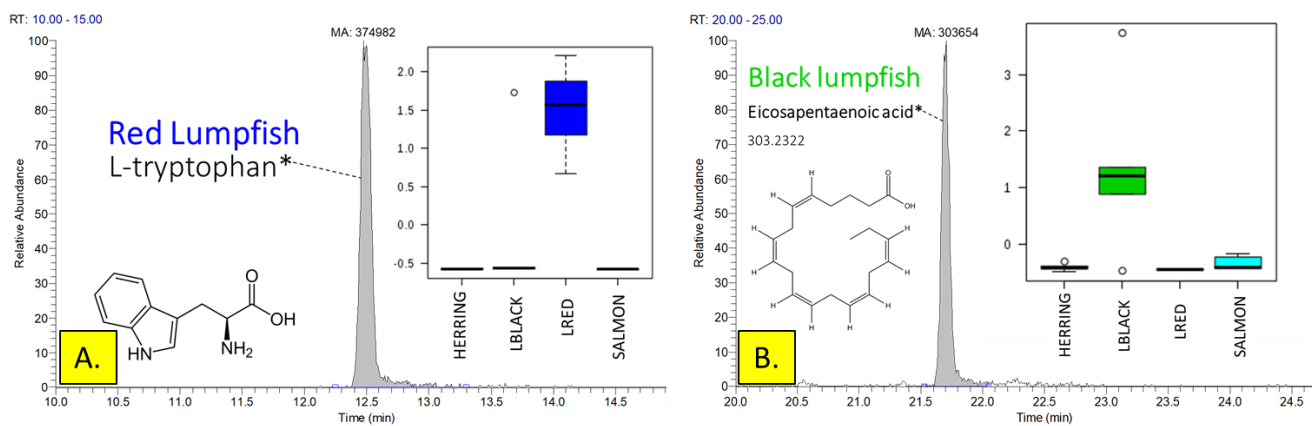
Figure 3.30 *Chromatographic peaks obtained for the untargeted metabolomic analysis of red and black lumpfish using SPME-HLB minitips and LC/HRMS. In **A.** and **B.**, tentatively identified L-tryptophan and eicosapentaenoic acid in red and black lumpfish can be observed. The boxplots with normalized concentrations of the detected values can also be observed in the inserts.*
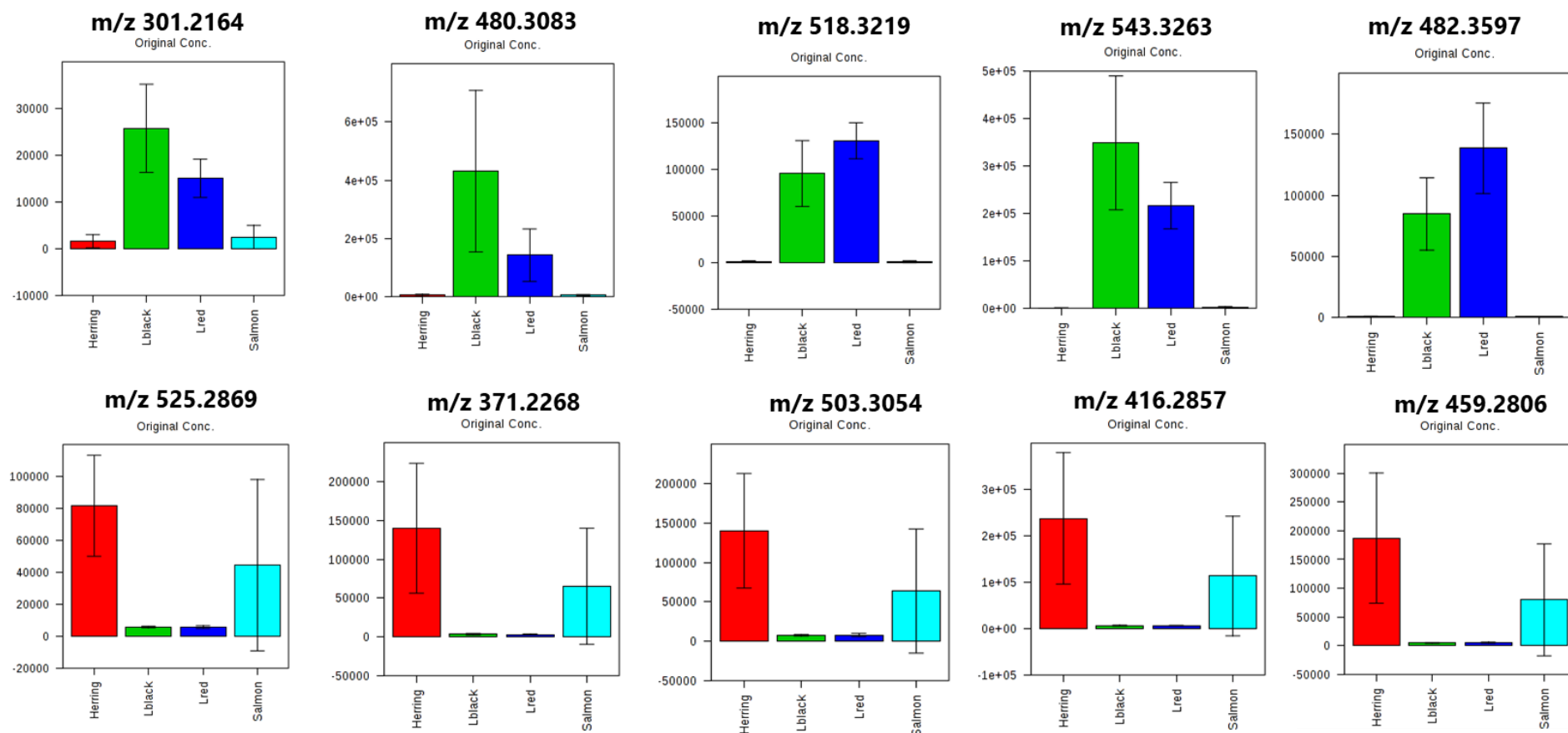
Figure 3.31 *Box plots of selected metabolites for black and red lumpfish (m/z 301.2164, 480.3083, 518.3219, 543.3263 and 482.3597) and herring and salmon (m/z 525.2869, 371.2268, 503.3054, 416.2857 and 459.2806).*

3.5 Conclusion

To the best of our knowledge, this chapter presents the first documented use of a 1 mm SPME minitip coating consisting of solid-coated HLB-PAN microporous particles. The results of our tests showed that our minitips provide good extraction efficiency and adequate repeatability. Furthermore, the results from the drug sampling test using 1 µL of blood and the subsequent nESI analysis demonstrated that the proposed tips are suitable for applications involving limited liquid volumes, which could have potential benefits for sample collection in clinical or forensic settings. We conducted metabolomic profiling on different types of caviar eggs and were able to achieve adequate discrimination and tentative identification among the tested samples. To the best of our knowledge, this is the first reported study that has successfully discriminated between caviar samples using a miniaturized SPME device and LC/HRMS analysis. This result is exceptional given the miniaturized size of the device, the dilution inherent to LC/MS, and the volume of the matrices tested. Unlike uncoated probes, HLB-coated SPME minitips can efficiently pre-concentrate analytes with lower MWs and differing physico-chemical properties. The availability of sampling devices that are capable of pre-concentration and non-selective extraction is highly important for metabolomics of single cells, as they can provide thorough insights into metabolism on a cellular scale. Our approach may be of potential interest to many fields, as the coating on the minitips can be altered in order to extract more challenging analytes more effectively.[309] While the majority of single-cell approaches utilise direct coupling, the use of a hyphenated technique with minitips could potentially allow relevant compounds to be separated more efficiently, thus making data interpretation easier. Indeed, SPME-HLB minitips promise great potential for small volume analyses, as they are easily convertible to accommodate small formats, while still providing quality data. However, one must keep in mind that minitips have certain limitations, such as bending/fragility at reduced tip diameters (d $\leq$ 30 µm), as well as poorer repeatability (i.e., 20-30% RSD) due to slight deviations that occur during tip preparation. As such, our future research is oriented towards establishing

a more reproducible fabrication protocol, as this will significantly enhance the performance of SPME-HLB minitips.

Chapter 4: Untargeted metabolomic analysis of patients afflicted with malignant hyperthermia using LC/HRMS and SPME

4.1   Preamble

Chapter 4 describes a collaboration between UW and Toronto General Hospital and has been submitted for potential publication to *Anaesthesia & Analgesia*. Tijana Vasiljevic completed the sampling, sample processing, instrumental runs, data processing and data interpretation of 2015 and 2016/17 patient cohort. Dr. Barbara Bojko completed the sampling, sample processing, instrumental run, data processing and data interpretation of mice cohort. Dr. Sheila Riazi provided the grant, the human samples and was vital in providing mice samples as a part of collaboration with the Baylor College of Medicine. Dr. Anna Roszkowska contributed to experimental work and provided significant scientific discussion. Dr. Ezel Boyaci contributed to experimental work and some discussion as well. Dr. Natalia Kraeva aided in sampling of 2015 and 2016/2017 patient cohort. Dr. Susan Hamilton and Dr. Amy Hanna of Baylor College of Medicine provided old heterozygous MH (Y524S, YS) and wild type (WT, control) mice and aided in their sampling. Tijana Vasiljevic also wrote this chapter (portions on mice sampling were written by Dr. Bojko with some input of Ms. Vasiljevic) and Dr. Riazi contributed to writing of some portions of the introduction. The manuscript for submission to Anaesthesia & Analgesia was also written by Tijana Vasiljevic, with some contributions from Dr. Bojko and Dr. Riazi. Tijana Vasiljevic and Dr. Barbara Bojko were assigned as equal contributors, whereby Dr. Bojko was assigned as first co-author based on alphabetical order of last names as requested by prof. Janusz Pawliszyn.

I, Barbara Bojko, authorize Tijana Vasiljevic to use this material in her thesis.

I, Sheila Riazi, authorize Tijana Vasiljevic to use this material in her thesis.

I, Anna Roszkowska, authorize Tijana Vasiljevic to use this material in her thesis.

I, Ezel Boyaci, authorize Tijana Vasiljevic to use this material in her thesis.

I, Natalia Kraeva, authorize Tijana Vasiljevic to use this material in her thesis.

I, Susan Hamilton, authorize Tijana Vasiljevic to use this material in her thesis.

I, Amy Hanna, authorize Tijana Vasiljevic to use this material in her thesis.

For this chapter it is important to emphasize that sample collection began in Spring 2015 and concluded in Spring 2017. While reading the chapter, one might note that the two human cohorts are described, 2015 and 2016/2017. The two cohorts were analysed separately. The 2015 cohort was analyzed first, since our goal was to examine whether meaningful information can be obtained from the muscle samples. In other words, we did not want to continue sampling for 2 years to find out that the results were non-informative. Hence, 2016/17 was analysed afterwards. The two were not analysed together due to a possibility of batch effect. Lastly, this chapter includes extensive statistical information pertaining to metabolomic analysis and validation of PLS-DA models. Section 1.4 of Chapter 1 includes key information on the basics of statistical workflow in metabolomics. Detailed overviews are available elsewhere.[436,437,439]

4.2   Introduction

Malignant hyperthermia (MH), a potentially deadly pharmacogenetic disease of skeletal muscle, is triggered by exposure to certain anesthetics. It results in a dysregulated, sustained elevation of myoplasmic calcium (Ca^{2+}) that leads, through as yet not fully identified pathways, to a hypermetabolic state.[354] Mutations in the ryanodine receptor-1 (RyR1) gene, the skeletal muscle L-type Ca^{2+} channel (CACNA1S) gene, and STAC3 gene have been associated with MH susceptibility.[355] Products of these genes play key roles in muscle contraction in the process of excitation-contraction coupling and in maintenance of Ca^{2+} homeostasis in skeletal muscle cells. While we know how mutations in these genes result in the production of massive dysregulated Ca^{2+} fluxes during an MH episode (by reducing the threshold for luminal Ca^{2+} activation and store overload-induced Ca^{2+} release (SOICR),[356] the details of the hypermetabolic processes associated with MH are not clear. Moreover, because the aforementioned genes only comprise ~60% of the population at risk, genetic diagnosis cannot be a sensitive, routine perioperative (pre-surgery) screen for MH susceptibility. The only test available for predicting MH susceptibility with a high sensitivity (i.e., >97%) is a contracture test, known in North America as caffeine-halothane contracture test (CHCT).[357] It involves measuring muscle strips contracture to increasing concentrations of caffeine or halothane. The principle of the test is based on the sensitivity of the muscle to the triggers that induce an increase in intracellular Ca^{2+} and result in skeletal muscle contraction. MH susceptible (MHS) individuals have a higher contracture response at lower trigger concentrations when compared to MH negative (MHN) individuals.

The emphasis on the episodic "MH event" obscures the fact that MH susceptibility is a pleomorphic (many formed) condition. MH is known to have variable penetrance,[358] delayed onset,[358] and is triggered by heat,[359] exercise,[360] and statin medications.[361] The pleiotropic (one gene influences two or several phenotypic traits) nature of clinical presentation makes the timely diagnosis of MH challenging, and therefore may result in delayed treatment both in operating room, and emergency department settings.

This is particularly troubling in the setting of fatal events like exercise related heat stroke in young athletes, where there is an inability to predict individuals at risk, and a lack of knowledge base to diagnose this entity and treat appropriately. Hence, there is a need to determine the characteristics of a potentially unique hypermetabolic pathophysiology in MH, which may ease perioperative or peri-event diagnosis, and also may account for the variety of clinical presentations.

Using pig models of MH, Fletcher and colleagues showed that free fatty acids (FtAs) enhance the effects of volatile anesthetics on Ca^{2+} regulation in skeletal muscle.[362] Studies on MHS RyR1-R163C knock-in mice exhibited an increase in mitochondrial matrix Ca^{2+}, increased reactive oxygen species (ROS) production, in conjunction with lower myoglobin and glycogen contents as well as lower glucose utilization, suggesting a switch to a compromised bioenergetics state characterized by both low oxidative phosphorylation and glycolysis.[363] With the exception of a study done by Chang et al., whereby respirometry was used to measure oxygen flux between MHS and MHN patients, comprehensive studies exploring the details of metabolic pathways of MH in humans are limited.[364]

Metabolomics, which is the study of changes in cellular metabolites occurring after an intervention that affects physiology, is an attractive way of determining biomarkers involved in metabolic reactions, such as MH.[278,365] SPME is a non-destructive sample preparation method that has recently been implemented for metabolite extractions in varying applications by using special solvent-resistant coatings which can be coupled to LC/MS. SPME allows one to identify subtle metabolic changes that typically occur within seconds or minutes.[278] This technology has been extensively tested for both hydrophobic, and hydrophilic metabolites, and has been shown to demonstrate adequate sensitivity, and specificity for cellular metabolites.[366–368]

We hypothesized that the differences between human MHS and MHN individuals are reflected in measurable differences in myoplasmic metabolites. We postulate that by defining the constellation of

metabolic pathways peculiar to MH, we can elucidate the role of these pathways in an MH-related hypermetabolic reaction and understand the phenotypic variability among MHS individuals. To accomplish this, SPME fibers were used to detect MHS and MHN muscle metabolites before and during exposure to caffeine, and halothane, with particular reference to lipid metabolism. Our goal was to define the metabolic pathways activated during an MHS-defining contracture response. Two human cohorts collected within different time periods were used (2015; 2016/17). Analysis was performed using LC-HRMS and when possible, semi-validation of features was performed using parallel reaction monitoring (PRM) and examination of their retention times (RTs) in comparison to those of standards. Tentatively identified metabolites corresponded to acylcarnitines (ACRs), vitamin-D metabolites, long chain fatty alcohols, fatty acids (FtAs), prostaglandins, amino acids as well as selected lipid species for the 2015 cohort. A single metabolite (16:0 LysoPC) was semi-validated, further suggesting involvement of lipid species with the MH condition. The second cohort produced limited information with regards to statistically significant metabolites but due to its value, "informative" features were extracted using heatmaps. Additional SLE extractions were performed on the muscle samples as a means of examining the robustness of the data, i.e., whether the same biomarkers would be obtained using a different sample preparation technique. Indeed, similarities were noted as elevation of several metabolites including amino acids, lipids and compounds related to muscle energy metabolism was evident in both studies. Certainly, differences were noted in the SLE extracts (potential biological and technical variations). Also, sampling of heterozygous MH (Y524S, YS) and wild type (WT, control) mice also confirmed presence of certain metabolites linked to the MH condition.

4.3 Experimental

Materials and methods

Following institutional research ethics board approval, all individuals undergoing muscle biopsy and CHCT at MH investigation unit at TGH were approached, and informed consent were obtained from the

participants. For CHCT, a piece of gracilis muscle is harvested and placed into a Krebs-Ringer (KR; saline solution). North American CHCT protocol was followed for all steps of CHCT.[357]

MS grade H_2O, ACN, MeOH and FA were all purchased from Thermo Fisher Scientific. SPME fibers with a MM extractive phase (C18 with benzenesulfonic acid, 7 mm length) were obtained from Millipore-Sigma. KR solution was made by mixing NaCl, KCl, $CaCl_2$ and $NaHCO_3$ obtained from MilliporeSigma. 16:0 LysoPC was obtained from Avanti Polar Lipids (Alabaster, AL, USA).

SPME sampling and SLE extraction

The excess part of the muscle which was not used for CHCT was utilized for this study. Muscle sizes between 5×5 mm to 10×25 mm were used due to inter-individual muscle size variability. Before the SPME sampling was done, the fibers were removed from preconditioning solution (MeOH/H_2O, 50/50) briefly washed with H_2O (to remove organic content) and using tweezers, carefully inserted into the muscle. Focus was placed on establishing proper contact between fiber and the muscle, since certain muscle samples were quite thin, which can potentially compromise the extraction process. Once inserted, the fibers were kept in the muscle for 15 minutes (n = 3). These samples were labeled as "baseline". Muscles exposed to halothane (3 %) and caffeine (2 mM) were also sampled. Once halothane and caffeine were administered to the CHCT chambers, the muscle strip was tied, penetrated with the SPME fiber and suspended into the chamber kept at 37 °C. See Figures 4.1-4.2 for schematic of the sampling for baseline, halothane and caffeine samples. Sampling was done for 15 minutes in triplicates. To avoid artifact identification, sampling was also done in the KR solution that was used to preserve the muscle sample (n = 3, 15 min extraction). These samples were simply labeled as "KR baselines". In total, n = 30 patient samples were examined (includes both cohorts). Once the sampling was completed, the fibers were carefully removed, washed briefly with H_2O and packed individually in vials. The vials were then placed on dry ice, transported to UW and stored at −80˚C until analysis. Remaining muscle samples were

subjected to SLE extraction. MeOH was added to the muscle samples, followed by rapid vortexing and

centrifugation. The excess organic solvent was removed and reconstituted for LC/MS analysis.
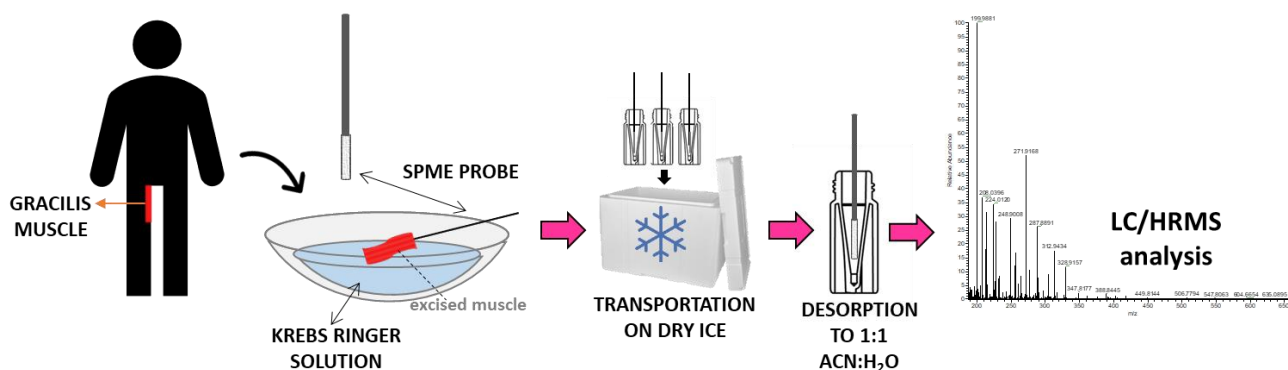
Figure 4.1 *Schematic representation of 'baseline' muscle sampling using SPME fibers.*

Chamber for exposure of muscle to 3 % halothane and 2 mM caffeine
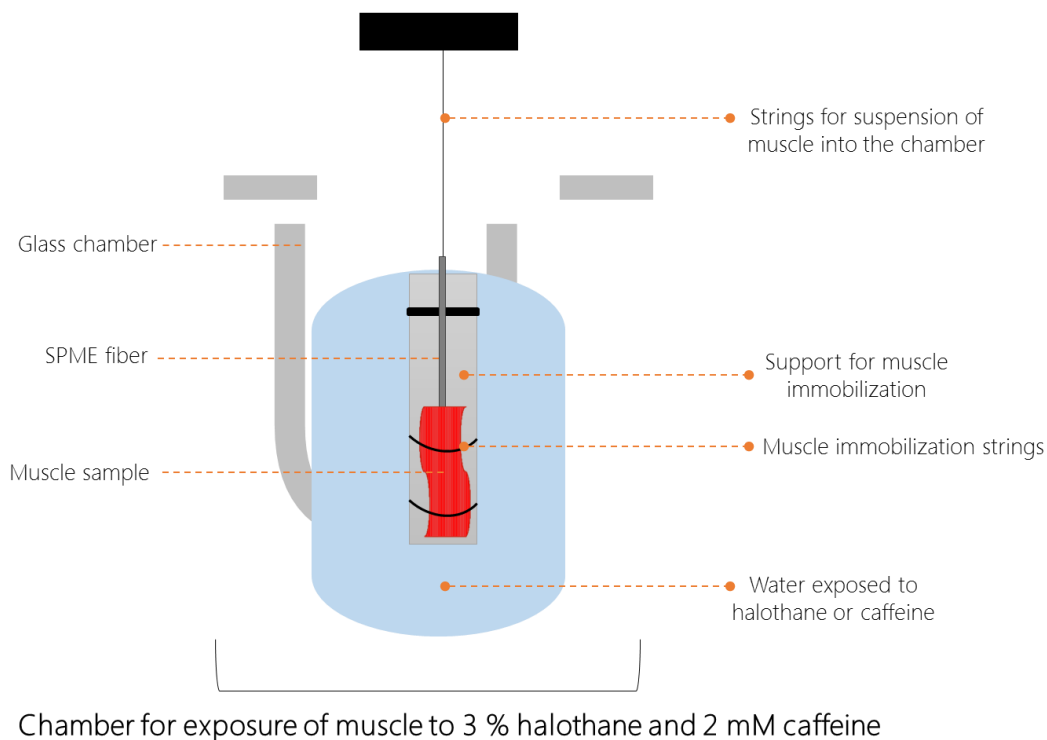
Figure 4.2 *Schematic showing sampling of the MH muscle during exposure to halothane and caffeine. Briefly, the muscle is immobilised to a metallic support and secured with strings. The top of the support is attached to a string which allows the support to be suspended within a glass chamber filled with H_2O. Once ready, the fiber is inserted into the immobilised muscle and suspended within the glass chamber while they are filled with either 3% halothane or 2mM caffeine.*

In vivo **mice SPME sampling**

Mice sampling was performed at the Department of Molecular Physiology and Biophysics at Baylor College of Medicine Houston. The *in vivo* experiment was done using 8 weeks old heterozygous MH (YS, Y524S mutation) and wild type (WT, control) mice (n = 6, each group). The mice were anaesthetized, and a 10-15 mm incision was made to expose the muscles of the upper hindlimb. A 28G needle was used to puncture the superficial muscles of the hindlimb and the extraction fiber (7 mm MM coating) was then inserted into the muscle and left in it for 15 min. After extraction, fibers were withdrawn, and mice were euthanized by cervical dislocation. All of the experiments had undergone ethics clearance and were done in triplicates (n = 3).

Analysis of samples by LC/MS and LC/MS/MS

Before the instrumental run, the fibers were removed from -80˚C and desorbed to 200 µL of ACN/H$_2$O (50/50) for 1 h on a vortex (1500 rpm). Immediately following desorption, a PQC sample was created by pooling predetermined volumes of the desorbed samples. The desorbed samples were analysed in +ve and −ve ionization modes in random order using an ESI source mounted on Exactive Orbitrap, coupled to an Accela autosampler and a binary pump. Additionally, instrumental QC was used to monitor instrument stability, and solvents blanks were used to establish system blanks. Due to the sample size and method length (40 min gradient) a PQC was injected every 10th sample to monitor the stability of the runs. The instrument was calibrated using Pierce™ LTQ Velos for +ve and Pierce™ ESI negative ion calibration solution for −ve ionization mode. The validation experiments were performed using PRM mode with 2 collision energies of 20 and 40 eV via LC-MS/MS done on Q-Exactive Quadrupole Orbitrap and a Dionex Ultimate 3000 UPLC system (Dionex Corporation, Bannockburn, IL, USA). Instrumental analysis of the extracts obtained for *in vivo* mice experiments was performed on Q-Exactive Focus orbitrap MS coupled to a Dionex UltiMate 3000 RS autosampler and a Dionex Ultimate 3000 RS pump

(Thermo Fisher Scientific). Same chromatographic method was used for all three instruments and the details have already been described in Section 3.3. Some instrumental details of Exactive-Orbitrap, Q-Exactive Orbitrap and Q-Exactive Focus Orbitrap can be seen in Table 4.1.

Table 4.1 *Details of MS acquisition specifications for Exactive-Orbitrap, Q-Exactive Orbitrap and Q-Exactive Focus*

Instrument	Exactive-Orbitrap	Q-Exactive Orbitrap	Q-Exactive Focus Orbitrap
Experiment	Full scan	PRM	Full scan
In-source CID	Disabled	0.0 eV	Disabled
Default charge state	-	1	0
Inclusion	-	On	Off
MS	-	-	-
Microscans	1	1	1
Resolution	100,000	70,000	70,000
AGC target	1e6	1e6	1e6
Maximum IT	100 ms	100 ms	100 ms
Loop count	-	1	-
MSX count	-	1	-
MSX isochronous Its	-	On	-
Isolation window	-	1.6 m/z	-
Isolation offset	-	0.0 m/z	-
Fixed first mass	-	-	-
(N) CE/ stepped (N) CE	-	Nce: 20	-
Spectrum data type	-	Profile	Profile

Data analysis

All the data was obtained in raw format of Thermo Xcalibur. The data was converted using MSconvert[345] (filter = peak picking, algorithm = vendor, MS level = 1, mass detector centroid noise: 1e3, data output= .mzXML). After conversion, the data was analysed using R-software[69] (R version 3.5.1 (2018-07-02) "Feather Spray"). Using R-software, features whose % RSD in the PQC was >30 % were removed, as per acceptance criterion proposed by Want et al.[369] Further, features whose S/N ratio was <5 in comparison to PQC were also removed. After data filtering, analysis was done using MetaboAnalyst.[346] Normalization of the data was done using the mean of PQC samples. After normalization, the data was further autoscaled (recommendation for biological interpretations).[370] Visual examination of data clustering was done using PCA and PLS-DA plots. PCA was used to observe general clustering of the

data and whether any outliers were present. Validation of the PLS-DA model was done by examining the maximum number of components (set to 5 max) and by using 10-fold cross-validation (CV) and Q2 for performance measure. The number of components for PLS-DA was chosen based on the result of the validation test. A permutation test (n = 2000) was done to assess the PLS-DA model validity using separation distance (B/W). Non-parametric tests (Wilcoxon's rank t-test or ANOVA, unequal group variance) were applied for the identification of significant features with p-value and false discovery rate (FDR) set at <0.05. Any features that appeared relevant were investigated by examining their chromatograms and comparing to signal from solvent blanks and KR solution. In order to evaluate whether some features were artifacts of KR solution, signal area of features elevated in KR of MHS patients were divided by signal area in KR of MHN patients. Features whose signal area ratio was < 3 were removed. Additionally, areas of chromatographic peaks found in MHS patients were divided by the signal areas found in the patient-specific KR solution. Any peaks that came from solvent blank and KR were removed. Tentative identification of the features was done using Metlin[73] or HMDB[72] whereby precursor m/z tolerance was set to 5 ppm. The following adducts were considered for +ve ionization mode: $[M+H]^+$, $[M+H-2H_2O]^+$, $[M+NH_4]^+$, $[M+Na]^+$ and $[M+K]^+$ while $[M+Na-2H]^-$, $[2M-H]^-$, $[M+FA-H]^-$, $[M-H, M-2H, M-3H]^-$, $[2M+FA-H]^-$, $[M-H2O-H]^-$ and $[M+Br]^-$ were considered for −ve ionization mode. Tentative IDs were assigned if the metabolite was of biological relevance. Metabolites deemed significant were examined by performing PRM on the PQC sample. Mass spectra obtained from the PRM analysis of features of interest was individually examined, and the fragments were searched using MS/MS spectrum mass search (precursor tolerance = 5 ppm, MS/MS tolerance = 0.02 Da) on Metlin.[73] Molecular formulas of the compounds were obtained using Thermo Xcalibur or Metlin and/or HMDB. When available, standards to confirm the presence of suspected metabolites were used to validate the data. Retention times (RTs) of the standards were compared against those of suspected metabolites. Metabolic pathway analysis was done using MetaboAnalyst.

For data processing of extracts of *in vivo* mice sampling, Compound Discoverer (CD) 2.1 software (Thermo Scientific) was used. The mass tolerance window was 3 ppm, S/N threshold was 3, max sample-to-blank ratio was 5. For PQC-based area correction, minimum 80% coverage and maximum 30% RSD was used. The processed dataset was submitted to MetaboAnalyst. Normalization of the data was done using sample median and autoscaling. Statistical analysis was done using fold change analysis, volcano plots, PCA and PLS-DA. Similar to human data, PLS-DA model was assessed by cross validation using 10-fold CV and validated by permutation test (n = 2000) using five components and based on separation distance (B/W).

4.4   Results/Discussion

Statistical analysis of 2015 cohort

Relevant patient details (age, gender, contracture of muscle at caffeine and halothane exposure and results of genetic testing) can be seen highlighted in blue in Table 4.2. Cohort from 2015 is highlighted in blue while 2016/17 is highlighted in yellow in Table 4.2. After analysis of the data with R-software, a total of 15945 features (m/z values) were obtained in +ve and 4985 in −ve ionization mode. Data filtering reduced the numbers to 4408 and 179, respectively. The −ve ionization mode for 2015 cases was filtered, and then analysed by Metaboanalyst but this led to significant reduction of information, yielding no statistically significant information. Hence, since results were considered non-informative results, they were excluded from further data interpretation. The PCA model (normalized using the PQC and autoscaling) for baseline samples can be seen in Figure 4.3A. with 3 PCs (9.5%) on the x-axis and 1 PC (31.5 %) on the y-axis. Cases diagnosed as MHS-halothane (MHH, positive CHCT test to halothane only) were excluded due to outlier behavior (excessively high signal areas pulling data in one direction, please see Figure 4.4A-B.). No clustering based on diagnosis was observed in the PCA plot. Figures 4.3B-C. show the plots obtained for muscle samples exposed to 3% halothane and 2 mM caffeine. Some clustering of MHS and MHN cases can be observed in samples exposed to halothane, while those

exposed to caffeine show a more prominent separation. Better clustering of data was obtained using PLS-DA (Figure 4.5), although some overlap was still present. Since PLS-DA tends to over-fit data (i.e. provide separation/clustering due to class assignment), a validation of the model is recommended.[371] The model was assessed by examining the results of a 10-fold CV and using Q2 as performance measure. According to the data obtained, the optimum number of components is 4, with R2 and Q2 value

Table 4.2 *Patient details including respective diagnostic (MHN, MHS-Both: caffeine and halothane positive, MHS-Halothane (MHH): halothane positive only), age at the time of biopsy, gender, contracture of muscle upon exposure to 2mM caffeine and 3 % halothane as well as result of genetic testing. Patients highlight in blue is 2015 cohort, and those highlighted in yellow represent the 2016-2017 cohort*

Diagnostic	Age at biopsy	Gender	Caffeine contracture	Halothane contracture	Genetic testing
MHN	27	F	0	0.4	-
	47	F	0.2	0.6	-
	58	F	0	0	-
	47	M	0	0.2	-
	64	M	0	1.1	Negative
	39	M	0	0	-
	38	M	0	0.6	-
	33	F	0	0.3	-
	42	F	0	0	-
	44	F	0	0.5	-
	27	F	0.1	0.5	-
	40	F	0	0	-
	41	M	0	0.6	-
	39	M	0	0.2	-
	36	M	0	0.6	-
	39	F	0	0.4	-
	43	M	0	0	-
	35	F	0	0	-
MHS-Both					
	27	M	0.3	1.6	RYR1+: p.Glu3583Gln
	46	F	0.7	1	Negative
	41	F	0.3	1.1	CACNA1S +: p.Tyr585Cys
	34	F	0.3	2	Negative
	37	M	0.3	1.1	-
	24	M	0.6	2.2	RYR1 c.526G>A p.Glu176Lys
	23	M	2	10.6	RYR1 c.526G>A p.Glu176Lys
	33	Male	3.4	6.6	p.His2204Gln
MHS-Halothane (MHH)					
	41	F	0	1.8	Negative
	22	F	0	2.5	Negative
	35	F	0.1	1.3	-
	52	M	0.2	1.2	-
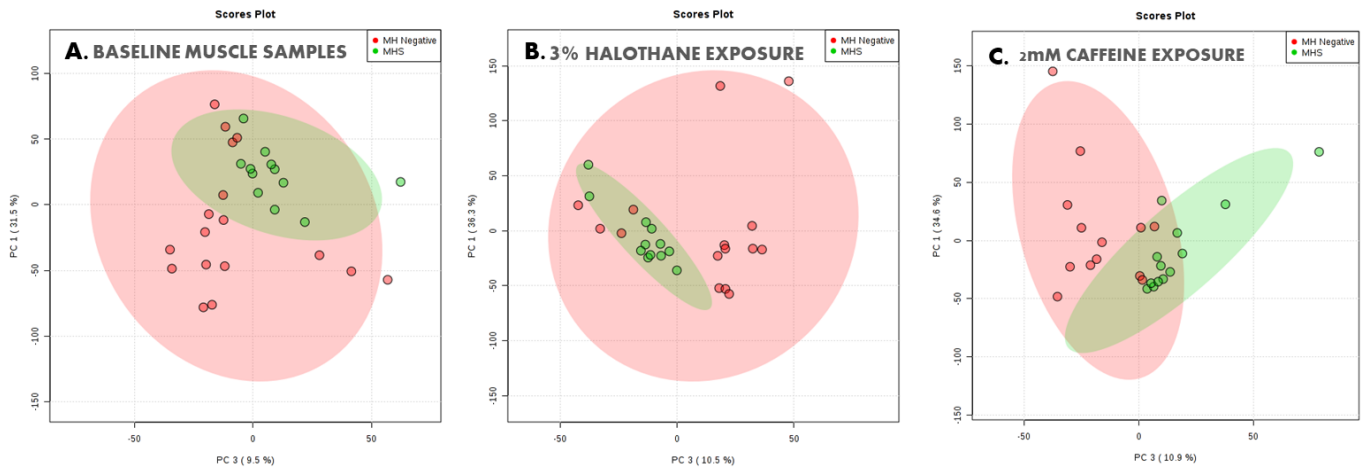
Figure 4.4 *PCA plots of the data obtained for the MHS and MHN patients for the 2015 cohort including (**A.**) baseline, (**B.**) 3 % halothane and (**C.**) 2 mM caffeine exposed samples. Data visualized in these plots has been constructed by normalising the features using mean of the PQC and autoscaling. Note in the PCA plot that positive cases cluster close to negative cases, but still provide acceptable separation (segregation of data is specific clusters) between the two.*

of 0.84 and 0.56, respectively (Figure 4.6; Table 4.3). The permutation test performed (n = 2000) resulted in a p value of 0.065 (Figure 4.7). While the p value is higher than 0.05, the test statistic lies on the right side of the permutation test, indicating that the PLS-DA model obtained is not entirely "forced" or obtained due to class assignment. PLS-DA plots of samples exposed to halothane and caffeine can be
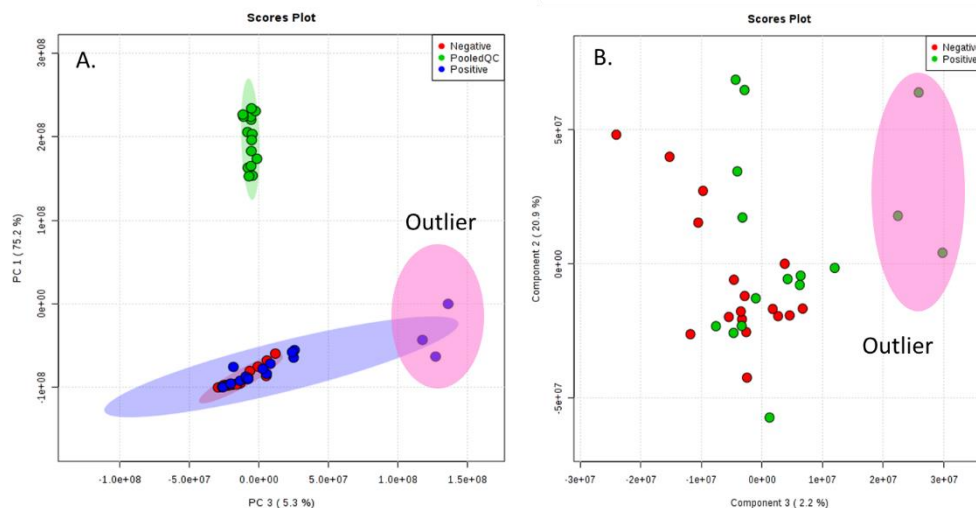
Figure 4.3 *PCA plots of the data indicating outlier presence. Figure **A.** shows the first outlier evident during preliminary data processing, while **B.** shows the outlier after removal of PQC. Indeed, attempting to process the data (i.e., find significant features) using outliers led to erroneous results. Likely cause of outlier behavior could be contributed to batch effects of sample storage.*

232

seen in Figure 4.8 with CV details in Tables 4.4-4.5. Optimum validation tests should be done using an external dataset, which is not always feasible.[372] Since only a limited number of patients were available for the study, CV and permutation tests may be considered useful towards validation , but are not satisfactory as a diagnostic method.[372]
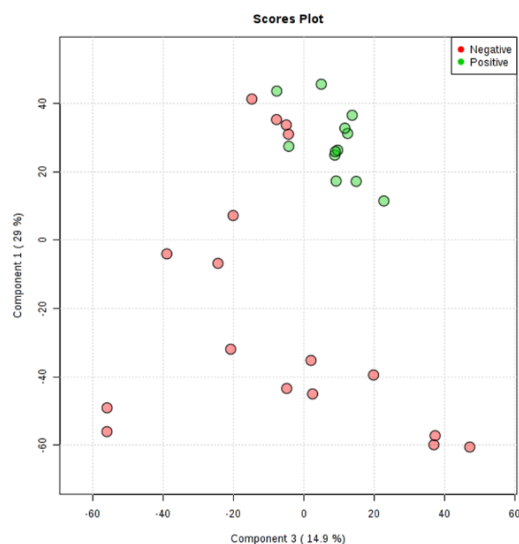
Figure 4.5 PLS-DA plot for baseline samples normalized with PQC and autoscaling. Two outliers have been removed from the plot due to excessively high signals in the samples which initially led to erroneous interpretation of the data (samples potentially compromised by external factors, such as storage for example).
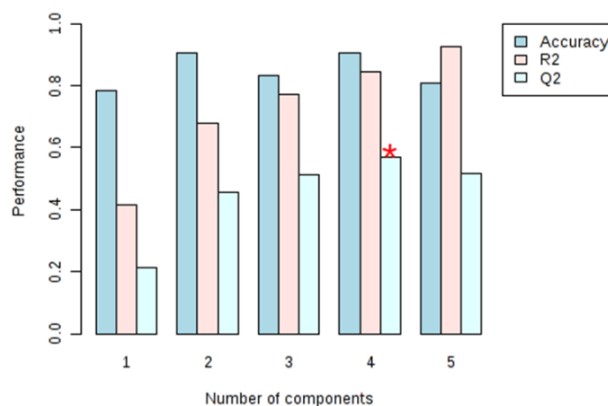
Figure 4.6 Results of cross-validation test done on Metaboanalyst for the PLS-DA model generated in Figure 4.5. The model was assessed by examining the results of a 10-fold CV and using Q2 as performance measure.. The red mark denotes the optimum number of components that should be used for the model. In this case, the optimum number of components is 4.
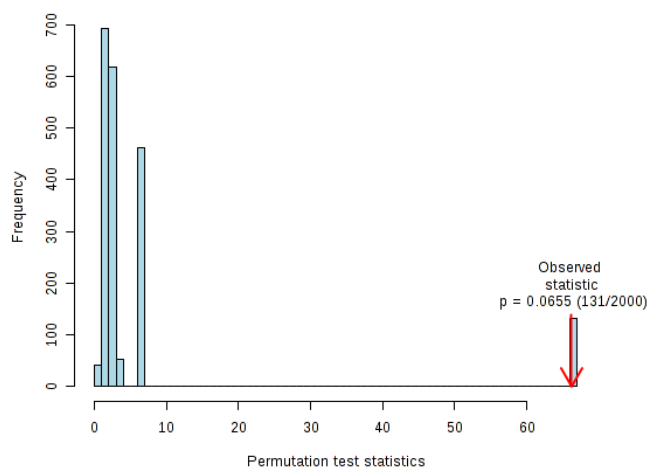
Figure 4.7 *Results of the permutation test done using separation distance (B/W) as the test statistic and permutation number set at 2000 for Figure 4.5. Results return p = 0.0655, which can be deemed acceptable to classification since the ratio B/W sum of squares dos not lie completely on the left side.*

Further evaluation using non-parametric Wilcoxon's rank T-test yielded a total of 829 significant features with 108 being elevated in susceptible cases. With the exception of carnitine, only up-regulated features were considered. The significant features elevated in MHS patients can be seen summarized in Table 4.6 with details that include accurate mass, RTs, ion, predicted formula, tolerance (in ppm), % RSD (mean PQC), p-value, FDR and database reference. Tentative identifications were assigned to these features and box-whisker plots can be found in Figures 4.9-4.11.

Table 4.3 *Detailed results obtained for the cross-validation test seen in Figure 4.5. According to the table shown below, the optimum number of components is 4, with R2 and Q2 value of 0.84 and 0.56, respectively.*

Measure	1 comps	2 comps	3 comps	4 comps	5 comps
Accuracy	0.78571	0.90476	0.83333	0.90476	0.80952
R2	0.41348	0.67660	0.77262	0.84634	0.92470
Q2	0.21425	0.45509	0.51244	0.56756	0.51642
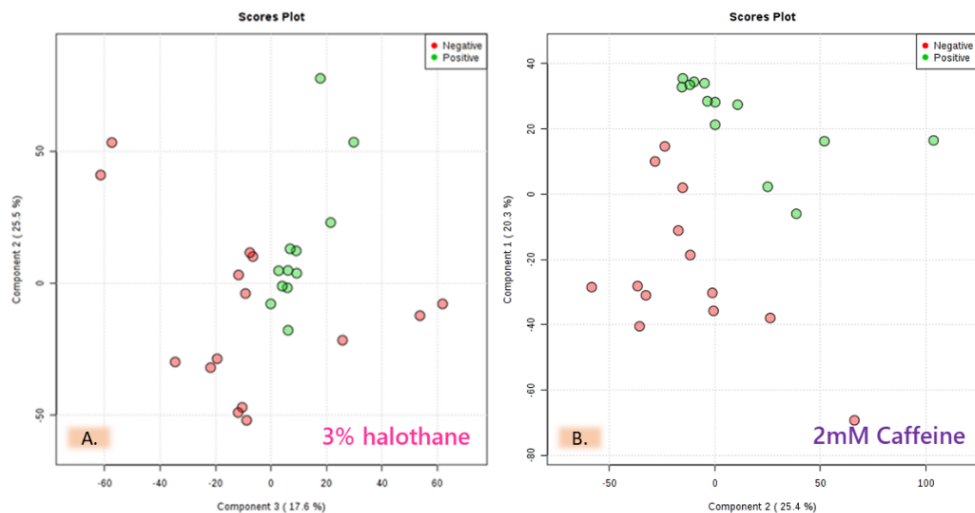
Figure 4.8 *PLS-DA plots of 3 % halothane* (**A.**) *and 2 mM caffeine* (**B.**). *Normalization done by PQC and autoscaling.*

Table 4.4 *Results obtained for cross-validation examination of the data in Figure 4.8.*

Measure	Accuracy		R2		Q2	
	Halothane	**Caffeine**	**Halothane**	**Caffeine**	**Halothane**	**Caffeine**
1 comp	0.77	0.77	0.54	0.63	0.28	0.40
2 comp	0.87	0.80	0.70	0.77	0.48	0.60
3 comp	0.85	0.88	0.81	0.84	0.59	0.65
4 comp	0.97	0.88	0.91	0.94	0.61	0.70
5 comp	0.95	0.94	0.97	0.97	0.64	0.70

Table 4.5 *Results of permutation test done (n = 2000) for samples exposed to 3 % halothane and 2 mM caffeine for Figure 4.8.*

Permutation test summary (n=2000)	
Group	p-value
3% halothane	0.64
2 mM caffeine	0.91

235

Statistical analysis of 2016/17 cohort

Second set of samples consisted of n = 19 patients, with n = 4 MHS-both, n = 2 MHH and the remainder being MHN. After processing of the data with R-software, a total of 10973 features for +ve and 5871 for −ve ionization mode were detected. Removal of peaks using S/N 5 and 30 % RSD led to significant reduction of data volume. Instead, S/N of 3 and RSD of 50% was used. Due to length of run (440 injections ~ 2 weeks of continual instrumental operation for one ionization mode mode) variability in PQC stability was observed in both ionization modes, although more prominent in +ve mode. Hence, only autoscaling was used to normalise the data. PCA plot of baselines for +ve ionization mode can be seen in Figure 4.12A., revealing a time dependent acquisition trend from negative to positive PC1. No clustering was observed based on diagnostics. Removal of first set of injected samples allows for a tighter cluster, but still does not achieve separation between MHH, MHS and MHN for PCA (Figure 4.13). Better separation for +ve ionization mode is observed using PLS-DA (Figure 4.14), but CV and permutation tests reveal that the model does not possess discriminating power (Table 4.7, Figure 4.15). Similar results with respect to PCA, PLS-DA and CV tests are observed in case of samples exposed to 3% halothane and 2mM caffeine in +ve ionization mode (Figure 4.16, Tables 4.8-4.9). Scarce number of significant features were found using the non-parametric ANOVA test. Hence, heatmaps were used to determine features of potential interest, whereby significant features were identified on the basis of their variable importance in projection (VIP) scores. The features with tentative identifications can be seen in Table 4.10. Features with no hits on HMDB, Metlin and of irrelevant biological significance were excluded. Detailed examination of peak areas for these features indicated some elevation in one to three susceptible patients. Examination of -ve ionization mode revealed less variability in the PQC, allowing its use for data normalization (alongside autoscaling). As it can be observed in Figure 4.11B., separation between MHH, MHS and MHN was not present. The MHS cases are clustering within MHN, while MHH is clustering towards negative PC2 with some intertwining with MHN. PLS-DA of baseline

Table 4.6 *List of tentatively identified features (+ve ionization mode) for the 2015 cohort. The table includes the accurate mass of the feature up to 4 decimals, Rt of the respective metabolite in minutes, its predicted formula, tolerance in ppm for the searched features, assigned identification (please note that some features produce more than one possible identity, hence the number of possible options was included under identification), % RSD based on the mean of the PQC samples (n=15), p-value and FDR value generated using non-parametric Wilcoxon's rank T-test and indication where the samples are elevated (i.e. baseline, caffeine or halothane exposed samples). In case of multiple options for adduct, formula and database reference "range" was used.*

TENTATIVELY IDENTIFIED COMPOUNDS

accurate mass (m/z)	Rt (min)	adduct	predicted formula	tolerance (ppm)	identification	% RSD (PQC)	p-value	FDR	database reference	elevation
253.2891	23.8	M+H-H_2O	$C_{18}H_{37}$	2	Octadecanol	11.5	0.00265	0.01959	HMDB0002350 METLIN6640	baseline ↑
289.1800	25.7	M+H	$C_{18}H_{24}O_3$	1	17-Epiestriol 4-hydroxyestradiol	26.8	0.00173	0.03911	HMDB0000356 HMDB0005896 METLIN5345 METLIN41825	halothane ↑
349.2380	23.4	M+H	$C_{21}H_{32}O_4$	0	15-(R)-15-methyl prostaglandin A2; PGA2 methyl ester	25.3	0.00060	0.02941	METLIN45403 METLIN45681 METLIN64888	halothane ↑
363.2534	23.9	M+H	$C_{22}H_{34}O_4$	1	(±)19,20-DiHDPA; 16,16-dimethyl-PGA2; 7(S),17(S)-dihydroxy-8(E),10(Z),13(Z),15(E),19(Z)-Docosapentaenoic Acid	6.2	0.00115	0.03692	HMDB0010214 METLIN36458 METLIN36154 METLIN64758 HMDB0001976	halothane ↑
368.3164	22.6	M+H-H_2O	$C_{22}H_{43}NO_4$	0	Pentadecanoylcarnitine	11.2	0.00422	0.04093	HMDB0062517	caffeine ↑
369.3509	25.0	M+H	$C_{27}H_{45}$	1	3-Deoxyvitamin D3	9.5	0.00926	0.04922	METLIN42544	baseline ↑
372.1009	27.4	M+Na	$C_{12}H_{19}N_3O_9$	1	Asp Thr Asp	28.76	0.00690	0.03948	METLIN21936	baseline ↑
377.2680	24.3	M+Na	$C_{21}H_{38}O_4$	4	MG(18:2(9Z,12Z)/0:0/0:0)[rac]	8.4	0.00434	0.02791	HMDB0011538 METLIN4252	baseline ↑
385.2352	23.9	M+Na	$C_{22}H_{34}O_4$	0	1a,1b-dihomo-15-deoxy-δ-12,14-PGD2; 1a,1b-dihomo-PGJ2	10.7	0.00309	0.04978	METLIN36208 METLIN36207 HMDB0002710 HMDB0001403	halothane ↑
387.2868	24	M+Na	$C_{23}H_{40}O_3$	0	2-AG ether; Noladin ether	15.4	0.00174	0.03912	HMDB0013657 METLIN64848 METLIN75560	halothane ↑

405.2037	23.4	M+K	$C_{21}H_{34}O_5$	0	Prostaglandins (10; Metlin)	18.5	0.00142	0.03912	n/a	halothane ↑
411.3235	22.9	M+Na	$C_{26}H_{44}O_2$	0	Vitamin D and derivatives (4; Metlin)	21.5	0.00370	0.02467	range	baseline ↑
417.3002	25.0	M+H	$C_{26}H_{40}O_4$	0	Vitamin D and derivatives (3; Metlin)	15.1	0.00001	0.00117	range	baseline ↑
422.3266	25.3	M+H	$C_{25}H_{43}NO_4$	0	Alpha-linolenyl carnitine	22.9	0.00314	0.02203	HMDB0006319	baseline ↑
426.2607	23.9	range	range	1	Phosphatidylethanolamine (1); Phosphatidic acid (1); Lysophosphatidylethanolamine (1); Phosphatidylcholine (3);	10.4	0.00265	0.01959	range	baseline ↑
439.2821	25.0	M+H	$C_{21}H_{43}O_7P$	0	LPA or PA	24.3	0.00023	0.02027	METLIN59310 METLIN40943	halothane ↑
441.3343	23.3	M+Na	$C_{27}H_{46}O_3$	0	(20R,22R)-20,22-dihydroxycholesterol	10.6	0.00191	0.02991	METLIN57643	caffeine ↑
443.3728	21.5	M+H (HMDB) M+NH$_4$ (Metlin)	$C_{26}H_{50}O_5$ (HMDB) $C_{27}H_{43}N_3O$ (Metlin)	1 (HMDB) 3 (Metlin)	Diacylglycerols (24; HMDB); 3-Deoxy-3-azido-25-hydroxyvitamin D3 (Metlin)	15.5	0.02478	0.02478	range	halothane ↑
450.3206	23.9	n/a	$C_{28}H_{38}O_3N_2$	n/a	Biologically irrelevant matches	15.8	0.00040	0.00647	n/a	baseline ↑
457.2718	25.3	M+K (Vitamin D); M+NH$_4$ (Leukotrienes)	$C_{26}H_{42}O_4$ (Vitamin D) $C_{23}H_{37}NO_5S$ (Leukotrienes)	0	Vitamin D and derivatives (9); Leukotrienes (4)	11.1	0.00001	0.00087	range	baseline ↑
468.3086	25.0	range	range	0 to 4	Range of lipids (8); Tyrosine and derivatives (2)	11.3	0.00003	0.00166	range	baseline ↑
471.2872	25.7	M+K	$C_{27}H_{44}O_4$	0	24-Hydroxycalcitriol	19.6	0.00287	0.03419	HMDB0006228 METLIN58368	caffeine ↑
478.2718	22.9	M+K	$C_{21}H_{46}NO_6P$	4	Phosphatidylcholines (2); Phosphatidylethanolamine (1)	24.9	0.00026	0.00493	range	baseline ↑
481.3657	24.7	M+Na; M+H	$C_{30}H_{50}O_3$; $C_{32}H_{48}O_3$	0; 3	Vitamin D and derivatives (5)	19.1	0.00314	0.02203	range	baseline ↑
492.3687	25.0	M+NH$_4$	$C_{29}H_{46}O_5$	0	18-acetoxy-1α,25-dihydroxyvitamin D3	17.9	0.00026	0.00493	METLIN42343	baseline ↑

496.3404	20.5, 25.2	M+H	$C_{24}H_{50}NO_7P$	1	16:0 LysoPC	20.36	0.002234	0.01749	HMDB0010382 METLIN182	baseline ↑
554.5149	24.8	M+NH$_4$	$C_{34}H_{64}O_4$	2	12-[[(9Z)-1-oxo-9-hexadecen-1-yl]oxy]-octadecanoic acid; 9-[[(9Z)-1-oxo-9-hexadecen-1-yl]oxy]-octadecanoic acid	18.5	0.00125	0.02822	HMDB0000827 METLIN263597 METLIN263594	caffeine ↑
700.5280	25.4	M+H-H$_2$O; M+H	$C_{39}H_{76}NO_8P$; $C_{39}H_{74}NO_7P$	0-1	Monomethylphosphatidylethanolamines phosphatidylethanolamines; 1-(1z-alkenyl),2-acylglycerophosphoethanolamines	29.0	0.00000	0.00101	range	halothane ↑
717.5559	20.7	M+NH$_4$; M+H	$C_{39}H_{77}N_2O_7P$		Phosphatidylethanolamines (9)	22.5	0.00093	0.03491	range	halothane ↑
724.5289	25.3	M+H-H$_2$O; M+H	$C_{41}H_{76}NO_8P$; $C_{41}H_{74}NO_7P$	1 to 2	Phosphatidylethanolamines (50)	11.7	0.00060	0.00800	range	baseline ↑
725.531	25.3	[M+H-2H$_2$O]	$C_{45}H_{77}O_7P$	4	PA(P-20:0/22:6(4Z,7Z,10Z,13Z,16Z,19Z))	16.7	0.00049	0.00714	METLIN82326	baseline ↑
726.5443	25.5	range	range	0-4	Phosphatidylethanolamines (50); Phosphatidylcholines (16); Phosphoserines (6); Phosphatidic acids (3)	23.3	0.00000	0.00085	range (METLIN)	caffeine ↑
742.5765	28.0	range	range	1 to 2	Phosphatidylcholines (41) Phosphatidylethanolamines (17) Phosphatidic acids (3)	15.9	0.00000	0.00198	range (METLIN)	caffeine ↑
750.5431	25.4	range	range	0-4	Phosphatidylethanolamines (62); Phosphatidylcholines (19)	13.8	0.00001	0.00087	range (METLIN)	baseline ↑
752.5596	26.2	range	range	0 to 4	Phosphatidylethanolamines (47); Phosphatidylcholines (15); Phosphatidic acids (3); Phosphatidic acids (2)	20.1	0.00287	0.03419	range (METLIN)	caffeine ↑
760.5859	29.2	range	range	0 to 1	Phosphatidylethanolamines (16) Phosphatidylcholines (31) Phosphatidic acids (12)	11.4	0.00157	0.01387	range (METLIN)	baseline ↑

766.575	27.3	range	range	0-3	Phosphatidylcholines (70); Phosphatidylethanolamines (15); Phosphocholine (1); Phosphatidylserines (6)	9.0	0.00349	0.03748	range (METLIN)	caffeine ↑
771.6443	22.6	range	range	3	Triglycerides (16)	27.7	0.00016	0.00415	range (METLIN)	baseline ↑
782.5687	26.5	range	range	0 -2	phosphatidylcholines (77); phosphatidylethanolamines (25); phosphatidic acids (7); phosphatidylserines (16)	6.5	0.00049	0.00714	range (METLIN)	baseline ↑
793.6308	22.6	range	range	1 to 4	Triglycerides (20)	18.7	0.00001	0.00117	range (METLIN)	baseline ↑
804.5496	24.6	range	range	2	Phosphatidylcholines (46); Phosphatidylethanolamines (10)	9.3	0.00257	0.04598	range (METLIN)	halothane ↑
805.5507	24.6	range	range	2	Phosphatidic acid (1); Phosphatidylethanolamines (21)	30.0	0.00093	0.03491	range (METLIN)	halothane ↑
824.6372	25.4	range	range	0	Phosphatidylglycerols (7)	15.8	0.00434	0.02792	range (METLIN)	baseline ↑
860.6104	25.4	range	range	4	Phosphatidylcholines (27); Phosphatidylethanolamines (2)	25.3	0.00000	0.0 64	range (METLIN)	baseline ↑
861.6133	25.3	range	range	3	Phosphatidylethanolamines (3)	19.8	0.00000	0.00051	range (METLIN)	baseline ↑
887.568	21.7	range	range	4	Phosphatidylinositols (24)	18.7	0.00212	0.04301	range (METLIN)	halothane ↑
934.6404	25.5	range	range	2	Phosphatidylinositols (11)	24.0	0.00157	0.01387	range (METLIN)	baseline ↑

241
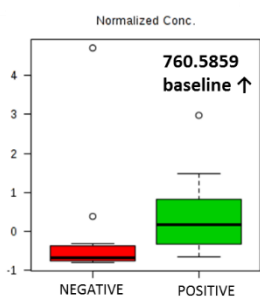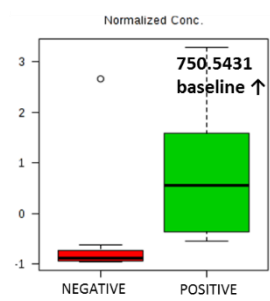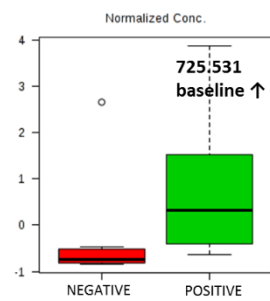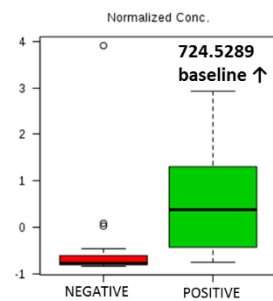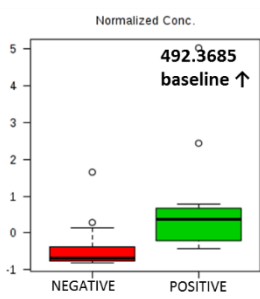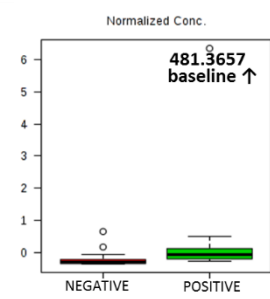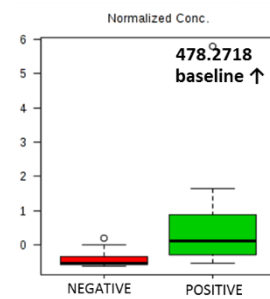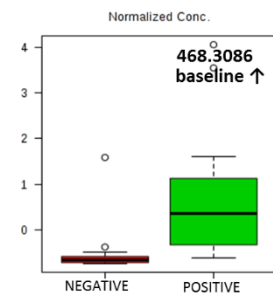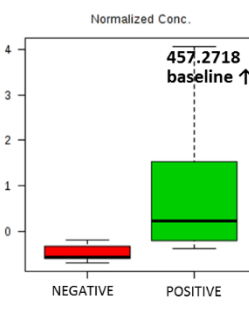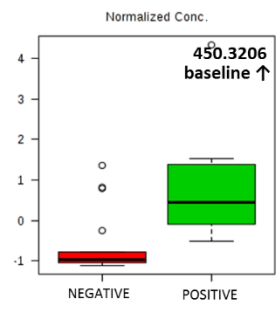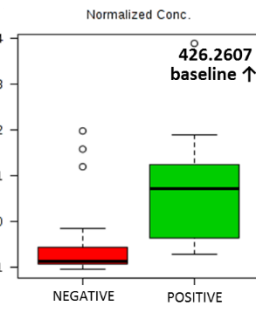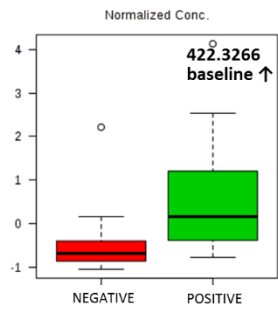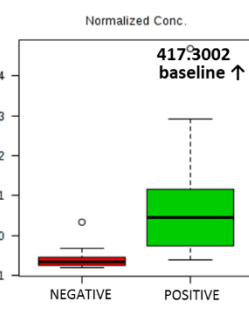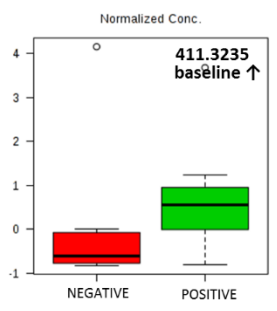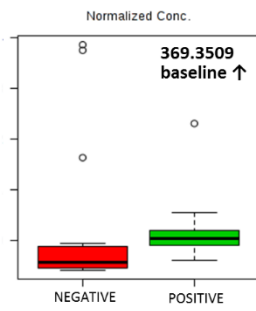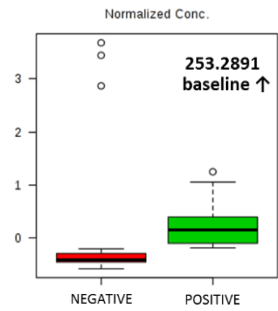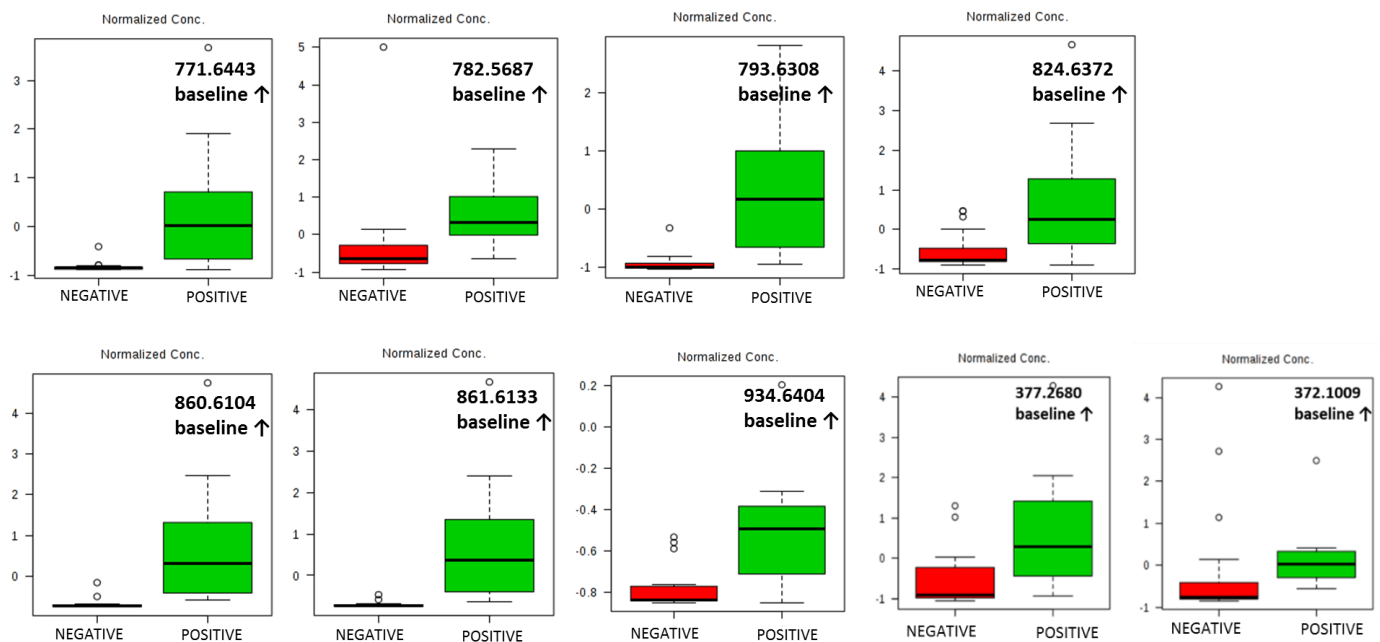
Figure 4.9 *Box-whisker plots of metabolites that were elevated only in baseline cases with the red bar representing MHN patients while the green bar represents MHS patients. Note that the concentration indicated in the plots was obtained from normalized values (i.e. values had been normalized by mean of PQC and autoscaled).*
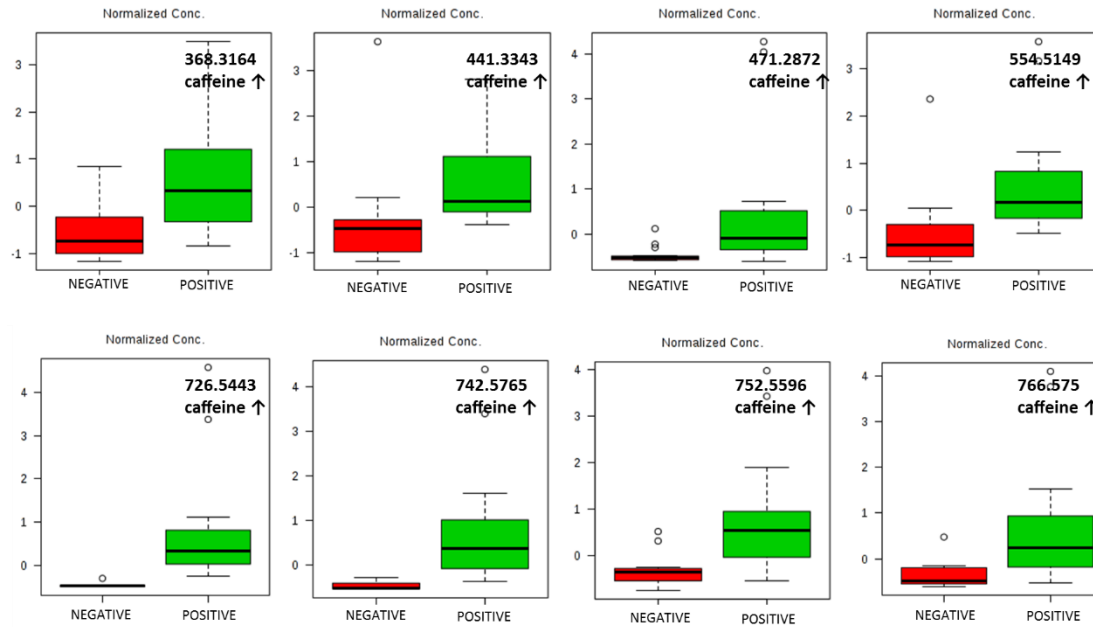
Figure 4.10 *Box-whisker plots of metabolites found to be elevated when the muscle samples (both MHN and MHS) are exposed to 2 mM caffeine. Note, these plots were also obtained using normalized concentrations.*
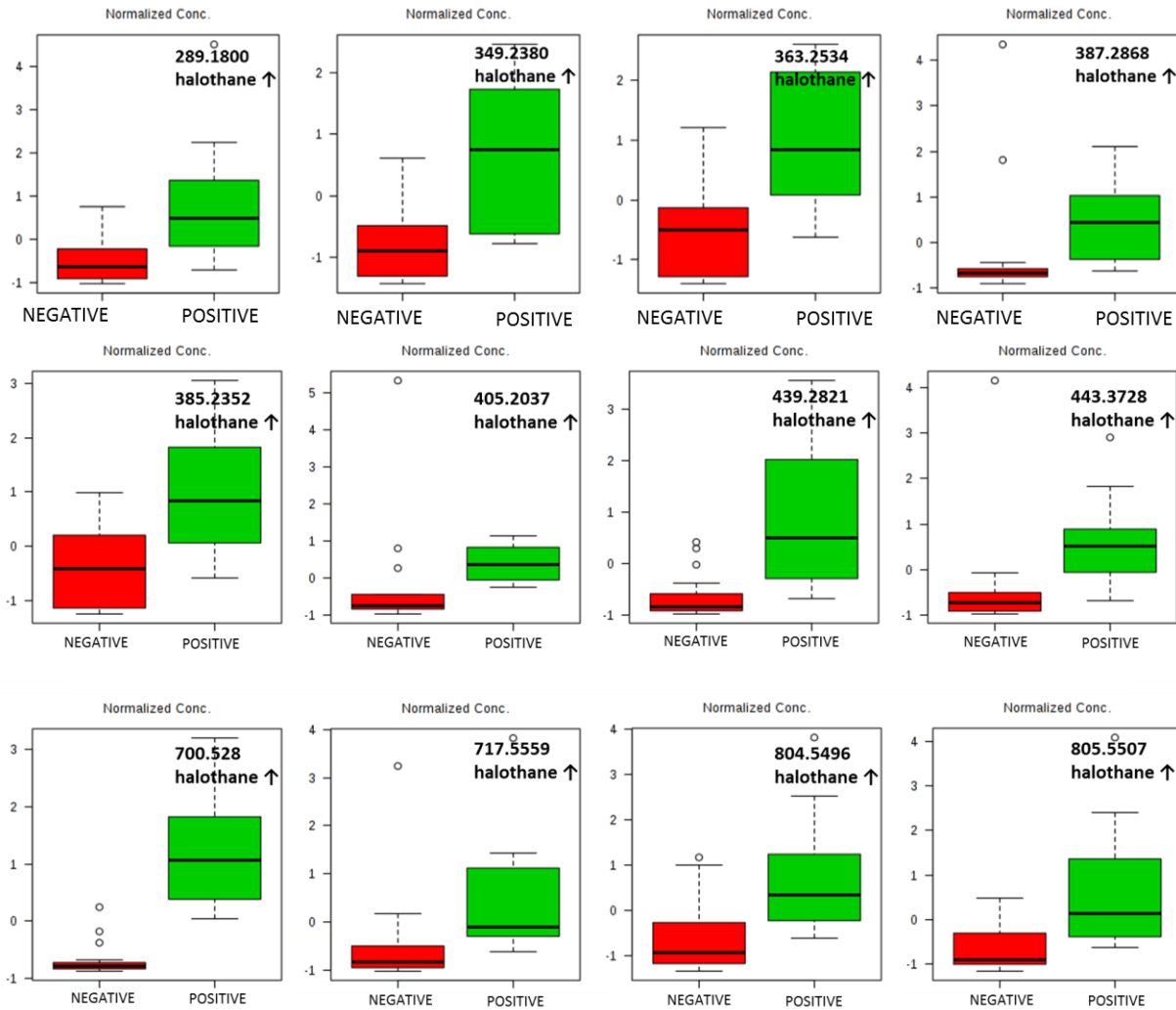
Figure 4.11 *Box-whisker plots of metabolites found to be elevated when the muscle samples (both MHN and MHS) are exposed to 3% halothane. Note, these plots were also obtained using normalized concentrations.*
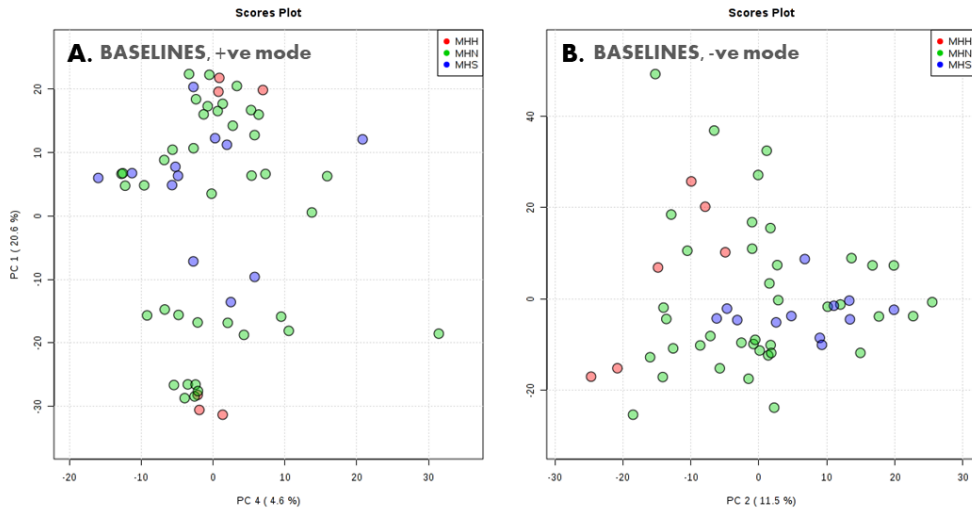
Figure 4.12 *PCA plots for the baselines of the 2016/17 cohort for +ve ionization mode in A., and -ve ionization mode in B. Plots constructed using autoscaling for +ve and mean of PQC and autoscaling for −ve ionization mode. Confidence intervals not shown for simplicity purpose (i.e. could overwhelm the plot visually).*
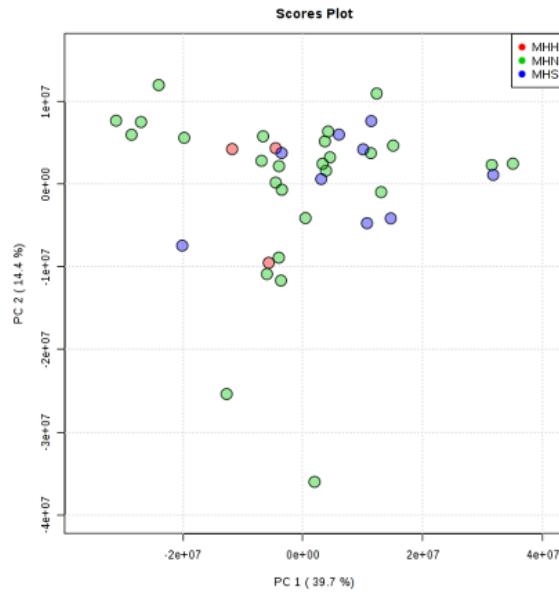
Figure 4.13 *Removal of the first set of injected samples does not efficiently separate the samples.*
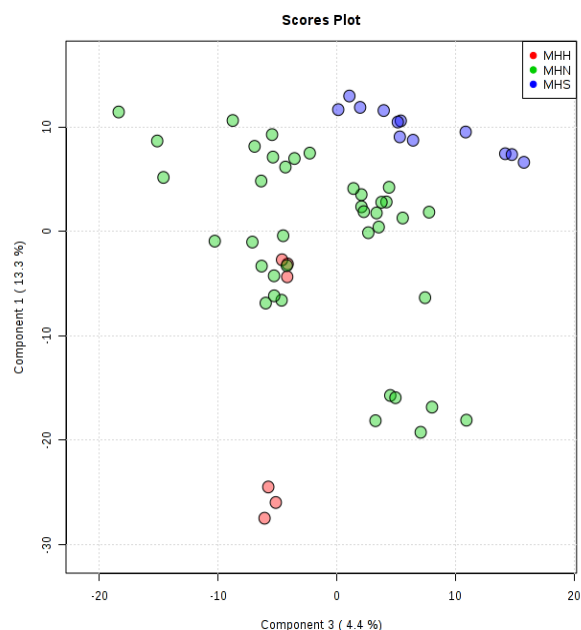
Figure 4.14 PLS-DA plot of baseline samples run in +ve ionization mode. Data is normalized by autoscaling and one case is removed as an outlier. This data reveals some separation between the cases, but a single MHH case is within the MHN cluster.

Table 4.7 Results of cross-validation test for Figure 4.14 done using 5 maximum searchable components, 10-fold CV as cross validation method and Q2 as performance measure.

Measure	1 comps	2 comps	3 comps	4 comps	5 comps
Accuracy	0.76000	0.76000	0.78667	0.81000	0.83000
R2	0.40176	0.66076	0.91381	0.97102	0.99499
Q2	0.00223	0.07522	0.20235	0.26361	0.29371

samples in −ve ionization mode (Figure 4.17) does provide for a better separation, with somewhat improved results of CV tests (Table 4.11, Figure 4.18). Examination of data for 3% halothane and 2 mM caffeine tested in −ve mode also reveals poor clustering based on diagnostics in PCA (Figure 4.19A. and C.). Better separation is observed in PLS-DA (Figure 4.19B. and D.) with improved CV results (Table 4.12-4.13). Features of importance were examined using a heatmap and can be seen in Table 4.14. Similar to +ve ionization mode, the signal area of these features was not elevated in all patients affected
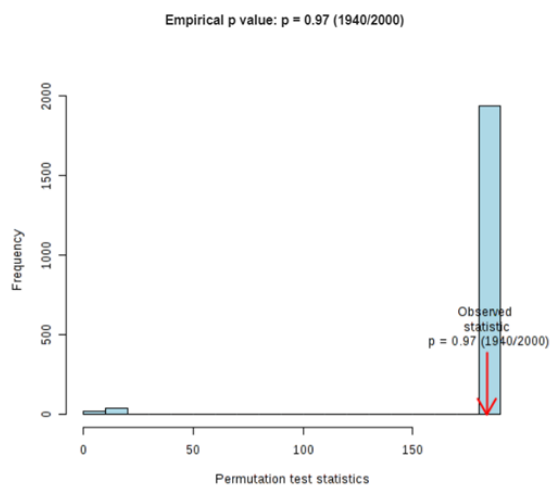
Figure 4.15 *Results of the permutation test (n = 2000) used to test the validity of the mode in Figure 4.14. Test statistic used was separation distance (B/W). The p value is 0.97, indicating a non-predictive model.*
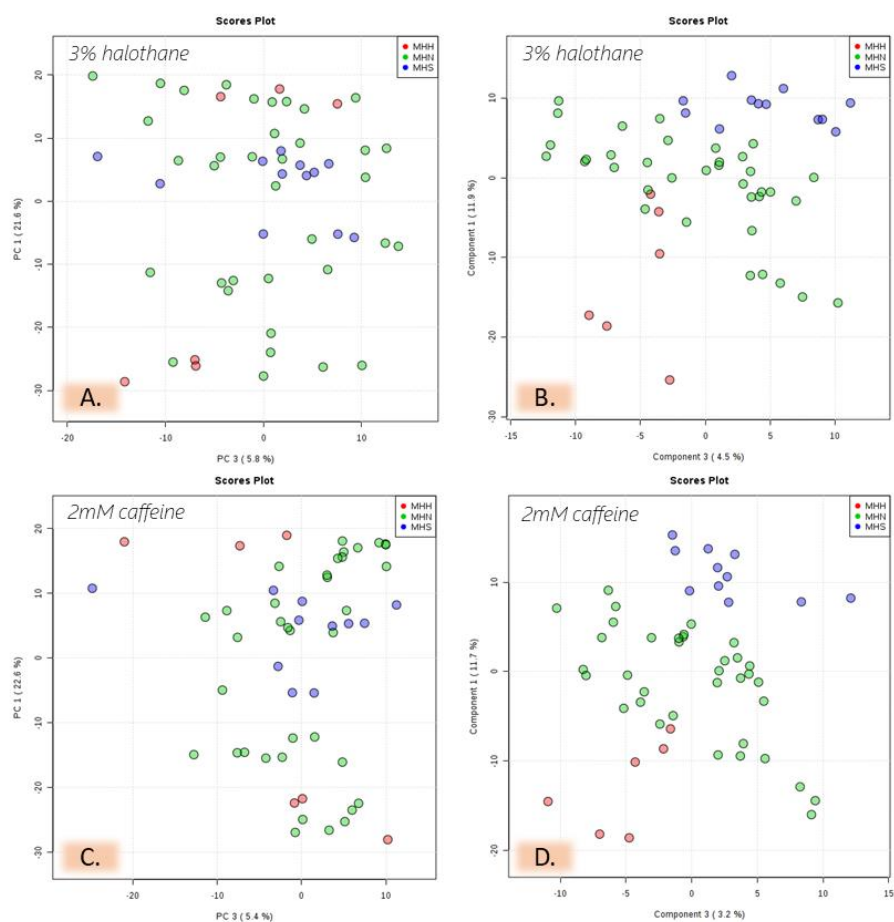
Figure 4.16 *PCA and PLS-DA plots of samples treated with 3% halothane (**A-B**.) and 2 mM caffeine (**C-D**.) for +ve ionization mode, respectively. In both instances, autoscaling was used as a form of data normalization and single outlier had been removed.*

Table 4.8 *Results obtained for cross-validation test of models in Figure 4.16.*

Measure	Accuracy		R2		Q2	
	Halothane	Caffeine	Halothane	Caffeine	Halothane	Caffeine
1 comp	0.70	0.78	0.50	0.59	0.21	0.25
2 comp	0.71	0.81	0.72	0.78	0.40	0.45
3 comp	0.77	0.76	0.93	0.95	0.55	0.50
4 comp	0.81	0.83	0.97	0.98	0.60	0.56
5 comp	0.83	0.89	0.99	0.99	0.61	0.57

Table 4.9 *Results of permutation test done (n = 2000) for models in Figure 4.16.*

Permutation test summary (n = 2000)	
Group	p-value
3% halothane	0.949
2 mM caffeine	0.966

Table 4.10 *Features tentatively identified for +ve ionization mode for baseline, halothane and caffeine exposed samples. Selection was done using a heatmap. Features which did not provide hits or were biologically relevant are not shown. Rts are in seconds.*

Feature (m/z vs Rt)	Tentative ID	Reference	Note	Elevation
244.1546/1112.82	Tiglylcarnitine	HMDB0002366	Acyl carnitines	MHH & MHS ↑, Caffeine (Both) ↑
244.2274/1066.77	5-Tetradecenoic acid	HMDB0000499	Linked to fatty acid chain oxidation diseases*	MHS ↑
305.2476/1354.14	Arachidonic acid	HMDB0001043	Linked to ischemia, lipid metabolism disorder, amino acid metabolic disorder, muscular dystrophy *	MHS (Halothane) ↑
378.2982/1289.32	Pristanoyl glycine	HMDB0013303	-	MHH (Halothane) ↑
156.0768/142.57	L-histidine	HMDB0000177	Linked to ischemia *	MHS (Caffeine) ↑
247.1389/265.71	Asparaginyl-Proline; Prolyl-Asparagine	HMDB0028739; HMDB0029012	-	MHH (Caffeine) ↑
147.1128/2389.1	N-Methyl proline; L-Lysine	HMDB0094696; HMDB0000182	Linked to ischemia, lipid metabolism disorder, amino acid metabolic disorder, muscular dystrophy *	MHH (Caffeine) ↑
* MalaCards: an amalgamated human disease compendium with diverse clinical and genetic annotation and structured search, https://www.malacards.org/				

with MH. Instead elevation was present in one to two cases. Possible contributors to difference in these results between the 2 cohorts could include phenotypic variability which in turn causes biomarker variation. Technical factors cannot be excluded as external contributors may also be responsible for the variations (instrumental effects, length of run, storage time). Hence, one must be careful in elimination of what appears as false positives, since different phenotypes could contribute to different biomarkers.
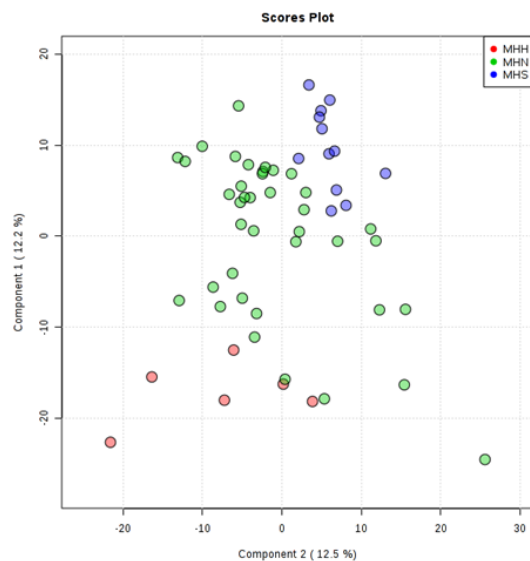
Figure 4.17 *PLS-DA model obtained for analysis of baseline samples done in -ve ionization mode on Exactive-Orbitrap. Normalization of the data done using the PQC and autoscaling.*
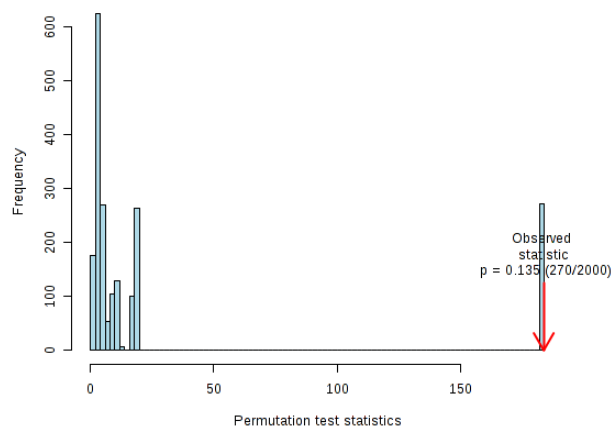
Figure 4.18 *Result of permutation test (n = 2000, separation distance B/W as test statistic) done for examination of the PLS-DA model in Figure 4.17.*

Table 4.11 *Results of cross-validation test done using 5 maximum searchable components, 10-fold CV as cross validation method and Q2 as performance measure for model in Figure 4.17.*

Measure	1 comps	2 comps	3 comps	4 comps	5 comps
Accuracy	0.72667	0.65667	0.71000	0.78000	0.82000
R2	0.44816	0.65134	0.84661	0.93176	0.96907
Q2	0.24973	0.33978	0.48210	0.55758	0.61138

249
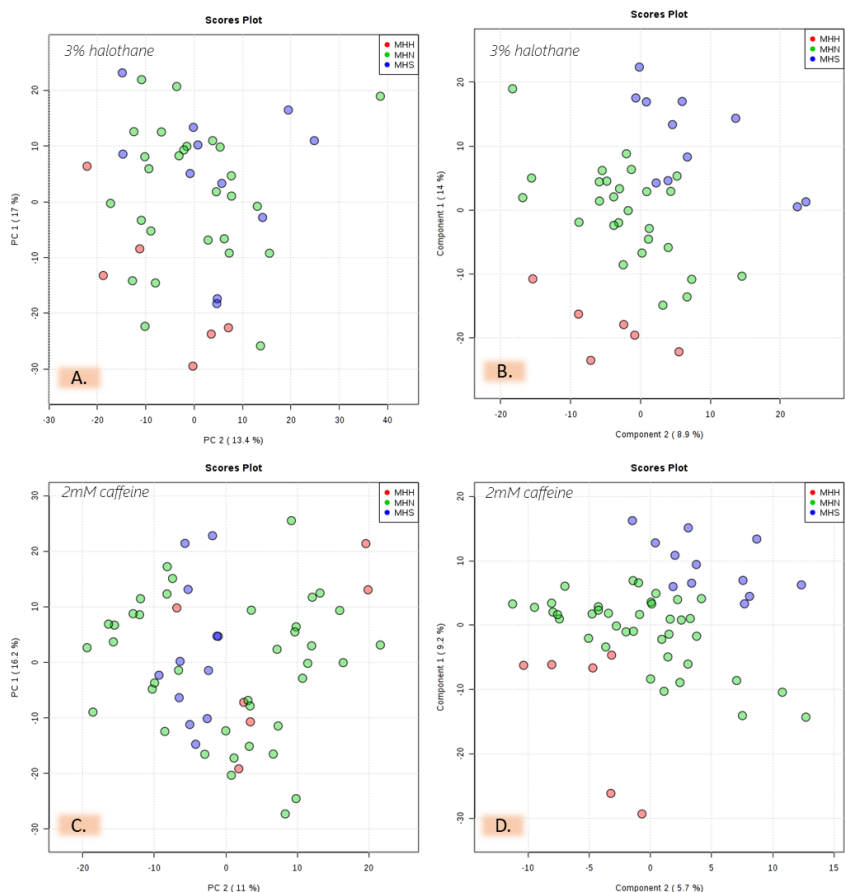
Figure 4.19 *PCA and PLS-DA plots of samples treated with 3 % halothane (**A.** and **B.**) and 2 mM caffeine (**B.** and **D.**) for −ve ionization mode. Normalization by PQC and autoscaling was used.*

Table 4.12 Results obtained for cross-validation examination of the data in Figure 4.19.

Measure	Accuracy		R2		Q2	
	Halothane	**Caffeine**	**Halothane**	**Caffeine**	**Halothane**	**Caffeine**
1 comp	0.63	0.78	0.59	0.50	0.39	0.26
2 comp	0.67	0.79	0.82	0.76	0.53	0.46
3 comp	0.77	0.77	0.90	0.84	0.60	0.51
4 comp	0.78	0.83	0.95	0.90	0.65	0.59
5 comp	0.81	0.84	0.98	0.95	0.66	0.62

Table 4.13 *Results of permutation test done (n=2000) for samples exposed to 3% halothane and 2 mM caffeine for Figure 4.18.*

Permutation test summary (n = 2000)	
Group	p-value
3% halothane	0.41
2 mM caffeine	0.05

Table 4.14 *Features tentatively identified for -ve ionization mode for baseline, halothane and caffeine exposed samples. Selection was done using a heatmap. Features which did not provide hits or were biologically irrelevant are not shown. Rt is in seconds.*

Feature (m/z vs Rt)	Tentative ID	Reference	Notes	Elevation
320.2196/1376.4	Pentadecanoylglycine	HMDB0013300	Linked to fatty acid oxidation disorder *	MHH ↑
239.0669/1246.61	4-Aminohippuric acid; L-beta-aspartyl-L-serine	HMDB0003269; HMDB0041912; HMDB0001867; HMDB0011168	Linked to fatty acid oxidation disorder *	MHH ↑
283.1135/120.2	4-Amino-3-hydroxybutyrate; L-Threonine; L-Homoserine	HMDB0061877; HMDB0000167; HMDB0000719	-	MHH (Halothane) ↑
125.0234/70.23	3-Hexenedioic acid; 3-Methylglutaconic acid;	HMDB0000393; HMDB0000522	3-Methylglutaconic acid linked to spasticity, muscle atrophy, myopathy, metabolic acidosis*	MHH (Halothane) ↑
196.0584/86.28	Hydroxyvalerylglycine	HMDB0094717	n/a	MHS (Caffeine) ↑
378.2000/1306.47	N-Palmitoylethanolamide (PEA)	HMDB0002100	Lipid linked to chronic pain, neuromuscular disease and spasticity*	MHS (Caffeine) ↑
325.2747/1334.23	Triglycerides	Range	n/a	MHH (Caffeine) ↑
307.2284/1335.21	Monoacylglycerols	Range	n/a	MHH (Caffeine) ↑
277.2176/1308.9	Triglycerides; Gamma-Linolenic acid; Alpha-Linolenic acid; a number of inflammatory related compounds	HMDB0003073; HMDB0001388	Inflammation related, linked to ischemia, lipid metabolism disorder*	MHH (Caffeine) ↑
279.2324/1345.21	Linoelaidic acid; bovinic acid; 9e,11e-octadecadienoic acid; 10e, 12z-octadecadienoic acid; linoleic acid; Octadecadienoate	HMDB0006270; HMDB0003797; HMDB0005047; HMDB0005048; HMDB0000673; HMDB0062784	Prostaglandins ↑- Inflammation related, inks to ischemia, metabolic acidosis, spasticity, lactic acidosis*	MHH (Caffeine) ↑

*MalaCards: an amalgamated human disease compendium with diverse clinical and genetic annotation and structured search, https://www.malacards.org/

PRM investigation of significant features

Significant features with matches on MS/MS spectra search included 17-Epiestriol, 4-hydroxyestradiol, 15-(R)-15-methyl prostaglandin A2, PGA2 methyl ester, (±)19(20)-DiHDPA; 16,16-dimethyl-PGA2, 7(S),17(S)-dihydroxy-8(E),10(Z),13(Z),15(E),19(Z)-Docosapentaenoic Acid, Aspartate Threonine

Aspartate (protein breakdown product), 1- Linoleoyl-rac-glycerol, 2-AG ether, Noladin ether and PC (16:0/0:0)U/PC(16:0/0:0, racemix) (Metlin scores: 32, 56, 37, 29, 36, 36, 50, 43, 20, 31 and 51, respectively. Standards were purchased to validate the metabolites, but promising results were obtained only for PC (16:0/0:0)U/PC(16:0/0:0). (Figure 4.20). Since PC(16:0/0:0)U/PC(16:0/0:0) is a racemix, 16:0 LysoPC was used to perform semi-validation since they are structurally identical. Additionally, feature annotation indicated this metabolite as a unique feature corresponding to 16:0 LysoPC. In the PQC, this metabolite eluted as a double peak at 20.5 and 25.2 min (Fig. 4.21a.). The standard eluted at 20.9 min which is close to the PQC peak at 20.5 min (Fig. 4.21b.). A second peak was not observed. Kyle et al. has shown that 16:0 LysoPC has two distinct LC peaks, which correspond to different acyl chain positions (i.e. sn-1 or sn-2 acyl chain position) with the more abundant later eluting peak correlating with a sn-1 position.[373] Ability to separate such isomers using RPLC has been demonstrated.[374] Lysophosphatidylcholines occur in two forms, with fatty acyl groups at positions 1 (sn-1) and 2 (sn-2).[375] The sn-1 LysoPCs are produced by phospholipase-A1 and sn-2 LysoPCs are produced by phospholipase-A2 (PLA$_2$).[376] The position of the acyl group is important in understanding their biological roles as lysoPCs with different sn-positions are responsible for different metabolic roles.[375] Interestingly, 16:0 LysoPC has been reported as a biomarker in lung cancer[375] and chronic renal failure.[377–381] Endogenous
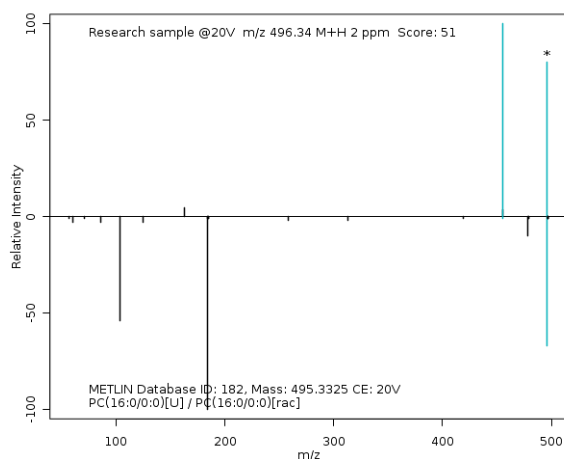
Figure 4.20 Result of MS/MS spectrum search done on Metlin with a positive match return for PC(16:0/0:0)U/PC(16:0/0:0)[rac].

252
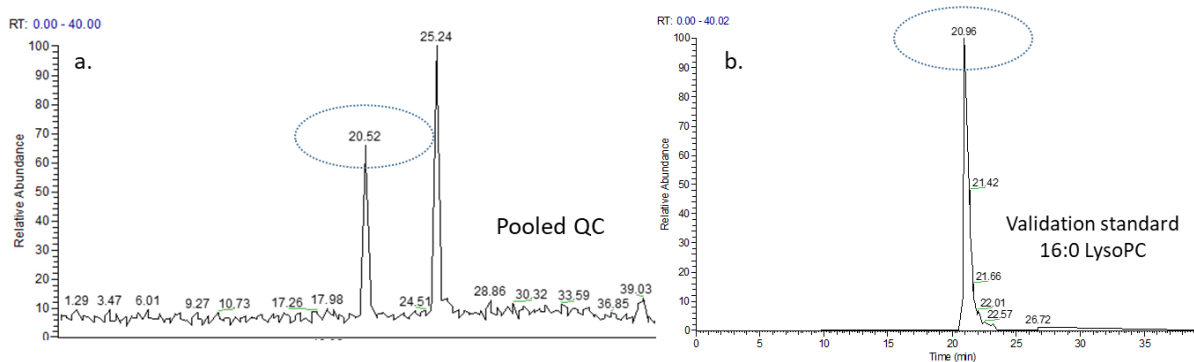
Figure 4.21 *Extracted ion chromatograms for 16:0 LysoPC (496.3390, [M+H]$^+$) in the pooled QC sample (a.) obtained from Q-Exactive at 20.5 and 25.2 minutes and validation standard (b.) obtained on Exactive Orbitrap at 20.9 minutes.*

phosphatidylcholines exist as isomers in biological matrices,[382] but there is some discord in chromatographic reporting of 16:0 LysoPC. Both single[383] and double peaks[384] have been reported. Additionally, reports of time and temperature related isomerization of 16:0 LysoPC factors also exist.[385,386] The isomerization may also depend on analyzed media, i.e., different tissues, cells, organelles or even phospholipid classes.[382] Hence, observation of a single peak in our case could be related to the use of a synthetic standard. Therefore, the evidence obtained points to possibility of up-regulated 16:0 LysoPC in the 2015 cohort. The metabolites that did not provide a MS/MS spectrum match during search possibly did not have enough intensity for the parent metabolite or could have potentially diminished due to storage- therefore not yielding sufficient fragmentation for fragment matches. Additionally, limitations in using commercially available databases exist, such as *in silico* predicted spectra which is obtained from different MS analysers and may not necessarily give the best prediction.[387] For example, a metabolite of particular interest in our study was 3-deoxyvitamin-d3, seen in Table 4.6. A search on Metlin revealed that this metabolite could be 3-deoxyvitamin-d3 (1 ppm accuracy). However, MS/MS fragmentation yielded an MS product (327.0771) whose accurate mass did not match that of the database (327.3050, *in silico* predicted fragmentation), making it difficult to confirm its identity (Figure 4.22). Additionally, a commercially available standard for this compound is not available, which adds another layer of difficulty in confirming the identity of this metabolite. Regardless, 3-deoxyvitamin-d3 could be

placed within the context of biological mechanism of MH, as vitamin-d3 is involved with regulation of Ca^{2+} levels in the body.[388] Additional tentatively identified metabolites (m/z 457.2718, 471.2872, 481.3657, and 492.3687) also point to vitamin D and its derivatives. However, it is important to point out that this information was not validated, and therefore could not be deemed entirely accurate.
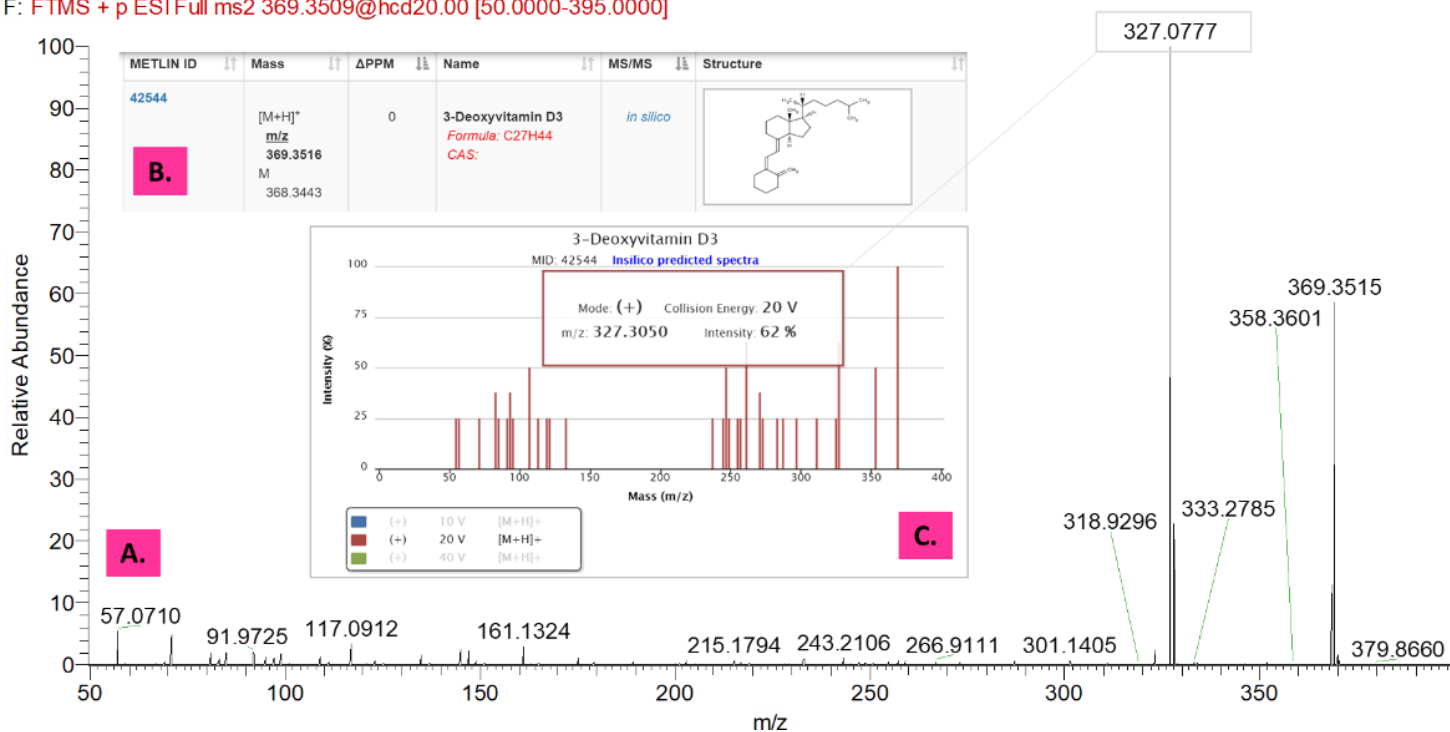
Figure 4.22 *Figure labeled A. shows the MS/MS spectra obtained at 20eV for fragmentation of a metabolite with m/z of 369.3515 with a predominant fragment ion of 327.0777. Insert B. shows the identification provided on Metlin by searching [M+H]$^+$ adducts only with a 0 ppm tolerance obtained for 3-Deoxyvitamin-d3. Insert C. shows the in silico predicted spectra of 3-Deoxyvitamin-d3 with a fragment ion of 327.3050, which did not match 327.0777.*

Statistical analysis of the *in vivo* mice data

After processing of the data obtained from *in vivo* SPME sampling of remaining mice, the number of features detected in +ve and −ve ionization mode was 2244 and 1248, respectively. After processing and filtering in CD 2.1, the final number of peaks underwent statistical analysis in MetaboAnalyst yielding 187 and 104 features for +ve and −ve ionization mode, respectively. No relevant information was found using −ve ionization mode, so the data will be focused on +ve ionization mode only. The PCA plot shown

in Figure 4.23 indicated separation between YS and WT groups by PC1 and PC3 explaining 23.2 and

12.1% of the variances. The PLS-DA model (Figure 4.24) subjected to 10-fold cross validation

assessment indicated PC3 as the best classifier with Q2 of 0.4006 and R2 of 0.9906 (Figure 4.25 and

Table 4.15). The permutation test failed the validation criteria thus not exhibiting statistical significance

in class discrimination (p = 0.9995, Figure 4.26). The fold change analysis resulted in identification of

18 important features differentiating the studied group, while the Volcano plot analysis showed four of

such features, which are all included in Tables 4.16-4.17. The tentative identification of the compounds

expressing biological relevance is presented in Table 4.18.
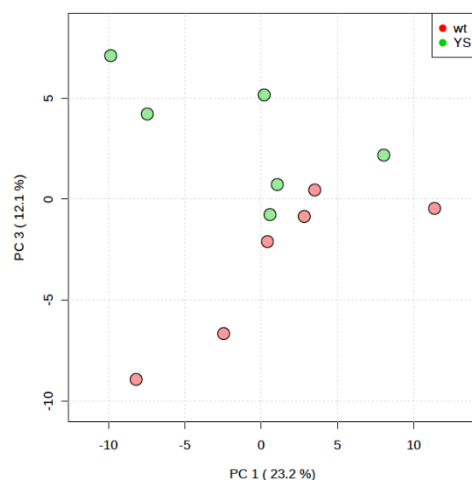
Figure 4.23 *PCA plot for the in vivo animal data in +ve ionization mode. Plot was constructed using autoscaling and normalized by sample median.*
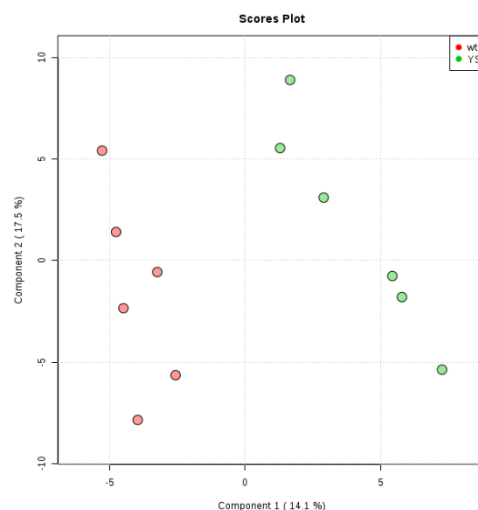
Figure 4.24 *PLS-DA plot of baseline samples. Data is normalized by autoscaling. This data reveals good separation between the cases, but the model fails the cross validation.*
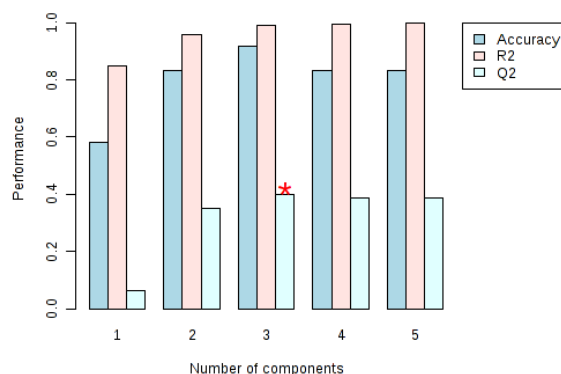
Figure 4.25 *Results of cross-validation test done on MetaboAnalyst for the PLS-DA model generated in Figure 4.23. The model was assessed by examining the results of a 10-fold CV and using Q2 as performance measure. Performance measurement of the PLS-DA model done on MetaboAnalyst detailing accuracy, R2 and Q2 values. The red mark denotes the optimum number of components that should be used for the model. In this case, the optimum number of components is 3.*

Table 4.15 *Results of cross-validation test done using five maximum searchable components, 10-fold CV as cross validation method and Q2 as performance measure for in vivo animal data in positive ionization mode.*

Measure	1 comps	2 comps	3 comps	4 comps	5 comps
Accuracy	0.58333	0.83333	0.91667	0.83333	0.83333
R2	0.84919	0.95776	0.99065	0.99588	0.99986
Q2	0.06243	0.35163	0.4006	0.38564	0.38597
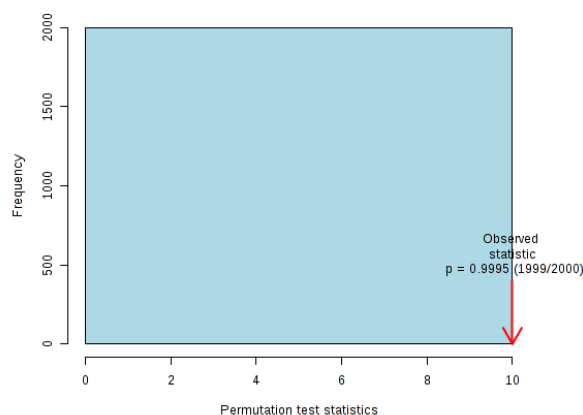
Figure 4.26 *Result of permutation test (n = 2000, separation distance B/W as test statistic) done for examination of the PLS-DA model for in vivo animal data in +ve ionization mode*

Table 4.16 *Important features differentiating YS and WT mice identified by fold change analysis.*

	Peaks (mass)	Fold Change	log2(FC)
1	140.95039/1.4	0.00411	−7.9267
2	704.49321/28.5	24.17800	4.5956
3	528.45439/27.6	10.99100	3.4582
4	724.40094/23.7	6.68580	2.7411
5	647.42471/23.4	5.80960	2.5384
6	652.38004/23.4	5.74630	2.5226
7	159.06844/10.9	0.18322	−2.4483
8	474.40752/27.2	5.03780	2.3328
9	109.01302/1.1	4.45850	2.1566
10	302.22442/19.3	0.24864	−2.0079
11	439.40255/23.9	3.51010	1.8115
12	97.97712/1.1	3.46850	1.7943
13	411.37117/23.1	2.65070	1.4064
14	418.30813/25.0	2.29600	1.1991
15	136.03853/6.9	0.45124	−1.1480
16	168.02854/1.5	0.45947	−1.1220
17	268.08046/6.9	0.46595	−1.1018
18	203.11586/9.1	0.49576	−1.0123

Table 4.17 *Important features differentiating YS and WT mice identified by volcano plot.*

	Peaks (mass)	FC	log2(FC)	raw.pval	-log10(p)
1	418.30813/25.0	2.2960	1.1991	0.00587	2.2309
2	704.49321/28.5	24.1780	4.5956	0.02132	1.6711
3	528.45439/27.6	10.9910	3.4582	0.04618	1.3355
4	474.40752/27.2	5.0387	2.3328	0.07868	1.1041

Table 4.18 *List of tentatively identified features of biological relevance for in vivo mice study. Rt is in seconds.*

Feature (m/z vs RT)	adduct	Predicted formula	Identified metabolite	FC	log2(FC)	-log10(p)	regulation
137.0459/88.2	M+H	C_5HN_4O	Hypoxanthine	1.97	0.98	1.30	up
169.0358/88.2	M+H	$C_5H_4N_4O_3$	Uric Acid	2.18	1.12	0.59	up
204.1231/546	M+H	$C_9H_{17}NO_4$	Acetylcarnitine	2.02	1.01	0.58	up
269.0879/88.2	M+H	$C_{10}H_{12}N_4O_5$	Inosine or Arabinosylhypoxanthine	1.75	0.81	0.92	up
412.3783/1383	M+H	$C_{25}H_{49}NO_3$	N-Tricosanoylglycine	0.38	-1.41	0.46	down
440.4099/1436	M+H	$C_{27}H_{53}NO_3$	N-Pentacosanoylglycine	0.28	-1.81	0.57	down

Discussion

Analysis of the extracts obtained from SPME sampling revealed that the levels of several classes of lipids, including phosphatidylethanolamines, phosphatidylcholines, and triglycerides were elevated in MHS patients from two cohort studies (Tables 4.6, 4.10 and 4.14), pointing to an affected lipid and FtA(s) metabolism. This observation is in accordance with previous studies, in which Cheah et al. were the first ones to report that the MH condition is influenced by an altered FtA metabolism, i.e., excessive production of FtA(s).[389] However, Fletcher has proposed that the observed alterations in the FtA(s) metabolism in MH are related more to synthesis and breakdown of triglycerides and not phospholipids.[390] The authors suggested that FtA(s) (primarily unsaturated) are responsible in part for modulation of Ca^{2+} channels.[390] However, the features found in our study (24 tentatively identified and 1 semi-validated) point to various lipid species, not only triglycerides. The semi-validated feature 16:0 LysoPC (Fig. 4.21 and Fig. 4.27A.) is a product of hydrolysis of phosphatidylcholine, a reaction catalyzed by the enzyme PLA_2, which is also involved in regulation of the metabolism of prostaglandins through modification of arachidonic acid. Interestingly, Wong et al. found that elevated Lyso:PC (particularly 16:0) in human endothelial cells led to enhanced arachidonate release, and subsequent increase of cellular Ca^{2+} and activation of protein kinase C,[391] which is involved with contraction of smooth muscle cells. In fact, Fletcher et. al. were the first ones to suggest a dysregulation of the lipid metabolism in MH[390,392] while

Wieland et al. proposed a potential abnormal function of hormone sensitive lipase.[393] In that study, it has been suggested that elevated PLA_2 activity may lead to greater concentrations of lysophosphatidylcholine and lysophosphatidylethanolamines,[393] a suggestion based on a greater free FtA release from MHS mitochondria.[389,390,392,394] As mentioned in the above section, 16:0 LysoPC was the early eluting peak in the PQC, thus suggesting that the acyl chain might be positioned on sn-2, and its production is controlled by PLA_2. The activity of PLA_2 is regulated by phosphorylation and Ca^{2+} concentrations.[376] The group of PLA_2 enzymes are classified into those that are calcium dependent ($cPLA_2$) and independent ($iPLA_2$).[395,396] PLA_2 also plays a role in ROS formation, influencing contractile properties and fatigue characteristics of skeletal muscles.[395,397] It has been already suggested that an increase in ROS is linked to hypermetabolic condition that occurs in MH. Oxidative stress occurs when formation of ROS exceeds the capacity of the anti-oxidant defense system.[395] In absence of PLA_2 regulation, pro-inflammatory mediators are produced[376] resulting in oxidative stress. Interestingly, Yoda et. al. found that $iPLA_2$-y null mice (i.e., no $iPLA_2$-y) exhibited increased mitochondrial dysfunction and oxidative stress which led to loss of skeletal muscle structure and function.[398] In a different study, Jurivich et. al.[399] found that PLA_2 may affect transcriptional switches which mediate thermal stress in some cells. Secretion of $cPLA_2$ is considered to induce inflammatory response in neighboring cells[376] and $iPLA_2$ is linked to lipid and energy metabolism,[396] skeletal muscle contractile function by modulating cytostolic oxidant activity,[400] mitochondrial integrity and phospholipid remodelling[396] and development of many diseases.[396] According to Carper et. al. acyl-CoA thioesterase activity of $iPLA_2$-β could be an important contributor for optimal FtA oxidation by skeletal muscle.[400] Even in the context of MH, Cheah et. al. obtained experimental evidence that supports the theory that increase in long chain FtA(s) by endogenous PLA_2 is responsible for enhanced release of Ca^{2+} from skeletal muscle mitochondria of porcine MH.[401] Interestingly, others have also noted connection between PLA_2 and its role in muscle physiology. Duncan has considered PLA_2 as a candidate which initiates changes in Ca^{2+} concentrations that trigger cellular

damage in skeletal muscle.[402] Boittin et. al.[403] showed that $iPLA_2$ enhances the entry of Ca^{2+} in dystrophic skeletal muscle fibers while Malhotra et. al.[404] identified $iPLA_2$-IV as a potential target for therapeutic intervention in patients afflicted with Barth syndrome.

In addition to the identification of 16:0 LysoPC, certain pro-inflammatory compounds were tentatively identified by our study (i.e.,1a,1b-dihomo-15-deoxy-δ-12,14-PGD2; 1a,1b-dihomo-PGJ2, arachidonic acid, etc.) indicating potentially elevated levels of prostaglandins and an affected arachidonic acid pathway (Figure 4.27B. shows box-whisker plot of one of such compounds). Prostaglandins belong to a group of oxidized FtA(s) and are involved in variety of physiological processes in the body, including the regulation of contraction of smooth muscle tissue.[405] They also promote entry of Ca^{2+} ions into cells, and an increased concentration of prostaglandins has been linked to muscle dystrophy.[406] Also, in the 2016/17 cohort, links to linoleic acid pathway (responsible for production of arachidonic acid and eicosanoids) were discovered (Figure 4.27F.). As mentioned in the introduction, free FtA(s) enhance the effects of volatile anesthetics on Ca^{2+} regulation in skeletal muscles. It is known that exposure of skeletal muscle to halothane increases the Ca^{2+} release from sarcoplasmatic reticulum.[407] In our study it can be noted that the level of prostaglandins were elevated in halothane exposed muscle samples, suggesting that the exposure to the volatile anesthetic may stimulate formation of such metabolites (Table 4.6, 4.10 and 4.14). Moreover, the level of arachidonate, a precursor of prostaglandins, was also elevated in halothane samples of MHS patients (Table 4.10). Indeed, oxidative metabolism of arachidonic acid generates ROS production[395] whereby $iPLA_2$-y also potentiates arachidonic acid release from various subclasses of lipids.[396] The use of anaesthetics is generally considered to have an anti-inflammatory effect during an inflammatory process such as surgery,[408] but this effect may be different in MHS individuals leading to increased metabolism of prostaglandins in skeletal muscles under halothane exposure. Other lipidomic features pointed to several different families of lipids, making tentative identification challenging. However, some features strictly returned hits for a family of lipids like

phosphoinositols. In fact, a study has shown that accumulation of inositol phosphate products was involved with the development of MH.[409] Inositol phosphate products were measured in MHN and MHS swine, and the latter showed a 304-1330 % increase in accumulation of the lipid species.[409]

Other tentatively identified species found in the baseline samples include octadecanol, a long chain fatty alcohol which has previously been detected in skeletal muscles of patients suffering from Sjögren-Larsson syndrome, a condition whose symptoms includes spasticity, i.e., muscle spasms and stiffness.[410] Interestingly, other compounds, whose level was elevated in skeletal muscles of MHS patients are AcR(s), a group of endogenous compounds that participate in muscle energy metabolism via β-oxidation (Figures 4.27C-D. show carnitines elevated in the 2015 and 2016/17 cohort). In fact, muscles are sound sources for AcR(s) generation.[411] In most tissues, including skeletal muscle, the rate of FtA β-oxidation is regulated by the carnitine-acylcarnitine shuttle. Among identified AcR(s) in this study, pentadecanoylcarnitine was present in the caffeine-exposed samples, and alpha-linolenyl carnitine was present in the baseline samples of MHS patients from 2015 cohort (Table 4.6), whereas tiglylcarnitine was extracted from skeletal muscles obtained from MHS patients in 2016/17 cohort (Table 4.10). The identified AcR(s) belong to long chain FtA(s), a group of compounds that are utilised by skeletal muscle during contraction[412,413] and are considered markers of disordered conditions of perixomal and mitochondrial oxidation[414] with a report linking elevated AcR levels to rhabdomyolysis.[415] It was observed that increases in levels of AcR(s) are also associated with an increase in concentration of ROS species and intracellular Ca^{2+}.[411,416] Therefore, elevated levels of certain AcR(s) may indicate dysregulation of FtA pathways, or FtA oxidation disorders. Consequently, these oxidation disorders affect enzymes involved in long chain FtA catabolism, which leads to accumulation of both plasma and tissue AcR(s).[411,416] Octadecanoic acids, found in MHS patients of 2015 are also involved in mitochondrial β-oxidation of long chain FtA(s). 5-tetradecenoic acid was found elevated in 2016/17 cohort as well (Figure 4.27E.), and it is connected to defects in long chain FtA disorders.[417] Interestingly,

levels of carnitine measured in 2015 MHS cases appeared to be down-regulated (Figure 4.28). Carnitine deficiency is linked to muscle weakness,[418] which could be another possible indication of MH susceptibility. Engel and Angelini found that carnitine deficiency in human skeletal muscle is associated with myopathy, and accumulation of lipids in the muscle tissue was considered to be a cause of excessive oxidative catabolism of FtA(s).[418] Apart from the disturbances in FtA(s), arachidonic acid and linoleic acid metabolic pathways, alterations in the metabolism of amino acids, and di- and tripeptides were observed in skeletal muscles of MHS patients in two cohort studies. Elevated levels of tyrosine and L-histidine pointed to potential dysregulations in the N_2 metabolism.[419] They also indicate increased protein synthesis or formation of neurotransmitters, whereas elevated level of lysine, one of the precursors of
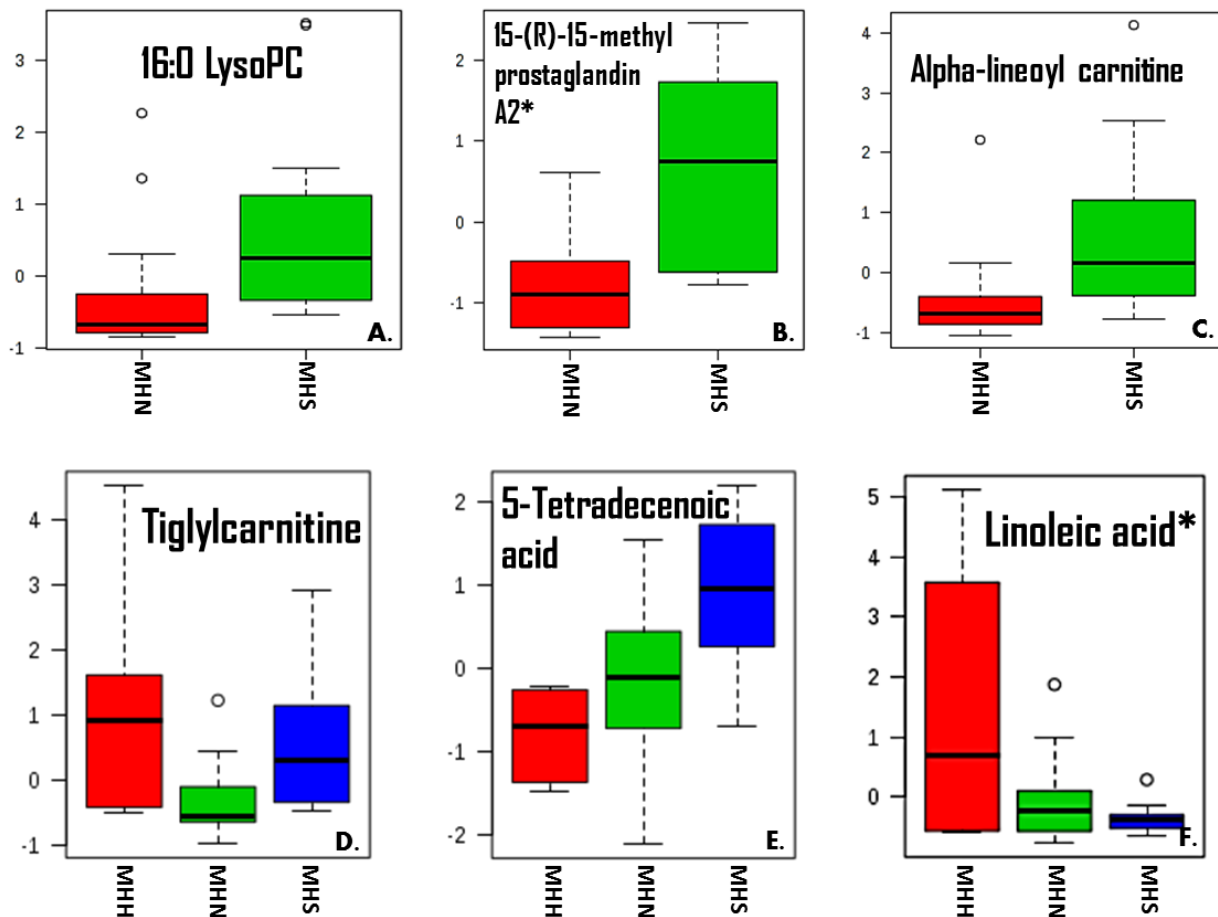

Figure 4.27 *Box-whisker plots of selected tentatively identified features, including 16:0 LysoPC, 15-(R)-15-methyl prostaglandin A$_2$ and alpha-lineoyl carnitine in **A.**, **B.** and **C.**, respectively (2015 cohort). Figures 4.26**D.**, **E.** and **F.** show plots of tiglylcarnitine, 5-tetradecenoic and linoleic acid, respectively (2016/17 cohort).*
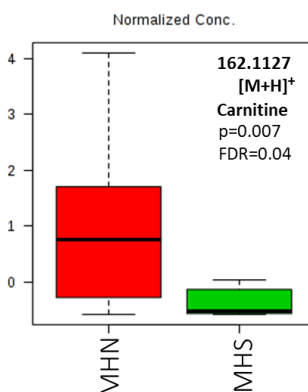
Figure 4.28 *Box-whisker plot of tentatively identified metabolite carnitine (162.1127, [M+H]$^+$) in negative (MHN) and positive (MHS cases). Carnitine deficiency is also linked to muscle myopathy, which is one of symptoms of MH.*

carnitine, may be related with observed alterations in carnitine-dependent oxidation of long chain FtA(s) in the skeletal muscles. L-histidine, L-threonine and L-lysine provided connections to amino-acyl tRNA biosynthesis pathway, whereby some synthetases are believed to regulate glucose metabolism and are connected to disruptive metabolic conditions.[420] N-palmitoylethanolamide was found in the 2016/17 cohort, and while research on its role is still under-going, this metabolite is considered to regulate functions involved in pain and inflammation.[421]

Interestingly, apart from the abovementioned compounds, SPME facilitated the extraction and identification of vitamin D and its multiple metabolites solely in human skeletal muscles obtained from MHS patients of 2015 cohort. The elevated level of those compounds was observed not only in the baseline samples, but also in the samples exposed to the action of halothane and caffeine. Vitamin D is well known compound involved in the regulation of Ca^{2+} homeostasis in the body, and its level is tightly regulated by parathormone (PTH) and fibroblast growth factor 23 (FGF23). In patients predisposed to develop the MH condition, the level of vitamin D3 was elevated and possibly not modulated by negative feedback loop by PTH and FGF23. In addition, increased level of vitamin D and its metabolites was not observed in SPME extracts obtained from the sampling of skeletal muscles of 2016/17 cohort and YT mice, therefore the underlying mechanism of altered vitamin D metabolism may not be related to genetic mutation in MH.

In vivo sampling of mice with RYR1 gene

Altered metabolism of small molecules, mainly metabolites involved in FtA(s) and purine metabolism was observed in SPME extracts obtained from the *in vivo* experiments performed on mice with knock-out RYR1 gene, pointing out that the reported imbalance in the metabolism of lipids in human skeletal muscles of MHS patients could be related to genetic basis of the disease (Table 4.18). The driving force to perform *in vivo* animal experiment was notable metabolic difference between MHS and MHN at baseline in human cohorts. At present, diagnostic of MH is based on CHCT, which is highly invasive. Therefore, alternative approach like SPME offering less invasive protocol would be desired. The results showed relatively good separation between YS and WT groups, but inter-animal variability was high in both groups. This is likely a result of technical issues related to sampling itself rather than biological variability. Simply, the muscle of the mouse is very small when compared to SPME probe. Therefore, it is very difficult to precisely control full penetration of the SPME fiber within the tight muscle. Nevertheless, the data showed number of features participating in separation of the MH and control cohorts. Some of the features could not be identified even putatively as the masses did not match any known metabolites from databases available. It was previously reported, that *in vivo* SPME may capture short-lived or unstable metabolites, but to draw conclusions of that matter, in-depth studies would have to be conducted. The metabolites presented in Table 4.18 indicate that genetic MH is associated with alteration in purine and FtA metabolism. Similar to human data, AcR(s) and acylglycines were found to be of particular importance. The AcR(s) in both human and animal studies showed increased muscular level, while in case of acylglycines the level was elevated in MHS patients but YS mice showed downregulation. The differences also concern the length of acyl chain of the acylglycines; with the longer ones being observed in mice data. To best of our knowledge, acylglycine were not discussed in the view of MH, but it was reported[422] that they might be a good complement to analysis of AcR(s) and organic acids in diagnosis of mitochondrial energy metabolism disorders.

Interestingly, the *in vivo* mice experiments showed direct link between MH and purine metabolism by increased level of inosine, uric acid and its precursor hypoxanthine in YS cohort. All these metabolites are known to be involved in muscle movement via energy consumption as they are by-products of ATP breakdown. Xanthine and inosine were proposed as early biomarkers of cardiac ischemia because their concentration significantly increases under hypoxia/ischemia.[423] The uric acid, which has strong antioxidative properties, was reported to be positively associated with muscle strength in older persons.[424,425] Although the chemometric models built based on the *in vivo* data did not pass the validation because of the reasons described above, the obtained results may suggest that in muscles of MH subjects oxygen deprive-like conditions occur. The alteration of purine metabolism was also found in MHS patients' muscles extracted with the solid liquid extraction (SLE) technique.

Comparison to data from SLE extractions

Similar results with respect to the changes in the metabolism of different lipid species, including phosphoethanolamines, amino acids and compounds involved in muscle energy metabolism were also observed in muscle samples obtained from MHS patients in comparison to MHN patients during the analysis performed using SLE. A summary of features that are biologically similar, i.e. shared between SPME and SLE can be observed in Figure 4.29. Based on the results obtained, it was observed that the level of AcR(s) was elevated in the baseline samples, as well as certain amino acids (glycine, histidine, asparagine for SLE and expected metabolite prolyl-asparagine for SPME) and a range of phosphoethanolamines and palmitoylethanolamides. As expected, there were also certain differences in features reported between the two techniques. For example, SLE provided links to metabolites involved with creatine, nicotinamide, purine metabolism and urea cycle. Since the SLE study is part of a larger on-going project being done at TGH, we will not represent all the features found in this study. The SLE information reported in this research is provided to affirm the findings accomplished via SPME. As it can be noticed, SPME provided links to vitamin D and arachidonic acid metabolism, while SLE did not.

SPME

Pristanoylglycine

L-histidine

Asparaginyl-proline:
Prolyl-asparagine

Alpha-lineoylcarnitine:
Pentadecanoylcarnitine:
Tiglylcarnitine

SLE

Glycine

Histidine

Asparagine

Acetylcarnitine:
Deoxycarnitine:
3-methylglutarylcarnitine

Range of phosphoethanolamines

N-palmitoylethanolamide

1-palmitoyl-2-oleyl-GPG
2-palmitoyl-GPC (16:0)
1-palmitoyl-GPC (16:0)
Palmitoylethanolamide

Figure 4.29 *Comparison of similar and shared metabolites obtained via SPME and SLE.*

Such discrepancy between the results obtained for the two techniques may be caused by different extraction mechanisms. SLE is an exhaustive sample preparation protocol which relies on tissue homogenization and protein precipitation. MeOH is also used, leading to tissue disruption and release of various metabolites from cellular binding. Such an approach facilitates the extraction of multiple endogenous compounds present in different forms (bound and unbound) in the living system but may not fully reflect the real metabolic profile of skeletal muscles. Variation in metabolite profiling via different techniques is recognized by the scientific community and for readers interested in this topic, detailed literature is available.[59,426–430]

Summary

The obtained results showed that, compared to the samples obtained from MHN patients, the levels of metabolites involved in different metabolic pathways, mostly related to lipid metabolism, were altered in skeletal muscle samples (baseline, halothane-exposed, and caffeine-exposed) collected from MHS patients in 2015 and 2016/2017 cohorts. The MHS group had elevated tissue levels of FtA(s) and AcR(s),

which could reflect inherent differences in muscle lipid metabolism in addition to providing evidence for a more readily utilization of β-oxidation as a source of energy in MH patients.

The exposure of skeletal muscle to inhaled anesthetic (halothane) and caffeine resulted in alterations in several metabolic pathways mainly related to energy metabolism and composition of membrane lipids (phospholipids, glycolipids, phosphoglycerides). Additionally, presence of 16:0 Lyso:PC suggested elevated PLA_2 activity which might lead to increased breakdown of membrane phospholipids. Moreover, the presence of elevated levels of vitamin D and its metabolites in skeletal muscles added the complexity to altered biochemical profile of MHS patients. Comparison of data obtained via SPME to that of SLE showed similarities with respect to several compound groups, but also highlighted the fact that utilization of different sample strategies could lead to different results. Employment of conventional protocol for sample preparation, including tissue homogenization and application of organic solvent, could introduce errors in the interpretation of the metabolite profile. When compared to traditional sample preparation protocol, SPME as non-exhaustive technique facilitated extraction of several endogenous compounds, including amino acids, peptides, lipids and metabolites of vitamin D present in free form in the tissue matrix. Hence, metabolomics profiling should implement several sample preparation strategies to obtain a truly robust perspective of the studied subject.

A novelty in the studies was implementation of *in-vivo* muscle sampling. This unique strategy may also provide insights into the involvement of intermediate or unstable compounds in MH, which are not easy to be preserved in biopsy samples. Moreover, the results from *in vivo* sampling are in good agreement with *ex-vivo* SPME and SLE indicating alteration of the same metabolic pathways i.e. FtA(s) and purine metabolism.

It is important to keep in mind that metabolites and their levels are influenced by a synergy of factors which define the phenotype.[431] Advancing our knowledge of MH from its metabolites to pathways would

allow for a better understanding of the disease mechanism as well as genetic, lifestyle and environmental risk factors.[431] This could aid in early disease detection, development of new therapy and patient centric model of care, also known as personalized medicine.[75,431] For example, findings with respect to dysregulation of muscle energy and lipid metabolism could be used to devise specific treatment options in clinical trials for MHS patients.[75] Additionally, combining metabolomic investigations of MH with genome wide association studies would allow one to better discern between metabolites associated with genetically determined metabotypes.[431] Indeed, MH is not always strictly expressed by individuals bearing the gene, so finding metabolites with consistent genetic association would be useful.

Limitations of the study

It must be kept in mind that this study was completed based on a small number of cases where control of patient samples was very random (different ages, genders, diets, environment, physical activity) which increases the chance of finding general biomarkers related to MH condition. One inherent limitation of studying a condition like MH is the small sample size. In other words, collection of MH samples from susceptible human cohorts is difficult because of the small number of cases which turn out to be susceptible after CHCT. In other words, the condition is rare. This means that collections of samples are done over extended periods of time and their storage in -80 ˚C freezers might have an impact on the quality of data obtained. Determining how many samples are required for metabolomic investigations is currently not well understood. Monte-Carlo simulations may be used to determine the appropriate number of samples,[371] but this requires high-level programming skills. Also, more controlled cohort studies are needed in the future to discern whether certain biomarkers are related to environment, lifestyle or are gene-associated.[432] It is known that metabolomics profiles can vary with gender[433] and genetics.[434] Our study did not have a sufficient number of patients to generate gender or gene specific patterns. A larger patient cohort is required for a more thorough study as variation can often be seen in biomarkers

reported by various investigators which could be due to a number of factors (both population and technical based).[433]

Features discovered in the 2016/17 cohort could be deemed informative (not strictly biomarker) due to concentration (sensitivity) differences between MHH and MHS and moderate differences in concentrations of some features between MHS/MHH and MHN patients. If the cause of this variability is phenotype related, then large groups of patient samples from various backgrounds should be used. Additionally, instrumental influence in metabolite discovery should not be ruled out as better understanding of recurring metabolites could be obtained by using a different analytical platform. Therefore, examination of both phenotype and technically-related variances would contribute in finding robust biomarkers for MH.

With respect to animal study, technical issues which influenced reproducibility of the data have been already mentioned. The mouse model was selected as a proof of concept, because of cost effectiveness and relative easiness to be organized. Large animal or preferably human sampling should be performed to eliminate the problems with small muscle size. Moreover, the animal models represent only the genetic factor for MH pathogenesis, therefore moving directly to human study would enable screening of all factors having impact on the mechanisms of the disease.

The analysis of the metabolites was done by focusing on a single platform (Metaboanalyst) as it is not uncommon to find that different biomarkers are reported by different analytical platforms.[372] Also, the effect of a single biomarker may not be great- rather multiple correlated metabolites related to pathophysiology of MH would prove to be more useful.[372,433] Also, as it was shown by our study, data variability was present in the analysis of the two cohorts and SLE extracts- hence robust investigations should make careful notes on both biological and technical data contributors.

Lastly, all the PLS-DA validation models provided in this chapter were strictly employed to assess relevant biological separation and applicability of SPME as a diagnostic tool. As shown, many of those PLS-DA models failed, and the answer why is not simple. Biology, sampling method, instrumental analysis and even data processing could have played a role. It is also important to acknowledge that disease pathophysiology of a large population is very complex. As such, it is rather difficult to imagine that a single biomarker (or even set of biomarkers) would always provide the correct diagnostic result for a group of individuals. This can downplay the use of SPME as a diagnostic tool, but it is important to acknowledge that the diagnostic potential of SPME does exist, but a lot of research and validation still must be done.

4.5 Conclusion

In conclusion, we were able to obtain some insights into the disease mechanism of MH. Our findings pointed to potential dysregulation of predominantly lipid metabolism. Further metabolomic studies should focus on larger patient cohorts and implementation of different analytical platforms to discover recurring metabolic characteristics of MH. In addition, future efforts will be directed at a more thorough investigation of the lipid profile of the patients as well as looking at a greater population as the small sample size is the major limitation of our study.

Chapter 5: Summary and future directions

5.1 Summary

This thesis was focused on the coupling of SPME to DART-MS and advancement of SPME technology for small volume analysis. In addition, current SPME technology (fibers) was investigated for metabolomics profiling of individuals affected by MH. Undeniably, DART-MS technology is simple to use, yielding rapid and sensitive results. DART-MS receives an additional benefit when coupled to a highly preconcentrating technique like SPME, which results in low detection limits in very complex matrices. In order to provide a better understanding of the mechanistic operation of SPME-DART-MS, several different experimental settings of DART and SPME were investigated. It was found that each factor has an impact on signal responses of SPME-DART-MS, but more importantly, there is a great likelihood of factor interaction, thus exhibiting somewhat of a synergistic effect. Analytical sensitivity of SPME-TM meshes and SPME fibers was also compared, and the evidence suggested that SPME-TM meshes of a very specific architecture (woven wire mesh) outperformed the SPME fibers. This highlighted the importance of using the appropriate format of SPME for the most sensitive detection. Applicability of SPME-TM-DART-MS was demonstrated for many scenarios, including coupling to portable MS instrumentation DART-QDa for simulated *in-vivo* detection of DoA(s) in OF. This could be particularly useful for law enforcement, as DUID accidents are expected to rise, particularly with the passing of the Cannabis Act. The prospect of using SPME-TM-DART-MS in small volume analysis was also successfully shown and can be of great benefit to TDM, animal welfare and forensic science. Within clinical settings, speedy results with high turnover rates are of great importance, especially with our ever-growing population. Hence, a HT 96-SPME-TM system for DART-MS was developed and applied for detection of opioids in human urine and plasma, yielding quantitative results in less than 1.5 hours for a set of 96 samples. Lastly, the use of alternative, biocompatible materials like PEEK for manufacturing

of SPME-TM meshes and use in quantitative detection of DoA(s) in OF and urine was demonstrated. PEEK, in comparison to SS, is easier to handle, single use and more comfortable for *in-vivo* buccal swabbing. As such, PEEK SPME-TM meshes have great potential for on site *in-vivo* detection.

Chapter 3 described the development of HLB coated SPME minitips and their subsequent application in small volume analysis. The problem of many approaches often used for small volume analysis is the implementation of poorly preconcentrating material on the probe surface. Certain published manuscripts had already demonstrated the use of preconcentrating materials on probe surface for compound isolation. However, the materials were selective, and the repeatability and limitations of the techniques were scarcely addressed. Hence, in chapter 3, the use of HLB microparticles for the manufacturing of SPME minitips was demonstrated in great detail, emphasizing the fact that microscale manufacturing is very challenging. The minitips developed had a 30 μm diameter on the tip apex and were coated 1 mm in length. Their accuracy, precision and technical problems were also discussed- particularly emphasizing the fact that microscale tip manufacturing can lead to deposition of slightly lower or higher amounts of the extractive phase, leading to pronounced errors. Use of IS can efficiently solve such problems, and this issue is not particularly problematic if probes are being used for extraction of highly concentrated compounds (ppm scale). However, the issue becomes more problematic if target analytes are present at lower concentrations. For example, a slightly "thicker" minitip could report a detection limit of 0.1 ppb, while a slightly "thinner" minitip could report a detection limit of 1 ppb. In chapter 3, a demonstration of analytical performance of SPME minitips coupled to LC/MS and nESI (AIMS) is provided for quantitation of DoA(s) in 1 μL of OF and 1 μL of blood, respectively. In addition, successful discrimination of four different types of fish eggs (caviar) is achieved, reporting over a hundred significant features. It is clear that LC/MS is a feasible instrumental analysis option, but its detection limits are much higher (due to dilution) when compared to nESI.

Chapter 4 was focused on investigation of metabolic markers of patients afflicted with MH. As explained, MH is hypermetabolic disorder, triggered by certain anesthetics which results in excessive release of calcium ions (Ca^{2+}) within muscle cells. The details of metabolic derangements during an MH reaction or even after are unknown. In this study, muscle samples of patients afflicted with MH were sampled using SPME while the instrumental analysis was performed using LC/HRMS. Two cohorts were collected at TGH hospital, one in 2015 and the second in 2016/17. The analysis yielded variable but promising results for the two groups; with statistically significant metabolites for 2015 cohort and insignificant but informative features for the 2016/17 cohort, which served to highlight potential involvement of phenotypic variability in manifestation of MH. Tentatively identified metabolites pointed (but are not limited) to dysregulation in metabolism of membrane lipids, FtA(s), arachidonic acid, N_2, amino-acyl-tRNA, long chain FA oxidation and linoleic acid metabolism in MH afflicted patients. Moreover, these results also pointed to potential involvement of PLA_2 and AcR(s) in pathophysiology of MH. SLE was additionally used on muscle samples to examine whether metabolites obtained by SPME would recur using an alternate technique. Indeed, similar (as well as different) features were found by both techniques. Additionally, *in-vivo* mice sampling was performed and confirmed alteration of lipids as well as purines metabolism. While potential to use SPME as a diagnostic tool was shown, more research is still required since MH phenotypes and biochemistry are highly complex, variable and unlikely to yield a straight-forward answer to a single set of biomarkers of the MH condition.

5.2 Future directions

While applicability of SPME-DART-MS has certainly been demonstrated, it is important to acknowledge that specific aspects of the technology would require further improvements and/or investigations. With respect to DART-MS technology, novel strategies should be implemented to enhance ionization of certain groups of analytes which traditionally yield poor results. A major hindrance of DART-MS is noise generated from the ambient air, which can interfere with detection capabilities of the device. In

other words, noise can overwhelm analyte signals at low concentrations or result in high detection limits for analytes of low MW(s). Hence, efforts should be made to improve and/or eliminate the generated noise by incorporating noise reduction components in the DART hardware. Lastly, DART would benefit from implementation of a fully robotic system which would be able to carry out all experimental steps, with minimal or no supervision since this would enable more efficient use of analyst's time because "nobody wants to sit in front of the MS".

With respect to SPME-DART-MS, it is important to carry out an investigation focusing on potential interaction of experimental factors which determine system response. Considering the number of different factors involved with the approach, it is likely that a full factorial design would be the best strategy to examine factor interaction. Understanding factor interaction would allow for improved experimental throughput as only important factors would be considered, thus resulting in better use of time.

The mechanism of thermal desorption of SPME devices during DART analysis should also be investigated, perhaps using modelling strategies, since it could potentially provide clues to optimum desorption conditions for the SPME devices. SPME is also capable of implementing derivatization strategies, which could be used concomitantly with DART-MS to improve ionization of thermally labile compounds, such as THC. Additionally, applicability of SPME-DART-MS has been insufficiently investigated for metabolomics. Coupling the two strategies together could lead to discovery of valuable information within a matter of minutes. Another aspect that should be considered is coupling of differential ion mobility MS (DIMS) with SPME and DART. While DART-MS has certainly shown that it can provide excellent analytical information, its lack of separation (chromatography) can be problematic if several target analytes have the same MRM transitions (i.e., isomers) or, if co-extracted components from working matrices (e.g., urine, OF, blood, plasma, etc.) have the same transition as the

target analytes. DIMS would not only aid in alleviating these issues, but also allow for further reduction of detection limits.

Lastly, it is important that SPME-DART-MS technology is compared against validated "golden" standard techniques such as GC and LC. Proving that same results could be obtained with both techniques would be an important step in establishing effectiveness and legitimacy of AIMS techniques.

With respect to SPME HLB minitips, further work should focus on improvement of protocol described in Chapter 3 to produce even smaller tips (i.e. tip apex ≤10 μm) which could penetrate tiny single cells. It is likely that the coating strategy would also have to change, as reduction of tip diameter would make it very challenging to use the existing dip-coating procedure. It is worthy to investigate formats other than acupuncture needles for the manufacturing of the minitips, but their cost must be considered, especially if minitip reusability is not an option. An example of this would be titanium. However, one must keep in mind that etching is often required for robust adherence of extractive particles to the SPME minitip. Hence, a careful and reproducible etching protocol should be devised as well for the titanium tips. While satisfactory results were obtained using HLB microparticles as the SPME minitip coating, it is worthy to investigate other coating chemistry options as they could yield even more information. Lastly, it is important to involve scientists from other fields to ensure the success of the SPME minitip. For example, devising a strategy to sample a single cell is not necessarily within the grasp of an analytical chemist, hence collaboration with researchers focusing on single cell analysis would be beneficial.

It is undeniable that metabolomics has great potential for capturing disease related markers and elucidating their biochemical pathways. However, many metabolomics publications which focus on disease investigation vary greatly with respect to sampling protocols and the manner of information presentation. There is a need to enforce some general standards with respect to the aforementioned. This also applies to statistical tools used to process the data. Greater focus should also be placed on using

different sampling strategies, instrumental analysis and data processing to examine whether if the same results can be obtained using varying approaches. Metabolomics is still largely limited by the number of features which can be searched on online databases such as Metlin and HMDB. Lastly, implementing SPME as a diagnostic tool via untargeted (and targeted) metabolomics may have some potential, but it is important to conduct studies with more patients, since disease pathophysiology is far from simple. SPME in combination with metabolomics could also be coupled to AIMS for point-of-care diagnostics within a clinical/medical setting, thus providing rapid results in urgent settings. However, AIMS techniques still require more validation. Finally, greater focus should also be placed on critical comparison of metabolite coverage of SPME vs other techniques like SPE and LLE.

Letter of Copyright Permission

277

278

Name : Tijana Vasiljevic
Address :

300 Keats Way- Unit 404

Tel : 2267504995
Fax :
Email : tijana.vasiljevic@hotmail.com

I am preparing the following work for publication:

Article/Chapter Title : Chapter 1: Introduction
Journal/Book Title : Doctoral thesis
Editor/Author(s) : Tijana Vasiljevic
Publisher : University of Waterloo

I would very much appreciate your permission to use the following material:

Journal/Book Title : Ambient Ionization Mass Spectrometry
Editor/Author(s) : Marek Domin, Rober Cody
Volume Number :
Year of Publication : 2015
Description of Material : Figure 2.1
Page(s) : 24

RE: Permission Request Form: Tijana Vasiljevic

CONTRACTS-COPYRIGHT (shared) <Contracts-Copyright@rsc.org>
2:21 AM

To: Tijana Vasiljevic

Hello Tijana

I must apologise for noticing it was a book from which you were requesting to reproduce material.

The Royal Society of Chemistry hereby grants permission for the use of the material specified below in the work described and in all subsequent editions of the work for distribution throughout the world, in all media including electronic and microfilm. You may use the material in conjunction with computer-based electronic and information retrieval systems, grant permissions for photocopying, reproductions and reprints, translate the material and to publish the translation, and authorize document delivery and abstracting and indexing services. The Royal Society of Chemistry is a signatory to the STM Guidelines on Permissions (available on request).

Please note that if the material specified below or any part of it appears with credit or acknowledgement to a third party then you must also secure permission from that third party before reproducing that material. Please ensure that the published article carries a credit to The Royal Society of Chemistry in the following format:
[Original citation] – Reproduced by permission of The Royal Society of Chemistry

and that any electronic version of the work includes a hyperlink to the article on the Royal Society of Chemistry website.

Best wishes

Gill

Reproducing material from a Royal Society of Chemistry journal

To request permission to reproduce material from a Royal Society of Chemistry journal please go to the Copyright Clearance Center. Please note that for open access articles published under a CC-BY licence no formal permission is needed as long as the reproduction includes a full acknowledgement to the Royal Society of Chemistry article. For open access articles published under a CC BY-NC article formal permission is needed to reproduce the material commercially, including but not limited to, all publishers.

✕

Solid phase microextraction (SPME)-transmission mode (TM) pushes down detection limits in direct analysis in real time (DART)

G. A. Gómez-Ríos and J. Pawliszyn, *Chem. Commun.*, 2014, **50**, 12937
DOI: 10.1039/C4CC05301J

Towards on-site analysis of complex matrices by solid-phase microextraction-transmission mode coupled to a portable mass spectrometer *via* direct analysis in real time

Rapid Communications in Mass Spectrometry

RESEARCH ARTICLE

High-Throughput Quantification of Drugs of Abuse in Biofluids via 96-Solid-Phase Microextraction–Transmission Mode (SPME-TM) and Direct Analysis in Real Time- Mass Spectrometry (DART-MS)

Tijana Vasiljevic, Germán Augusto Gómez-Ríos, Frederick Li, Paul Liang, Janusz Pawliszyn ✉

References

(1)   Nychas, G. J. E.; Skandamis, P. N.; Tassou, C. C.; Koutsoumanis, K. P. *Meat Sci.* **2008**, *78*, 77–89.

(2)   Nciri, N.; Kim, J.; Kim, N.; Cho, N. *Materials (Basel).* **2016**, *9* (859), 1–20.

(3)   Hirayama, A.; Kami, K.; Sugimoto, M.; Sugawara, M.; Toki, N.; Onozuka, H.; Kinoshita, T.; Saito, N.; Ochiai, A.; Tomita, M.; Esumi, H.; Soga, T. *Cancer Res.* **2009**, *69* (11), 4918–4926.

(4)   Government of Canada. Mandatory cannabis testing for pesticide active ingredients https://www.canada.ca/en/public-health/services/publications/drugs-health-products/cannabis-testing-pesticide-requirements.html (accessed Feb 19, 2019).

(5)   Government of Canada. Cannabis Act (S.C. 2018, c. 16) https://laws-lois.justice.gc.ca/eng/acts/C-24.5/ (accessed Feb 19, 2019).

(6)   Wolf, C. E.; Poklis, J. L.; Poklis, A. *J. Anal. Toxicol.* **2017**, *41*, 153–157.

(7)   Pawliszyn, J. *Handbook of Solid Phase Microextraction*; Chemical Industry Press: Beijing, 2009.

(8)   Qi, M.; Philip, M. C.; Yang, N.; Sweedler, J. V. *ACS Chem. Neurosci.* **2018**, *9*, 40–50.

(9)   Agilent. *Sample Preparation Fundamentals for Chromatography*; Agilent Technologies: Santa Clara, CA, USA, 2013.

(10)   Marin, S. J.; Keith, L.; Merrell, M.; McMillin, G. A. *J. Anal. Toxicol.* **2009**, *33* (April), 148–154.

(11)   US Department of Health and Human Services Food and Drug Administration; Center for Drug Evaluation and Research and Center for Veterinary Medicine. Bioanalytical Method Validation Guidance for Industry http://www.fda.gov/Drugs/GuidanceComplianceRegulatoryInformation/Guidances/default.htmand/orhttp://www.fda.gov/AnimalVeterinary/GuidanceComplianceEnforcement/GuidanceforIndustry/default.htm.

(12)   Pawliszyn, J. *Anal. Chem.* **2003**, *75* (11), 2543–2558.

(13)   Smith, R. M. *J. Chromatogr. A* **2003**, *1000*, 3–27.

(14)   Szultka, M.; Pomastowski, P.; Railean-Plugaru, V.; Buszewski, B. *J. Sep. Sci.* **2014**, *37*, 3094–3105.

(15)   Reyes-Garcés, N.; Gionfriddo, E.; Gómez-Ríos, G. A.; Md. Alam, N.; Boyacı, E.; Bojko, B.; Singh, V.; Grandy, J.; Pawliszyn, J. *Anal. Chem.* **2018**, *90*, 302–360.

(16)   Arthur, C. L.; Pawliszyn, J. *Anal. Chem.* **1990**, *62* (19), 2145–2148.

(17)   Budziak, D.; Martendal, E.; Carasek, E. *J. Chromatogr. A* **2007**, *1164* (1–2), 18–24.

(18)   Es-haghi, A.; Hosseininasab, V.; Bagheri, H. *Anal. Chim. Acta* **2014**, *813*, 48–55.

(19)   Reyes-Garcés, N.; Bojko, B.; Hein, D.; Pawliszyn, J. *Anal. Chem.* **2015**, *87* (19), 9722–9730.

(20)   Eisert, R.; Pawliszyn, J. *Anal. Chem.* **1997**, *69* (16), 3140–3147.

(21)   Jiang, R.; Cudjoe, E.; Bojko, B.; Abaffy, T.; Pawliszyn, J. *Anal. Chim. Acta* **2013**, *804*, 111–119.

(22)   Du, T.; Cheng, J.; Wu, M.; Wang, X.; Zhou, H.; Cheng, M. *J. Chromatogr. B* **2014**, *951–952*, 104–109.

(23)   Jiang, R.; Pawliszyn, J. *Trends Anal. Chem.* **2012**, *39*, 245–253.

(24)   Poole, J. J.; Grandy, J. J.; Yu, M.; Boyaci, E.; Gómez-Ríos, G. A.; Reyes-Garcés, N.; Bojko, B.; Heide, H. Vander; Pawliszyn, J. *Anal. Chem.* **2017**, *89*, 8021–8026.

(25) Piri-Moghadam, H.; Ahmadi, F.; Gómez-Ríos, G. A.; Boyacı, E.; Reyes-Garcés, N.; Aghakhani, A.; Bojko, B.; Pawliszyn, J. *Angew. Chemie* **2016**, *55*, 7510–7514.

(26) Gómez-Ríos, G. A.; Pawliszyn, J. *Chem. Commun.* **2014**, *50*, 12937–12940.

(27) Gómez-Ríos, G. A.; Pawliszyn, J. *Angew. Chemie* **2014**, *53* (52), 14503–14507.

(28) Kremser, A.; Jochmann, M. A.; Schmidt, T. C. *Anal. Bioanal. Chem.* **2016**, *408*, 943–952.

(29) Baltussen, E.; Sandra, P.; David, F.; Cramers, C. *J. Microcolumn Sep.* **1999**, *11* (10), 737–747.

(30) Tascon, M.; Singh, V.; Huq, M.; Pawliszyn, J. *Anal. Chem.* **2019**, *91* (7), 4762–4770.

(31) Atkins, P.; De Paula, J. *Atkins' Physical Chemistry*, 8th ed.; W.H. Freeman: New York, NY, 2006.

(32) Musteata, F. M.; Pawliszyn, J.; Qian, M. G.; Wu, J.-T.; Miwa, G. T. *J. Pharm. Sci.* **2006**, *95* (8), 1712–1722.

(33) Ahmadi, F.; Sparham, C.; Boyacı, E.; Pawliszyn, J. *Environ. Sci. Technol.* **2017**, *51*, 3929–3937.

(34) Bai, Z.; Pilote, A.; Sarker, P. K.; Vandenberg, G.; Pawliszyn, J. *Anal. Chem.* **2013**, *85*, 2328–2332.

(35) Roszkowska, A.; Tascon, M.; Bojko, B.; Gory, K.; Reck dos Santos, P.; Cypel, M.; Pawliszyn, J. *Talanta* **2018**, *183*, 304–310.

(36) Ouyang, G.; Pawliszyn, J. *Anal. Chim. Acta* **2008**, *7*, 184–197.

(37) Know, Y. In *Handbook of Essential Pharmacokinetics, Pharmacodynamics and Drug Metabolism for Industrial Scientists*; Kluwer Academic/Plenum Publishers: New York, NY, 2001.

(38) Risticevic, S.; Lord, H.; Górecki, T.; Arthur, C. L.; Pawliszyn, J. *Nat. Protoc.* **2010**, *5* (1), 122–139.

(39) Xie, L.; Liu, S.; Han, Z.; Jiang, R.; Liu, H.; Zhu, F.; Zeng, F.; Su, C.; Ouyang, G. *Anal. Chim. Acta* **2015**, *853* (1), 303–310.

(40) Zang, X.; Zhang, G.; Chang, Q.; Zhang, X.; Wang, C.; Wang, Z. *Anal. Methods* **2015**, *7* (3), 918–923.

(41) Koster, E. H. M.; Crescenzi, C.; dan Hoedt, W.; Ensing, K.; de Jong, G. J. *Anal. Chem.* **2007**, *79*, 3099–3104.

(42) Bagheri, H.; Ayazi, Z.; Naderi, M. *Anal. Chim. Acta* **2013**, *767*, 1–13.

(43) Ho, T. D.; Canestraro, A. J.; Anderson, J. L. *Anal. Chim. Acta* **2011**, *695*, 18–43.

(44) Mirnaghi, F. S.; Chen, Y.; Sidisky, L. M.; Pawliszyn, J. *Anal. Chem.* **2011**, *83* (15), 6018–6025.

(45) Vuckovic, D.; Pawliszyn, J. *Anal. Chem.* **2011**, *83*, 1944–1954.

(46) Lashgari, M.; Yamini, Y. *Talanta* **2019**, *191*, 283–306.

(47) Giffen, J. E.; Rosati, J. Y.; Longo, C. M.; Musah, R. A. *Anal. Chem.* **2017**, *89*, 7719–7726.

(48) Musteata, M. L.; Musteata, F. M.; Pawliszyn, J. *Anal. Chem.* **2007**, *79* (18), 6903–6911.

(49) Mirnaghi, F. S.; Pawliszyn, J. *Anal. Chem.* **2012**, *84* (19), 8301–8309.

(50) Mousavi, F.; Bojko, B.; Pawliszyn, J. *Anal. Chim. Acta* **2015**, *892*, 95–104.

(51) Alam, M. N.; Pawliszyn, J. *Anal. Chem.* **2018**, *90* (4), 2430–2433.

(52) Amiji, M.; Park, K. *Biomaterials* **1992**, *13* (10), 682–692.

(53) Werner, C.; Maitz, M. M.; Sperling, C. *J. Mater. Chem.* **2007**, *17*, 3376–3384.

(54) Musteata, F. M.; Musteata, M. L.; Pawliszyn, J. *Clin. Chem.* **2006**, *52* (4), 708–715.

(55) Bessonneau, V.; Vasiljevic, T.; Pawliszyn, J. *Am. Fish. Soc. Symp.* **2017**, *85*, 161–165.

(56) Taylor, P. J. *Clin. Biochem.* **2005**, *38*, 328–334.

(57) Bessonneau, V.; Bojko, B.; Pawliszyn, J. *Bioanalysis* **2013**, *5* (7), 783–792.

(58) Patti, G. J.; Yanes, O.; Siuzdak, G. *Nat. Rev. Mollecular Cell Biol.* **2013**, *13* (4), 263–269.

(59) Vuckovic, D. *Anal. Bioanal. Chem.* **2012**, *403*, 1523–1548.

(60) Bessonneau, V.; Zhan, Y.; Lannoy, I. A. M. De; Saldivia, V.; Pawliszyn, J. *J. Chromatogr. A* **2015**, *1424*, 134–138.

(61) Bojko, B.; Marcin, W.; Pawliszyn, J. *J. Pharm. Anal.* **2014**, *4* (1), 6–13.

(62) Roszkowska, A.; Yu, M.; Bessonneau, V.; Bragg, L.; Servos, M.; Pawliszyn, J. *Environ. Sci. Technol. Lett.* **2018**, *5* (7), 431–435.

(63) Boyaci, E.; Gorynski, K.; Rodriguez-Lafuente, A.; Bojko, B.; Pawliszyn, J. *Anal. Chim. Acta* **2014**, *809*, 69–81.

(64) Boyaci, E.; Pawliszyn, J. *Anal. Chem.* **2014**, *86* (18), 8916–8921.

(65) Lankadurai, B. P.; Nagato, E. G.; Simpson, M. J. *Environ. Rev.* **2013**, *21* (3), 180–205.

(66) Kim, S.; Kim, J.; Yun, E. J.; Kim, K. H. *Curr. Opin. Biotechnol.* **2016**, *37*, 16–23.

(67) Vuckovic, D.; Risticevic, S.; Pawliszyn, J. *Angew. Chem. Int. Ed. Engl.* **2011**, *50*, 5618–5628.

(68) Gowda, H.; Ivanisevic, J.; Johnson, C. H.; Kurczy, M. E.; Benton, H. P.; Rinehart, D.; Nguyen, T.; Ray, J.; Kuehl, J.; Arevalo, B.; Westenskow, P. D.; Wang, J.; Arkin, A. P.; Deutschbauer, A. M.; Patti, G. J.; Siuzdak, G. *Anal. Chem.* **2014**, *86* (14), 6931–6939.

(69) R Development Core Team. *R Foundation for Statistical Computing*. Vienna, Austria 2008.

(70) Haines, N. R.; Manoharan, N.; Olson, J. L.; D'Alessandro, A.; Reisz, J. A. *J. Proteome Res.* **2018**, *17* (7), 2421–2427.

(71) Worley, B.; Powers, R. *Curr. Metabolomics* **2015**, *1* (1), 92–107.

(72) Wishart, D. S.; Knox, C.; Guo, A. C.; Eisner, R.; Young, N.; Gautam, B.; Hau, D. D.; Psychogios, N.; Dong, E.; Bouatra, S.; Mandal, R.; Sinelnikov, I.; Xia, J.; Jia, L.; Cruz, J. A.; Lim, E.; Sobsey, C. A.; Shrivastava, S.; Huang, P.; Liu, P.; Fang, L.; Peng, J.; Fradette, R.; Cheng, D.; Tzur, D.; Clements, M.; Lewis, A.; de souza, A.; Zuniga, A.; Dawe, M.; Xiong, Y.; Clive, D.; Greiner, R.; Nazyrova, A.; Shaykhutdinov, R.; Li, L.; Vogel, H. J.; Forsythei, I. *Nucleic Acids Res.* **2009**, *37*, 603–610.

(73) Guijas, C.; Montenegro-burke, J. R.; Domingo-almenara, X.; Palermo, A.; Warth, B.; Hermann, G.; Koellensperger, G.; Huan, T.; Uritboonthai, W.; Aisporna, A. E.; Wolan, D. W.; Spilker, M. E.; Benton, H. P.; Siuzdak, G. *Anal. Chem.* **2018**, *90*, 3156–3164.

(74) Tefera, T. W.; Borges, K. *Front. Neurosci.* **2017**, *10*, 1–15.

(75) Lanznaster, D.; de Assis, D. R.; Corcia, P.; Pradat, P.-F.; Blasco, H. *Front. Neurol.* **2018**, *9*, 1–7.

(76) Blasco, H.; Mavel, S.; Corcia, P.; Gordon, P. H. *Curr. Med. Chem.* **2014**, *21* (31), 3551–3575.

(77) Smith, D.; Spanel, P. *Mass Spectrom. Rev.* **2005**, *24*, 661–700.

(78) Arneborgl, J.; Heinemeier, J.; Lynnerup, N.; Nielsen, H. L.; Rude, N.; Sveinbjörnsdóttir, Á. E.

Radiocarbon **1999**, *41* (2), 157–168.

(79)   Guthrie, R. D. *Nature* **2006**, *441*, 207–209.

(80)   Diamandis, E. *Mollecular Cell. Proteomics* **2004**, *3* (4), 367–378.

(81)   Petrie, S.; Bohme, D. K. *Mass Spectrom. Rev.* **2007**, *26*, 258–280.

(82)   Iwamoto, N.; Shimada, T. *Pharmacol. Ther.* **2018**, *185*, 147–154.

(83)   Alberici, R. M.; Simas, R. C.; Sanvido, G. B.; Romão, W.; Lalli, P. M.; Benassi, M.; Cunha, I. B. S.; Eberlin, M. N. *Anal. Bioanal. Chem.* **2010**, *398* (1), 265–294.

(84)   Venter, A. R.; Douglass, K. A.; Shelley, J. T.; Hasman, G. J.; Honarvar, E. *Anal. Chem.* **2014**, *86* (1), 233–249.

(85)   Takáts, Z.; Wiseman, J. M.; Gologan, B.; Graham Cooks, R. *Sci. Mag.* **2004**, *306*, 471–473.

(86)   Gibson, G. T. T.; Mugo, S. M.; Oleschuk, R. D. *Mass Spectrom. Rev.* **2009**, *28*, 918–936.

(87)   Cody, R. B.; Laramee, J. a; Durst, H. D. *Anal. Chem.* **2005**, *77* (8), 2297–2302.

(88)   *New Developments in Mass Spectrometry: Ambient Ionization Mass Spectrometry*; Domin, M., Cody, R. B., Eds.; Royal Society of Chemistry: Cambridge, UK, 2015.

(89)   *Direct Analysis in Real Time Mass Spectrometry: Principles and Practices of DART-MS*, 1st ed.; Dong, Y., Ed.; Wiley-VCH: Weinheim, 2018.

(90)   National Institute of Standards and Technology. NIST Chemistry WebBook, SRD 69 (Water) https://webbook.nist.gov/cgi/cbook.cgi?ID=C7732185&Mask=20 (accessed Feb 19, 2019).

(91)   Gross, J. H. *Anal. Bioanal. Chem.* **2013**, *406*, 63–80.

(92)   Correa, D. N.; Santos, J. M.; Eberlin, L. S.; Eberlin, M. N.; Teunissen, S. F. *Anal. Chem.* **2016**, *88*, 2515–2526.

(93)   Hajslova, J.; Cajka, T.; Vaclavik, L. *Trends Anal. Chem.* **2011**, *30* (2), 204–218.

(94)   Zhou, S.; Forbes, M. W.; Abbatt, J. P. D. *Anal. Chem.* **2015**, *87* (9), 4733–4740.

(95)   Manfredi, M.; Robotti, E.; Bearman, G.; France, F.; Barberis, E.; Shor, P.; Marengo, E. *J. Anal. Methods Chem.* **2016**, *2016*, 1–11.

(96)   He, T.; Chambers, M. I.; Musah, R. A. *Anal. Chem.* **2018**, *90* (21), 12802–12809.

(97)   Srbek, J.; Klejdus, B.; Douša, M.; Břicháč, J.; Stasiak, P.; Reitmajer, J.; Nováková, L. *Talanta* **2014**, *130*, 518–526.

(98)   JeolUSA. *Rapid Analysis of p-Phenylenediamine Antioxidants in Rubber*.

(99)   Banerjee, S.; Madhusudanan, K. P.; Khanuja, S. P. S.; Chattopadhyay, S. K. *Biomed. Chromatogr.* **2008**, *22*, 250–253.

(100)   Cajka, T.; Danhelova, H.; Vavrecka, A.; Riddellova, K.; Kocourek, V.; Vacha, F.; Hajslova, J. *Talanta* **2013**, *115*, 263–270.

(101)   Crawford, E.; Musselman, B. *Anal. Bioanal. Chem.* **2012**, *403*, 2807–2812.

(102)   Jones, R. W.; Cody, R. B.; McClelland, J. F. *J. Forensic Sci.* **2006**, *51* (4), 915–918.

(103)   Nilles, J. M.; Connell, T. R.; Durst, H. D. *Anal. Chem.* **2009**, *81* (16), 6744–6749.

(104) Vaclavik, L.; Cajka, T.; Hrbek, V.; Hajslova, J. *Anal. Chim. Acta* **2009**, *645*, 56–63.

(105) World Anti-Doping Agency. 2017 Anti-Doping Testing Figures https://www.wada-ama.org/sites/default/files/resources/files/2017_anti-doping_testing_figures_en_0.pdf (accessed Apr 10, 2019).

(106) Bridoux, M. C.; Malandain, H.; Leprince, F.; Progent, F.; Machuron-Mandard, X. *Anal. Chim. Acta* **2015**, *869*, 1–10.

(107) Jagerdeo, E.; Abdel-Rehim, M. *Am. Soc. Mass Spectrom.* **2009**, *20*, 891–899.

(108) Bai, Y.; Zhang, J.; Bai, Y.; Liu, H. *Anal. Bioanal. Chem.* **2012**, *403*, 2307–2314.

(109) Chernetsova, E. S.; Morlock, G. E. *Int. J. Mass Spectrom.* **2012**, *314*, 22–32.

(110) Duvivier, W. F.; van Beek, T. A.; Pennings, E. J. M.; Nielen, M. W. F. *Rapid Commun. Mass Spectrom.* **2014**, *28* (7), 682–690.

(111) Grange, A. H. *Rapid Commun. Mass Spectrom.* **2013**, *27*, 305–318.

(112) Zhao, Y.; Lam, M.; Wu, D.; Mak, R. *Rapid Commun. Mass Spectrom.* **2008**, *22*, 3217–3224.

(113) Yu, S.; Crawford, E.; Tice, J.; Musselman, B.; Wu, J.-T. *Anal. Chem.* **2009**, *81*, 193–202.

(114) Maeno, K.; Shida, Y.; Shimada, H. *Anal. Methods* **2017**, *9*, 4851–4857.

(115) Perez, J. J.; Harris, G. A.; Chipuk, J. E.; Brodbelt, J. S.; Green, M. D.; Hampton, C. Y.; Fernandez, F. M. *Analyst* **2010**, *135*, 712–719.

(116) Rodriguez-Lafuente, A.; Mirnaghi, F. S.; Pawliszyn, J. *Anal. Bioanal. Chem.* **2013**, *405* (30), 9723–9727.

(117) Gómez-Riós, G. A.; Gionfriddo, E.; Poole, J.; Pawliszyn, J. *Anal. Chem.* **2017**, *89*, 7240–7248.

(118) Chapman, K.; Burnett, J.; Corvaro, M.; Mitchell, D.; Robinson, S.; Sangster, T.; Sparrow, S.; Spooner, N.; Wilson, A. *Bioanalysis* **2014**, *6*, 2965–2968.

(119) Henion, J.; Oliveira, R. V. *Bioanalysis* **2013**, *5*, 2547–2565.

(120) Wilhelm, A. J.; den Burger, J. C. G.; Swart, E. L. *Clin. Pharmacokinet.* **2014**, *53*, 961–973.

(121) Goldsmith, B. M. *Lab. Med.* **1997**, *28* (10), 659–663.

(122) Workman, P.; Aboagye, E. O.; Balkwill, F.; Balmain, A.; Bruder, G.; Chaplin, D. J.; Double, J. A.; Everitt, J.; Farningham, D.; Glennie, M.; Kelland, L.; Robinson, V.; Stratford, I.; Tozer, G.; Watson, S.; Wedge, S.; Eccles, S. *Br. J. Cancer* **2010**, *102* (11), 1555–1577.

(123) Duncan, K. D.; Fyrestam, J.; Lanekoff, I. *Analyst* **2019**, *144* (3), 782–793.

(124) Wang, L.; Wang, B.; Chadwick, K. D.; Su, T.; Mangipudy, R.; Pillutla, R. C.; Ji, Q. C. *Bioanalysis* **2019**, *11* (3), 175–184.

(125) Verheijen, R. B.; Thijssen, B.; Atrafi, F.; Schellens, J. H. M.; Rosing, H.; de Vries, N.; Beijnen, J. H.; Mathijssen, R. H. J.; Steeghs, N.; Huitema, A. D. R. *J. Chromatogr. B* **2019**, *1104* (August 2018), 234–239.

(126) Joye, T.; Sidibé, J.; Déglon, J.; Karmime, A.; Sporkert, F.; Widmer, C.; Favrat, B.; Lescuyer, P.; Augsburger, M.; Thomas, A. *Anal. Chim. Acta* **2019**, *1063*, 110–116.

(127) Saha-Shah, A.; Weber, A. E.; Karty, J. A.; Ray, S. J.; Hieftje, G. M.; Baker, L. A. *Chem. Sci.* **2015**, *6*, 3334–3341.

(128) Gholipour, Y.; Erra-balsells, R.; Hiraoka, K.; Nonami, H. *Anal. Biochem.* **2013**, *433*, 70–78.

(129) Nakashima, T.; Wada, H.; Morita, S.; Erra-balsells, R.; Hiraoka, K.; Nonami, H. *Anal. Chem.* **2016**, *88*, 3049–3057.

(130) Pan, N.; Rao, W.; Kothapalli, N. R.; Liu, R.; Burgett, A. W. G.; Yang, Z. *Anal. Chem.* **2014**, *86*, 9376–9380.

(131) Tsuyama, N.; Mizuno, H.; Tokunaga, E.; Masujima, T. *Anal. Sci.* **2008**, *24*, 559–561.

(132) Culbertson, C. T. *Microchip Capill. Electrophor.* **2006**, *339*, 203–216.

(133) Lin, L.; Mawatari, K.; Morikawa, K.; Kitamori, T. *Anal. Sci.* **2016**, *32*, 75–78.

(134) Gómez-Ríos, G. A.; Vasiljevic, T.; Gionfriddo, E.; Yu, M.; Pawliszyn, J. *Analyst* **2017**, *142*, 2928–2935.

(135) Vasiljevic, T.; Gómez-Ríos, G. A.; Li, F.; Liang, P.; Pawliszyn, J. *Rapid Commun. Mass Spectrom.* **2019**.

(136) Vasiljevic, T.; Gómez-Ríos, G. A.; Pawliszyn, J. *Anal. Chem.* **2018**, *90*, 952–960.

(137) Bee, M. Y.; Jastrzembski, J. A.; Sacks, G. L. *Anal. Chem.* **2018**, *90*, 13806–13813.

(138) Jastrzembski, J. A.; Bee, M. Y.; Sacks, G. L. *J. Agric. Food Chem.* **2017**, *65* (42), 9353–9359.

(139) Jastrzembski, J. A.; Sacks, G. L. *Anal. Chem.* **2016**, *88*, 8617–8623.

(140) Kpegba, K.; Spadaro, T.; Cody, R. B.; Nesnas, N.; Olson, J. A. *Anal. Chem.* **2007**, *79* (14), 5479–5483.

(141) Sanchez, L. M.; Curtis, M. E.; Bracamonte, B. E.; Kurita, K. L.; Navarro, G.; Sparkman, O. D.; Linington, R. G. *Org. Lett.* **2011**, *13* (15), 3770–3773.

(142) Dane, A. J.; Cody, R. B. *Analyst* **2010**, *135*, 696–699.

(143) Xu, B.; Zhang, D.-Y.; Liu, Z.-Y.; Zhang, Y.; Liu, L.; Li, L.; Liu, C. C.; Wu, G.-H. *J. Pharm. Biomed. Anal.* **2015**, *114*, 447–454.

(144) Zhou, M.; McDonald, J. F.; Fernández, F. M. *J. Am. Soc. Mass Spectrom.* **2010**, *21*, 68–75.

(145) Harris, G. A.; Fernández, F. M. *Anal. Chem.* **2009**, *81*, 322–329.

(146) Harding, L. P.; Parkes, G. M. B.; Townend, J. D. *Analyst* **2014**, *139*, 4176–4180.

(147) Maleknia, S. D.; Vail, T. M.; Cody, R. B.; Sparkman, D. O.; Bell, T. L.; Adams, M. A. *Rapid Commun. Mass Spectrom.* **2009**, *23*, 2241–2246.

(148) Saang'onyo, D. S.; Smith, D. L. *Rapid Commun. Mass Spectrom.* **2012**, *26*, 385–391.

(149) Chernetsova, E. S.; Revelsky, A. I.; Morlock, G. E. *Rapid Commun. Mass Spectrom.* **2011**, *25*, 2275–2282.

(150) Ackerman, L. K.; Noonan, G. O.; Begley, T. H. *Food Addit. Contam.* **2009**, *26* (12), 1611–1618.

(151) Morlock, G.; Ueda, Y. *J. Chromatogr. A* **2007**, *1143*, 243–251.

(152) Duvivier, W. F.; Beek, T. A. Van; Nielen, M. W. F. *Rapid Commun. Mass Spectrom.* **2016**, *30*, 2331–2340.

(153) Zhang, W.; Wang, X.; Xia, Y.; Ouyang, Z. *Theranostics* **2017**, *7* (12), 2968–2981.

(154) Dittrich, M. Determination of proton affinities https://www.ks.uiuc.edu/Training/SumSchool/materials/sources/tutorials/05-qm-tutorial/qm_tutorial.html (accessed May 27, 2019).

(155) Lundstedt, T.; Seifert, E.; Abramo, L.; Thelin, B.; Nystrom, A.; Pettersen, J.; Bergman, R. *Chemom. Intell. Lab. Syst.* **1998**, *42* (1–2), 3–40.

(156) Kim, S.; Chen, J.; Cheng, T.; Gindulyte, A.; He, J.; Li, Q.; Shoemaker, B.; Thiessen, P.; Yu, B.; Zaslavsky, L.; Zhang, J.; Bolton, E. *Nucleic Acids Res.* **2019**, *47* (D1), D1102-1109.

(157) PerkinElmerInformatics. ChemDrawJS. https://chemdrawdirect.perkinelmer.cloud/js/sample/index.html# (accessed May 20, 2019).

(158) Waters. Oasis Sample Extraction Products https://www.waters.com/waters/en_CA/Waters-Oasis-Sample-Extraction-SPE-Products/nav.htm?cid=513209&locale=en_CA (accessed May 20, 2019).

(159) Gómez-Ríos, G. A.; Mirabelli, M. F. *Trends Anal. Chem.* **2019**, *112*, 201–211.

(160) Newsome, G. A.; Kayama, I.; Brogdon-Grantham, S. A. *Anal. Methods* **2018**, *10*, 1038–1045.

(161) Wishart, D. S.; Feunang, Y.; Guo, A.; Lo, E.; Marcu, A.; Grant, J.; Sajed, T.; Johnson, D.; Li, C.; Sayeeda, Z.; Assempour, N.; Iynkkaran, I.; Liu, Y.; Maciejewski, A.; Gale, N.; Wilson, A.; Chin, L.; Cummings, R.; Le, D.; Pon, A.; Knox, C.; Wilson, M. *Nucleic Acids Res.* **2017**.

(162) Li, X.; Ma, W.; Li, H.; Ai, W.; Bai, Y.; Liu, H. *Anal. Bioanal. Chem.* **2018**, *410*, 715–724.

(163) Wang, X.; Li, X.; Li, Z.; Zhang, Y.; Bai, Y.; Liu, H. *Anal. Chem.* **2014**, *86* (10), 4739–4747.

(164) Haunschmidt, M.; Klampfl, C. W.; Buchberger, W.; Hertsens, R. *Anal. Bioanal. Chem.* **2010**, *397*, 269–275.

(165) LaPointe, J.; Musselman, B.; O'Neill, T.; Shepard, J. R. E. *J. Am. Soc. Mass Spectrom.* **2014**, *26*, 159–165.

(166) Cajka, T.; Riddellova, K.; Tomaniova, M.; Hajslova, J. *J. Chromatogr. A* **2010**, *1217* (25), 4195–4203.

(167) Park, H. M.; Kim, H. J.; Jang, Y. P.; Kim, S. Y. *Biomol. Ther.* **2013**, *21* (6), 470–475.

(168) Qin, Z.; Bragg, L.; Ouyang, G.; Pawliszyn, J. *J. Chromatogr. A* **2008**, *1196–1197*, 89–95.

(169) BankerWire. Woven Wire Basics https://www.bankerwire.com/content/resources/basics/woven-wire-basics-percent-open-area-poa-and-mesh-diameter-ratio-md (accessed Apr 30, 2019).

(170) Grange, A. H.; Sovocool, G. W. *Rapid Commun. Mass Spectrom.* **2011**, *25*, 1271–1281.

(171) Cudjoe, E.; Bojko, B.; de Lannoy, I.; Saldivia, V.; Pawliszyn, J. *Angew. Chem. Int. Ed. Engl.* **2013**, *52*, 12124–12126.

(172) Roszkowska, A.; Yu, M.; Bessonneau, V.; Bragg, L.; Servos, M.; Pawliszyn, J. *Environ. Sci. Technol. Lett.* **2018**, *5*, 431–435.

(173) Vasiljevic, T.; Singh, V.; Pawliszyn, J. *Talanta* **2019**, *199*, 689–697.

(174) Lawton, Z. E.; Traub, A.; Fatigante, W. L.; Mancias, J.; Leary, A. E. O.; Hall, S. E.; Wieland, J. R.; Oberacher, H.; Gizzi, M. C.; Mulligan, C. C. *J. Am. Soc. Mass Spectrom.* **2017**, *28*, 1048–1059.

(175) Badman, E. R.; Cooks, R. G. *J. Mass Spectrom.* **2000**, *35*, 659–671.

(176) de Araujo, W. R. D.; Cardoso, T. M. G.; da Rocha, R. G.; Santana, M. H. P.; Munoz, R. A. A.; Richter, E. M.; Paixao, T. R. L. C.; Coltro, W. K. T. *Anal. Chim. Acta* **2018**, *1034*, 1–21.

(177) O'Leary, A. E.; Hall, S. E.; Vircks, K. E.; Mulligan, C. C. *Anal. Methods* **2015**, *7*, 7156–7163.

(178) O'Leary, A. E.; Oberacher, H.; Hall, S. E.; Mulligan, C. C. *Anal. Methods* **2015**, *7* (8), 3331–3338.

(179) Mach, P. M.; McBride, E. M.; Sasiene, Z. J.; Brigance, K. R.; Kennard, S. K.; Wright, K. C.; Verbeck, G. F. *Anal. Chem.* **2015**, *87*, 11501–11508.

(180) Bruno, A. M.; Cleary, S. R.; O'Leary, A. E.; Gizzi, M. C.; Mulligan, C. C. *Anal. Methods* **2017**, *9*, 5015–5022.

(181) Chen, C.-H.; Chen, T.-C.; Zhou, X.; Kline-Schoder, R.; Sorensen, P.; Cooks, R. G.; Ouyang, Z. *J. Am. Soc. Mass Spectrom.* **2015**, *26*, 240–247.

(182) Zhang, Z.; Xu, W.; Manicke, N. E.; Cooks, R. G.; Ouyang, Z. *Anal. Chem.* **2012**, *84*, 931–938.

(183) Ren, Y.; Chiang, S.; Zhang, W.; Wang, X.; Lin, Z.; Ouyang, Z. *Anal. Bioanal. Chem.* **2016**, *408*, 1385–1390.

(184) Brown, H.; Oktem, B.; Windom, A.; Doroshenko, V.; Evans-Nguyen, K. *Forensic Chem.* **2016**, *1*, 66–73.

(185) Bernier, M. C.; Li, F.; Musselman, B.; Newton, P. N.; Fernández, F. M. *Anal. Methods* **2016**, *8*, 6616–6624.

(186) Waters. DART QDa System Instrument Specifications http://www.waters.com/waters/library.htm?locale=en_US&cid=134983082&lid=135009099 (accessed Apr 22, 2019).

(187) Samyn, N.; Boeck, G. De; Verstraete, A. G. *J. Forensic Sci.* **2002**, *47* (6), 1–8.

(188) Bosker, W. M.; Huestis, M. A. *Clin. Chem.* **2009**, *55* (11), 1910–1931.

(189) SAMHSA. Analytes and their cut- offs. https://www.samhsa.gov/sites/default/files/workplace/2010GuidelinesAnalytesCutoffs.pdf (accessed Aug 25, 2017).

(190) Schulze, H.; Schumacher, M.; Urmeew, R.; Auerbach, K. DRUID, Final report: work performed, main results and recommendations https://www.oisevi.org/a/archivos/estudios-especificos/ong/Union-Europea-Druid-Final-Report.pdf (accessed Apr 1, 2019).

(191) Wright, S.; Malcolm, A.; Wright, C.; Prey, S. O.; Crichton, E.; Dash, N.; Moseley, R. W.; Zaczek, W.; Edwards, P.; Fussell, R. J.; Syms, R. R. A. *Anal. Chem.* **2015**, *87*, 3115–3122.

(192) Li, L.; Chen, T. C.; Ren, Y.; Hendricks, P. I.; Cooks, R. G.; Ouyang, Z. *Anal. Chem.* **2014**, *86* (6), 2909–2916.

(193) Ferreira, C. R.; Yannell, K. E.; Jarmusch, A. K.; Pirro, V.; Ouyang, Z.; Cooks, R. G. *Clin. Chem.* **2016**, *61* (1), 99–110.

(194) Denniff, P.; Spooner, N. *Anal. Chem.* **2014**, *86*, 8489–8495.

(195) Shokry, E.; Villanelli, F.; Malvagia, S.; Rosati, A.; Forni, G.; Funghini, S.; Ombrone, D.; Della, M.; Guerrini, R. *J. Pharm. Biomed. Anal.* **2015**, *109*, 164–170.

(196) Wang, H.; Liu, J.; Cooks, R. G.; Ouyang, Z. *Angew. Chem. Int. Ed. Engl.* **2010**, *49*, 877–880.

(197) Corso, G.; Paglia, G.; Garofalo, D.; D'Apolito, O. *Rapid Commun. Mass Spectrom.* **2007**, *21*, 3777–3784.

(198) Kolocouri, F.; Dotsikas, Y.; Loukas, Y. L. *Anal. Bioanal. Chem.* **2010**, *398*, 1339–1347.

(199) Abdel-Rehim, A.; Abdel-Rehim, M. *Biomed. Chromatogr.* **2014**, *28*, 875–877.

(200) Zhang, C.; Manicke, N. E. *Anal. Chem.* **2015**, *87* (12), 6212–6219.

(201) Manicke, N. E.; Bills, B. J.; Chengsen, Z. *Bioanalysis* **2016**, *8* (6), 589–606.

(202) Yannell, K. E.; Kesely, K. R.; Chien, H. D.; Kissinger, C. B.; Cooks, R. G. *Anal. Bioanal. Chem.* **2017**, *409*, 121–131.

(203) Huang, C. M.; Zhu, Y.; Jin, D. Q.; Kelly, R. T.; Fang, Q. *Anal. Chem.* **2017**, *89*, 9009–9016.

(204) Ren, Y.; McLuckey, M. N.; Liu, J.; Ouyang, Z. *Angew. Chem. Int. Ed. Engl.* **2014**, *53*, 14124–14127.

(205) Tascon, M.; Md. Alam, N.; Gómez-Ríos, G. A.; Pawliszyn, J. *Anal. Chem.* **2018**, *90*, 2631–2638.

(206) Gómez-Ríos, G. A.; Reyes-Garcés, N.; Bojko, B.; Pawliszyn, J. *Anal. Chem.* **2016**, *88*, 1259–1265.

(207) Lee, C. W.; Su, H.; Chen, P. Y.; Lin, S. J.; Shiea, J.; Shin, S. J.; Chen, B. H. *J. Mass Spectrom.* **2016**, *51*, 97–104.

(208) Wang, C.; Zhu, H.; Cai, Z.; Song, F.; Liu, Z.; Liu, S. *Anal. Bioanal. Chem.* **2013**, *405*, 3159–3164.

(209) Crawford, E.; Gordon, J.; Wu, J.-T.; Musselman, B.; Liu, R.; Yu, S. *Bioanalysis* **2011**, *3* (11), 1217–1226.

(210) Khaled, A.; Gionfriddo, E.; Acquaro, V.; Singh, V.; Pawliszyn, J. *Anal. Chim. Acta* **2019**, *1056*, 34–46.

(211) Reyes-Garcés, N.; Bojko, B.; Pawliszyn, J. *J. Chromatogr. A* **2014**, *1374*, 40–49.

(212) Øiestad, E. L.; Øiestad, Å. M. L.; Gjelstad, A.; Karinen, R. *Bioanalysis* **2016**, *8*, 691–710.

(213) Humphrey, S. P.; Williamson, R. T. *J. Prosthet. Dent.* **2001**, *85* (2), 162–169.

(214) Brutin, D.; Sobac, B.; Loquet, B.; Sampol, J. *J. Fluid Mech.* **2011**, *667*, 85–95.

(215) BCcampus-OpenStax. 18.1 An Overview of Blood https://opentextbc.ca/anatomyandphysiology/chapter/an-overview-of-blood/ (accessed Mar 14, 2019).

(216) Bevel, T.; Gardner, R. M. *Bloodstain Pattern Analysis with an Introduction to Crime Scene Reconstruction (Practical Aspects of Criminal and Forensics Investigations)*, 3rd Editio.; CRC Press: Boca Raton, Florida, USA, 2008.

(217) Lavalle, P.; Stoltz, J.; Senger, B.; Voegel, J.; Schaaf, P. *Proc. Natl. Acad. Sci. U. S. A.* **1996**, *93*, 15136–15140.

(218) Ramsthaler, F.; Schmidt, P.; Bux, R.; Potente, S.; Kaiser, C.; Kettner, M. *Int. J. Legal Med.* **2012**, *126*, 739–746.

(219) Mirnaghi, F. S.; Pawliszyn, J. *Anal. Chem.* **2012**, *84*, 8301–8309.

(220) Huang, H.; Wu, Q.; Zeng, L.; Wan, L.; Lai, S.; Yin, X.; Huang, J.; Yang, B.; Liu, J. *Anal. Methods* **2017**, *9*, 4282–4287.

(221) Gómez-Ríos, G. A.; Tascon, M.; Reyes-Garcés, N.; Boyacı, E.; Poole, J.; Pawliszyn, J. *Sci. Rep.* **2017**, *7* (16104), 1–7.

(222) Annesley, T. M.; Clayton, L. *Clin. Chem.* **2004**, *50* (10), 1845–1848.

(223) Clinical Laboratory Reference: Cutoff and Toxicity Levels for Drugs-of-Abuse Testing http://www.clr-online.com/CLR2017-13_Table-of-Cutoff-Toxicity-DOA.pdf (accessed Aug 26, 2017).

(224) Takats, Z.; Strittmatter, N.; Mckenzie, J. S. In *Ambient Mass Spectrometry in Cancer Research*; Drake, R. R., McDonnell, L. A., Eds.; Elsevier Inc., 2017; Vol. 134, pp 231–256.

(225) Shevlin, M. *ACS Med. Chem. Lett.* **2017**, *8*, 601–607.

(226) Medina-Remón, A.; Barrionuevo-González, A.; Zamora-Ros, R.; Andres-Lacueva, C.; Estruch, R.;

Martínez-González, M. Á.; Diez-Espino, J.; Lamuela-Raventos, R. M. *Anal. Chim. Acta* **2009**, *634*, 54–60.

(227) Baz-Lomba, J. A.; Löve, A. S. C.; Reid, M. J.; Ólafsdóttir, K.; Thomas, K. V. *J. Chromatogr. A* **2018**, *1531*, 32–38.

(228) Zhang, N.; Yang, A.; Rogers, J. D.; Zhao, J. J. *J. Pharm. Biomed. Anal.* **2004**, *34*, 175–187.

(229) Watt, A. P.; Morrison, D.; Locker, K. L.; Evans, D. C. *Anal. Chem.* **2000**, *72* (5), 2340–2345.

(230) Lehotay, S. J.; Mastovska, K.; Lightfield, A. R.; Nuñez, A.; Dutko, T.; Ng, C.; Bluhm, L. *J. Chromatogr. A* **2013**, *1313*, 103–112.

(231) Jannetto, P. J.; Langman, L. J. *Clin. Biochem.* **2016**, *49*, 1032–1034.

(232) Grote-Koska, D.; Czajkowski, S.; Brand, K. *Ther. Drug Monit.* **2015**, *37*, 400–404.

(233) Prabhu, G. R. D.; Urban, P. L. *Trends Anal. Chem.* **2017**, *88*, 41–52.

(234) Jones, C. M.; Fernández, F. M. *Rapid Commun. Mass Spectrom.* **2013**, *27*, 1311–1318.

(235) Danhelova, H.; Hradecky, J.; Prinosilova, S.; Cajka, T.; Riddellova, K.; Vaclavik, L.; Hajslova, J. *Anal. Bioanal. Chem.* **2012**, *403*, 2883–2889.

(236) Grange, A. H. *Environ. Forensics* **2008**, *9*, 127–136.

(237) Jastrzembski, J. A.; Bee, M. Y.; Sacks, G. L. *J. Agric. Food Chem.* **2017**, *65*, 9353–9359.

(238) Mirabelli, M. F.; Wolf, J.-C.; Zenobi, R. *Anal. Chem.* **2016**, *88*, 7252–7258.

(239) Strittmatter, N.; Düring, R.; Takáts, Z. *Analyst* **2012**, *137*, 4037–4044.

(240) Walles, M.; Gu, Y.; Dartiguenave, C.; Musteata, F. M.; Waldron, K.; Lubda, D.; Pawliszyn, J. *J. Chromatogr. A* **2005**, *1067*, 197–205.

(241) Mirabelli, M. F.; Zenobi, R. *Anal. Chem.* **2018**, *90*, 5015–5022.

(242) Gómez-Ríos, G. A.; Mirabelli, M. F. *TrAC Trends Anal. Chem.* **2019**, *112*, 201–211.

(243) Williamson, R.; Gura, S.; Tarifa, A.; Almirall, J. R. *Forensic Chem.* **2018**, *8*, 49–56.

(244) Li, F.; Musselman, B. *Methods Mol. Biol.* **2018**, *1810*, 97–106.

(245) Tascon, M.; Gómez-Ríos, G. A.; Reyes-Garcés, N.; Poole, J.; Boyacı, E.; Pawliszyn, J. *Anal. Chem.* **2017**, *89*, 8421–8428.

(246) Vuckovic, D.; Cudjoe, E.; Hein, D.; Pawliszyn, J. *Anal. Chem.* **2008**, *80*, 6870–6880.

(247) The Engineering ToolBox https://www.engineeringtoolbox.com/thermal-conductivity-d_429.html (accessed Nov 13, 2018).

(248) National Institute of Standards and Technology. No Title https://webbook.nist.gov/cgi/formula?ID=U137060&Mask=200 (accessed Jan 13, 2019).

(249) Little, J. L. *J. Chromatogr. A* **1999**, *844*, 1–22.

(250) Zhou, M.; Guan, W.; Walker, L. D.; Mezencev, R.; Benigno, B. B.; Gray, A.; Fernández, F. M.; Mcdonald, J. F. *Cancer Epidemiol. Biomarkers Prev.* **2010**, *19*, 2262–2272.

(251) Busman, M. *J. Assoc. Off. Agric. Chem.* **2018**, *101* (3), 643–646.

(252) Hayeck, N.; Ravier, S.; Gemayel, R.; Gligorovski, S.; Poulet, I.; Maalouly, J.; Wortham, H. *Talanta*

2015, *144*, 1163–1170.

(253) Zhang, L.; Yong, W.; Liu, J.; Wang, S.; Chen, Q.; Guo, T.; Zhang, J.; Tan, T.; Su, H.; Dong, Y. *J. Am. Soc. Mass Spectrom.* **2015**, *26*, 1414–1422.

(254) Häbe, T. T.; Morlock, G. E. *Rapid Commun. Mass Spectrom.* **2015**, *29*, 474–484.

(255) Madras, B. *JAMA Psychiatry* **2017**, *74* (5), 441–442.

(256) United Nations. *World Drug Report 2018*; Vienna, 2018.

(257) Cooks, R. G.; Ouyang, Z.; Takats, Z.; Wiseman, J. M. *Detect. Technol.* **2006**, *311*, 1566–1570.

(258) Wu, C.; Dill, A. L.; Eberlin, L. S.; Cooks, R. G.; Ifa, D. R. *Mass Spectrom. Rev.* **2013**, *32*, 218–243.

(259) *Clarke's Analytical Forensic Toxicology*; Jickells, S., Negrusz, A., Eds.; Pharmaceutical Press: London, 2008.

(260) Tarté, R. In *Handbook of Food Proteins*; Phillips, G. O., Williams, P. A., Eds.; Woodhead Publishing: Sawston, 2011; pp 56–91.

(261) Marin, S. J.; Hughes, J. M.; Lawlor, B. G.; Clark, C. J.; McMillin, G. A. *J. Anal. Toxicol.* **2012**, *36* (7), 477–486.

(262) Espy, R. D.; Teunissen, S. F.; Manicke, N. E.; Ren, Y.; Ouyang, Z.; Asten, A. Van; Cooks, R. G. *Anal. Chem.* **2014**, *86*, 7712–7718.

(263) Liu, J.; Wang, H.; Manicke, N. E.; Lin, J.-M.; Cooks, R. G. *Anal. Chem.* **2010**, *82* (6), 2463–2471.

(264) Qian, Z.; Le, J.; Chen, X.; Li, S.; Song, H.; Hong, Z. *J. Sep. Sci.* **2018**, *41*, 618–629.

(265) Sobolesky, P. M.; Smith, B. E.; Hubbard, J. A.; Stone, J.; Marcotte, T. D.; Grelotti, D. J.; Grant, I.; Fitzgerald, R. L. *Clin. Chim. Acta* **2019**, *491*, 30–38.

(266) Meng, J.; Lai, M.-T.; Munshi, V.; Grobler, J.; McCauley, J.; Zuck, P.; Johnson, E. N.; Uebele, V. N.; Hermes, J. D.; Adam, G. C. *J. Biomol. Screen.* **2015**, *20* (5), 606–615.

(267) Romm, M. V; Parikh, N.; Miller, V. P. Ultra Fast Analysis of Hydroxymidazolam in Plasma Using the Agilent RapidFire High-Throughput Mass Spectrometry System https://www.agilent.com/cs/library/applications/5990-9767EN.pdf (accessed Apr 4, 2019).

(268) Canadian Centre on Substance Abuse. Facts about drug impaired driving. http://www.ccsa.ca/Resource Library/CCSA-Drug-Impaired-Driving-Toolkit-Facts-2016-en.pdf (accessed Aug 25, 2017).

(269) Smink, B. E.; Mathijssen, M. P. M.; Lusthof, K. J.; de Gier, J. J.; Egberts, A. C. G.; Uges, D. R. A. *J. Anal. Toxicol.* **2006**, *30* (7), 478–485.

(270) Laloup, M.; del Mar Ramirez Fernandez, M.; Wood, M.; De Boeck, G.; Maes, V.; Samyn, N. *Forensic Sci. Int.* **2006**, *161*, 175–179.

(271) Wood, M.; De Boeck, G.; Samyn, N.; Morris, M.; Cooper, D. P.; Maes, R. A. A.; De Bruijn, E. A. *J. Anal. Toxicol.* **2003**, *27*, 78–87.

(272) Strano-Rossi, S.; Anzillotti, L.; Castrignanò, E.; Felli, M.; Serpelloni, G.; Mollica, R.; Chiarotti, M. *Anal. Bioanal. Chem.* **2011**, *401* (2), 609–624.

(273) Wood, M.; Laloup, M.; Ramirez Fernandez, M. D. M.; Jenkins, K. M.; Young, M. S.; Ramaekers, J. G.; De Boeck, G.; Samyn, N. *Forensic Sci. Int.* **2005**, *150*, 227–238.

(274) Badawi, N.; Simonsen, K. W.; Steentoft, A.; Bernhoft, I. M.; Linnet, K. *Clin. Chem.* **2009**, *55* (11), 2004–2018.

(275) Jung, J.; Kempf, J.; Mahler, H.; Weinmann, W. *J. Mass Spectrom.* **2007**, *42*, 354–360.

(276) Maralikova, B.; Weinmann, W. *J. Chromatogr. B* **2004**, *811*, 21–30.

(277) Newton, P. N.; Fernandez, F. M.; Plancon, A.; Mildenhall, D. C.; Green, M. D.; Ziyong, L.; Christophel, E. M.; Phanouvong, S.; Howells, S.; McIntosh, E.; Laurin, P.; Blum, N.; Hampton, C. Y.; Faure, K.; Nyadong, L.; Soong, C. W. R.; Santoso, B.; Zhiguang, W.; Newton, J.; Palmer, K. *PLoS Med.* **2008**, *5* (2), 0209–0219.

(278) Bojko, B.; Cudjoe, E.; Gómez-Ríos, G. A.; Gorynski, K.; Jiang, R.; Reyes-Garcés, N.; Risticevic, S.; Silva, É. A. S.; Togunde, O.; Vuckovic, D.; Pawliszyn, J. *Anal. Chim. Acta* **2012**, *750*, 132–151.

(279) Caris, J. A.; Chaves, A. R.; Queiroz, M. E. C. *J. Brazilian Chem. Soc.* **2012**, *23* (1), 57–64.

(280) Musteata, F. M.; de Lannoy, I.; Gien, B.; Pawliszyn, J. *J. Pharm. Biomed. Anal.* **2008**, *47* (4–5), 907–912.

(281) Vuckovic, D.; Cudjoe, E.; Musteata, F. M.; Pawliszyn, J. *Nat. Protoc.* **2010**, *5* (1), 140–161.

(282) Souza-Silva, É. A.; Reyes-Garcés, N.; Gómez-Ríos, G. A.; Boyaci, E.; Bojko, B.; Pawliszyn, J. *TrAC - Trends Anal. Chem.* **2015**, *71*, 249–264.

(283) Li, X.; Li, Z.; Wang, X.; Nie, H.; Zhang, Y.; Bai, Y.; Liu, H. *Analyst* **2016**, *141*, 4947–4952.

(284) Wu, M.; Wang, H.; Dong, G.; Musselman, B. D.; Liu, C. C.; Guo, Y. *Chinese J. Chem.* **2015**, *33*, 213–219.

(285) Wang, X.; Li, X.; Li, Z.; Zhang, Y.; Bai, Y.; Liu, H. *Anal. Chem.* **2014**, *86*, 4739–1747.

(286) Liu, Y.; Shen, Y.; Lee, M. L. *Anal. Chem.* **1997**, *69* (2), 190–195.

(287) Djozan, D.; Abdollahi, L. *Chromatographia* **2003**, *57* (11–12), 799–804.

(288) Hashemi, P.; Shamizadeh, M.; Badiei, A.; Poor, P. Z.; Ghiasvand, A. R.; Yarahmadi, A. *Anal. Chim. Acta* **2009**, *646* (1–2), 1–5.

(289) Panayotov, I. V.; Orti, V.; Cuisinier, F.; Yachouh, J. *J. Mater. Sci. Mater. Med.* **2016**, *27* (188), 1–11.

(290) Abu Bakar, M. S.; Cheang, P.; Khor, K. A. *Mater. Sci. Eng. A345* **2003**, *345* (1–2), 55–63.

(291) Fan, J. P.; Tsui, C. P.; Tang, C. Y.; Chow, C. L. *Biomaterials* **2004**, *25* (23), 5363–5373.

(292) Ha, S. W.; Kirch, M.; Birchler, F.; Eckert, K. L.; Mayer, J.; Wintermantel, E.; Sittig, C.; Pfund-Klingenfuss, I.; Textor, M.; Spencer, N. D.; Guecheva, M.; Vonmont, H. *J. Mater. Sci. Mater. Med.* **1997**, *8* (11), 683–690.

(293) Zoidis, P.; Papathanasiou, I. *J. Prosthet. Dent.* **2016**, *116* (5), 637–641.

(294) Staal, F.; Pluijmers, B.; Wolvius, E.; Koudstaal, M. *Craniomaxillofac. Trauma Reconstr.* **2016**, *9* (3), 264–267.

(295) Ponnappan, R. K.; Serhan, H.; Zarda, B.; Patel, R.; Albert, T.; Vaccaro, A. R. *Spine J.* **2009**, *9* (3), 263–267.

(296) Sobieraj, M. C.; Kurtz, S. M.; Rimnac, C. M. *Biomaterials* **2009**, *30* (33), 6485–6494.

(297) Leat, M. E.; Fisher, J. *Med. Eng. Phys.* **1994**, *16* (6), 470–476.

(298) Liguori, A.; Hughes, J. R.; Grass, J. A. *Pharmacol. Biochem. Behav.* **1997**, *58* (3), 721–726.

(299) Mercolini, L.; Protti, M. *J. Pharm. Biomed. Anal.* **2016**, *130*, 202–219.

(300) So, P. K.; Ng, T. T.; Wang, H.; Hu, B.; Yao, Z. P. *Analyst* **2013**, *138* (8), 2239–2243.

(301) Saha, S.; Mandal, M. K.; Hiraoka, K. *Anal. Methods* **2013**, *5*, 4731–4738.

(302) Pirro, V.; Jarmusch, A. K.; Vincenti, M.; Cooks, R. G. *Anal. Chim. Acta* **2015**, *861*, 47–54.

(303) B Cody, R. *Mass Spectrom. (Tokyo, Japan)* **2013**, *2* (Spec Iss), S0007.

(304) Sviridov, D.; Hortin, G. L. *Clin. Chim. Acta* **2009**, *404* (2), 140–143.

(305) *Caffeine: Chemisty, Analysis, Function and Effects*; Preedy, V., Ed.; Royal Society of Chemistry: London, 2012.

(306) Zhang, L.; Vertes, A. *Angew. Chem. Int. Ed. Engl.* **2018**, *57*, 4466–4477.

(307) Gong, X.; Zhao, Y.; Cai, S.; Fu, S.; Yang, C.; Zhang, S.; Zhang, X. *Anal. Chem.* **2014**, *86*, 3809–3816.

(308) Korfmacher, W.; Ho, S.; Wang, J.; Wu, Z.; Shea, T. O. *Bioanalysis* **2015**, *7*, 449–461.

(309) Yang, Y.; Huang, Y.; Wu, J.; Liu, N.; Deng, J. *Trends Anal. Chem.* **2017**, *90*, 14–26.

(310) Mizuno, H.; Tsuyama, N.; Harada, T.; Masujima, T. *J. Mass Spectrom.* **2008**, *43*, 1692–1700.

(311) Hiyama, E.; Ali, A.; Amer, S.; Harada, T.; Shimamoto, K.; Furushima, R.; Abouleila, Y.; Emara, S.; Masujima, T. *Anal. Sci.* **2015**, *31*, 1215–1217.

(312) Tejedor, M. L.; Mizuno, H.; Tsuyama, N.; Harada, T.; Masujima, T. *Anal. Sci.* **2009**, *25*, 1053–1055.

(313) Deng, J.; Li, W.; Yang, Q.; Liu, Y.; Fang, L.; Guo, Y.; Guo, P.; Lin, L.; Yang, Y.; Luan, T. *Anal. Chem.* **2018**, *90*, 6936–6944.

(314) Deng, J.; Yang, Y.; Xu, M.; Wang, X.; Lin, L.; Yao, Z. P.; Luan, T. *Anal. Chem.* **2015**, *87*, 9923–9930.

(315) Huang, X.; Zhu, X.; Pei, M. *Microchim. Acta* **2018**, *185*, 1–8.

(316) Cheng, H.; Song, Y.; Bian, Y. *Microchim. Acta* **2018**, *185*, 1–8.

(317) Bagheri, H.; Manouchehri, M.; Allahdadlalouni, M. *Microchim. Acta* **2017**, *184*, 2201–2209.

(318) Li, J.; Liu, Y.; Su, H.; Wong, Y. E.; Chen, X.; Chan, T. D.; Chen, Q. *Microchim. Acta* **2017**, *184*, 3809–3815.

(319) Cabrera, K.; Altmaier, S. High Resolution and Ultra Trace Analysis of Pesticides Using Silica Monoliths https://www.chromatographytoday.com/article/chromatography/1/merck-kgaa/high-resolution-and-ultra-trace-analysis-of-pesticides-using-silica-monoliths/1492 (accessed Nov 19, 2018).

(320) Zhang, S.; Yang, Q.; Yang, X.; Wang, W.; Li, Z.; Zhang, L.; Wang, C.; Wang, Z. *Talanta* **2017**, *166*, 46–53.

(321) Abolghasemi, M. M.; Habibiyan, R.; Jaymand, M.; Piryaei, M. *Microchim. Acta* **2018**, *185*, 1–6.

(322) Vikrant, K.; Tsang, D. C. W.; Raza, N.; Giri, B. S.; Kukkar, D.; Kim, K. *ACS Appl. Mater. Interfaces* **2018**, *10*, 8797–8817.

(323) Woonton, B. W.; Smithers, G. W. *Separation, Extraction and Concentration Processes in the Food, Beverage and Nutraceutical Industries*; Woodhead Publishing Series in Food Science, Technology and Nutrition: Sawston, Cambridge, 2013.

(324) Madaan, K.; Kumar, S.; Poonia, N.; Lather, V.; Pandita, D. *J. Pharm. Bioallied Sci.* **2014**, *6*, 139–150.

(325) Pearson, R. M.; Sunoqrot, S.; Hsu, H. J.; Bae, J. W.; Hong, S. *Ther. Deliv.* **2012**, *3*, 941–959.

(326) Anbia, M.; Haghi, A.; Shariati, S. *Anal. Methods* **2012**, *4*, 2555–2561.

(327) Rahimi, A.; Hashemi, P.; Badiei, A.; Arab, P.; Reza, A. *Anal. Chim. Acta* **2011**, *695*, 58–62.

(328) Hanke, M.; Arslan, H. K.; Bauer, S.; Zybaylo, O.; Christophis, C.; Gliemann, H.; Rosenhahn, A.; Wo, C. *Langmuir* **2012**, *28*, 6877–6884.

(329) Kwak, J.-H.; Min, J.; Kim, N.-H.; Valan, M.; Kim, S.; Kyoung, M.; Kim, S.-J. *Saudi J. Biol. Sci.* **2017**, *24*, 1387–1391.

(330) Singh, V.; Kumar, A.; Chinthakindi, S.; D, R. G.; Tak, V.; Pardasani, D.; Roy, A.; Kumar, D. *J. Chromatogr. A* **2016**, *1434*, 39–49.

(331) Matuszewski, B. K.; Constanzer, M. L.; Chavez-Eng, C. M. *Anal. Chem.* **2003**, *75*, 3019–3030.

(332) Brinker, C. J.; Frye, G. C.; Hurd, A. J.; Ashley, C. S. *Thin Solid Films* **1991**, *201*, 97–108.

(333) Fang, H. W.; Li, K. Y.; Su, T. L.; Yang, T. C. K.; Chang, J. S.; Lin, P. L. *Mater. Lett.* **2008**, *62*, 3739–3741.

(334) Landau, L.; Levich, B. *Acta Physicochim. URSS* **1942**, *17* (42), 42–54.

(335) Reyes-Garcés, N.; Gionfriddo, E.; Gómez-Ríos, G. A.; Md. Alam, N.; Boyaci, E.; Bojko, B.; Singh, V.; Grandy, J.; Pawliszyn, J. *Anal. Chem.* **2018**, *90*, 302–360.

(336) Simões, R.; Bonato, P.; Mirnaghi, F.; Bojko, B.; Pawliszyn, J. *Bioanalysis* **2015**, *7*, 65–77.

(337) Gorynski, K.; Bojko, B.; Kluger, M.; Jerath, A.; Wasowicz, M.; Pawliszyn, J. *J. Pharm. Biomed. Anal.* **2014**, *92*, 183–192.

(338) Jones, D. R.; Wu, Z.; Chauhan, D.; Anderson, K. C.; Peng, J. *Anal. Chem.* **2014**, *86*, 3667–3675.

(339) Chetwynd, A. J.; Abdul-Sada, A.; Hill, E. M. *Anal. Chem.* **2015**, *87*, 1158–1165.

(340) Bailey, D. *Am. J. Clin. Pathol.* **1995**, *104*, 180–186.

(341) Yamamoto, I.; Iwata, K.; Nakashima, M. *J. Pharmacobiodyn.* **1985**, *8*, 385–391.

(342) Bojko, B.; Reyes-Garcés, N.; Bessonneau, V.; Goryński, K.; Mousavi, F.; Silva, E. A. S.; Pawliszyn, J. *Trends Anal. Chem.* **2014**, *61*, 168–180.

(343) Zhang, B.; Xie, M.; Brüschweiler-Li, L.; Brüschweiler, R. *Metabolites* **2018**, *8*, 1–14.

(344) Porcari, A. M.; Fernandes, G. D.; Belaz, K.; Schwab, N.; Santos, V.; Alberici, R.; Gromova, V.; Eberlin, M.; Lebedev, A.; Tata, A. *Anal. Methods* **2014**, *6*, 2436–2443.

(345) Chambers, M. C.; Maclean, B.; Burke, R.; Amodei, D.; Ruderman, D. L.; Neumann, S.; Gatto, L.; Fischer, B.; Pratt, B.; Egertson, J.; Hoff, K.; Kessner, D.; Tasman, N.; Shulman, N.; Frewen, B.; Baker, T. A.; Brusniak, M.; Paulse, C.; Creasy, D.; Flashner, L.; Kani, K.; Moulding, C.; Seymour, S. L.; Nuwaysir, L. M.; Lefebvre, B.; Kuhlmann, F.; Roark, J.; Rainer, P.; Detlev, S.; Hemenway, T.; Huhmer, A.; Langridge, J.; Connoly, B.; Chadick, T.; Holly, K.; Eckels, J.; Deutsch, E. W.; Moritz, R. L.; Katz, J. E.; Agus, D. B.; MacCoss, M.; Tabb, D. L.; Mallick, P. *Nat. Biotechnol.* **2012**, *30* (10), 918–920.

(346) Chong, J.; Soufan, O.; Li, C.; Caraus, I.; Li, S.; Bourque, G.; Wishart, D. S.; Xia, J. *Nucleic Acids Res.* **2018**, *46*, 486–494.

(347) Viczek, S. A.; Jensen, K. B.; Francesconi, K. A. *Angew. Chemie* **2016**, *128*, 5345–5348.

(348) Schug, K. A. Does Mass Spectrometry Need Chromatography? https://www.chromacademy.com/chromatography-Does-mass-spectrometry-need-chromatography.html (accessed Nov 19, 2018).

(349) Panuwet, P.; Hunter, R. E. J.; D'Souza, P. E.; Chen, X.; Radford, S. A.; Cohen, J. R.; Marder, M. E.;

Kartavenka, K.; Ryna, P. B.; Boyd Barr, D. *Crit. Rev. Anal. Chem.* **2016**, *46*, 93–105.

(350) Schmidt, A.; Karas, M.; Dülcks, T. *J. Am. Soc. Mass Spectrom.* **2003**, *14*, 492–500.

(351) Kajiyama, S.; Harada, K.; Fukusaki, E.; Kobayashi, A. *J. Biosci. Bioeng.* **2006**, *102*, 575–578.

(352) Zhang, Z.; Sun, L.; Zhu, G.; Cox, O. F.; Huber, P. W.; Dovichi, N. J. *Anal. Chem.* **2015**, *88*, 877–882.

(353) Sun, L.; Bertke, M. M.; Champion, M. M.; Zhu, G.; Huber, P. W.; Dovichi, N. J. *Sci. Rep.* **2014**, *4*, 1–9.

(354) Rosenberg, H.; Davis, M.; James, D.; Pollock, N.; Stowell, K. *Orphanet J. Rare Dis.* **2007**, *2* (21), 1–14.

(355) Brandom, B. W. *Anesth. Analg.* **2014**, *116* (5), 1078–1086.

(356) Jiang, D.; Chen, W.; Xiao, J.; Wang, R.; Kong, H.; Jones, P. P.; Zhang, L.; Fruen, B.; Chen, S. R. W. *J. Biol. Chem.* **2008**, *283* (30), 20813–20820.

(357) Larach, M. G. *Anesth. Analg.* **1989**, *69* (4), 511–515.

(358) Riazi, S.; Larach, M. G.; Hu, C.; Wijeysundera, D.; Massey, C.; Kraeva, N. *Anesth. Analg.* **2014**, *118* (2), 381–387.

(359) Capacchione, J. F.; Sambuughin, N.; Bina, S.; Mulligan, L. P.; Lawson, T. D.; Muldoon, S. M. *Anesthesiology* **2010**, *112*, 239–244.

(360) Tobin, J. R.; Jason, D. R.; Challa, V. R.; Nelson, T. E.; Sambuughin, N. *J. Am. Med. Assoc.* **2001**, *286* (2), 2–7.

(361) Vladutiu, G. D.; Isackson, P. J.; Kaufman, K.; Harley, J. B.; Cobb, B.; Christopher-Stine, L.; Wortmann, R. L. *Mol. Genet. Metab.* **2011**, *104* (1–2), 167–173.

(362) Fletcher, J.; Rosenberg, H.; Beech, J. In *Mechanisms of Anesthetic Action in Skeletal, Cardiac, and Smooth Muscle*; Blanck, T., Wheeler, D., Eds.; Plenum Press: Baltimore, 1991; pp 57–69.

(363) Giulivi, C.; Ross-Inta, C.; Omanska-Klusek, A.; Napoli, E.; Sakaguchi, D.; Barrientos, G.; Allen, P. D.; Pessah, I. N. *J. Biol. Chem.* **2011**, *286* (1), 99–113.

(364) Chang, L.; Daly, C.; Miller, D. M.; Allen, P. D.; Boyle, J. P.; Hopkins, P. M.; Shaw, M.-A. *Br. J. Anaesth.* **2019**, 1–9.

(365) Collins, F. *Nature* **2010**, *464*, 674–675.

(366) Cudjoe, E.; Togunde, P.; Pawliszyn, J. *Bioanalysis* **2012**, *4* (21), 2605–2619.

(367) Goryński, K.; Bojko, B.; Nowaczyk, A.; Bucinski, A.; Pawliszyn, J.; Kaliszan, R. *Anal. Chim. Acta* **2013**, *797*, 13–19.

(368) Bojko, B.; Gorynski, K.; Gómez-Ríos, G. A.; Knaak, J. M.; Machuca, T.; Spetzler Nikolaus, V.; Cudjoe, E.; Hsin, M.; Cypel, M.; Selzner, M.; Liu, M.; Keshavjee, S.; Pawliszyn, J. *Anal. Chim. Acta* **2013**, *803*, 75–81.

(369) Want, E. J.; Wilson, I. D.; Gika, H.; Theodoridis, G.; Plumb, R. S.; Shockcor, J.; Holmes, E.; Nicholson, J. K. *Nat. Protoc.* **2010**, *5* (6), 1005–1018.

(370) van den Berg, R. A.; Hoefsloot, H. C. J.; Westerhuis, J. A.; Smilde, A. K.; van der Werf, M. J. *BMC Genomics* **2006**, *15* (142), 1–15.

(371) Westerhuis, J. A.; Hoefsloot, H. C. J.; Smit, S.; Vis, D. J.; Smilde, A. K.; Velzen, E. J. J.; Duijnhoven, J. P. M.; Dorsten, F. A. *Metabolomics* **2008**, *4*, 81–89.

(372) Madsen, R.; Lundstedt, T.; Trygg, J. *Anal. Chim. Acta* **2010**, *659*, 23–33.

(373) Kyle, J. E.; Zhang, X.; Weitz, K. K.; Monroe, M. E.; Ibrahim, Y. M.; Moore, R. J.; Cha, J.; Sun, X.; Lovelace, E. S.; Wagoner, J.; Polyak, S. J.; Metz, T. O.; Dey, S. K.; Smith, R. D.; Burnum-Johnson, K. E.; Baker, E. S. *Analyst* **2016**, *141*, 1649–1659.

(374) Fang, N.; Yu, S.; Badger, T. M. *J. Agric. Food Chem.* **2003**, *51*, 6676–6682.

(375) Dong, J.; Cai, X.; Zhao, L.; Xue, X.; Zou, L.; Zhang, X.; Liang, X. *Metabolomics* **2010**, *6*, 478–488.

(376) Qiu, Z. H.; Gijo, M. A.; Carvalho, M. S. De; Spencer, D. M.; Leslie, C. C. *J. Biol. Chem.* **1998**, *273* (14), 8203–8211.

(377) Zhao, Y. Y.; Lin, R. C. *Chem. Biol. Interact.* **2014**, *215*, 7–16.

(378) Zhao, Y. Y.; Feng, Y. L.; Bai, X.; Tan, X. J.; Lin, R. C.; Mei, Q. *PLoS One* **2013**, *8* (3), 1–10.

(379) Zhao, Y. Y.; Cheng, X. L.; Wei, F.; Xiao, X. Y.; Sun, W. J.; Zhang, Y.; Lin, R. C. *Biomarkers* **2012**, *17* (1), 48–55.

(380) Zhao, Y. Y.; Cheng, X. L.; Cui, J. H.; Yan, X. R.; Wei, F.; Bai, X.; Lin, R. C. *Clin. Chim. Acta* **2012**, *413*, 1438–1445.

(381) Zhao, Y. Y. *Clin. Chim. Acta* **2013**, *422*, 59–69.

(382) Nakanishi, H.; Iida, Y.; Shimizu, T.; Taguchi, R. *J. Biochem.* **2010**, *147* (2), 245–256.

(383) Suárez-García, S.; Arola, L.; Pascual-Serrano, A.; Arola-Arnal, A.; Aragonès, G.; Bladé, C.; Suárez, M. *J. Chromatogr. B* **2017**, *1055–1056*, 86–97.

(384) Lee, J. Y.; Min, H. K.; Moon, M. H. *Anal. Bioanal. Chem.* **2011**, *400*, 2953–2961.

(385) Sugasini, D.; Subbaiah, P. V. *PLoS One* **2017**, 1–13.

(386) Liebisch, G.; Drobnik, W.; Lieser, B.; Schmitz, G. *Clin. Chem.* **2002**, *48* (12), 2217–2224.

(387) Watson, D. G. *Comput. Struct. Biotechnol.* **2013**, *4* (5), 1–10.

(388) DeLuca, H. F. In *Steroid Hormone Resistance*; Chrousos, G. P., Loriaux, L. D., Lipsett, M. B., Eds.; Springer: Boston, MA, 1986; pp 361–375.

(389) Cheah, K. S.; Cheah, A. M.; Fletcher, J. E.; Rosenberg, H. *Int. J. Biochem.* **1989**, *21* (8), 913–920.

(390) Fletcher, J. E.; Mayerberger, S.; Tripolitis, L.; Yudkowsky, M.; Rosenberg, H. *Life Sci.* **1991**, *49* (22), 1651–1657.

(391) Wong, J. T.; Tran, K.; Pierce, G. N.; Chan, A. C.; Karmin, O.; Choy, P. C. *J. Biol. Chem.* **1998**, *273* (12), 6830–6836.

(392) Fletcher, E.; Tripolitis, L.; Erwin, K.; Hanson, S.; Rosenberg, H.; Conti, P.; Beech, J. *Biochem. Cell Biol.* **1990**, *68* (10), 1195–1201.

(393) Wieland, S. J.; Fletcher, J. R.; Gong, Q.; Rosenberg, H. In *Mechanisms of Anesthetic Action in Skeletal, Cardiac, and Smooth Muscle*; Blanck, T. J., Wheeler, D. M., Eds.; Plenum Press: New York, 1991; pp 9–19.

(394) Fletcher, J.; Rosenberg, H.; Michaux, K.; Tripolitis, L.; Lizzo, F. *Eur. J. od Anaesthesiol.* **1989**, *6* (5), 355–362.

(395) Adibhatla, R. M.; Hatcher, J. F. *Free Radic. Biol. Med.* **2006**, *40*, 376–387.

(396) Ramanadham, S.; Ali, T.; Ashley, J. W.; Bone, R. N.; Hancock, W. D.; Lei, X. *J. Lipid Res.* **2015**, *56*, 1643–1668.

(397) Gong, M. C.; Arbogast, S.; Guo, Z.; Mathenia, J.; Su, W.; Reid, M. B. *J. Appl. Physiol.* **2006**, *100*, 399–405.

(398) Yoda, E.; Hachisu, K.; Taketomi, Y.; Yoshida, K.; Nakamura, M.; Ikeda, K.; Taguchi, R.; Nakatani, Y.; Kuwata, H.; Murakami, M.; Kudo, I.; Hara, S. *J. Lipid Res.* **2010**, *51*, 3003–3015.

(399) Jurivich, D. A.; Pangas, S.; Welk, J. F. *J. Immunol.* **1996**, *157*, 1669–1677.

(400) Carper, M. J.; Zhang, S.; Turk, J.; Ramanadham, S. *Biochemistry* **2008**, *47* (46), 12241–12249.

(401) Cheah, K. S.; Cheah, A. M. *Biochim. Biophys. Acta* **1981**, *638*, 40–49.

(402) Duncan, C. J. *Cell Tissue Res.* **1988**, *253*, 457–462.

(403) Boittin, F. X.; Petermann, O.; Hirn, C.; Mittaud, P.; Dorchies, O. M.; Roulet, E.; Ruegg, U. T. *J. Cell Sci.* **2006**, *119*, 3733–3742.

(404) Malhotra, A.; Edelman-Novemsky, I.; Xu, Y.; Plesken, H.; Ma, J.; Schlame, M. *Proc. Natl. Acad. Sci. U. S. A.* **2008**, *106* (7), 2337–2341.

(405) Horton, E. W. *Br. Med. Bull.* **1979**, *35* (3), 295–300.

(406) Horrobin, D. F.; Morgan, R.; Karmali, R. A.; Manku, M. S.; Karmazyn, M.; Ally, A.; Mtabaji, J. P. *Med. Hypotheses* **1977**, *3* (4), 150–153.

(407) Ohnishi, S. T.; Katsuoka, M. In *Mechanisms of Anesthetic Action in Skeletal, Cardiac, and Smooth Muscleheric Acrion in Skeletal, Cardiac, and Smooth Muscle*; Blanck, T. J., Wheeler, D. M., Eds.; Plenum Press: New York, 1991; pp 73–87.

(408) Cruz, F. F.; Rocco, P. R. M.; Pelosi, P. *Crit. Care* **2017**, *21* (67), 1–7.

(409) Scholz, J.; Roewer, N.; Troll, U.; Patten, M.; Shmitz, W.; Scholz, H.; Schulte, am E. *Anasthesiol. Intensivmed. Notfallmedizin, Schmerztherapie* **1991**, *26* (8), 450–453.

(410) Rizzo, W. B.; Craft, D. A. *J. Lipid Res.* **2000**, *41*, 1077–1081.

(411) McCoin, C. S.; Knotts, T. A.; Ono-Moore, K. D.; Oort, P. J.; Adams, S. H. *Am. J. Physiol. Endocrinol. Metab.* **2015**, *308* (11), 1–21.

(412) Kiens, B.; Roepstorff, C. *Acta Physiol. Scand.* **2003**, *178*, 391–396.

(413) Makrecka-Kuka, M.; Sevostjanovs, E.; Vilks, K.; Volska, K.; Antone, U.; Kuka, J.; Makarova, E.; Pugovics, O.; Dambrova, M.; Liepinsh, E. *Sci. Rep.* **2017**, *7* (17528), 1–11.

(414) Giesbertz, P.; Ecker, J.; Haag, A.; Spanier, B.; Daniel, H. *Methods* **2015**, *56*, 2029–2039.

(415) Topçu, Y.; Bayram, E.; Karaoğlu, P.; Yiş, U.; Kurul, S. H. *Ann. Indian Acad. Neurol.* **2014**, *17* (4), 437–440.

(416) McCoin, C. S.; Knotts, T. A.; Adams, S. H. *Nat. Rev. Endocrinol.* **2015**, *11*, 617–625.

(417) Divry, P.; Vianey-Saban, C.; Mathieu, M. *J. Inherit. Metab. Dis.* **1999**, *22*, 286–288.

(418) Engel, A. G.; Angelini, C. *Science (80-.).* **1973**, *179* (4076), 899–902.

(419) KEGG. Nitrogen metabolism https://www.genome.jp/dbget-bin/www_bget?map00910 (accessed Apr 17, 2019).

(420) Park, S. G.; Schimmel, P.; Kim, S. *Proc. Natl. Acad. Sci. U. S. A.* **2008**, *105* (32), 11043–11049.

(421) Hesselink, J. M. K.; Boer, T. De; Witkamp, R. F. *Hindawi Pub. Corp. Int. J. Inflamm.* **2013**, *ID 151028*,

1–8.

(422)   Bonafe, L.; Troxler, H.; Kuster, T.; Heizmann, C. W.; Chamoles, N.; Burlina, A. B.; Blau, N. *Mol. Genet. Metab.* **2000**, *69*, 302–311.

(423)   Farthing, D. E.; Farthing, C. A.; Xi, L. *Exp. Biol. Med.* **2015**, *240*, 821–831.

(424)   Macchi, C.; Molino-Lova, R.; Polcaro, P.; Guarducci, L.; Lauretani, F.; Cecchi, F.; Bandinelli, S.; Guralnik, J. M.; Ferrucci, L. *Mech. Ageing Dev.* **2008**, *129*, 522–527.

(425)   Molino-Lova, R.; Sofi, F.; Pasquini, G.; Vannetti, F.; Del Ry, S.; Vassalle, C.; Clerici, M.; Sorbi, S.; Macchi, C. *Eur. J. Intern. Med.* **2017**, *41*, 39–43.

(426)   Kim, S.; Lee, D. Y.; Wohlgemuth, G.; Park, H. S.; Fiehn, O.; Kim, K. H. *Anal. Chem.* **2013**, *85*, 2169–2176.

(427)   Bruce, S. J.; Tavazzi, I.; Veronique, P.; Rezzi, S.; Kochhar, S.; Guy, P. A. *Anal. Chem.* **2009**, *81*, 3285–3296.

(428)   Teahan, O.; Gamble, S.; Holmes, E.; Waxman, J.; Nicholson, J. K.; Bevan, C.; Keun, H. C. *Anal. Chem.* **2006**, *78*, 4307–4318.

(429)   Canelas, B.; Pierick, A.; Ras, C.; Seifar, R. M.; van Dam, J. C.; van Gulik, W. M.; Heijnen, J. J. *Anal. Chem.* **2009**, *81*, 7379–7389.

(430)   Duportet, X.; Aggio, R. B. M.; Carneiro, S.; Villas-Boas, S. G. *Metabolomics* **2012**, *8*, 410–421.

(431)   Ivanisevic, J.; Thomas, A. In *Clinical Metabolomics: Methods and Protocols, Methods in Molecular Biology*; Giera, M., Ed.; Humana Press: New York, 2018; Vol. 1730, pp 3–28.

(432)   Kind, T.; Tolstikov, V.; Fiehn, O.; Weiss, R. H. *Anal. Biochem.* **2007**, *363*, 185–195.

(433)   Farshidfar, F.; Weljie, A. M.; Kopciuk, K. A.; Hilsden, R.; Mcgregor, S. E.; Buie, W. D.; Maclean, A.; Vogel, H. J.; Bathe, O. F. *Br. J. Cancerh J. Cancer* **2016**, *115* (7), 848–857.

(434)   Yet, I.; Menni, C.; Shin, S.-Y.; Mangino, M.; Soranzo, N.; Adamski, J.; Suhre, K.; Spector, T. D.; Kastenmüller, G.; Bell, J. T. *PLoS One* **2016**, *11* (4), 1–13.

(435)   Górecki, T.; Yu, X.; Pawliszyn, J. *Analyst* **1999**, *124*, 643–649.

(436)   Triba, M.N.; Le Moyec, L.; Amathieu, R.; Goossens, C.; Bouchemal, N.; Nahon P.; Rutledge, D.N.; Savarin, P. *Mol. BioSyst.*, **2015**, *11*, 13-19.

(437)   Szymańska, E.; Saccenti, E.; Smilde, A.K.; Westerhuis, J.A. *Metabolomics* **2012**, *8*, 3-16.

(438)   Viswan, A.; Singh, C.; Rai, R.K.; Azim, A.; Sinha, N.; Kumar Baronia, A. *PLOS ONE* **2017** 12(11): e0187545

(439)   Umetrics, User Guide SIMCA (Version 13) 2012. http://chemsrv0.pph.univie.ac.at/scripten/EDV/Software/Simca13/User%20Guide%20to%20SIMCA%2013.pdf (accessed 15 August 2019)